Exploring Weather and Climate

Glen Sampson

First Edition

CC BY NC SA

TABLE OF CONTENTS

PREFACE 6

CHAPTER 1 - INTRODUCTION AND ATMOSPHERIC STRUCTURE 7

Overview 7

1.1 - Scientific Method 7

1.2 - Units of Measure Used in Atmospheric Science 8

1.3 - Using Maps 10

1.4 - Weather Basics 12

1.5 - Atmospheric Composition 21

1.6 - Atmospheric Pressure 23

1.7 - Layers of the Atmosphere 25

Chapter 1 Review Questions 28

CHAPTER 2 - ENERGY AND EARTH'S ENERGY BALANCE 29

Overview 29

2.1 - Types of Energy 29

2.2 - Causes of Earth's Seasons 38

2.3 - Atmospheric Influences on Insolation 42

2.4 - Earth's Energy Balance (Shortwave and Longwave Radiation) 46

Chapter 2 Review Questions 51

CHAPTER 3 – PRESSURE AND WIND 52

Overview 52

3.1 - Space Weather Essentials 52

3.2 - Concepts Associated with Pressure 57

3.3 – Applying the Forces Which Affect Wind 66

Chapter 3 Review Questions 74

CHAPTER 4 - ATMOSPHERIC MOISTURE I 75

Overview 75

4.1 – The Changing States of Water 75

4.2 – Measuring Water Vapor 78

4.3 – How Do Cloud Droplets Occur? 83

4.4 – Concepts for Lowering the Air Temperature 87

4.5 – Atmosphere Stability 93

Chapter 4 Review Questions 99

CHAPTER 5 – ATMOSPHERIC MOISTURE II 100
Overview 100
5.1 – Cloud Types 100
5.2 – Growth of Cloud Droplets for Precipitation 108
5.3 - Water (Hydrologic) Cycle 114
5.4 – Measuring and Tracking Surface Water 118
5.5 – Floods 124
Chapter 5 Review Questions 129

CHAPTER 6 - GLOBAL CIRCULATIONS 130
Overview 130
6.1 – Concept of Scale 130
6.2 – Global Scale 132
6.3 – Synoptic Scale 141
6.4 – Air masses 144
6.5 – Fronts 147
Chapter 6 Review Questions 157

CHAPTER 7 – MIDLATITUDE CYCLONES AND WIND SYSTEMS 158
Overview 158
7.1 – Midlatitude Cyclones 158
7.2 – Concept of Vorticity 169
7.3 – Local Wind Systems - Sea Breeze 172
7.4 – Monsoons – Asian Monsoon 176
Chapter 7 Review Questions 180

CHAPTER 8 – LIGHTNING AND THUNDERSTORMS 181
Overview 181
8.1 - Lightning 181
8.2 - Thunderstorms 189
8.3 - How a Weather Radar Works 200
8.4 - Radar Reflectivity Observations 204
Chapter 8 Review Questions 213

CHAPTER 9 – TORNADOES AND HURRICANES 214
Overview 214
9.1 – Tornadoes 214
9.2 – Tropical Storms and Hurricanes 225
9.3 – Hurricane Hazards 238
Chapter 9 Review Questions 246

CHAPTER 10 – OPTICAL PHENOMENA AND WEATHER FORECASTING 247
Overview 247
10.1 – Atmospheric optics 247
10.2 – Weather Forecasting 257
Chapter 10 Review Questions 270

CHAPTER 11 – EARTH'S CLIMATES 272
Overview 272
11.1 – Temperature and Climate 272
11.2 – Weather Factors Affecting Temperature 280
11.3 – Climate Classification 283
Chapter 11 Review Questions 299

CHAPTER 12 – HUMAN INFLUENCES ON THE ATMOSPHERE 300
Overview 300
12.1 – Atmospheric Pollutants 300
12.2 – The Interactions Between Weather and Pollution 312
12.3 – Heat Islands 315
12.4 – Earth's Climate System 321
12.5 – Energy Resources 329
Chapter 12 Review Questions 334

CHAPTER 13 – PALEOCLIMATES AND CLIMATE VARIABILITY 335
Overview 335
13.1 – Paleoclimate and Short-term Climate Proxies 335
13.2 – Long-term Climate Proxies 341
13.3 – Natural Climate Variability 350
13.4 – Natural Ocean Circulations and Oscillations 357
Chapter 13 Review Questions 369

CHAPTER 14 – ANTHROPOGENIC CLIMATE CHANGE AND EARTH'S FUTURE CLIMATE 371
Overview 371
14.1 – Observed Anthropogenic Climate Changes 371
14.2 – Global Circulation Models (GCMs) 386
14.3 – Climate Projections 391
Chapter 14 Review Questions 400

CHAPTER 15 – CLIMATE CHANGE AND EXTREME WEATHER 401
Overview 401
15.1 – Attribution of Climate Changes to Weather Events 401

15.2 – Confidence in Attribution Studies 402
15.3 – Approaches for Dealing with Climate Change 415
Chapter 15 Review Questions 420

CHAPTER 16 – AMERICA'S CLIMATE CHOICES 421
Overview 421
16.1 – The Unique Challenges of Climate Change 421
16.2 – A Framework for Making Climate Choices 422
16.3 – Key Elements in Making Climate Choices 423
Chapter 16 Review Questions 426

REFERENCES, OER, AND PUBLIC DOMAIN MATERIALS USED 427

Exploring Weather and Climate © 2025 by Glen Sampson is licensed under CC BY-NC-SA 4.0. To view a copy of this license, visit https://creativecommons.org/licenses/by-nc-sa/4.0/.

Preface

This textbook is oriented toward a first or second year college science class, or an advanced high school course. Sixteen chapters are present which fits a 16-week college semester. These chapters may be divided into three sections:

1. Atmospheric processes including structure, composition, energy balance, pressure forces, moisture, stability, and precipitation processes in Chapters 1 through 5.
2. Weather systems including global circulation, tropical and extratropical cyclones, thunderstorms, tornadoes, atmospheric optics, and weather forecasting in Chapters 6 through 10.
3. Climate topics including classification, human influences on the atmosphere, natural climate variability, paleoclimate, climate change due to anthropogenic influences, climate projections, and a changing climate's affect on extreme weather in Chapters 11 through 16.

The book is written to build upon a person's knowledge from Chapter 1 to the end. The chapters do not need to be used in a numerical order, but some knowledge "gaps" may need to be filled for cohesiveness if a person skips around.

At the end of each chapter there are review questions, which highlight many important topics in that chapter. At the end of the book is a references section which contains information on the origin of the materials used in this book. The efforts of many people went into creating the materials assembled in this book. This reference section highlights their efforts, and provides a person with easy access if more details on a topic are desired.

Chapter 1 - Introduction and Atmospheric Structure

Overview

This chapter covers the scientific method, basic techniques for interpreting weather data, an introduction to atmospheric pressure, and the composition and structure of the atmosphere.

Chapter objectives:

1. Understand the scientific method.
2. Interpret basic weather data.
3. Distinguish between permanent and variable gases in the atmosphere and list the major gases in each category.
4. Describe how pressure is created.
5. Identify and describe the layers of the Earth's atmosphere.

1.1 - Scientific Method

At the core of science lies a problem-solving approach called the scientific method. The **scientific method** is a scheme for answering scientific questions. The scientific method is used in all the sciences, and has six steps (Figure 1-1):

1. Make an observation.
2. Ask a question about this observation.
3. Form a hypothesis, or testable explanation, to answer this question.
4. Make a prediction based on the hypothesis.
5. Test the prediction and analyze the results.
6. Make a conclusion.

Scientists in different fields ask different questions and perform different tests, but everyone uses the same core approach to find answers that are logical and supported by evidence. Each step in the scientific method can be repeated or redone as new understanding occurs. This method is not rigid and allows a scientist to move back and forth between the steps as needed. This diagram illustrates the scientific method.

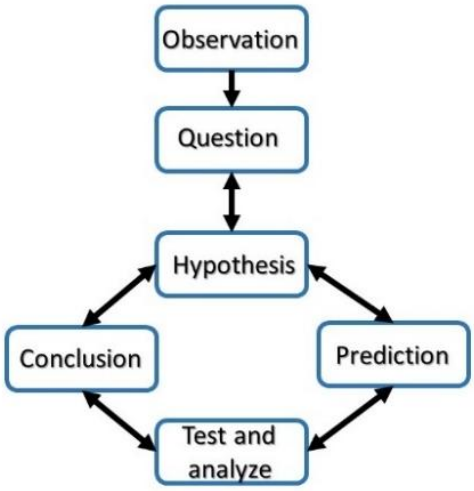

Figure 1-1: Steps used in the scientific method.

Here is an example of the scientific method. Say you live in a cold climate in Northern Europe. You have observed (step 1) that a pond nearby freezes faster than the ocean. Both the pond and ocean have similar weather, which raises the question (step 2), why does the pond freeze

before the ocean? After pondering this question, you hypothesize (step 3) that the ocean has salt in it. The prediction (step 4) is that salt lowers the temperature at which the water will freeze. A good hypothesis must be testable, and the test must be repeatable (step 5). To test this hypothesis and prediction, other factors which could affect the water freezing must be removed. Other factors could be wind, waves, or boat traffic. If we were to take two containers of water, one with salt and one without, these other factors would be removed when testing the hypothesis.

This example provides the means to design an experiment, run the experiment, analyze the results of the experiment, and then make a conclusion (step 6). While running the experiment, data could be gathered on what temperature each container starts to freeze. This information would allow a prediction with more detail than was originally proposed. The double pointed arrows in the diagram illustrate this ability to easily go between steps and adjust steps when warranted.

When using the scientific method, these three precautions should be noted:

1. The scientific method can only disprove hypotheses. A scientific theory can never be proven to be 100% correct, because new information may become available which contradicts previous tests and results.

2. Correlation is not causation. A correlation is an analysis of data without any understanding of the conditions causing that data to occur. The best science tries to determine the cause behind what is being observed.

3. Selective windowing should be avoided. Selective windows pick and choose which facts or data to examine, so a desired conclusion is achieved. The whole truth and all aspects of the tests should be present in the scientific method.

1.2 - Units of Measure Used in Atmospheric Science

This section reviews the units that will be used in this course. Most scientific fields use the metric system and atmospheric science is not an exception. However, the United States uses some English system units when measuring surface parameters. These exceptions are noted below.

The information in section 1.2 does not need to be memorized, rather it is presented as an introduction to the notation and terms used throughout the course.

Scientific Notation

Long form		Scientific notation	Name	Symbol
1,000,000,000	=	10^9	giga	G
1,000,000	=	10^6	mega	M
1,000	=	10^3	kilo	k
100	=	10^2	hecto	h

Long form		Scientific notation	Name	Symbol
10	=	10^{1}	deka	da
1	=	10^{0}		
0.1	=	10^{-1}	deci	d
0.01	=	10^{-2}	centi	c
0.001	=	10^{-3}	milli	m
0.000001	=	10^{-6}	micro	μ

Units of Length

Unit	Symbol	Relationship	English system
micron	μ	10^{6} μ = 1 m	
millimeter	mm	1000 mm = 1 m	1 mm = 0.03937 in
meter	m		1 m = 1.0936 yd
kilometer	km	1 km = 1000m	1 km = 0.6214 mi

Units of mass

Unit	Symbol	Relationship	English system
gram	g		1 g = 0.03527 oz
kilogram	kg	1 kg = 1000 g	1 kg = 2.2046 lb

Temperature

Unit	Symbol	Conversion equation
degree Celsius	ºC	1ºC = 5/9 (ºF - 32)
degree Fahrenheit	ºF	1ºF = 9/5 (ºC) + 32

In the United States surface temperatures are reported in Fahrenheit, and everything aloft is reported in Celsius. Most other countries report all temperatures in Celsius.

Speed

Unit	Symbol	Relationship	English system
meters/second	m/s		1 m/s = 2.24 mph
kilometers/hour	kph	1 km/hr = 0.278 m/s	1 km/hr = 0.6214 mph
knots	kn	1 kn = 0.514 m/s	1 kn = 1.151 mph

A knot is a nautical mile per hour and is not part of the metric system. Traditionally all wind speeds were reported in knots. With the advent of computers, wind speeds at the surface

frequently are given in miles per hour (mph) or kilometers per hour (kph). Winds aloft are always reported in knots in the United States.

Pressure

Unit	Symbol	Relationship	English system
atmosphere	atm	1 atm = 1013.2 mb	1 atm = 14.7 lb/in^2
millibar	mb		1 mb = 0.6895 lb/in^2
kilopascal	kPa	1 kPa = 10 mb	1 kPa = 6.895 lb/in^2

Most of the world, including the United States, uses millibar (mb) as the atmospheric pressure measurement. Some countries use kilopascal (kPa), which is essentially the same as millibar with the decimal moved one place to the left.

Energy

Unit	Symbol	Relationship
joule (Newton meter)	J (N m)	1 J = 0.239 calorie
watt	W	1 W = 1 J/sec

Most energy measurements are based in the metric system. The defining unit of energy is the calorie. One calorie is the amount of energy required to raise 1 gram of water 1 degree Celsius. Food nutritional labels use the calorie as an indication of how much energy a person will get from this product. The watt is commonly used as a measurement when dealing with electricity. Light bulbs post their energy consumption in watts.

1.3 - Using Maps

Earth is almost a perfect sphere, which makes accurately representing it on a paper or computer screen difficult. Earth is three-dimensional while a piece of paper has two dimensions. Thus, all maps have distortions inherent in them.

The first step in representing Earth on a map is to establish a coordinate system. This coordinate system uses longitude and latitude lines. Longitude lines (also called meridians) go from the North Pole across the equator to the South Pole. By convention, a Prime Meridian (Figure 1-2) was established as 0°. The Prime Meridian is situated on Greenwich, England. Traveling east or west of the Prime Meridian provides a degrees east or west longitude location.

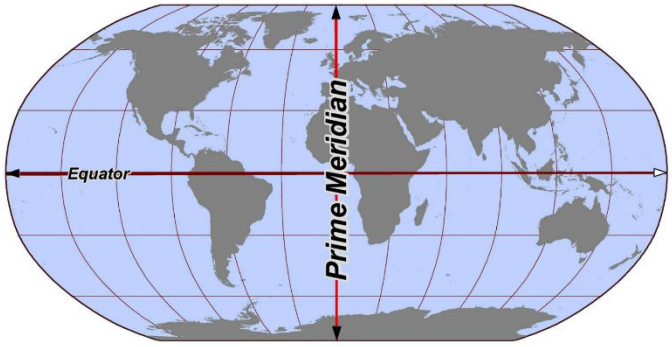

Figure 1-2: Prime Meridian location at 0 degrees longitude. East (right) of the Prime Meridian are east longitude and west longitude is towards the left. The North Pole is at the top and the South Pole is at the bottom.

Latitude lines (also called parallels) are oriented east and west with the zero latitude being the equator. Latitude lines north of the equator increase up to 90°N at the North Pole. Likewise, latitude lines south of the equator are designated with a “S”.

The latitude-longitude coordinates provide a grid to create maps and place features on these maps. Since all maps have some distortion, many different map projections have been developed. Each map projection has advantages and disadvantages. Several types of maps used in this course are Mercator, Robinson, and Mollweide.

The Mercator map projection (Figure 1-3) was originally developed for nautical navigation and places a route at a constant angle to the lines. Representation of features near the equator are good, while accurate representation near the poles is poor. Notice that Greenland is extremely large. In actuality, Greenland is about three times the size of Texas.

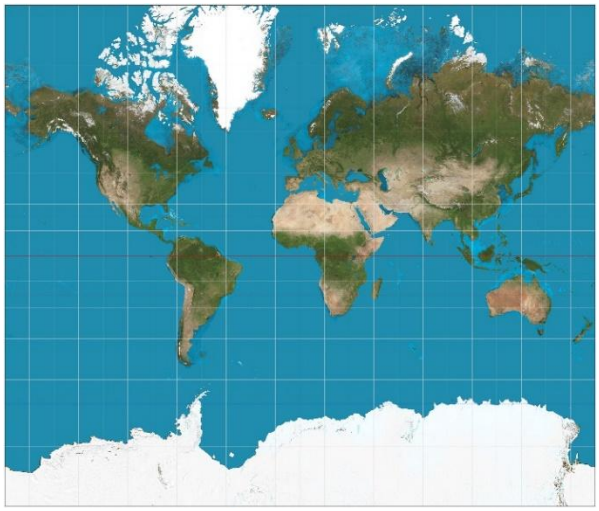

Figure 1-3: Mercator map projection.

To reduce the distortion near the poles, a Robinson projection (Figure 1-4) was developed. This projection curves the longitude lines near the poles inward. The actual size of Greenland is now better represented.

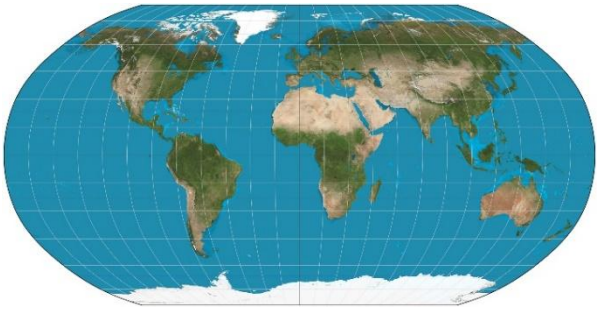

Figure 1-4: Robinson map projection.

Following this approach further, the Wollmeide projection (Figure 1-5) was developed. This projection curves the longitude lines all the way into the pole. Greenland is even smaller in this projection.

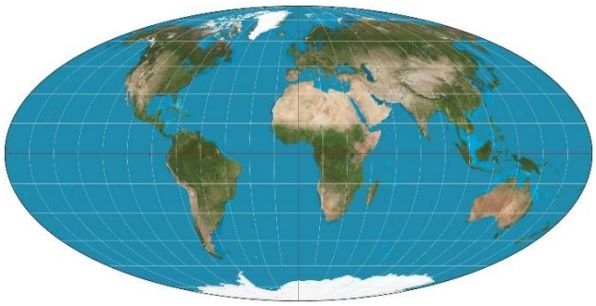

Figure 1-5: Wollmeide map projection.

1.3.1 - Topographical Maps

With the essentials about maps covered, data is ready to be placed on them. One type of data widely used on maps is elevation data. Maps with elevation data are called topographical maps.

Understanding topographical maps lends itself to the process of interpreting weather maps. Thus, taking a quick look at topographical maps is useful.

A topographical map of the Big Island in Hawaii is a good illustration. Since the Big Island is surrounded by water, the elevation at the coast is sea-level or zero. There are two high volcanic summits: Mauna Loa and Mauna Kea at 13,452 feet and 13,796 feet. Hence, the change in elevation on the Big Island is dramatic.

A topographical map of Hawaii (right) gives a representation of elevation. The more contour lines, the greater the change in elevation. Note the two volcanic peaks on the contour map and compare them with the image of Hawaii taken from space (left).

Figure 1-6: Modis satellite image of the Big Island, Hawaii. Credit: NASA

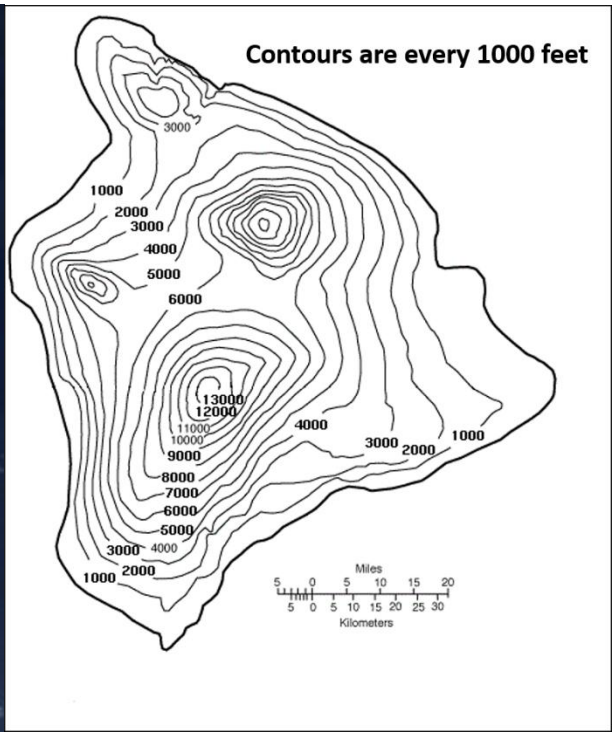

Figure 1-7: Topographical map of the Big Island, Hawaii. Contours are at 1000 feet intervals with the highest point at 13,000 feet.

Each contour on the map is an **isopleth**, which is a contour connecting points of equal value ("iso" translates to "equal" and "pleth" means "value"). In this case, the isopleths connect points of equal elevation above sea-level, and are drawn for every 1,000 feet of elevation above sea level. Isopleths can be drawn at any interval. The lower the interval between isopleths the higher the resolution of the map.

1.4 - Weather Basics

When weather data is collected or disseminated, a key component is the time stamp of the data. Everyone needs to know when the data was collected or when the forecast is supposed to be valid. Since there are 24 hours in a day, there are 24 time zones across the world. Each time zone is 15^{o} longitude in width, although these boundaries are modified at a country's discretion.

Notice in Figure 1-8 China (a yellow country) has one time zone although covers over 60° longitude.

The time stamp for weather data has been universally agreed upon as the time at the Prime Meridian. This time is referred to as a Coordinated Universal Time (UTC), Zulu (Z) or Greenwich Mean Time (GMT). All three of these acronyms refer to the time at the Prime Meridian. Additionally, a 24-hour clock is used with UTC rather than 12 hours in the morning (a.m.) and 12 hours in the evening (p.m.) clock.

Figure 1-8: Time zones of the world.

To determine the UTC time at your current time zone, count the number of time zones between you and Greenwich (suburb of London), England. UTC is 5 hours (+5) ahead of New York City, 6 hours (+6) ahead of Dallas, 7 hours (+7) ahead of Denver, and 8 hours (+8) ahead of Los Angeles when all of these cities are on standard time. Many local time zones also have daylight savings time, rather than standard time, which shifts the difference between local time and UTC by 1 hour.

1.4.1 - Interpreting a Station Model

Figure 1-9 contains a typical surface weather map with observation data. As you can see, placing weather data on a map with the ability to read all the data may be difficult.

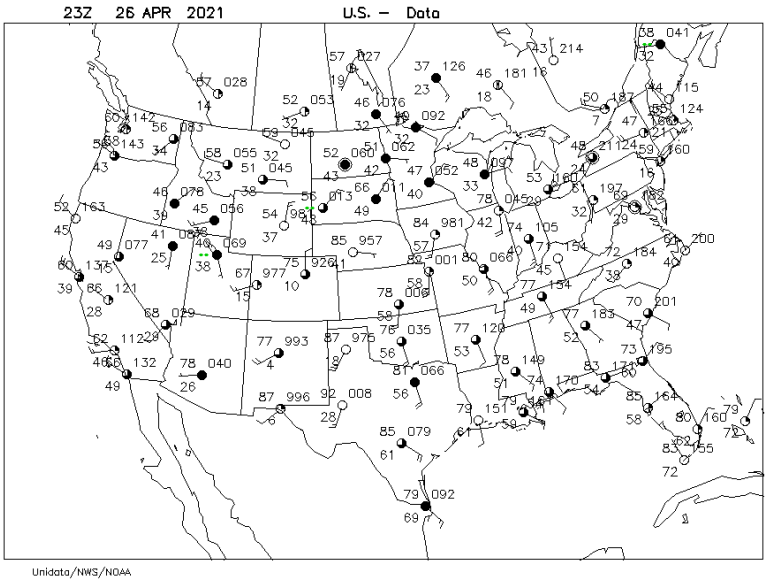

Figure 1-9: A typical map containing surface weather information at cities across the U.S.

Commonly, observations are arranged in a format called a station model. A **station model** is a graphical template showing current weather conditions at a weather station. Key variables displayed in a station model are temperature, dew point, type of weather occurring, pressure, wind, and sky cover. See Figure 1-10.

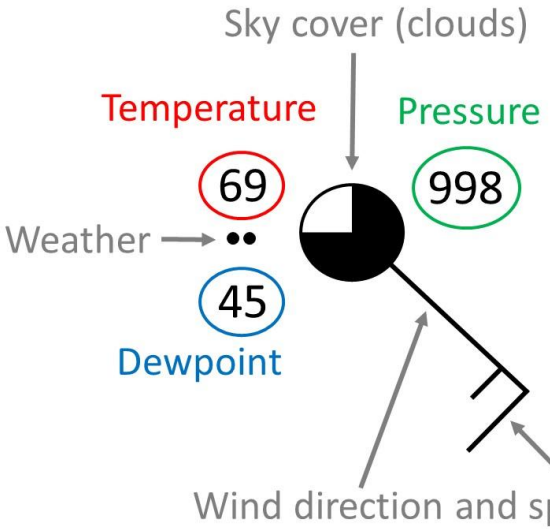

Figure 1-10: Station model used to place weather data on a map for each observation site.

Temperature is the air temperature in degrees Fahrenheit. Dewpoint is a new term for most people.

Dewpoint is the temperature at which water will start to condense out of the atmosphere. For example, in the station model diagram if the air temperature was cooled to 45 degrees, water would begin forming on nearby objects such as plants and cars. Dewpoint is a measure of humidity. This textbook has two chapters on atmospheric moisture, so humidity is examined in much more detail later.

Pressure is a measure of the amount of atmosphere above the weather observation station and is reported in millibars (mb). To save space, the first digit of pressure is usually omitted from the station model. Sea-level pressure on average is 1013.2 mb or about 1000 mb. A pressure value is generally reported to a tenth (0.1) of a millibar. Combining this information gives us a pressure value of 99.8 mb. Since we know the pressure should be close to 1000 mb and the first digit may be omitted, the omitted digit must be a "9". Inserting the missing digit gives an actual pressure of 999.8 mb. Another example would be if the pressure value in the station model was given as 046. In this example the missing digit(s) would be "10" for a pressure value of 1004.6 mb. The missing digit will be a "9" or a "10" for surface pressure to get close to 1000 mb.

Sky cover simply describes the portion of sky covered by clouds. The circle at the center of the station model is filled in to represent this value. Clear skies have an empty circle. Clouds across the entire sky has the circle filled. Clouds are reported in one eighth (1/8) increments.

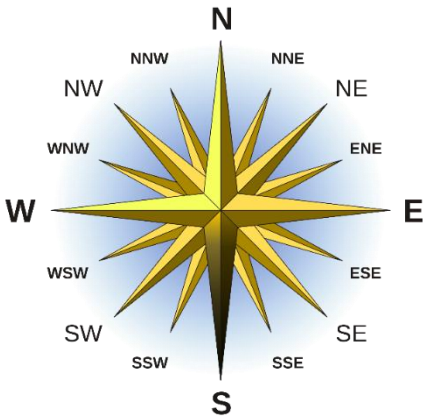

Figure 1-11: A compass rose, or wind rose, indicates the direction wind is blowing from.

Wind speed and direction is given in the lines attached to the sky cover circle. These lines are called a flag. The flag points in the direction the wind is coming from (see Figure 1-11). The direction is always expressed as the direction from which the wind blows. If facing into the wind, the direction you are facing is the wind direction. Wind direction follows a compass with north as up, west to the left, east to right and south down. In the station model the wind is coming from the southeast or simply stated as a southeast wind. The smaller lines on the flag indicate wind speed. A long line indicates 10 knots and a shorter line 5 knots. In the station model

diagram (figure 1-10) the wind speed is 15 knots. When a calm wind is occurring, that is no wind at all, the wind flag is omitted and a second circle is placed around the sky cover circle.

Weather is a description of what is occurring. If the weather field is blank, no weather is occurring. In the station model diagram (Figure 1-10), the two dots represent that rain is occurring. A dot is the symbol for rain. Some other symbols are an asterisk for snow, commas for drizzle and horizontal lines for fog.

A summary of the station model symbols is found in Figure 1-12.

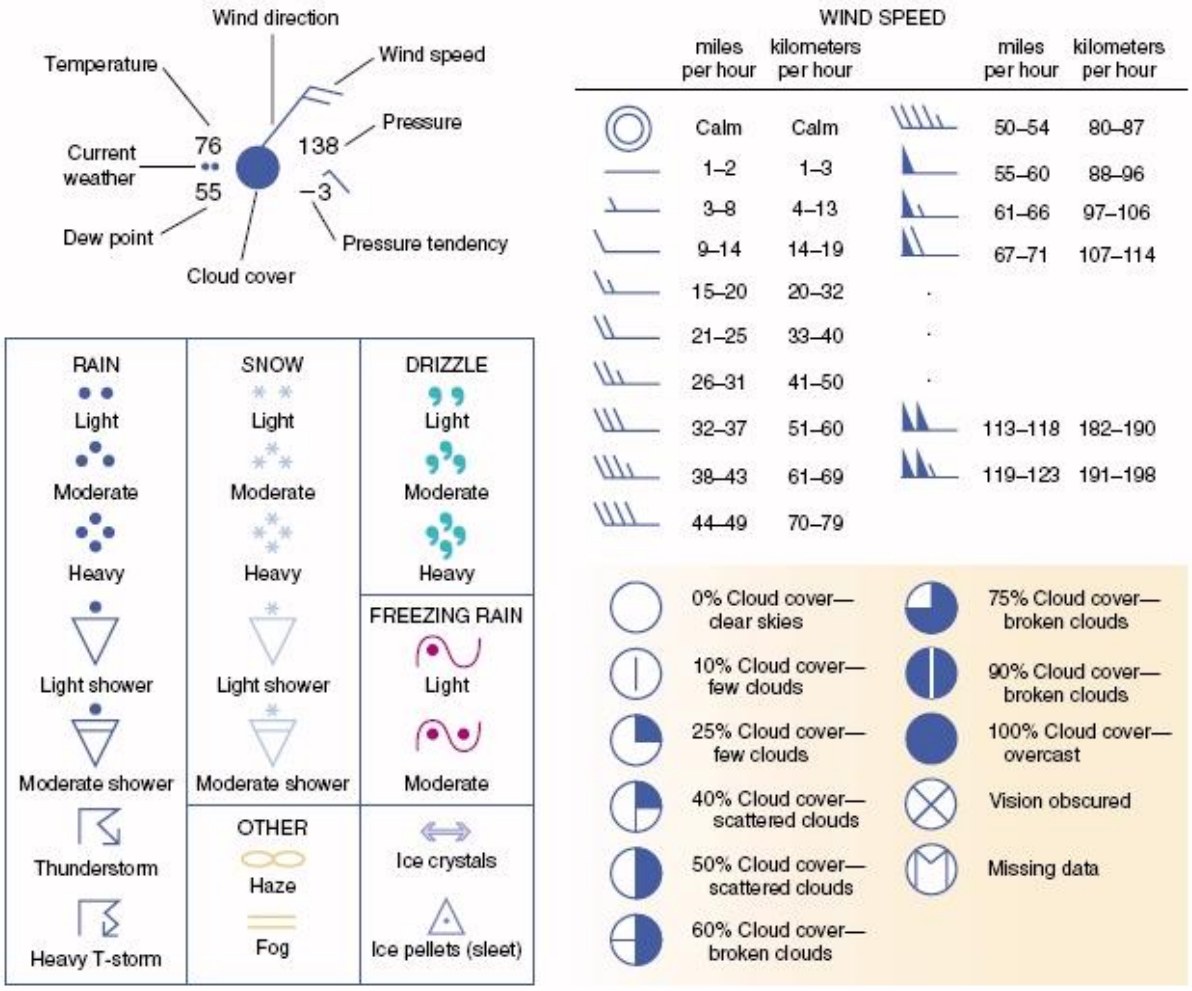

Figure 1-12: Station model key containing the symbols used in the station model and their values.

1.4.2 - Contour Maps

Meteorologists use contour maps to see how weather variables (temperature or pressure, for example) change over large areas, but they also use them to estimate values of weather variables at individual points. To get us started on interpreting contour maps, revisiting the topographical map of Hawaii will help.

How would a person determine the elevation of the point marked "P"? First, the two contours that lie on either side of "P" must be identified. In some cases, the contours needed are clearly

labeled; however, in other instances, the contour interval (1,000 feet, in this case) is needed to "count" up or down from a labeled contour. On this map, point "P" lies between 3000 feet and 4000 feet, so the elevation at point "P" is greater than (but not equal to) 3000 feet but less than (but again, not equal to) 4000 feet. Point "P" is not equal to either of these values because it does not lie on a contour line.

Technically, all that can be accurately stated about the elevation at point "P" is it between 3,000 and 4,000 feet. Often a single number is preferred instead of a range of elevations. An interpolation can be done between the two known elevations. In this case, “P” appears to be half-way between the contours so an estimated elevation of 3,500 feet is possible. Keep in mind that interpolation is only an estimated value.

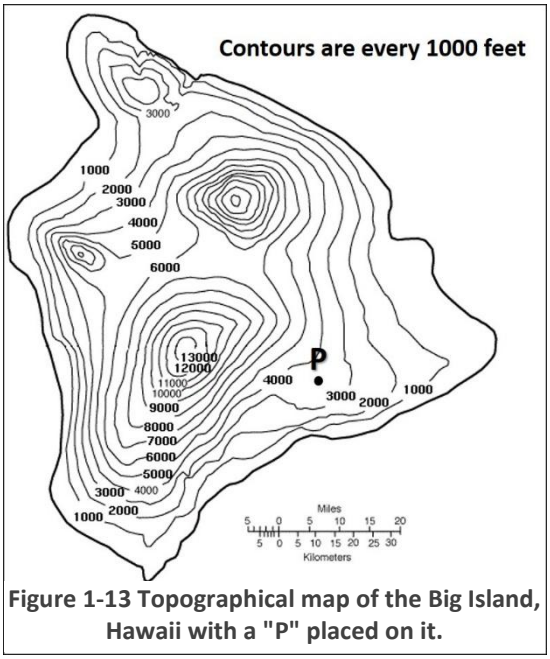

Figure 1-13 Topographical map of the Big Island, Hawaii with a "P" placed on it.

Two variables commonly contoured by meteorologists are temperature and air pressure. Isopleths of temperature are called **isotherms** (contours of constant temperature), and isopleths of pressure are called **isobars** (contours of constant pressure). Do not confuse the two! It would be incorrect to look at a map that shows contours of constant temperature and call them isobars.

Figure 1-14 is an isobar contour analysis for the surface observation data shown previously. This map has the surface pressures in black and the contour values in blue. The contour interval is 4 millibars (mb). As you can see, finding an area of higher pressure “H” or lower pressure “L” is much easier than looking at plotted data.

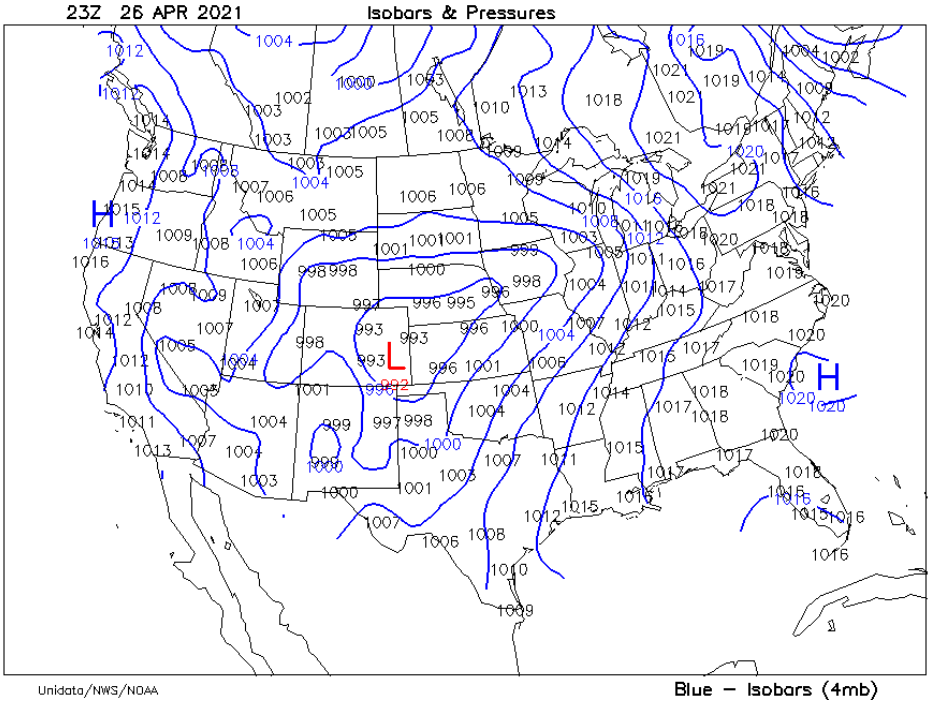

Figure 1-14: Surface pressure contour map. The pressure values are in millibars (mb).

An isotherm analysis for the same time is Figure 1-15. Again, individual station temperatures are in black, and the temperature contours are red. The contour interval is 10º F. Similarly, the contours make finding warm and cold areas much easier.

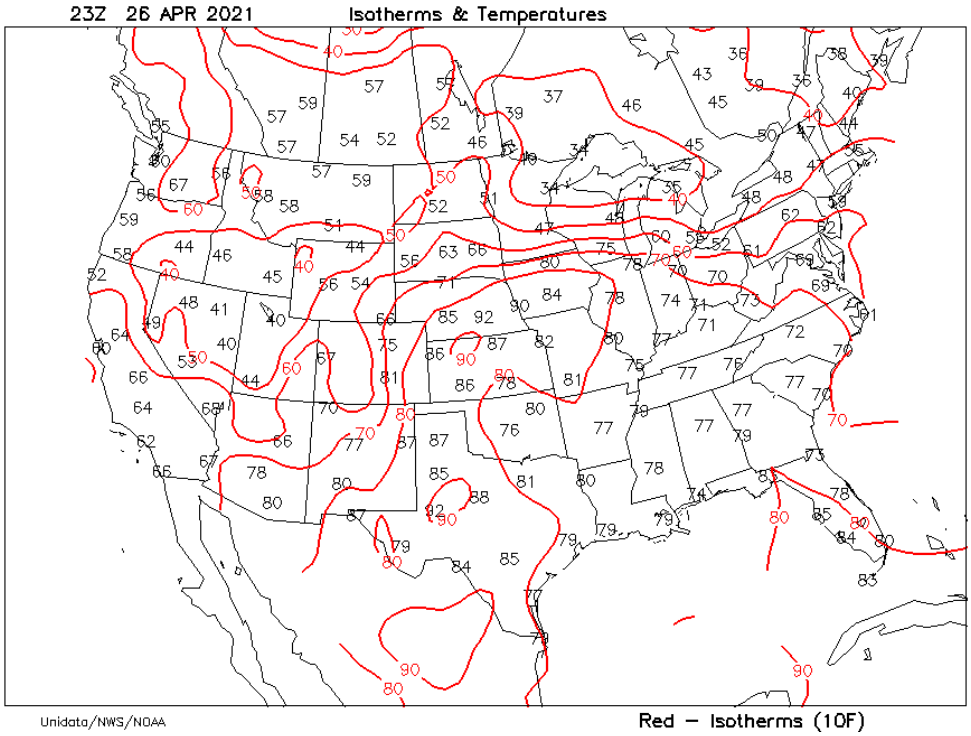

Figure 1-15: Surface temperature contour map. Th temperature contours are in 10°F

1.4.3 - Types of Weather Satellites

The two types of satellite used to track weather are called polar orbiting and geostationary as illustrated in Figure 1-16.

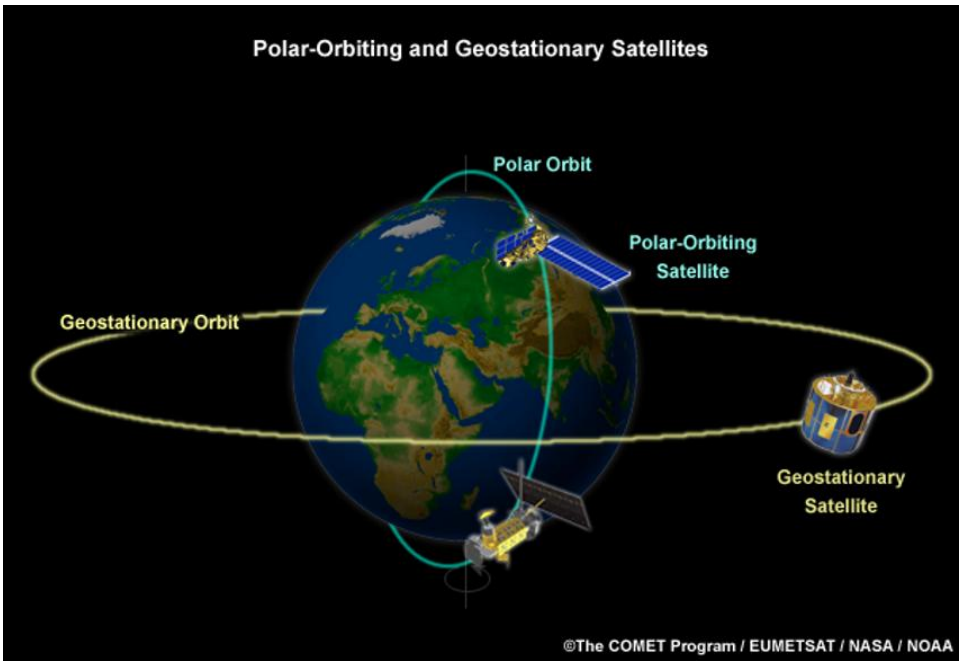

Figure 1-16: Diagram depicting the path of polar-orbiting and geostationary satellites.

A polar orbiting satellite circles the Earth around the poles. These satellites are located closer to Earth and as such can obtain higher resolution imagery than geostationary satellites. As the Earth rotates a polar orbiter satellite travels from north to south or south to north and observes a strip of the planet. An observation of a polar orbiting satellite has an appearance as shown in Figure 1-17.

Geostationary satellites are established at a fixed location over the Earth's equator. These satellites are at a higher orbit and generally provide lower resolution than polar orbiters. Since these satellites are at a fixed location imagery is always available for that region of the Earth. This aspect makes geostationary satellites the most widely used in weather analysis and forecasting. The United States has two GOES (Geostationary Orbiting Environmental Satellites); one located over the eastern U.S. and one over the West. The western satellite is typically referred to as GOES-West; the eastern one as GOES-East. Figure 1-18 is an image from GOES-West.

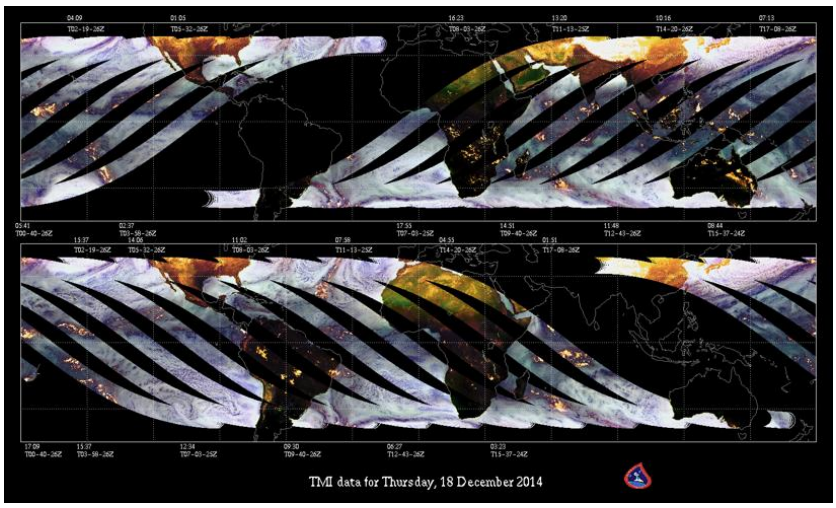

Figure 1-17: Imagery from a polar orbiting satellite as it tracks across the poles.

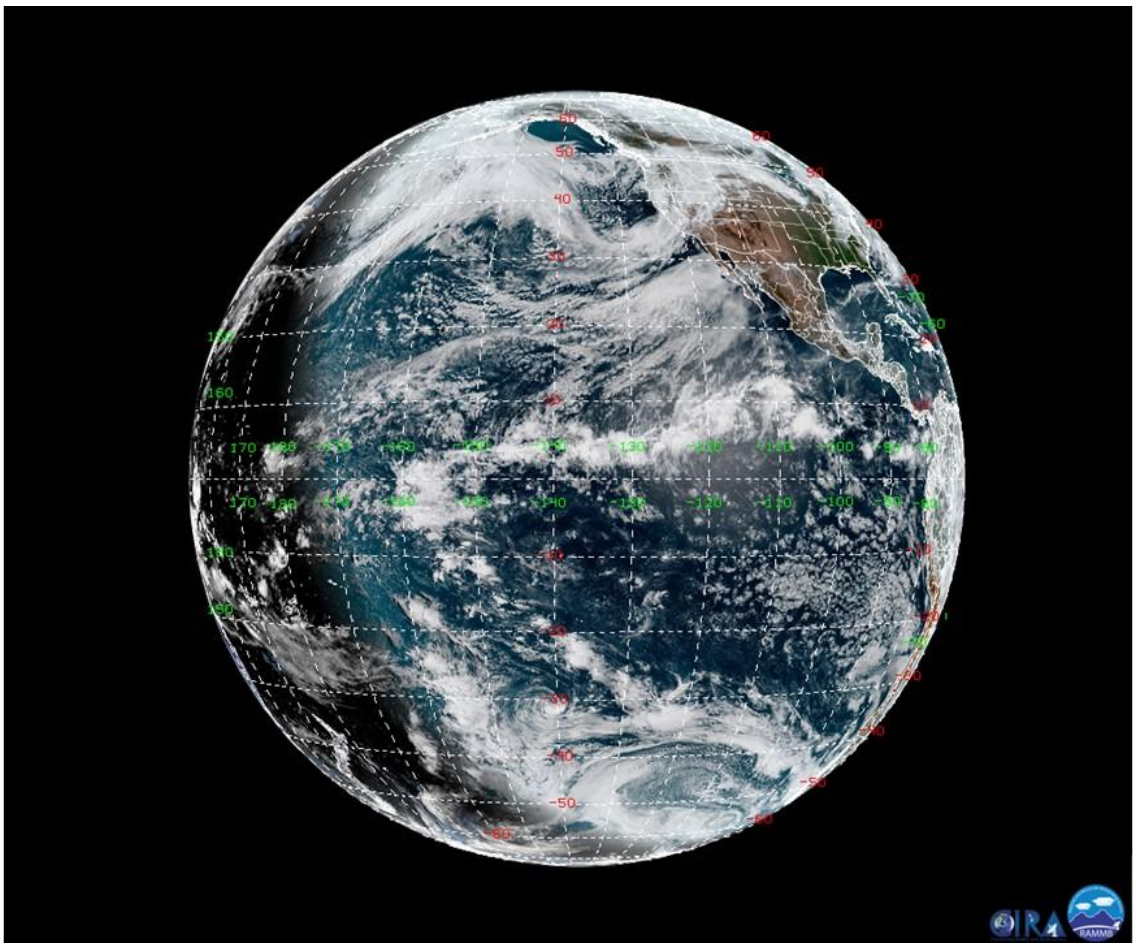

Figure 1-18: Satellite image from the geostationary satellite GOES-west.

Imagery from satellites is an essential component of understanding weather and climate. Satellites can measure temperature, moisture, winds, and even precipitation estimates or wildfire intensity among other things. With the background on the different types of satellites covered, the next section focuses on interpreting this imagery.

1.4.4 - Interpreting Weather Satellite Imagery

The three types of imagery examined in this book are visible, infrared and water vapor. Most satellite images are animated showing a time sequence of images. This animation provides the motion and evolution of the clouds and their associated weather system.

Visible imagery is what a person would see if they were sitting on the satellite. During the night visible images do not contain much information because it is dark. During the day, visible images depict the tops of the clouds. Figure 1-19 is an example of a visible image from GOES-East.

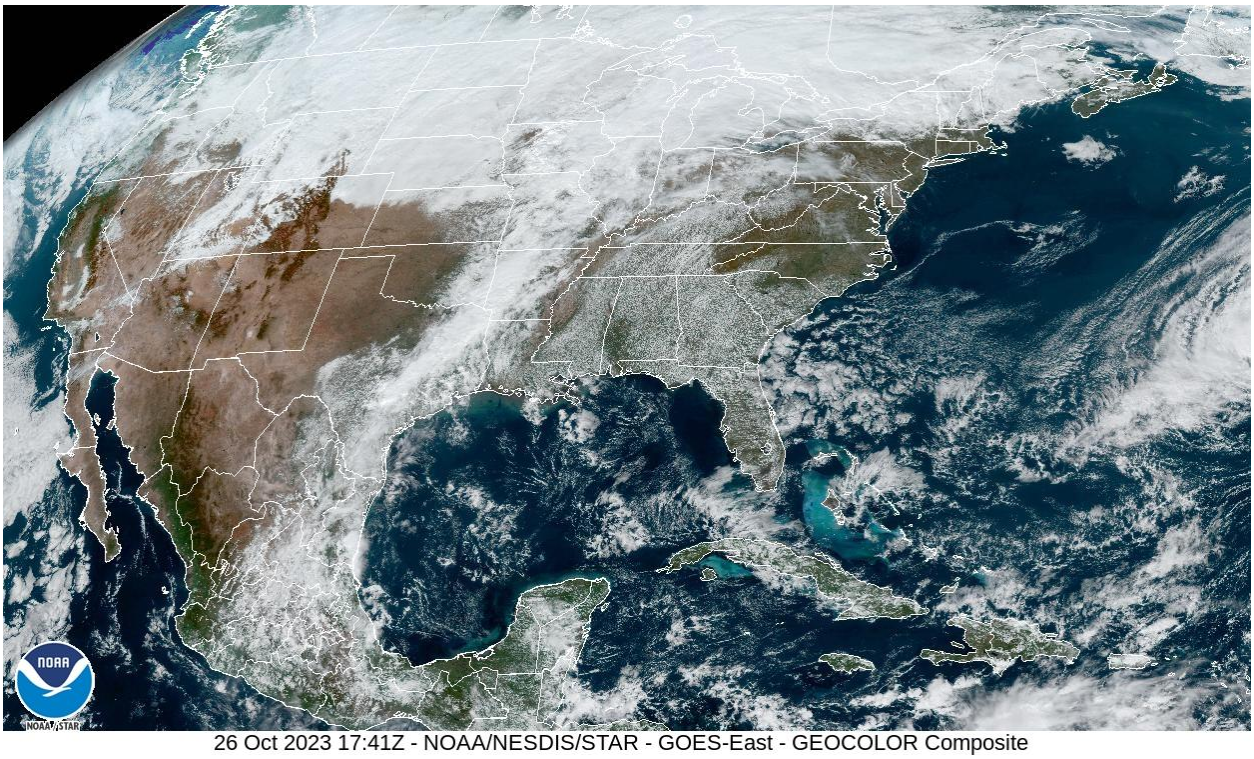

26 Oct 2023 17:41Z - NOAA/NESDIS/STAR - GOES-East - GEOCOLOR Composite

Figure 1-19: A visible satellite image from the geostationary satellite GOES-East.

Infrared imagery depicts the temperatures sensed by the satellite. The “infrared” notation describes the wavelength of radiation observed by the satellite. More details on wavelength and radiation are in an upcoming section. The important detail to remember is that the imagery contains temperature data. Temperature data is available during the night! Hence infrared imagery contains useful data 24 hours a day.

If skies are clear over an area, infrared imagery will sense the temperature of the ground. Since temperatures decrease as altitude increases in the atmosphere, higher clouds have colder temperatures. This decreasing temperature aspect of the atmosphere is observed when a

person travels to a mountain top. The temperatures on the mountain are always lower than a valley location. Therefore, the height of a cloud can be inferred from its temperature. Figure 1-20 is an infrared image from GOES-East for the same time as the previous visible image.

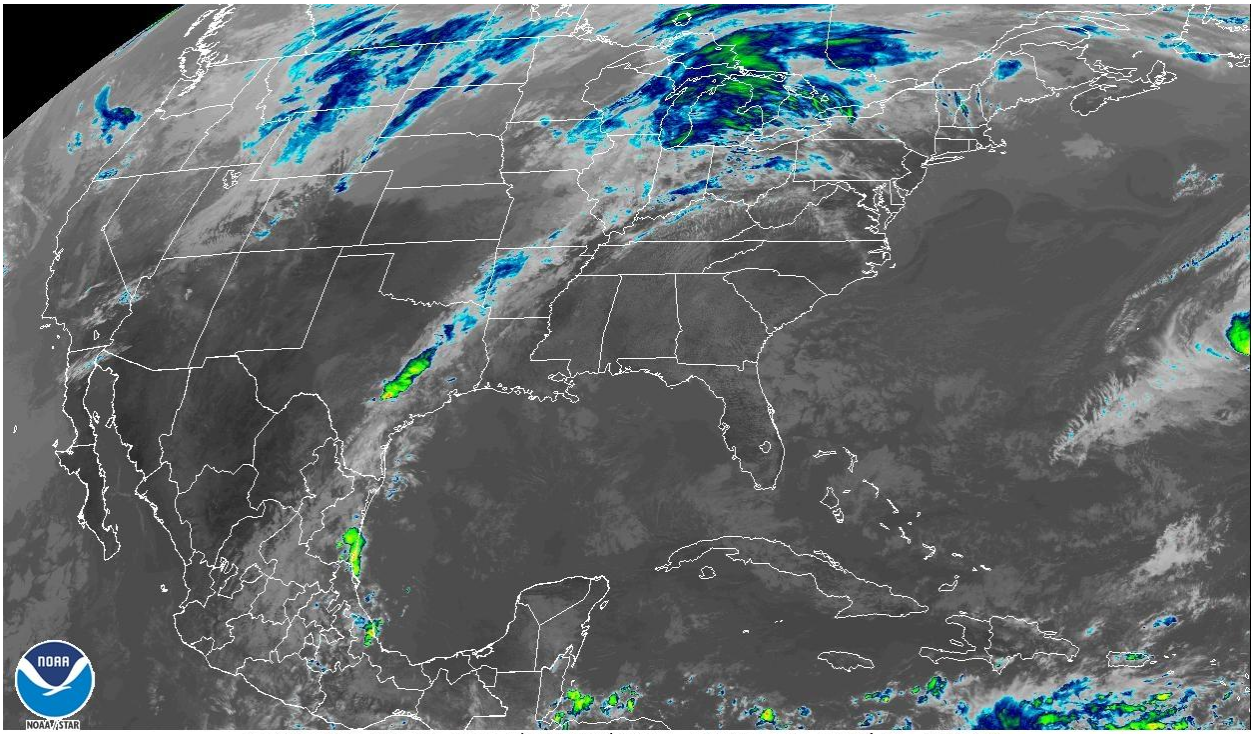

26 Oct 2023 17:41Z - NOAA/NESDIS/STAR - GOES-East - Band 13 - CONUS

Figure 1-20: An infrared satellite image from the GOES-East satellite.

Notice the color included in the infrared image. Since temperature data is present across this entire image, specific temperatures can be enhanced with color. The temperature scale for this infrared image is given in Figure 1-21.

Figure 1-21: An infrared temperature scale for GOES imagery (Band 13).

The temperature of the lighter blue clouds is about -35°C. Enhanced images allow any specific temperature to be assigned a color for fast and easy identification. The gray portions of this image contain temperature data too, although obtaining a temperature value from a gray scale is more difficult.

Water vapor imagery is another type of infrared imagery that observes wavelengths sensitive to the humidity in the atmosphere. Water vapor images depict where dry and moist air is present. This example highlights the moisture in the mid layers of the atmosphere. Yellow and red areas are dry. White areas indicate clouds and higher humidity with the highest humidity in green. The bluish areas have intermediate moisture values which may or may not have clouds. All three of the images in this section are at the same time, so a person can compare the different aspects and details of each.

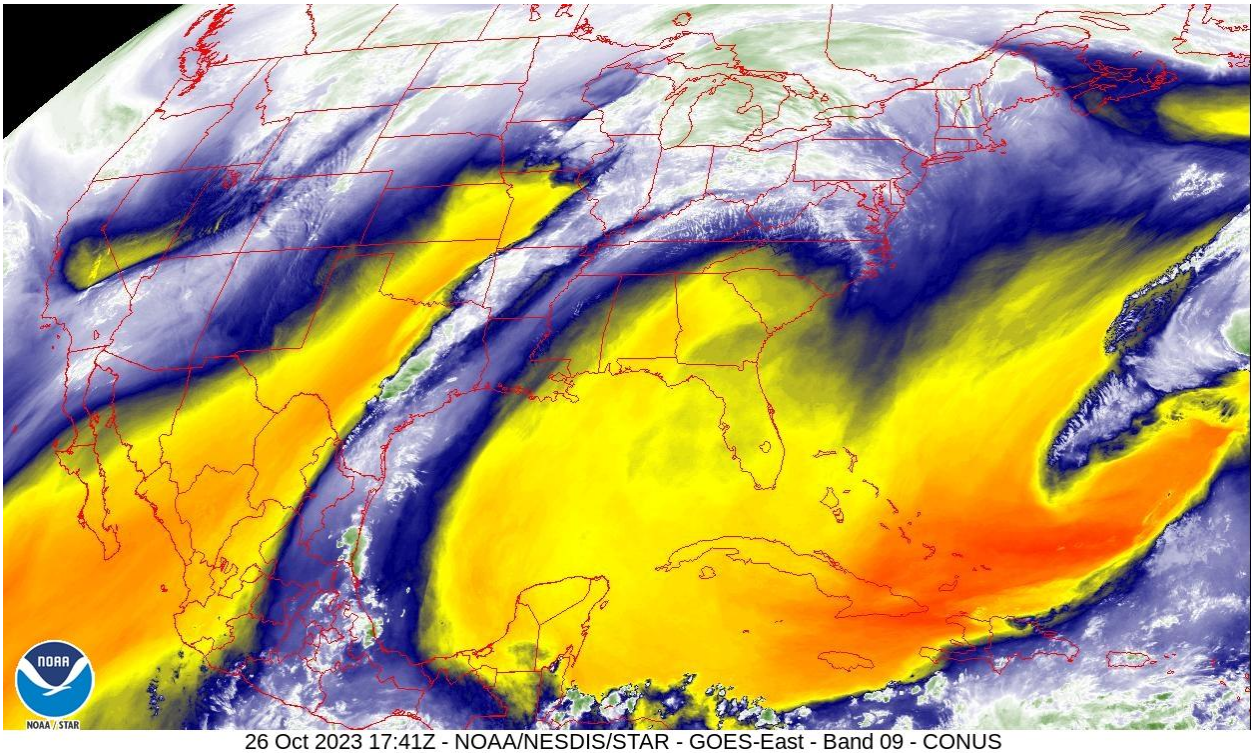

26 Oct 2023 17:41Z - NOAA/NESDIS/STAR - GOES-East - Band 09 - CONUS

Figure 1-22: A water vapor satellite image which depicts moisture in the mid-layers of the atmosphere. The lowest humidity has the colors red and yellow. Highest humidity is white and greenish.

1.5 - Atmospheric Composition

The atmosphere is a cloud of gas and suspended solids extending from the Earth's surface outward many thousands of miles. The atmosphere becomes increasingly thinner with distance, but is always held by the Earth's gravitational pull. The atmosphere is relatively thin compared to the Earth. An analogy would be the atmosphere is like the skin on an apple. The atmosphere can be seen from this International Space Station picture (Figure 1-23) taken over the Middle East. The light blue (called airglow) shown on the edge of the Earth is the atmosphere. The airglow is caused by light interacting with the atmosphere.

Figure 1-23: The light blue (airglow) is Earth's atmosphere.

The atmosphere surrounds the Earth and holds the air needed for life on our planet. It protects this life from outer space; and holds moisture (clouds), gases, and tiny particles. In short, the atmosphere is a protective bubble over Earth.

The gases comprising the atmosphere can be divided into two categories: permanent and variable. The permanent gases are the most abundant and are relatively constant over time. The permanent gases and their volumes in a dry atmosphere are listed in this table.

Gas - Permanent	Percentage of volume	Molecular symbol
Nitrogen	78.08%	N_2
Oxygen	20.95%	O_2
Argon	0.934%	Ar
Neon	0.018%	Ne
Other permanent gases	less than 0.009%	

Notice that when added together, the two largest permanent gases comprise over 99% of the atmosphere. Nitrogen is the most prevalent gas. Other than oxygen, the permanent gases generally do not interact with the Earth nor each other and change little over time.

Since most of the atmosphere is “taken” with permanent gases, the remaining portion available for variable gases is small. The variable gases are listed in this table.

Gas - Variable	Percentage of volume	Molecular symbol
Water vapor	up to 4%	H_2O
Carbon dioxide	0.039%	CO_2
Ozone	0.0015%	O_3
Methane	0.00017%	CH_4

While these gases are a small percentage of the atmosphere, they play an important role in keeping the planet warm. All these gases capture heat and are also called greenhouse gases. The variable gases are continually interacting with Earth’s surface, and do not stay in the atmosphere long. The average residence time in the atmosphere is about 100 years.

Water vapor (water in a gas state) is nearly always present and can vary from near 0% up to about 4% of the total volume. In the Earth's deserts, the water vapor contribution to the composition of the atmosphere will be near zero. Water vapor contribution climbs to near 3% on extremely hot/humid days. The upper limit, approaching 4%, is found in tropical climates. As water vapor increases, the percentage of permanent gases decreases. Water vapor is extremely important in weather and will be examine in more detail.

Carbon dioxide is a critical component in plant growth (photosynthesis) and has been increasing in the atmosphere for years. Much of this increase is from human caused activities

(anthropogenic) associated with combustion. An observatory at Mauna Loa, Hawaii has been measuring CO_2 since 1959. Figure 1-24 (left side) depicts these carbon dioxide measurements.

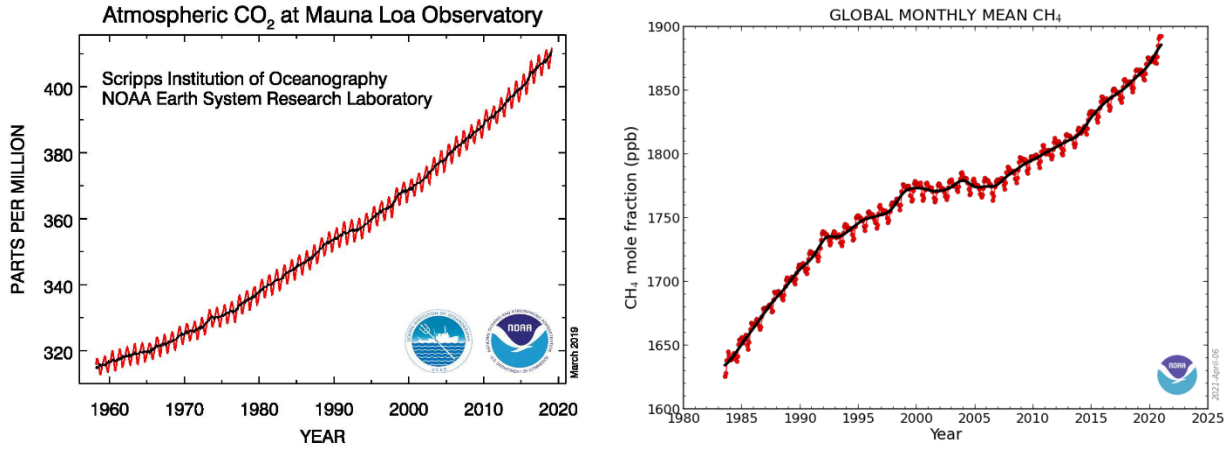

Figure 1-24: Carbon dioxide measurements at Mauna Loa Observatory in Hawaii (left). Global mean methane measurements (right).

Ozone in the lower portion of the atmosphere near the surface is considered bad because it harms respiration systems and vegetation. However, higher level ozone is essential for life on our planet. Higher-level ozone absorbs lethal ultra-violet (UV) radiation. In the 1970s, a decrease in higher-level ozone over the South Pole was discovered. This ozone hole was expanding due to use of CFCs (chlorofluorocarbons). Subsequent legislation reduced the use of CFCs and this higher-level ozone layer appears to be slowly healing.

Methane, also known as natural gas, has been steadily increasing in the atmosphere. Most of these increases are anthropogenic in nature, and include activities such as rice cultivation, raising livestock, burning of vegetation and fossil fuel (oil and coal) extraction. Global measurements of methane concentrations have a graph similar to carbon dioxide. Figure 1-24 (right side) depicts the increasing levels of methane in the atmosphere.

1.6 - Atmospheric Pressure

Atmospheric pressure is the weight of an air column that extends from an area on the ground to the top of the atmosphere. This weight is caused by gravity pulling gas molecules towards the Earth (Figure 1-25). At sea level, the weight of a column on one square inch of area is roughly 14.7 pounds, resulting in an air pressure of 14.7 pounds per square inch. Think about this value. An average human body has a

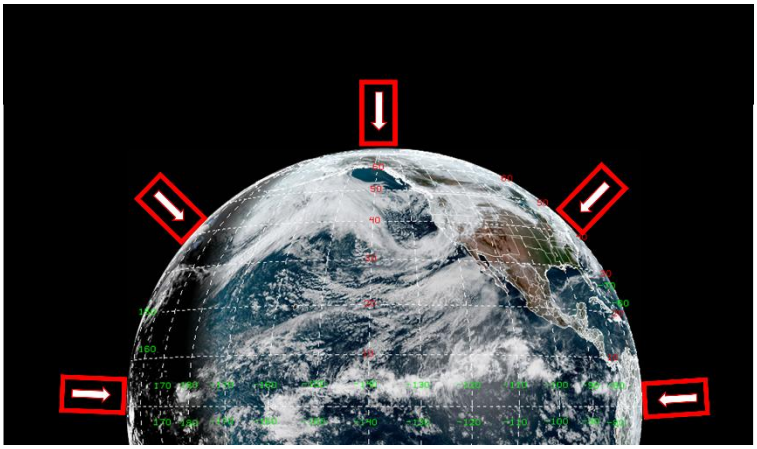

Figure 1-25: Illustration of air pressure on Earth.

surface area of about 3000 square inches. Thus, your body has force of over 40,000 pounds of air pressure on it. Right now!

One of the first instruments to measure air pressure was the mercurial barometer. A mercurial barometer has a dish of mercury with a vertical tube placed in it (Figure 1-26). As the atmospheric pressure changes, the force exerted on the mercury changes and the level of mercury in the tube changes.

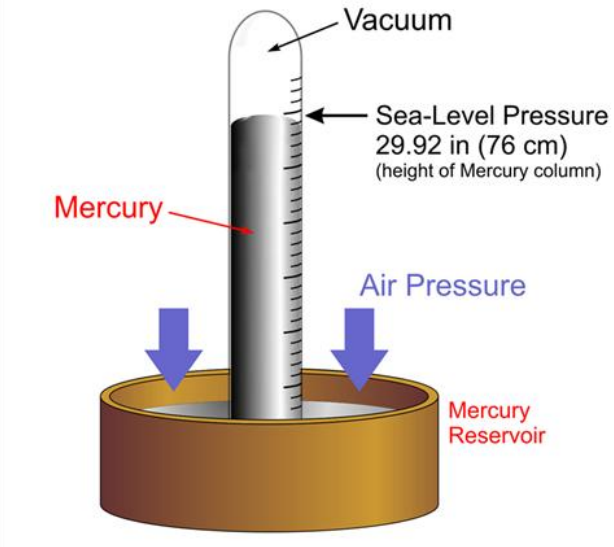

Figure 1-26: A diagram of a simple mercurial barometer to measure air pressure.

Since air is a compressible gas, the density of gas molecules in a valley (lower elevation) is higher than at mountaintop location. A valley location has more atmosphere over it and hence a higher atmospheric pressure. This characteristic is why physical exertion at a higher elevation will cause a person to breathe more. A body recognizes the lower density of oxygen molecules at the higher elevation. Figure 1-27 illustrates this change in atmospheric pressure with height.

Pressure decreases about 50% for every 5 km (16,400 feet). Likewise, the density of air decreases as altitude increases. A person can think of air being thinner (less dense) on a mountain, which is correct. Pressure is much easier to measure than density, so pressure values are used universally in the atmospheric sciences. The graph in Figure 1-27 illustrates this decrease in atmospheric pressure with height.

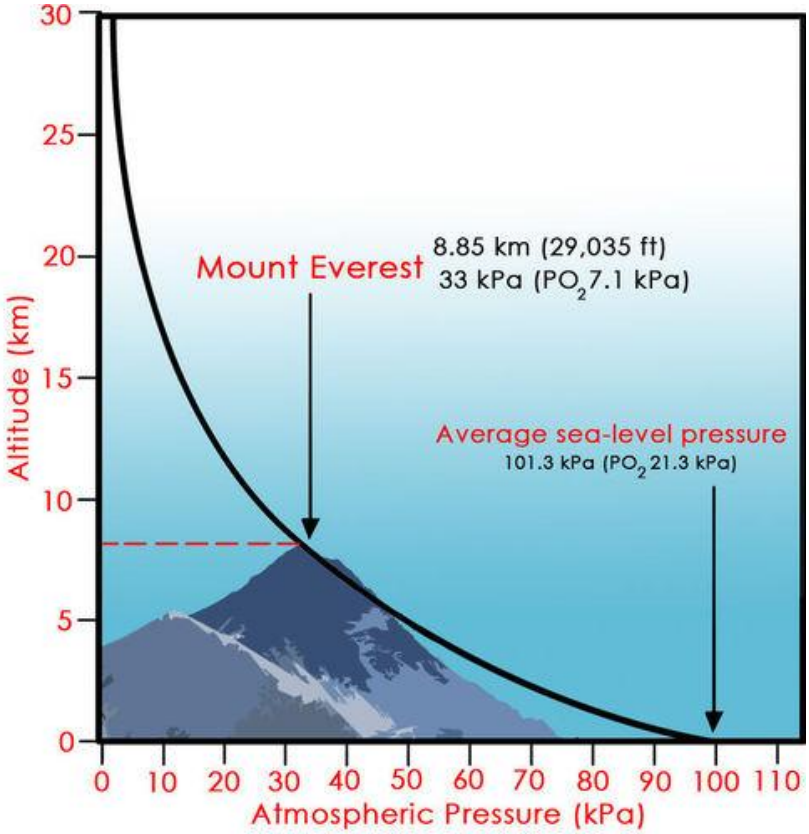

Figure 1-27: A graph depicting the decrease in atmospheric pressure with height.

1.7 - Layers of the Atmosphere

The atmosphere has five distinct layers defined primarily by their temperature. These layers, starting with the lowest, are called the (1) troposphere, (2) stratosphere, (3) mesosphere, (4) thermosphere, and (5) exosphere. Figure 1-28 illustrates these five layers.

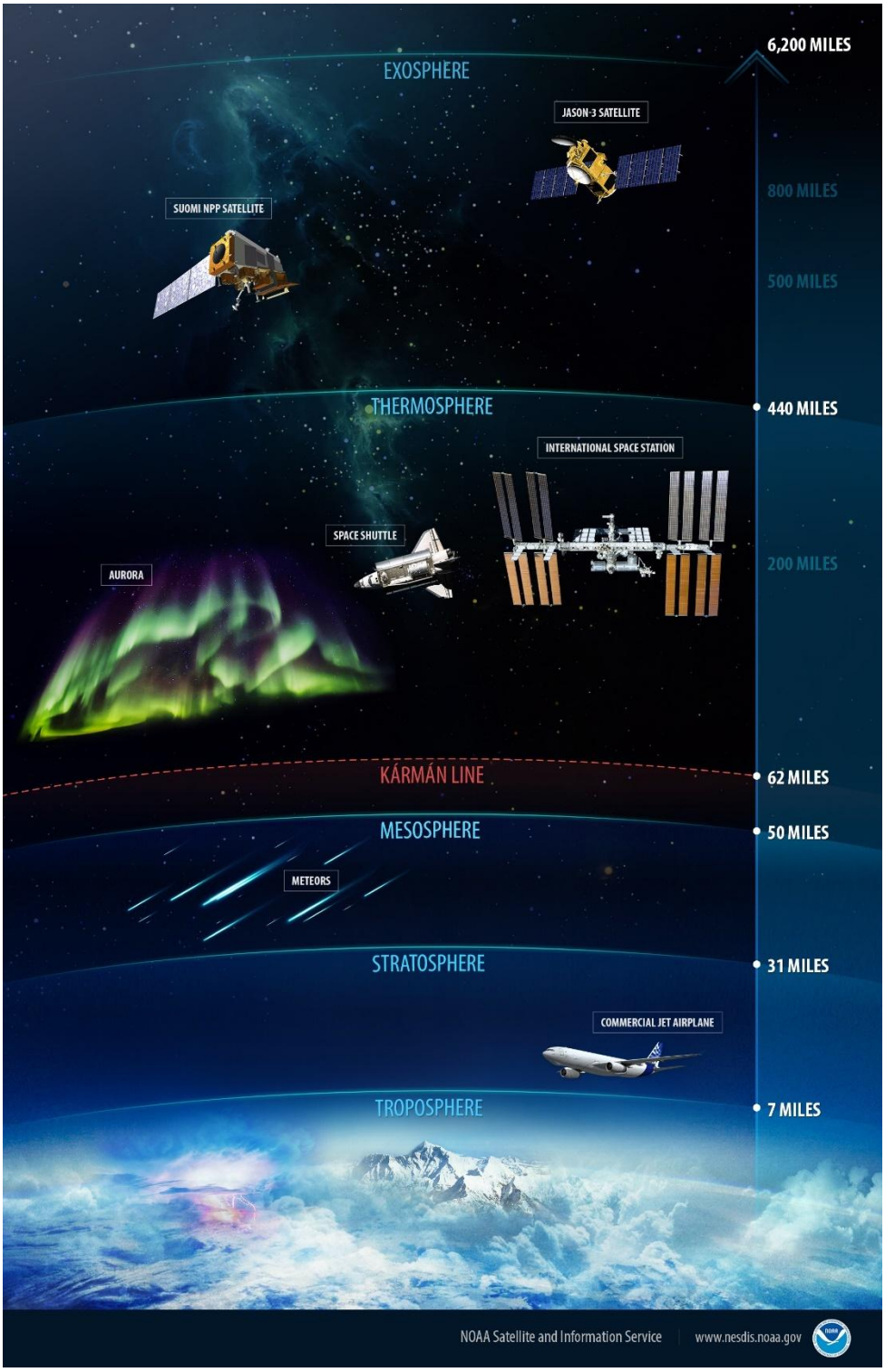

Figure 1-28: The five different temperature layers of the atmosphere.

The troposphere extends from Earth's surface about 12 kilometers (7.5 miles) in height. Yet this very shallow layer is tasked with holding all the air needed for plants and animals, and contains about 99 percent of all water vapor. In the troposphere, temperatures typically go down as altitude increases, since most of the heat found in the troposphere is generated by the transfer of energy from Earth's surface. The troposphere is the densest atmospheric layer, containing about 85% of the atmosphere's mass. Most of Earth's weather happens in the troposphere, and this course focuses on the troposphere.

The stratosphere is located between approximately 12 and 50 kilometers (7.5 and 31 miles) above Earth's surface. This layer is perhaps best known as the home of Earth's ozone layer, which protects the Earth from the Sun's harmful ultraviolet radiation. Because of the heat generated by ozone interacting with UV radiation, temperatures increase with altitude in the stratosphere. The stratosphere is nearly cloud- and weather-free. It is also the highest part of the atmosphere that jet planes can reach.

The mesosphere is located between about 50 and 80 kilometers (31 and 50 miles) above Earth's surface. The mesosphere gets progressively colder with altitude. In fact, the top of this layer is the coldest place found within the Earth system, with an average temperature of about -85°C (-120°F). Most meteors burn up in this layer. Rocket-powered aircraft can reach the mesosphere.

The thermosphere is located between about 80 and 700 kilometers (50 and 440 miles) above Earth's surface. The lower portion of the thermosphere contains what is called an ionosphere. The ionosphere can capture sub-atomic particles from the Sun to create an aurora. In this layer, temperatures increase with altitude due to the very low density of molecules found here. It is both cloud- and water vapor-free. The International Space Station orbits in the thermosphere.

The exosphere is located between about 700 and 10,000 kilometers (440 and 6,200 miles) above Earth's surface. The exosphere is the highest layer of Earth's atmosphere and merges with the solar wind at its top. The solar wind consists of subatomic particles emitted by the Sun. Molecules found here are of extremely low density and can escape to space. The aurora borealis and aurora australis are sometimes seen in its lowest part. Most Earth satellites orbit in the exosphere. Many times, when studying the atmosphere, the exosphere is omitted and is just considered as space outside the planet.

Figure 1-29 illustrates the four lowest layers and their temperature profiles. Notice temperatures cool as altitude increases in the troposphere and mesosphere, while temperatures warm with altitude in the stratosphere and thermosphere. Each layer is separated by what is called a "pause" where the greatest change in thermal characteristics occur. These "pause" layers are given the prefix of the layer below it; that is tropopause, stratopause, and mesopause.

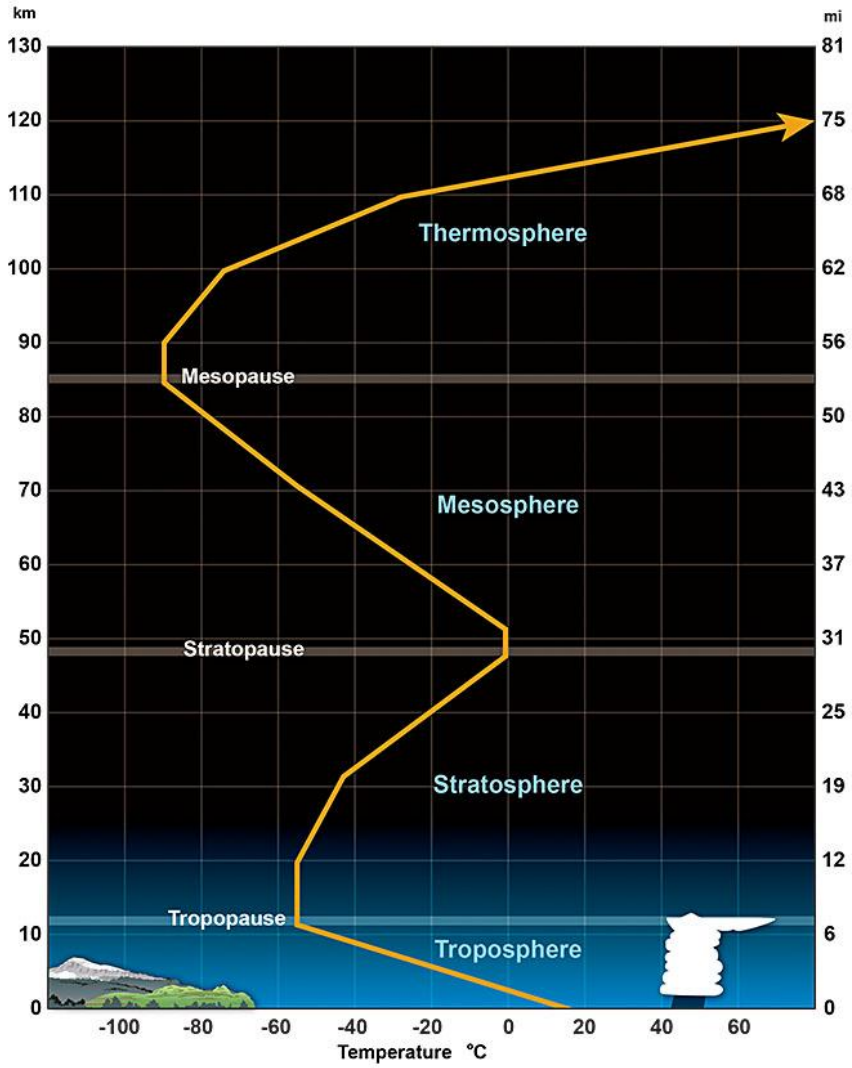

Figure 1-29: A graph of atmospheric temperature for the lowest four layers of the atmosphere.

Chapter 1 Review Questions

1. Describe each step of the scientific method.
2. Why are weather observations all taken at the same time?
3. Draw a station model and label the locations of each observation parameter.
4. Describe the advantages of geostationary weather satellites.
5. Describe the advantages of polar orbiting weather satellites.
6. Which type of weather satellite is most commonly used in weather operations?
7. Describe the characteristics of visible, infrared, and water vapor satellite imagery.
8. What are the three most predominate permanent gases?
9. What are the three most predominate variable gases?
10. Which of the variable gases capture heat?
11. What is an isobar on a weather map?
12. What causes atmospheric pressure?
13. Why does the temperature in the stratosphere increase with altitude?
14. List the temperature layers of the atmosphere from lowest to highest.

Chapter 2 - Energy and Earth's Energy Balance

Overview

This chapter covers the energy received from the Sun as electromagnetic radiation: how the atmosphere and Earth interact with the Sun's energy and radiate heat back to space. Methods for transferring energy are presented. This chapter explores Earth's energy balance from the perspective that the Earth's temperature is constant.

Chapter objectives:

1. Identify the types of energy and how they are transferred.
2. Understand the cause of Earth's seasons.
3. Explain how incoming solar radiation is affected by the atmosphere.
4. Describe the Earth's energy balance through incoming and outgoing radiation.

2.1 - Types of Energy

This section examines energy, specifically how energy is transferred from the Sun to the Earth. A good place to start with this topic is with definitions. **Energy** is traditionally described as the ability to do work. The unit of energy is a joule (pronounced "jewel"). One joule is equal to 0.237 calories. This "calories" is the same "calories" found on the nutritional labels of food. Eating food or calories provides energy for a person to do work.

Radiation is the emission and transfer of energy via particles or waves. Many people think of radiation as coming from nuclear reactors or bombs. This type of radiation transfers energy with subatomic particles. In addition, an everyday light bulb, radio, and microwaves are all examples of devices that produce and use radiation. This type of radiation uses waves; there is no mass or charge but there is energy. The energy packets in the waves are called photons. The entire range of these waves is called the **electromagnetic spectrum**.

How is the electromagnetic spectrum created? You probably know that the building blocks of all matter are atoms and molecules. Within these atoms and molecules are smaller particles which have positive and negative charges -- protons and electrons. These charged particles tend to oscillate or vibrate. Without getting into more detail, physics tells us that any charged particle like an electron has an electrical field surrounding it. Furthermore, moving charges also possess magnetic fields. Thus, when an electron oscillates, its surrounding electric and magnetic fields change. Like moving your hand rapidly back and forth in a pool of water, oscillating electrons send out ripples of energy (that is, "waves") that have both electrical and magnetic properties. Hence, the name *electro - magnetic* radiation.

The last definition needed is thermodynamics. Studying the movement of molecules and their energy for an atmosphere is overwhelming. Instead, thermodynamics is studied.

Thermodynamics examines the relationship between heat and energy. Understanding aspects of thermodynamics helps in determining why at times the atmosphere is stable and at other times when it is not.

2.1.1 - Looking at Energy and Thermodynamics

Energy has many forms such as electrical, nuclear, or chemical. All forms of energy fall into the two categories of kinetic and potential. **Kinetic** energy is a result of motion. Some examples of kinetic energy are the Sun (electromagnetic radiation), moving water, electricity, the burning of fuel or the vibration of molecules which is measured as temperature.

Potential energy is stored and has the capacity to do work under the correct conditions. Some examples of potential energy are water behind a dam, gasoline, food, a battery, or firewood. Potential energy is frequently converted into kinetic energy when work is performed.

Energy, heat and temperature are all related but not identical to each other. Thermodynamics helps define the relationship between them, and has two laws which are important. The First Law of Thermodynamics states that energy is a conserved property that is neither created nor destroyed. Essentially energy is converted from one form to another. This concept is also called the conservation of energy.

Temperature is a measure of the heat of an object. At a molecular level, temperature measures how fast the molecules are moving or vibrating. Air with a high temperature has gas molecules moving much faster than colder air. The Second Law of Thermodynamic states that heat is always transferred from hot to cold objects. Hot objects tend to cool down and cold objects warm up.

Two temperature scales are widely used, Fahrenheit and Celsius. Fahrenheit has the temperature at which water freezes as 32^{o}F, whereas this temperature in Celsius is 0^{o}C. The boiling point of water at a standard air pressure is 212^{o}F and 100^{o}C.

Thermodynamics is an important concept when studying the atmosphere because the Sun transfers energy to the Earth. The Earth in turn transfers energy to the atmosphere in the form of heat. How does this transfer of heat occur? The next section examines this question.

2.1.2 - Transfer of Heat Energy

The primary heat source for our planet is the Sun. Energy from the sun is transferred through space and through the Earth's atmosphere to the Earth's surface. Since this energy warms the Earth's surface and atmosphere, some of it becomes heat energy. There are three ways heat is transferred into and throughout the atmosphere: conduction, convection, and radiation.

Conduction is the transfer of heat energy without the appreciable movement of molecules. The transfer of heat energy occurs by the kinetic energy translating from one particle to another within the materials. Have you ever left a metal spoon in a pot of soup being heated on a stove? After a short time, the handle of the spoon becomes hot. This is due to the conduction of heat energy from molecule to molecule within the spoon. Conduction is a very effective method of heat transfer in metals. However, conduction of heat through air is poor.

Convection is the transfer of heat by the mixing of a fluid. An example of convection is the heating of water in a pot. As the water heats, water at the bottom becomes hot and rises. As the hot water rises, its space is replaced by cooler water from above. Both liquids and gases are considered fluids. Thus, the atmosphere behaves like a fluid. The mixing of heat in a fluid is associated with buoyancy, which in turn is related to density. Hot air rises because it is less dense than surrounding air. Cold air sinks because it is denser. As the Sun heats the Earth's surface, the air molecules near the surface gain heat by conduction. This hot air then rises from the surface through convection.

Figure 2-1: A pot of boiling water illustrates the transfer of heat by convection; the transfer of heat by the mixing of a fluid.

The type of radiation most important in studying the atmosphere is electromagnetic radiation. Electromagnetic waves travel from the Sun to the Earth through a vacuum and gives energy and life to everything on our planet. From this perspective, the best definition for **radiation** is the transfer of heat without a transfer medium.

Figure 2-2 illustrates these three methods of heat transfer on our planet. Electromagnetic radiation from the Sun travels to Earth through the atmosphere to heat the ground. As the ground warms, the gas molecules touching the ground warm and start to rise. The rising hot air mixes this heat throughout the atmosphere.

The details associated with electromagnetic radiation are extremely important in warming the Earth, and are the primary topic of the next section.

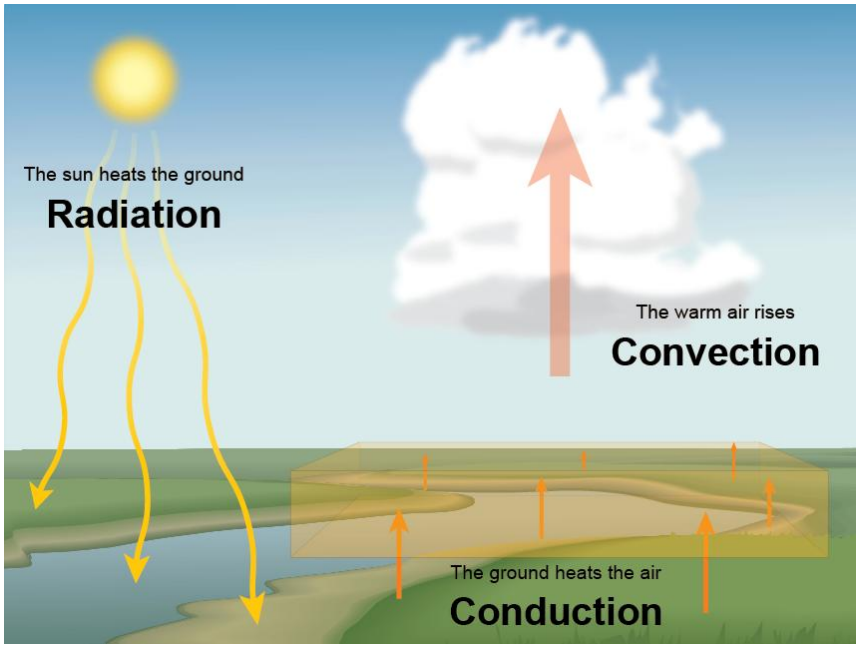

Figure 2-2: Diagram illustrating the three methods of heat transfer on Earth.

2.1.3 - Characteristics of Electromagnetic Radiation

Before examining electromagnetic radiation in detail, a general review of waves is useful. Waves have two important characteristics called wavelength and frequency, as is illustrated on the left side of Figure 2-3.

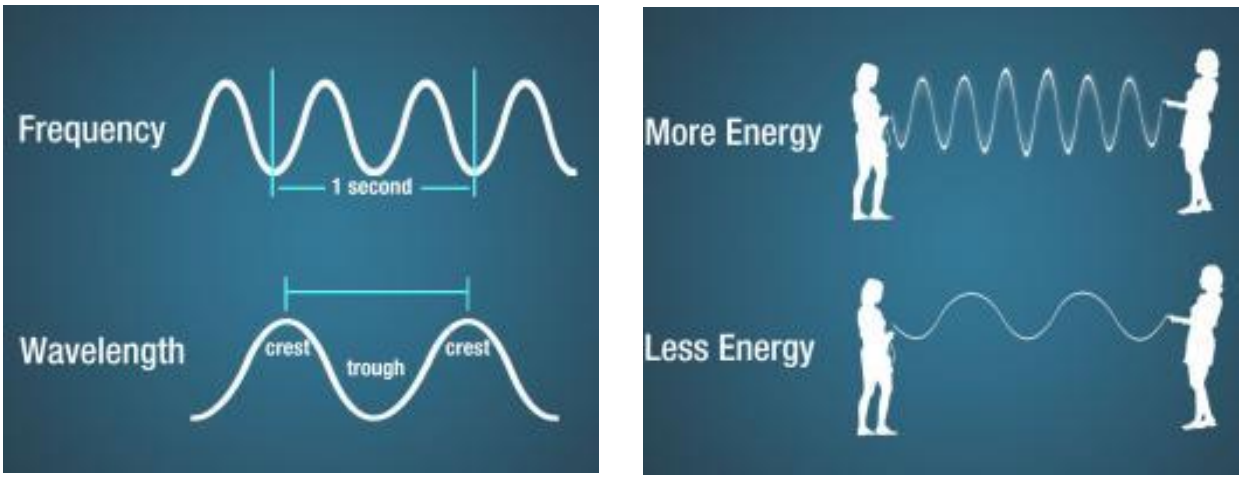

Figure 2-3: (left side) The frequency and wavelength characteristics of waves. (right side) Energy contained in a wave decreases as the wavelength increases.

Electromagnet waves have crests and troughs like ocean waves. The distance between the crests is called wavelength. The number of crests that pass a given point within one second is described as the frequency of the wave. Moving along the spectrum from short to long wavelengths, energy decreases as the wavelength increases. Consider a jump rope with its ends being pulled up and down. More energy is needed to make the rope have more waves as illustrated on the right side of Figure 2-3.

Wavelength is associated with the type of radiation. Types of radiation are gamma ray, X-ray, ultraviolet, visible, infrared, microwave, and radio. Figure 2-4 illustrates the types of radiation and their relative wavelength. The types of radiation (such as radio waves, infrared, visible light, etc.) are also referred to as bands. Shorter wavelengths (gamma rays at 10^{-23}m) transfer higher energy than longer wavelengths (radio waves at 10 to 100m).

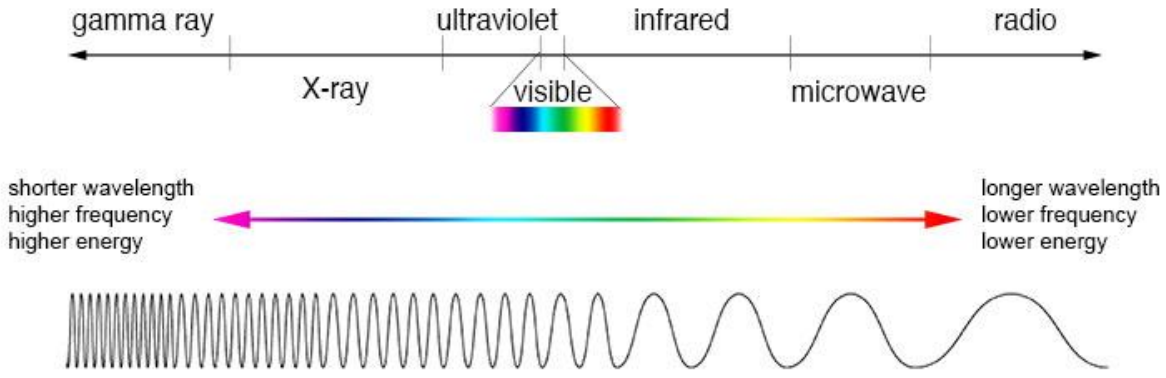

Figure 2-4: The types of radiation and their associated wavelengths. Shorter wavelengths have higher energy and vice versa.

As mentioned previously, electromagnetic waves have both electrical and magnetic properties. Electromagnetic waves are formed when an electric field (which is shown in red arrows) couples with a magnetic field (which is shown in blue arrows). Magnetic and electric fields of an electromagnetic wave are perpendicular to each other and to the direction of the wave.

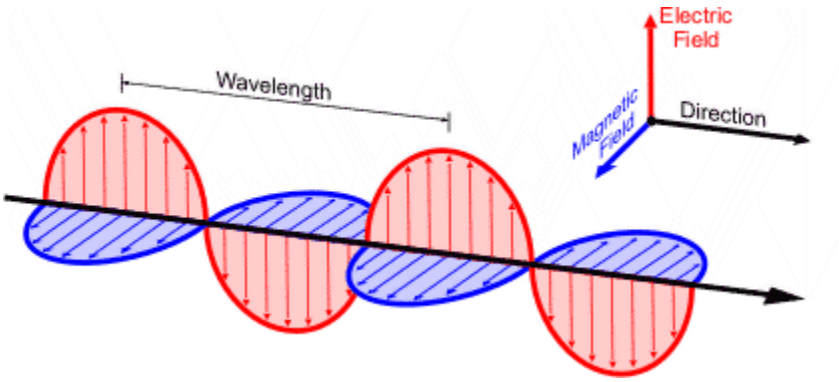

Figure 2-5: Electromagnetic waves have both electrical and magnetic properties which are oriented perpendicular to each other.

This NASA video on YouTube provides a 5 minute overview of electromagnetic radiation with examples of its uses.

By understanding the fundamentals of electromagnetic radiation, this knowledge is used to examine the energy transferred from the Sun to the Earth. The Sun transfers energy in the ultraviolet (6.7%), visible (46.8%) and the near infrared (46.5%) bands. The Earth absorbs this energy and radiates energy (heat) in the far infrared band. Figure 2-6 describes the incoming wavelengths from the Sun and outgoing wavelengths from the Earth. This figure also depicts the entire electromagnetic spectrum wavelengths and bands.

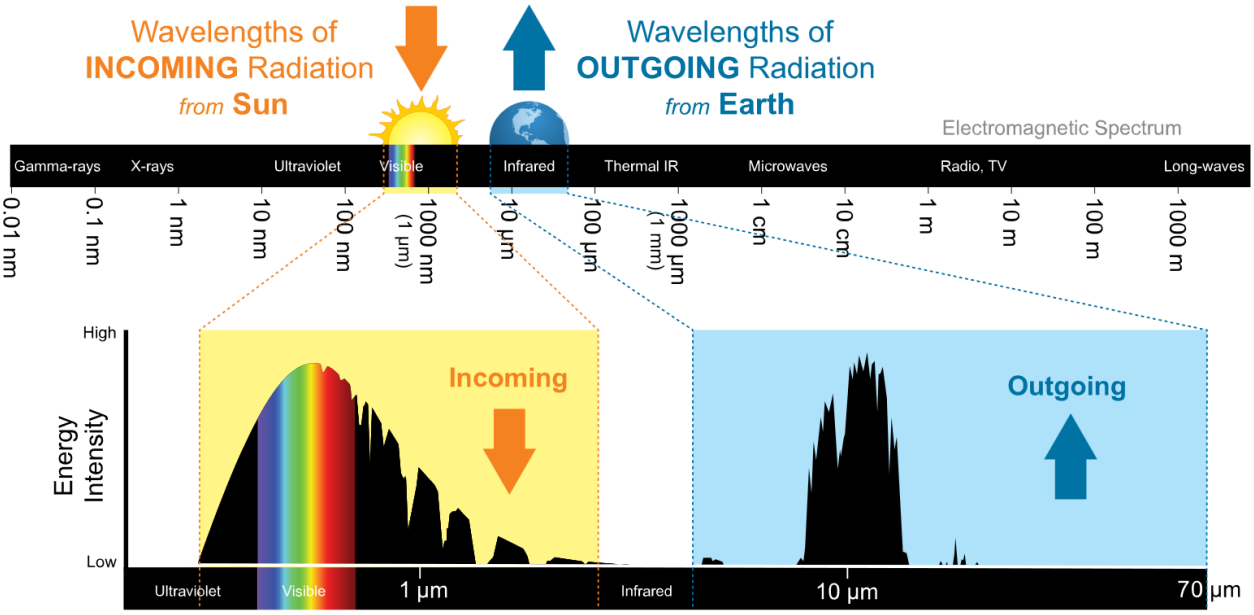

Figure 2-6: Incoming wavelengths from the Sun and outgoing wavelengths (as heat) from the Earth.

Electromagnetic radiation travels at the speed of light (186,000 miles/sec) in space. With the Earth being 92,900,000 miles from the Sun, energy from the Sun takes 8 minutes and 20 seconds to arrive at the Earth.

2.1.4 - Laws of Radiation

A **blackbody** is a theoretical object which absorbs all radiation falling upon it. Likewise, blackbodies can also emit a maximum amount of radiation. Both emission and absorption can be applied using the blackbody concept. The emissions from a blackbody are directly related to its temperature. The concept of a blackbody is useful because the Sun and Earth are close to blackbodies, and follow the laws of radiation.

Scientific laws are generally expressed as mathematical equations. The equation reflects the conditions that occur without exception. Assuming an object has blackbody properties simplifies these equations, which in turn makes understanding them easier.

The single variable which determines how much energy a blackbody emits is temperature. The Stefan-Boltzmann Law is expressed as

$$I = \sigma T^4$$

The intensity of radiation (I) equals a constant (σ) times temperature (T) to the fourth power. The constant (σ) is 5.67×10^{-8} watts/m^{2}K^4**.** The temperature is given in degrees Kelvin. Basically, this equation indicates that the higher the temperature the more energy (in watts) an object emits.

Putting some numbers into the Stefan-Boltzmann Law, the average temperature of the Earth is 289^{o}K (16^{o}C or 61^{o}F). Therefore, the Earth emits about 395 watts/m^2. The Sun has a much higher average temperature of 5800^{o}K. This temperature gives an emission value of about 64 million watts/m^2.

Wein's Law is another useful law of radiation and states that the wavelength of an object's peak emission is inversely related to its temperature. The equation expressing this relationship is

$$\lambda_{max} = c / T$$

The wavelength of energy emitted with the greatest intensity is λ_{max}. The other side of the equation has a constant (c = 0.0029 for wavelengths measured in meters) and temperature (T), which is in Kelvin. Wein's (pronounced "weens") Law physically states that hotter objects emit shorter wavelengths. Placing numbers into this equation gives the wavelength of peak emission of the Sun at 0.5 μm and the Earth at 10 μm.

These laws of radiation are applied in extracting information from weather satellite imagery. The satellite measures the intensity of radiation emitted from a cloud top. This intensity can be translated to temperature through the Stefan-Boltzmann Law. All infrared satellite imagery, like Figure 1-20, uses this law to extract and display detailed temperature information.

Applying the blackbody concept and these laws of radiation to the Sun-Earth interactions produces this graph in Figure 2-7 Notice the energy output scale is different for the Sun (left side) and Earth (right side). Both emission curves assume blackbody properties. These energy

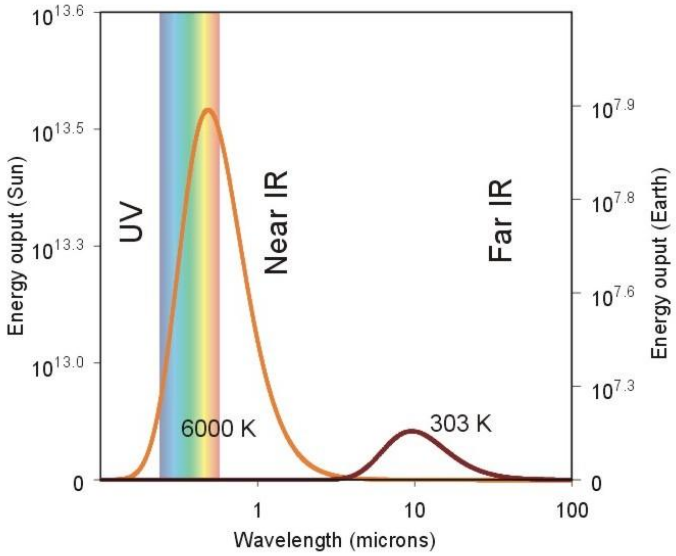

Figure 2-7: Graph of blackbody radiation for the Sun (T=6000 K) and Earth (T=303 K).

scales are as expected from the Stefan-Boltzmann Law. The Sun puts out a lot of energy. The shorter wavelengths associated with the Sun, and the longer wavelengths from the Earth follow Wein's Law. As a cooler object, the Earth emits longer wavelengths.

2.1.5 - How Radiation Interacts with the Earth

Previous sections described how electromagnetic radiation behaves and what is emitted by both the Sun and the Earth. A missing piece of information is how the Earth interacts with the radiation received from the Sun. Additionally, we need to know how the atmosphere interacts with incoming radiation from the Sun, and outgoing radiation from the Earth. The graphs in Figure 2-8 are an expansion of a previous diagram and provides some of these details.

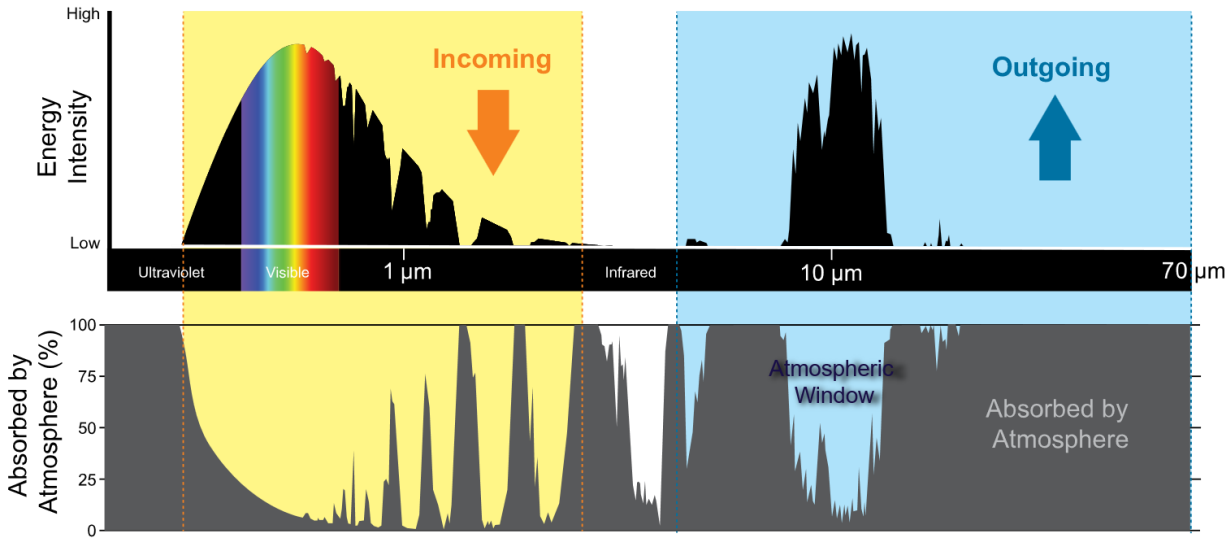

Figure 2-8: Top portion is the radiation received from the Sun (yellow) and emitted by the Earth (blue). The gray portion of the lower graph is the percentage of radiation absorbed by the atmosphere.

To simply the terminology describing this physical process, all wavelengths less than 4 μm are referred to as **shortwave radiation**. **Longwave radiation** are wavelengths greater than 4 μm. Hence, all incoming radiation from the Sun is shortwave radiation. All outgoing radiation from the Earth is longwave radiation when using this terminology.

The gray portion of the bottom graph is what the atmosphere absorbs from the incoming and outgoing radiation. Thankfully, the incoming radiation from the Sun is not absorbed by the atmosphere, and largely passes through to the surface where people live. This situation is good in that the energy from the Sun is needed to sustain life on our planet. Notice on the outgoing side, the atmosphere behaves very differently and absorbs much of the energy being emitted by the Earth. The area centered around 10 μm has minimal absorption by the atmosphere, and is called a window. Radiation with wavelengths around 10 μm can pass through this window to space and leave the Earth. This absorption aspect of the atmosphere is good! If the Earth were to lose all its heat to space, our planet would be in perpetual winter.

What causes this absorption of radiation in the atmosphere? The short answer is the gas molecules composing the atmosphere. The atmosphere is mostly transparent to shortwave radiation from the Sun, and opaque to longwave radiation from the Earth. Most of the absorption of outgoing radiation is due to the variable or greenhouse gases (GHGs). Water vapor is the most abundant GHG and carbon dioxide is a distant second. The other greenhouse gases of ozone and methane also contribute to this absorption. Figure 2-9 illustrates the absorption by these atmospheric gases. Notice the absence of absorption by permanent gases, since the total absorption is essentially the sum of the GHG absorptions.

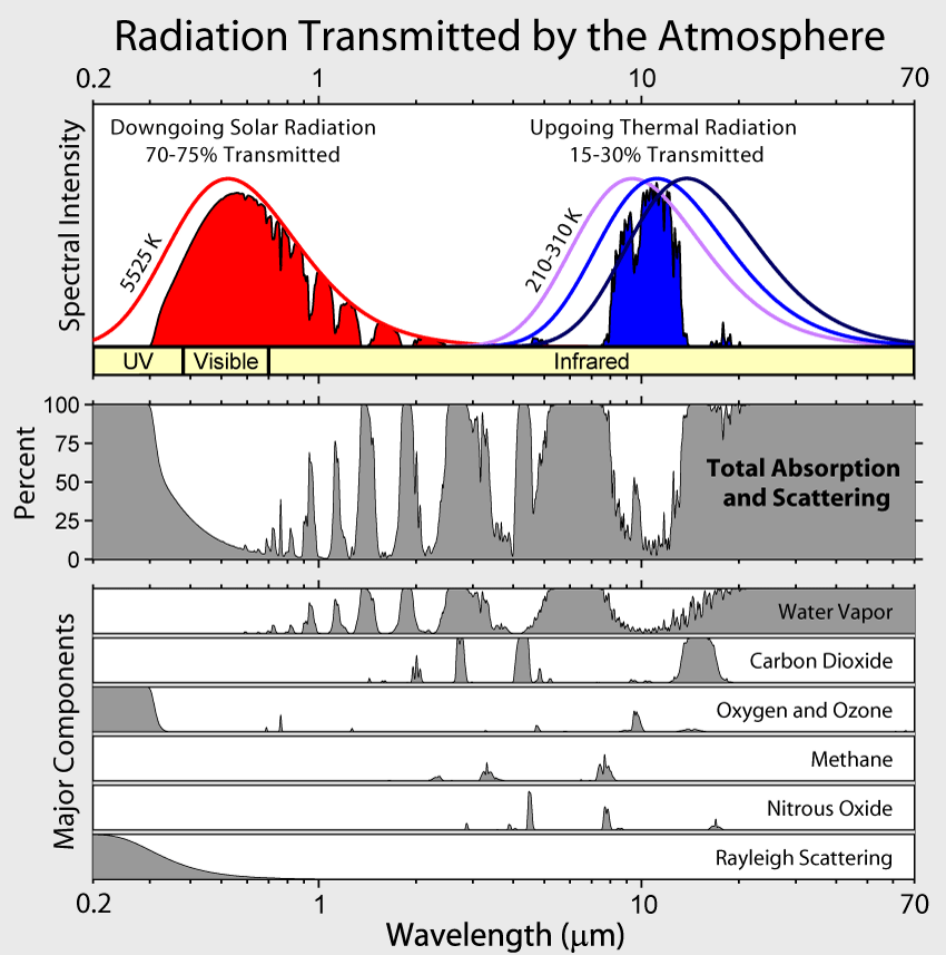

Figure 2-9: Top graph is the radiation received from the Sun (red) and emitted by the Earth (blue). Bottom portion is the total absorption by the atmosphere followed by the individual absorption of each greenhouse gas (GHG).

The last categories in Figure 2-9 are nitrous oxide and Rayleigh scattering. Nitrous oxide is a by-product of combustion, and is frequently observed as a brownish pollution layer over metropolitan areas. Rayleigh scattering is not a gas, but rather how light interacts with gas molecules. More details on Rayleigh scattering are given later in this chapter (Section 2.3.2).

While the bulk of the Sun's electromagnetic radiation is in the visible and infrared bands, the Sun can transmit radiation across the entire electromagnetic spectrum. How does the atmosphere interact with wavelengths other than short and longwave radiation? Figure 2-10 answers this question. In Figure 2-10 the purple and red lines extending from the top of the atmosphere to the Earth indicate that the atmosphere is transparent to that band of radiation. If the purple or red lines stop within the atmosphere, absorption is occurring. Gamma, X-ray and a portion of the ultraviolet spectrum are absorbed in the mesosphere and stratosphere. The far infrared (longer) wavelengths and longer radio waves are also absorbed by the atmosphere. This figure further illustrates the protective shell the atmosphere provides us, since the higher energy portions of the electromagnetic spectrum (purple) are detrimental to life.

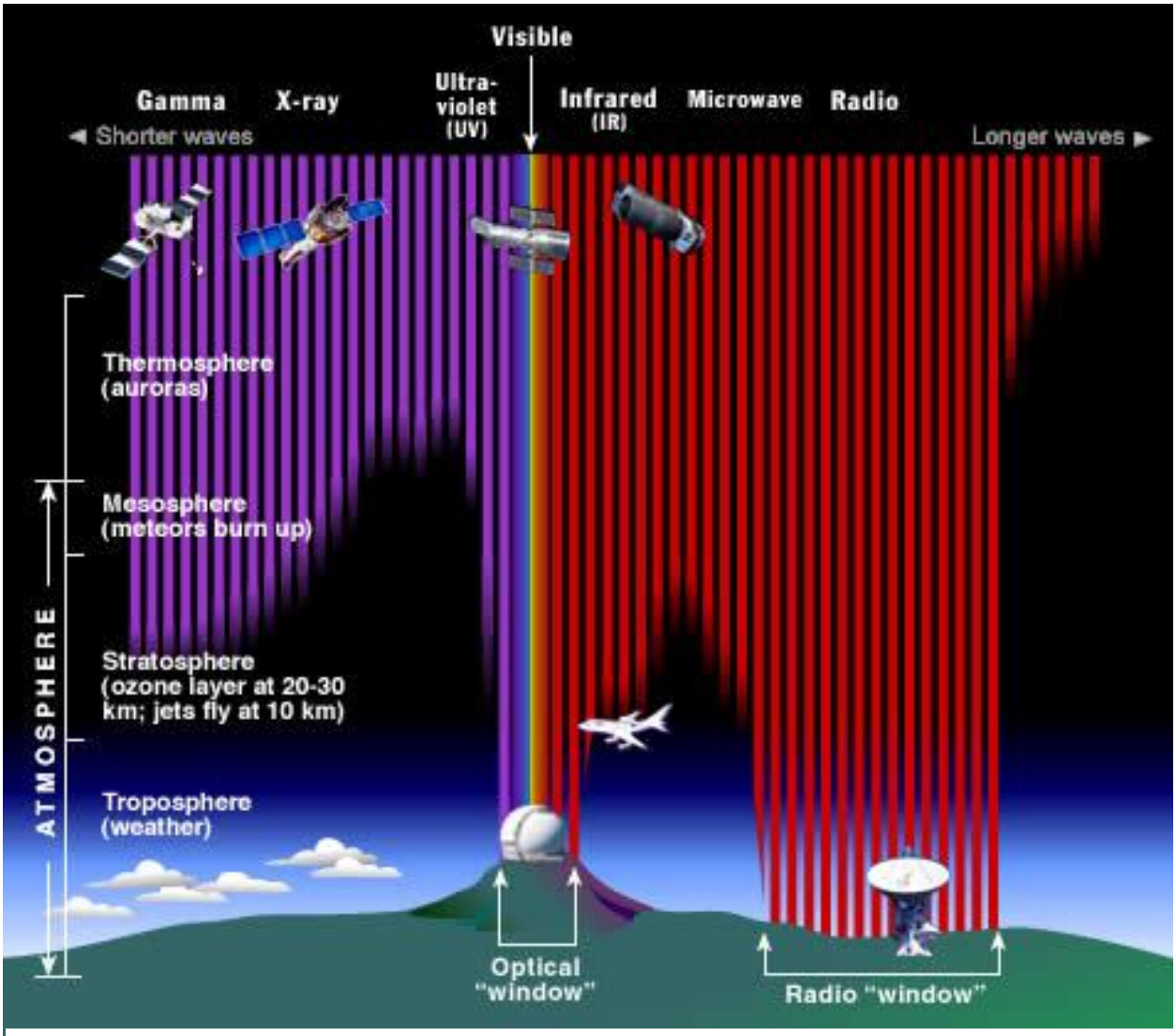

Figure 2-10: Absorption by the atmosphere across the entire electromagnetic spectrum. When the red or purple lines reach the surface, little absorption is occurring. Lines ending in the atmosphere are absorbed. The temperature layers of the atmosphere are given on the left side.

2.2 - Causes of Earth's Seasons

During the year, seasons are observed with winter being colder and summer being hotter. What causes these seasons? The Earth's orbit around the Sun and the tilt of the Earth's axis are looked at to answer this question. The answer is the tilt of the Earth's axis causes the seasons. Seasonal solar radiation conditions across the globe are then examined to determine why winter is colder and summer is hotter. These details allow a person to further hypothesize why weather occurs on our planet.

2.2.1 - Earth's Orbit Around the Sun

The Earth orbits the Sun on a flat plane called the ecliptic (or orbital) plane. The average distance from the Sun to the Earth is 150 million km. Since this orbit is elliptical, the nearest point from the Earth to the Sun is 147 million km and is called perihelion. The farthest point from the Sun is 152 million km and is called aphelion. Since the closest distance to the Sun occurs in our winter, these variations in distance to the Sun are **not** the cause of the seasons.

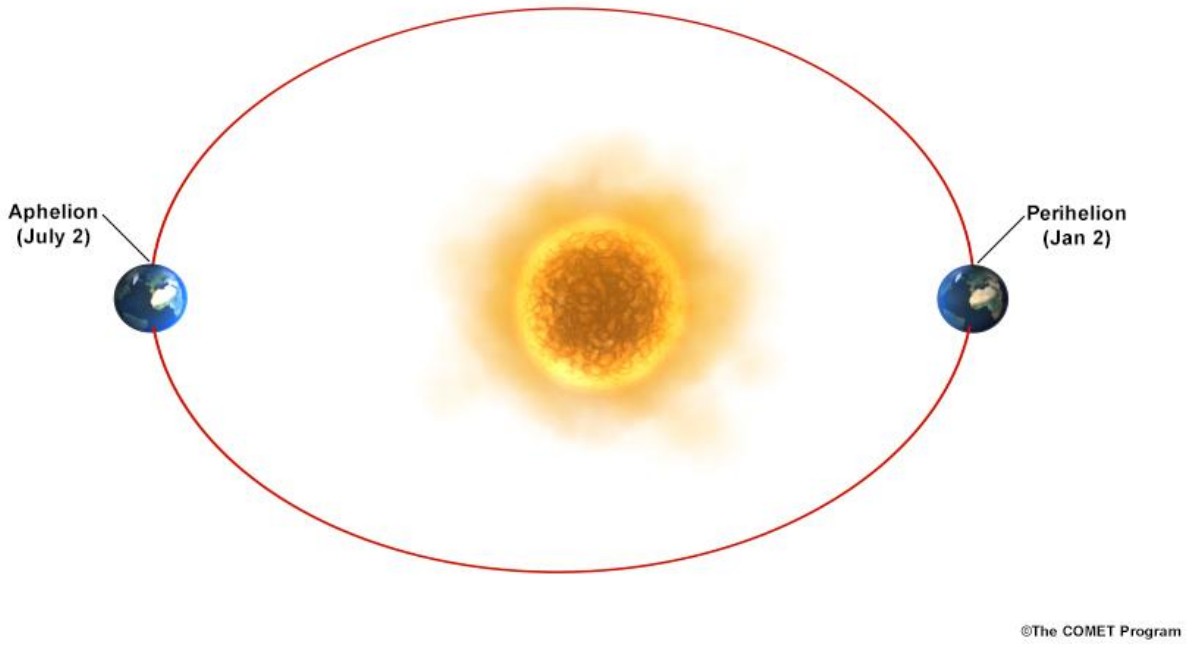

Figure 2-11: Elliptical orbit of the Earth around the Sun. The Earth is closest to the Sun on January 2 and furthest from the Sun on July 2.

2.2.2 - Earth's Rotation and Axis Tilt

The Earth has a spinning motion called **rotation**. A complete rotation occurs about every 24 hours. This rotation is not perpendicular to the ecliptic plane of the Earth's orbit around the Sun. Rather the axis is tilted at 23.4°. This axis tilt is also called **obliquity**. The tilt does not change as the Earth orbits the Sun. Thus, a hemisphere (Northern or Southern) is tilted towards the Sun for half a year and away from the Sun the other half of the year. This tilt is what causes the seasons! Figure 2-12 illustrates the Earth's rotation and axis tilt.

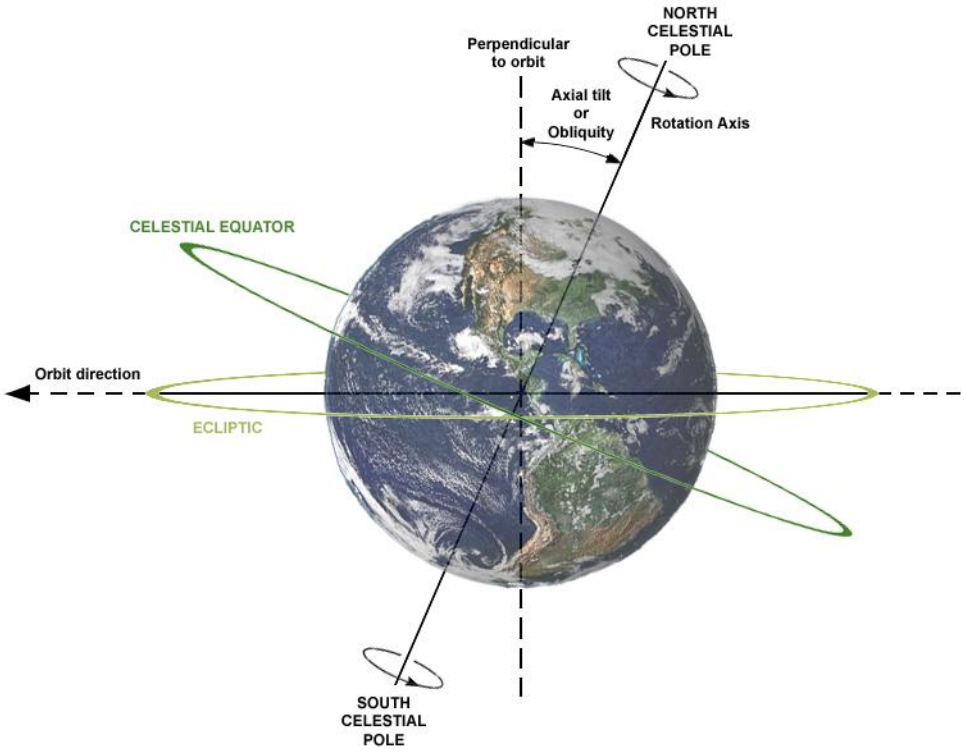

Figure 2-12: Earth's rotation and axis tilt. This tilt does not change as the Earth rotates around the Sun.

Additionally, the spherical shape of the Earth causes beam spreading at higher latitudes. **Beam spreading** is an increase in the surface area over which radiation is distributed. At higher latitudes, the Sun has a lower angle in the sky, and sunlight is spread out over a larger area. This sunlight also passes through more atmosphere before reaching the Earth. These characteristics cause the poles to be cold and the equator hot. Additionally, beam spreading can occur at any location on the Earth whenever the sun angle is low like sunrise or sunset.

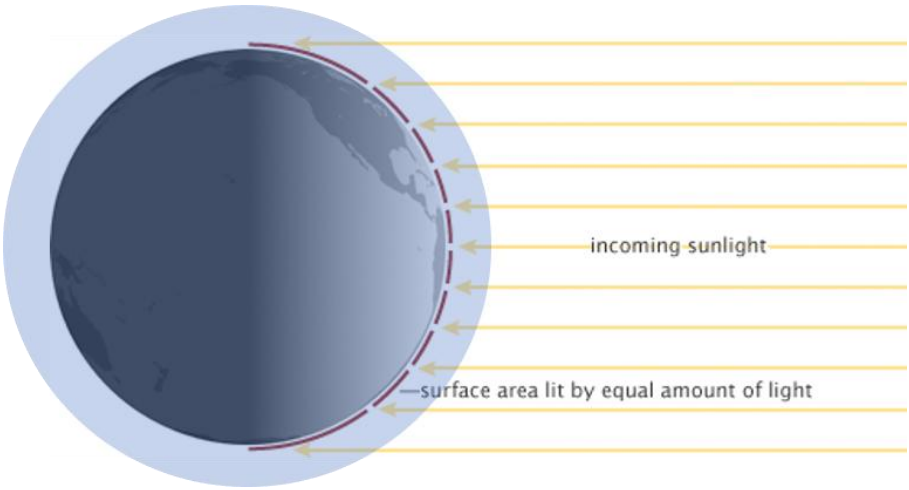

Figure 2-13: Red lines on the Earth indicate the spreading of sunlight over the surface, which is called beam spreading. Beam spreading at the pole is much more pronounced than at the equator.

2.2.3 - Earth's Orientation for Solstices and Equinoxes

Summer in the Northern Hemisphere is when the Earth's axis is tilted towards the Sun and it receives more sunlight. The name given this position is the summer solstice and it occurs

around June 21. Likewise, this time of year is winter in the Southern Hemisphere because it receives less sunlight. Figure 2-14 illustrates the summer solstice in the Northern Hemisphere. During the summer solstice, days are longer and the angle of the Sun is higher in the sky. The North Pole experiences 24 hours of daylight. The Southern Hemisphere has the reverse of these conditions with the South Pole experiencing perpetual night. Labels have been placed at important latitudes to highlight these daylight conditions. The Arctic Circle is at 66.6°N and the Antarctic Circle is at 66.6°S. From the Circles to the pole, this region experiences either 24 hours of day or night depending on which solstice is occurring.

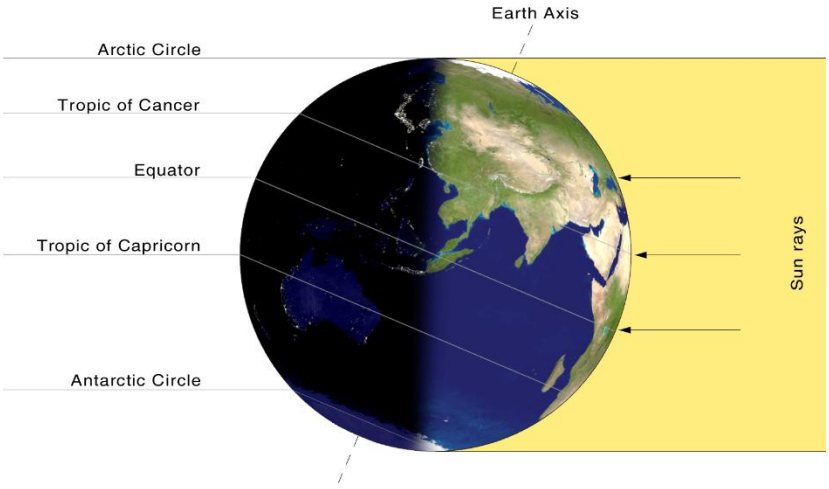

Figure 2-14: Summer solstice in the Northern Hemisphere.

The Tropic of Cancer at 23.4°N is where the Sun is perpendicular to the Earth (directly overhead) during the summer solstice. Therefore, the Tropic of Cancer is getting the most intense sunlight during the summer solstice. Beam spreading and absorption of incoming solar radiation by the atmosphere is minimal.

Figure 2-15 illustrates the winter solstice for the Northern Hemisphere. This solstice occurs around December 21. The Southern Hemisphere receives substantially more sunlight. The Sun is overhead at the Tropic of Capricorn (23.4°S) which is getting the most intense solar radiation. Days are shorter in the Northern Hemisphere and the incoming shortwave radiation is less intense because the Sun angle is lower.

Figure 2-15: Winter solstice in the Northern Hemisphere.

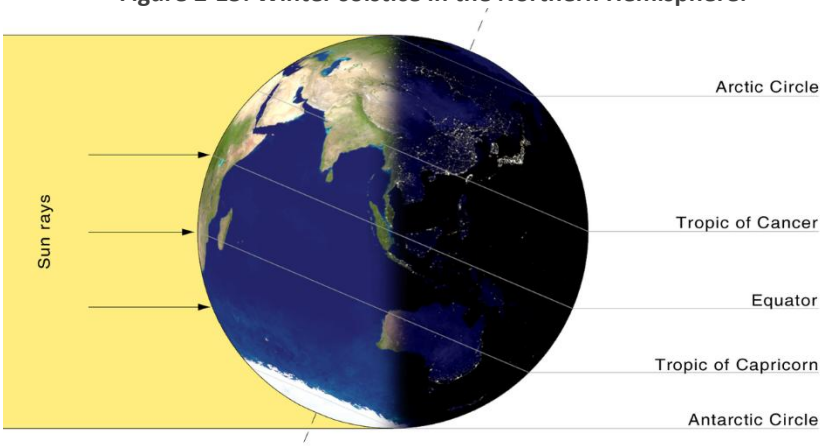

The spring and fall equinoxes are when the Sun is directly overhead at the equator. Every location on Earth gets 12 hours of day and night. These equinoxes occur around March 22 and September 22.

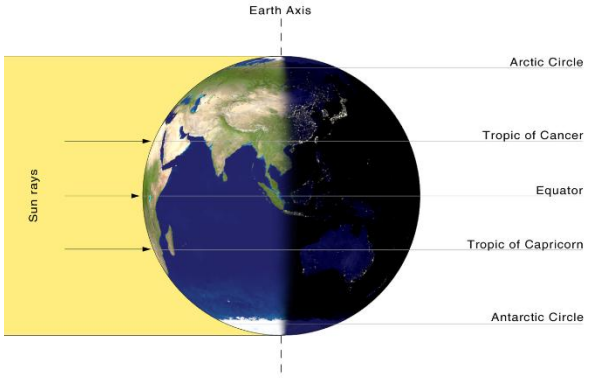

Figure 2-16: Fall and spring equinoxes for both hemispheres.

The angle at which the Sun's rays strike the Earth is important and has specific terminology associated with describing it. The **solar noon** is when the Sun is highest in the sky or the sun angle is highest. Solar noon is not necessarily at noon (12:00 pm). Solar noon is when a person can get sunburned the fastest.

The **solar declination** is the latitude the Sun is directly overhead at noon. The solar declination varies between -23.4ºS and 23.4ºN. For the summer solstice, the solar declination is the Tropic of Cancer. For the equinoxes, the solar declination is the equator.

The angle of the Sun above the horizon varies throughout the day. In the early morning and late evening, the Sun angle is at the horizon or near zero. The highest sun angle during the day is at solar noon. The sun angle at solar noon for any location can be found by (1) subtracting the location latitude from 90º and (2) adding the current solar declination latitude. For example, the sun angle at solar noon during the summer solstice at Denver, Colorado is (90º – 39.7º) + 23.5º = 73.8º.

A solar calculator with information on the Sun for any location on the Earth for any day can be found at https://www.esrl.noaa.gov/gmd/grad/solcalc/index.html.

2.2.4 - What Causes Weather?

The changing orientation of the Earth with respect to Sun (because of the axis tilt) affects the incoming solar radiation received in three ways:

1. The length of day (sunshine) at a location. Summer days are longer than winter days.

2. The angle at which the Sun strikes the Earth. The summer Sun has higher sun angles than winter.

3. The amount of atmosphere sunlight must penetrate to reach the Earth changes with the seasons. Lower sun angles cause the radiation to pass through more atmosphere before reaching the surface.

These effects cause the poles to have a "deficit" of incoming shortwave radiation and the tropics to have a "surplus" of radiation. In other words, the poles are cold and the tropics are hot. The atmosphere tries to equalize these temperatures differences across the Earth with weather. Warm air from the tropics is transported north and cold air from the poles is transported south. Figure 2-17 from NASA illustrates the radiation imbalance between the poles and tropics.

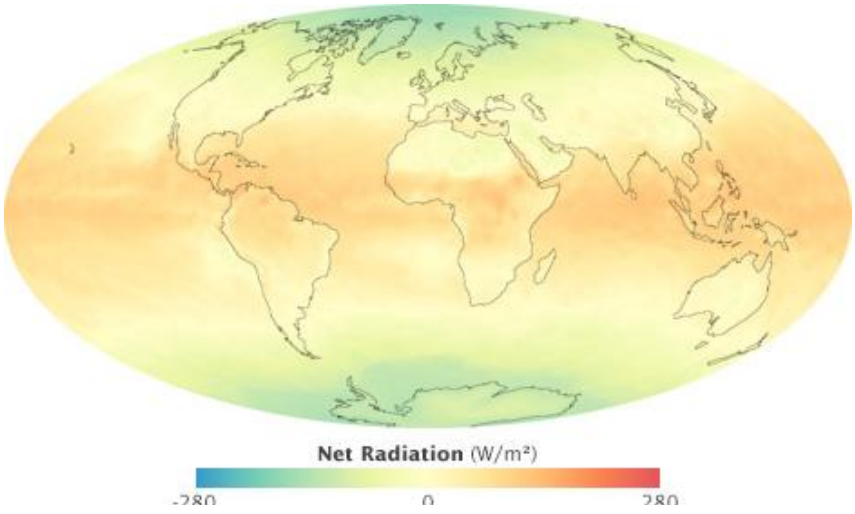

Figure 2-17: Net solar radiation received over the Earth. Notice the highest amounts at the equator with the poles being much lower.

2.3 - Atmospheric Influences on Insolation

Another word for incoming solar radiation is **insolation**. Since shortwave radiation comes from the Sun, insolation can also be thought of as incoming shortwave radiation. Section 2.1 examined details of electromagnetic radiation as it exits through the atmosphere. The variable gases were important in these analyses since they absorb heat. However, a definition of "absorb" has never been given. This section corrects that omission, along with examining the reflection and scattering characteristics of the atmosphere. Additionally, this section completes the knowledge needed to understand how the atmosphere interacts with shortwave and longwave radiation.

2.3.1 - Absorption and Reflection

Absorption is when the atmosphere intercepts radiation, gains energy, and warms. The gas molecules in air are not all equal in absorbing every wavelength. As covered previously, most of the insolation reaching the Earth's surface passes through the atmosphere. However, the atmosphere does absorb some incoming radiation as is shown in Figure 2-18.

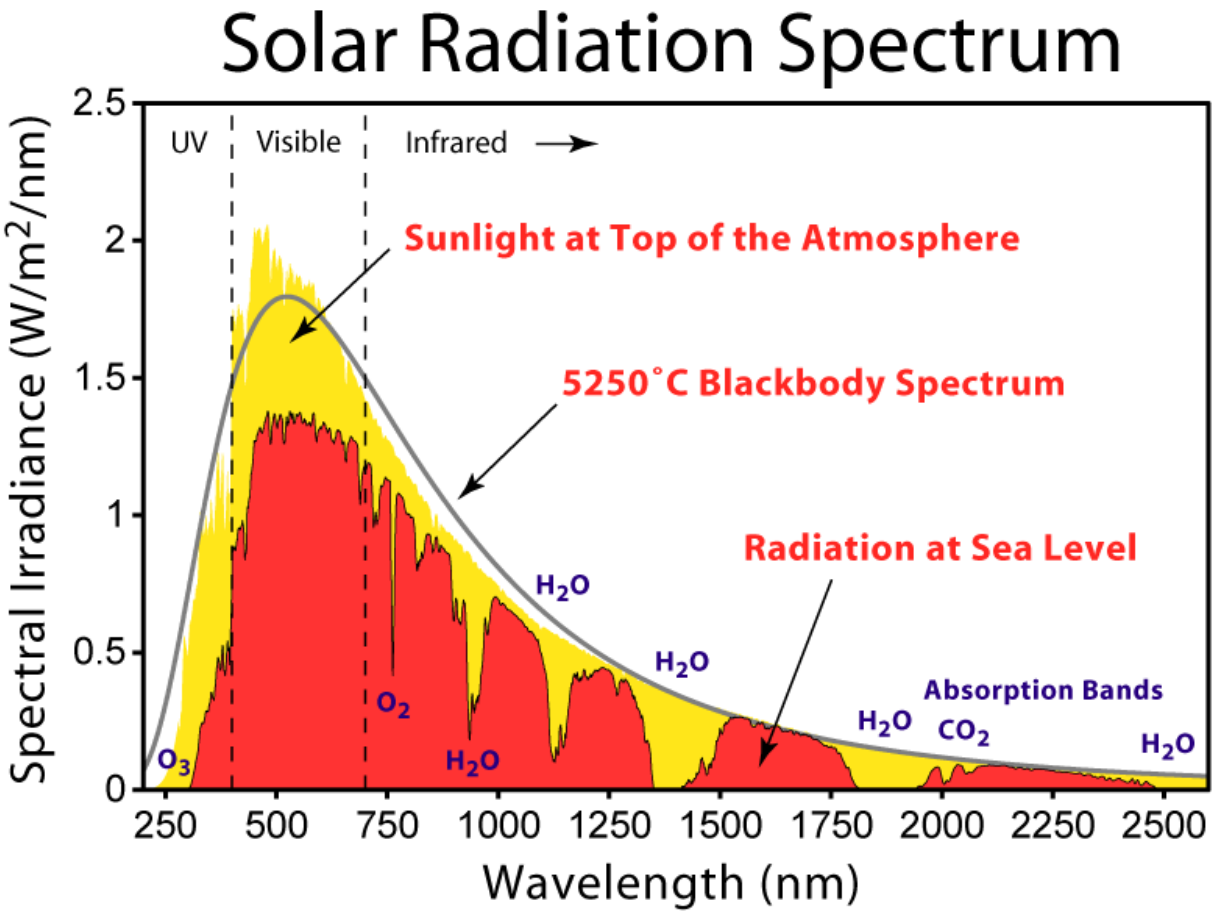

Figure 2-18: The solar radiation spectrum received at the top of the atmosphere (yellow) and at the surface after traveling through the atmosphere (red).

In Figure 2-18 the yellow area is insolation at the top of the atmosphere. The red area is what is received at the surface. Water vapor (H_2O) has the largest absorption of insolation in the near

infrared band (greater than 780 nm). You may notice that the Sun does not feel as hot on humid days, because water vapor is absorbing some of the Sun's infrared energy. Additionally, carbon dioxide absorbs a little in the near infrared wavelengths and of course ozone (far left) absorbs ultraviolet.

Reflection occurs when radiation strikes an object and is redirected away from it. The best analogy of reflection is a mirror. All objects reflect some light which enables us to see them. Clouds are both an absorber and a reflector as illustrated in Figure 2-19.

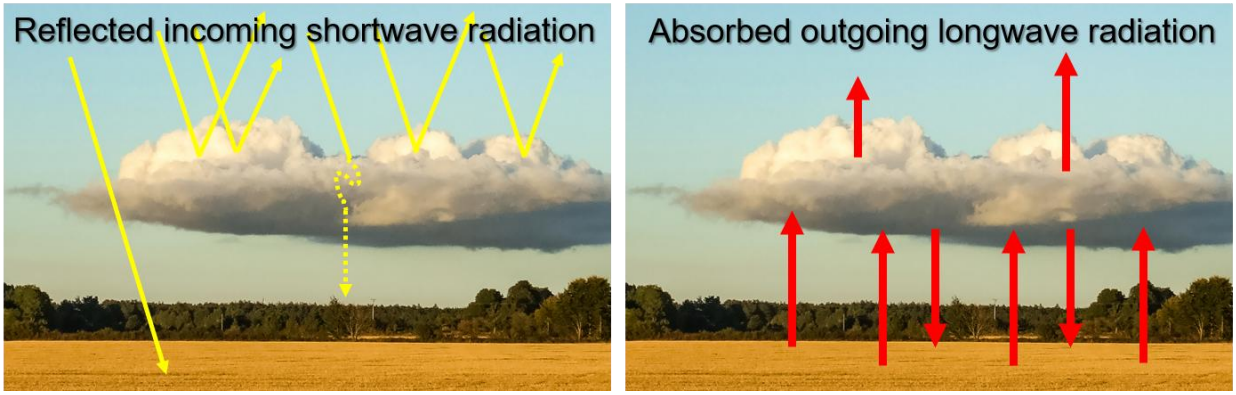

Figure 2-19: A cloud photo illustrating the reflection of incoming insolation and the absorption of outgoing heat.

Albedo is the percent of insolation reflected by an object. Fresh snow has the highest albedo at 75 to 90%. Asphalt has one of the lowest at 5 to 10%. The following table contains the various albedos of objects. Notice that Earth's average albedo is 30%. Hence, 30% of incoming shortwave radiation is reflected by the Earth.

Surface	Albedo
asphalt road	5 – 10%
Cities	14 – 18%
Forest	14 – 20%
crops and grassland	10 - 25%
lakes and ocean	10 – 60% varies with Sun angle
fresh snow	75 – 90%
Earth as an average	30%

2.3.2 – Scattering

Scattering is the dispersion of radiation in multiple directions when it strikes an object. Figure 2-10 illustrates the scattering of light in the atmosphere.

The characteristics of this scattering are determined by the size of the suspended atmospheric particles. Three general categories of scattering are:

1. Rayleigh (pronounced “ray-lee”) scattering happens with the smallest size particles like molecules.
2. Mie (pronounced “me”) scattering occurs with medium size particles like dust.
3. Nonselective scattering happens with the largest size particles like water droplets.

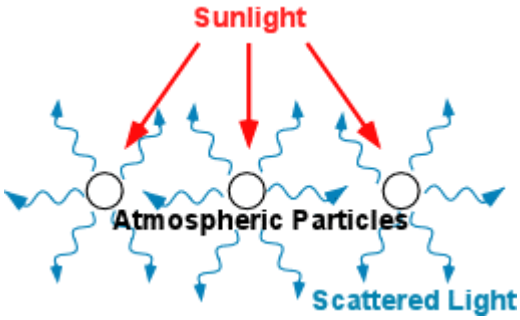

Figure 2-20: Illustration of the scattering of light in the atmosphere.

Rayleigh scattering occurs when the object is smaller than about 1/10 the wavelength of the incoming shortwave radiation. The gas molecules in air fit this category. Rayleigh scattering affects shorter wavelengths more than longer wavelengths, and is more effective with visible light. Shorter wavelengths are the blue and violet colors, although our eyes see blue much better than violet. The wavelengths of light are illustrated in Figure 2-21.

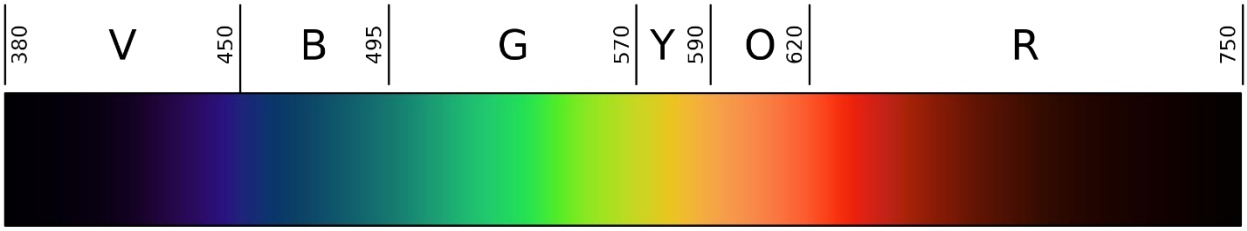

Figure 2-21: The entire visible light spectrum and the wavelengths (in nanometers) associated with each color. Rayleigh scattering affects the shorter wavelengths more than the longer ones.

Light from the Sun consists of all wavelengths. As this light interacts with the atmosphere, blue light is scattered more than the other colors. This scattering is why the sky is blue. The question now is why are sunsets and sunrises sometimes red? The answer to this question is that the light is passing through more atmosphere with a low sun angle at sunrise and sunset. The more atmosphere affecting the scattering of the light, the more the shorter wavelengths are scattered. Eventually only the predominate red and orange colors are left in the light.

Mie scattering occurs when atmospheric particle diameters are larger than the wavelength of the radiation. Most atmospheric particles of this size fall in the aerosol (dust) category. Mie scattering disperses light predominately forward, rather than omnidirectional like Rayleigh scattering. Figure 2-22 illustrates Mie scattering of sunlight.

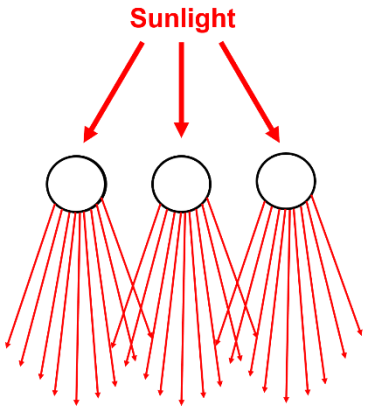

Figure 2-22: Mie scattering disperses light in a forward direction.

Mie scatters do not favor any wavelength and tend to amplify the existing light. When Mie scattering is occurring a whitish or grayish color is present. Many times, Mie scattering can be observed when looking towards the Sun in the morning and noticing a haze is present. Turn around so the Sun is at your back and the haze disappears. Landscape photographers are aware of this visual aspect and prefer the Sun behind them for a clearer picture.

Nonselective scattering occurs with all particles larger than aerosols, like cloud droplets. Non-selective scatters reflect all wavelengths equally, and clouds are the most important particle in this category. The reflection of incoming shortwave radiation due to clouds is due to nonselective scatters (Figure 2-23). The scatters tend to be white or gray in color.

Figure 2-23: Clouds are an example of nonselective scattering.

An interesting aspect of nonselective scattering is when clouds occur during the night. Do you remember Figure 2-8 from section 2.1.5? (See the left side of Figure 2-24) During the night, outgoing longwave radiation (heat) primarily escapes to space through the 10 μm window.

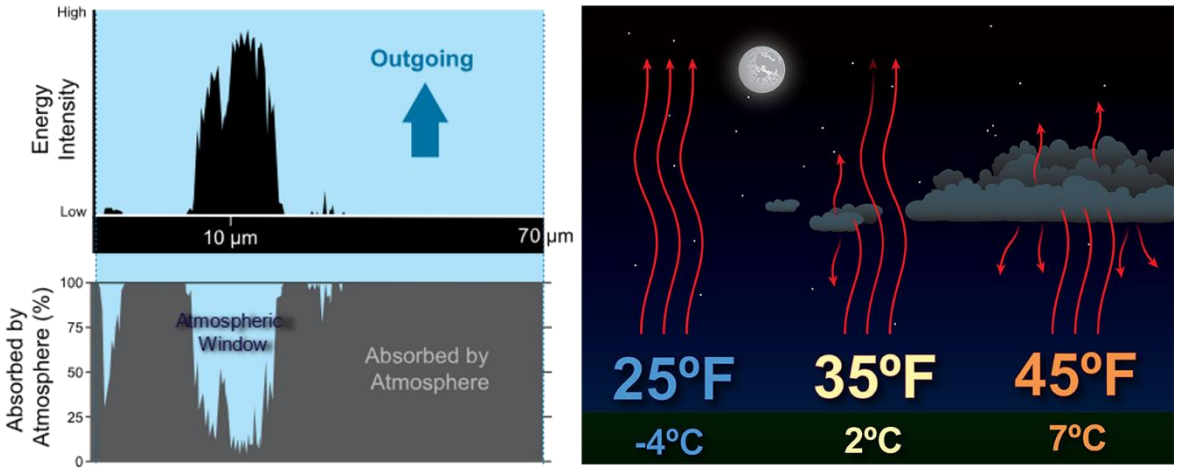

Figure 2-24: The graphs (a portion of Figure 2-8) on the left are the longwave energy absorbed by the atmosphere (bottom) and the energy emitted to space (top). The diagram on the right depicts clouds closing this

As clouds come overhead, their nonselective scattering property closes this 10 μm window. Outgoing longwave radiation is greatly reduced, which in turn increases the temperatures during the night. The right side of Figure 2-24 illustrates the change in nighttime temperatures associated with cloud cover. A simple way to remember this concept is “clouds act like a blanket at night”.

2.4 - Earth’s Energy Balance (Shortwave and Longwave Radiation)

For the Earth to remain at a constant temperature the incoming radiation must equal outgoing radiation. If incoming exceeds outgoing, the Earth will warm. If outgoing exceeds incoming, the Earth will cool. This section exams Earth’s energy balance from the perspective of keeping the Earth at constant temperature in that incoming equals outgoing (See figure 2-25).

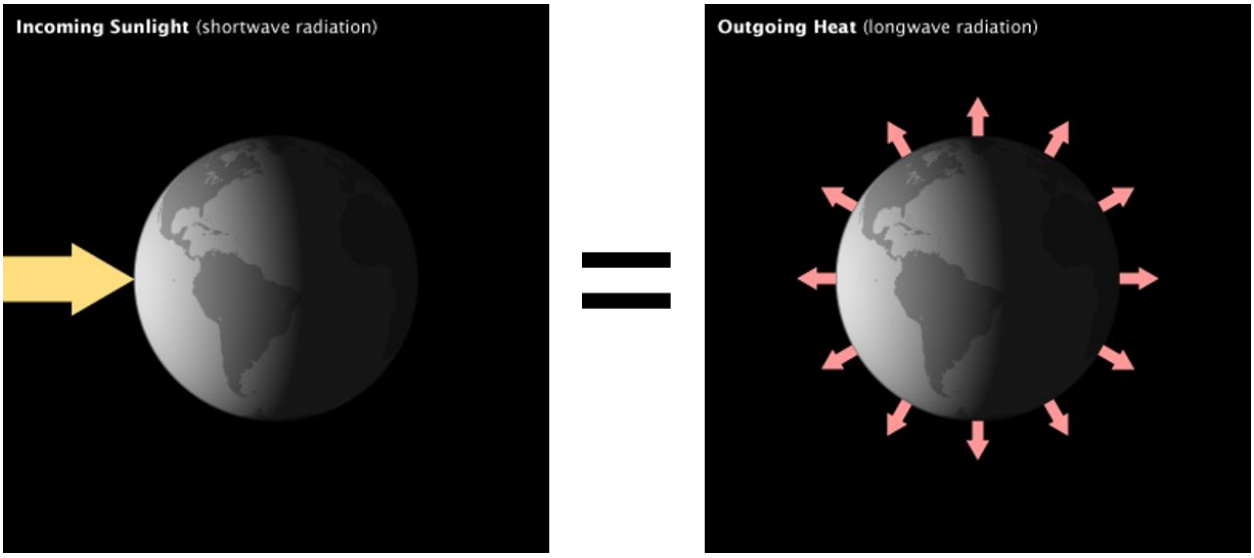

Figure 2-25: Incoming solar radiation balances outgoing heat for the Earth to remain at a constant temperature.

This NASA video introduces the concept of Earth’s energy balance.

2.4.1 - Incoming Radiation

For simplicity, the amount of radiation entering the atmosphere is designated as 100 units. If 100 units are incoming, then 100 units should be outgoing to maintain a constant temperature. An incoming shortwave energy analysis reveals:

- 19 units are absorbed by the atmosphere
- 4 units are absorbed by clouds
- 23 units are reflected by clouds
- 7 units are reflected by the Earth’s surface
- 47 units are absorbed by the Earth’s surface

Adding these numbers gives us 100 units. The Earth's albedo is 30%, so the analysis should have 30 units reflected. From the above numbers, adding 23 (reflected by clouds) and 7 (reflected by surface) gives an albedo of 30. Yay! These numbers are all consistent with our previous knowledge. Figure 2-26 summarizes these numbers. Satellites are the largest source of data associated with tracking Earth's energy balance.

Here is another video from NASA on energy balance with more details.

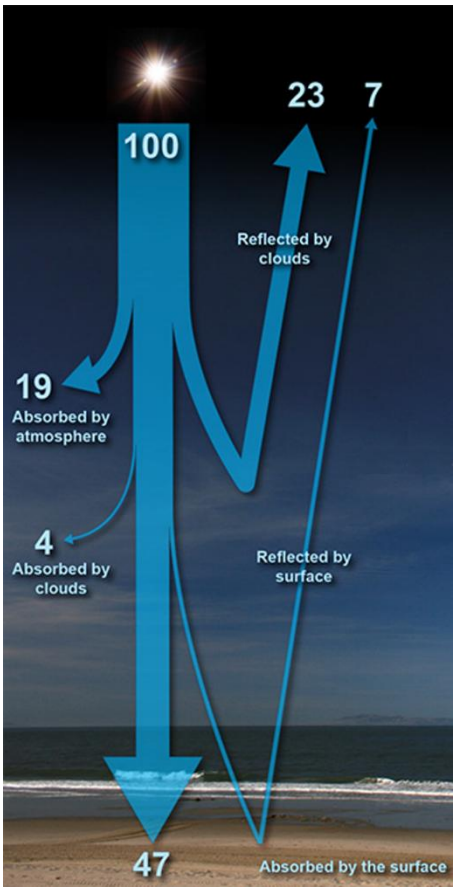

Figure 2-26: An analysis of energy coming from the sun into the atmosphere and to Earth.

2.4.2 - Outgoing Radiation

Outgoing longwave radiation is more complicated than incoming. However, to keep the Earth at a constant temperature, 100 unit should be emitted to space from the Earth. An analysis of outgoing energy going directly to space has:

- 49 units emitted by the atmosphere
- 9 units emitted by clouds
- 12 units emitted by the surface going directly to space

Adding these units together (49 + 9 +12) equals 70. This analysis at first glance seems to be short 30 units. Looking back at the incoming shows that 30 units were reflected into space before entering the atmosphere. Therefore, the requirement to have 100 units going to space is satisfied (70 + 30 incoming reflected = 100).

Now looking at the lower right portion of the outgoing energy diagram (Figure 2-27) indicates some large numbers of 98, 116 and 104. If we started with 100, where do these large numbers come from? The answer to this question is the atmosphere is storing heat. These numbers indicate the amount of heat residing in the atmosphere prior to receiving the 100 units of insolation. However, these numbers should still balance, so the Earth's temperature does not change. In other words, the 47 units originally absorbed by the surface should be emitted by the surface. Looking at the units emitted by the surface, 116 is emitted by the surface. Twelve (12)

units go directly to space, leaving 104 in the atmosphere. Of this 104 in the atmosphere, 98 goes back to the surface from the atmosphere. This process leaves 6 units residing in the atmosphere (104 – 98 = 6). The diagram has 24 units of latent heat and 5 units of sensible heat. More details on latent and sensible heat are in the next section. For now, these two types of heat are processes occurring at the surface to release heat other than emitting longwave radiation (116 units). Summarizing the energy emitted by the surface:

- 24 units latent heat
- 5 units sensible heat
- 6 units emitted by the surface remain in the atmosphere (104 – 98)
- 11 units go directly to space from the surface

Adding these numbers gives 47 units, which is exactly what was originally absorbed by the surface. These numbers are all balanced! Our accounting is good and the Earth has a balance of incoming and outgoing energy. Figure 2-27 summarizes all these numbers associated with Earth's energy balance.

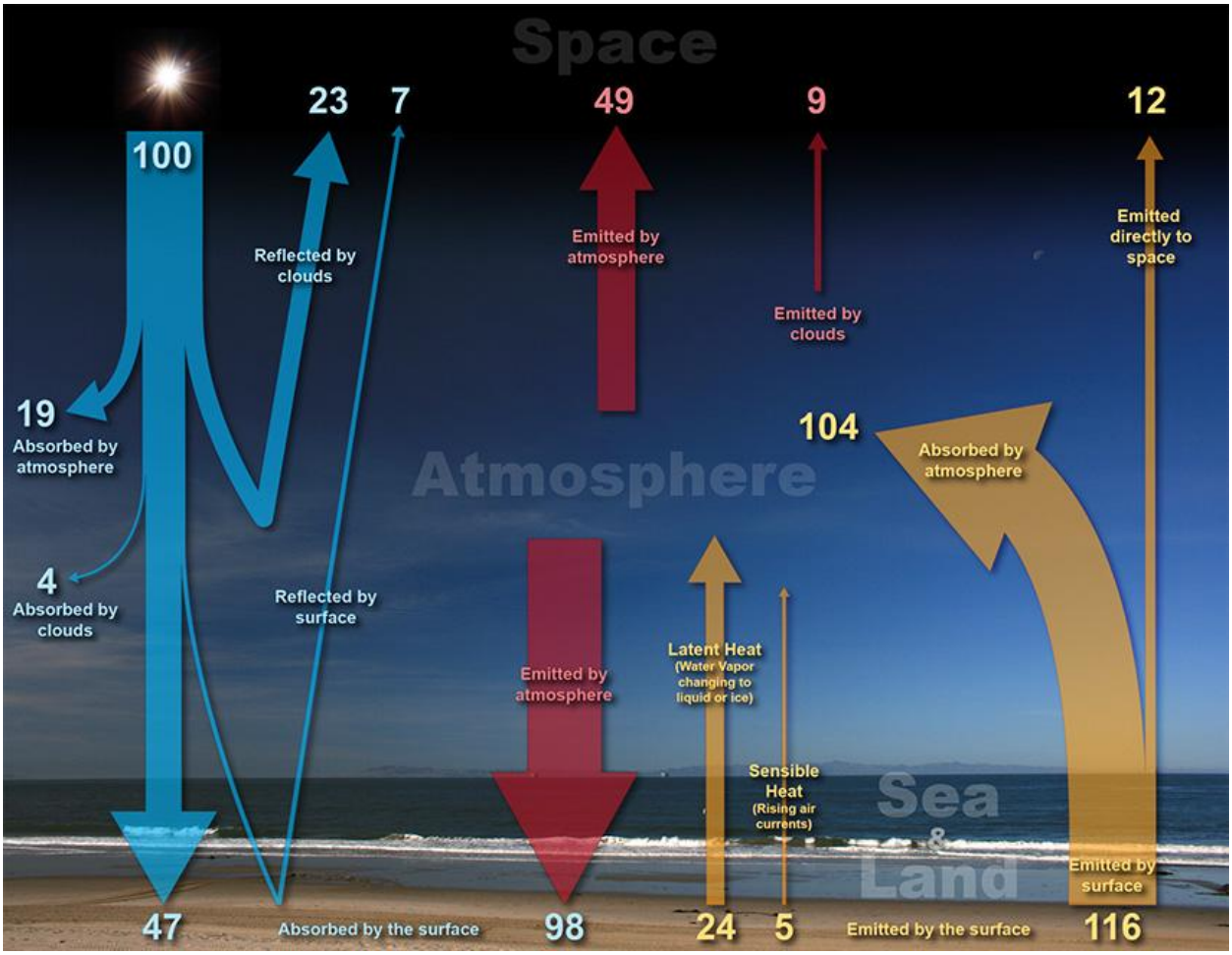

Figure 2-27: A summary of Earth's energy balance. Blue arrows are incoming shortwave energy from the sun. Red arrows are energy emitted and absorbed by the atmosphere. The yellow arrows are energy (heat) emitted by the Earth.

The storage of heat in the atmosphere is called the greenhouse effect, and is a result of greenhouse gases. More on the greenhouse effect upcoming in section 2.4.4.

2.4.3 - Sensible and Latent Heat

Sensible heat is the transfer of heat from one substance to another that results in a change in temperature. For the Earth and the atmosphere, the substances are land, water and air. If you go outside on a hot day, the increase in the temperature you *feel* is your body gaining sensible heat. Sensible heat transfers by conduction.

Associated with this heat transfer is another term called specific heat. **Specific heat** is the amount of energy required to produce a temperature change. Different substances have different specific heats. For example, Figure 2-28 illustrates the differences between the specific heat of water and soil.

Water has a higher specific heat than soil; more energy is required to raise its temperature. This difference in specific heat between water and soil is important! If the Sun is shining equally on an ocean (water) and nearby land (soil), the land will heat up faster and to a higher temperature than the ocean. The higher specific heat causes water bodies to generally cool slower than land during the night too.

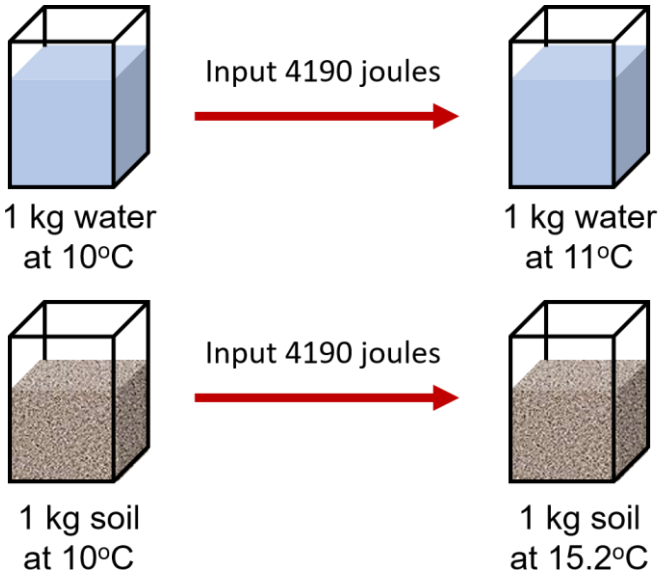

Figure 2-28: Illustration of the differences between the specific heat of water and soil. The same amount of energy (4190 joules) raises the temperature of water 1°C, whereas soil is raised 5.2°C.

Latent heat is the energy required to change the phase (gas, liquid or solid) of a substance. Water is the substance of most interest in the atmosphere. One gram of water requires 1 calorie to raise its temperature 1°C. For 1 gram of water to go from 0°C to 100°C requires 100 calories. The phase change for 1 gram of water to freeze (or melt) requires 80 calories. The phase change for 1 gram of water to evaporate (or condense) requires a whopping 540 calories.

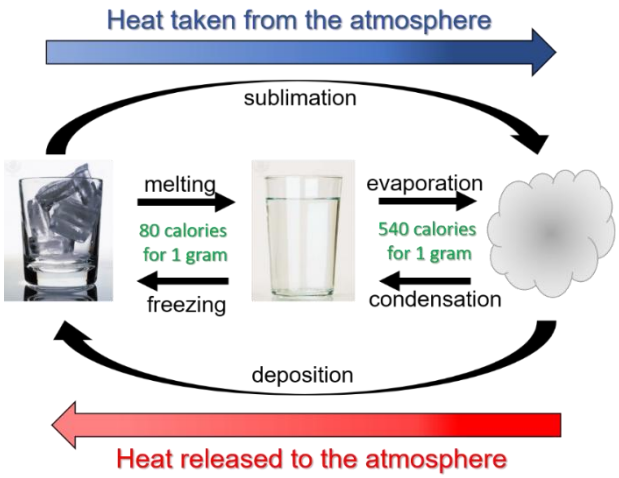

Figure 2-29: The latent heat of water as it changes phase (ice, liquid, and gas).

Additionally, water can skip the intermediate step of being a liquid and go straight from a solid to a gas (water vapor), which is called sublimation. The reverse of going from water vapor to ice is deposition. The latent heat associated with these changes is either taken from the atmosphere or released to the atmosphere. For rain to occur, water vapor must condense. The latent heat associated with condensation releases a lot of heat into the atmosphere. Most people do not think of rain as heating the atmosphere, but from a thermodynamic perspective this is occurring. The latent heat of condensation will be referenced repeatedly in this textbook, because it dramatically affects atmospheric stability.

2.4.4 – Greenhouse Effect

The name "greenhouse effect" was dubbed in the early 1800s when it was thought that greenhouses stayed warmer because the panes of glass allowed solar radiation to enter, but prevented radiation emitted from plants and other objects inside the greenhouse from escaping. Actually, the reason why greenhouses stay warmer inside has to do with the fact that the air inside cannot mix with cooler air outside. The warm air in a greenhouse essentially gets trapped inside the panes of glass.

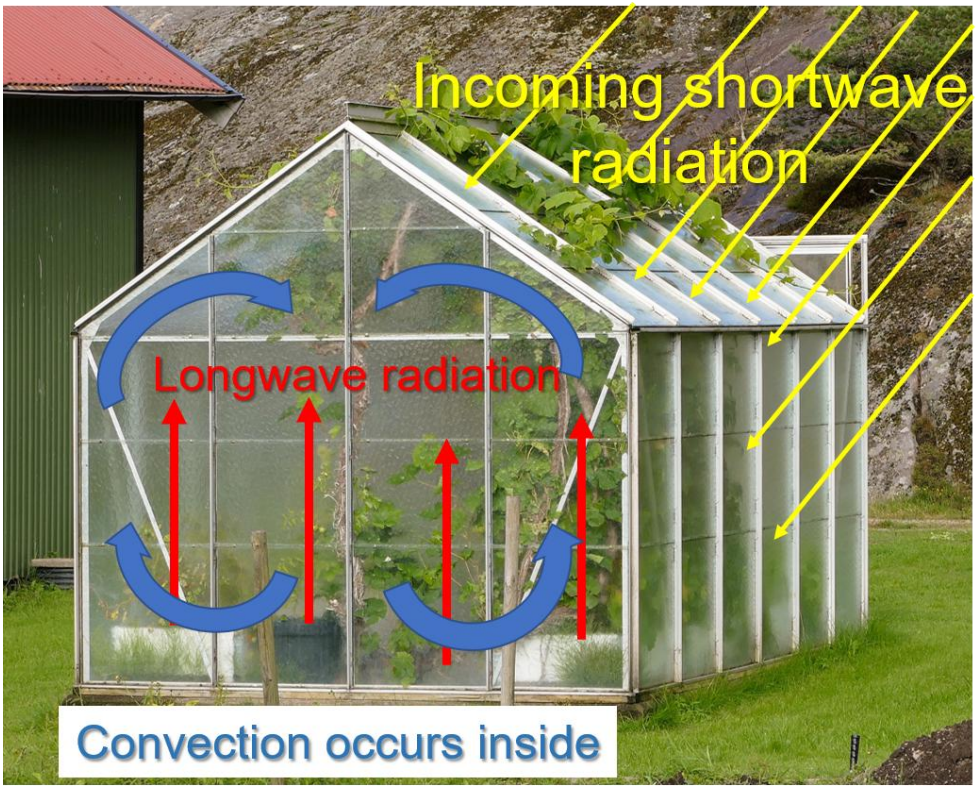

Figure 2-30: Photo of a greenhouse depicting warm air being trapped inside.

The atmospheric “greenhouse effect” is all about the absorption and emission of radiation by atmospheric gases. The physical processes in a greenhouse are much different than the atmospheric “greenhouse effect”. The variable gases associated with capturing heat are now referred to as greenhouse gases (GHGs), which indicates that the greenhouse terminology will be used for decades.

Chapter 2 Review Questions

1. What does the Stefan-Boltzmann Law quantify?
2. In what form is most of the energy from the Sun transferred to the Earth?
3. Once the Earth's surface is heated by the Sun, how is this energy transferred to the atmosphere?
4. Electromagnetic radiation is divided into types (like gamma rays and radio waves). What is the characteristic that defines these types of radiation?
5. What type of radiation has the shortest wavelength? Longest wavelength?
6. What are the wavelengths of the visible light spectrum?
7. How long does light take from the Sun to reach the Earth?
8. Why is summer a warmer season than winter?
9. What causes weather?
10. At what time of day is beam spreading greatest?
11. At what latitude is the Sun directly overhead on the summer solstice? During an equinox? On the winter solstice?
12. Why is the sky blue?
13. What is albedo?
14. What is the Earth's albedo?
15. What is the greenhouse effect?
16. How much energy is required to change 1 gram of liquid water at 100^{o}C into water vapor?
17. Does condensation warm or cool the atmosphere?
18. What gas is an efficient absorber of longwave radiation between about 5 and 7 microns?
19. What is an atmospheric window?
20. What wavelengths does carbon dioxide absorb?
21. What is the most abundant and important greenhouse gas in the atmosphere?

Chapter 3 – Pressure and Wind

Overview

This chapter examines space weather, which is associated with everything other than ultraviolet, visible and infrared radiation that the Sun sends to the Earth. Space weather is the concluding topic associated with the Sun's energy.

The remainder of this chapter discusses air pressure and wind. Wind is a result of differences in pressure. Obviously, wind is a fundamental concept associated with weather, which makes pressure a fundamental concept too. The forces associated with pressure are examined and how these forces combine to create the wind we all experience.

Chapter objectives:

1. Describe impacts associated with space weather.
2. Explain how surface pressure is measured and compared at multiple locations.
3. Understand how pressure gradients in the upper atmosphere are mapped.
4. Explain the forces that affect wind speed and direction.
5. Describe the vertical motions associated with cyclones and anticyclones.

3.1 - Space Weather Essentials

What is space weather? Space weather is activity on the Sun that sends pulses of subatomic particles and full spectrum electromagnetic radiation to Earth. These solar storms can impact everyday technology like Global Positioning Systems (GPS), satellites, and electric power grids. Space weather is a consequence of the behavior of the Sun, the nature of Earth's magnetic field and atmosphere, and our location in the solar system. Outbursts from huge explosions on the Sun—solar flares and corona mass ejections (CMEs)—send space weather storms hurtling outward through our solar system. The Sun also emits a continuous stream of radiation in the form of charged particles that make up the plasma of the solar wind.

A dramatic example of the effects of space weather occurred in March 1989 when a solar storm knocked out power in Quebec for up to 36 hours. The Hydro-Quebec electrical utility went from full operating capacity to blackout status in 92 seconds. Six million people were plunged into cold and darkness.

3.1.1 - Features of the Sun

The Sun is a gas ball of hydrogen and helium. The Sun's enormous mass is held together by gravity, producing immense pressure and temperature at its core. The Sun has six regions: the core, the radiative zone, and the convective zone in the interior; the visible surface, called the photosphere; the chromosphere; and the outermost region, the corona. Figure 3.1 illustrates these six regions. The Sun is not featureless, but has storms much like the Earth has weather.

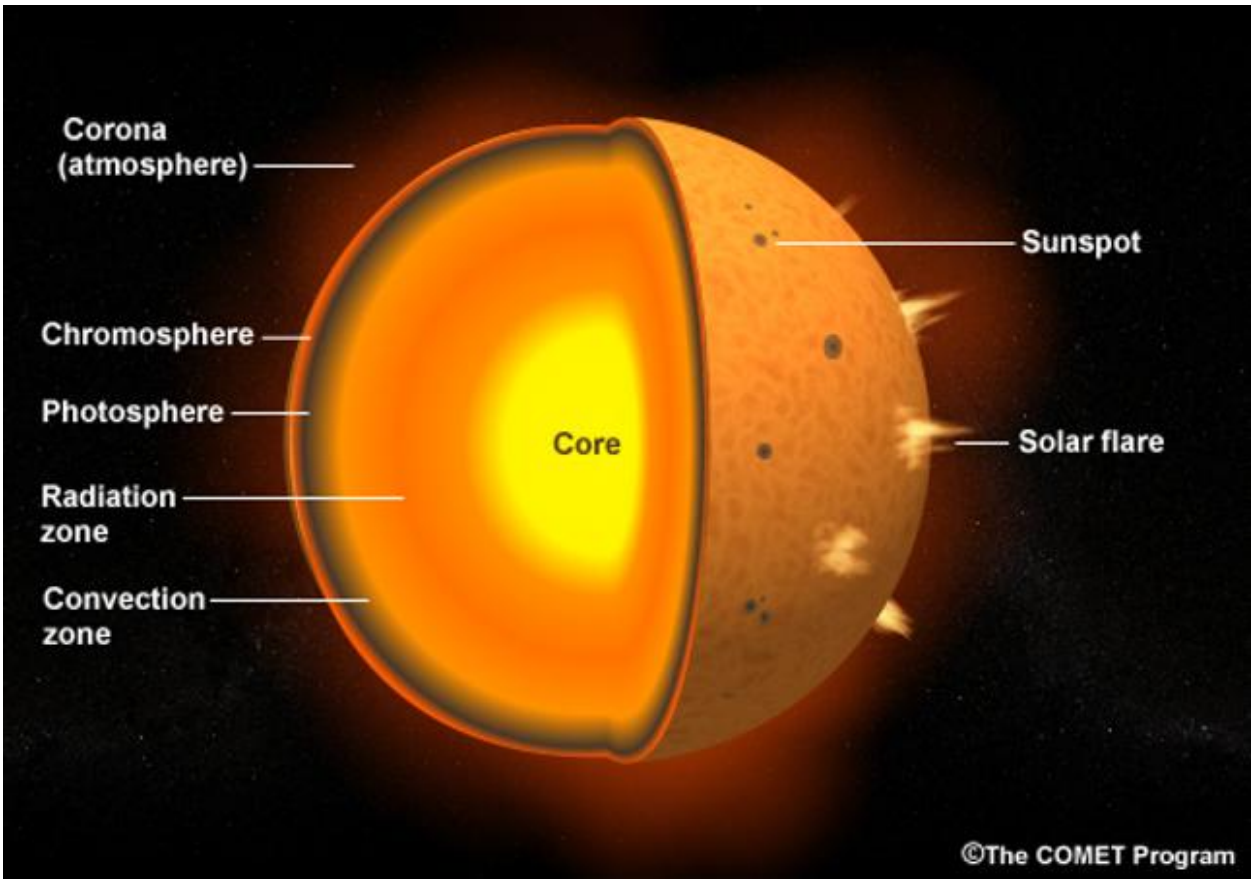

Figure 3-1: Features of the Sun.

At the core, the temperature is about 27 million degrees Fahrenheit (15 million degrees Celsius), which is sufficient to sustain thermonuclear fusion. This is a process in which smaller atoms combine to form larger atoms and in the process release staggering amounts of energy. Specifically, in the Sun's core, hydrogen atoms fuse to make helium. The energy manufactured is 3.8×10^{23} kilowatts (kilojoules/sec). One second of the Sun's energy could power the United States for 9 million years.

The Sun is constantly releasing subatomic particles, predominately protons and electrons, into the solar system. These particles are called the **solar wind**. A solar storm can release larger quantities of high energy charged particles, which are accelerated close to the speed of light. These particles may arrive at the Earth between 30 minutes and several days after leaving the Sun. These particle events and similar electromagnetic radiation bursts are associated with sunspots, solar flares and corona mass ejections (CMEs).

3.1.2 - Sunspots, Solar Flares and Corona Mass Ejections

Sunspots are visible spots on the surface of the Sun that are cooler than their surrounding area (4500ºC versus 5800ºC). These cooler areas appear as dark spots on the Sun . See Figure 3-2. As the Sun rotates, sunspots on its surface appear to move from left to right. The Sun takes 27 days to make one complete rotation; whereas the Earth takes 24 hours to complete a rotation. Sunspots occur when strong magnetic fields emerge through the solar surface and allow the surrounding area to cool slightly.

Sunspot activity is not constant, but has a quasi-periodic variation of eleven years. An increase in sunspots corresponds to an increase in solar activity, such as solar flares and CMEs. Sunspots were recorded as early as 325 B.C. The sunspot cycle going back to the 1930s is shown in Figure 3-2 with a peak in 2024 and 2025.

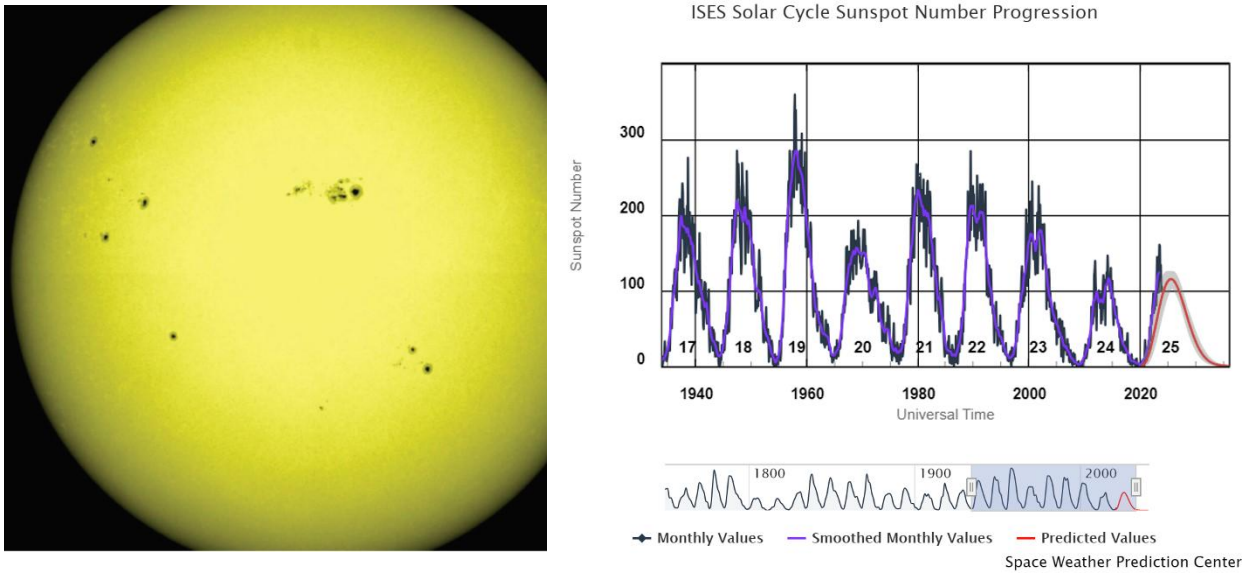

Figure 3-2: (left side) Cooler temperatures on the Sun are seen as darker areas called sunspots. (right side) Graph containing the number of sunspots occurring back to the 1930s. Sunspots have a cyclic nature with a maximum occurring about every 11 years.

This NASA video describes how sunspots occur and are tracked along with the solar cycle.

Solar flares are huge explosions on the Sun. A flare appears as a sudden, intense, brightening region on the Sun typically lasting several minutes to hours. An image of a solar flare is shown in Figure 3-3. Flares produce bursts of electromagnetic radiation in the optical and radio wavelengths. The primary source of their energy is the tearing and reconnection of strong magnetic fields. The electromagnetic emissions produced during flares travel at the speed of light, taking 8 minutes and 20 seconds to reach the Earth; thus, rapidly affecting the dayside portion of our planet.

Corona Mass Ejections (CMEs) are explosive outbursts of plasma from the Sun's outer atmosphere, the corona. The blast of a CME typically carries roughly a billion tons of material outward from the Sun at speeds as fast as hundreds of kilometers per second. A CME contains particle radiation (mostly protons and electrons) and powerful magnetic fields. An image of a CME is shown in Figure 3-3. In contrast to solar flares, CMEs are not particularly bright, may take hours to fully erupt from the Sun, and typically take 1-4 days to travel to Earth. The subatomic particles in a CME have mass, which is why they take days to reach the Earth. Figure 3-3 (right side) captures a relatively minor CME. With Earth at 7900 miles in diameter, this eruption is about 20 times the diameter of our planet.

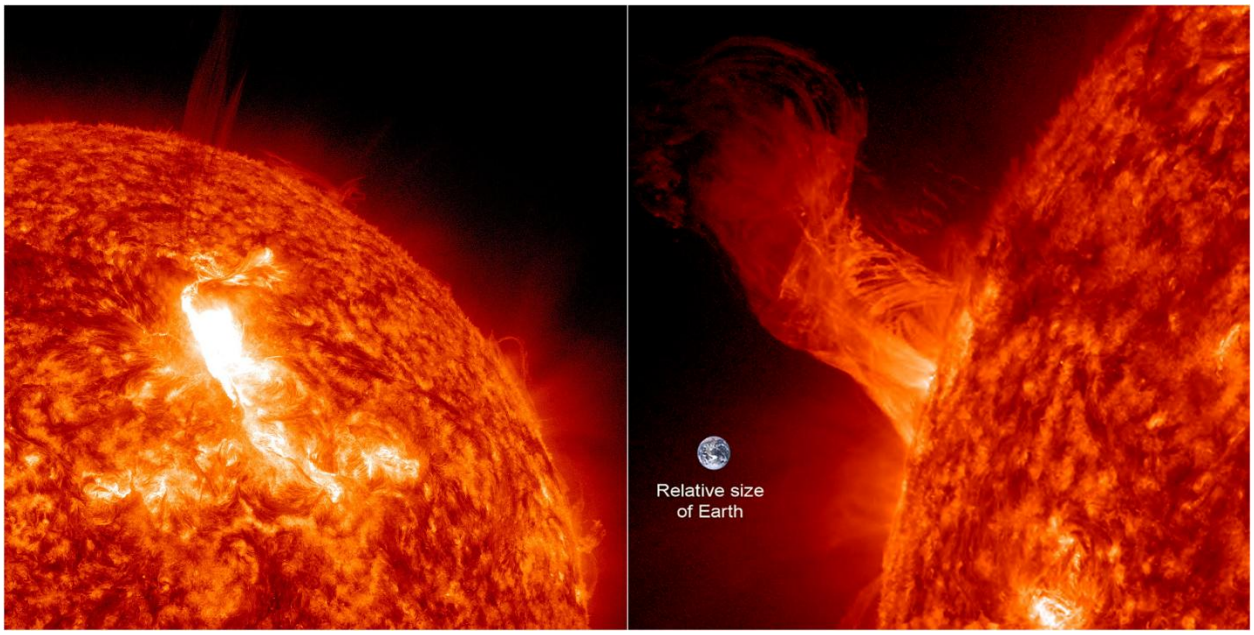

Figure 3-3: (left image) A solar flare as seen as a bright area on the sun. (right image) A corona mass ejection (CME) leaving the Sun. Notice the relative size of the Earth in this image.

This short video from NASA discusses CMEs, solar flares and the Sun's magnetic fields involved in these events.

3.1.3 - Interactions with Earth's Magnetic Field

Surrounding Earth is a giant magnetic field called the magnetosphere. Its shape is defined not only by the planet's north and south magnetic poles, but also by the solar wind from the Sun. The magnetosphere is buffeted by this wind and can change shape dramatically when a CME occurs.

The solar wind interacts with Earth's ionosphere. Most of the ionosphere resides in the lower portion of the thermosphere and upper portion of the mesosphere. The atmosphere frequently absorbs these particles without noticeable effects. During a CME the increased solar wind excites the gas molecules in the ionosphere and causes them to glow. This light is referred to as an aurora or aurora borealis in the Northern Hemisphere (Figure 3-4). The charged gas molecules tend to align themselves with Earth's magnetic field, which gives a wavy appearance to an aurora. Auroras usually occur between 60 and 80 degrees latitude, although in 1909 an aurora was seen in Singapore (1.3°N).

Figure 3-4: A photo of an aurora. Notice the wavy appearance as the charged molecules align themselves to the Earth's magnetic field.

A large CME can also strengthen the ionosphere by increasing the number of charged gas molecules (ions). During normal activity, radio waves can be bounced off the ionosphere to extend their transmission range. However, a strengthened ionosphere, as depicted in Figure 3-5, will absorb or dampen radio signals and can cause transmissions to fail.

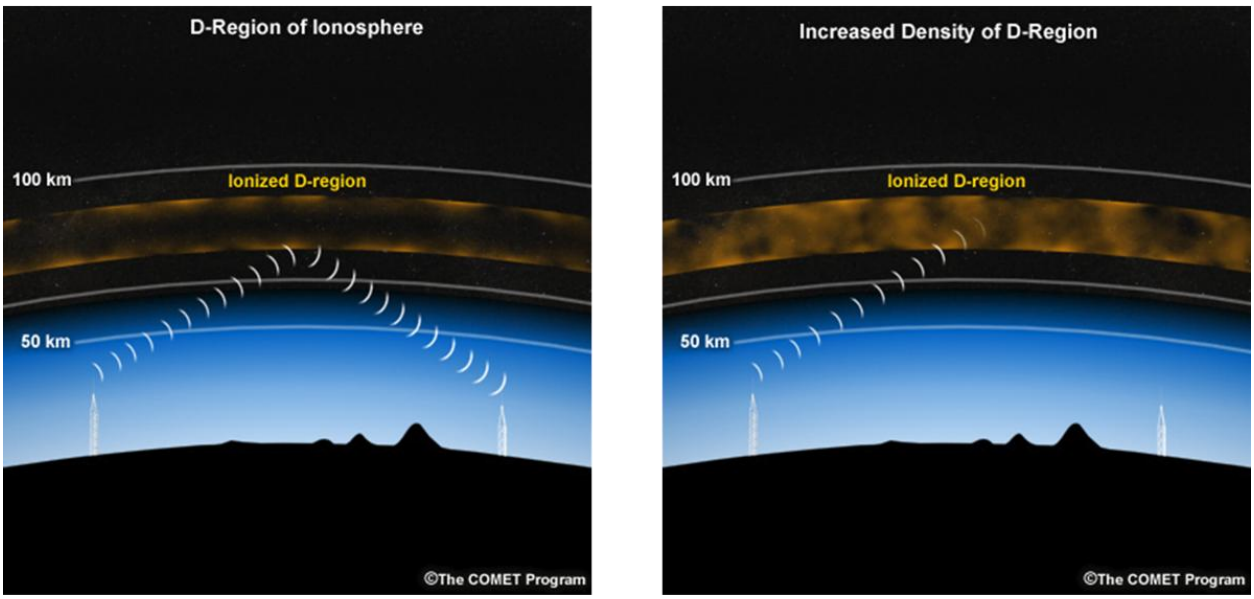

Figure 3-5: A comparison of radio signals in a normal ionosphere (left) and an ionosphere strengthened with more charged molecules (right).

Other problems associated with storms from the Sun are induced electrical current in long metal pipelines or electrical power transmission lines. Remember, electrical and magnetic fields are closely tied together. Changing the magnetic field surrounding a metal conductor changes the electrical properties of the conductor. All these impacts are associated with space weather.

3.1.4 - Space Weather Effects

Space weather can impact seven aspects of modern society:

Electric Power
Large currents in the ionosphere can induce currents in power lines. Surges from these induced currents can cause massive network failures and permanent damage to electric grid components.

Navigation Systems
Disturbances in the ionosphere can cause degradation in GPS range measurements and, in severe circumstances, loss of lock by the receiver on the GPS signal.

Aviation
Space weather storms can cause lost or degraded communications, radiation hazards to crew and passengers, unreliable navigational information, and problems with flight-critical electronic systems.

Human Space Exploration
Energetic particles present a health hazard to astronauts on space missions as well as threats to electronic systems. During space missions, astronauts outside spacecraft are less protected and more exposed to space radiation.

Satellite Operations
Highly energetic ions penetrate electronic components, causing bit-flips in a chain of electronic signals that can result in improper commands within the spacecraft or incorrect data from an instrument. Less energetic particles contribute to a variety of spacecraft surface charging problems, especially during periods of high geomagnetic activity.

Surveying
Magnetic field changes associated with geomagnetic storms directly affect operations that use the Earth's magnetic field for guidance, such as magnetic surveys, directional drilling, or the use of magnetic compasses. Ionospheric disturbances cause errors in location obtained from GPS signals.

Communications
Communications at all frequencies may be affected by space weather. High frequency (HF) radio communications are more routinely affected because this frequency band depends on reflection by the ionosphere to carry signals great distances.

This video summarizes the impacts of space weather, and what NOAA's National Weather Service is doing to protect us.

3.2 - Concepts Associated with Pressure

In Chapter 1, the concept of air pressure was introduced. Air pressure is a critical aspect of weather, because differences in pressure cause the wind. Wind can lead to storms, dramatic temperature changes and much more. Obviously, we need to know much more about pressure to understand weather. This section and the next provide those details.

3.2.1 - Measuring Pressure

Air pressure is the weight of an air column that extends from the ground to the top of the atmosphere. This statement is from Chapter 1 and defines surface pressure. **Surface pressure** is the measure of air pressure at the surface.

As elevation increases, the mass of atmosphere above a location on the surface decreases. Air pressure on a high mountain will always be less than in a valley. Pressure is a unique atmospheric parameter in that it always decreases vertically. Figure 3.6 illustrates this concept of air pressure decreasing with height.

The pressure at P1 will be the weight of the air above the mountain. The pressure at P2 will be the pressure at P1 plus the weight of the air between P1 and P2. This aspect of pressure presents a problem, because we would like to compare the surface pressure at every location. Every location has a different elevation, so comparing surface pressures will not work. A new definition will fix this surface pressure conundrum. **Sea-level pressure** is the surface pressure of a location as if that location were at sea-level. Taking the surface pressure and converting it

to sea-level allows a person to compare pressures at all locations without regard to elevation. These comparisons will increase our understanding of the air motion associated with changes in weather.

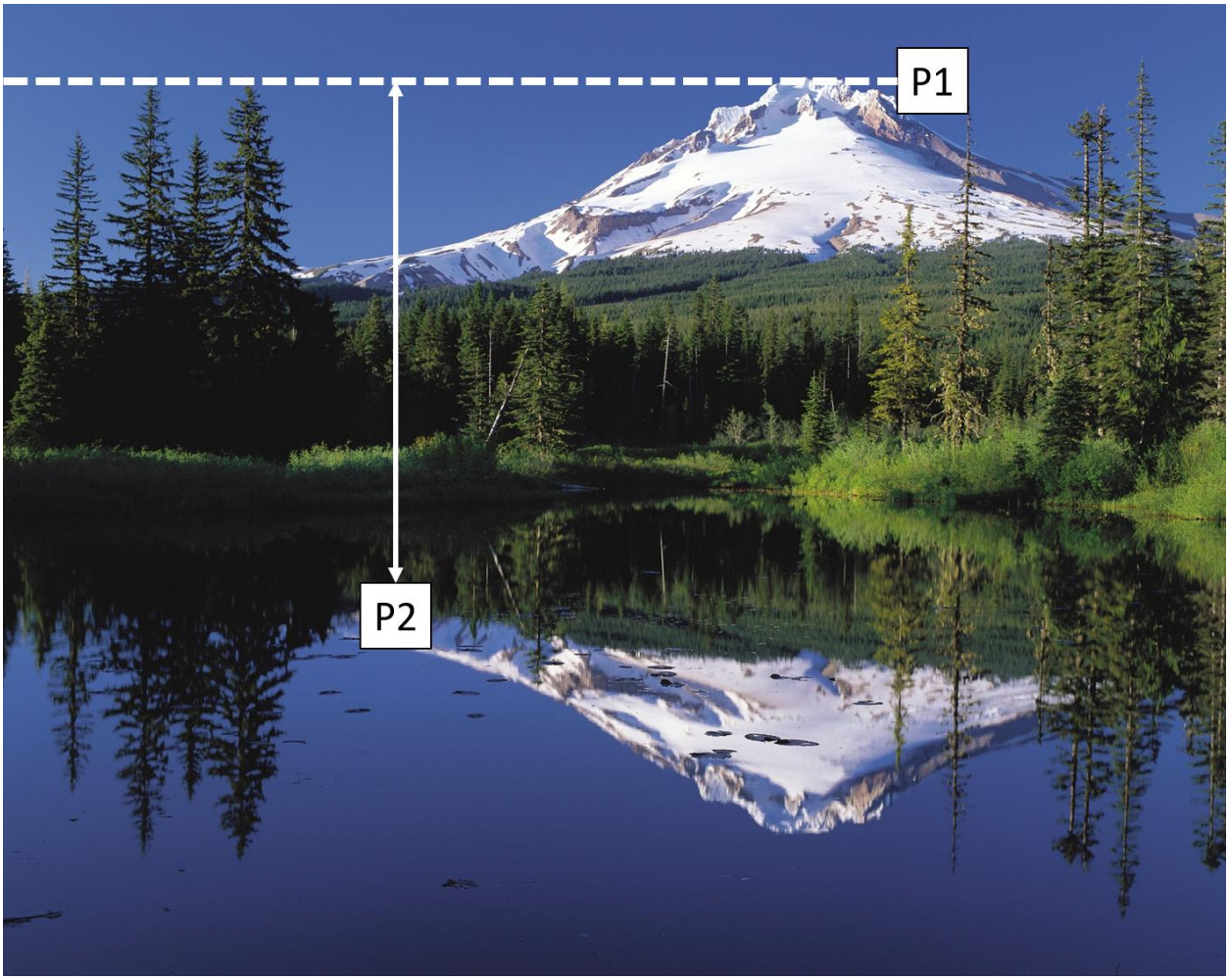

Figure 3-6: Photo depicting the pressure difference between a mountain and a valley. The pressure at P2 will be the pressure at P1 plus the weight of the air between P1 and P2.

When comparing surface pressure to sea-level pressure, surface pressure is almost always the lower of the two. Taking an average of sea-level pressures over the globe gives a value of 1013.2 mb. This value is called standard sea-level pressure or 1 atmosphere (1 atm).

The most common method to measure surface pressure is with an aneroid barometer (Figure 3-7). An aneroid barometer consists of a sealed metal cylinder (box) that expands and contracts as the air pressure changes. This cylinder is connected to a needle and calibrated to a dial for taking readings.

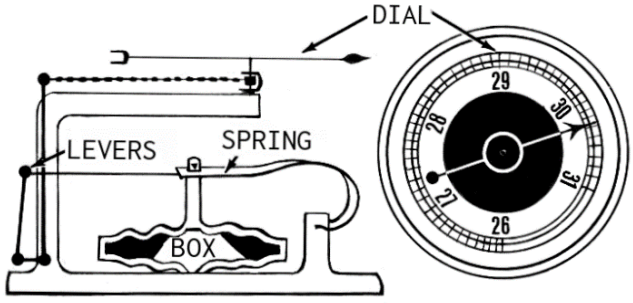

Figure 3-7: Diagram of an aneroid barometer.

3.2.2 - Ideal Gas Law

The pressure in a sealed container can be changed by either (1) putting more air in the container or (2) heating or cooling the container. Hence, pressure is related to both density and temperature. In Figure 3-8, which of these boxes containing air has the highest pressure?

When looking at these boxes, “C” appears to have the most air molecules and appears to have the highest pressure. “C” is the correct answer if the boxes all have the same temperature. However, information on temperature is not known. If “A” was much warmer than “B” or “C”, it could have the highest pressure. This example illustrates that pressure is dependent upon *both* density and temperature.

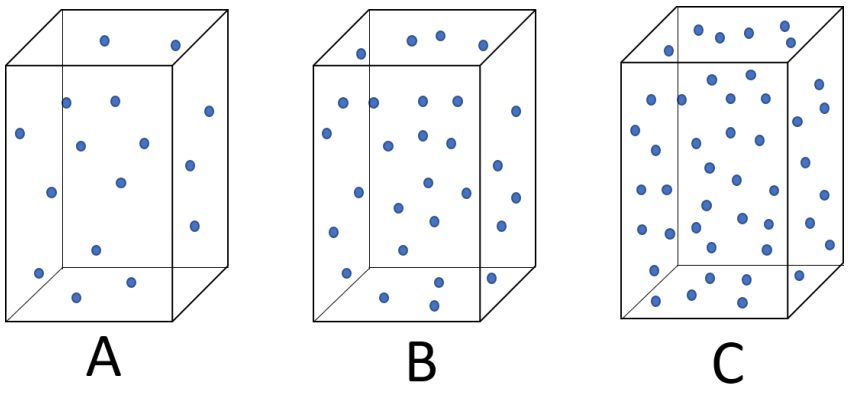

Figure 3-8: Three equal size boxes with a different number of air molecules in each. Which box has the highest pressure inside?

The Ideal Gas Law, also referred to as the Equation of State, relates pressure (P), density (ρ) and temperature (T). In this equation, “R” is a constant.

$$P = \rho RT$$

The general form of the Ideal Gas Law used in many science courses is PV = nRT. In this form V is volume and n is the number of moles of gas. The composition of the atmosphere is relatively constant, so n/V is translated into the density (ρ) variable. Density does decrease with height in the atmosphere, although much, much slower than pressure or temperature. Pressure changes dramatically with height and is easy to measure. Likewise, temperature changes with height and it is easy to measure too. Thus, this form of the Ideal Gas Law (using density) is the best form for the atmospheric sciences.

The physical aspect of the Ideal Gas Law tells us that pressure varies directly with temperature. If the temperature increases, then pressure increases. If the temperature decreases, then pressure decreases. The effects of the Ideal Gas Law can be observed in many situations. For example, when pumping up a bicycle tire with a hand pump, the pump gets warm. The pressure increases which causes a corresponding temperature increase in the pump. When using a can of spray paint, the pressure inside the can decreases and the can cools.

3.2.3 - Vertical Versus Horizontal Pressure Characteristics

The sea-level pressure at a location is constantly varying. To monitor these variations, surface weather maps are created with isobars (lines of constant pressure) analyzed every 4 mb. A typical sea-level pressure map has an “H” or “L” placed over higher or lower pressure areas. Figure 3-9 contains a typical surface weather map. The isobars are brown lines. The colored

lines with triangles and half circles are called fronts. The fronts on the map can be ignored for now. The important aspect of this figure is the isobars.

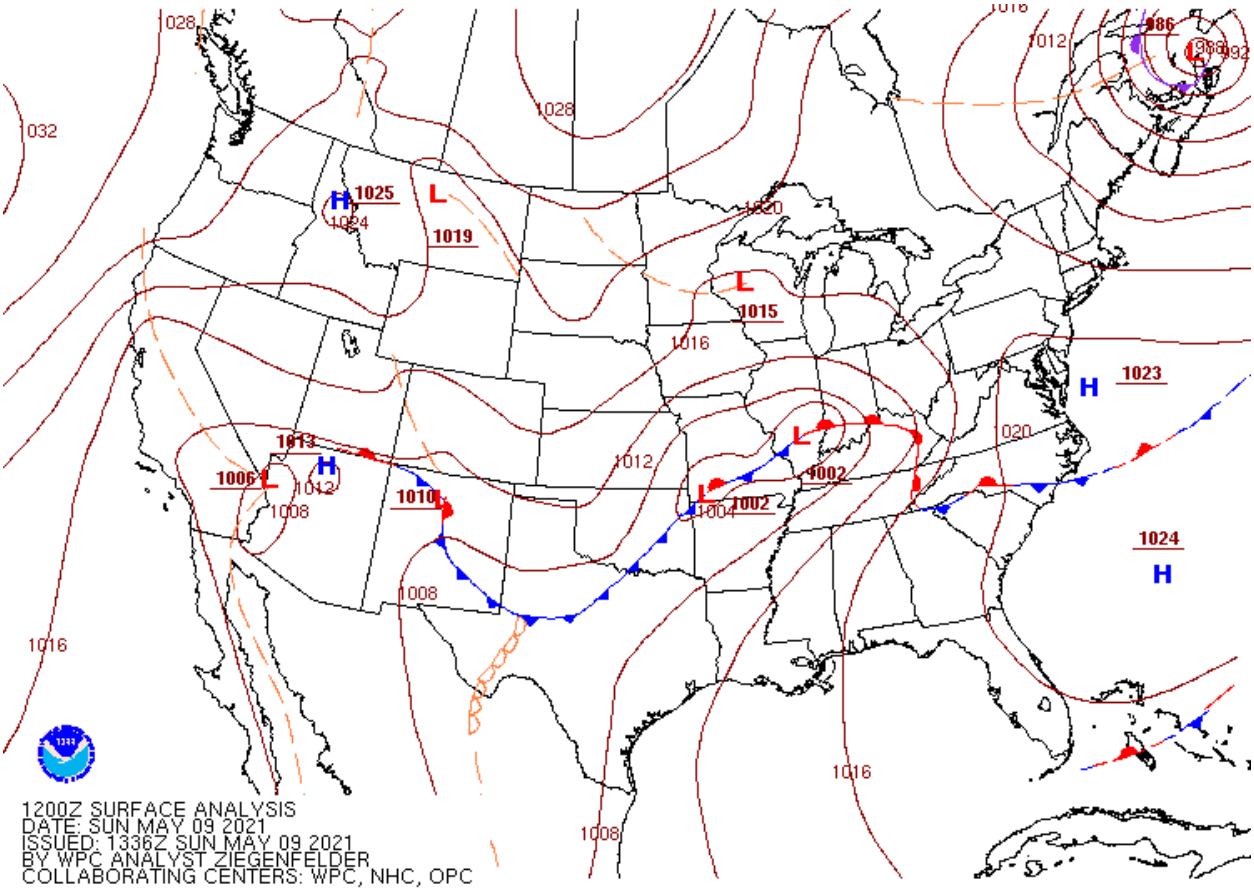

Figure 3-9: A typical surface weather map of the United States. The brown lines are lines of constant pressure called isobars. The colored lines with half circles and triangles are called fronts.

The lowest pressure in the U.S. on the above map is 1002 mb in Illinois and Missouri. The highest pressure is 1025 mb in northern Idaho. The distance between these two locations is over 3000 km with a change of 23 mb. Pressure changes across a horizontal distance are not large. Pressure changes over a similar distance in the vertical are much larger. From the Earth's surface to 3000 km in the vertical (into the exosphere), the pressure is near zero, a change of over 1000 mb.

Contour maps can be thought of as topographical maps in some respects. The low pressure area in Illinois and Missouri can be visualized in three dimensions as a valley, and the high pressure in Idaho as a hill. Air flows from higher pressure areas (hills) into lower pressure areas (valleys). This aspect of air movement (wind) is the topic of the next section.

3.2.4 - Pressure Gradient Force

A **pressure gradient** is the rate of change in pressure across a distance. Pressure gradients are easy to determine in a sea-level pressure analysis. The closer the isobars are to each other,

the higher the pressure gradient. The further apart the isobars are to each other, the lower the pressure gradient. These pressure gradients are important because they create a force which generates wind. The **pressure gradient force** is a force that results from a difference in pressure. The difference in pressure causes air to move and creates wind.

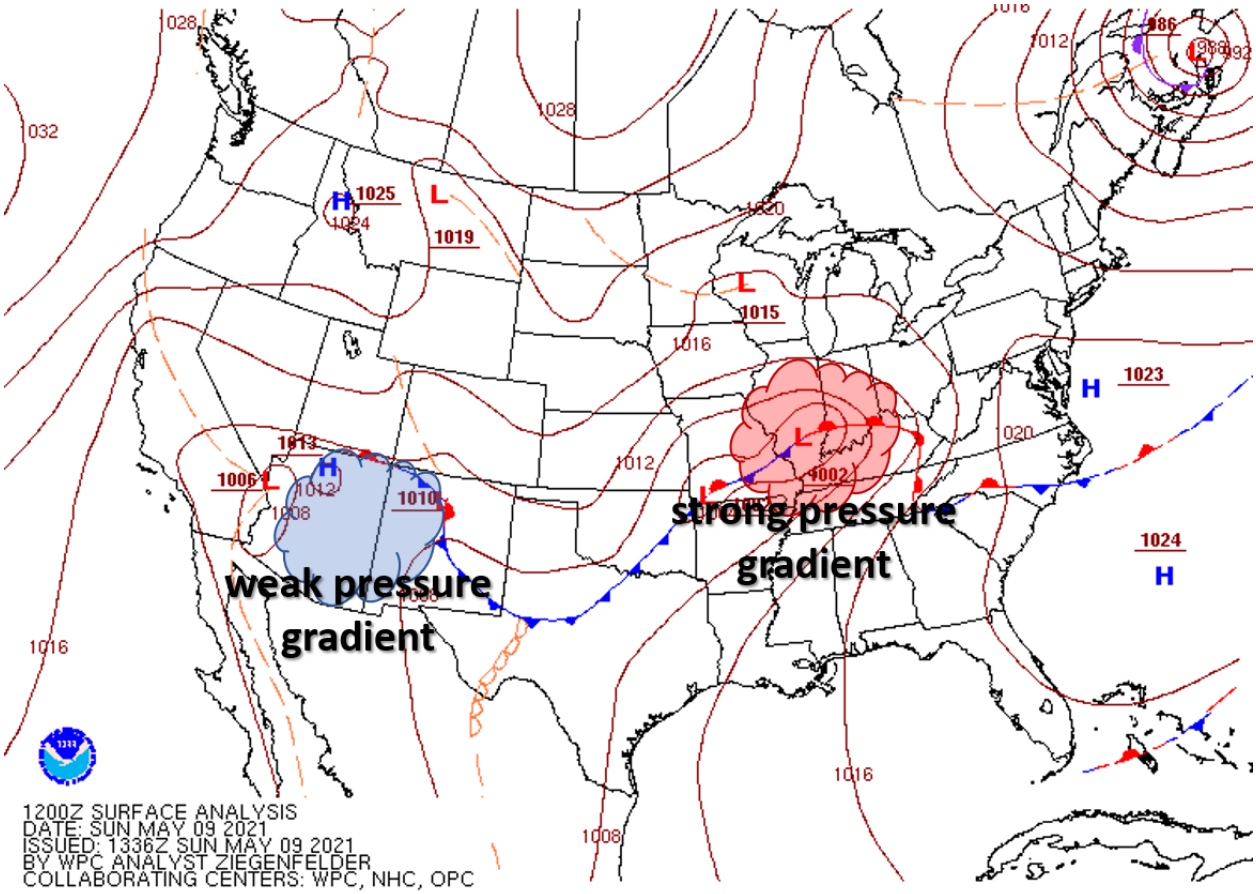

Figure 3-10: The same surface weather map shown in Figure 3-9 with the areas of weak and strong pressure gradients highlighted. Notice the lack of isobars in the weak pressure gradient area, and the abundance of isobars in the strong pressure gradient area.

Air (wind) always moves from high pressure to low pressure. Always! You already know this fact if you have ever had a flat tire. A normal tire has higher pressure inside it than outside. If the tire is punctured, the higher pressure air moves to the lower pressure outside until the pressures are equal inside and out.

Figure 3-11: Air always moves from higher to lower pressure. Typical tire (left) with a higher pressure inside than outside. A flat tire (right) where the pressures inside and outside the tire are equal.

Since we now know wind moves from high to low pressure, what keeps air from leaving the Earth? The pressure outside the atmosphere is zero. A strong pressure gradient force exists from sea-level at 1013.2 mb to 0 mb outside the atmosphere. The answer to this question is the gravitational force, which is what creates air pressure in the first place. The gravitational force balances the pressure gradient force in the vertical. This balance of forces is called *hydrostatic equilibrium*. Hydrostatic equilibrium is normally maintained at all altitudes in the atmosphere.

3.2.5 - Upper Atmosphere Pressure Gradients

All the pressure gradients examined so far have been on the surface. Obviously, pressure gradients exist aloft, since winds occur aloft and a pressure gradient force is associated with these winds. Let us now explore pressure gradients aloft. This exploration will be confined to the troposphere, because that is where most of the atmosphere resides and where weather occurs.

Examining a cool and warm column of air at the same pressure, the warmer column of air must have a larger volume. Applying the Ideal Gas Law ($P = \rho RT$), the pressure (P) is same in both columns. The temperature is not the same, one is warmer than the other. The only variable left to balance the equation in this Law is density (ρ). If the temperature is higher, density must be slightly lower. If both columns have the same number of air molecules, the height of the warmer air column must be higher to offset the warmer temperature. The higher column has a larger volume, which causes the density to be lower. Remember the number of gas molecules in each column is the same.

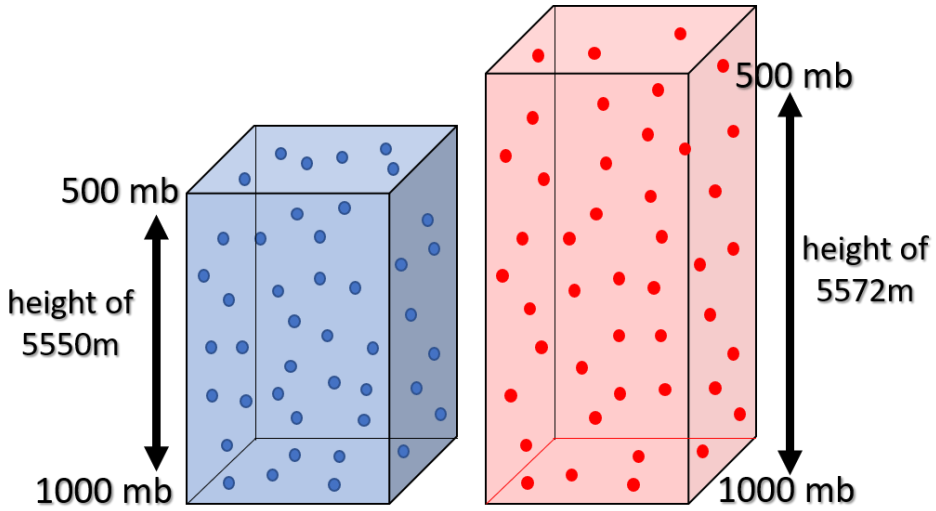

Figure 3-12: Two columns of air at the same pressure, but having different temperatures. The number of air molecules in each column is identical, so the height of the warmer column must be higher.

In a sea-level pressure analysis, all surface pressures are converted to sea-level to avoid problems with elevation. Once off the surface of the Earth, analyses are performed on constant pressure surfaces. The height of a specific pressure for a site is placed on the map. An analysis is done on the height data as shown in the 500 mb map in Figure 3-13.

The station model (Figure 1-12) is used to display data on constant pressure maps, the same as surface maps. The temperature and dewpoint value are in the same location. Since this map is for a constant pressure of 500 mb, the height value is placed in the pressure location.

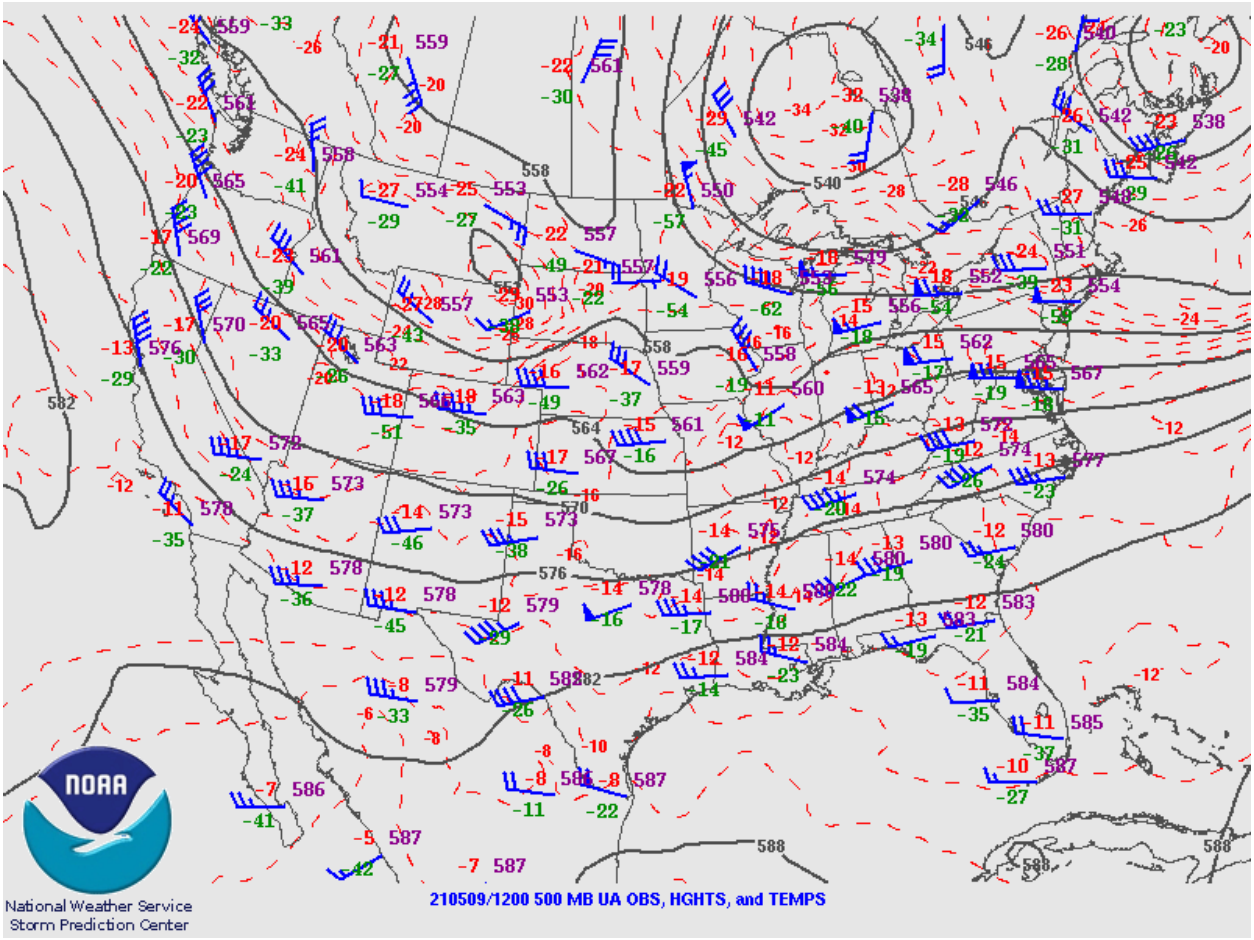

Figure 3-13: A 500 mb weather map of the United States. The height of the 500 mb pressure is plotted on the map and the dark lines are contours of equal height. Lines of equal temperature (isotherms) are red dashes.

Commonly used pressure surface values and their approximate heights are below. The actual height of these pressures at a location varies because the temperature of the air is always changing.

Pressure level	850 mb	700 mb	500 mb	300 mb
Approximate height	5000 feet	10,000 feet	18,000 feet	30,000 feet

A 500 mb map looks like a sea-level pressure analysis. Can these maps be used to determine pressure gradients? The answer is "yes". Air flows from higher to lower heights. When height lines are closer together, they indicate a stronger pressure gradient and stronger winds. Conceptually height lines can be treated as if they were isobars. Additionally, higher heights (pressure) aloft indicates warmer air resides in that area than an area with lower heights, which is accurate.

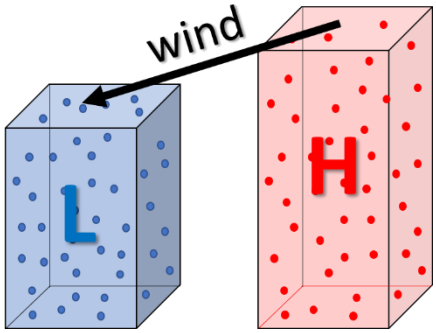

Figure 3-14: Wind flow between different heights on a constant pressure surface.

3.2.6 - Pressure Gradients Across a Hemisphere

If accurate, the height and temperature concepts presented in the section 3.2.5 should be present on the Earth. The tropics are always warmer than the poles. Therefore, the tropics should have higher 500 mb heights and the poles lower heights. The pattern should look like Figure 3-15 with the height of 500 mb values getting lower towards the pole.

Figure 3-15: Theoretical 500 mb heights from the tropics to the poles based on temperature differences.

Examining the actual average 500 mb data for the winter of 2021 provides us Figure 3-16. Notice that higher heights are present towards the tropics and lower heights are near the poles. A wave or dip exists in these heights across the central U.S., but the basic concept of pressure gradient force and using the height of a pressure surface for an analysis of the atmosphere is valid.

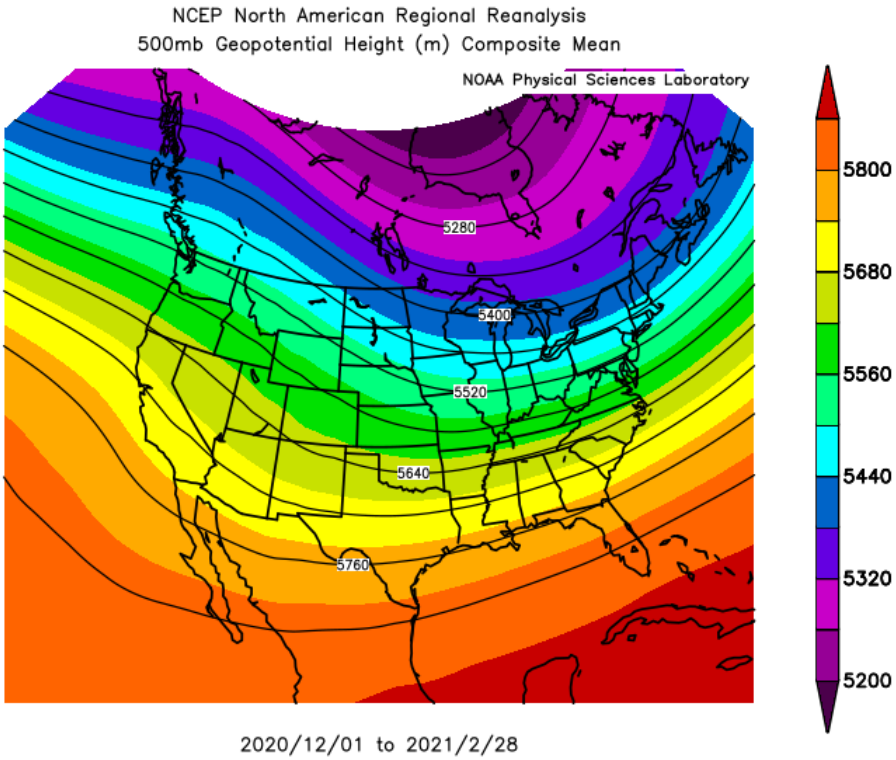

Figure 3-16: The 500 mb height values over North America for the winter of 2021.

The primary force affecting the wind is the pressure gradient force. However, two other forces or effects can influence the wind. These other forces are the Coriolis Effect and friction. The next two sections discuss these forces to complete the fundamentals of pressure and wind.

3.2.7 - Coriolis Effect

The **Coriolis Effect** results from the Earth's rotation and alters only the wind direction, not the wind speed. Frequently the Coriolis Effect is referred to as the Coriolis force. Both terms are correct. The Coriolis Effect influences everything traveling long distances over the earth, like airplanes, wind and ocean currents, missiles, or migrating birds. The Coriolis Effect deflects objects to the right in the Northern Hemisphere and to the left in the Southern Hemisphere. The reason for this deflection is that locations on the Earth move at different speeds.

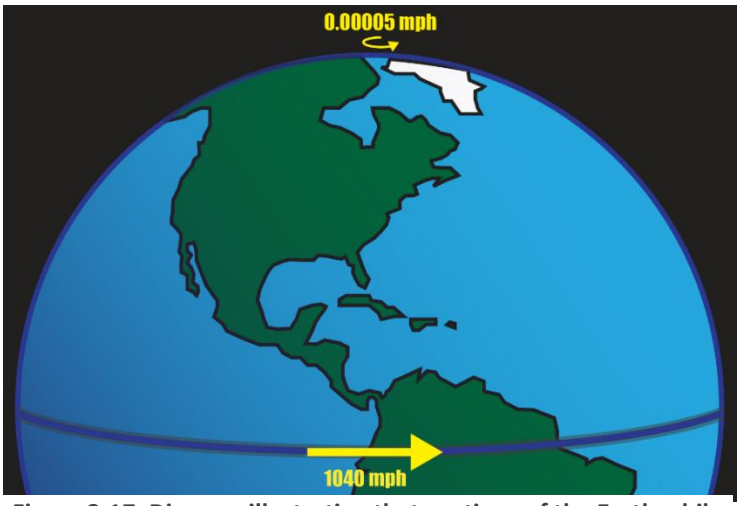

Figure 3-17: Diagram illustrating that portions of the Earth while rotating move at different speeds.

The Earth takes 24 hours to complete a rotation. If you are standing 1 foot to the right of the North or South Pole, that means it takes 24 hours to move in a circle about 6 feet in circumference. Your speed would be about 0.00005 mph. At the equator, the 24 hours rotation is still present, but you would travel the entire circumference of the Earth in this time. The Earth's circumference is about 25,000 miles so your speed is almost 1040 mph. The farther from the equator, the slower a person moves (Figure 3-17).

How does this speed difference prevent objects from traveling in a straight line? Good question! Now think about this: You are on a train traveling at top speed and are passing a train which is moving slower. You see a soccer goal on this slower train and have a soccer ball along. You take an incredible shot directly at the goal when you are across from it. Even though your aim is perfect, the ball travels to the side and misses the net. The reason the ball misses is because it is traveling not only towards the goal, but it also has the faster speed of your train. A short animation of this scenario can be seen at this link.

These trains are similar to the Earth. The faster train is near the equator and the slower train is closer to the pole. If the Earth was not rotating, everything would move in a straight line. A rotating Earth causes the deflection as shown in Figure 3-18.

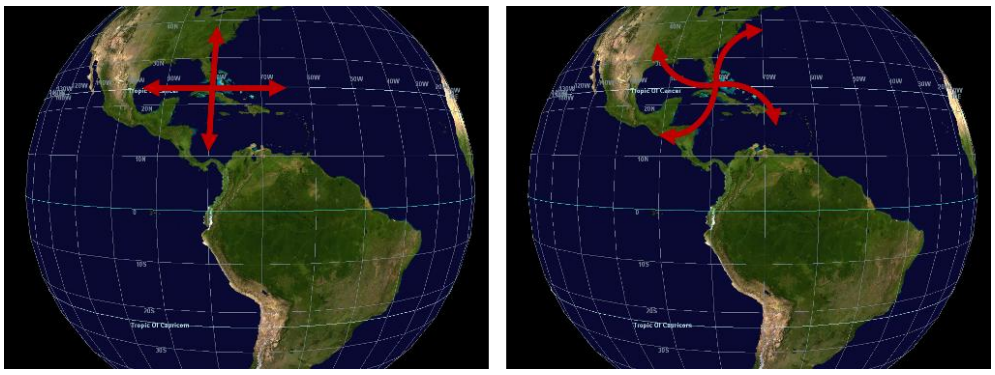

Figure 3-18: (left) Motion on a non-rotating Earth. (right) Motion on a rotating Earth which causes a deflection. This deflection is called the Coriolis Effect.

A summary of the important aspects of the Coriolis Effect are:

1. Deflects an object to the right in the Northern Hemisphere.
2. Increases the deflection as the speed of the object increases.
3. Only changes the direction, never the speed of an object.
4. Is zero at the equator and reaches a maximum near the poles.

3.2.8 - Friction Force

The third force affecting wind in the atmosphere is friction. The frictional force is always in the opposite direction of motion as illustrated in Figure 3-19.

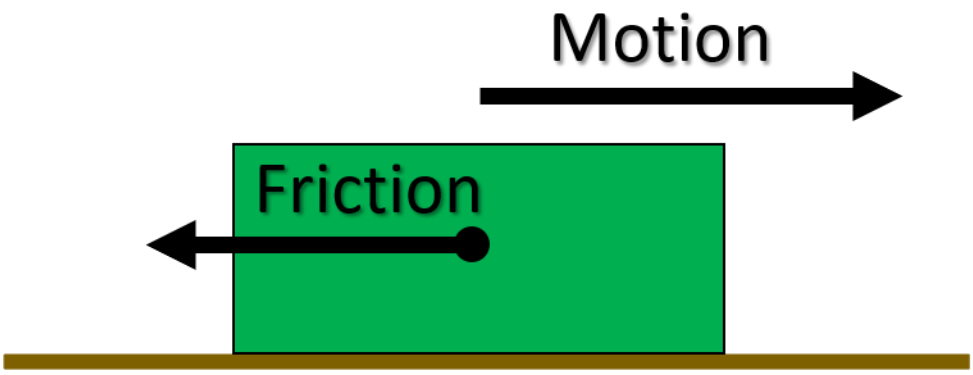

Figure 3-19: Illustration that friction is a force opposite in direction to the motion of an object.

In the atmosphere, friction occurs where air interacts with or contacts the Earth. The bottom layer of the troposphere in contact with the Earth is called the **boundary layer**. The depth of the boundary layer varies with temperature and weather conditions, and can range from less than 100 feet to over a mile. The conductive transfer of heat and the evaporation of moisture into the atmosphere occur in the boundary layer.

Friction occurs in the boundary layer as air moves over and around obstacles like vegetation, trees, buildings, hills and mountains. Friction is always in the opposite direction of the wind. Once outside the boundary layer and into the “free” atmosphere, friction is negligible. The atmosphere is assumed to be frictionless at higher altitudes.

3.3 – Applying the Forces Which Affect Wind

Three forces affecting wind have been examined:

1. Pressure gradient force
2. Coriolis force
3. Friction

Additionally, we have these methods for analyzing pressure (1) at the surface using sea-level pressure isobars and (2) aloft using heights at a set pressure value (like 500 mb). Applying these techniques and knowledge will enable us to expand our understanding of the atmosphere even further. This section applies these principles to accomplish that goal.

3.3.1 – Winds Aloft

The wind above the boundary layer is assumed to be frictionless. These winds do not encounter the Earth or any vegetation or structure on the Earth. With no friction only two forces are left to analyze: (1) the pressure gradient force and (2) the Coriolis force. Examining the pressure gradient force, we know that wind moves from high to low pressure. We also know that higher heights are present closer to the tropics and lower heights closer to the poles. This situation has air moving from higher to lower or from south to north as shown in Figure 3-20.

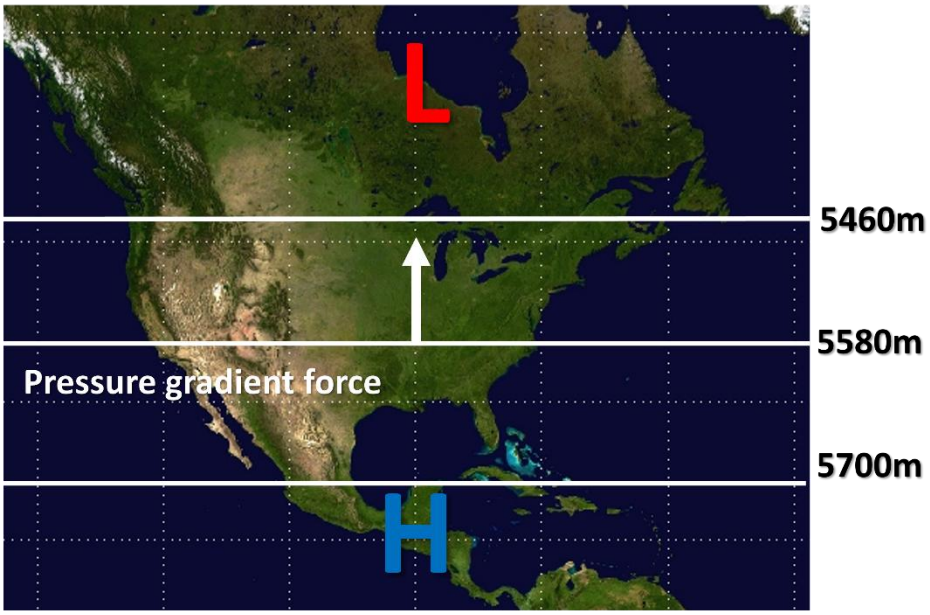

Figure 3-20: Air motion above the boundary layer associate with just the pressure gradient force.

Now considering the Coriolis force, the direction of the wind will be deflected to the right (see Figure 3-21). The wind speed associated with the pressure gradient force remains the same. However, the stronger the wind speed the more deflection to the right due to the Coriolis force.

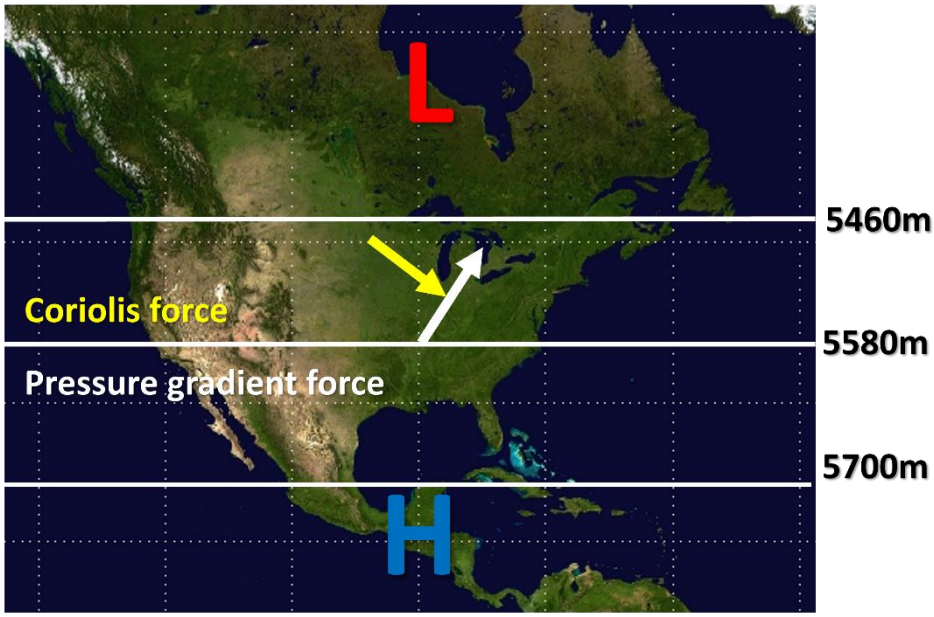

Figure 3-21: The Coriolis force deflects the wind to the right (in the Northern Hemisphere).

Eventually the pressure gradient and Coriolis forces must balance. When balance occurs, the wind will be *parallel* to the height contours as shown in Figure 3-22. If the wind were to turn further south, its speed would decrease going against the pressure gradient force. A slower wind speed reduces the Coriolis force. A weaker Coriolis force would shift the wind back north to restore the balance.

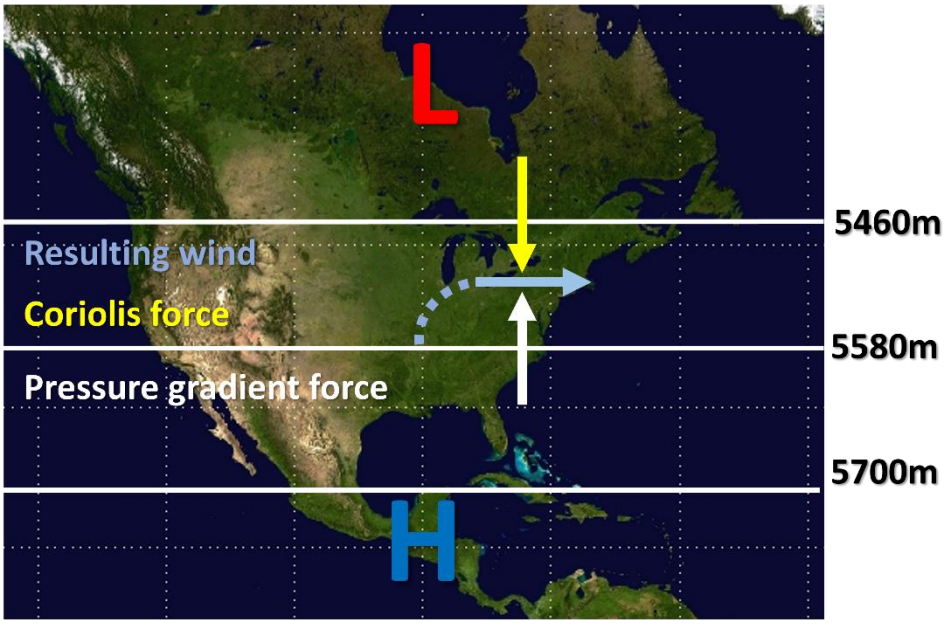

Figure 3-22: A balance between the pressure gradient and Coriolis forces causes the wind to flow parallel to the height contours. This condition is called geostrophic flow.

Geostrophic flow or **geostrophic balance** is defined as when the pressure gradient and Coriolis forces are equal and the wind is at a constant speed. Once established, geostrophic flow is very stable and can be observed in the upper atmosphere.

The real atmosphere, unlike the previous illustrations, does not have a uniform pressure gradient with straight lines. Variations in the pressure gradient cause the wind to speed up and slow down. These changes in speed also result in changes in the Coriolis force. A balance between the Coriolis and pressure gradient forces, including these wind speed changes, is called **gradient flow**. Gradient flow is much more common in the atmosphere and the wind still flows *parallel* to the height contours. The biggest difference between geostrophic and gradient flows is that the wind speed varies in the gradient flow.

Examining the 500 mb map shown previously in this section provides an illustration of both geostrophic and gradient flows. Notice the wind and heights over Arizona and New Mexico. The height lines are straight and the winds are at constant speed. These characteristics are associated with geostrophic flow. Looking further east, the height contours have a wavy appearance and the wind speed varies from 15 to 60 knots in this area. These characteristics are associated with gradient flow. In both examples, the winds are *parallel* to the height contours.

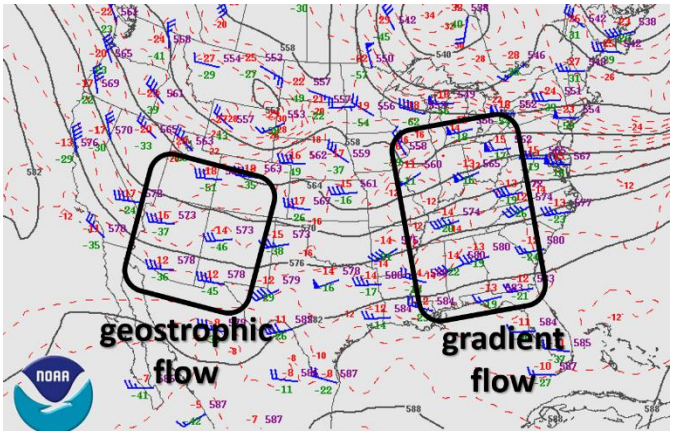

Figure 3-23: An example of geostrophic and gradient flow in the atmosphere.

3.3.2 – Winds Near the Surface

Winds at the surface within the boundary layer include the frictional force. Thus, all the forces are present: (1) pressure gradient, (2) Coriolis and (3) friction forces. Friction acts as a force opposite to the pressure gradient force. Friction slows down the speed of the wind. The direction remains unchanged. With a slower wind speed the pressure gradient and Coriolis forces cannot balance each other. The pressure gradient force is always stronger. This change causes the wind to cross the isobars rather than be parallel to the isobars.

As you can see in Figure 3-24, adding friction makes the situation more complicated. The important aspect to remember in a surface analysis is that the wind crosses the isobars. In the upper atmosphere without friction, the wind tends to be parallel to the heights.

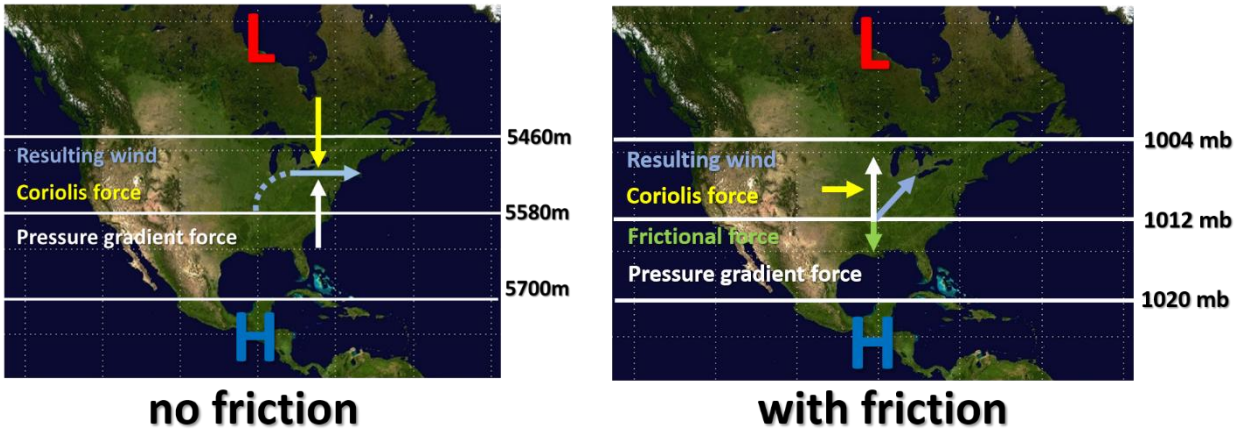

Figure 3-24: Comparison of the wind aloft without friction and wind at the surface with friction.

Looking at the surface analysis previously shown (Figure 3-25), while adding the observations shows that the winds do cross the isobars. Friction causes this fundamental difference between the surface and upper air pressure and wind fields.

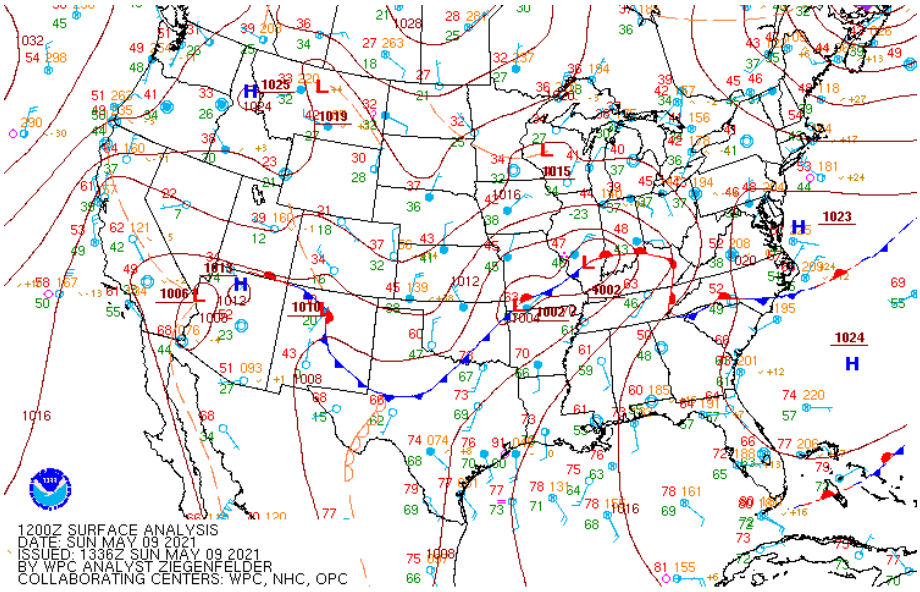

Figure 3-25: A surface pressure analysis with observations showing winds crossing the isobars. This concept is best depicted in the central U.S.

3.3.3 – Vertical Motions Associated With Wind

We know that air still moves from higher to lower pressure due to the pressure gradient force. Friction at the surface causes wind to cross the isobars. With wind crossing the isobars, air truly does move away from a high pressure center and into a low pressure center. In Figure 3-26, the black lines are isobars at the surface. The blue and red arrows represent the wind motion.

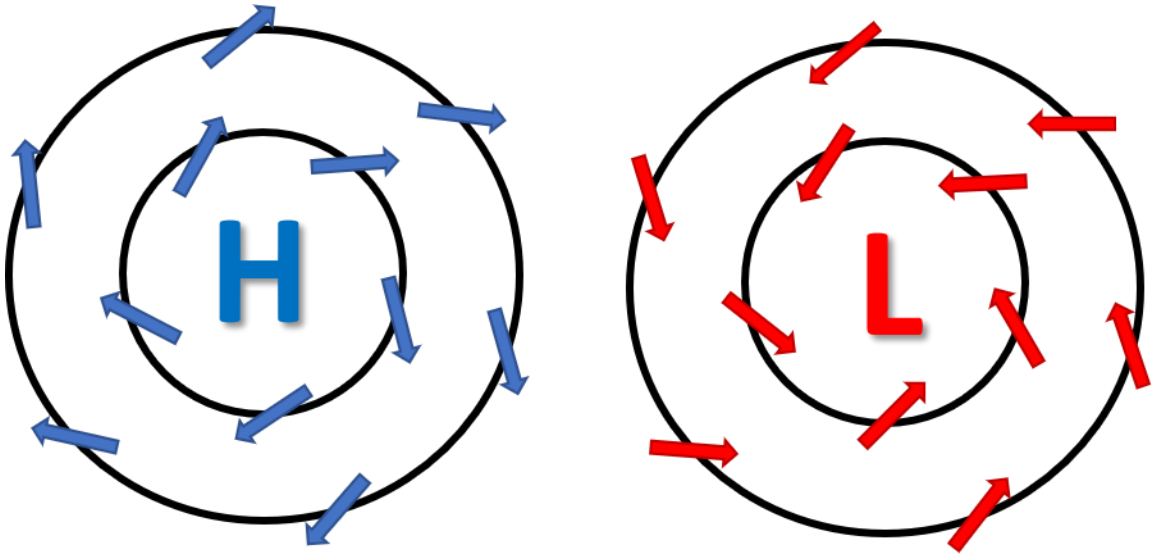

Figure 3-26: Air motion associated with surface high and low pressures. The black lines are isobars, and the colored arrows are the wind motion.

Looking at the surface pressure analysis again in Figure 3-27, notice the winds circle into the low pressures over Illinois and Missouri. Hence, real data supports these conceptual models of pressure and wind.

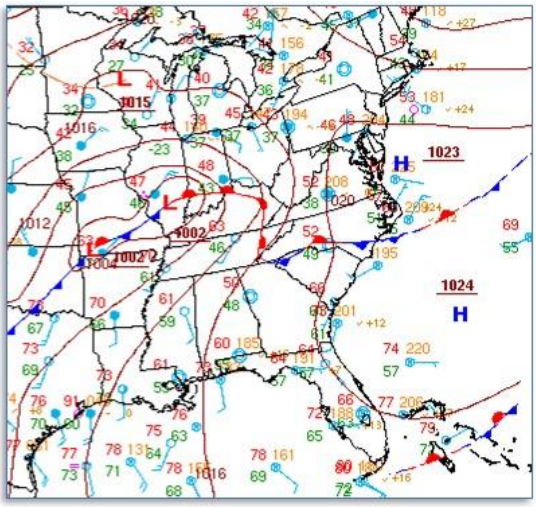

Figure 3-27: Real data in a surface pressure analysis supports the conceptual model of pressure and wind. Notice the winds are blowing into the low pressure centers.

When air leaves a high pressure center, it must be replaced. The only available air is from above. Therefore, air descends from aloft to replace the surface air moving away from a high pressure. Descending air in the atmosphere warms. Remember the Ideal Gas Law, if pressure increases a corresponding temperature increase should occur. Air aloft is at a lower pressure than air at the surface. As air descends the pressure on it increases which causes a corresponding increase in temperature. These circumstances are why fair weather is often associated with high pressure.

A low pressure center has the opposite situation. As air comes into a low pressure center, it needs to go somewhere. The air cannot go into the ground, which means it must rise. Therefore, the air associated with a surface low pressure must be ascending. Ascending air cools. As air cools, condensation is favored which promotes clouds and possible precipitation. Low pressure areas are often associated with inclement weather. These vertical air motions are illustrated in Figure 3-28.

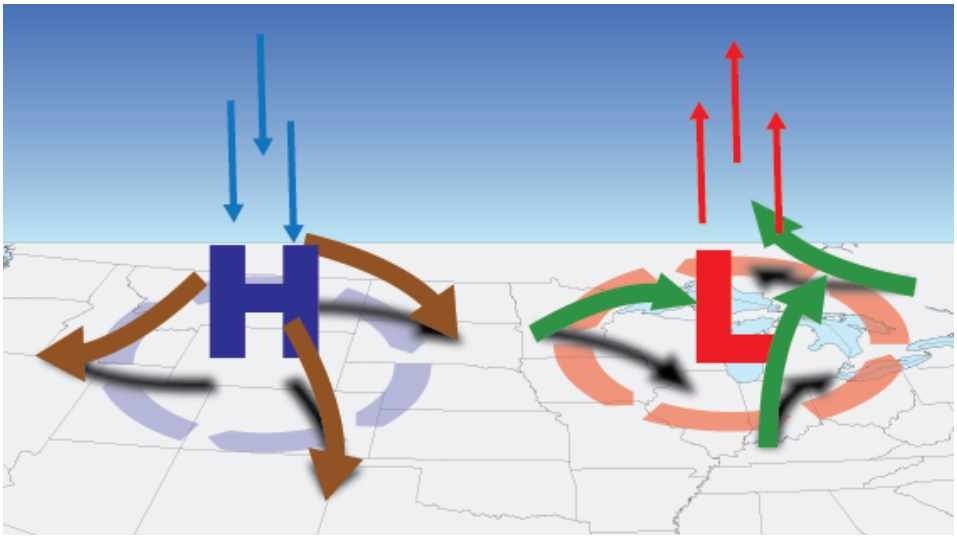

Figure 3-28: Vertical air flow associated with surface pressure centers.

3.3.4 – Cyclones and Anticyclones Defined

High and low pressure centers are present across the globe every day. They are not randomly distributed but usually alternate with each other across an area. Because of their common occurrence, these pressure centers have been named. **Cyclones** are enclosed circular isobars or heights of low pressure. **Anticyclones** are enclosed circular isobars or heights of high pressure. Cyclones is also a generic name associated with hurricanes, winter storms, thunderstorms or any stormy weather in general. Most inclement weather is associated with a low pressure area, which is why “cyclones” are often in the news.

In the northern hemisphere, anticyclones rotate in a clockwise manner; cyclones in a counterclockwise direction. This rotation direction is due to the Coriolis Effect. For the southern hemisphere, everything rotates in the opposite direction. This change in direction based on a hemisphere can be confusing. Hence, all the illustrations in this textbook are based on the northern hemisphere to reduce confusion.

At the surface, cyclones and anticyclones normally have a circular isobar or height associated with them. Aloft these pressure areas tend to “open up” into a larger area of high or low pressure without an enclosed circular contour. An area of low pressure aloft is called a **trough**. An area of high pressure aloft is called a **ridge**. Figure 3-29 helps visualize troughs and ridges at the 500 mb level. The center or axis of a trough is designated with a dashed line. The ridge axis is designated with a zigzag line.

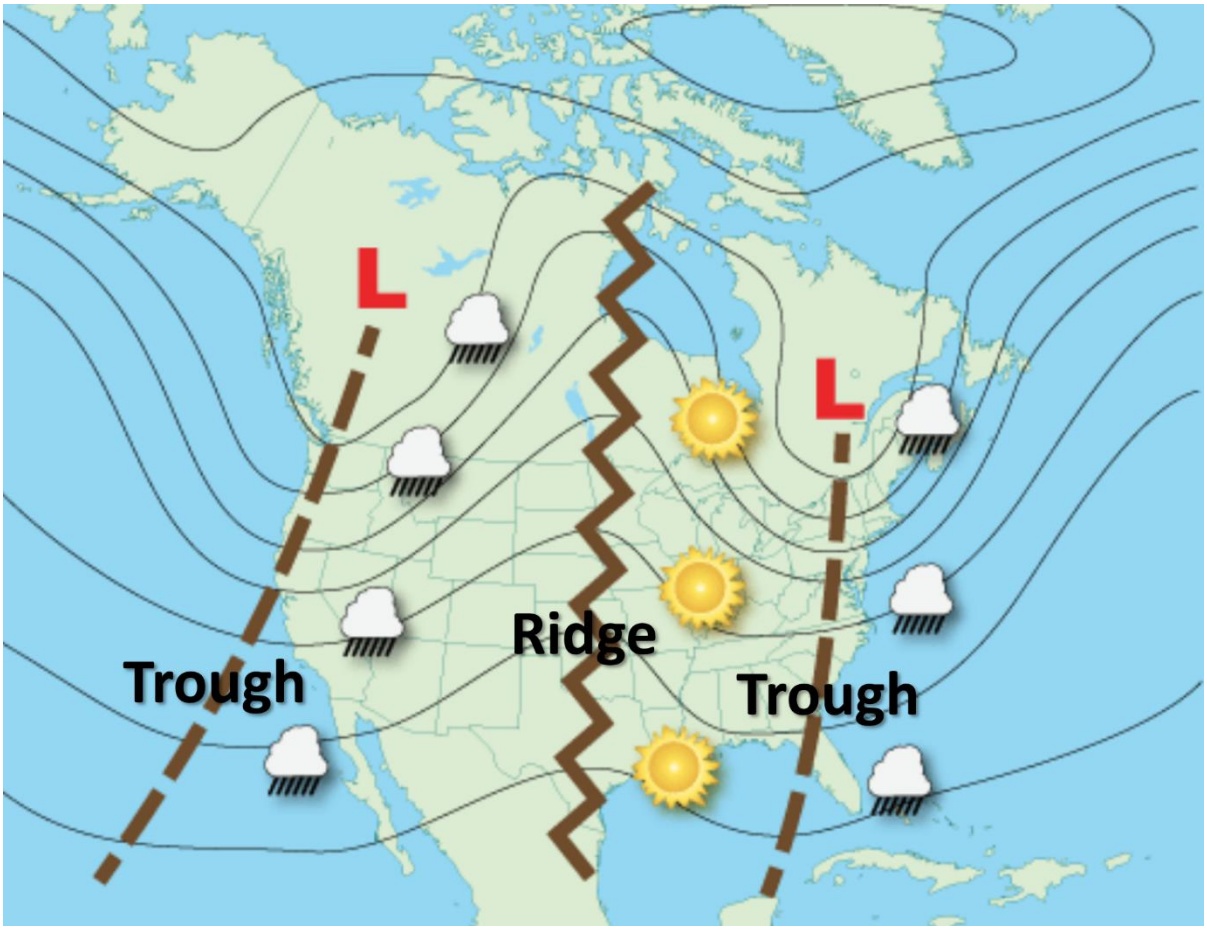

Figure 3-29: Troughs and ridges at 500 mb. The center or axis of a trough is designated with a dashed line. Ridges are designated with a zigzag line.

A trough has lower heights and the cooler air associated with it. A ridge has higher heights and warmer air. These troughs and ridges vary in shape and areal coverage depending on the level of the atmosphere where they reside. Troughs and ridges at the surface frequently have closed contours. Aloft the contours are not closed but "open up" to form waves. Many times, troughs at 500 mb tend to be further west than the surface low pressure. This vertical tilt is conducive to maintaining the strength of a storm and will be discussed in more detail in a future chapter.

Figure 3-30 demonstrates these characteristics. Notice the closed contours on the 1000 to 700 mb layers in the central U.S. From 500 mb and up, the low pressure trough has no closed contours and a wave like appearance associated with the lower heights.

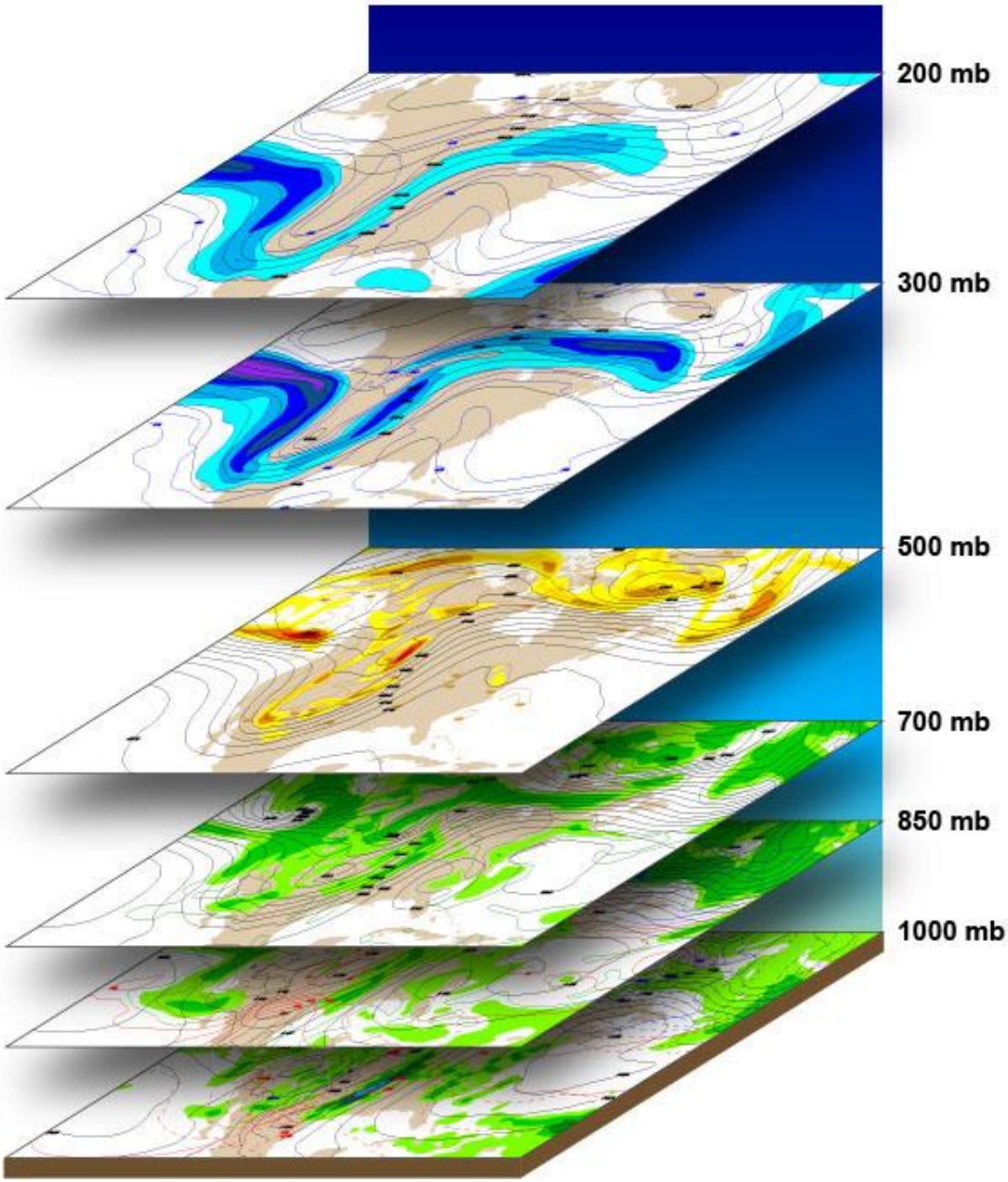

Figure 3-30: Layers of the atmosphere associated with a trough over the central U.S. Notice the closed contours at the lower levels and a lack of them at higher levels.

Chapter 3 Review Questions

1. What activities can space weather influence or impact?
2. What is a sunspot?
3. How many years are associated with the quasi-periodic variation of sunspot activity?
4. What are explosive outbursts of plasma from the Sun's corona called?
5. What atmospheric parameters always decrease with altitude?
6. Why is sea-level pressure used on weather maps instead of surface pressure?
7. What does the close spacing of isobars on a sea-level pressure map indicate?
8. How is a moving object in Earth's atmosphere deflected as a result of Earth's rotation?
9. What causes the Coriolis force?
10. Which direction would a plane be deflected if flying from the west to east coasts of the United States?
11. Where does the wind move when influenced by the pressure gradient force?
12. What are enclosed areas of high pressure (circular isobars) at the surface called?
13. What is a geostrophic wind?
14. What is a gradient wind?
15. What is an area of low pressure aloft called?
16. What forces are balanced in winds aloft?
17. What forces are balanced in surface winds?
18. What type of surface pressure can cause ascending or vertically rising air?
19. What is the boundary layer?
20. What type of vertical motion is associated with an anticyclone?

Chapter 4 - Atmospheric Moisture I

Overview

This chapter is the first of two related to atmospheric moisture. Understanding the technical details about water and humidity is an essential aspect in understanding weather and climate. Hence, the reason this textbook has two chapters on atmospheric moisture. The states of water, measuring humidity, cloud formation and atmospheric stability are covered in this chapter.

Chapter objectives:

1. Define the states of water.
2. Explain how the atmosphere's water vapor content is measured.
3. Explain the processes that lead to saturation and condensation.
4. Describe the concepts associated with lowering the air temperature.
5. Understand and determine atmospheric stability.

4.1 – The Changing States of Water

Water is an essential atmospheric element in transferring heat, determining stability and creating active weather. We briefly examined the states of water associated with latent and sensible heat in chapter 2. Due to the importance of water, the changes associated with its state are reviewed and expanded in this section.

4.1.1 – Evaporation, Condensation, and Saturation

To examine the properties of water (liquid) and water vapor (gas), as an experiment we can fill half a container with water. A barrier is placed between the water and the remaining space in the container. All the water vapor molecules are removed from the "empty" portion of the container. The experiment begins by removing the barrier between the two sections of the container.

Water molecules leave the liquid and become airborne (water vapor) which is called **evaporation**. The rate of molecules leaving the liquid is the evaporation rate. Likewise, water molecules can again become liquid which is called **condensation**. Initially the evaporation exceeds the condensation rate. Eventually an equilibrium is reached where the evaporation and condensation rates are the same. This equilibrium between the two rates is called **saturation**. This experiment is illustrated in Figure 4-1.

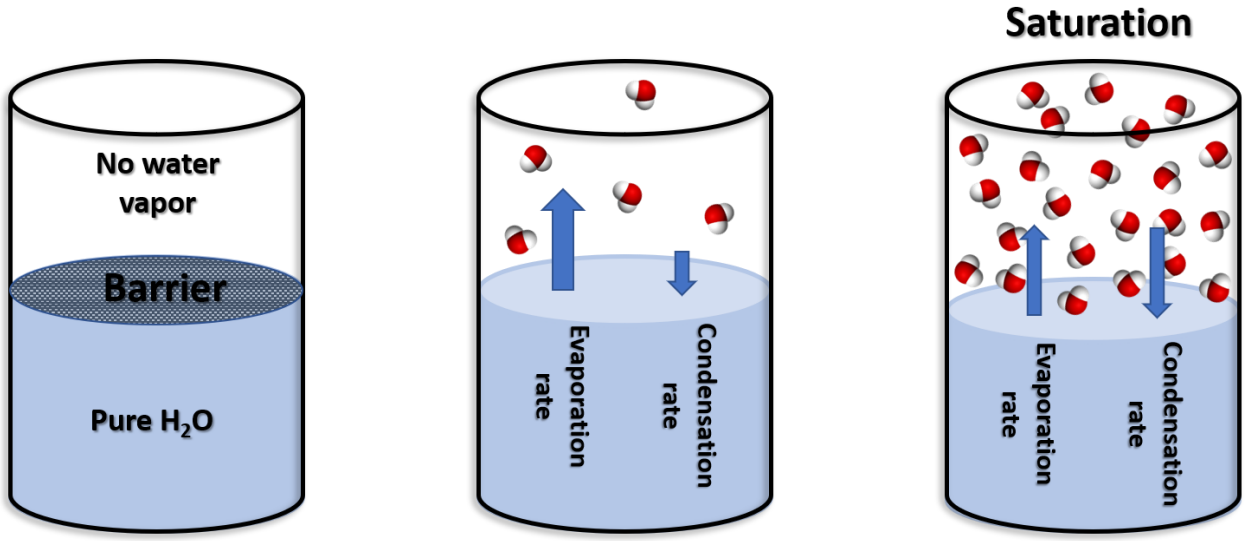

Figure 4-1: An experiment in which half a container is filled with water. As the barrier between the air and water is removed, evaporation and condensation occur. Once the evaporation and condensation rates are equal, the air portion of the container holds the maximum concentration of water vapor molecules.

Saturation, evaporation rate and condensation rate are related to the kinetic energy of the water molecules. Temperature is a measure of this kinetic energy. Water vapor (gas) has the highest kinetic energy and has the highest temperatures. Like any gas, water vapor is compressible. At the molecular level, water consists of two hydrogen atoms and one oxygen atom. The hydrogen atoms have a positive charge while the oxygen has a negative charge as shown in Figure 4-2.

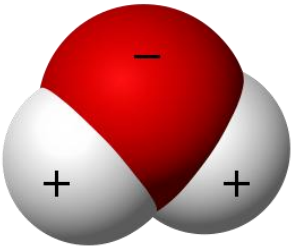

Figure 4-2: A water molecule has two hydrogen atoms with positive charges, and one oxygen with a negative charge.

These charges determine the structure of water as it undergoes changes in state. Water vapor as a gas consists of individual molecules mixed in with the other atmospheric gases. Water as a liquid has the molecules aligned with positive and negative charges adjacent to each other (see Figure 4-3). The liquid form is very compact and water is densest at 4°C or 39°F

Water as a solid (ice) has a six-sided crystalline structure. This structure requires more space as the hydrogen and oxygen molecules align themselves into "fixed" locations. Hence, the reason that water pipes burst when frozen. The density of ice is less than the density of water, and is the reason ice cubes float in a cold drink. Water is the only substance on our planet that naturally exists in all three states.

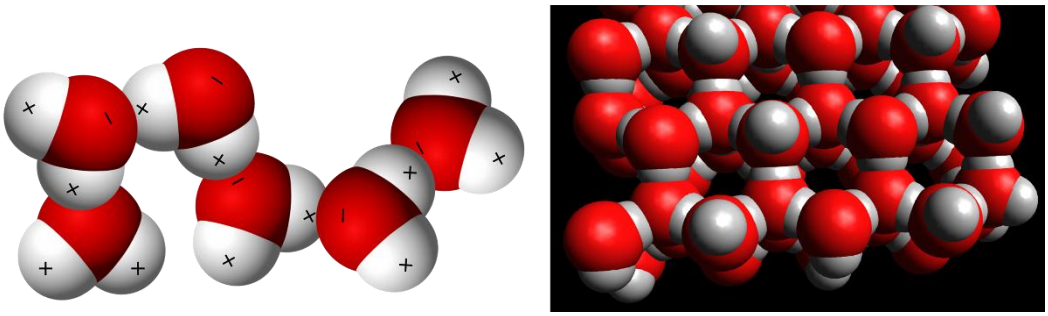

Figure 4-3: (left) The molecular structure of liquid water. (right) The molecular structure of ice.

4.1.2 – Sublimation and Deposition

The orderly change of state for water is to go from ice to liquid to vapor and vice versa. However, once a water molecule has enough energy it can skip this sequence of steps. The phase change of water going directly from ice to water vapor is called **sublimation**. **Deposition** is going straight from water vapor to ice. Deposition is a crucial step in creating precipitation which will be examined later. Figure 4-4 illustrates sublimation and deposition as water molecules bypass the liquid state.

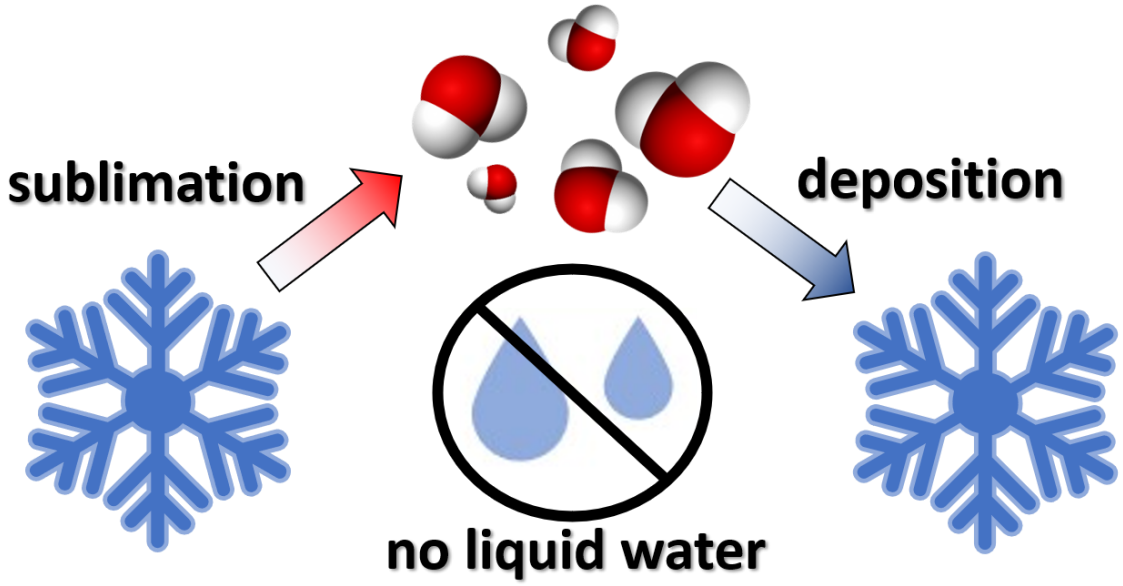

Figure 4-4: Illustration of sublimation and deposition where water molecules bypass the liquid state.

4.1.3 – Freezing and Melting

The last two changes of state for water are the most common. **Freezing** is the change from liquid water to ice. **Melting** is the change from ice to liquid water. The freezing or melting temperature of water is 0°C or 32°F. The boiling (or vaporization) temperature of water is 100°C (212°F). The Metric scale was established with water as the standard. One gram of water takes 1 calorie to raise its temperature 1°C.

At a temperature of 0°C water can exist as both a liquid and a solid (ice). While the Celsius temperature was established with 0°C as the freezing point, this is the temperature at which water starts to freeze. Keeping a container of water fully frozen with no liquid present requires much colder temperatures. This characteristic is why food freezers are kept at colder temperatures from about 0°F (-18°C) to -10°F (-23°C). These temperatures are required to keep food fully frozen to avoid spoilage. The atmosphere has similar conditions with water droplets not starting to freeze in a cloud until temperatures of -10°C or colder are present.

The boiling point of water has similar conditions. While water boils at 100°C, it does not instantly evaporate or vaporize into a gas at this temperature. Once a pan of water starts boiling, time and more heat is required to change all the liquid into water vapor. The energy required for these phase changes is called latent heat. Latent heat was mentioned in connection with Earth's energy balance, and is analyzed more in the next section.

4.1.4 – Energy Required to Change State

Latent heat is the energy required to change the phase (gas, liquid or solid) of a substance. This definition was given in Chapter 2. This heat energy is labeled as latent because it is hidden. Water can exist as both ice and liquid at 0°C, although latent heat is required to go from one state to another. The latent heat associated with these phase changes is given in Figure 4-5. The energies associated with the phase or temperature change are for 1 gram of water.

Melting or freezing takes 80 calories. The temperature change for liquid water to go from 0°C to 100°C is 100 calories. The latent heat of evaporation (or vaporization) is a whopping 540 calories. Likewise, the latent heat of condensation is 540 calories. More important than these values is how latent heat changes the environment. The environment in our case is the atmosphere or the Earth's surface.

The latent heat of condensation releases 540 calories per gram of water, which is an enormous amount of heat. One gram of water equals a milliliter. A normal size bottle of water contains 500 ml. The energy required to evaporate this bottle or condense water into it is 270,000 calories. A person's normal food calorie intake in a day is 3000 calories or less. When one bottle of water precipitates out of the atmosphere, the atmosphere has gained heat energy comparable to over 3 months of food (calories) for one person. The latent heat released through condensation is a fundamental driver in hurricanes and strong thunderstorms. Figure 4-5 captures all of this information in one diagram.

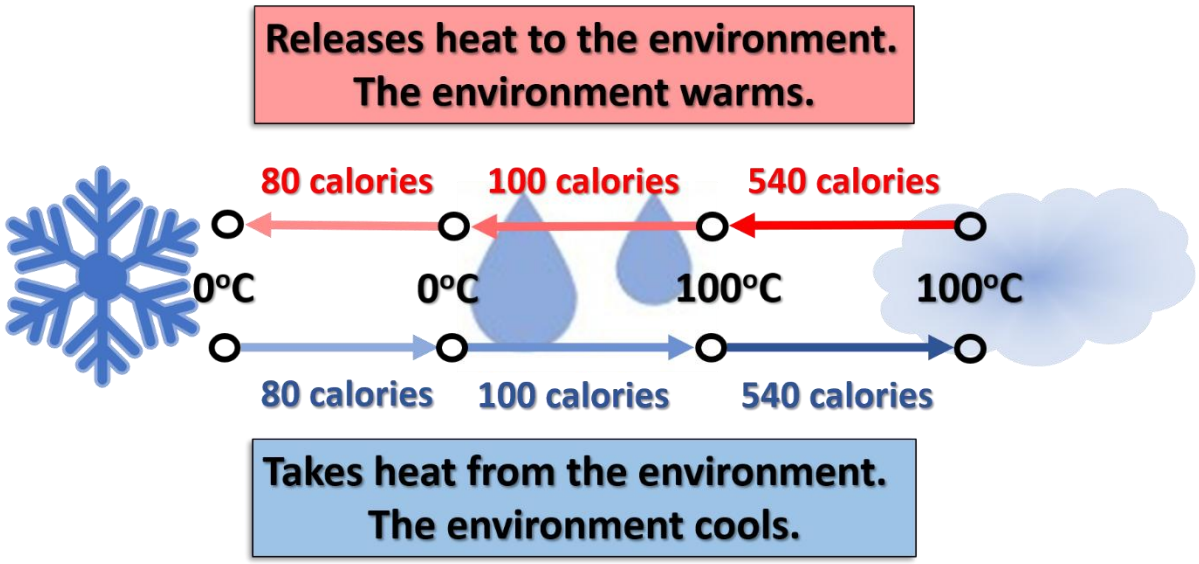

Figure 4-5: The latent heat required for water to change states. Notice the latent heat for water to go from liquid to gas and vice versa is significantly higher than the other state changes.

4.2 – Measuring Water Vapor

Humidity is a general word that refers to the amount of water vapor in the air. Humidity is so important in the atmosphere that numerous methods are available to quantify the amount of water vapor present. These measures of humidity include vapor pressure, absolute humidity, specific humidity, mixing ratio, relative humidity and dew point. Absolute humidity is not too useful nor widely used, so we will skip that one. The rest of these humidity terms are covered in

this section. The two most important and widely used humidity measures are relative humidity and dew point.

4.2.1 – Vapor Pressure

Vapor pressure is the portion of air pressure exerted by water vapor. Vapor pressure (e_s) is measured in millibars like air pressure. The vapor pressure of a volume depends on temperature. Vapor pressure follows the Ideal Gas Law which directly relates pressure to temperature. As temperature increases, the amount of water vapor in the air can increase. Once the water vapor is in equilibrium with liquid water, saturation has been reached. These conditions are similar to the hypothetical experiment conducted at the beginning of this chapter. Figure 4-6 has vapor pressure (e_s) on the y-axis and temperature on the x-axis. This graph demonstrates an increase in water vapor (moisture) in the air as temperatures increase.

The air is unsaturated if the evaporation and condensation rates are not equal, and the air can hold more water vapor. Saturation is an equilibrium state where the evaporation and condensation rates are balanced. Supersaturation is a transient condition where excess water vapor is present in the volume because no liquid water or ice surface is available to promote condensation. Supersaturation is unlikely to occur in our hypothetical experiment. However, slightly supersaturated conditions are possible in the atmosphere, and will be examined in more detail.

Figure 4-6: A graph of vapor pressure (e_s) and temperature. As the temperature increases, the amount of moisture in the air can increase.

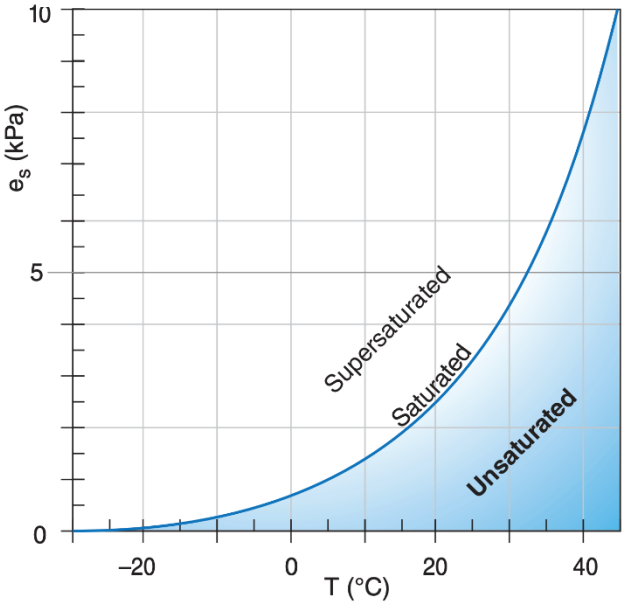

4.2.2 – Specific Humidity and Mixing Ratio

Specific humidity is the grams of water vapor in 1 kg of air. Specific humidity is a ratio or percentage of how much water is in the air. Mixing ratio is very similar to specific humidity. **Mixing ratio** is the grams of water vapor in 1kg of air after the water vapor has been removed. Mathematically the denominator associated with specific humidity has 1 kg of air with water vapor included. Mixing ratio has the denominator as only dry air. These definitions in an equation format are:

$$\text{specific humidity} = \frac{\text{grams of water vapor}}{\text{1 kilogram of air}}$$

$$\text{mixing ratio} = \frac{\text{grams of water vapor}}{\text{1 kilogram of air - grams of water vapor}}$$

An example may clarify the minor differences between these two measures of humidity. Let us analyze 1 kg of air. In this air, 10 grams of water are present. The specific humidity is 10 grams divided by 1 kg which equals 10 g / kg. The mixing ratio is 10 grams divided by .990 (1 – 0.01) kg of dry air which equals 10.1 g / kg. The final numbers are very similar. Of these two measures, mixing ration is used more often.

A graph of specific humidity and mixing ratio is like the graph for vapor pressure. They are all influenced by temperature with a rapidly sloping curve at warmer temperatures. They all have unsaturated, saturated and supersaturated conditions. This table contains the saturated mixing ratio at various temperatures. The higher the temperature, the more moisture the air can hold. The dew point temperature in this table will be explained in section 4.2.4.

Temperature (°C) or Dew point (°C)	Saturation Mixing Ratio (g/kg) or Mixing Ratio (g/kg)
-40	0.1
-30	0.3
-20	0.8
-10	1.8
0	3.8
5	5.4
10	7.6
15	10.6
20	14.7
25	20.1
30	27.2
35	36.6
40	49.0

4.2.3 – Relative Humidity

Relative humidity (RH) is a percentage of how much water vapor is present in the air compared to how much could be present if saturated. Relative humidity is the most widely used measurement of humidity. Like all humidity measurements, relative humidity is sensitive to temperature. An equation form of relative humidity is:

$$\text{relative humidity} = \frac{\text{mixing ratio}}{\text{saturation mixing ratio}} \text{ X } 100\%$$

Relative humidity varies throughout the day because temperature varies throughout the day, even if the amount of moisture (mixing ratio) remains constant. The following graph of temperature and relative humidity illustrates this point. Relative humidity is highest in the morning when the temperature is the lowest. As the temperature increases through the day, relative humidity decreases.

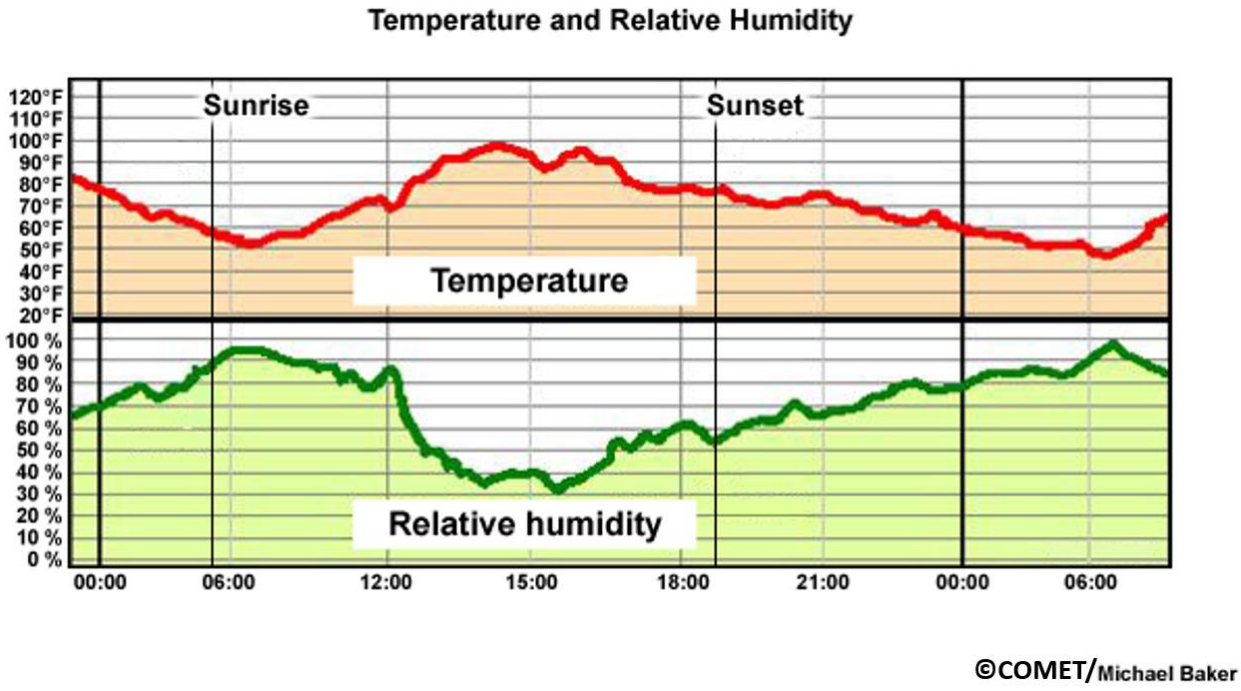

Figure 4-7: A graph of temperature and relative humidity (RH) throughout 36 hours. Notice relative humidity is the highest when temperature is the lowest and vice versa.

4.2.4 – Dew Point

Dew point is the temperature at which saturation occurs. Dew point is a widely used measurement expressed in degrees Celsius or Fahrenheit. Dew point is not an actual measure of water vapor, but it does largely depend on the amount of water vapor present. A high dew point number implies lots of moisture is in the air. A lower dew point implies drier air.

Dew point temperature is *always* less than or equal to the air (ambient) temperature. Why cannot the dew point be higher than the air temperature? When the dew point equals the ambient temperature, the air is saturated and condensation can occur. Condensation releases latent heat causing the air temperature to increase. Thus, the ambient temperature will always be greater than or equal to the dew point.

The following illustration demonstrates the relationships between temperature, dew point, mixing ratio, saturated mixing ratio and relative humidity. The mixing ratio numbers were obtained from the table in the specific humidity and mixing ratio section (4.2.2).

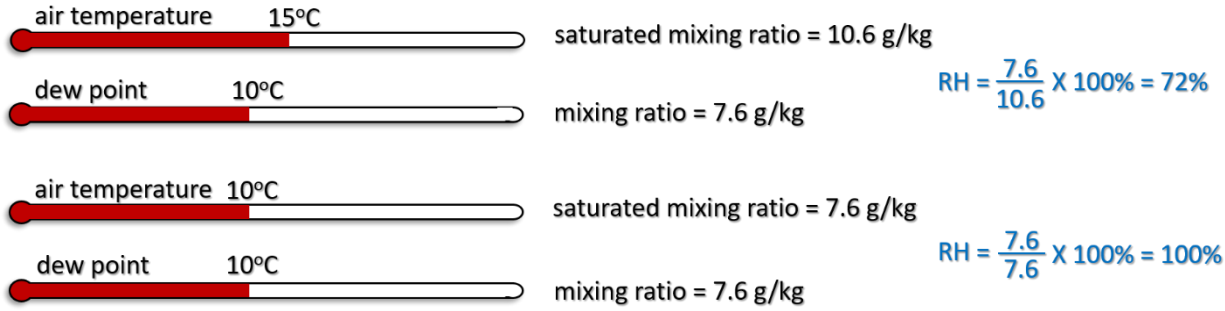

Since dew point is the temperature at which saturation occurs, when the dew point and temperature are the same the relative humidity is 100%. Saturation is a relative humidity of 100% by definition. Dew point and relative humidity calculators are available as apps or on a web page like this one https://www.wpc.ncep.noaa.gov/html/dewrh.shtml.

4.2.5 – Instruments for Measuring Humidity

As you have probably noticed, all the humidity measurements are closely related. When one humidity value is known the others can be calculated. Two types of instruments used to measure humidity are (1) a sling psychrometer and (2) electronic sensors.

The sling psychrometer is a manual method for remote locations. Wildland fire fighters use sling psychrometers to track weather conditions near wildfires.

A sling psychrometer has a wet bulb and a dry bulb thermometer (Figure 4-8). The dry bulb is just a normal thermometer. The wet bulb has a cotton wick attached to the end. This wick is dipped in water and spun to get a temperature reading based on evaporating water into the air. A handle to spin the thermometer frame (not shown) is attached to the hole at the end. These two temperatures can easily be used to determine the dew point.

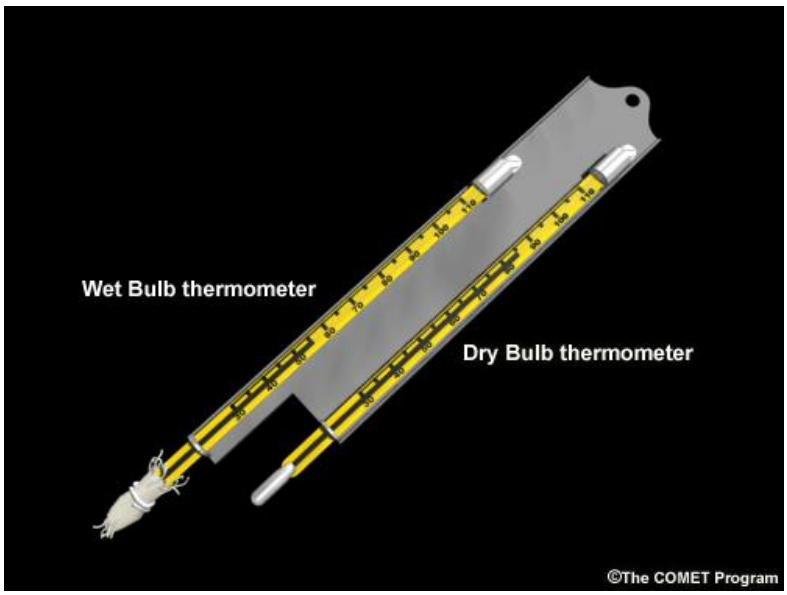

Figure 4-8: A sling psychrometer used to take humidity measurements in remote locations.

Electronic sensors tend to measure the relative humidity (RH), since an RH sensor is reliable and accurate. These devices look like typical boxes containing electronics, such as this sensor from a company called Vaisala. The widespread use of these electronic sensors makes RH a common parameter included in a weather observation.

Figure 4-9: A typical electronic relative humidity sensor.

4.3 – How Do Cloud Droplets Occur?

What is the difference between water vapor and a cloud droplet? The difference is one is a gas and the other is liquid. For a liquid cloud droplet to form, the air must first reach saturation and then condensation can occur. Unfortunately, condensation does not happen spontaneously. Specific conditions must be present for condensation to occur. This section examines processes that lead to saturation. Once saturation is present then we will examine the conditions leading to condensation.

4.3.1 - Processes Causing Saturation

Three processes in the atmosphere can cause saturation:

1. Cooling the air temperature to the dew point. This process is the most common.

2. Mixing cold air with warm, moist air.

3. Adding moisture (water vapor) to the air. Evaporation is the primary mechanism for this process, which is linked to precipitation.

An example of lowering the air temperature to the dew point is air rising over a mountain. As the air flows over mountains, its altitude increases and temperature decreases. In this picture (Figure 4-10), saturation has occurred along with condensation to form a cloud as the air moves over the mountain.

Figure 4-10: Photo of air moving over a mountain causing both saturation and condensation off the coast of Kurile, Russia. This process associated with rising air is very common in the atmosphere.

(Photo courtesy of COMET and NOAA)

A classic example of mixing cold air with warm, moist air is present in the condensation trail seen behind a jet plane. Combustion of fuel in a jet engine creates exhaust and warm, moist air. This water vapor is much warmer than the surrounding environment, so saturation occurs rapidly followed by condensation.

An example of adding water vapor to the air is when a person takes a shower. The shower puts water vapor into the air. Saturation in the room can be reached and condensation starts to occur on the mirror and walls. Rain is the most common method for adding moisture to air. Obviously, water vapor needs to be in the air before rain can occur, and this entire process of evaporation and precipitation is called the hydrologic (water) cycle. The photos in Figure 4-11 illustrate these other two processes.

Figure 4-11: Other examples of situations causing saturation and condensation. (left) Mixing cold air with warm moist air. (right) Adding moisture to the air, such as rain.

4.3.2 – Factors Affecting Condensation (Liquid Water)

After the atmosphere is saturated (the relative humidity equals 100%), two additional factors affect whether condensation occurs. These factors are (1) supersaturation conditions and (2) the presence of cloud condensation nuclei.

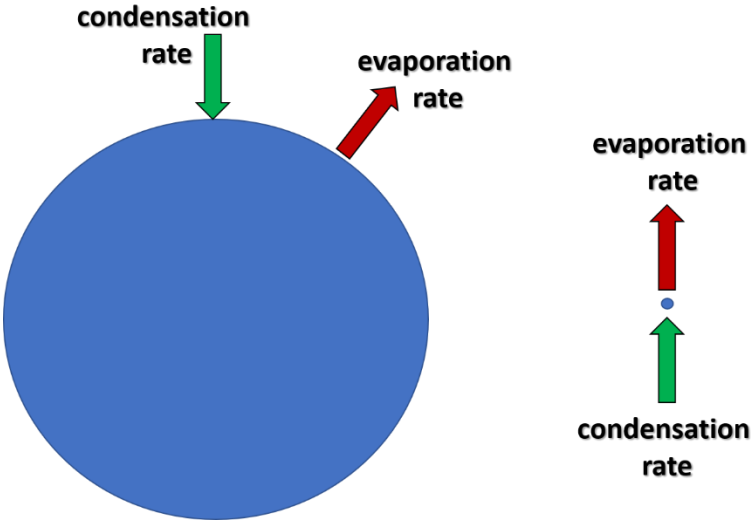

Figure 4-12: Small water droplets evaporate quickly when compared to larger droplets. For small droplets to grow into large droplets, supersaturated conditions are necessary.

As a water droplet begins to form, both the evaporation and condensation rates influence it. The water molecules on the surface of the droplet are affected by these rates. The molecules inside the droplet are somewhat isolated from these conditions. Thus, smaller droplets can easily evaporate and disappear. Larger droplets are much more likely to remain droplets, as illustrated in Figure 4-12. For a droplet to reach a sustainable size, supersaturated conditions must be present for smaller droplets to grow larger. **Supersaturation** is defined as relative humidity greater than 100%. In other words, the evaporation rate must be reduced and the condensation rate increased. A relative humidity higher than 100% provides this environment.

The graph in Figure 4-13 shows that droplets less than 1 μm in radius require a supersaturation environment to grow. If supersaturation is not present the droplet evaporates.

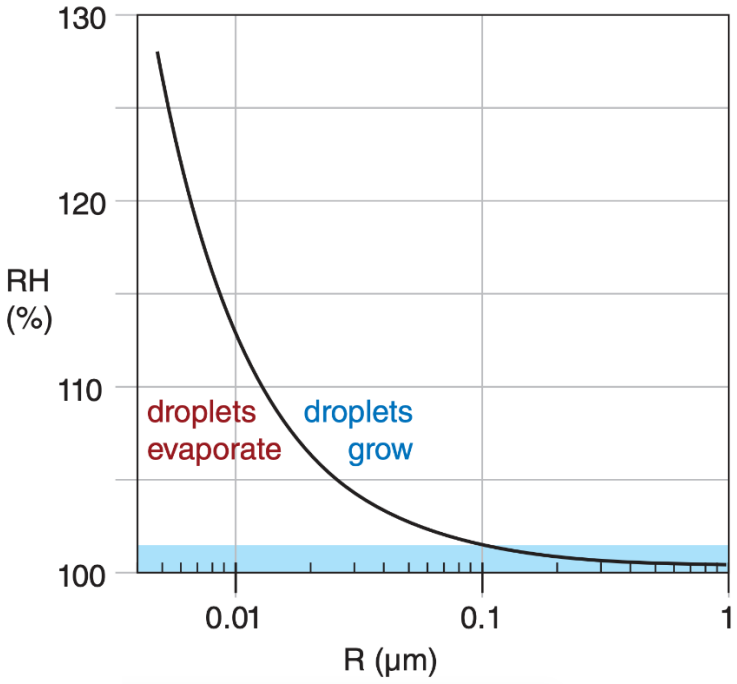

Figure 4-13: A graph of relative humidity and water droplet radius. The black line is where the condensation and evaporation rates are in equilibrium, and no change in the droplet size occurs. Small droplets less than 1μm radius grow when supersaturated conditions are present.

The blue shaded region highlights the range of relative humidity normally found in clouds.

Water vapor molecules themselves tend not to condense into a liquid when cooled. The key word in this sentence is “themselves”. If a chamber is filled with pure water vapor and nothing else, a relative humidity of 300% or higher is present before condensation starts. The atmosphere is not a pristine chamber nor has a relative humidity of over 300% been observed. Therefore, something else must be contributing to the formation of water droplets. This “something else” is called cloud condensation nuclei. Cloud condensation nuclei are aerosols (small particles) in the atmosphere. Most people refer to aerosols as dust or haze when visible. These aerosols attract water vapor molecules and readily bond with them. Aerosols are very abundant and are a critical ingredient for condensation to occur. Figure 4-14 shows the effect of cloud condensation nuclei in the atmosphere.

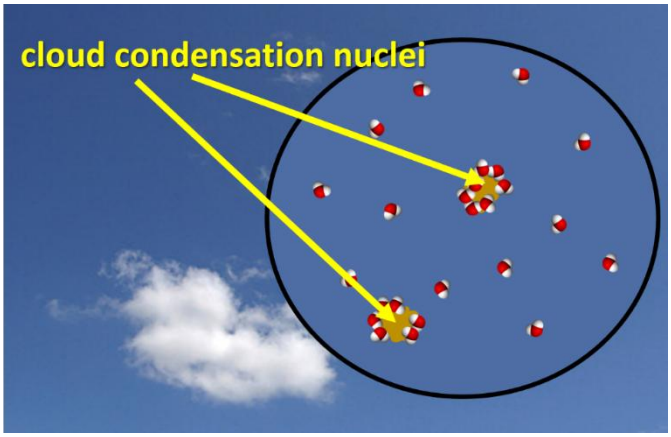

Figure 4-14: The effect of cloud condensation nuclei allows condensation to occur at lower humidity.

Both supersaturation and cloud condensation nuclei are required for condensation in the atmosphere. All the information in this section is associated with liquid water or above freezing temperatures. Condensation and deposition also occur with temperatures below zero, and that is the topic of the next section.

4.3.3 – Factors Affecting Deposition (Ice and Supercooled Water)

As mentioned in the previous section, aerosols act as cloud condensation nuclei in the atmosphere when temperatures are above freezing. However, supersaturation conditions can occur when conditions are below freezing. These cold conditions bring ice and vapor deposition, rather than liquid droplets and condensation, as a method for growing clouds. Colder temperatures introduce another level of complexity, because water vapor does not freeze at 0°C in the atmosphere.

Supercooled water is liquid water below freezing (0°C). Ice does not spontaneously form in the atmosphere between 0°C and -4°C, but water vapor can still condense at these temperatures. Supercooled water needs ice nuclei to form ice, much like liquid water needs cloud condensation nuclei. Ice nuclei, other than ice itself, are not abundant in the atmosphere. Hence, little ice is present at -10°C and warmer. Between -10°C and -20°C, saturation conditions can lead to ice crystals or supercooled droplets. At -10 °C, one ice crystal exists per one million water droplets. At -20°C, the ratio of ice to liquid water tends to be 50% or higher. All liquid has become ice when temperatures are below -40°C Figure 4-15 depicts the ice and supercooled water temperature ranges.

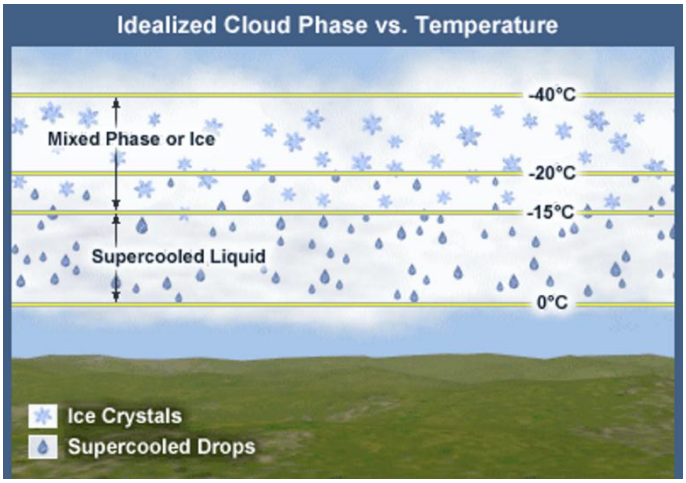

Figure 4-15: The temperature ranges associated with ice and supercooled water (less than 0°C).

The shape of the ice crystals which form are determined by the temperature and supersaturation conditions. The six-sided molecular structure of ice causes an underlying hexagonal shape. This hexagonal configuration maximizes the attractive forces between the molecules, and minimizes the repulsive forces. The small crystal variations due to temperature help make every snowflake that reaches the ground somewhat unique.

The graph in Figure 4-16 shows how supersaturation (excess water vapor over ice) and temperature form various ice crystal shapes. Rapid ice formation can occur between the temperatures of -10°C to -20°C. Figure 4-17 contains photos of various ice crystals grown under different temperature and supersaturation conditions.

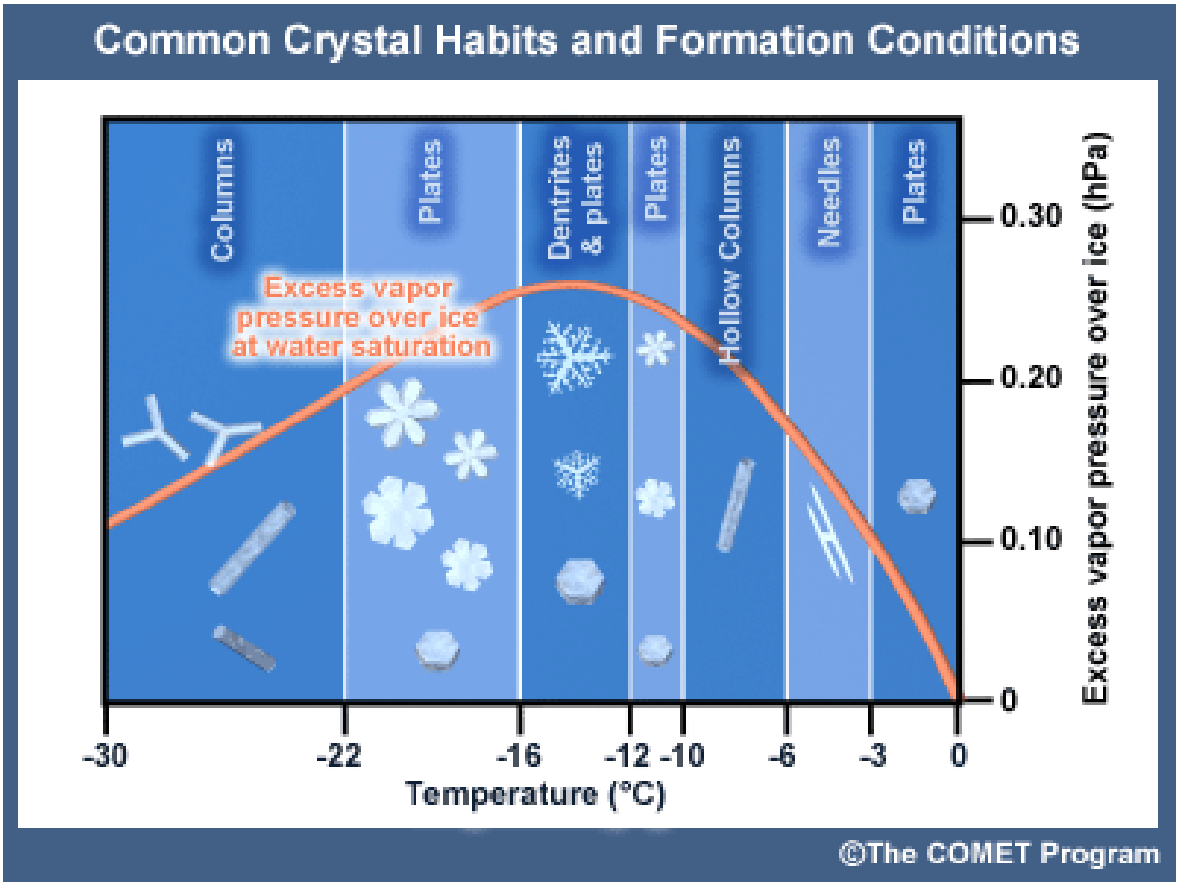

Figure 4-16: Graph of supersaturation (excess water vapor pressure) and temperature. The temperatures for maximum ice crystal growth are -10 to -20°C.

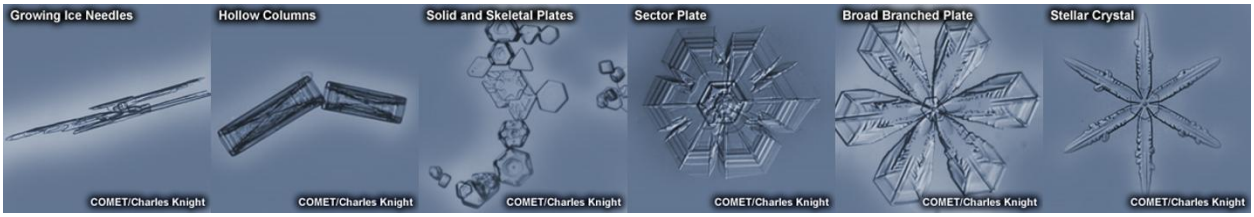

Figure 4-17: Photos of ice crystals grown in a lab under different temperature and humidity conditions.

4.4 – Concepts for Lowering the Air Temperature

As mentioned previously, the most common method by which saturation occurs in the atmosphere is cooling the air until the dew point temperature is reached. All methods involve heat and must follow the Laws of Thermodynamics. Hence, this section looks at these processes from a thermodynamic aspect. We will then examine common mechanisms in the atmosphere that cause cooling and air saturation.

4.4.1 – Diabatic versus Adiabatic Processes

When looking at cloud formation, air temperature changes can be divided into two categories (1) diabatic (pronounced die-uh-ba-tic) and (2) adiabatic (pronounced ay-dee-uh-ba-tic) processes.

A **diabatic process** involves the exchange of energy with its surroundings. An **adiabatic process** occurs without the exchange of energy. “Energy” in these sentences is generally referring to a heat or temperature difference between the process and its surroundings. Both of these processes occur in the atmosphere. An example of a diabatic process is the Sun shining on the Earth to heat its surface. This surface heat is transferred to the atmosphere through a diabatic process. The Earth’s surface and the atmosphere have an exchange of heat energy.

An adiabatic process has no exchange of heat with its environment. Any changes in the system are internal and solely a consequence of work. An example of an adiabatic process is seen when applying the Ideal Gas Law. When compressing air with a bicycle pump, its pressure increases. This increase in pressure results in a corresponding temperature increase. Hence, a bicycle pump is an example of an adiabatic process, no heat has been added from an outside source.

In the atmosphere, an adiabatic process is used to understand changes associated with parcels of air. Air parcels can be thought of as a balloon containing a sample of atmosphere. This parcel can move up and down in the atmosphere. The pressure and temperature inside the parcel may change depending on its altitude. The parcel size may expand or contact. However, no energy exchange is allowed from the outside into the parcel. Any changes to the parcel must come from within itself.

An adiabatic process is an ideal condition for increasing our understanding of atmospheric air motions. The next two sections look at two cases of adiabatic motion, without and with condensation.

4.4.2 – Dry Adiabatic Lapse Rate (DALR)

As an air parcel moves up and down in the atmosphere, its temperature will change because the pressure surrounding it changes. As the parcel rises, the size of it will increase to match the decrease in “outside” pressure. A decrease in pressure causes a temperature change per the Ideal Gas Law. This change in temperature with altitude is called a **lapse rate**. The rate at which a rising parcel of unsaturated air cools is called the **dry adiabatic lapse rate (DALR)**. Notice this definition states the parcel is unsaturated, which implies no condensation is occurring. Thus, the DALR occurs without condensation. The dry adiabatic lapse rate in the atmosphere is -1°C / 100m, which means for every 100 meter of ascent the temperature cools 1°C. Figure 4-18 demonstrates the DALR of a rising and sinking air parcel.

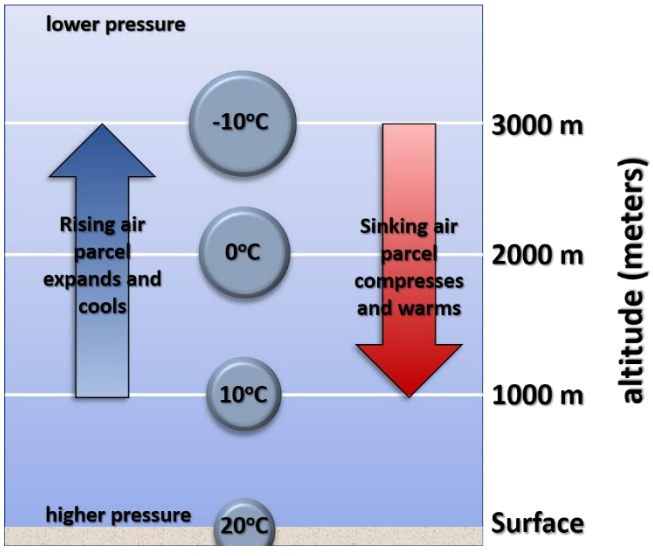

Figure 4-18: Air parcels following the dry adiabatic lapse rate (-1°C / 100m) as they rise and fall. The dry adiabatic lapse rate (DALR) occurs without condensation.

4.4.3 – Moist Adiabatic Lapse Rate (MALR)

Sometimes as air parcels change position in the atmosphere, saturation occurs followed by condensation. Like the dry adiabatic lapse rate, temperature will decrease as the altitude increases. However, when condensation occurs latent heat is released which warms the parcel. The rate at which a rising parcel of saturated air cools is called the **moist adiabatic lapse rate (MALR)**. The amount of water vapor present determines the exact lapse rate. On average, the moist adiabatic lapse rate in the atmosphere is -0.5ºC / 100m. The MALR is half of the DALR due to the latent heat of condensation. The moist adiabatic lapse rate is also called the saturated adiabatic lapse rate or the wet adiabatic lapse rate. All three names are the same. In this textbook, we will only use the moist adiabatic lapse rate (MALR) to avoid confusion.

As air parcels rise, condensation does not begin immediately. The parcel must rise, cool, reach saturation and then condensation can begin. The altitude at which condensation starts is called the **lifting condensation level (LCL)**. This altitude is when clouds start to form, so the height at the bottom of a cloud is the LCL. Figure 4-19 demonstrates the LCL, DALR and MALR.

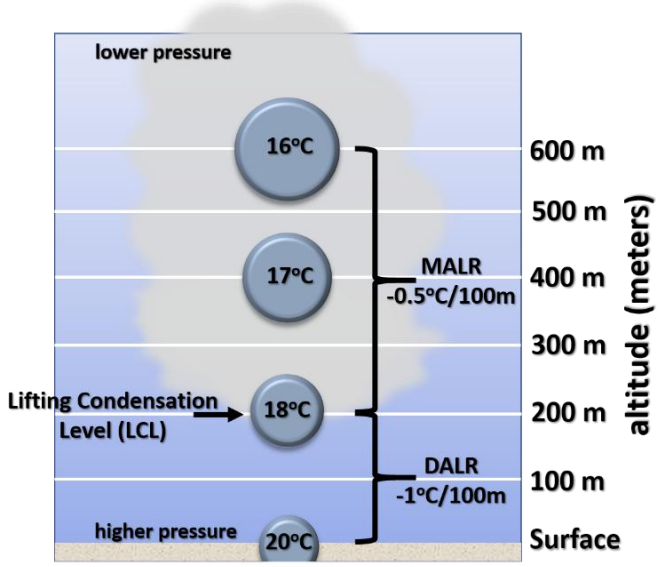

Figure 4-19: When condensation occurs, the moist adiabatic lapse rate -0.5ºC / 100m () is followed. In this diagram, the DALR occurs from the surface to 200 m. From 200 m and higher the moist adiabatic lapse rate (MALR) occurs as clouds form. The level at which clouds start to form is the Lifting Condensation Level (LCL).

4.4.4 – Environmental Lapse Rate (ELR)

When air parcels move vertically in the atmosphere, the temperature of the parcels follows the appropriate lapse rate. The DALR is the appropriate lapse rate when the parcel has no condensation and it is the MALR when condensation is occurring. These lapse rates are important because atmospheric stability is directly related to them when the environmental lapse rate of the atmosphere is known. The **environmental lapse rate (ELR)** is the actual rate of change of temperature with altitude. The environmental lapse rate is constantly changing, and varies at every location.

The environmental lapse rate is obtained through the use of weather balloons and is called an **upper air sounding** or just **sounding**. A radiosonde is the weather instrument attached to the weather balloon and released into the atmosphere. The radiosonde measures temperature, dewpoint, pressure, altitude, and wind while sending this information back to the launch site through a built-in radio transmitter. Weather balloons are launched twice a day (00Z and 12Z) in

the United States and most other countries. The map in Figure 4-20 contains the upper air sites across the world. Is an upper air site located close to you?

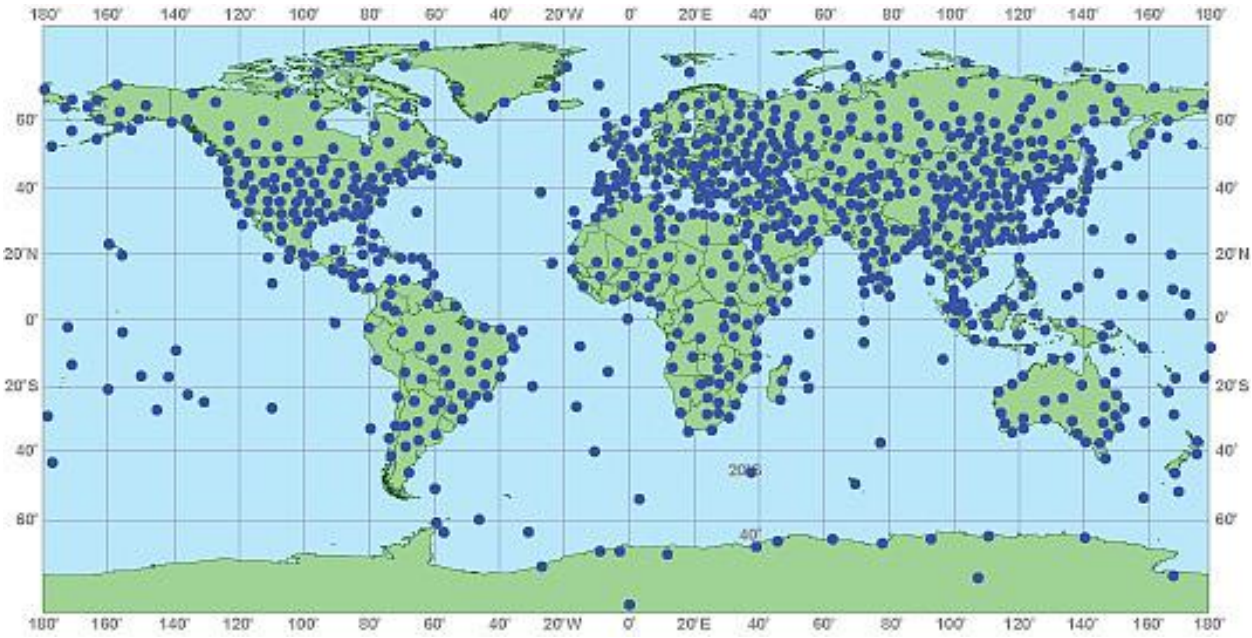

Figure 4-20: The location of upper air sites across the world.

Sounding data is the highest quality data available on the atmosphere, and is widely shared through international agreements. This video shows the details of a weather balloon launch in the United States.

Sounding data is plotted on thermodynamic diagrams, which allow for a quick stability analysis of the atmosphere. Many thermodynamic diagrams exist. The two most widely used are called a Stüve diagram (Figure 4-21) and Skew-T. The Skew-T diagram is almost identical to the Stüve except the temperature lines are skewed (at an angle).

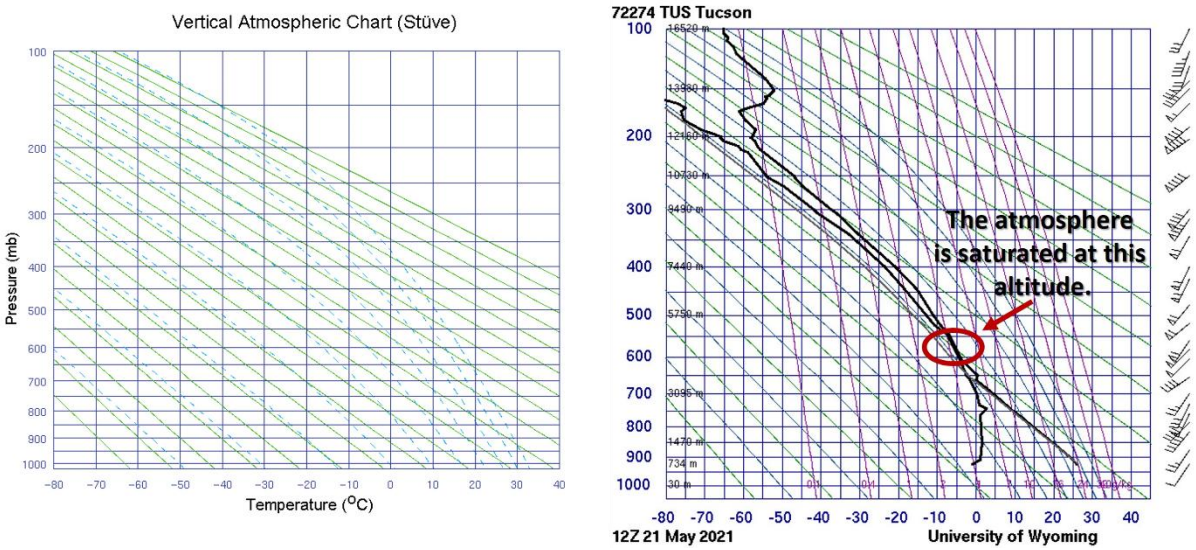

Figure 4-21: (left) A blank Stüve diagram. (right) A diagram with temperature, dew point, and wind data plotted on it.

The two most important lines on a Stüve diagram are the vertical temperature lines on the x-axis and the horizontal pressure lines on the y-axis. Unlike many graphs, the y-axis pressure values decrease with height. The temperature and dew point values are plotted in the body of the graph. The wind information is placed on the right side.

In Figure 4-21, the solid black line on the right is the temperature plot. The solid black line on the left is the dew point plot. Remember dew point must always be less than the ambient temperature, which is shown in this example. The dew point and ambient temperature are the same value around 550 to 600 mb. This indicates the atmosphere is saturated at this level, and a few light sprinkles of rain were occurring in Tucson, Arizona on this day.

4.4.5 – Four Mechanisms that Lift Air and Cause Cooling

The primary method to achieve saturation in the atmosphere is to cool the air parcel, or to lift the air parcel vertically. As the parcel ascends, cooling takes place at a rate similar to either the dry or moist adiabatic lapse rates. The unanswered question now is what lifts these air parcels? There are four mechanisms that can lift air and cause condensation: (1) orographic lifting, (2) convergence at the surface, (3) frontal lifting and (4) convection due to surface heating.

Orographic lifting occurs when air encounters a mountain and is forced to rise over it, as described in Figure 4-22.

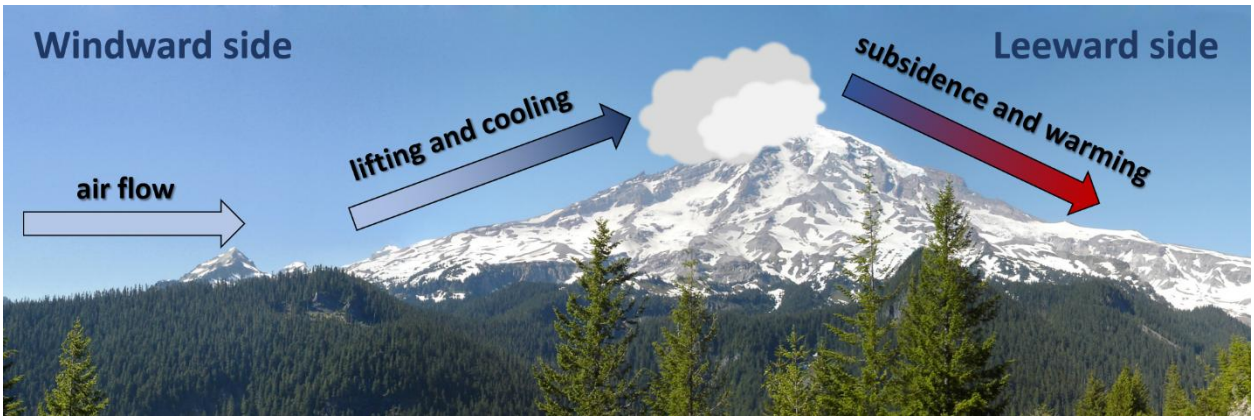

Figure 4-22: Orographic lifting occurs as air moves over a mountain. Precipitation is greater on the windward side, and decreases on the leeward side as the descending air warms.

The windward side of the mountain is cooler and wetter. As the air rises, the pressure decreases causing cooling, saturation, condensation and frequent precipitation. On the leeward side, air descends (subsides) to a lower altitude and experiences an increase in pressure. This increase in pressure causes warming. Since moisture in the air flow is removed on the windward side, precipitation is greatly reduced on the leeward side of an orographic barrier. This area of reduced precipitation is called a **rain shadow**.

A rain shadow is easily seen in the vegetation differences across Washington and Oregon (Figure 4-23). The coastal mountains receive much more precipitation than the interior portions of these states.

Figure 4-23: Image depicting the vegetation due to a rain shadow.

The second type of lifting is convergence at the surface, generally associated with a low pressure. We already know wind moves from high to low pressure, and a low pressure at the surface leads to rising air. Therefore, this rising air will cool air parcels and cause saturation and condensation.

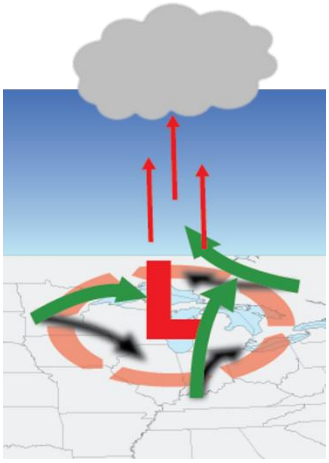

Figure 4-24: Lifting due to convergence at the surface. This type of convergence is frequently associated with a surface low pressure.

The third type of lifting is frontal lifting. Frontal lifting is when colder air slides underneath warmer air, or warmer air rises over cooler air. Cooler air is more dense than warmer air, so when air masses of difference densities meet, the denser one is on the bottom. The boundary separating these areas of different temperatures is called a front. We will cover fronts in more detail in Chapter 6.

The fourth type of lift is heating of the Earth's surface leading to convection. As the surface of the Earth warms from sunshine, the air near the surface rises and mixes this heat into the atmosphere. This situation is the same as the convective heat transfer covered in Chapter 2. The warm rising air is called a thermal. Evaporation from soil moisture is also carried into the atmosphere through convection. These concepts are shown in Figure 4-25.

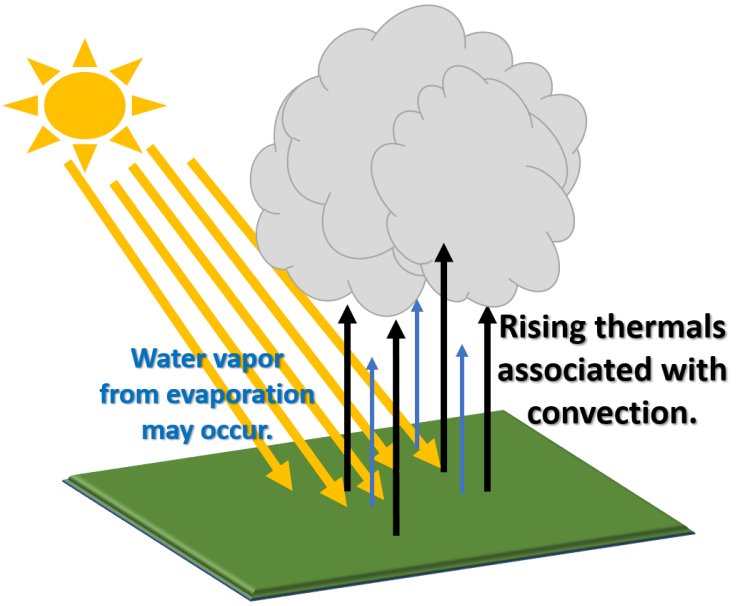

Figure 4-25: Surface heating warms the air which then rises. This lifting mechanism is called convection.

Thermals tend to have an upward moving area next to a downward area as the air mixes. This pattern generates small clouds evenly spaced apart from each other (Figure 4-26).

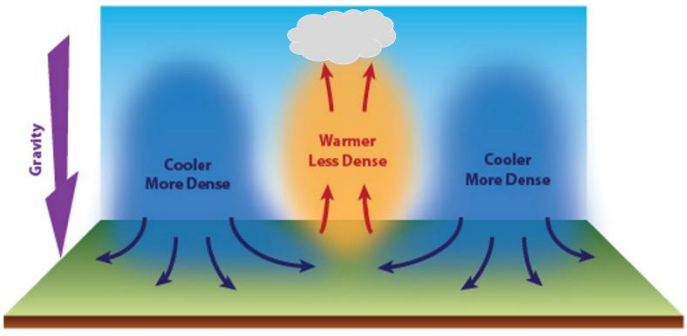

Figure 4-26: Thermals and the clouds they produce.

4.5 – Atmosphere Stability

So far in this chapter, we have covered material on understanding atmospheric moisture, saturation, condensation and the mechanisms within the atmosphere causing these conditions. However, once an air parcel has been lifted and the lifting mechanism stops, what happens? Does the air continue to rise? Does the air stop at the point where it was lifted? Does the air sink back down to where it originated? All these questions are related to atmosphere stability. Stability is related to buoyancy and answers these questions. This section covers the types of stability which are possible in the atmosphere.

4.5.1 – Buoyancy and Stability

The reason for looking at air parcels in the previous section is to help determine the stability of the atmosphere. As a parcel starts to rise, its density determines whether it is less dense (warmer) than the surrounding air or denser (cooler). Warmer air rises, similar to a hot air balloon. Colder air sinks because it is heavier than the surrounding air. These density differences determine the buoyancy of the parcel. Buoyancy is the tendency of an air parcel to rise. Gravity is the force that pulls air parcels downward. Examining the possible combinations of buoyancy and gravity in the atmosphere defines four possible categories of stability

1. Absolutely stable – The air parcel is denser (colder) than the atmosphere and returns to its initial altitude before it was lifted. Gravity wins! The pink ball in Figure 4-27 represents an air parcel with absolute stability.

Figure 4-27:

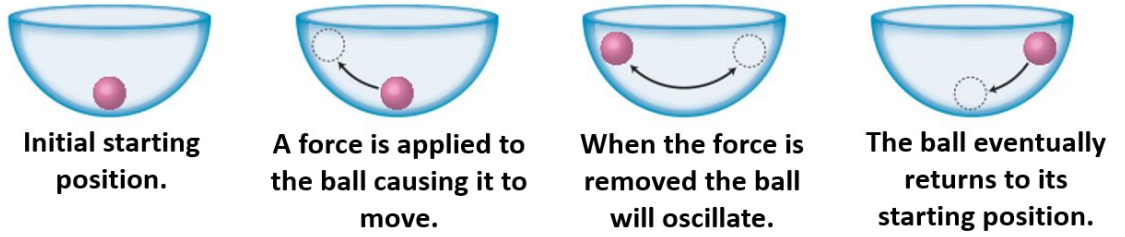

2. Absolutely unstable – The air parcel is less dense (warmer) than the atmosphere and continues to rise. Buoyancy wins! Figure 4-28 illustrates absolute instability with the pink ball on the top of a bowl. The ball always rolls away and keeps moving.

Figure 4-28:

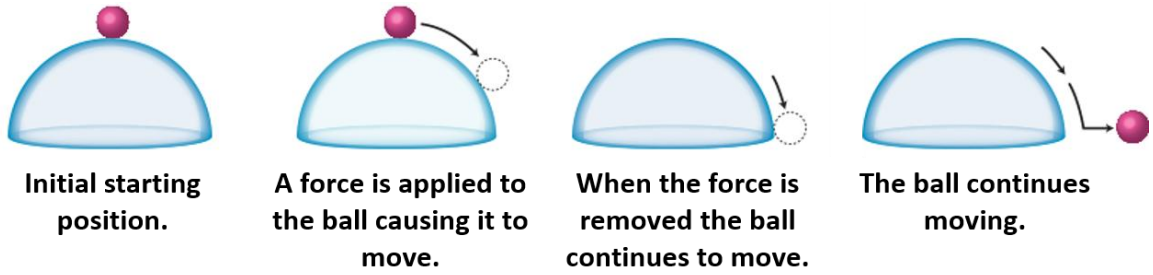

3. Neutral stability – The air parcel once lifted is the same temperature as the surrounding atmosphere and remains at that altitude. Gravity and buoyancy are equal and the contest is

a tie. Neutral stability rarely happens in the atmosphere since air is constantly in motion. This stability is illustrated with a ball on a flat surface as in Figure 4-29.

Figure 4-29:

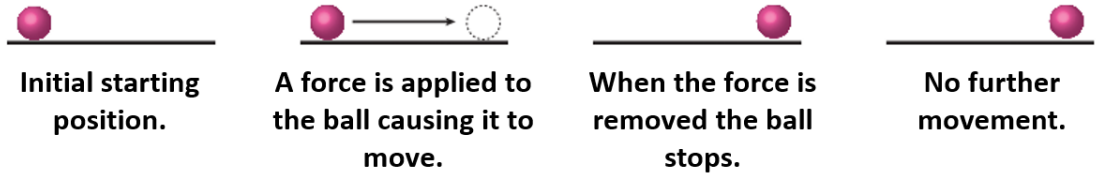

4. Conditional instability – The atmosphere is unstable if certain conditions are met, otherwise it is stable. Conditional stability is a common state of the atmosphere. Figure 4-30 illustrates this "maybe, maybe not" situation.

Figure 4-30:

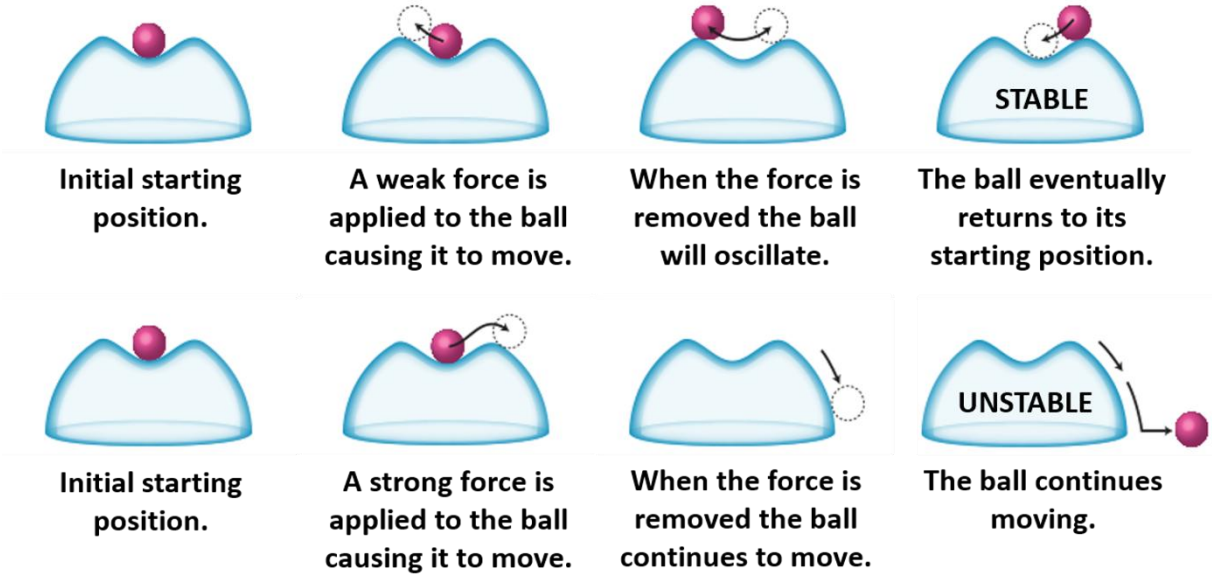

4.5.2 – Unstable Conditions

Unstable conditions are when the air parcel continues rising on its own with no need for a lifting mechanism. The air parcel is warmer than the environment, and once nudged upward continues rising. Figure 4-31 illustrates unstable conditions.

The left side of Figure 4-31 is the dry adiabatic lapse rate without condensation. The right side is for a moist environment with condensation. The environmental lapse rate in this example is 1.5°C / 100m, which is a very cold atmosphere. The air parcel is warmer at all altitudes as it rises. Warm air rises on its own as is depicted. The latent heat associated with condensation causes the parcel to gain even more heat as it rises on the right side.

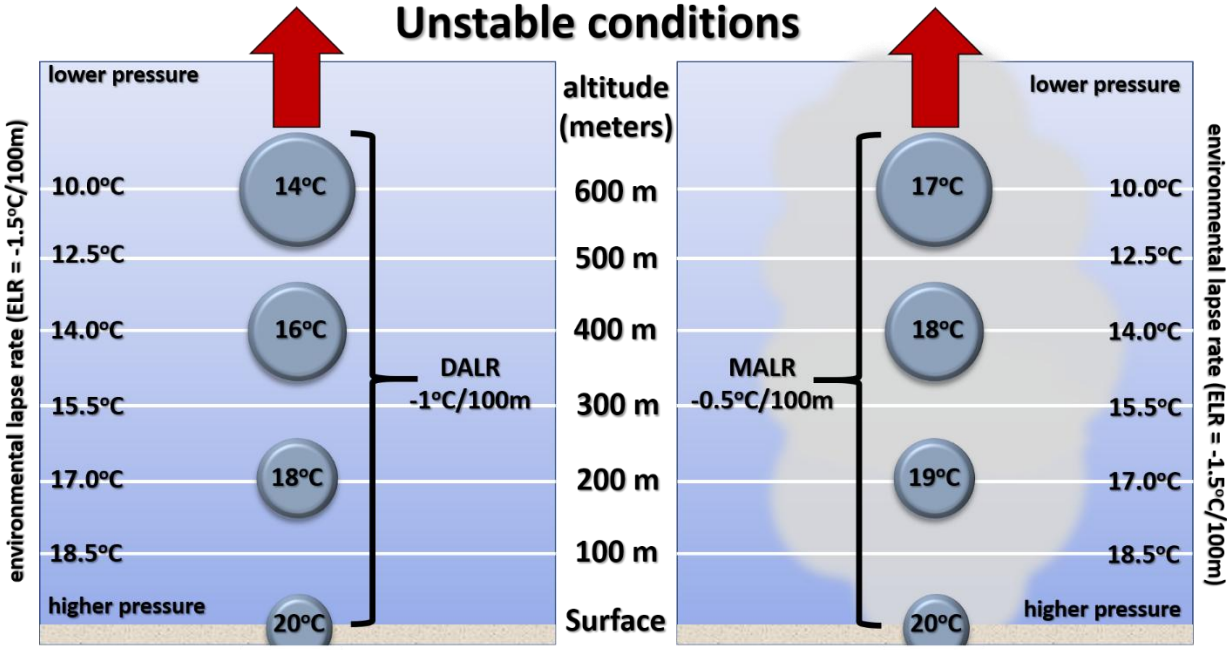

Figure 4-31: A rising air parcel is always warmer than the surrounding air with unstable conditions. The left side gives the air parcel details with a dry adiabatic lapse rate. The right side has condensation and follows a moist adiabatic lapse rate.

Thermodynamic diagrams allow for a quick analysis of stability conditions. So far, we have looked at the vertical (temperature) and horizontal (pressure) lines on a Stüve diagram. The other curved and slanted lines on the diagram are dry and moist adiabats. These adiabatic lines enable a person to determine what happens when a parcel is lifted. The quantity of adiabatic lines allows the lifting of an air parcel from any starting temperature or height.

The DALR and MALR lines on Figure 4-32 are associated with a specific air parcel as it is lifted and rises. Additionally, the regions of unstable, conditionally stable and stable conditions are labeled. When the temperature data from a weather balloon is plotted on a Stüve diagram, it will fall into one of these regions. Unstable conditions occur when the environmental lapse rate is colder than the DALR. Figure 4-31 has the ELR (-1.5°C / 100m) decreasing faster than the DALR (-1.0°C / 100m), and falls into the unstable region.

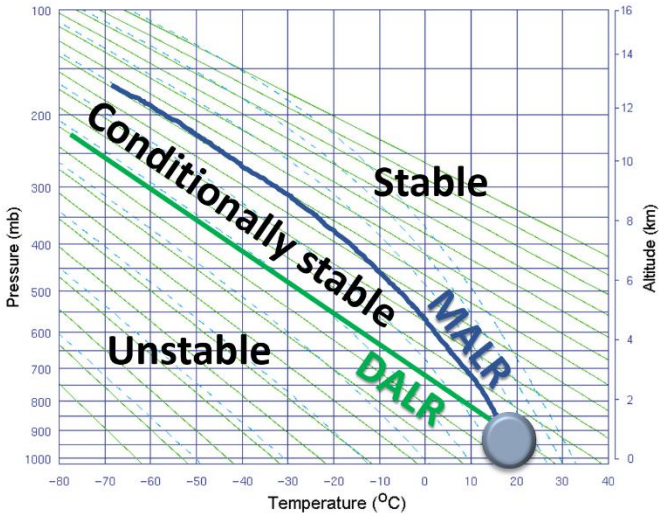

Figure 4-32: Atmospheric stability associated with a rising air parcel. The dry adiabatic lapse rates (DALR) are the slanted green lines. The moist adiabatic lapse rates (MALR) are the curved, dashed blue lines. The abundance of these lines on the diagram allows a person to determine the stability of any air parcel as it rises.

While theoretically possible, unstable conditions in the atmosphere are rarely

observed. Why? Physically what would be happening in unstable conditions is the bottom layer of the atmosphere is rising to the top. The atmosphere would essentially be flipping itself upside down. However, prior to these conditions happening the atmosphere is already adjusting itself to remain stable. The closest to unstable conditions observed is when the ELR equals the DALR, which can occur in the desert Southwest or other desert regions during intense summer surface heating.

4.5.3 – Stable Conditions

Stable conditions are present when the atmosphere is very warm. The environmental lapse rate is decreasing less than either the dry or moist adiabatic lapse rates. Figure 4-33 illustrates stable conditions. A rising air parcel always sinks back to its original position.

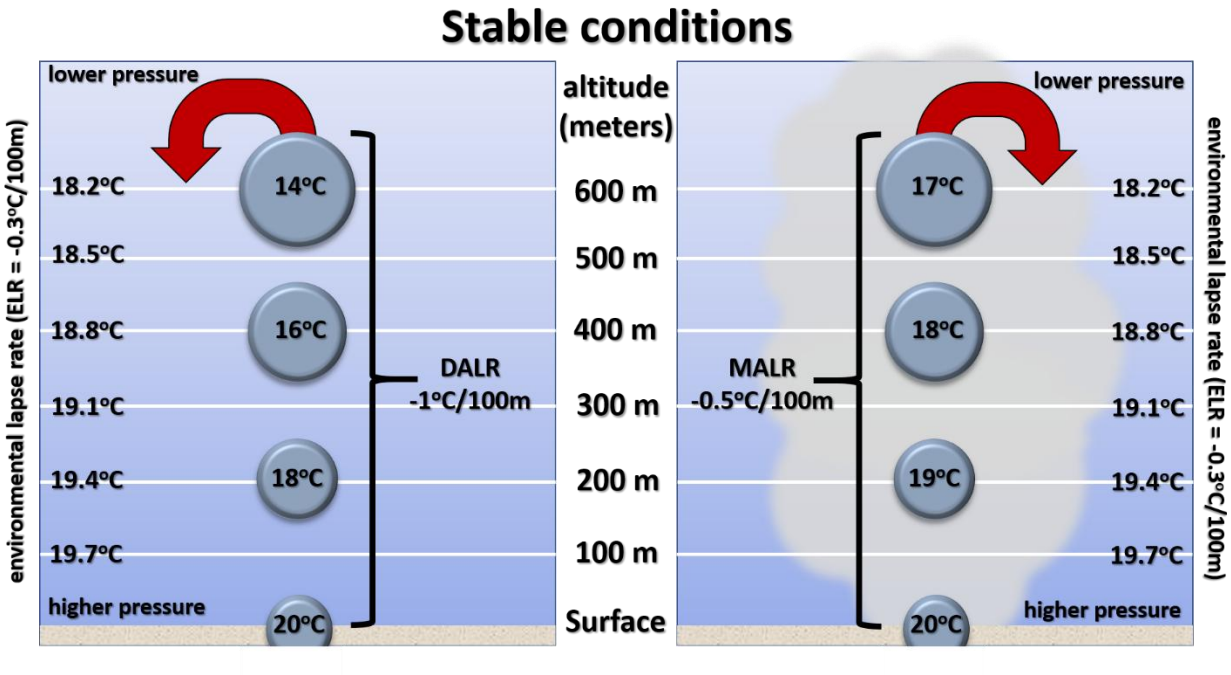

Figure 4-33: A rising air parcel is always cooler than the surrounding air with stable conditions. The left side gives the air parcel details with a dry adiabatic lapse rate. The right side has condensation and follows a moist adiabatic lapse rate.

The left side of Figure 4-33 is the dry adiabatic lapse rate without condensation. The right side is for a moist environment with condensation. The environmental lapse rate (ELR) in this example is -0.3°C / 100m, which is a warm atmosphere. The air parcel is cooler at all altitudes as it rises. Colder air parcels are denser and sink. The latent heat associated with condensation causes the parcel on the right side to be warmer than the left, but still cooler than the environment.

4.5.4 – Conditionally Stable (or Unstable) Conditions

At times, the atmosphere may be stable or unstable. Stable conditions occur if the air parcel once lifted returns to its original position. Unstable conditions occur if the air parcel once lifted continues to rise. This “uncertain” state of the atmosphere is designated as conditionally stable (or conditionally unstable). The determining factor on stability in this situation is whether the

latent heat associated with condensation warms the parcel enough for it to continue rising. Figure 4-34 illustrates a conditionally stable situation.

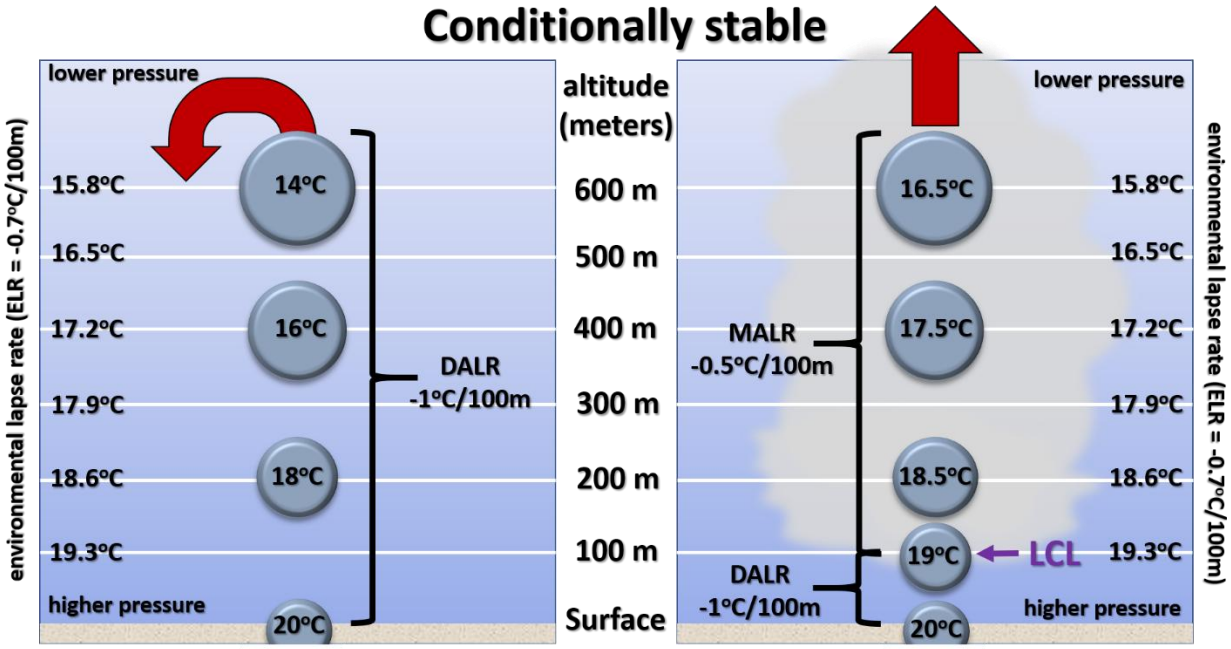

Figure 4-34: A rising air parcel with conditionally stable conditions. The determining factor on stability is whether condensation warms the parcel enough to continue rising. The left side raises the air parcel with a dry adiabatic lapse rate and it returns to its original position. The right side has condensation and follows a moist adiabatic lapse rate which allows the parcel to continue rising.

The left side of this diagram is the dry adiabatic lapse rate without condensation. The right side is for a moist environment with condensation. Since air parcels at the surface do not normally have condensation occurring, a Lifting Condensation Level (LCL) has been added on the right to indicate when condensation starts. Before condensation happens, the air parcel is lifted according to the dry adiabatic lapse rate. The environmental lapse rate (ELR) in this example is -0.7°C / 100m. Notice the ELR is between the DALR (-1.0°C / 100m) and the MALR (-0.5°C / 100m). On the left side with no condensation, the air parcel is cooler at all altitudes as it rises. These colder air parcels sink. On the right side with condensation occurring, the parcel is cooler than the environment at both the 100 and 200 meter altitudes. Once higher than 200 meters, the parcel becomes warmer than the environment and can continue to rise on its own. The latent heat of condensation has warmed the parcel enough to become unstable.

The difficult factor in determining whether a conditionally stable parcel becomes unstable is whether the lifting mechanism can push the parcel high enough to cause condensation. The height of the Lifting Condensation Level (LCL) is essential in determining stability, and the Stüve diagram can be used to find the LCL in addition to the buoyancy of the air parcel.

4.5.5 – Extremely Stable Air (Inversions)

Once an air parcel becomes unstable and continues to rise on its own, what stops it? Two common conditions can stop a parcel from rising: (1) a dry layer of air aloft and (2) a warmer layer of air aloft. Unstable conditions are usually a result of condensation occurring and warming the parcel. Theoretically these rising parcels contain air from where they originated. In reality,

these parcels are affected by the surrounding atmosphere as they rise. If an air parcel encounters a dry layer, this drier air can halt condensation which results in the parcel becoming cooler than the environment. Thus, a parcel may rise to a certain level on its own, but then sink once it encounters dry air.

The second condition which halts a rising air parcel is an inversion. Temperatures that increase with height are called an **inversion**. When an inversion is present, the parcel encounters air that is warmer than itself. Thus, the parcel is suddenly cooler than the environment and starts to sink. Inversions can be detected in a sounding by a kink in the temperature plot. Normally temperatures decreases with height in the troposphere. When an inversion is present this normal decrease in temperature is reversed, resulting in a zig or kink in the temperature line. The ultimate inversion for the troposphere is the stratosphere. Remember that temperatures increase with height in the stratosphere. Strong thunderstorms push up against the stratosphere and flatten out. Hence, if you have seen a healthy thunderstorm, you have likely seen the location of the stratosphere and the effects of an inversion (Figure 4-35).

Figure 4-35: Photo of a thunderstorm with vertical development stopping at the stratosphere.

The sounding from Bismark, North Dakota in Figure 4-36 illustrates multiple inversions in the troposphere. Inversions are fairly common in the atmosphere and their ramifications will be discussed in subsequent chapters.

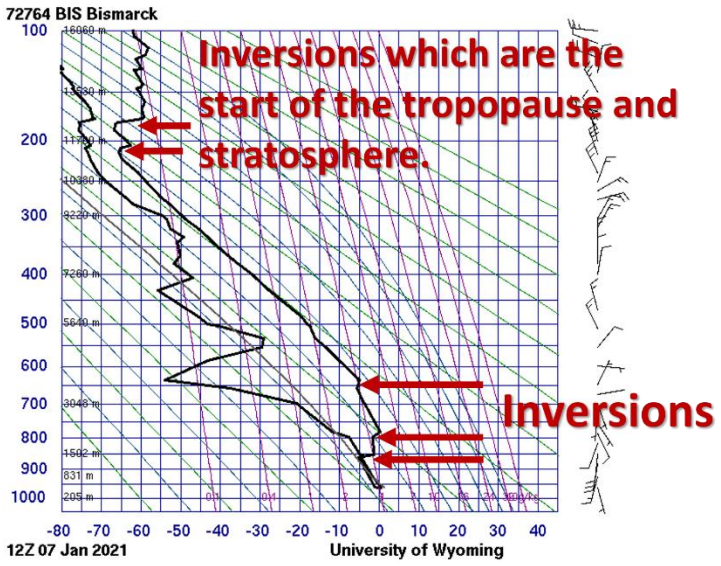

Figure 4-36: Sounding from Bismark, North Dakota with the inversions highlighted.

Chapter 4 Review Questions

1. What is the state of water when it
    a. is the densest?
    b. is the most energetic?
    c. has the molecules in a fixed location?
    d. is compressible?
    e. has a crystalline structure?
2. What is the change of state for water molecules going from a gas to a solid called?
3. Which change of state for water molecules releases the most energy?
4. What is the energy required to change the phase of a substance called?
5. At what temperature do water droplets start to freeze in a cloud?
6. What is the definition of dew point temperature?
7. How much more moisture is in 1 kg of saturated air at a tropical location with a temperature of 40^{o}C than a polar location at -10^{o}C?
8. What is the definition of relative humidity?
9. In what portion of a day is relative humidity generally the highest?
10. What is a relative humidity greater than 100% called?
11. What is the name of aerosols in the atmosphere that contribute to the formation of water droplets?
12. What is liquid water below freezing called?
13. What determines the shape of an ice crystal?
14. What is the underlying shape of an ice crystal?
15. At what temperature in a cloud is the ration of liquid water to ice about 50%?
16. What is the name of the process in which energy is added to or removed from a system?
17. Name and describe the lifting mechanisms for air in the atmosphere.
18. What is the lifting condensation level (LCL)?
19. What happens to an air parcel that is warmer than the surrounding air?
20. What is the atmosphere condition called where temperatures increase with altitude?
21. In a conditionally stable environment, what warms the air parcel enough to become unstable?
22. What conditions can halt an unstable air parcel from rising?
23. How is the environmental lapse rate observed?
24. Is a very cold atmosphere more unstable than a very warm atmosphere (Yes/No)?

Chapter 5 – Atmospheric Moisture II

Overview

This chapter completes the study of atmospheric moisture. Since details about saturation and condensation are known, we move onto clouds and their classification. Clouds are a pre-requisite for precipitation, and precipitation is examined in detail. Precipitation can be divided into two processes: warm cloud processes above freezing, and cold cloud processes where a portion of the cloud is below freezing. We will finally learn how rain happens.

After the precipitation topic, the hydrologic cycle is briefly reviewed along with groundwater and surface water. This chapter finishes with information on streamflow and floods. After completing it, the basics on how the atmosphere works have been covered. Chapters 6 through 10 look at weather patterns and storm systems, or what most people traditionally think of as weather.

Chapter objectives:

1. State how clouds are classified.
2. Describe the processes involved in the growth of cloud droplets.
3. Understand the relationship between drainage basins and rivers.
4. Explain the relationship between river stage, rating table, discharge and a hydrograph.
5. Understand the definition of a recurrence interval and how to calculate it.

5.1 – Cloud Types

Clouds form from the same mechanisms that lift air and cause cooling. These four mechanisms were explored in section 4.4.5. The types of clouds present in a region provide visual clues as to the state and stability of the atmosphere. Two characteristics define all the types of clouds: appearance (or shape) and height. A cloud appearance or shape falls into one of four categories: (1) cirro-form, (2) strato-form, (3) nimbo-form, and (4) cumulo-form.

Figure 5-1: A typical shape of cirro-form clouds.

Cirro-form clouds are composed of ice crystals, and are whitish and hair-like. The Latin word 'cirro' means curl of hair. They are the high, wispy clouds to first appear in advance of a storm system and are usually the remnants of a storm after it decayed. See Figure 5-1.

Figure 5-2: A typical shape of strato-form clouds.

Strato-form clouds are generally a broad, flat layer of cloud. The Latin word ‘strato’ means layer. These clouds tend to occur where air is lifted and cooled slowly. The edges of strato-form clouds are frequently diffuse. See Figure 5-2.

Nimbo-form clouds have precipitation originating from them. The Latin word 'nimbus' means rain. Nimbus is added to the other cloud forms when precipitation is occurring such as nimbostratus (a layer cloud with rain) or cumulonimbus (a vertically developed cloud with rain). See Figure 5-3.

Figure 5-3: A typical shape of nimbo-form clouds.

Cumulo-form clouds have vertical development, usually originating from thermals and convective heating. Cumulus clouds start out looking like fluffy cotton balls, and can rise to great heights. They are dense in appearance and have sharp outlines during development See Figure 5-4.

Figure 5-4: : A typical shape of cumulo-form clouds.

Cloud heights fall into one of four categories: (1) high, (2) middle, (3) low, and (4) vertically developed or covering multiple heights. The physical height of a cloud is determined by the depth of the troposphere at that location. Remember, a constant pressure surface is higher at the warmer equator than at the cooler poles. These temperature differences cause the troposphere to be deeper in the tropics and shallower at higher latitudes. The troposphere is divided into three heights for clouds based on its total depth as is described in Figure 5-5.

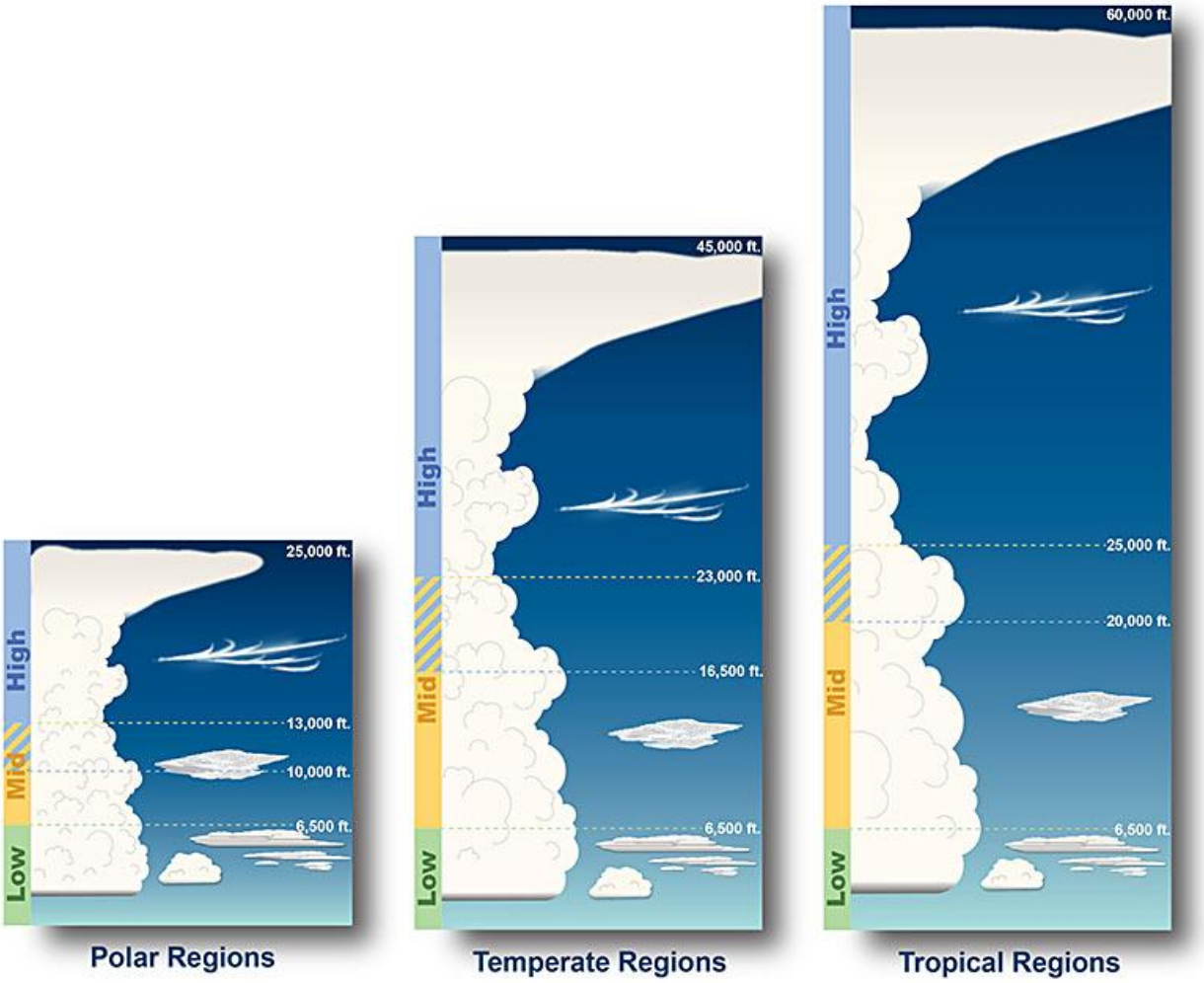

Figure 5-5: Cloud height classifications (high, middle, and low) vary with the depth of the troposphere from the polar to tropical regions.

The actual latitudes of these regions vary seasonally. However, the polar region is generally from 60° latitude to the pole. The temperate region from 30° to 60°, and the tropical from 30° to the equator. This table contains the cloud height categories based on latitude. Notice that all latitudes and regions have the same heights for low clouds.

Level	Polar Regions	Temperate Regions	Tropical Regions
High Clouds	10,000-25,000 feet	16,500-45,000 feet	20,000-60,000 feet
Mid Clouds	6,500-13,000 feet	6,500-23,000 feet	6,500-25,000 feet
Low Clouds	Surface-6,500 feet	Surface-6,500 feet	Surface-6,500 feet

Figure 5-6 contains all the different types of clouds in one graphic. The remainder of this section examines all these types of clouds and their associated appearance/shape and height.

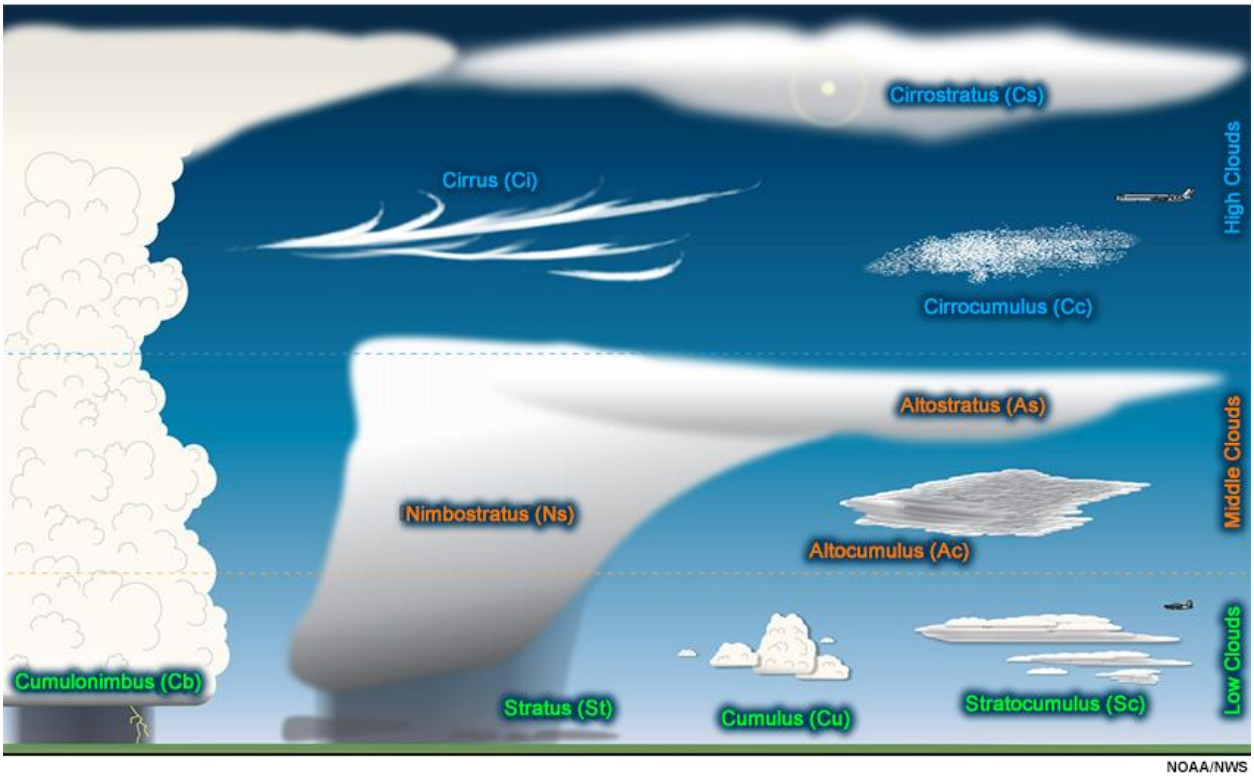

Figure 5-6: A graphic containing all the types of clouds examined in Section 5.1.

5.1.1 – High Clouds

Cirrus, cirrocumulus, and cirrostratus are high level clouds. They are typically thin and white in appearance, but can appear in a magnificent array of colors when the Sun is low on the horizon.

Cirrus are detached clouds in the form of white, delicate filaments, mostly white patches or narrow bands. They may have a fibrous (hair-like) or silky sheen appearance. See Figure 5-7.

Cirrus clouds are always composed of ice crystals, and their transparent character depends upon the degree of separation of the crystals. As a rule, when these clouds cross the Sun, they

barely diminish its brightness. When they are exceptionally thick, they may mask the Sun's light and blot out its contour.

Before sunrise and after sunset, cirrus is often colored bright yellow or red. These clouds are lit up long before other clouds and fade out much later; some time after sunset they become gray. At all hours of the day, cirrus near the horizon (a long distance away) often have a yellowish color.

Figure 5-7: Photo of cirrus clouds.

Cirrostratus is a transparent, whitish cloud with a fibrous (hair-like) or smooth appearance. A sheet of cirrostratus is large and usually covers the entire sky at some point. During the day, when the sun is sufficiently high above the horizon, the sheet is never thick enough to prevent shadows of objects on the ground. See Figure 5-8.

Figure 5-8: Photo of cirrostratus clouds.

A milky thin stratus (a low cloud) can be distinguished from a cirrostratus with a similar appearance by the halo which the Sun or the moon creates. A halo is a bright ring around the Sun or moon, and will be covered in more detail in Chapter 10. Cirrostratus is able to create a halo because it is composed of ice crystals. A lower stratus cloud is composed of water droplets and cannot create a halo. A faint halo is seen in this picture of cirrostratus.

Cirrocumulus is a thin, white patch or layer of clouds composed of very small elements in the form of grains or ripples. Cirrocumulus may be composed of supercooled water droplets, as well as small ice crystals, or a mixture of both. See Figure 5-9.

Figure 5-9: Photo of cirrocumulus clouds.

In general, cirrocumulus represents a degraded state of cirrus and cirrostratus. Cirrocumulus may be attached to cirrus or cirrostratus and has some of the characteristics associated with these other ice crystal clouds.

5.1.2 – Middle Clouds

Altostratus, altocumulus and nimbostratus are middle clouds. These clouds are primarily composed of water droplets. Altostratus is a gray or bluish cloud layer with a striated or fibrous appearance. They are thin enough to regularly reveal the Sun. Altostratus clouds do not produce shadows of objects on the ground. Sometimes precipitation that evaporates before reaching the ground can be seen hanging from altostratus. See Figure 5-10.

Figure 5-10: Photo of altostratus clouds.

Altocumulus are a white or gray cloud layer composed of small elements in the form of grains or ripples. The cloud elements are well-defined and have an appearance like cirrocumulus, although are at a lower altitude. These clouds are generally composed of water droplets. See Figure 5-11.

Figure 5-11: Photo of altocumulus clouds.

Nimbostratus is a result of thickening altostratus or stratus. This cloud is a dark gray layer with no well-defined cloud elements. Falling rain or snow blur the cloud definition and it is thick enough to hide the Sun. The cloud base lowers as precipitation continues, making it possible for nimbostratus to be both a middle and a low cloud. Lightning and hail are not present in a nimbostratus cloud. See Figure 5-12.

Figure 5-12: Photo of nimbostratus clouds.

5.1.3 - Low Clouds

Stratocumulus and stratus are low clouds composed of water droplets. Stratocumulus is a gray or white layered cloud, which almost always has a dark honeycomb appearance. They are generally non-fibrous and may or may not merge together. Stratocumulus have regularly arranged small elements in groups, lines or a wavy pattern. See Figure 5-13.

Stratus is a gray cloud layer with a uniform base. These clouds generally do not produce precipitation, but if they do the droplets are very small and appear to be floating slowly downward. This type of precipitation is called drizzle. Often when a layer of stratus dissipates blue sky can be seen overhead. See Figure 5-14.

Figure 5-13: Photo of stratocumulus clouds.

Nimbostratus is a result of thickening altostratus or stratus. This cloud is a dark gray layer with no well-defined cloud elements. Falling rain or snow blur the cloud definition and it is thick enough to hide the Sun. The cloud base lowers as precipitation continues, making it possible for nimbostratus to be both a middle and a low cloud. Lightning and hail are not present in a nimbostratus cloud. See Figure 5-12 in the middle clouds section.

Figure 5-14: Photo of stratus clouds.

5.1.4 – Vertically Developed Clouds

Two vertically developed clouds are cumulus and cumulonimbus. Both of these cloud types start out as a low cloud and can build up through higher levels. Cumulo-form clouds tend to be diurnal in nature in that they develop and build from the morning into the afternoon and dissipate in the evening.

Cumulus clouds are detached, generally dense clouds with sharp outlines. They develop vertically in the form of rising mounds, domes or towers with bulging upper parts often resembling a cauliflower. The sunlit parts of these clouds are mostly brilliant white, while their bases are relatively dark and horizontal. See Figure 5-15.

Figure 5-15: Photo of cumulus clouds.

On a satellite image, cumulus appear to be small cotton balls evenly spaced apart. Figure 5-16 contains a satellite image of cumulus clouds.

A cumulonimbus cloud is commonly called a thunderstorm and is a heavy, dense cloud in the form of a mountain or huge tower. The upper portion is usually smooth, fibrous or striated and frequently flattens into the shape of an anvil or large plume.

The base of this cloud is often very dark. When precipitation is present, low ragged clouds can occur that may or may not be attached to the primary cloud body. Thunderstorms can produce heavy precipitation, hail, strong winds and tornadoes. Figure 5-17 contains a photo of a mature cumulonimbus cloud.

Developing thunderstorms start out on satellite imagery as a large round cloud. Once the storm encounters the tropopause, it spreads outward with cirrus clouds. Figure 5-18 contains a satellite image of thunderstorms in the South China Sea. The cumulonimbus builds during the day and decays after sunset. Notice the shadows on the east side of these storms prior to sunset. Vertically developed storms in visible satellite imagery have noticeable shadows when the Sun angle is low. More than one thunderstorm can be seen in this satellite image (Figure 5-18).

Figure 5-16: Satellite image of cumulus along the shore of a lake. Cumulus clouds from above appear as cotton balls.

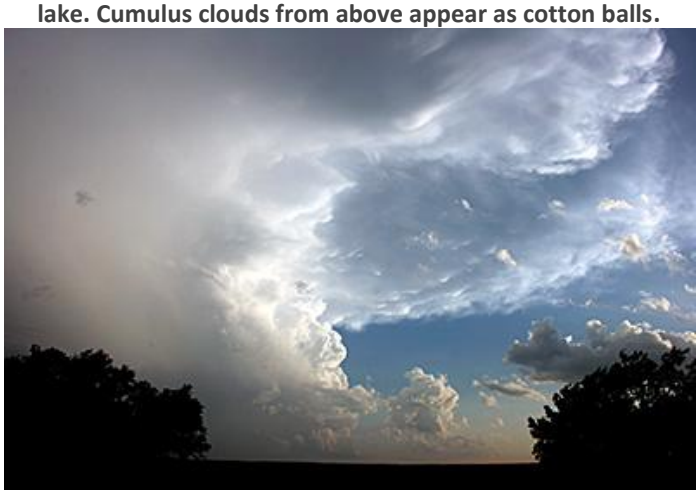

Figure 5-17: Photo of a mature cumulonimbus cloud.

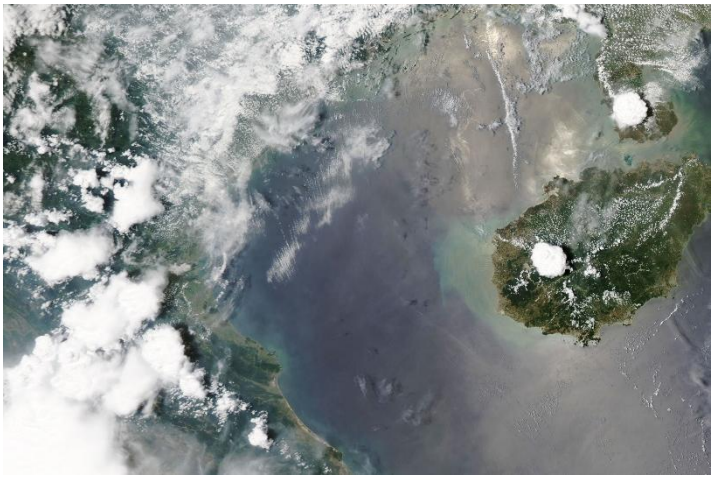

Figure 5-18: Visible satellite imagery of thunderstorms. Growing thunderstorms have a circular appearance as on right side. As a thunderstorm matures, cirrus forms which can be seen on the left side as the circular cloud becomes fuzzy. These thunderstorms have cloud shadows on their east (right sides).

5.1.5 – Fog

Fog consists of water droplets suspended in the air which are in contact with the ground. The difference between fog and a cloud is the cloud is suspended above the ground. Fog restricts visibility and occurs when the temperature and dew point are close to equaling each other. Fog rarely forms when the temperature and dew point are separated by more than about 2°C or 4°F.

Two common types of fog are (1) advection and (2) radiation fog. Advection fog occurs when moist air moves over a cold surface. The air cools to the dewpoint which allows for condensation to occur. Advection fog is common near seas and oceans as warm moist air moves northward over cooler water. This satellite image from NASA shows advection fog moving into the San Francisco Bay area (Figure 5-19).

Figure 5-19: Advection fog moving into the San Francisco Bay area.

Radiation fog occurs at night when the ground cools the lower layer of air to the dewpoint. This type of fog needs a moist layer of air near the ground, which can occur when the ground is damp. Hence if it rains during the day and skies clear at night, radiation fog can form. During the night, the ground cools which in turn cools the air closest to the ground. Radiation fog frequently forms in the early morning hours. When the Sun comes up in the morning, radiation fog tends to thin and dissipate from the outer edges first. This satellite image (Figure 5-20) from NASA shows radiation fog in California.

Figure 5-20: Radiation fog in the Central Valley of California occurs frequently in the winter months.

5.2 – Growth of Cloud Droplets for Precipitation

We have discussed saturation, condensation and the types of clouds which can form by these processes. However, we have not explored the processes necessary for precipitation to occur. This section looks at how precipitation is created in the atmosphere.

Condensation can create water droplets, but how do these droplets fall out of the cloud to the Earth as precipitation? When examining cloud droplets, two forces are acting on a droplet (1) drag and (2) gravity as illustrated in Figure 5-21.

Figure 5-21: Two forces affect a water droplet's vertical motion: drag and gravity. Drag is the air around the droplet impeding its motion.

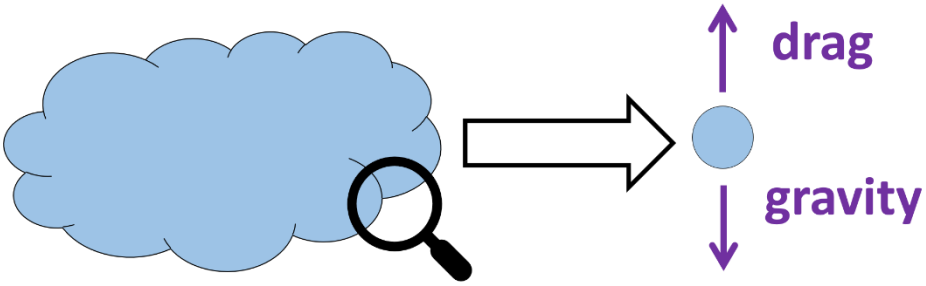

Gravity is pulling the droplet towards the Earth. Drag can be thought of as the resistance resulting from the droplet needing to move air molecules out of the way to descend. Cloud

droplets remain suspended when gravity cannot overcome this opposing air resistance. If gravity cannot overcome drag the droplet remains suspended.

If gravity can overcome drag the droplet begins falling. The speed of this descending droplet is called its terminal velocity. The terminal velocity of a 100μm droplet is about 1 meter per second or 2.2 mph. As a droplet falls it must still contend with condensation and evaporation rates. Many times, droplets falling out of a cloud evaporate before reaching the surface. Precipitation evaporating before reaching the ground is called **virga**. The photo in Figure 5-22 is an example of virga.

Figure 5-22: Photo of virga. Virga is water droplets evaporating before they reach the ground.

5.2.1 – Size Differences between Cloud and Rain Droplets

A cloud is a visible suspension of water droplets. Knowing the droplet sizes would be helpful in investigating how precipitation forms. Figure 5-23 illustrates the various sizes, from the cloud condensation nuclei up to a small rain drop. A drizzle drop is a very small droplet that appears to float as it slowly descends to the surface.

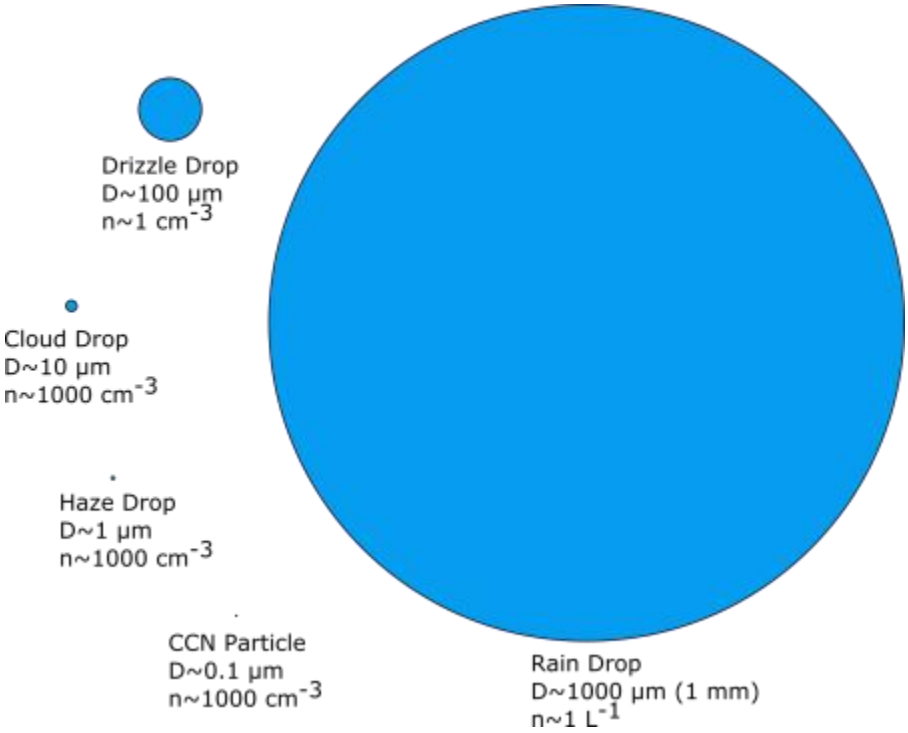

Figure 5-23: Diagram illustrating droplet size from cloud condensation nuclei (CCN) to a small rain drop. "D" the diameter and "n" is the typical number found in a cubic centimeter or liter of air.

Note the wide range in size, volume, and number of particles in Figure 5-23. “D” is the diameter of the drop, “n” is the typical number found in a cubic centimeter (cm^3) or liter (L^{-1}) of air. The smallest, the cloud condensation nuclei (CCN), is a particle to which water can attach itself (called hydrophilic). These particles grow by adding water molecules, but still contain the original CCN upon which they formed. As Figure 5-23 illustrates, a small raindrop is huge compared to a cloud water droplet.

An important piece of information we need to know is how large can a raindrop grow through condensation? Figure 5-24 contains the answer to this question, and shows that the cloud drop radius increases rapidly through condensation at the beginning, but slows down within minutes. A cloud drop can grow to about 20 μm in 15 minutes. After 15 minutes, growth is much slower. Since the lifetime of a cloud drop is in the tens of minutes range, it is not possible for cloud drops to grow into rain drops by condensation alone. Some other processes must be occurring to generate precipitation. To examine these other processes, we are going to categorize them by temperature. The **warm cloud process** occurs in clouds above freezing or warmer than 0°C. The **cold cloud process** occurs in clouds where a portion or the entire cloud is below freezing or less than 0°C.

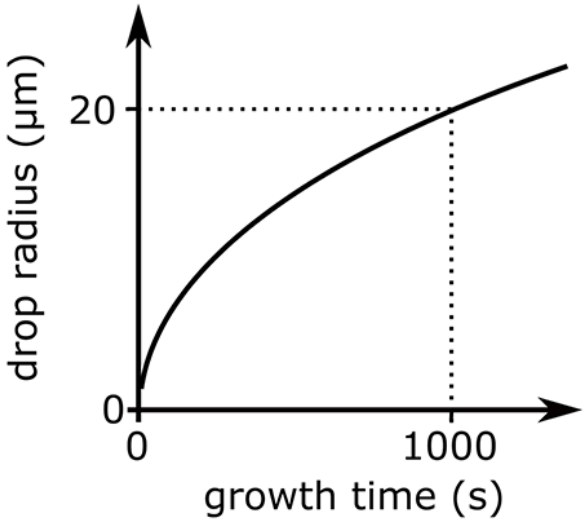

Figure 5-24: A graph of water droplet radius and growth time in seconds. A droplet can grow to 20μm in about 15 minutes, which is much less than a small rain drop size.

5.2.2 – Warm Cloud Droplet Growth Process

The warm cloud droplet growth process involves droplets colliding with each other and coalescing. This process is called **collision-coalescence**. Collision-coalescence is the only process for creating precipitation in a cloud warmer than 0°C.

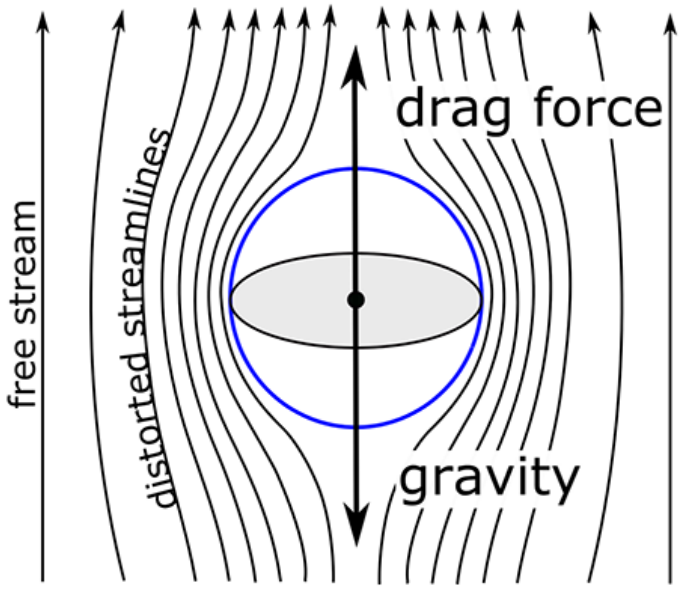

Figure 5-25 shows the air flow around a water droplet as it falls. The shaded area is the cross-sectional area of the droplet. Note the movement of air around the particle. This air flow is indicated by the lines around the droplet, which are called streamlines. Only the innermost streamline collides with the droplet. The remaining streamlines do not touch it.

Figure 5-25: Air flow around a water droplet as it falls.

The left side of Figure 5-26 utilizes the air flow around a droplet to illustrate how collisions occur with smaller droplets. Droplet A avoids a collision; droplet B collides with the larger droplet. These larger droplets are called collector drops.

The right side of Figure 5-26 indicates that once a collecting drop has reached a radius of a few hundred microns (μm), it falls fast and its collision–coalescence efficiency is close to 100%. These graphs indicate that growth by condensation occurs up to about 20 μm, then collision-coalescence starts and produces a few big drops. These collector drops then grow exponentially with time.

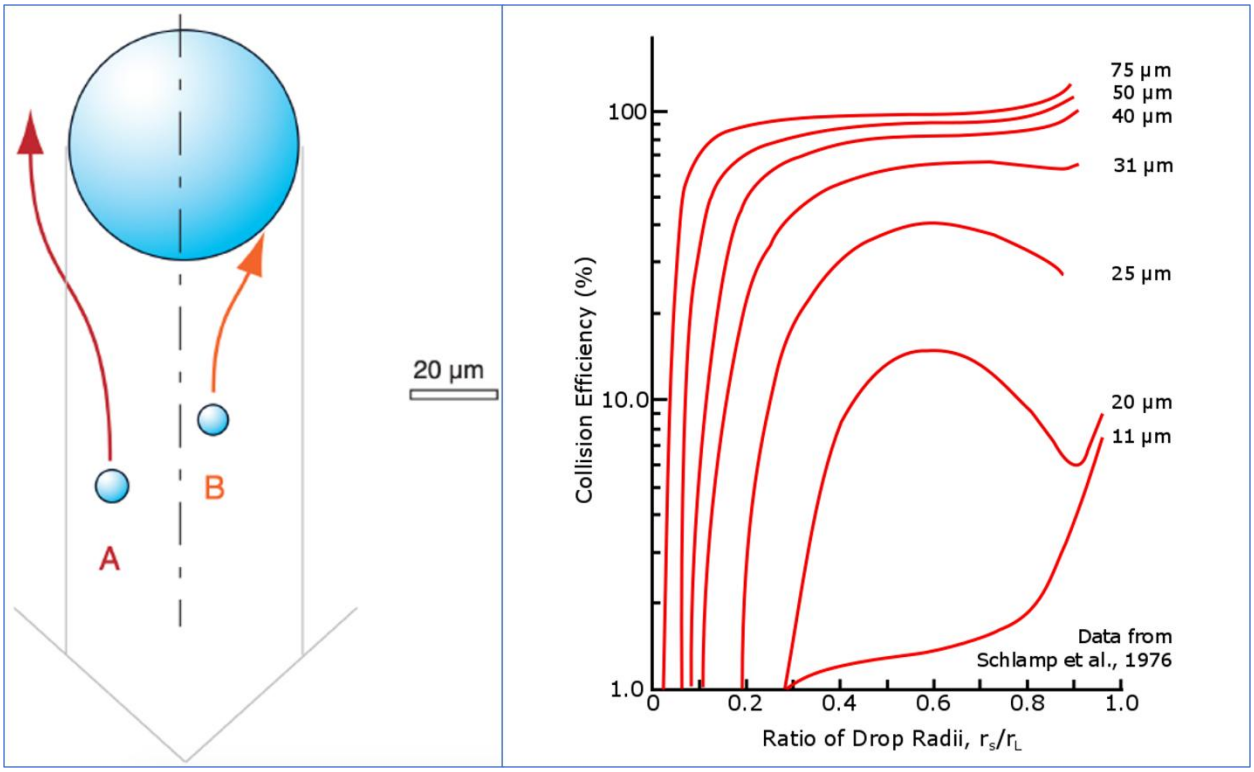

Figure 5-26: Left side depicts the mechanics of smaller droplet colliding with a larger droplet. The right side is the efficiency of this collision process. Once a droplet reaches 20 in size through condensation, collision-coalescence continues the growth to larger droplets.

As a collector drop gets larger its spherical shape flattens. This flattening is a result of air resistance (drag) and the raindrop changes from spherical to a mushroom shape. As the drop continues to grow, the flattening becomes extreme and the droplet splits. This splitting results in a maximum collector raindrop size of about 5mm or ¼ inch, as illustrated in Figure 5-27.

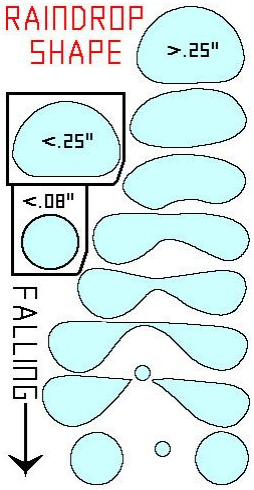

Figure 5-27: As a droplet increases in size, the air drag moving around the droplet splits it into smaller pieces. This situation results in a maximum collector raindrop size of about 5 mm or ¼ inch.

5.2.3 – Cold Cloud Ice Growth Process

When a portion of a cloud is below freezing (0°C) ice crystals and supercooled water are present in the cloud. Ice crystals add a new perspective in growing particles fast enough to gain a terminal velocity for reaching the ground.

The basis for this **ice process of precipitation** is that the saturation vapor pressure for ice is less than that for liquid water at the same temperature, as shown in Figure 5-28.

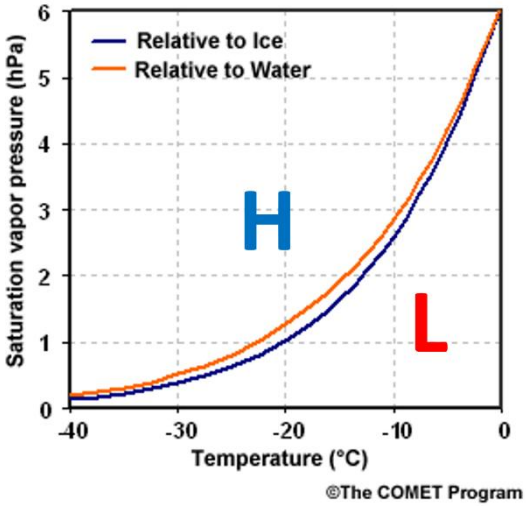

Figure 5-28: A graph of saturation vapor pressure and temperature. This graph indicates that ice crystals grow faster than water droplets.

Okay, Figure 5-28 is a nice graph but why is this important? The physical meaning of this graph is that when ice crystals and supercooled water droplets are competing for water vapor to grow, the ice crystals will always win. Ice crystals will grow at the expense of the water droplets. The pressure gradient force is valid in a saturated water vapor environment, and the vapor will travel from a higher to a lower pressure. Ice has the lower pressure (blue line) and will always win in a growth contest with liquid water.

Figure 5-29 illustrates this ice growth process in action. Crystal growth rates by deposition are at a maximum between about -10°C to -20°C, as was shown in Figure 4-16.

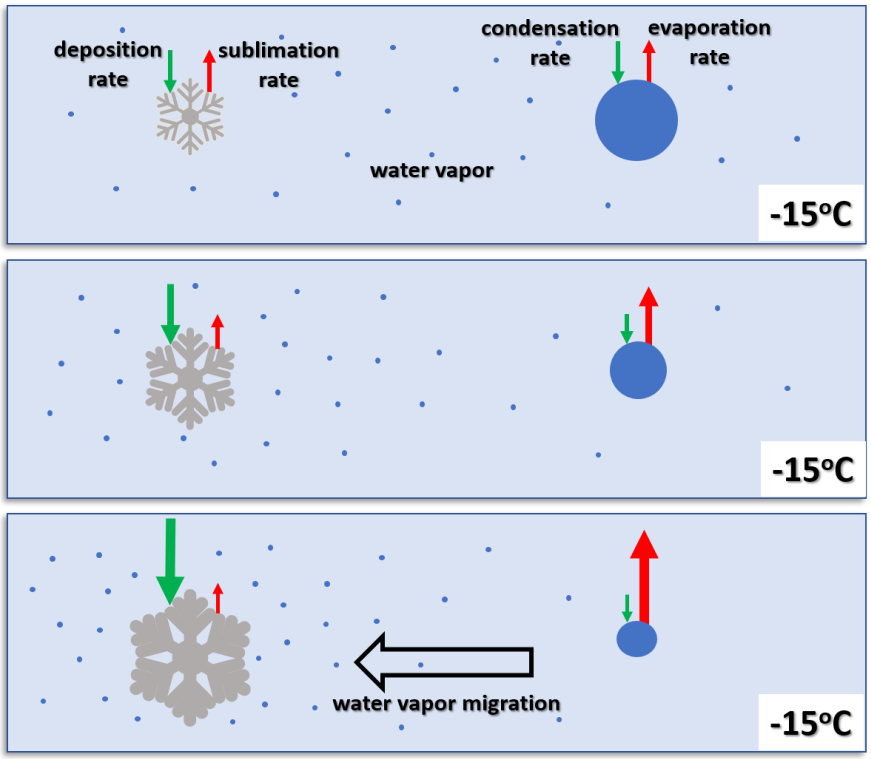

Figure 5-29: Diagram describing the ice process of precipitation.

(top panel) The ice crystal and water droplet are the same size. Water vapor exists around both.

(middle panel) The water vapor is attracted to the ice crystal as it grows and the evaporation rate on the water droplet has increased.

(bottom panel) Most of the water vapor has deposited itself on the ice crystal.

The mixed states of ice, liquid water and water vapor are present in many clouds. The best example of a mixed state cloud is the cumulonimbus, or a thunderstorm. Between 0°C to -40°C a mixture of ice and supercooled liquid droplets and water vapor is present. When the precipitation falls into temperatures above freezing everything melts. While liquid water will not instantly freeze at temperatures colder than freezing, ice does quickly melt in the atmosphere when temperatures are above freezing. Figure 5-30 depicts the states or phases of water in a thunderstorm. Everything colder than -40°C is ice. Everything warmer than 0°C is water or melting ice soon to be liquid.

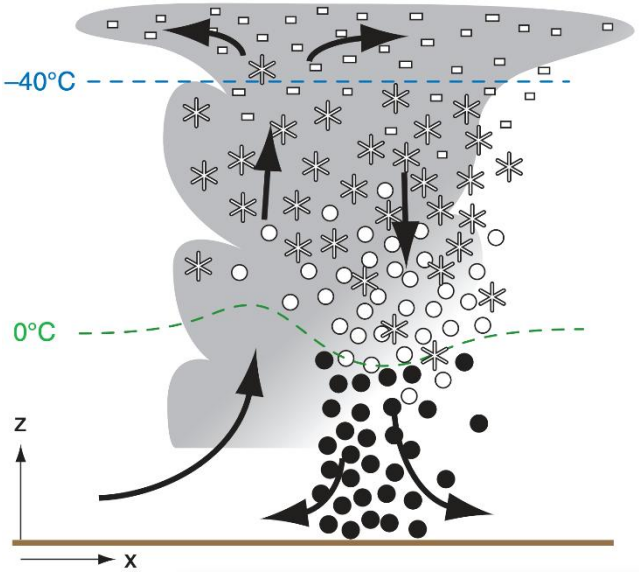

Figure 5-30: The states of water in a thunderstorm cloud.

The ice process of precipitation is also referred to as the Bergeron-Findeisen-Wegener process. T. Bergeron, W. Findeisen and A. Wegener were the researchers working on this theory in the first half of the 1900s. In this textbook, we will refer to it as the ice process of precipitation or just ice process for simplicity.

This video demonstrates the ice process of precipitation in a cloud chamber. The video starts with a chamber of liquid water droplets (about 20-30 μm in diameter) and cools them to -15°C. The droplets remain liquid and are thus supercooled. An ice crystal is introduced into the chamber which rapidly freezes all the supercooled droplets. The ice crystals sparkle as light reflects off of them. This video is best viewed in HD, and only the first 2-3 minutes needs to be viewed to see the ice process of precipitation in action.

5.2.4 – Cold Cloud Riming and Aggregation

As water droplet collide and coalesce in the liquid water environment, collisions between ice crystals and water droplets can occur in a supercooled environment. **Riming** is when water droplets collide with ice and freeze. Riming is also called accretion. **Aggregation** is when ice crystals collide and stick together. Most snow falling to the ground is a collection of ice crystals formed through aggregation and riming. Figure 5-31 depicts all of these collisions that can occur to increase the size of a water droplet or ice crystal.

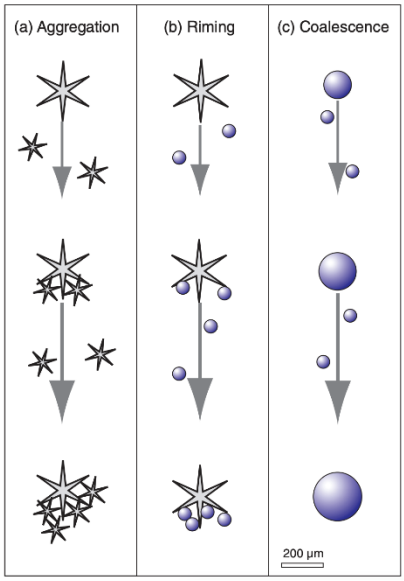

Figure 5-31: Diagram with all the collisions that can occur to increase the size of a water droplet or ice crystal.

Rime ice is a common occurrence in mountain locations. The supercooled water droplets in the cloud come in contact with cold objects on the ground and freeze. The left side of Figure 5-32 is a photo of rime ice on a tree. Riming is most efficient between the temperatures of 0°C to -10°C.

The right side of Figure 5-32 is a photo of aggregation. Additionally, some of the snow crystals in this picture appear to exhibit the effects of riming. All these types of collisions can occur simultaneously and are not mutually exclusive. Aggregation is most efficient with temperatures near 0°C. The liquid water on the outside of ice crystals near freezing increases the bonding when they collide.

Figure 5-32: Rime ice on a tree branch (left photo). Aggregation of snow crystals (right photo).

5.3 - Water (Hydrologic) Cycle

Now that we understand how precipitation occurs, we are going to explore the water cycle from a global perspective.

Most of the Earth's surface (about 70%) is covered with water. Most of this water (about 97%) contains salt and is in the oceans. This amount leaves about 3% of Earth's water as fresh water (without salt). Slightly less than 69% of this fresh water is frozen in glaciers and the polar ice caps. Another 30% is underground which leaves about 1% of this fresh water above the surface in

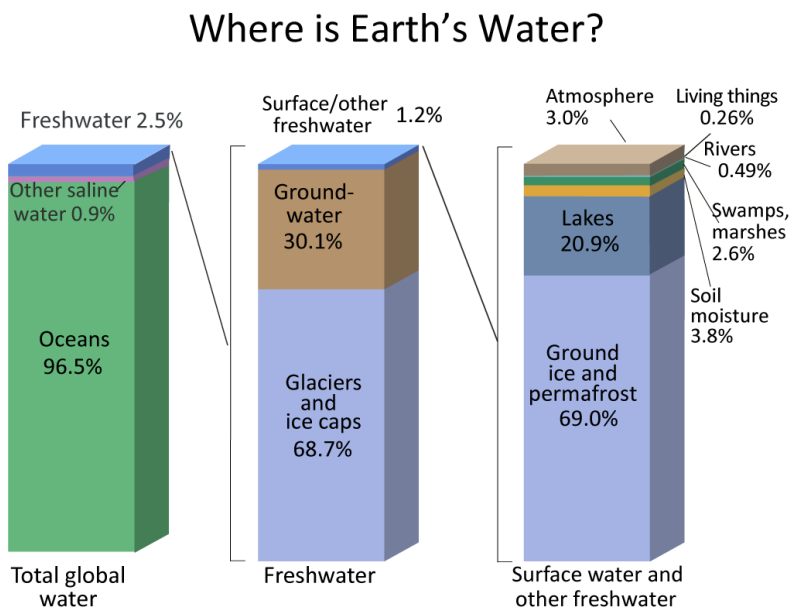

Figure 5-33: Description of where Earth's water resides.

the atmosphere, lakes, rivers and ice on the ground. The percentage of total water in the Earth's atmosphere is about 0.001: only a small percentage compared to the total amount of water on the Earth. Figure 5-33 contains the details of this information in a bar graph format.

Hydrology is the science of water and its global circulation, distribution, and properties. Hence, the water cycle is also frequently referred to as the hydrologic cycle. Figure 5-34 describes this water cycle. Nearly 86% of evaporation originates from the oceans. The remaining 14% originates from the land through transpiration from plants and evaporation from the soil. Plants evaporate water to maintain their temperature which is called transpiration.

Since the oceans cover most of our planet, 78% of global precipitation occurs over the oceans. This leaves 22% of the remaining precipitation occurring over land. Since evaporation from land and plants is 14%, only 8% of the Earth's total precipitation goes into groundwater and surface runoff. Our main interest from an atmospheric perspective is surface runoff, because we would like to know how excess precipitation creates a flood. In this section, we will examine ground water and surface runoff. Subsequent sections in this chapter will look at measuring surface runoff and any flooding that may occur.

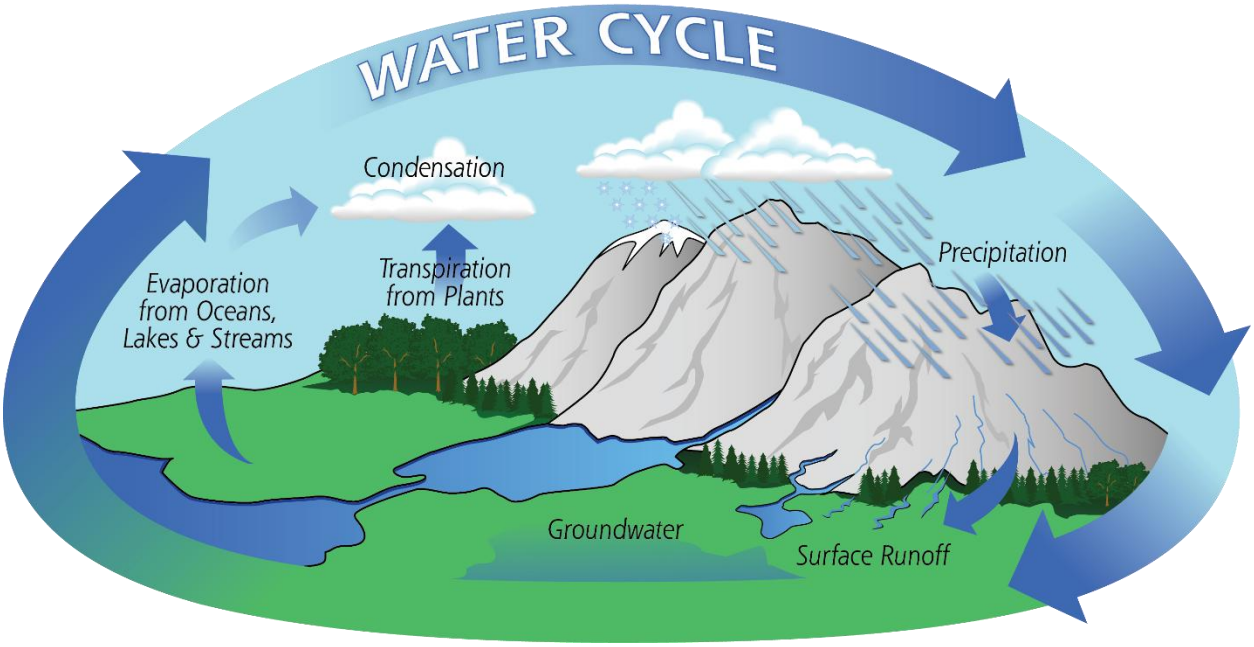

Figure 5-34: A diagram of the water cycle.

5.3.1 – Ground Water

Precipitation can either become groundwater, surface runoff or it can evaporate. This section focuses on groundwater. Groundwater begins when precipitation infiltrates through the soil to a saturated zone. The **water table** is the top of this saturated zone beneath the Earth's surface. Figure 5-35 shows the location of the water table.

The upper layer of the soil is the unsaturated zone, where water is present in varying amounts but does not saturate the soil. Below this layer is the saturated zone, where all of the pores, cracks, and spaces between soil particles are filled with water. The term groundwater is used to describe this area. Another term for groundwater is aquifer. However, the term aquifer is usually

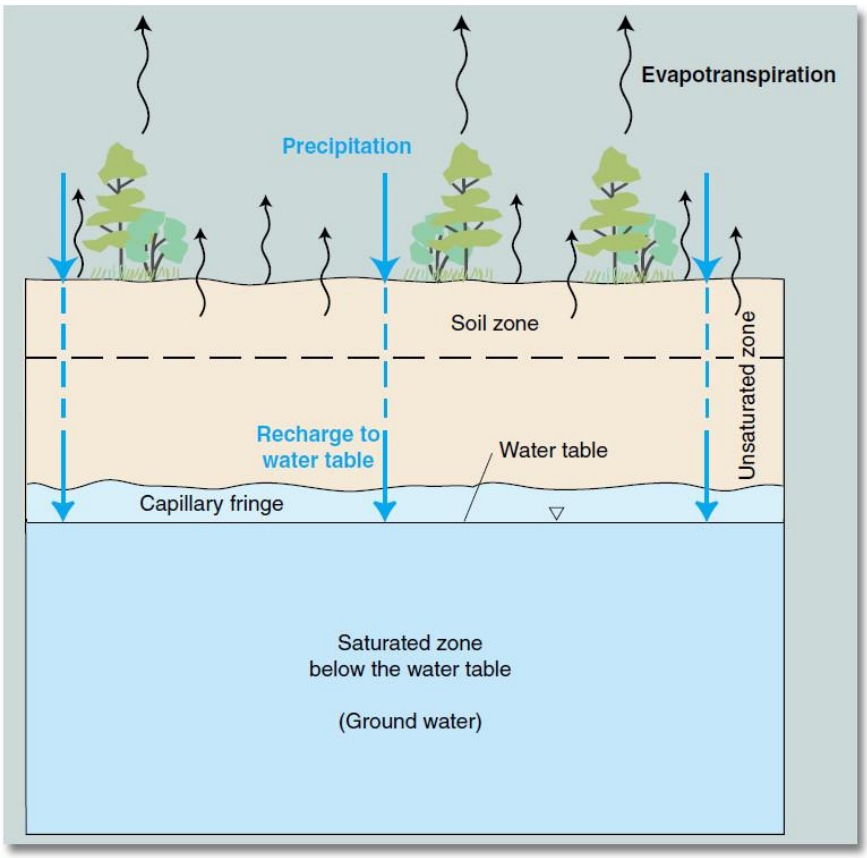

Figure 5-35: Cross section depicting the water table and ground water.

used to describe formations capable of yielding enough water to supply a population. Aquifers are a huge storehouse of Earth's water, which many people depend on in their daily lives. Precipitation and infiltration replenish an aquifer.

If the aquifer is permeable enough to allow water to move through it, then water can be withdrawn from it through wells. The level of the water table changes naturally over time due to changes in precipitation patterns, streamflow and geologic changes, and even human-induced changes.

The pumping of wells can have a big influence on water levels below ground, especially in the vicinity of the well, as shown in figure 5-36. Depending on geologic and hydrologic conditions of the aquifer, the impact on the level of the water table can be short-lived or last for decades. Excessive pumping can lower the water table so much that the wells and nearby streams go dry.

"Base flow" is the sustained flow of a stream in the absence of precipitation. A natural base flow is maintained largely by groundwater. Notice in Figure 5-36 that the water table intersects the top of the stream level. If the pumping well were to continue to lower the water table, the water in the stream would eventually disappear.

Land subsidence occurs when large amounts of groundwater have been withdrawn from certain

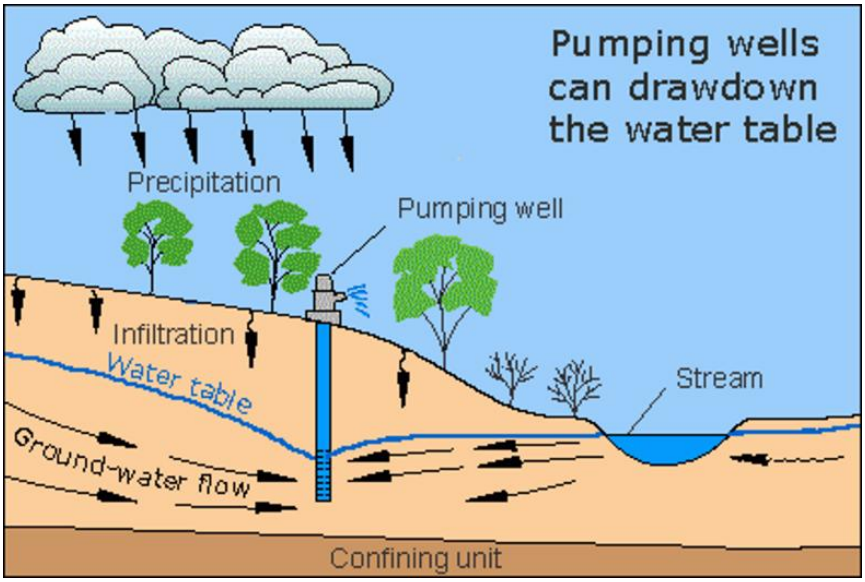

Figure 5-36: Diagram depicting a dropping water table due to a pumping well.

types of sediments. The ground compacts because the water is partly responsible for holding the ground up. When the water is withdrawn, the upper layers fall on themselves. Land subsidence can be difficult to notice, because it occurs over large areas supporting the aquifer. States like California, Texas, and Florida have suffered millions of dollars in damages over the years due to land subsidence.

5.3.2 – Surface Water

When rain occurs, the water can either (1) infiltrate into the soil, (2) evaporate, or (3) flow downhill overland. Overland flow occurs when rain falls on saturated soil or the ground is impervious to infiltration (like an asphalt street). Water always flows downhill under the force of gravity into smaller tributaries, rivers and then usually into a sea or ocean. Figure 5-37 contains an information graphic explaining the various components of a river, from the headwaters into tributaries and the main river channel. Rivers typically exit into an ocean.

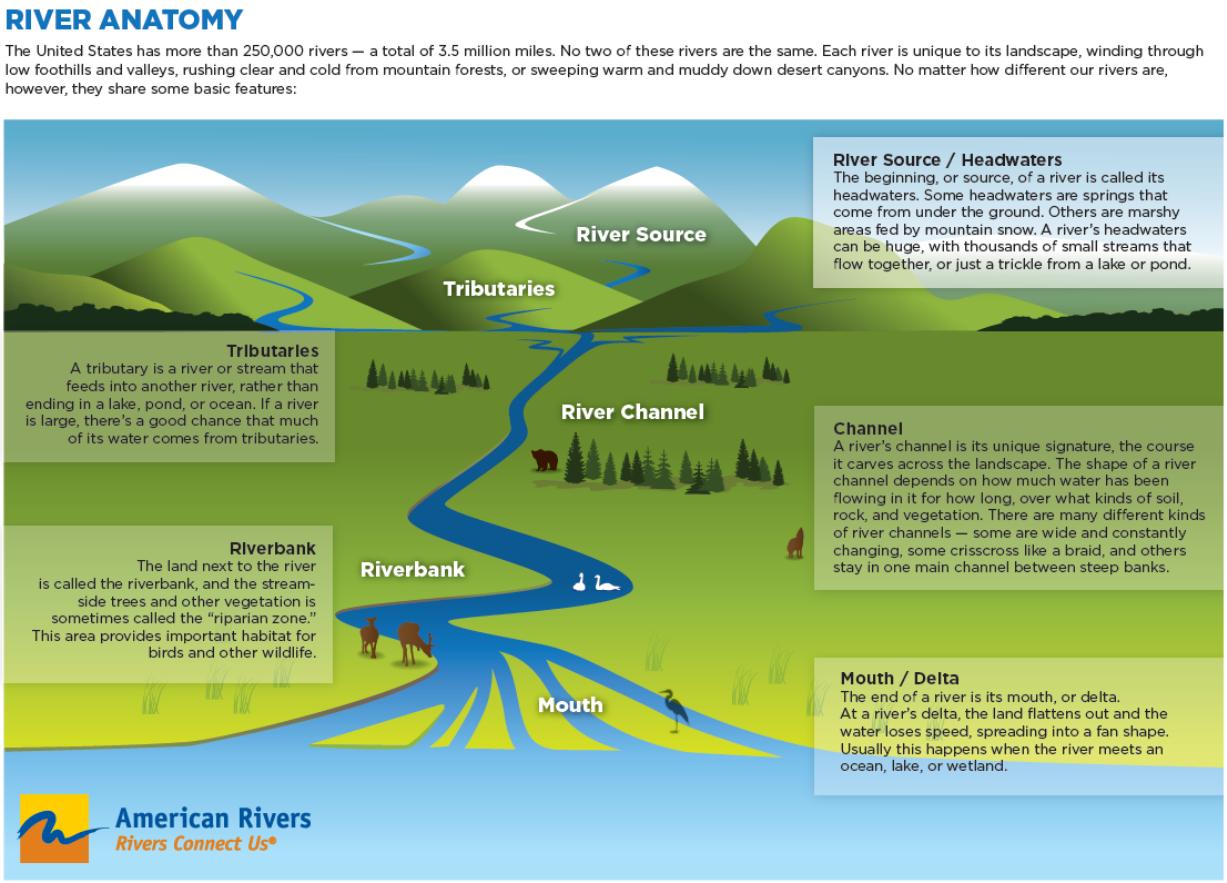

Figure 5-37: Anatomy of a river. Rivers start at the headwaters, flowing through tributaries into the main river channel. Rivers generally exit into a larger body of water (ocean) through their mouth or delta.

A **drainage basin** or **watershed** is an area of land that drains all the streams and rainfall to a common outlet. Drainage basins can be as small as a canyon or as large as a portion of a continent. The map in Figure 5-38 shows the larger watersheds in North America. The top or highest portion of a basin where surface flow first originates is called its headwater. The end or lowest portion of river when it empties into a larger body of water is called the river's mouth or delta.

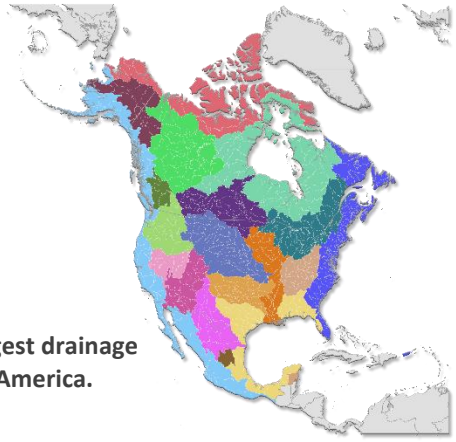

Figure 5-38: The largest drainage basins in North America.

5.4 – Measuring and Tracking Surface Water

Streamflow is the amount of water flowing in a channel. Measuring streamflow is important for multiple reasons:

- To determine how much water is available to supply population and agricultural needs.
- To ensure interstate agreements, compacts and court decrees are met.
- To design transportation facilities (roads, bridges, culverts) and water treatment plants for normal and extreme variations in streamflow.
- To manage power generation facilities in an efficient and optimal manner.
- To plan for floods and flood warning systems.

Measuring streamflow involves three steps:

1. Measure the stage or gage height of the water surface at a location on the river.
2. Obtain periodic discharge measurements at this location. **Discharge** is the streamflow volume passing a location over a given time period.
3. Create a stage-discharge relationship from the data obtained in steps 1 and 2.

The photograph in Figure 5-39 shows U.S. Geological Survey employees obtaining discharge data (step 2) for a river in Montana. This approach works well for a shallow river with light flow that allows a person to stand in the water. For deeper rivers or higher flows, this approach will not work. The remainder of this section examines the details associated with each of these three steps, and how the resulting streamflow data is displayed.

Figure 5-39: Photo of USGS employees taking discharge measurements for a river in Montana.

5.4.1 – Stream Stage (Gage) Measurement

Figure 5-40: A measuring board in a river for obtaining a stream gage measurement.

Stage, sometimes called gage height, can be measured using a variety of methods (step 1). The most basic method is to place a measuring board in the river (Figure 5—40). While easy to implement, this method is not the most accurate as the board decays. Additionally, getting a manual reading of the river height can be hazardous at night or during a flood.

Another common approach is with a stilling well embedded in the riverbank or attached to a bridge pier. Water from the river enters and leaves the stilling well through underwater pipes allowing the water surface in the stilling well to be at the same elevation as the water surface in the river. This approach removes the waves normally observed in a river from affecting the measurement. The stage is measured inside the stilling well. The stage value is stored in an electronic data recorder at a regular interval, usually every 15 minutes. Figure 5-41 shows a cross section of a stilling well along with a photograph of an operational one.

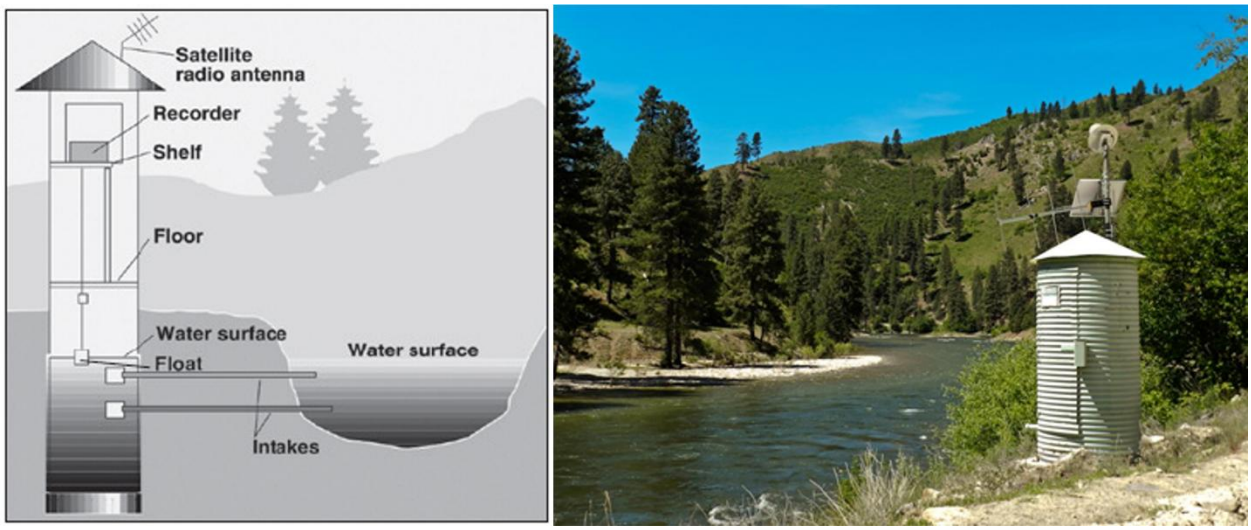

Figure 5-41: A cross section of a stilling well (left) along with a photograph (right) of an operational one.

At some stream gage sites, a stilling well is not feasible or is not cost effective to install. As an alternative, stage can be determined by measuring the pressure required to maintain a small flow of gas through a tube that is bubbled out at a fixed location under the water. The measured pressure is directly related to the height of water over the tube outlet in the stream. As the depth of water above the tube outlet increases, more pressure is required to push the gas bubbles through the tube. This type of stream gage is called a pressure transducer (Figure 5-42).

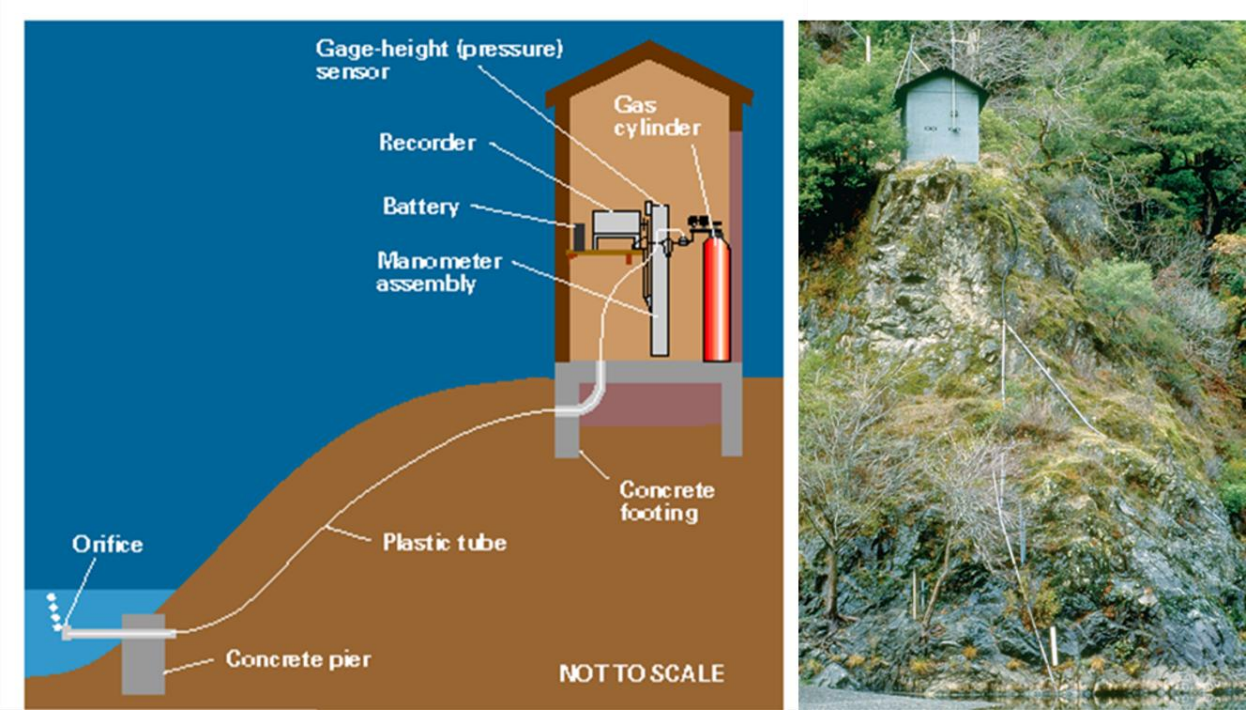

Figure 5-42: A pressure transducer cross section and a photograph of an operational one.

A fourth approach to measuring water level is to use noncontact sensors. These devices use acoustic or light waves that reflect off the water below (Figure 5-43). They are generally mounted to bridges above the water channel. These type of stream gages have fewer moving parts which simplifies long-term maintenance. Noncontact sensor gages are widely used in portions of the U.S.

Figure 5-43: A photograph of a noncontact sensor gage.

Stage at a stream gage must be measured with respect to a constant reference elevation, known as a datum. Sometimes stream gage structures are damaged by floods or can settle over time. To maintain accuracy, the elevations of gage structures are routinely surveyed relative to permanent elevation benchmarks.

Although stage is valuable information, most people are interested in streamflow or discharge. However, it is not practical for a stream gage to continuously measure discharge. Fortunately, there is a strong relation between river stage and discharge, and a continuous record of river discharge can be determined from the continuous record of stage. Determining discharge from stage requires defining the stage-discharge relationship by measuring discharge over a wide range of river stages.

5.4.2 – Discharge Measurements

Discharge is the volume of water moving down a stream or river per unit of time, commonly expressed in cubic feet per second. In general, river discharge (step 2) is computed by multiplying the area of water in a channel cross section by the average velocity of the water in that cross section. An illustration describing this discharge equation is in Figure 5-44.

discharge = area x velocity

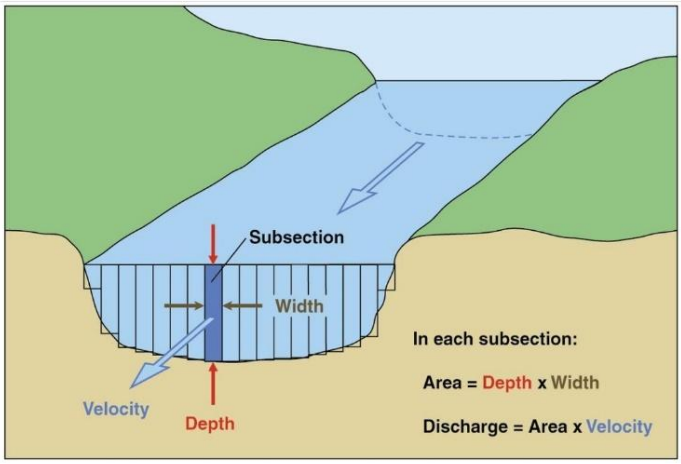

Figure 5-44: An illustration for determining discharge in a river. The river area equals the depth times the width. The discharge equals this area times the water velocity.

The most common method used for measuring velocity is with a current meter (Figure 5-45, left side). The current meter is used to measure water velocity at predetermined points (subsections) along a marked line, suspended cableway, or bridge across a river. The depth of the water is also measured at each point. These velocity and depth measurements are used to compute the total volume of water flowing past the line during a specific interval of time.

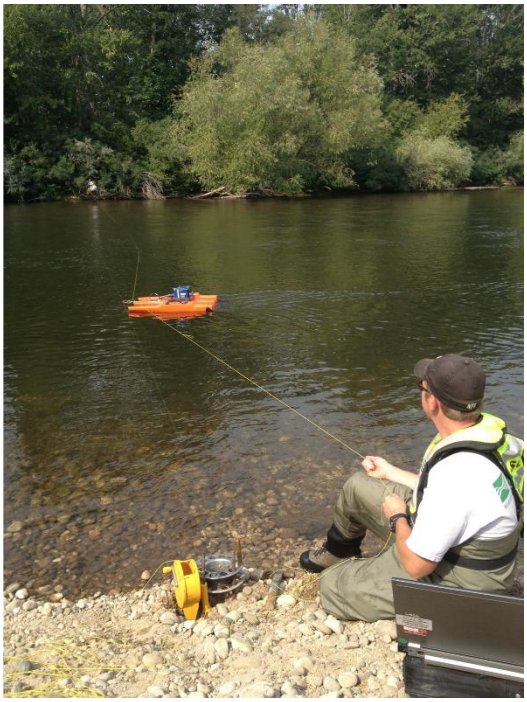

Figure 5-45: Devices used to measure discharge in a river. Left side is a current meter. Right side is a Doppler current profiler.

Another method to measure the discharge is with an acoustic Doppler current profiler. The Doppler Effect is the phenomenon we experience when passed by a car or train that is sounding its horn. As the car or train passes, the sound of the horn seems to drop in frequency. The profiler is mounted on a small watercraft with its acoustic beams directed into the water. The profiler is then guided across the water surface to obtain measurements of velocity and depth (Figure 4-45, right side).

With stage height and discharge measurements taken, the stage-discharge relationship (step 3) can be created, and is called a rating table or curve.

5.4.3 – Rating Table (Curve)

Stream gages continuously measure stage (step 1). This continuous record of stage is translated to river discharge by applying a stage-discharge relationship (also called rating). A **rating table** or **rating curve** contains the relationship between stream gage height and discharge. The difference between a rating table and a rating curve is the first one is a table of data, the second one is a graph of the data. Both a rating table and a rating curve contain the same information in a different format.

Rating tables are developed for stream gages by physically measuring the flow of the river with a mechanical current meter or acoustic profiler at a wide range of river heights (step 2). For each measurement of discharge there is a corresponding measurement of stage (step 3). Special effort is made to measure extremely high and low stages and corresponding flows because these measurements occur less frequently. The stage-discharge relation depends upon the shape, size, slope, and roughness of the channel at the stream gage location and is different for every gage. Unfortunately, river channels are continuously changing through erosion, deposition of soil materials, vegetation and other debris. This situation causes a need to continually take new discharge measurements, which ensures the most accurate information is available.

Figure 5-46 depicts a rating curve. A rating curve relates the stage to discharge. Stage is on the y-axis and discharge is on the x-axis.

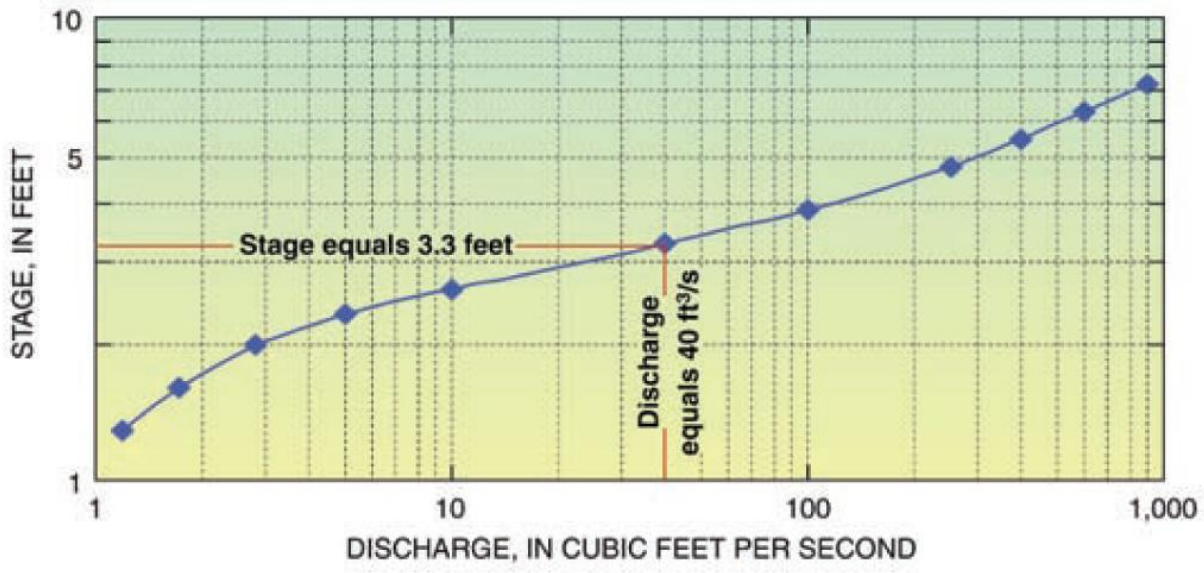

Figure 5-46: A graph of river stage height and discharge, which is called a rating curve.

Stage heights are continuously available for rivers. With a rating curve, discharges are continuously available too. In this example (Figure 5-46), a stage height of 3.3 feet equals a discharge of 40 cfs. River flow is expressed as cubic feet per second (cfs) in the United States. A cubic foot is about the size of a basketball. Hence, 40 cfs visually would have 40 basketballs passing this location on the river every second.

Much like weather data, real-time river data is available in the United States. This web site has the current river flows for the entire U.S. The surface runoff from precipitation is being tracked just like the precipitation itself.

5.4.4 – Hydrographs

A **hydrograph** is a graph that shows changes in discharge or river stage over time. Figure 5-47 shows a hydrograph (solid line) along with the precipitation (bar graphs) that caused the creek to rise.

A hydrograph always has time on the x-axis. This hydrograph has discharge on the left side of the y-axis, and precipitation amounts on the right side. The precipitation amounts allows us to see how fast the river flow changes when precipitation occurs. The maximum precipitation occurred at about 6:00 am. The highest flow in the creek occurred around 9:30 am. Over three hours lapsed between the time of the highest rainfall rate and the peak in streamflow. A peak discharge after a precipitation event is called a **crest**. If several high precipitation amounts occur, then several crests in the river may also occur. Every river has different characteristics for how fast it reacts to precipitation and how fast a crest flows downstream.

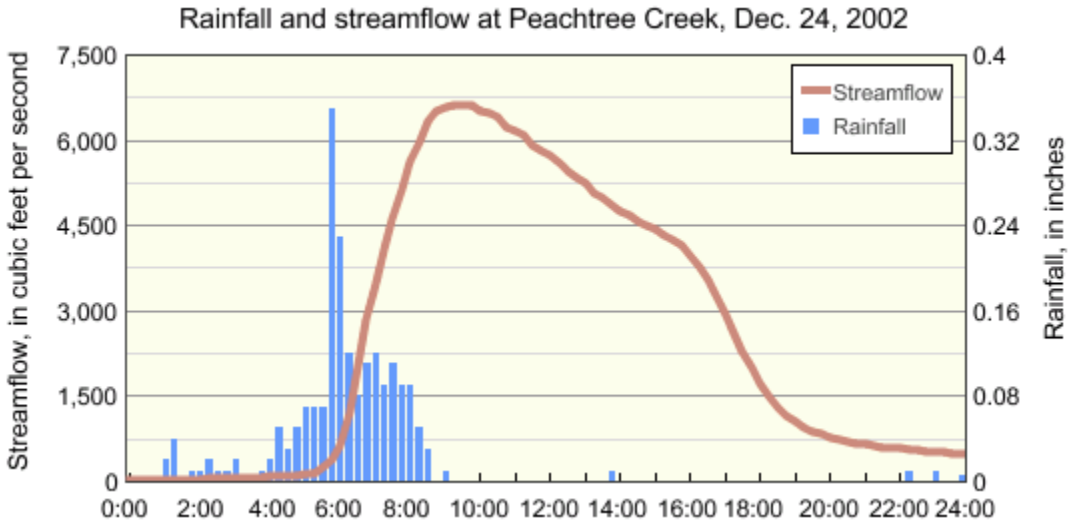

Figure 5-47: A hydrograph shows the discharge (streamflow) of a river over time. This hydrograph has precipitation in the bar graphs to indicate the lag between precipitation and discharge changes.

Figure 5-48 is a hydrograph for the Santa Cruz River at the Cortaro Farms Road bridge in Tucson, Arizona. This hydrograph has gage height on the left side rather than discharge. In early October 2014, the remnants of Hurricane Norbert provided precipitation across the Santa Cruz Basin. The water level rose about 3 feet due to this precipitation. Additionally, two crests are shown which are due to two episodes of heavier precipitation.

Another aspect to notice about Figure 5-48 is the red line at about 6.3 feet. This red line indicates essentially the bottom of the river channel. Most people assume a stage or gage height starts at the bottom of the channel and measures up. That assumption is frequently incorrect, because the bottom of the channel is not designated as zero. Never assume the bottom of the channel starts at zero for any gage location. In this example, the Santa Cruz River normally has about a foot to a foot and a half water at this location, not 7 feet.

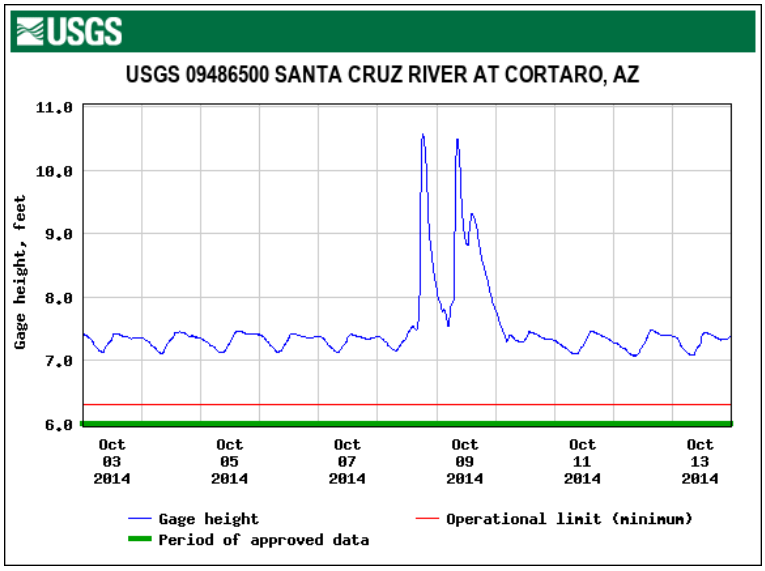

Figure 5-48: A hydrograph at the Santa Cruz River in Tucson, Arizona for early October 2014.

The last aspect to notice in Figure 5-48 is the diurnal variation in the flow. Much like temperatures in weather, the water level goes down to a minimum and up to some maximum during a day. These changes occur naturally based on evaporation, groundwater flows, snow melting or other local conditions.

5.5 – Floods

A **flood** is the flow of water onto land adjacent to a river, stream, lake or ocean not normally covered by water. A flood plain is a strip of relatively flat and normally dry land along a river that is covered by water during a flood. All major rivers have a flood plain somewhere along a portion of their channel. The flood plain can be seen as a low area next to the river. Many times, flood plains are used for farming, since the land in very fertile in a flood plain. If a flood occurs, crops will be lost but can be regrown which is easier than replacing flooded structures.

Two conditions are responsible for many floods. These conditions are (1) saturated soils and (2) excessive precipitation. The saturated soils are associated with increased surface runoff, because water cannot infiltrate into the ground. The excessive precipitation is essentially an abundance of water in the basin.

When flooding is forecast to occur or is occurring, three questions arise from those impacted:

1. How deep with the water get?
2. What areas will be flooded?
3. When will the flood crest or crests arrive?

Historical information on past floods associated with a river are essential to answering these questions. River gages, rating tables, and hydrographs provide a portion of this historical information. Another critical piece of information are high water marks. After a flood, hydrologists often visit streams to check for high-water marks. If, for example, records show that the stage reached 17 feet during a storm, a high-water mark will show the hydrologist what was

affected by that amount of water. High water marks can be used to estimate how much land alongside a stream will be inundated at various stream levels. These facts are valuable in developing maps showing the impact of floods on the adjacent landscape, structures, and people. Figure 5-49 is a photo of a high-water mark.

Figure 5-49: Photo of a high-water mark created during a flood.

Maps designating areas which will be flooded at various river stage heights are called inundation maps. Figure 5-50 illustrates an inundation map and the areas affected by the flood are highlighted in blue. The hydrograph on the left has both observed and forecast data. As the stage height rises, larger areas near the river are flooded.

Inundation maps take time and abundant data to develop. Many communities partner with government agencies to create these maps. However, most rivers do not have them. For this reason, a statistical approach is used to define the flood magnitude as a frequency of occurrence. Trying to place a context associated with a flood is where terms such as a "100-year flood" came into being. A 100-year flood is a flood that has a 1% chance of happening every year. Another way to state a flood frequency is a 100-year flood has a 1 in 100 chance of happening every year.

Statistical techniques, through a process called frequency analysis, are used to estimate these recurrence intervals. Recurrence intervals can be calculated for any type of event, such as rainfall over a certain amount, or snow accumulation, and of course flood intervals.

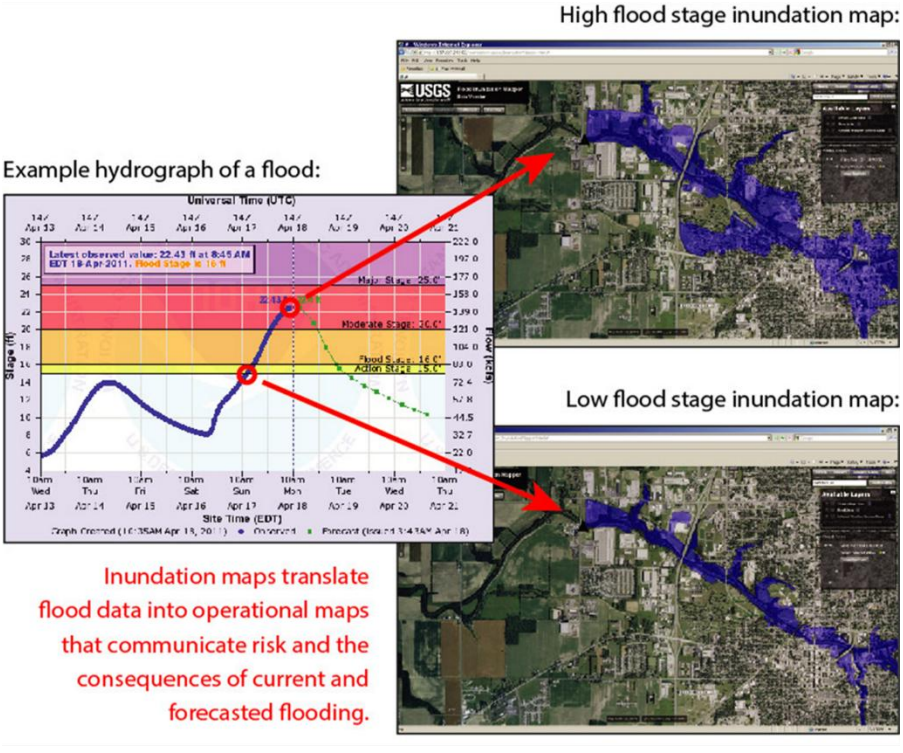

Figure 5-50: Inundation maps for both a high and low flood stage (right side). A hydrograph indicating the stage these flood levels occur (left side).

5.5.1 - Recurrence Intervals

You may never have heard of "recurrence interval", but the terminology associated with it may still be familiar to you. When a major flood occurs, terms like “the river reached the 100-year flood level" are used. This term means that a flood of that magnitude has a 1 in 100 chance of occurring in any year or a 1% chance of occurring every year.

Two pieces of information are needed to calculate a recurrence interval for a river:

- The number of years that records were taken (N).
- The number of flows above a certain level that occurred during this period of time (M).

A recurrence interval (RI) tells a person the number of years between when a flow of a certain magnitude is expected to occur. The equation to calculate a recurrence interval is:

$$\text{Recurrence Interval (RI)} = (N + 1) / M$$

N is found by taking the last year of records and subtracting the first year of records. M is found by listing the highest annual peak flows from the highest to the lowest. The highest annual peak flow is labeled “1”, the second highest is labeled “2”, and so on down to the lowest annual peak flow. Put these numbers into the equation to get RI.

The plus one (+1) is needed because when the last year of observations is subtracted from the first year of observations, a year is lost. For example, if we have ten years of records (1, 2, 3, 4, 5, 6, 7, 8, 9, 10) subtracting the last year from the first year (10 - 1) only gives us 9 years. However, we actually have 10 years of data which is 9 + 1 or N + 1.

Streamflow recurrence intervals are based solely on the magnitude of the annual peak flow or the highest flow occurring on a river in one year. Ten or more years of data are required to perform this type of frequency analysis. More confidence can be placed in the results of an analysis that has more years of data. A recurrence interval analysis with 100 years of data is much, much better than one with only 10 years of data.

The units for a recurrence interval are years, which is the number of years between floods of the specified magnitude to occur. The probability that a flood will occur is given by this equation:

$$\text{Probability} = 1 / RI \times 100\%$$

Will a 10-year flood occur once every 10 years? The answer to this question is “no”. On average a 10-year flood will occur once every 10 years, but the floods are rarely spaced exactly 10 years apart. Figure 5-51 shows the incidence of the 10-year flood for the Embarras River at Ste. Marie, IL. The magnitude of the 10-year flood was determined through a recurrence interval analysis to be approximately 31,100 cubic feet per second (cfs). The variability in time between "10-year floods" ranges from 4 to 28 years. The average of these intervals is about 10 years. Figure 5-51 highlights the irregularity of a 10 year flood.

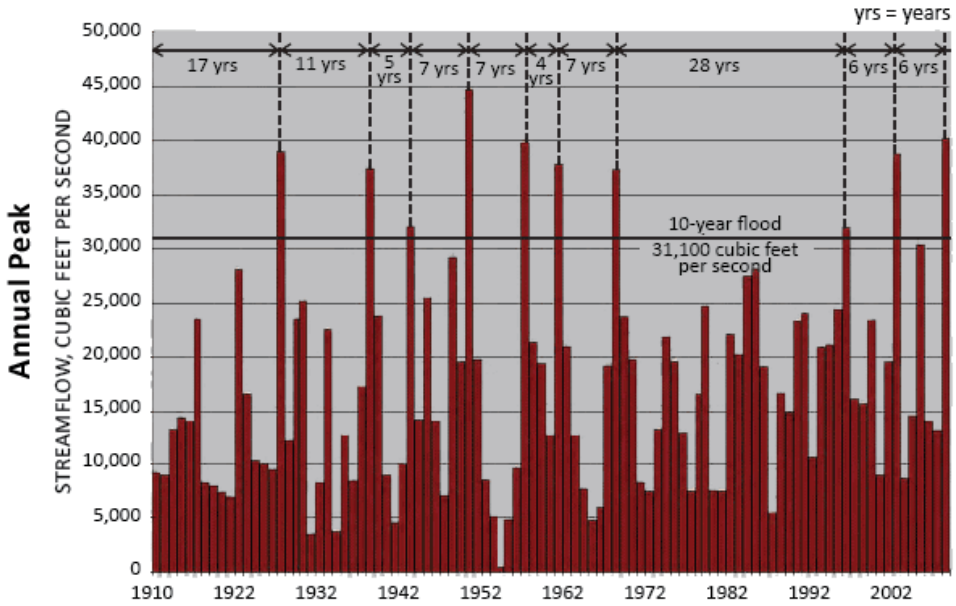

Figure 5-51: Bar graph for the annual peak flow for the Embarras River at Ste. Marie, Illinois versus time.

5.5.2 – Basin Changes Affecting Floods

Drainage basins and rivers are in a constant state of change, and the data associated with a river system needs to be constantly updated for accuracy. Common changes that affect flooding or annual exceedance probabilities are:

1. Additional river flow data becomes available.
2. Installation of flood controls like a dam or reservoir.
3. Urbanization of the drainage basin.

Every year new stage data becomes available for a river. As mentioned previously, a longer data set is much better than a shorter one. Over many years, this larger data set will allow better statistical analysis calculations. The peak annual streamflow graph in Figure 5-52 shows the first 20 years (1903 to 1922) of data has a 100-year flood of about 70,000 cfs. Enlarging this data set to over 100 years (1903 to 2008) indicates a 100-year flood is now closer to 85,000 cfs. The one flood in 2008 with 140,000 cfs significantly changed the statistical analysis.

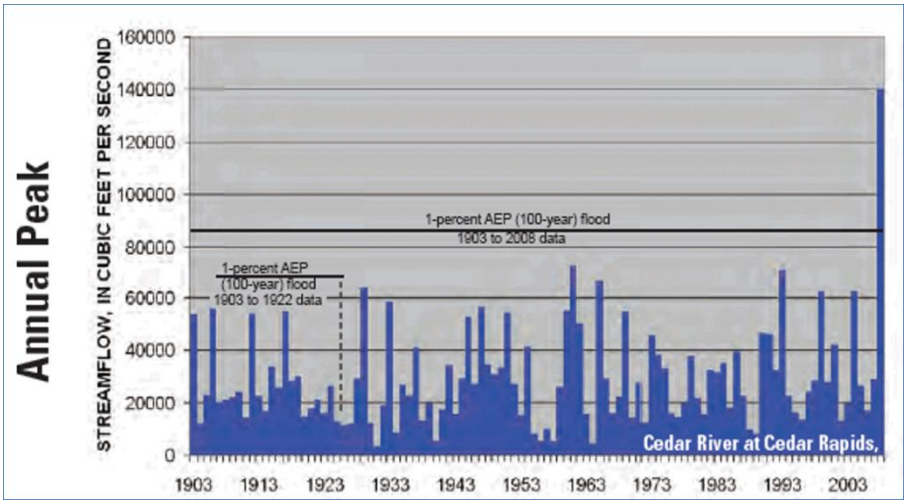

Figure 5-52: A longer data set provides better analysis as shown. A 100-year flood using the first 20 years of data is much different than an analysis with 100 years of data.

Urbanization of a river basin increases the amount of impervious surfaces present. Impervious surfaces like roads, parking lots and buildings causes surface runoff to occur faster and to increase in volume. A hydrograph will depict urbanization changes by (1) shortening the time between when precipitation fell and the flow crested in the river, and (2) increasing the height of the crest. Both of these changes occur because precipitation infiltration is inhibited. Figure 5-53 shows the effects of urbanization on a 100-year flood. The urbanization of Urbana, Illinois (near Chicago) almost doubled the magnitude of a 100-year flood since the 1960s.

The implementation of flood control structures, such as dams or reservoirs, significantly changes the flood characteristics of a river system. When flood waters flow downstream and enter a dam, the flood essentially stops. This aspect of flood control must be considered when managing the amount of water in a dam. These structures frequently serve as both flood control and sources of water supply. The flood control aspects would like the dam to be empty when flood water arrives. The water supply aspects would always like the dam full. Hence, water managers must consider these competing priorities when storing or releasing water. Figure 5-54 shows the flow changes associated with building flood control structures in the 1960s in Auburn, WS. These structures reduced the magnitude of a 100-year flood from 28,000 cfs to less than 15,000 cfs.

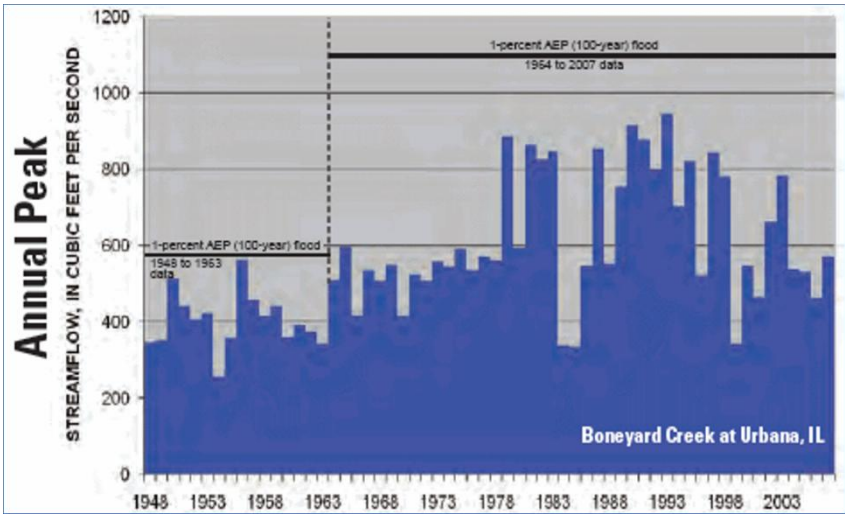

Figure 5-53: Change in a 100-year flood due to the ubanization of a basin. Urbanization shortens the time between when precipitation falls and the flow crest, and increases the height of this crest.

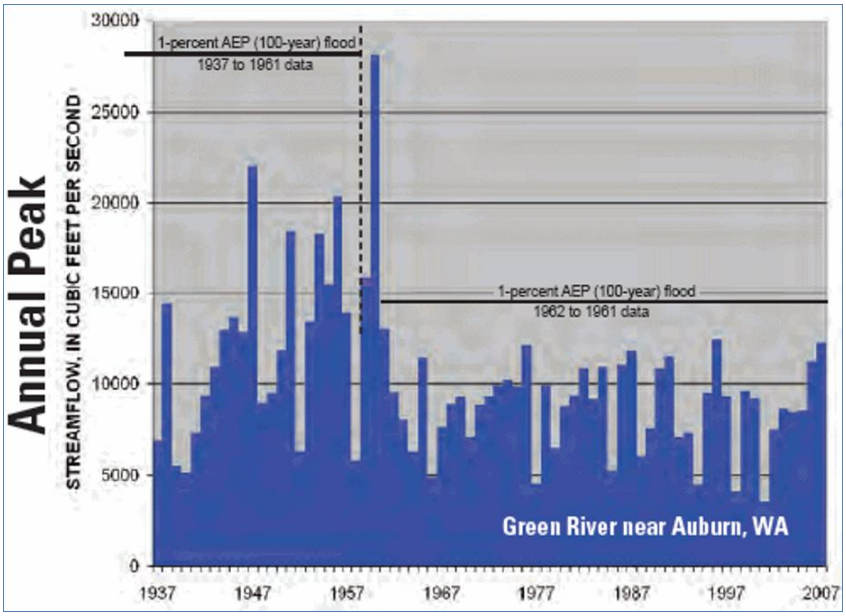

Figure 5-54: Change in a 100-year flood due to the construction of flood control structures (dams and reservoirs).

Chapter 5 Review Questions

1. What two characteristics define all types of clouds?
2. High clouds composed primarily of ice crystals are in what category?
3. Clouds that have precipitation originating from them are in what category?'
4. Describe the appearance of a cumulonimbus cloud.
5. Why does the ice process of precipitation have the fastest droplet growth?
6. What is the maximum size of a collector drop?
7. What determines the shape of an ice crystal?
8. At what temperatures is the ice process of precipitation most efficient?
9. What is the water table?
10. What percentage of Earth's total precipitation goes into groundwater and surface runoff?
11. What percentage of Earth's total water is in the atmosphere?
12. What is an area of land that drains the streams and rainfall to a common outlet called?
13. How is a river stage (height of the water in a river channel) used to determine the flow in the river?
14. What is the streamflow volume passing a location over a given time period called?
15. What is the definition of a hydrograph?
16. What is required to measure flow in a river?
17. What are two common conditions responsible for a flood?
18. How does urbanization change a hydrograph?
19. How is a flood defined?
20. What is the definition of a 100-year flood?

Chapter 6 - Global Circulations

Overview

This chapter starts putting together our knowledge of the atmosphere to better understand weather systems. The global circulation is examined first, and how air moves from the tropics to the poles. The concept of air masses is defined and how they move and interact. The midlatitudes, latitudes between 30° and 60°, are where air masses collide. The boundaries between these air masses creates fronts. The Norwegian Cyclone Model is discussed. This conceptual model explains the life cycle of these fronts, and the weather associated with them.

Chapter objectives:

1. List the terms used to describe the spatial scales of weather phenomena.
2. Describe the three-cell model of atmospheric general circulation.
3. Describe synoptic scale phenomena.
4. Describe the types of air masses and explain how they form.
5. Identify the types of fronts and their characteristics, such as the cloud and weather conditions associated with a front.

6.1 – Concept of Scale

Scientists who study the atmosphere must be aware of both the spatial and time scale of the weather phenomena being examined. The larger the area affected by a weather system, the longer time this system takes to move or change. An example would be the persistent global circulation patterns observed around the Earth. Smaller systems have the opposite characteristics. An example would be a thunderstorm, which can be “born”, wreak havoc and decay within several hours, but only affect a neighborhood within a city.

The largest scale is called global scale. **Global scale** features affect the entire Earth or a hemisphere and are persistent year after year. Any changes occurring on a global scale are usually related to the seasons. A persistent global scale weather feature are the trade winds in the tropics and subtropics from the equator to about 30° latitude. Trade winds are the easterly surface winds that exist in both the Northern and Southern Hemisphere. Commerce relied on the trade winds for hundreds of years prior to the invention of the steam and internal combustion engines. Even today the trade winds are a factor when navigating the tropics.

The next size scale is synoptic scale. **Synoptic scale** covers a portion of a continent and persists from several days to several months. The cyclones and troughs associated with a winter storm are a classic synoptic scale weather feature. When examining a surface weather map, the annotation of fronts are synoptic scale features. Figure 6-1 depicts synoptic scale surface fronts across the Atlantic Ocean and Europe.

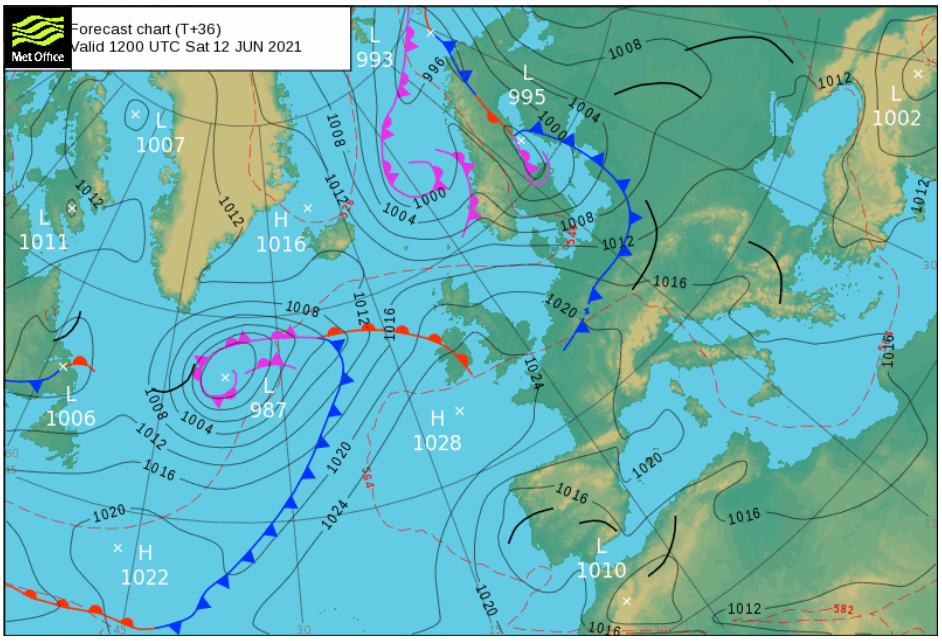

Figure 6-1: A synoptic scale weather map with surface fronts. The colored lines with half circles and triangles depict the front locations.

The smaller scale is called the mesoscale. **Mesoscale** phenomena cover from a few to several hundred kilometers and may last up to a day. Other terms which may be used when examining these smaller scales are microscale (2km or less) and misoscale (4 km or less). A thunderstorm is a mesoscale phenomenon. Strong winds exiting a thunderstorm are called a microburst, which is based on these smaller scales nomenclature. Microburst wind damage with estimated wind speed over 100 mph is shown in Figure 6-2.

Figure 6-2: Microburst wind damage that toppled two trees. Notice the surrounding trees and mailbox remain.

6.2 – Global Scale

A spatial imbalance between radiative inputs and outputs exists on the Earth. The Earth loses energy at all latitudes due to outgoing longwave radiation. Near the tropics, more solar radiation enters than leaves. Near the poles more radiation leaves than is received. The result is differential heating, creating warm equatorial air and cold polar air. This imbalance drives the global scale general circulation of wind which is unceasing. Figure 6-3 illustrates this imbalance in temperatures.

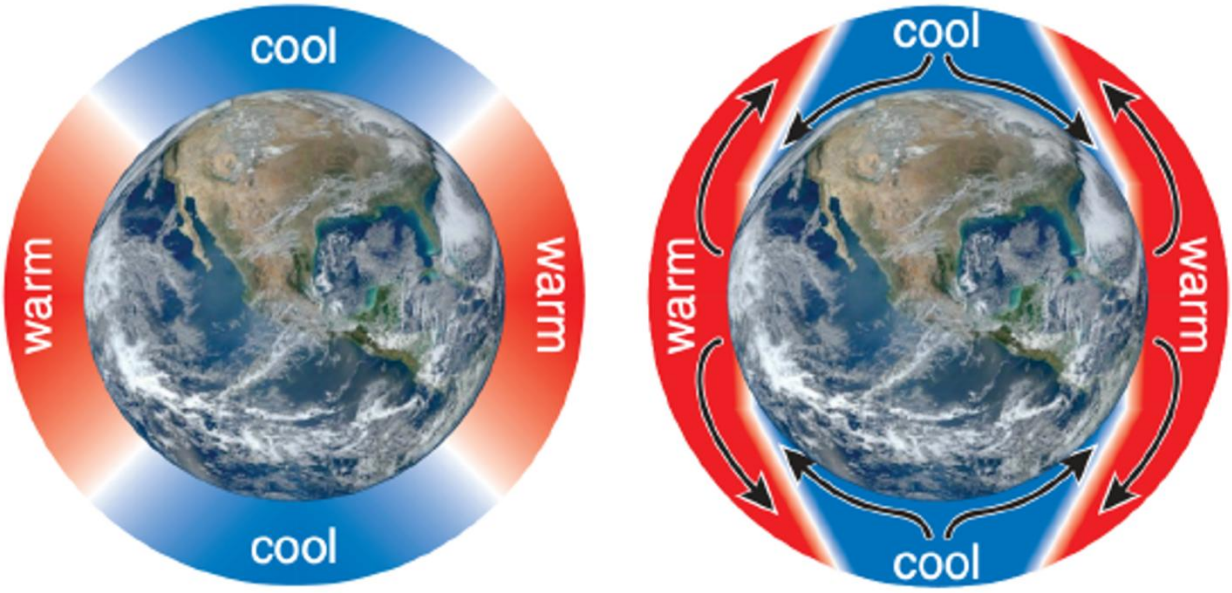

Figure 6-3: Illustration of the imbalance in temperatures between the tropics and poles. This imbalance drives the global circulation.

People have known about the cold north and warm tropics for a long time. A simple concept to equalize these temperatures is to move the cold air south and the warm air north. When buoyancy is considered, the warm air would be aloft and the cooler air near the surface.

In 1735, George Hadley understood that solar radiation drives all weather. He proposed that the surplus of heating at the equator would flow towards the poles. This single-cell migration of energy in both hemispheres was proposed to explain the trade winds. The Hadley cell or the single-cell model was trying to take this differential heating and balance it, while fitting in the observations of the trade winds and rising air near the equator.

In 1856, William Ferrel proposed a circulation in the midlatitudes with westerly winds as the middle of three circulation cells in each hemisphere. This three-cell model is in use today and is described next.

This first video from the United Kingdom Met Office explains the causes of the global circulation.

6.2.1 – Three-cell Model

The three-cell model has three meridional circulations in both the Northern and Southern Hemisphere. Figure 6-4 illustrates the three-cell model.

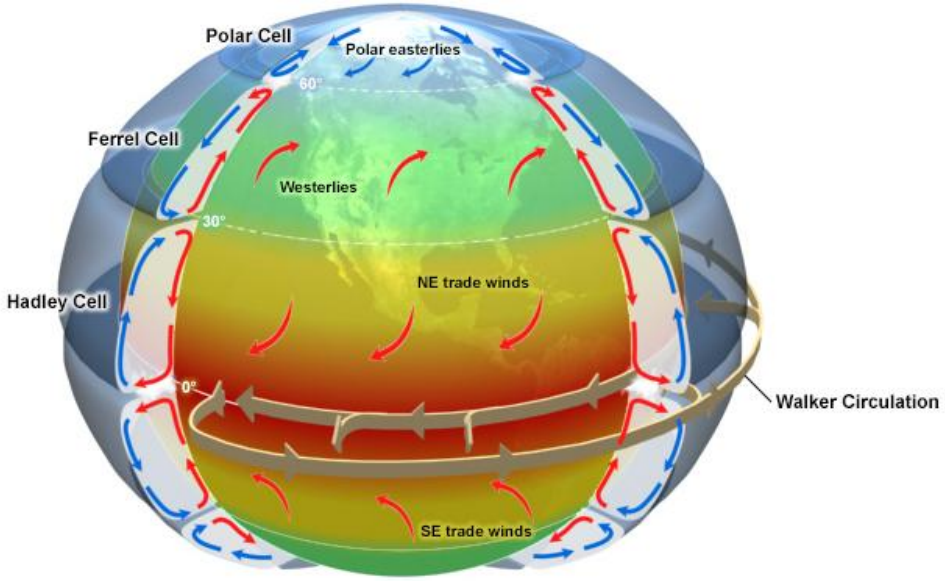

©The COMET Program

Figure 6-4: The three-cell model of Earth's general circulation. The wind pattern in each cell (Hadley, Ferrel and Polar) are shown with the relative temperatures colored as red (warm) or blue (cool).

The **Hadley cell** circulates air between the tropics and subtropics (0º to 30º latitude). The **Ferrel cell** circulates air in the midlatitudes. The midlatitudes extend from 30º to 60º latitude. The weak third circulation cell from 60º latitude to the pole is called the **polar cell**. Before examining these cells in more detail, two new terms must be introduced. **Zonal flow** occurs when the wind is parallel to the latitude lines. Zonal flow describes winds in an east or west direction. **Meridional flow** occurs when the wind is parallel to the longitude lines or meridians. Meridional flow describes winds in a south or north direction as illustrated in Figure 6-5.

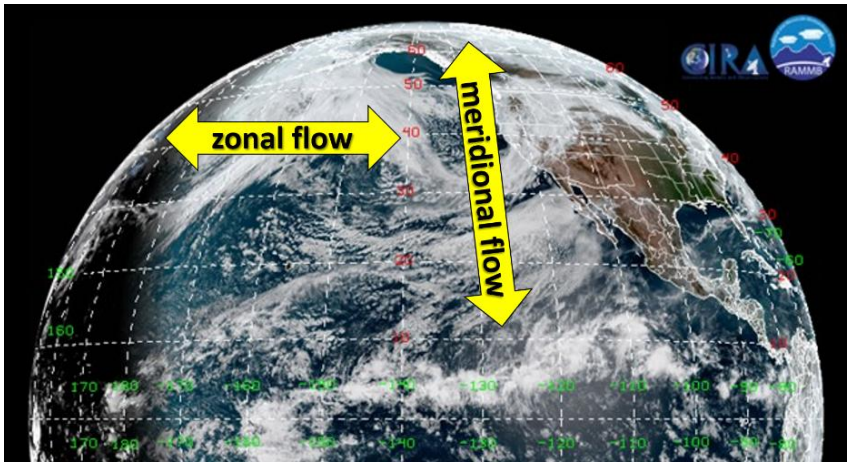

Figure 6-5: Illustration of meridional and zonal flow. Meridional flow crosses latitude lines (meridians) and zonal flow crosses longitude lines.

Associated with these cell circulations are regions of upward and downward air motions. Near the equator where the Hadley cells from each hemisphere collide is a region of upward motion. The pressure gradient force is active in all of these air motions. Thus, a region of ascending air is physically linked to a persistent surface low pressure. Where the Ferrel and Hadley cells meet near 30° is associated with descending air and a persistent surface high pressure. Where the Ferrel and polar cells meet is another area of ascending air and another low surface pressure. Figure 6-6 illustrates these regions of vertical air motion between the cells.

Figure 6-6: Vertical air motions between the three general circulation cells. Slanted yellow lines are downward moving air. Slanted blue lines are upward moving air.

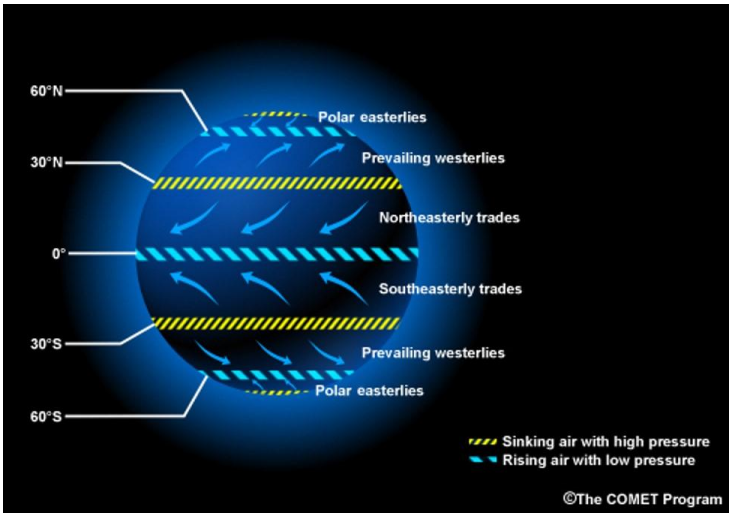

On a hypothetical planet with no contrast between the land and oceans, the long-term average winds would closely resemble the three-cell model. Actual winds on any day may differ due to transient weather systems, but the long term average would remain intact. Seasonal variations would still be present as the temperature contrasts shift north and south.

This second video from the United Kingdom Met Office further describes the global circulation on our rotating planet.

6.2.2 – Hadley Cell and the ITCZ

The Hadley cell consists of hot air rising near the equator. This rising air forms a low pressure at the surface called an equatorial low. After the air rises, it moves poleward and eventually descends around 30°. This area of descending air is called the subtropical high since a persistent surface high pressure resides at this latitude. To complete this circulation, surface winds move from 30° back towards the equator. This circulation forms a convection cell that dominates the tropical and sub-tropical regions.

The Coriolis force turns these large scale air movements towards the right in the Northern Hemisphere. Surface winds in the Northern Hemisphere are from the northeast and from the southeast in the Southern Hemisphere. These winds are referred to as the Trade Winds due to their extensive use by sailing ships crossing the oceans.

The equatorial low assists in creating a convergence area associated with thunderstorms and heavy precipitation called the **intertropical convergence zone (ITCZ)**. The ITCZ roughly forms a band that circumnavigates the Earth near the equator where the northeast and southeast trade winds from each hemisphere converge. Sailors have often referred to this area as the

doldrums due to its generally light winds. Yet, the ITCZ is an important part of the global circulation as it forms the ascending branch of the Hadley circulation. This entire pattern is driven by incoming solar radiation, which peaks near the Equator.

This rising moist air in the convergence zone condenses and releases latent heat, which further drives the upward motion. Locations under the ITCZ can experience some of the heaviest rainfall rates on Earth. Clouds and precipitation form, revealing the ITCZ as a band of rainfall that wraps around the Earth near to the Equator. Figure 6-8 is a satellite precipitation estimate from NASA, and highlights the ITCZ well. The precipitation values are in mm per hour and the red band is associated with the ITCZ.

Figure 6-7: Three-cell model with the high and low pressure areas between the cells highlighted. The Intertropical Convergence Zone (ITCZ) results from the convergence of the northern and southern Hadley cells.

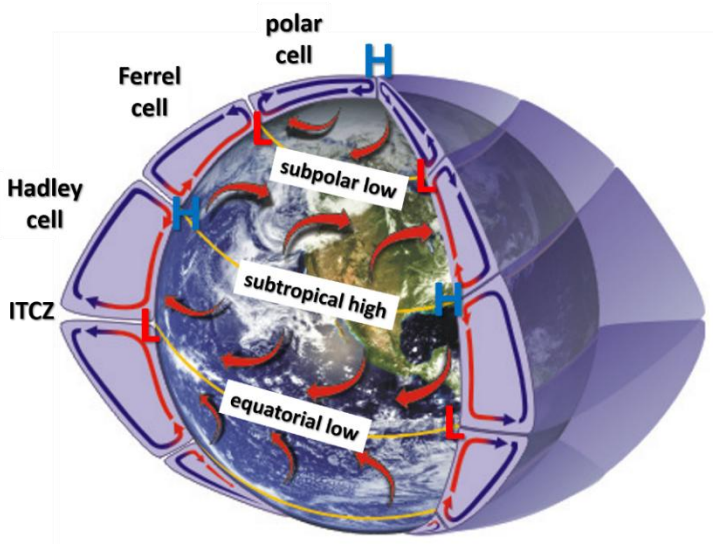

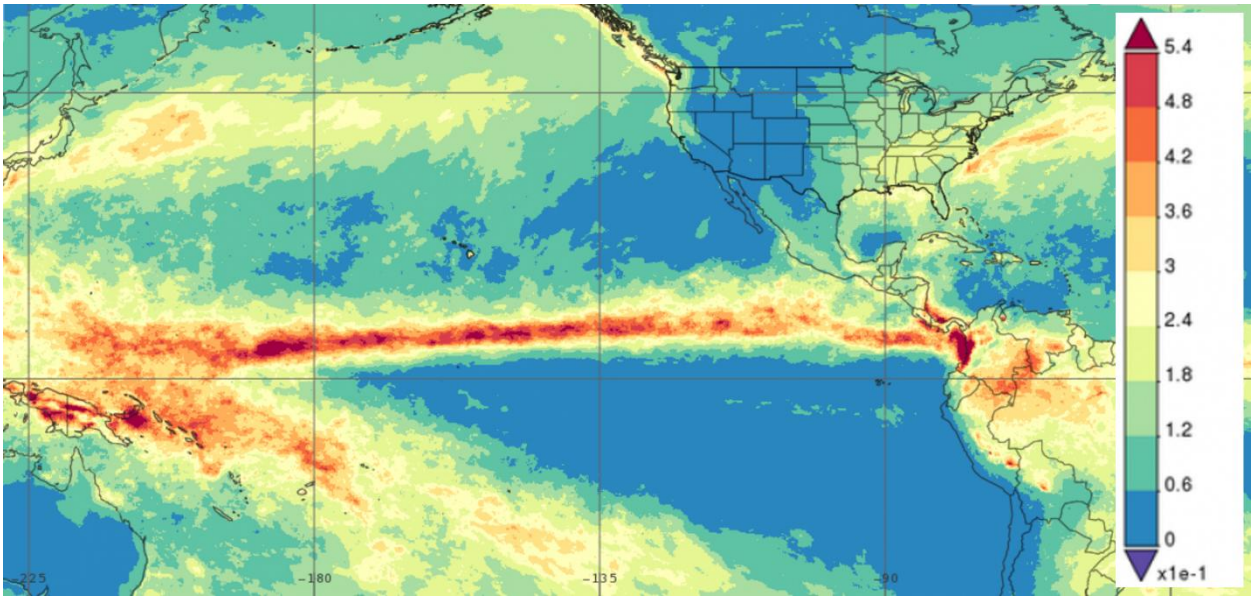

Figure 6-8: Satellite precipitation estimate. The color scale is mm per hour. The higher precipitation red band across the Pacific Ocean is associated with the ITCZ.

The ITCZ is always present somewhere on the globe. Portions of the ITCZ intensify and decay throughout the year. Additionally, the ITCZ has a seasonal shift between 15°N and 15°S towards the hemisphere experiencing summer, and can wander even further at times. Figure 6-9 contains a visible satellite image with the ITCZ circled in red, and a cross section of the atmosphere near the ITCZ A **cross section** is defined as a vertical slice of the atmosphere across a linear distance.

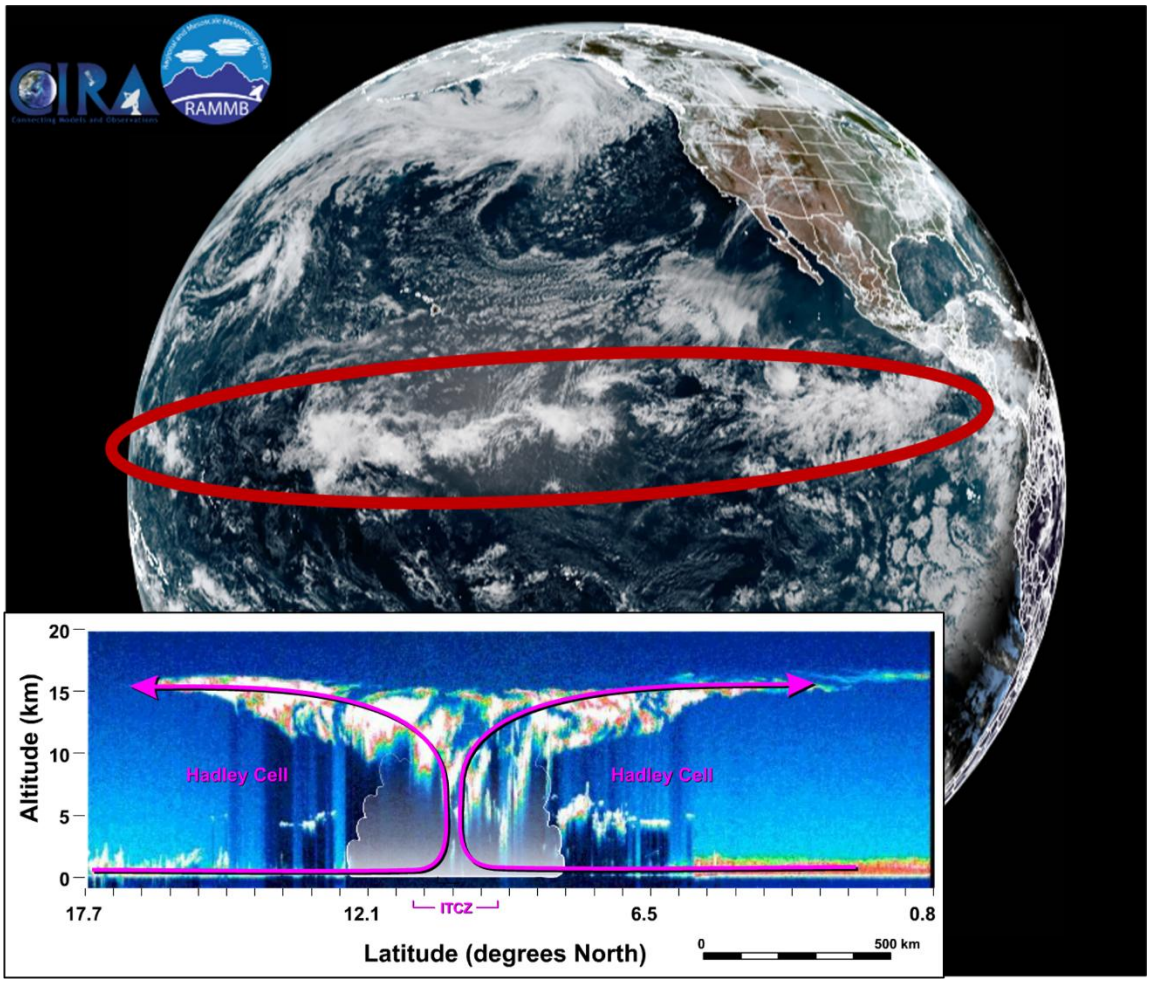

Figure 6-9: A visible satellite image with the ITCZ circled in red. The insert is a vertical cross section of the atmosphere from 0.8°N to 17.7°N across the ITCZ.

6.2.3 – Subtropical High, Ferrel and Polar Cells

The subtropical high is associated with descending air located between the Hadley and Ferrel cells around 30° latitude. This surface high pressure area is semi-permanent. As the air descends in altitude, it compresses and warms. These conditions discourage condensation and many areas near the subtropical high are deserts or have dry climates due to the subtropical high. Figure 6-10 contains a vegetation map of Africa and highlights the effects of the subtropical high in forming desert areas.

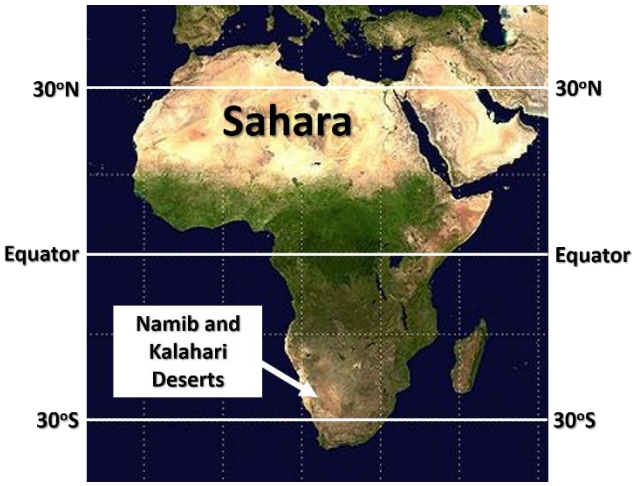

Figure 6-10: Deserts across Africa associated with the subtropical high.

The Sahara, Namib and Kalahari Deserts are all a result of this semi-permanent

subtropical high. Likewise, the lusher vegetation near the equator is a result of the precipitation associated with the ITCZ.

The subtropical high is characterized by calm winds and sunny skies, and is sometimes referred to as the horse latitudes. This term comes from ships sailing to the New World that would often become stalled for days or even weeks when they encountered calm winds. Many of these ships carried horses to the Americas as part of their cargo. Unable to sail and resupply due to lack of wind, crews often ran out of drinking water. To conserve scarce water, sailors on these ships would at times throw the horses they were transporting overboard. Thus, the phrase 'horse latitudes' was born.

In the Ferrel cell, the air flows poleward from the subtropical high to a surface subpolar low near 60°. The Coriolis force again shifts these winds towards the right into a zonal flow pattern. The Coriolis force is balanced with the pressure gradient force. These winds are referred to as the westerlies since they originate from the west. Whereas the Hadley cell is driven directly by solar radiation (convection), the Ferrel cell is an indirect circulation as a result of the polar and Hadley cells. A person could think of the Ferrel cell as going along with the flow, since it is stuck in the middle. See Figure 6-7 for the location of the Ferrel cell.

A subpolar surface low resides between 50° and 70° latitude with ascending air. Air motion aloft in the polar cell is towards the pole where it descends. A surface high pressure resides at the pole called the polar high. Air motion at the surface is equatorward. Since many transient weather systems pass through this area, the polar cell is barely detectable when examining average cross sections of the Arctic. The polar cell is a thermally driven circulation caused by the temperature differences between the pole and lower latitudes.

This third video from the United Kingdom Met Office describes how the Coriolis force influences the global circulation patterns and the winds within each cell. The concept of jet streams is introduced and is explored further in section 6.3.1.

6.2.4 – Three-cell Model Reality Check

How well does the three-cell model fit what is actually observed? To answer this question, a good first step is to examine the average sea-level pressure maps across the globe. Since a seasonal variation is likely present, examining maps for the months of July and January will provide details on these variations. Figure 6-11 contains the average sea-level pressure map (SLP) for July. In this figure, the warm yellow to red colors are higher pressure and the cool blue colors are lower pressure. The lime green areas essentially depict the areas of neither high nor low pressure values.

Looking at the Southern Hemisphere first. The Antarctic has a strong high pressure over the pole with a strong low pressure around 60°S. This surface pressure pattern fits the polar high and subpolar low extremely well. Moving equatorward, the subtropical high near 30°S is again depicted well. Near the equator, we should see a band of lower pressure associated with the ITCZ. Lower pressure blue colors are present across the western Pacific Ocean into Asia and Africa, but not elsewhere. Normal rather than lower pressures are present in the eastern Pacific and Atlantic Oceans and across South America.

Examining the Northern Hemisphere, the subtropical high can be seen closer to 40°N across the eastern Pacific and Atlantic Oceans into Europe, but not so much across Asia. The subpolar low

is present with slightly lower pressures across 70ºN. The surface polar near the pole is not seen.

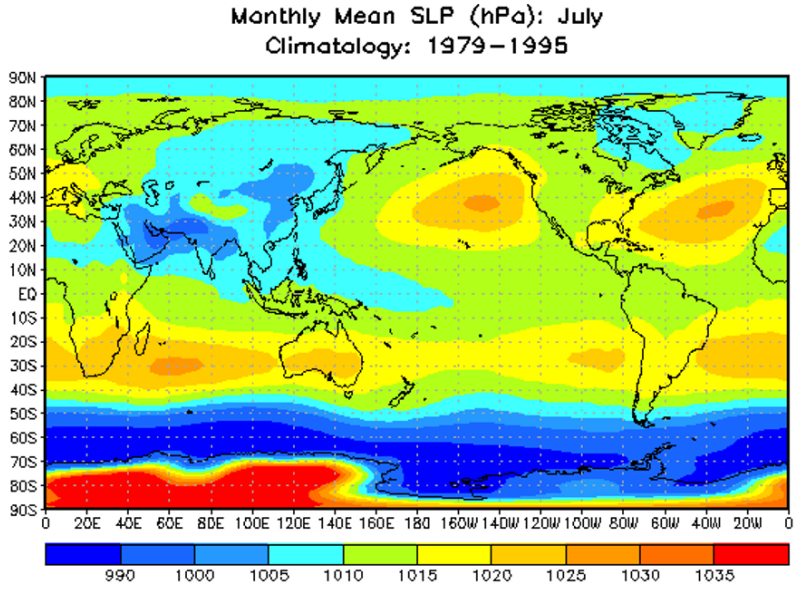

Figure 6-11: Mean sea-level pressure across the globe for July. The yellow to red colors represent higher pressures. The blue colors represent lower pressures. The green areas are neutral; neither high nor low pressures.

Figure 6-12 contains the average sea-level pressure map for January, and uses the same color scale as the July map. Starting the analysis with the Southern Hemisphere again. No polar high is present in the Antarctic, instead an area of low pressure extends from 50ºS to the pole. This large low pressure certainly encompasses the area where the subpolar should be present. At about 35ºS the subtropical high can be seen. Low pressures associated with the equatorial low or ITCZ are present in the western Pacific Ocean near Indonesia and weakly in Africa. The ITCZ is not seen in the Atlantic nor Indian Oceans. North of the equator, high pressure is observed around 30ºN with a huge high pressure over Asia. Subpolar low pressures are shown at 50ºN in the northern Atlantic Ocean near Iceland and the Pacific Ocean. The land masses of Asia and North America do not indicate subpolar low pressures. No Arctic high pressure is present at the pole.

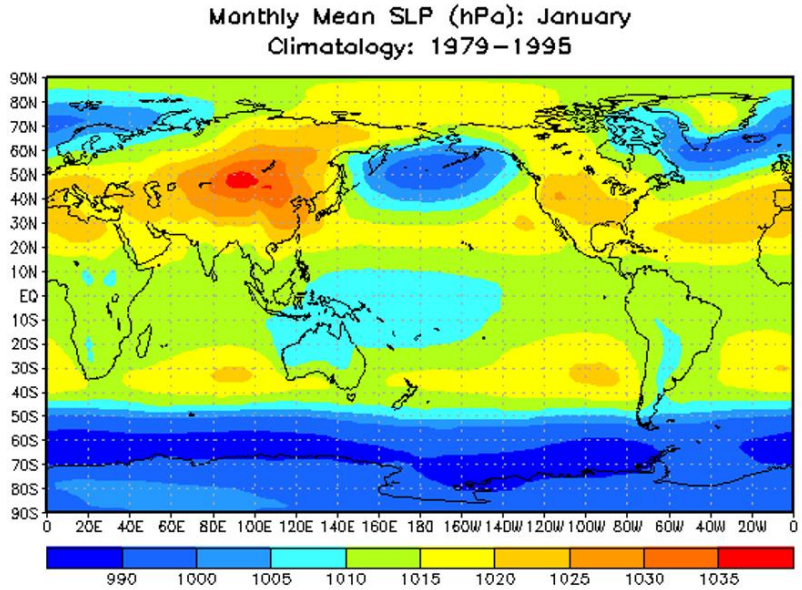

Figure 6-12: Mean sea-level pressure across the globe for January. The color scale is the same as Figure 6-11.

One last map will help complete this surface analysis. Figure 6-13 contains the average location of the ITCZ for January (blue) and July (red). This map helps explain some of the variability noted in the sea-level pressure maps. The ITCZ seasonally wanders across the western Pacific and Indian Oceans, Asia and eastern Africa. This convective zone shifts much less from west Africa, across the Atlantic Ocean and into South America.

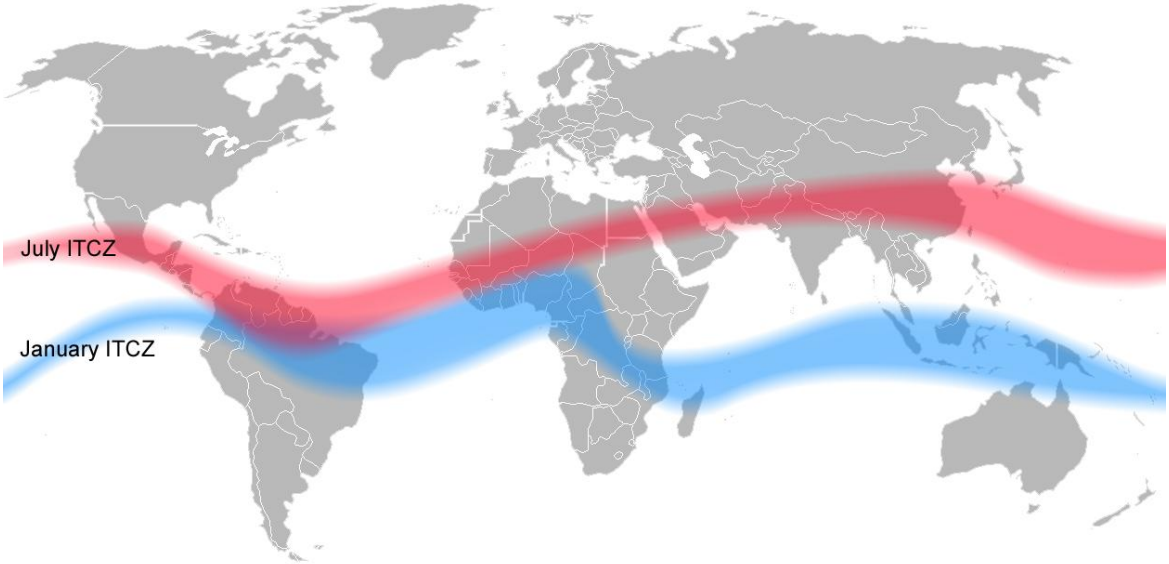

Figure 6-13: The average location of the ITCZ across the globe in July and January.

As you can see from these analyses, the three-cell model fits some of what it describes well, but does not account for everything. The July (winter) surface patterns in the Southern Hemisphere are the closet match. Many of these variations from what the conceptual model predicts are due to the land masses. The Southern Hemisphere is largely water. This flat water surface allows air to move with few disruptions. The Northern Hemisphere has most of the land mass on our planet. As the air flows over vegetation, hills and mountains, the atmosphere adjusts to these obstacles accordingly.

6.2.5 – Upper Level Characteristics Reality Check

The reality check of the three-cell model so far has centered on surface analyses. How does this model relate to upper level analyses? Figure 6-14 is a 500 mb height average for July in the Northern Hemisphere. Each different color on this map is a 100 meter change in the height field. The larger black circle is 30°N and the smaller circle 60°N. From the equator to 30°N the height field does not change much; it is orange across most of the area. Remember the height gradient translates to the pressure gradient and a corresponding wind speed. Little change in the height field indicates winds are light. Since the surface pressure gradient also indicates lighter winds, the winds aloft appear to balance the surface winds in the Hadley cell. The Ferrel cell in the middle should have the westerlies. Wind flows parallel to the height field as is indicated by the arrows. These winds agree with the

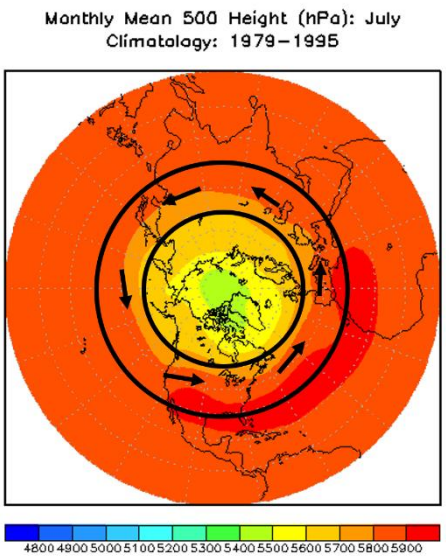

Figure 6-14: Mean 500 mb heights in the Northern Hemisphere for July.

three-cell model expectations. The lowest heights are at the North Pole with continued westerly flow, which does not fully match the polar cell concept.

Figure 6-15 is a 500 mb average height field for January. The height gradient in the midlatitudes between 30ºN and 60ºN is stronger which in turn makes the wind stronger in winter. Everything else is similar to the July analysis.

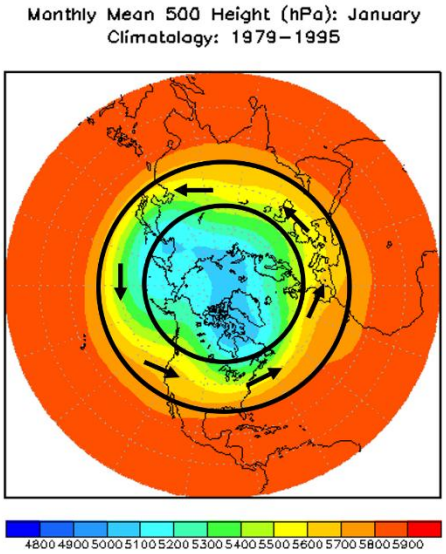

Figure 6-15: Mean 500 mb height in the Northern Hemisphere for January.

So far, we have examined monthly average analyses. How does a snapshot of a 500 mb chart for one day fit the three-cell model? Figure 6-16 is a 500 mb height chart for a single day in June. The black circles again highlight 30ºN and 60ºN. The height field is depicted in thin black lines rather than colors. Winds are still parallel to the height contours. From the equator to 30ºN, light winds are present since few height lines exist. This observation agrees with the monthly mean charts previously. In the midlatitudes, between the circles, the westerlies and zonal flow are not present. Arrows indicate the wind directions. Significant meridional flow is seen, which does not fit the three-cell model. However, an underlying objective in learning about global circulations is to understand how weather equalizes the temperature differences between the poles and the equator. Meridional flow is needed to accomplish this heat transfer. Zonal flow can transfer heat east or west, but not north and south. These troughs (lower pressure) and ridges (higher pressure) in the midlatitudes will need further investigation because they are important. Lastly the area around the North Pole has several low pressure systems which match what was seen on the monthly means.

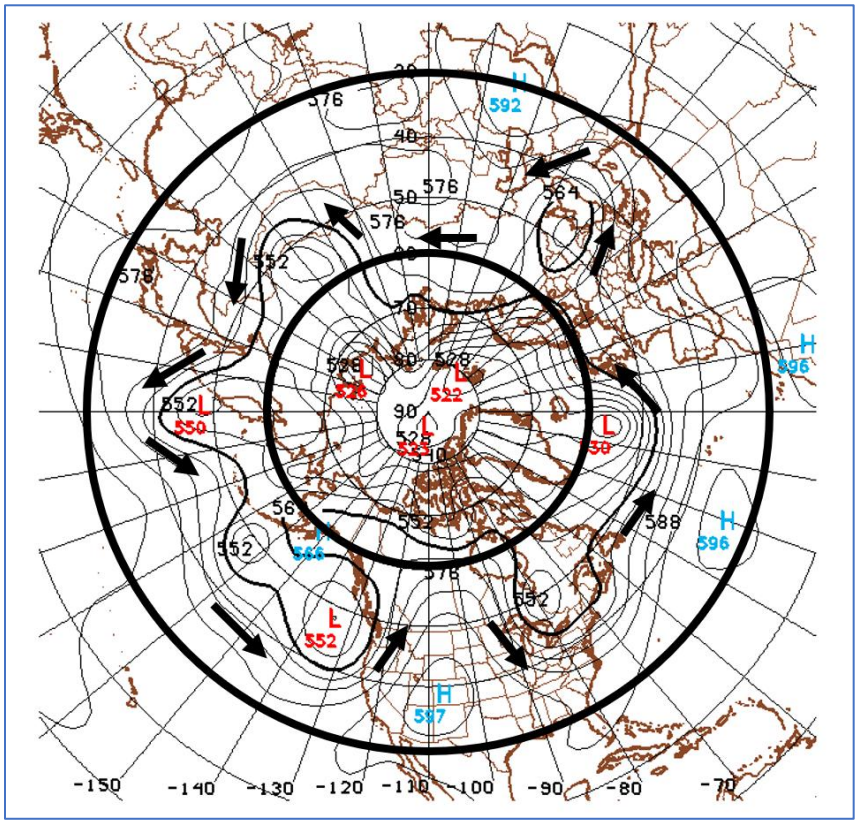

Overall, the three-cell model coincides with many of the observations for the upper levels, but some discrepancies are still present. The Hadley cell is verified the best in this reality check.

Figure 6-16: A 500 mb height map of the Northern Hemisphere for a single day in June. Notice the zonal and meridional flow between the think black lines, which represent the latitudes associated with the Ferrel cell.

6.3 – Synoptic Scale

Mean 500 mb westerly flows for July and January in the midlatitudes agreed with the three-cell conceptual model. However, looking at a single day 500 mb map (Figure 6-16) did not show a zonal westerly flow. Rather troughs and ridges were shown across the globe as both zonal and meridional flow were present.

These troughs and ridges are no longer a global scale phenomenon, but fall into the synoptic scale category. For example, the ridge of high pressure over the United States (Figure 6-16) covers a portion of the continent. These synoptic scale features are discussed in this section.

6.3.1 – Jet Streams

Jet streams are relatively narrow bands of strong wind in the upper levels (9 to 15 km) of the troposphere. The winds generally blow from west to east in jet streams. Jet streams follow the boundaries between the hot and cold air. Since these hot and cold air boundaries are most pronounced in winter, jet streams are the strongest during the winter months.

The boundaries between the three global circulation cells is where the temperatures changes are the greatest. Hence, jet streams tend to follow these boundaries near latitudes 30° and 50° to 60°. The jet stream closest to the equator is called the subtropical jet and the one closest to the pole is called the polar jet. The left side of Figure 6-17 illustrates these locations and this naming convention.

Jet streams meander around the globe, dipping and rising in altitude and latitude, splitting at times, and even disappearing altogether to appear somewhere else. Additionally, the subtropical and polar jets may merge into one. This erratic nature is illustrated on the right side of Figure 6-17.

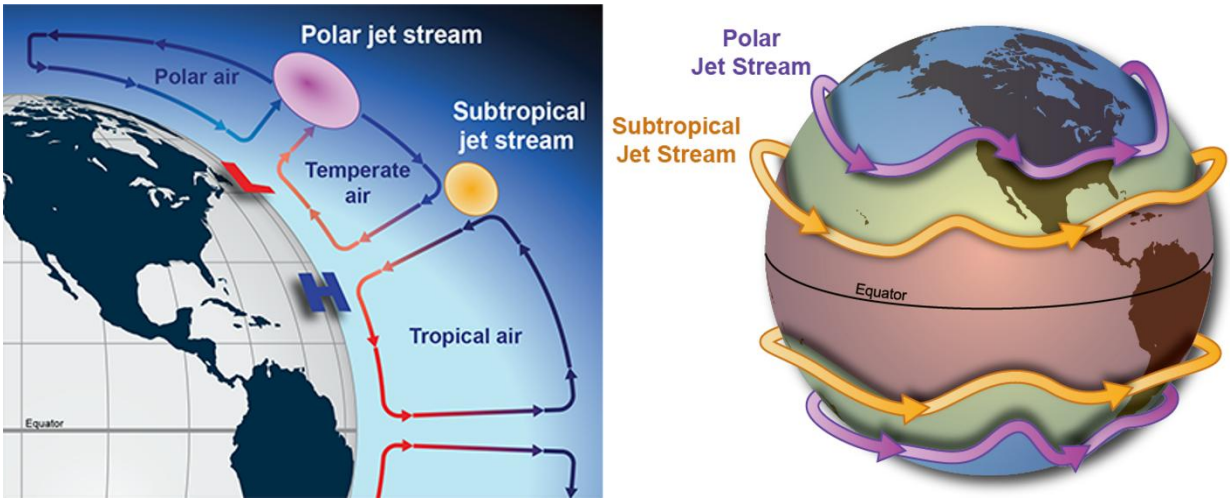

Figure 6-17: (left side) The location of the polar and subtropical jet streams with respect to the three-cell model. (right side) The meandering nature of the jet streams around the globe.

Jet streams do not have a constant speed around the globe. Instead, the wind increases towards a central core of greatest strength, and then weakens into the general wind field, and

then strengthens again. The diagrams in Figure 6-18 depict these wind speed variations in a jet stream.

This video, again from the United Kingdom Met Office, discusses the origin of jet streams and how they may affect the weather.

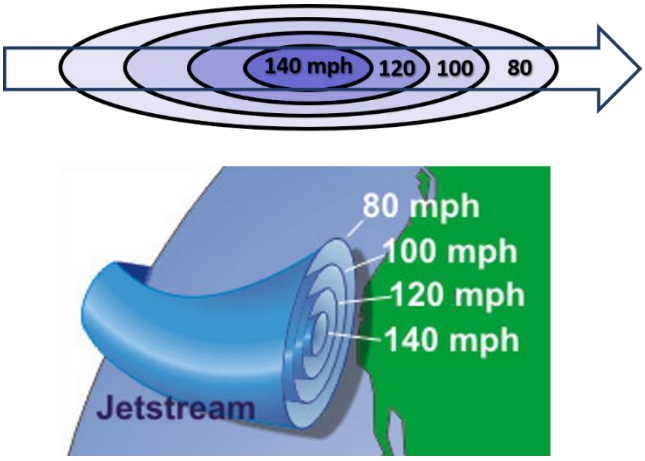

Figure 6-18: The horizontal (top) and vertical (bottom) variation of wind speeds within a jet stream. Jet streams are not a constant wind speed around the globe.

6.3.2 – Rossby Waves

Rossby waves, also known as planetary waves, are the flow pattern between troughs and ridges in the midlatitudes. These waves occur naturally in rotating fluids within Earth's atmosphere and oceans. The atmosphere behaves very much like a fluid, although it is considerably less dense than water in an ocean. These waves form as a result of the rotation of our planet. Rossby waves help transfer heat from the tropics toward the poles and cold air toward the tropics in an attempt to equalize temperatures across the Earth. They determine the location of the jet stream and influence the track of surface low pressure systems. Rossby waves are named after Carl Rossby who determined the mathematics describing them.

These waves in the midlatitudes can be categorized into two sizes (1) longwaves which cover around 3700 to 5000 miles and (2) shortwaves which are less than 3700 miles in length. The number of longwaves at any one time in a hemisphere varies from 3 to 7, though it is typically 4 or 5. Figure 6-19 depicts 5 longwaves.

Shortwaves are embedded within longwaves, and are much faster moving with an average speed of 23 mph. Shortwaves are the chief instigator of episodes of precipitation. Their main precipitation bands will be typically localized near the short wave as it passes overhead.

Figure 6-20 illustrates both longwaves and shortwaves on a 500 mb chart. In this illustration, the height contours are black. The brown arrows indicate the direction of airflow. The large red dashed lines represent the location of the longwave troughs.

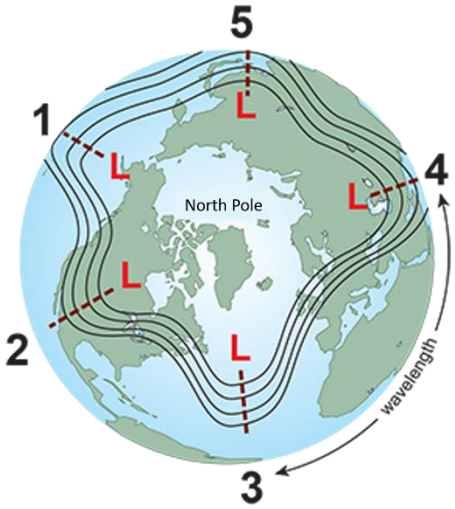

Figure 6-19: Five longwaves are depicted in the Northern Hemisphere.

Longwave troughs take many days or weeks to move. The shorter blue dashed lines represent the location of the more prominent shortwaves. Shortwaves move much faster and pass through an area in a day or two. The green areas represent precipitation amounts with the light green at 0.01 inches. The areas of precipitation are mainly associated with the shortwaves as they pass through the longwaves. Like railroad cars on a train track, shortwaves will generally follow the height contours.

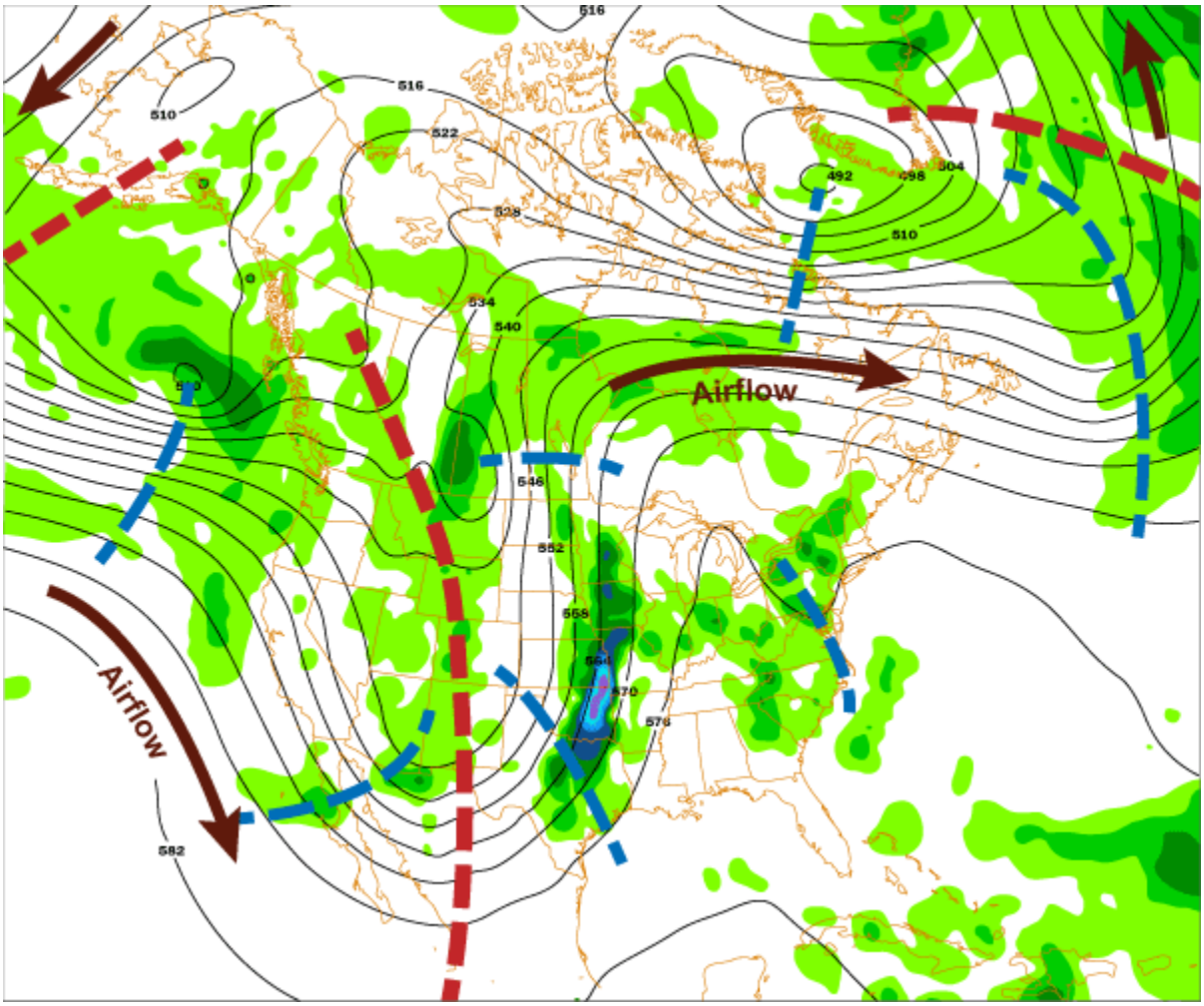

Figure 6-20: A 500 mb map highlighting the longwaves and shortwaves. Height contours are in black. The brown arrows indicate the direction of airflow. The red dashed lines are the location of long wave troughs. The blue dashed lines are the short wave troughs embedded in the flow. The green areas are precipitation. Notice the higher amounts of precipitation are associated with the shortwaves.

6.3.3 – Atmospheric Rivers

Atmospheric rivers are relatively long, narrow regions in the atmosphere that transport water vapor from the tropics to higher latitudes. On average, atmospheric rivers are 250 to 370 miles wide. These bands of water vapor interact with Rossby waves and their associated subtropical jet streams. When an atmospheric river encounters land, it often releases this water vapor in the form of rain or snow. A strong atmospheric river transports an amount of water vapor roughly equivalent to 7.5–15 times the average flow of water at the mouth of the Mississippi River.

Figure 6-21 shows an atmospheric river moving from the tropics onto the West Coast of the U.S. and Mexico in January 2017. The color key is in centimeters of liquid water present in a vertical column of atmosphere. This column is from the surface to the top of the atmosphere.

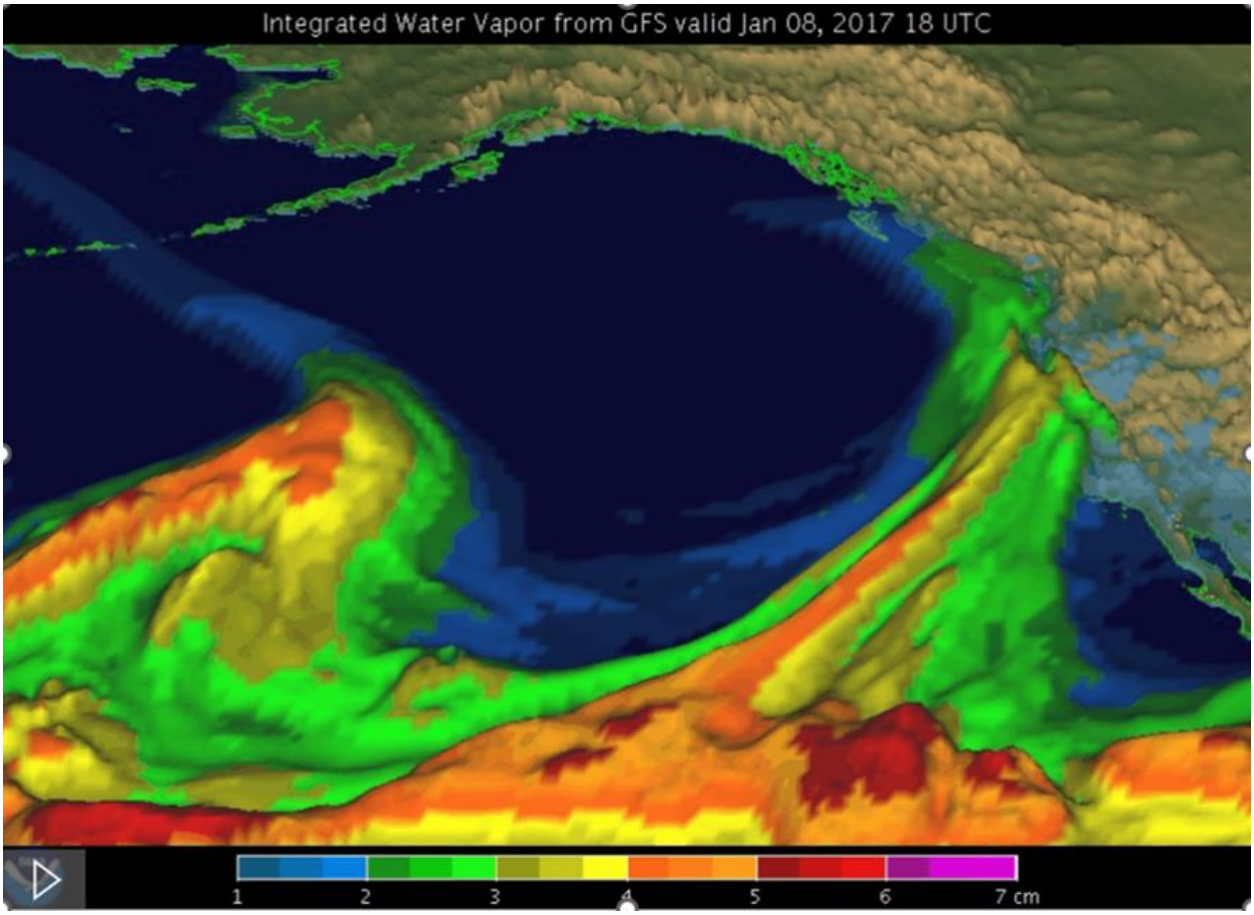

Figure 6-21: An atmospheric river affecting the West Coast of the United States and Mexico.

6.4 – Air masses

An **air mass** is a large body of air with similar temperature and humidity characteristics. The area over which an air mass originates is called a **source region**. The longer the air mass stays over its source region, the more likely it will acquire the properties of that surface. Air masses exhibit the properties of their source regions within one or two weeks of residing there. They form within the boundary layer, or that portion of the atmosphere interacting with the Earth's surface, and under an upper level high pressure. The high pressure assists in keeping the air from migrating out of the source region.

Air masses are classified using two letters. The first letter is lower case and designates the moisture content of the air:

c (continental) forms over land and is dry
m (maritime) forms over water and is moist.

The second letter is upper case and designates the temperature of the air:

A (Arctic or Antarctic) is very cold
P (Polar) is cold but not as cold as Arctic
T (Tropical) is warm to hot
E (Equatorial) is hot

The temperature characteristic corresponds to the latitude over which the air mass formed. Figure 6-22 illustrates the air masses affecting North America. The source regions, air mass names, and the direction they tend to move are depicted in this figure. The colder air masses tend to travel towards the south and the warmer air masses travel towards the north.

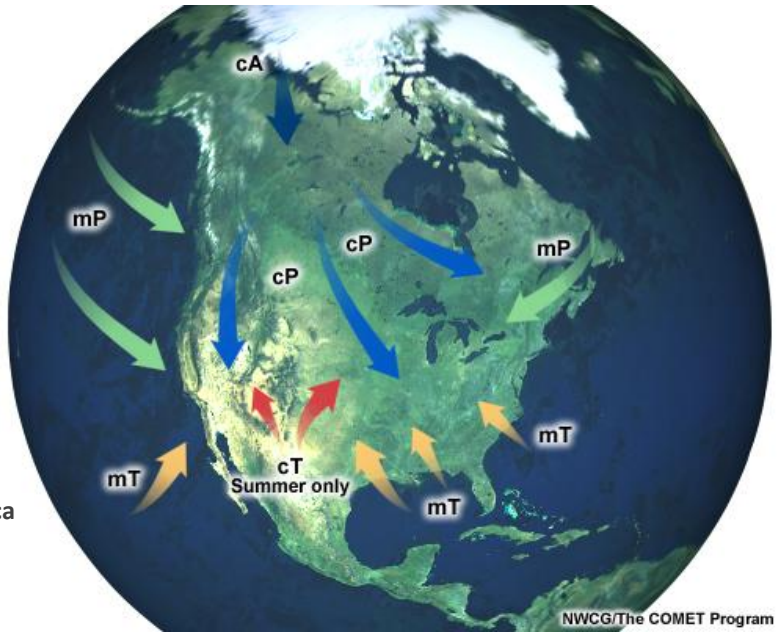

Figure 6-22: Air mass over North America and their direction of movement.

This second map in Figure 6-23 depicts all the source regions around the globe.

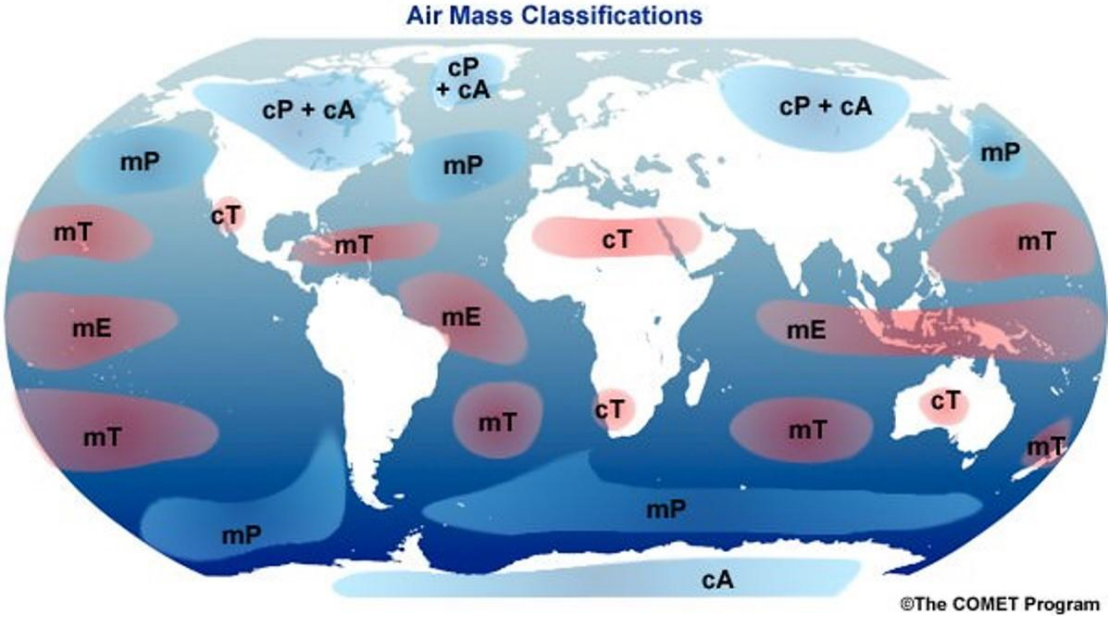

Figure 6-23: Air mass source regions around the globe.

Whenever air masses start to move their characteristics begin to modify. A continental polar (cP) moving south over North America will begin to warm. If a maritime polar or tropical (mP or mT) air mass moves inland, it will start to dry out.

Notice that no air masses form over land in the midlatitudes. Air masses collide and mix in the midlatitudes, which discourages air from residing unperturbed for a week or two. Air masses form over a source region only when the air can remain in that location.

6.4.1 – Characteristics of cA, cP and mP

The continental polar (**cP**) air masses form over the large, high latitude land masses such as Canada and Siberia. Notice no cP air masses exist in the Southern Hemisphere. The Southern Hemisphere has no high latitude land masses.

These regions have short days and low Sun angles in the winter. These areas lose more energy than they receive. The cold temperatures make the air extremely dry. This cold air resides near the surface with a strong inversion above it, which makes for stable conditions. During the summer, cP conditions are not as extreme and the air masses tend not to migrate from where they form.

The continental arctic (**cA**) air masses are more extreme than the cP air masses, and originate over the poles. They have much colder air with a much stronger inversion above it for extremely stable conditions. Arctic air masses tend to be shallower in depth than polar ones.

The maritime polar (**mP**) air masses contain moisture, since they originate over the higher latitude oceans. The temperatures are slightly moderated from the cP air masses, because they formed over water. These moisture laden air masses tend to drop precipitation when they move inland. Figure 6-24 illustrates the precipitation that occurs over the mountain ranges of western North America associated with an mP air mass moving over land.

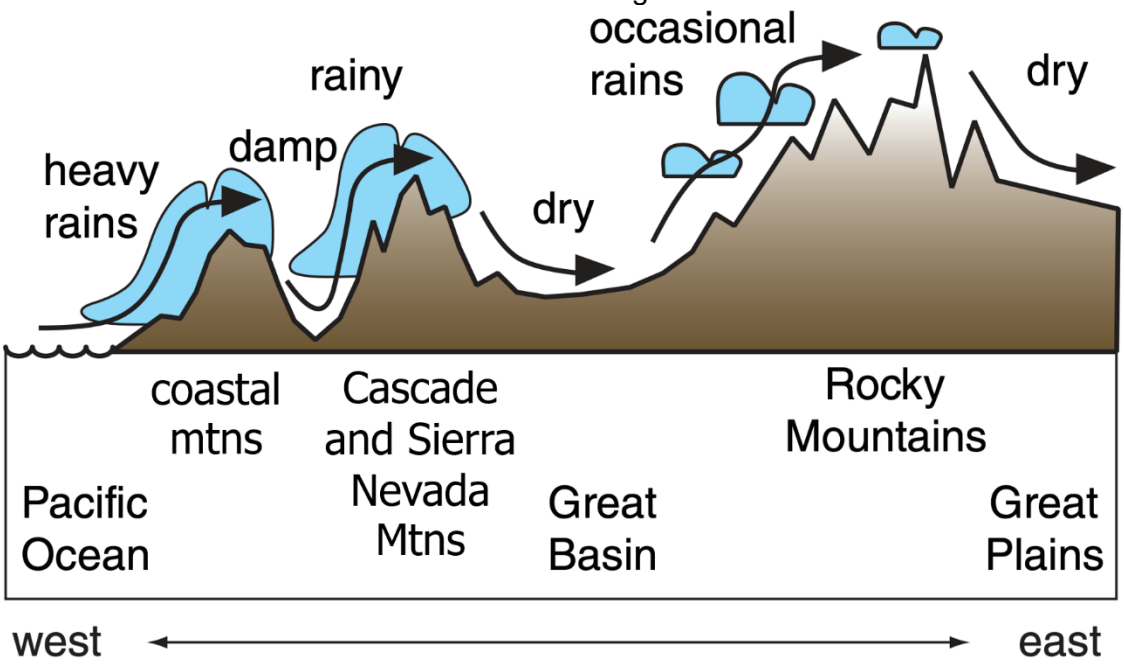

Figure 6-24: Precipitation associated with an mP air mass moving over the mountains of western North America.

The eastern portion of North America has a similar situation with mP air masses. These air masses are a key component in the Nor'easters which form off the New England coast.

6.4.2 – Characteristics of cT, mT and mE

The continental tropical (**cT**) air masses develop under the subtropical high near 30^{o} latitude during the summer months. These air masses form due to intense surface heating of the desert landscape. The hot air created near the surface rises to great heights on its own, and is thus extremely unstable. These source regions lack moisture, so hot and sunny conditions can prevail for many days. Once moisture enters the area, usually from an mT air mass, intense thunderstorms can occur.

Maritime tropical (**mT**) and maritime equatorial (**mE**) air masses develop over tropical waters and are warm, hot and humid. Tropical air masses on the equator are referred to as maritime equatorial (mE), but are essentially the same as mT. The difference between the two is the location where they form. Since these air masses contain warm to hot and moist air near the surface, they can be unstable. Hurricanes form in these air masses.

During the winter when mT air masses migrate north over land, they invariably collide with cP air masses moving south. This clash between the two air masses creates significant weather in the midlatitudes.

6.5 – Fronts

During World War I, Vilhelm Bjerknes, a Norwegian physicist with expertise in radio science and fluid mechanics, was asked to form a Geophysical Institute in Bergen, Norway. Cut-off from weather data due to the war, he arranged for a dense network of 60 surface weather stations to be installed. Some of his students were C.G. Rossby, H. Solberg, T. Bergeron, V. W. Ekman, H. U. Sverdrup, and his son Jacob Bjerknes.

Jacob Bjerknes used the weather station data to identify and classify cold, warm, and occluded fronts. He published his results in 1919, at age 22. The term "front" supposedly came by analogy to the battle fronts during the war. He and Solberg later explained the life cycle of cyclones. Their description is known as the Norwegian Cyclone Model.

The Bergen School of Meteorology still exists today, although it no longer has the notoriety of the 1900s. Figure 6-25 is a photo of Bergen, Norway. The school is spread throughout the city, so this picture depicts the current university.

Figure 6-25: Photo of Bergen, Norway.

The remainder of this chapter and Chapter 7 on midlatitude cyclones examine the concepts in the Norwegian Cyclone Model. This conceptual model was first developed when only surface observations were available. As weather balloon data became available, and researchers could analyze the vertical structure of the atmosphere, the Norwegian Cyclone Model was expanded to include the vertical structure of the atmosphere.

6.5.1 – What Happens When Air Masses Collide?

In an effort to balance the differential heating across the planet, the tropical (T and E) air masses move north and the polar (P and A) air masses move south. These air masses collide and the transition zone between different air masses is called a **front**.

Since air masses have different temperature and humidity characteristics, a front signifies a change in:

1. Temperature
2. Dew point or humidity
3. Wind direction
4. Surface pressure
5. Clouds and precipitation

Remember frontal lift is a mechanism for adiabatic cooling, clouds and sometimes precipitation. As air masses collide, the denser or colder one ends up on the bottom and the lighter or warmer one is lifted. The most important fronts in the Norwegian Cyclone Model are cold fronts, warm fronts, stationary fronts, and occluded fronts. Three other boundaries which appear on surface analysis weather maps in the United States are dry lines, squall lines and troughs. We will examine all of these fronts and boundaries.

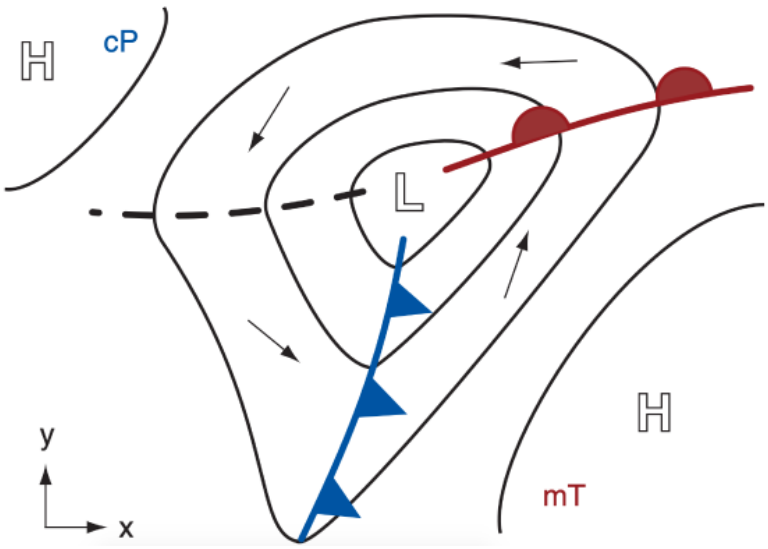

Figure 6-26: The classic (mature) structure of a cold and warm front centered around a surface low pressure. The cold front is the blue line with triangles. The warm front is the red line with half circles. The black lines are isobars with the arrows indicating wind flow direction. A low surface pressure ("L") is frequently located near the intersection of the warm and cold fronts.

Fronts are typically associated with a low pressure center, and are rarely isolated from each other. A typical configuration in the Northern Hemisphere has a counterclockwise rotation around the low pressure center. The fronts connect to each other at this low pressure center where the highest precipitation amounts usually occur. Figure 6-26 illustrates a classic cold front (blue) and warm front (red) configuration. Notice the high pressure associated with the cP and mT air masses.

Taking a vertical slice, called a cross section, through the cold front (blue) yields a diagram shown in Figure 6-27. The strongest winds (jet) are aloft over the cold front. This particular jet would then connect into the

hemispheric jet stream pattern. Hence, jet streams, Rossby waves, and fronts are all interconnected in a storm system. Fronts are more surface based phenomena. Rossby waves and jet streams are aloft. The movement of air masses creates all of these phenomena at different levels in the atmosphere.

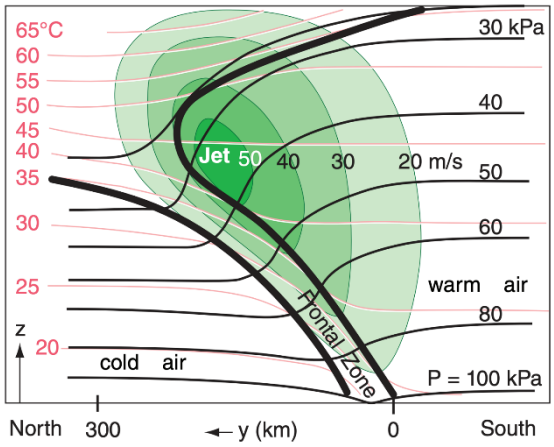

Figure 6-27: Vertical slice, called a cross section, through a cold front.

6.5.2 – Cold Front

The leading edge of a cold air mass is called a **cold front**. As seen in Figure 6-28, the symbol for a cold front is a blue line with triangles on one side. The triangles point in the direction the front is moving. In the Northern Hemisphere, cold, drier air (cP) is frequently behind the cold front and warm, moist air (mT) is frequently ahead of the front.

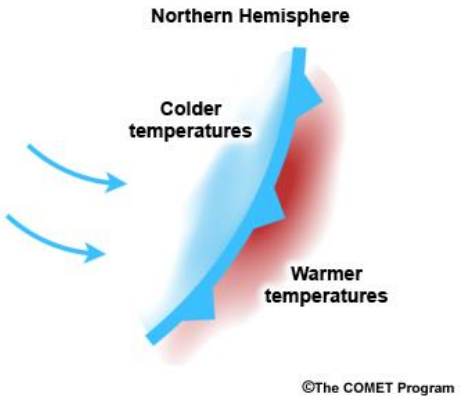

Figure 6-28: Symbols for a cold front.

Surface pressures are lowest at the front. Winds switch from a southerly direction ahead of the cold front to a northerly direction behind it. The movement of a cold front on average is 20 to 25 mph. The exact speed is determined by the wind speed behind the front. A cold front frequently has an abrupt vertical boundary, which can cause cumulonimbus to develop near the front. These thunderstorms may be associated with heavier precipitation. Ahead of the cold front is warm, moist air which can have a hazy appearance. Behind the cold front in the drier air are clear skies or scattered cumulus clouds. The cold air behind the front is relatively dry and stable. Precipitation primarily occurs with the frontal boundary. These characteristics are illustrated in Figure 6-29.

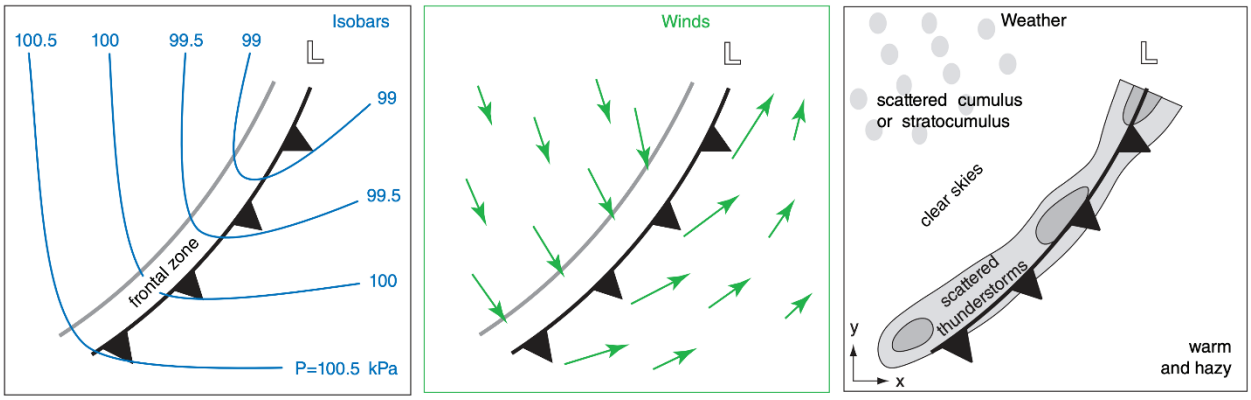

Figure 6-29: Diagrams showing the surface pressure (left), wind direction (center), and clouds (right) associated with a cold front.

Figure 6-30 illustrates the abrupt nature of the frontal boundary, which can cause thunderstorms. Notice the abrupt slope at the leading edge of the cold air. Further behind the cold front the slope of the cold air decreases significantly. The boundary between the cold and warm air extends vertically into the atmosphere.

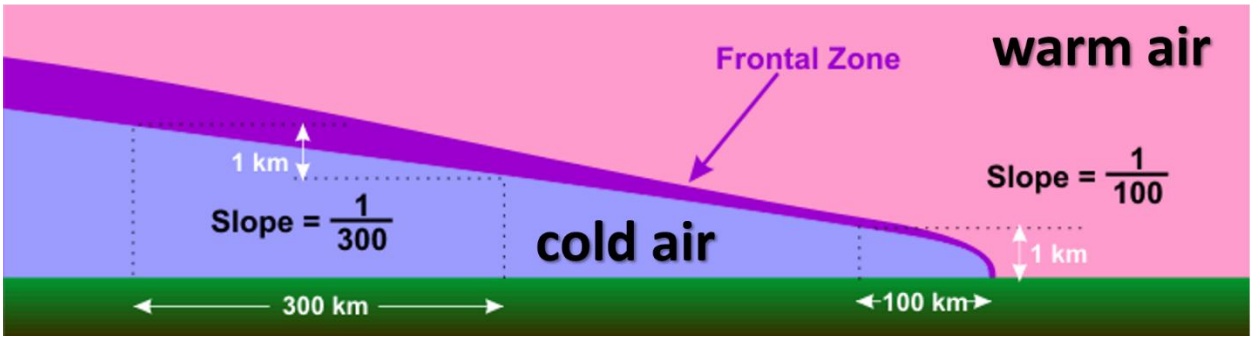

Figure 6-30: The vertical structure associated with a cold front. Notice the sharp boundary at leading edge of the cold air, which can create thunderstorms as the front moves forward.

6.5.3 – Warm Front

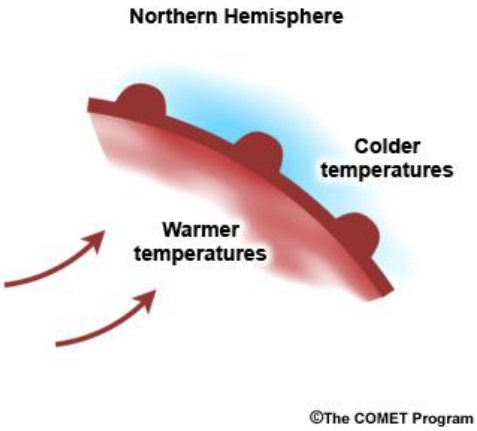

Figure 6-31: Symbols for a warm front.

The leading edge of a warm air mass is called a **warm front**. The symbol for a warm front is a red line with half circles (Figure 6-31). The half circles are on the side of the line towards which the warm air is moving. In the Northern Hemisphere, warm, moist air (mT) is frequently behind the warm front.

Surface pressures have a relative minimum at the front, although the change in pressure is much less than what is observed with a cold front. Winds ahead of a warm front have an easterly component and behind the front more of a southerly component. These southerly winds advect in warm, humid air. The movement of a warm front is much slower than a colder front and is about 10 to 15 mph. This speed is determined by the winds behind the warm front, and the winds in the cooler air ahead of the front. Since the cooler air is denser, the warm front air will override this cooler air rather than move it out of the way. The warm air mass rises slowly over a cooler air mass as shown in Figure 6-32.

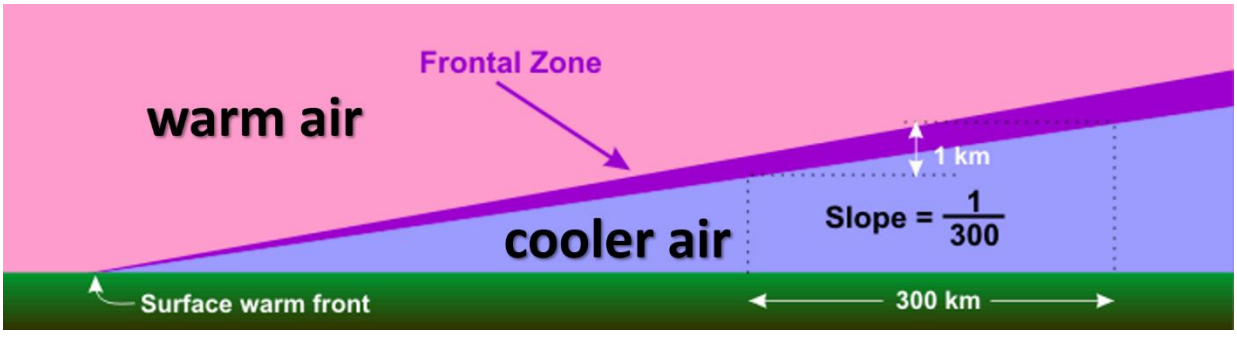

Figure 6-32: The vertical structure associated with a warm front. Notice the gradual slope associated with the frontal zone as the warm air rises over the cooler air.

Since an abrupt vertical boundary is not present in a warm front, no cumulonimbus or thunderstorms are present. Precipitation is in the form of uniform rain from a strato-form type of cloud ahead of the front. The gradual rising of the warm air can cause a variety of clouds near or ahead of the warm front. For example, fog, nimbostratus, stratus, altostratus, and cirrus. All the clouds and precipitation occurs ahead of a warm front, which is much different than a cold front. These characteristics are illustrated in Figure 6-33.

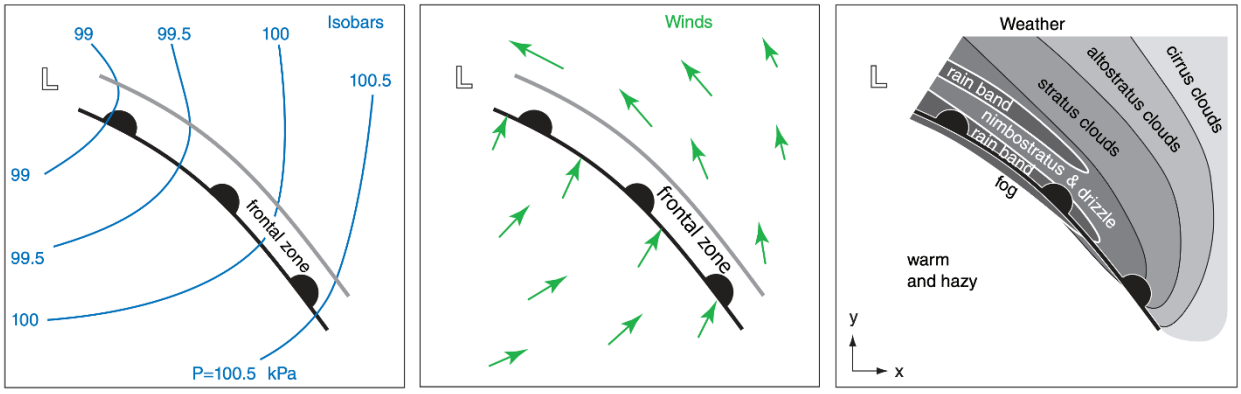

Figure 6-33: Diagrams showing the surface pressure (left), wind direction (center), and clouds (right) associated with a warm front.

6.5.4 – Stationary Front

A **stationary front** is a front that is not moving or is moving less than 5 mph. One side of the stationary front has cooler air and the other side warmer air, as depicted in Figure 6-34. The stationary front symbol has alternating cold front and warm front symbols. Surface winds are frequently parallel to a stationary front when the two air masses initially meet.

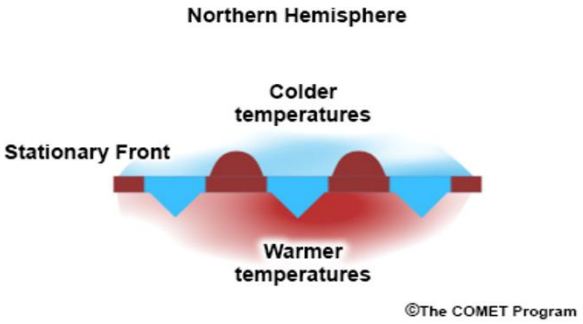

Figure 6-34: Symbols for a stationary front.

Figure 6-35 provides a broader view of two air masses meeting, the winds associated with each air mass, and the stationary front between them. By default, stationary fronts form in regions of lower pressure which is true for all fronts. Clouds associated with a stationary front depend on how much lift the warm air experiences as it flows over the cooler, denser air. If lift is substantial, precipitation can occur in the frontal zone. Since stationary fronts do not move quickly, the extended duration of precipitation may lead to flooding.

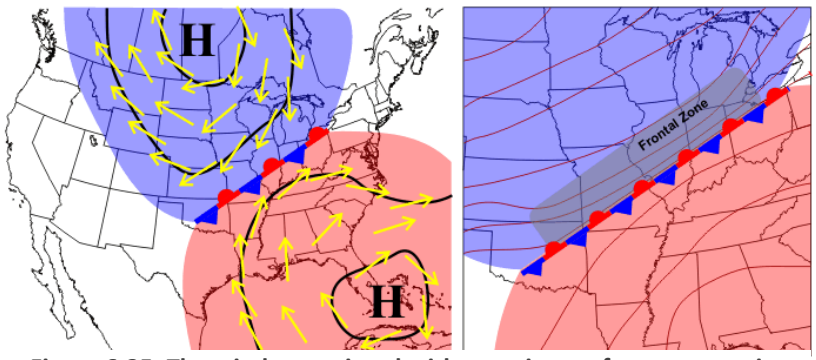

Figure 6-35: The winds associated with a stationary front as two air masses meet. Clouds and precipitation can occur in the frontal zone.

6.5.5 – Occluded Front

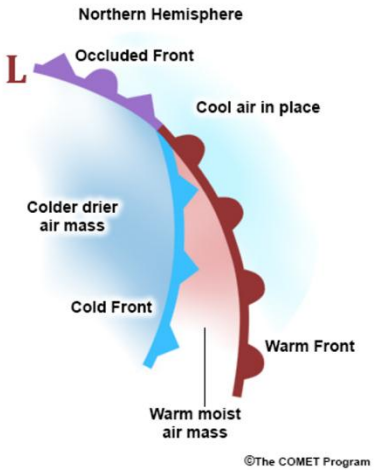

Figure 6-36: Symbols for an occluded front.

Cold fronts typically move faster than warm fronts, so in time they can "catch up" to warm fronts. As they do, the warm air mass is fully lifted off the surface forming an occlusion. An **occluded front** occurs when the warm air mass is lifted aloft.

The surface location of the occluded front is directly below the convergence point of the warm, cool and cold air masses. Occluded fronts point to a decrease in intensity of the parent weather system, and are indicated by a purple line with alternating triangles and half circles. The triangles and half circles point in the direction of its movement, as illustrated in Figure 6-36.

While there is no difference in how they are depicted on a weather map, there are two types of occlusions: cold and warm. Cold occlusions are the most common where the cold front overtakes the warm front and also undercuts the cooler air mass ahead of the warm front.

Warm occlusions occur when the air associated with the "cold" front is actually not as cold as the air mass associated with the warm front. The warm air is forced up as before, but the colder, denser air mass ahead of the warm front remains at the surface forcing the air mass associated with the cold front up as well. Figure 6-37 illustrates a cold and warm occlusion. While the process to form a cold or warm occlusion is slightly different, the end result of both is to lift the warm air aloft.

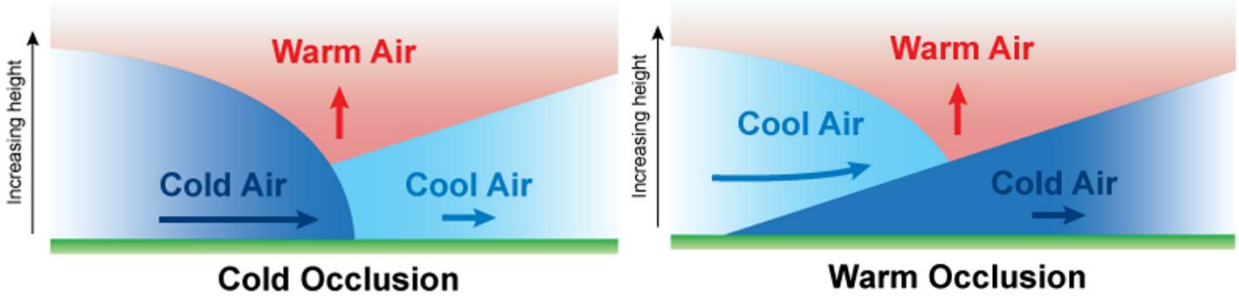

Figure 6-37: (left) A cold occlusion where the coldest air is behind the cold front. (right) A warm occlusion where the coldest air is ahead of the warm front. Both types of occlusion lift the warm air aloft.

Occluded fronts generally have abundant precipitation from cumulonimbus and nimbostratus clouds as the warm, moist air is lifted to higher altitudes. The surface low pressure traditionally moves from a location where the cold and warm fronts intersect to a more northerly position along the occluded front. The cross section in Figure 6-38 describes the clouds and precipitation associated with a cold occlusion.

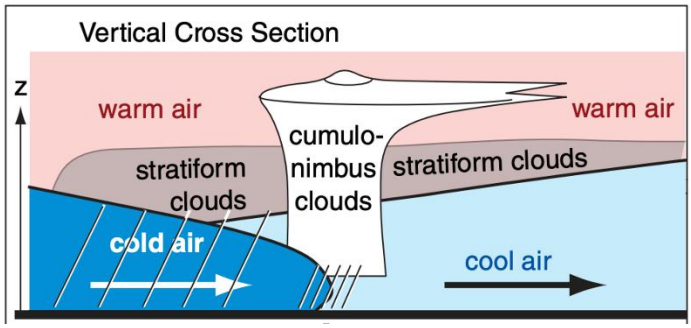

Figure 6-38: Clouds and precipitation associated with a cold occlusion.

This video from the United Kingdom Met Office shows air mass interactions and the weather associated with cold, warm and occluded fronts.

6.5.6 – Norwegian Cyclone Model Life Cycle

The Norwegian Cyclone Model has a particular life cycle that storm systems undergo. This life cycle has these stages:

1. Initial conditions
2. Beginning stage
3. Intensification
4. Mature stage
5. Dissipation

Initial conditions are for a stationary front to exist first. Cold air is on one side and warm air is on the other side. Winds are generally parallel to the front as is shown in Figure 6-39. On the left side is a weather map view as if looking at it from above. The right side is a three-dimensional view. Both views represent the same conditions, just with a different perspective.

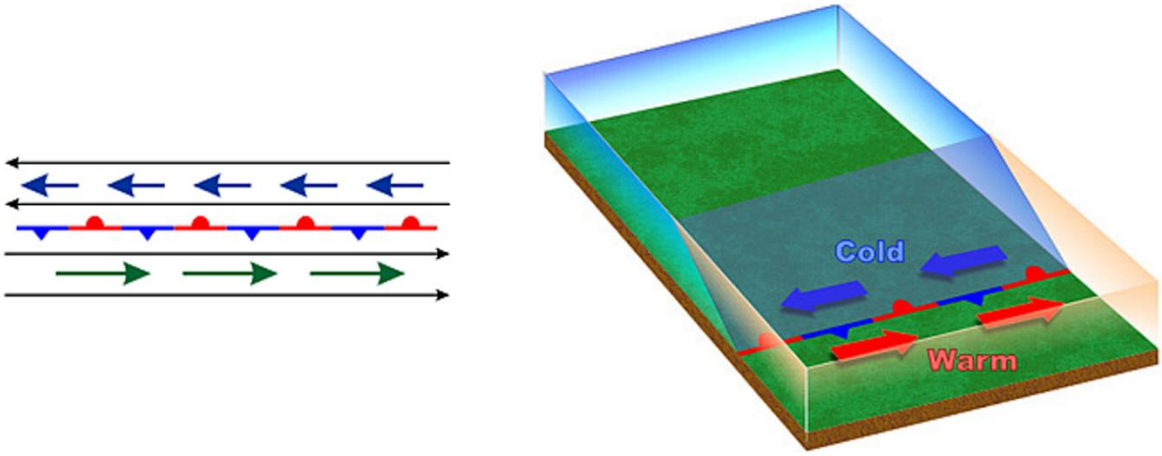

Figure 6-39: Initial conditions in the Norwegian cyclone model start with a stationary front.

The beginning stage is a wave or kink develops on the stationary front. This kink is associated with a weak surface low pressure. Winds start to move cyclonically around this low pressure with a cold and warm front forming. Precipitation will begin to develop with the heaviest near the low center. Figure 6-40 depicts this beginning stage. The green area indicates precipitation in the map view (left side) with the heaviest along the front (dark green). The black lines in the map view are isobars.

Intensification sees the low pressure deepening along with well-defined cold and warm fronts. The winds are northerly behind the cold front and southerly behind the warm front. The area of precipitation has expanded with the heaviest precipitation still associated with the low center. Figure 6-41 depicts this stage in the life cycle.

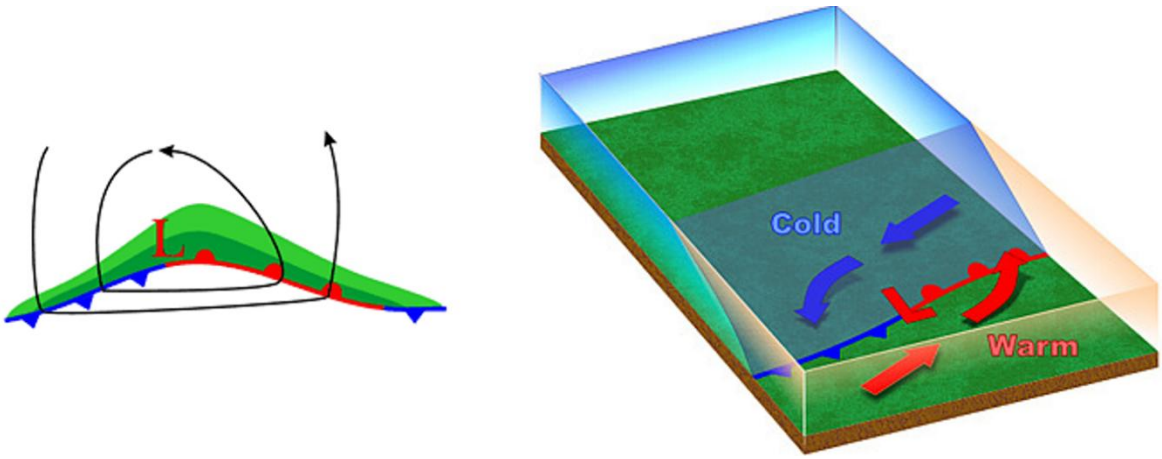

Figure 6-40: Beginning stage as a kink associated with a surface low pressure forms on the stationary front.

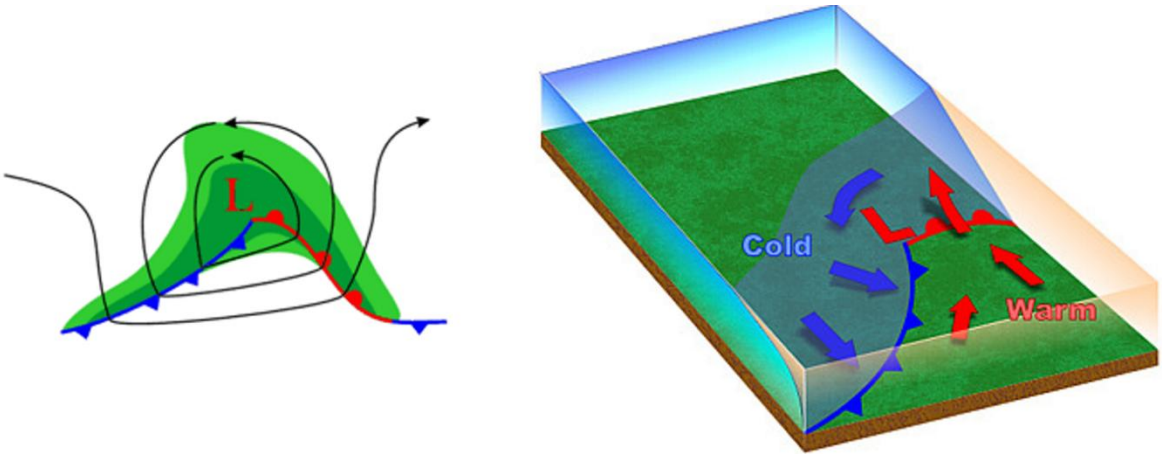

Figure 6-41: Intensification as the low pressure deepens and precipitation increases.

The mature stage has the cold front starting to lift the warm air aloft, which is the beginning of an occluded front. The low pressure center stays with the formation of the occlusion. Precipitation wraps around this low center. Figure 6-42 depicts the mature stage.

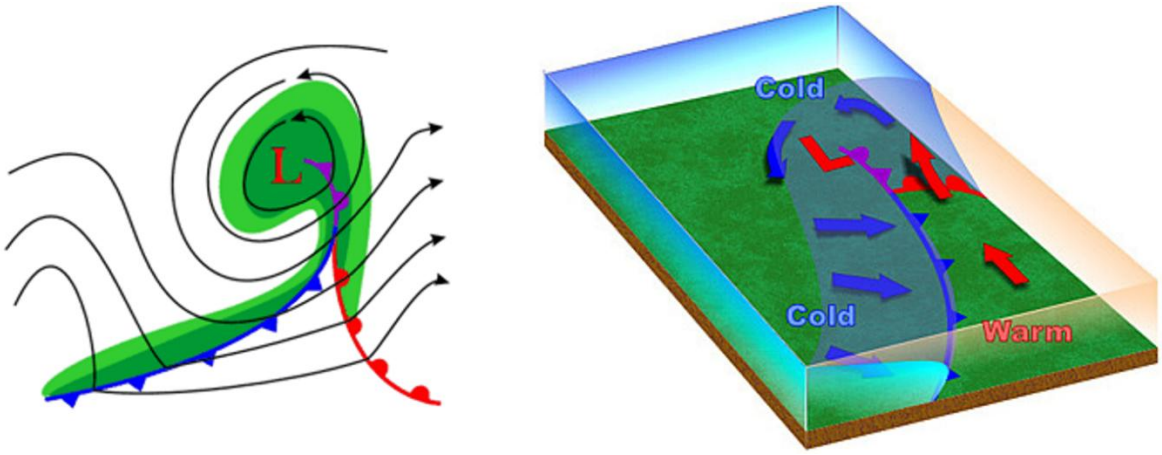

Figure 6-42: Mature stage as the cold front starts to lift the warm air aloft as an occluded front forms.

Dissipation occurs as the cold front continues to advance on the warm front. The occluded front lengthens which eventually removes the supply of warm, moist air. The low pressure weakens and gradually dissipates. Figure 6-43 depicts the final dissipation stage of the storm system.

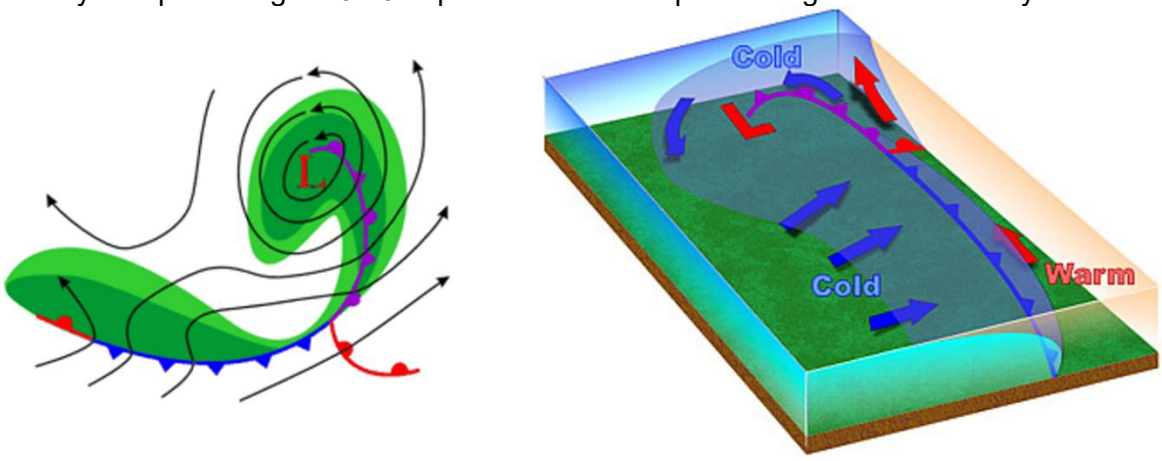

Figure 6-43: The final dissipation of the cyclone as the low pressure weakens.

6.5.7 – Other Boundaries Found on a Surface Map

Three other boundaries are seen on weather surface analysis maps in the United States. These boundaries are a dry line, squall line and a trough. A dry line marks the boundary between a moist air mass and a dry air mass. It typically lies north-south across the central and southern high Plains states (NM, CO, TX, KS and OK) during the spring and early summer, where it separates moist air from the Gulf of Mexico (to the east) and dry desert air from the southwestern states (to the west).

The dry line typically advances eastward during the afternoon and retreats westward at night. A dry line passage results in a sharp drop in humidity, a rise in temperatures, clearing skies, and a wind shift from south or southeasterly to west or southwesterly. These changes occur in reverse order when the dry line retreats westward.

Which is heavier, dry air or moist air? We know colder air is denser (or weighs more) than warm air; thus, colder air always slides under warmer air when the two collide. To determine how dry and moist air interact, we need to know which one weighs more. This question can be answered by looking at the molecular weights of air and water. From Chapter 1, we know air is largely comprised of 78% nitrogen and 21% oxygen. Taking the molecular weights of N_2 (28) and O_2 (32) along with their percentages (0.78 and 0.21) gives a molecular weight of dry air as 29. Water (H_2O) has a molecular weight of 18 (2 + 16). Water vapor is much lighter than dry air. Therefore, dry air with little or no moisture will be heavier than moist air.

Since drier air weighs more than moist air, as the dryline moves east it lifts moist air. Therefore, severe and sometimes tornadic thunderstorms can develop along a dry line or in the moist air just to the east of it. A dry line is represented by a brown line with unfilled half circles on the side the dry air is moving towards. Figure 6-44 depicts the dry line symbol and how it interacts with moist air.

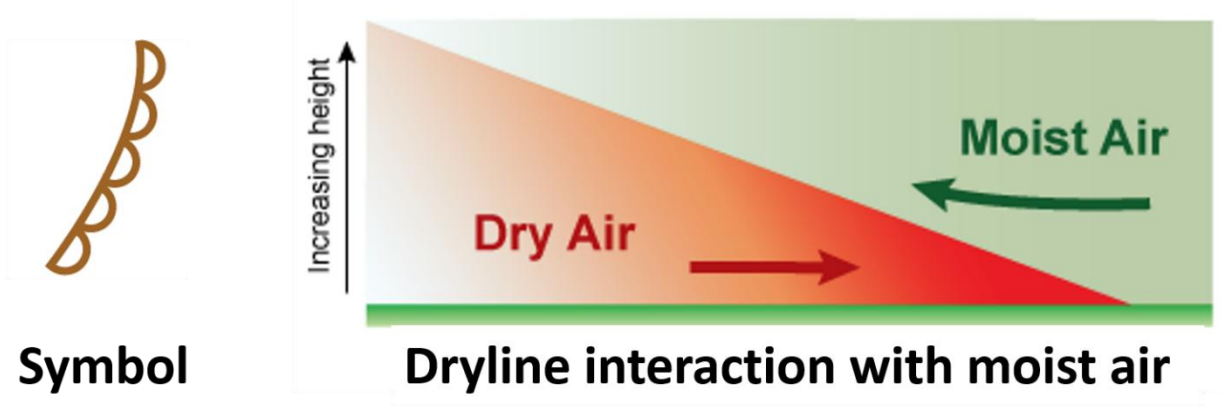

Figure 6-44: Dry line symbol, and the interaction of moist lighter air with heavier dry air lifts the moist air.

The second boundary seen on surface maps is a squall line. A line of thunderstorms that moves ahead of an approaching cold front is called a squall line. A squall line only proceeds a cold front when certain atmospheric conditions are present. A secondary line of weaker thunderstorms or showers would then be associated with the actual cold front passage. Squall lines will be discussed in more detail in Chapter 9.

The third symbol commonly depicted on surface weather maps is a trough. A trough is an area of low pressure aloft. This definition is the same one used in Chapter 3, so no new terminology here. The wind changes direction across a trough, but there is not a change in air mass. While not specifically a surface boundary, troughs reflect a change in atmospheric conditions aloft. Hence, troughs can be areas where clouds and precipitation may form. Figure 6-45 depicts the symbols for a squall line and trough.

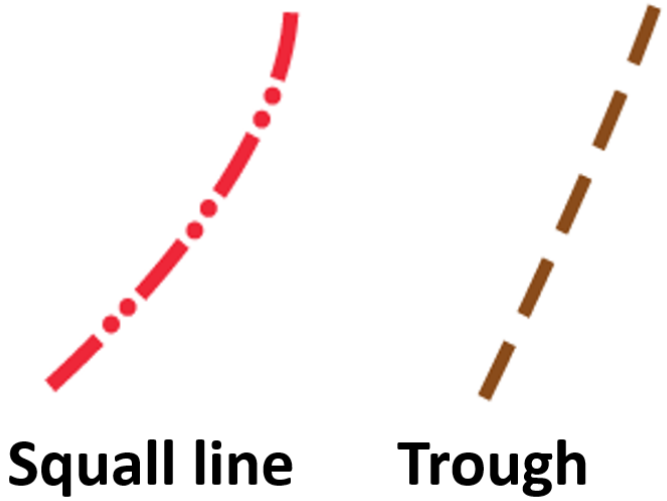

Figure 6-45: Symbols for a squall line and trough.

Chapter 6 Review Questions

1. Describe synoptic scale and the weather features associated with this scale.
2. In what scale is a thunderstorm?
3. What is a conceptual model?
4. What is the primary cause of Earth's global circulation?
5. What is a zonal wind? A meridional wind?
6. What global circulation feature causes dry climates to occur near 30 degrees latitude?
7. What causes the Intertropical Convergence Zone (ITCZ)?
8. Describe the characteristics of a jet stream.
9. In what direction do jet streams usually travel?
10. Name two characteristics of longwaves and two characteristics of shortwaves.
11. What is the definition of an air mass?
12. Which air mass has the highest dew point or moisture content?
13. What is the definition of a front?
14. Label each of the symbols on the following weather map.

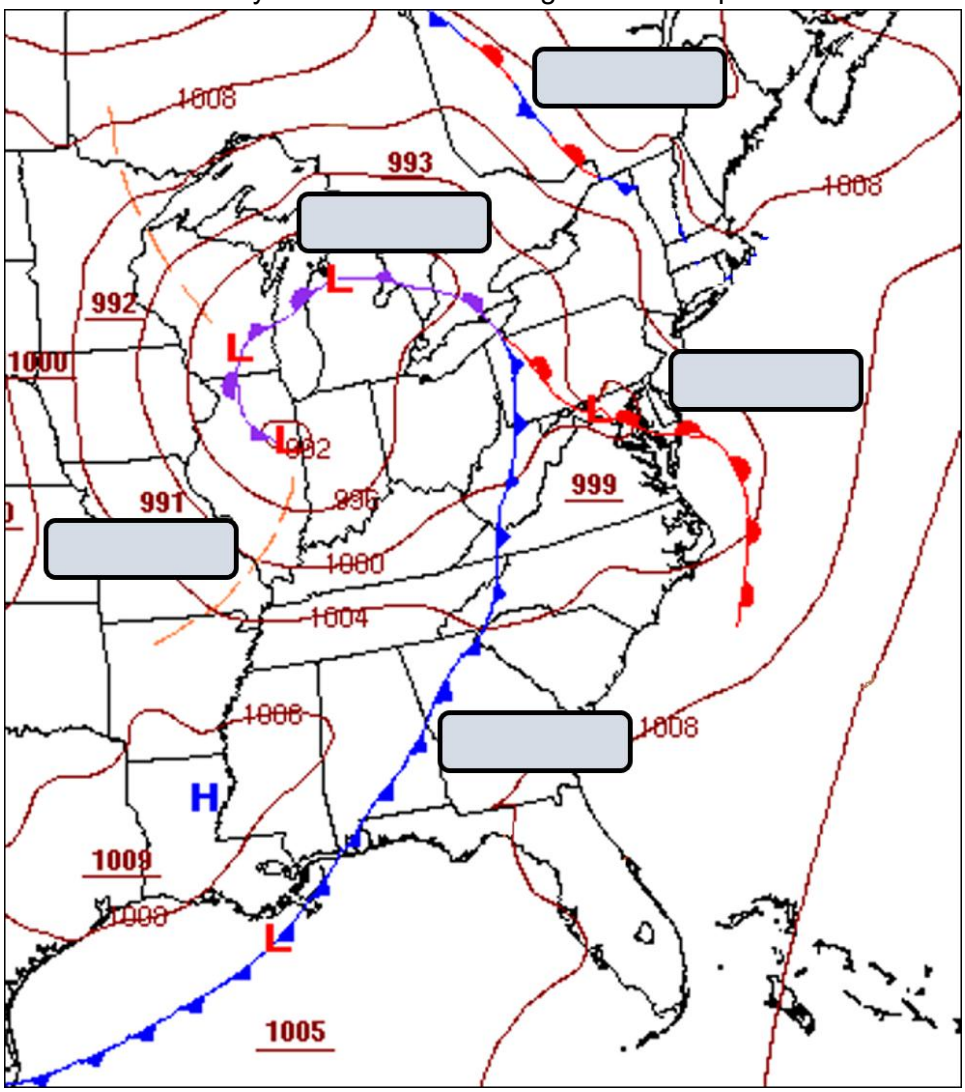

Chapter 7 – Midlatitude Cyclones and Wind Systems

Overview

This chapter explores the vertical structure of midlatitude cyclones. We look at the jet stream, divergence, upper level troughs and ridges that support the stages in the life cycle of midlatitude cyclones. Vorticity is introduced, which is important in understanding vertical motion and the strengthening of storms.

Local and synoptic scale wind systems are discussed. These wind systems, such as a monsoon, are driven by temperature differences as a thermally driven circulation. The wind regimes examined are the sea/land breezes, mountain/valley breezes, the Asian Monsoon and the North American Monsoon.

Chapter objectives:

1. Outline the lifecycle of a midlatitude cyclone.
2. Understand the vertical structure of midlatitude cyclones.
3. Name the paths that midlatitude cyclones frequently travel across North America.
4. Describe the characteristics of a monsoon.
5. Describe the mechanisms which cause sea/land and mountain/valley breezes.

7.1 – Midlatitude Cyclones

In Chapter 6, the Norwegian Cyclone Model was presented. The Norwegian model was originally formulated using surface observations. As more data aloft became available, this model evolved to account for the vertical structure of atmosphere associated with these cyclones. These storm systems migrate in the westerlies of the midlatitude, and are now referred to as midlatitude cyclones or extratropical cyclones.

Cyclone was defined previously as enclosed circular isobars or heights of low pressure, which is correct. Unfortunately, the word “cyclone” is used in many situations and a look at this terminology may be helpful. The formal name for these low pressure areas in the midlatitudes is extratropical cyclones. The word “extratropical” essentially means not in the tropics. In this course, we will use the terminology midlatitude cyclone, because we are examining storms that occur in the midlatitudes between 30º and 60º. Other commonly used names for extratropical cyclones are low-pressure center, low, storm system or cyclone. Tropical storms have a similar situation with common names such as hurricanes, typhoons or cyclones. North America prefers hurricanes, which is what will be used in this book. Hopefully, this brief description of the “cyclone” terminology helps reduce confusion.

Cyclogenesis is when cyclones are born and intensify. Cyclolysis is when they weaken and die. During cyclogenesis three conditions occur simultaneously: (1) winds rotating around the

surface low center increase, (2) vertically motion associated with the surface low center increases and (3) the surface pressure decreases.

Cyclogenesis is favored where one or more of these conditions occur:

1. At frontal zones where the temperature gradients are large.
2. East of a longwave trough in the polar jet stream.
3. East of mountain ranges where the terrain slopes downhill under the jet stream.
4. Where cold air moves over warm water such as the Gulf Stream (increases the instability).
5. At locations where weak instability favors vertical motions.
6. At locations further from the equator where the Coriolis force is greater (not zero).

If cyclogenesis is rapid, with a decrease of over 24 mb in a 24 hour period, this condition is called explosive cyclogenesis, cyclone bomb or bombogenesis. Explosive cyclogenesis usually occurs when multiple conditions favoring cyclogenesis are present.

7.1.1 – Vertical Structure for the Initial Conditions

The first two stages in the Norwegian Cyclone Model (section 6.5.6) are the initial conditions of a stationary front, and the beginning stage with a kink developing on this stationary front. However, for cyclogenesis to begin on a stationary front, a polar jet should reside aloft over it, as illustrated in Figure 7-1.

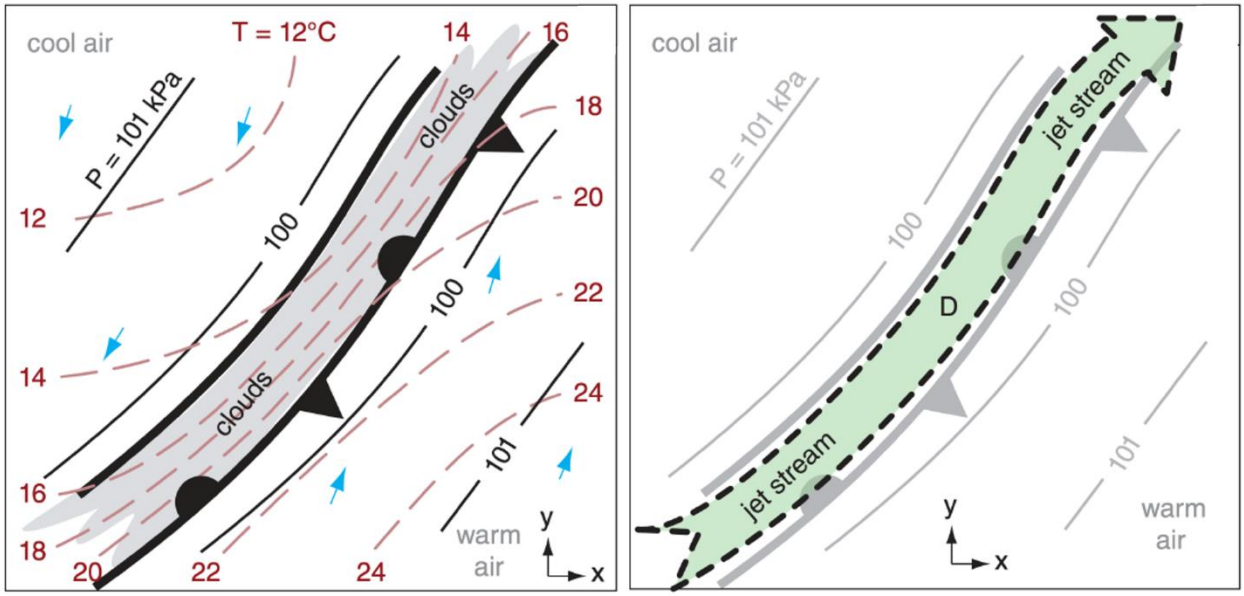

Figure 7-1: Cyclogenesis begins when a jet stream resides over a stationary front. (left) A cloud band and temperature gradient associated with a stationary front. (right) The location of the jet stream with respect to the stationary front. The "D" is associated with divergence.

The left side of Figure 7-1 has isotherms in red. Notice the temperature gradient near the stationary front. The right side of this figure has the jet stream aloft overlaid on the frontal zone. Notice the "D" on the jet stream. The "D" stands for divergence. Divergence is where the wind spreads out into a larger area or increases in speed upstream. Convergence is where the wind is funneled into a smaller area or slows down upstream. Convergence is the exact opposite of

divergence. Figure 7-2 depicts three ways to get divergence in a wind field. The thickness of the arrows in Figure 7-2 represents wind speed.

Divergence aloft promotes the formation of a low pressure at the surface. From previous chapters, we know that a surface low center has air flowing into it or convergence. This convergence of air at the surface causes air to rise over the low pressure center. As the air rises, it will eventually run into the tropopause and spread out. This process works in reverse too. If divergence exists aloft, air must be rising from below to fill that area. The best mechanism to support this rising air is a surface low pressure. Thus, a surface low pressures promotes divergence aloft forming, and divergence aloft promotes a surface low pressure forming. Figure 7-3 depicts what is happening vertically in the troposphere with low and high pressures at the surface.

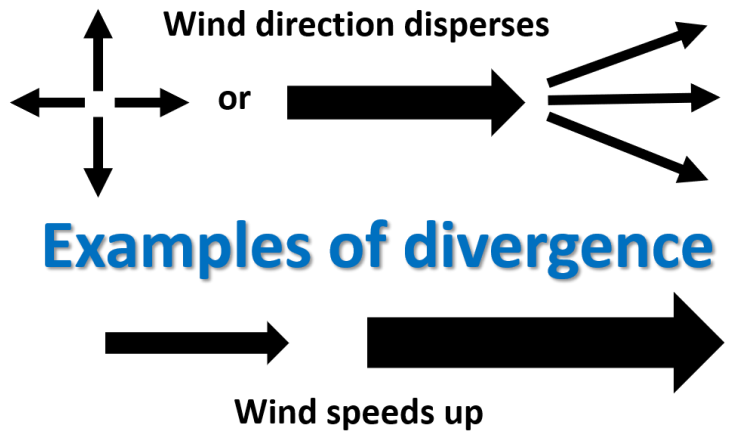

Figure 7-2: Three ways to get divergence in a wind field. Divergence occurs when the wind spreads out into a larger area or increases in speed.

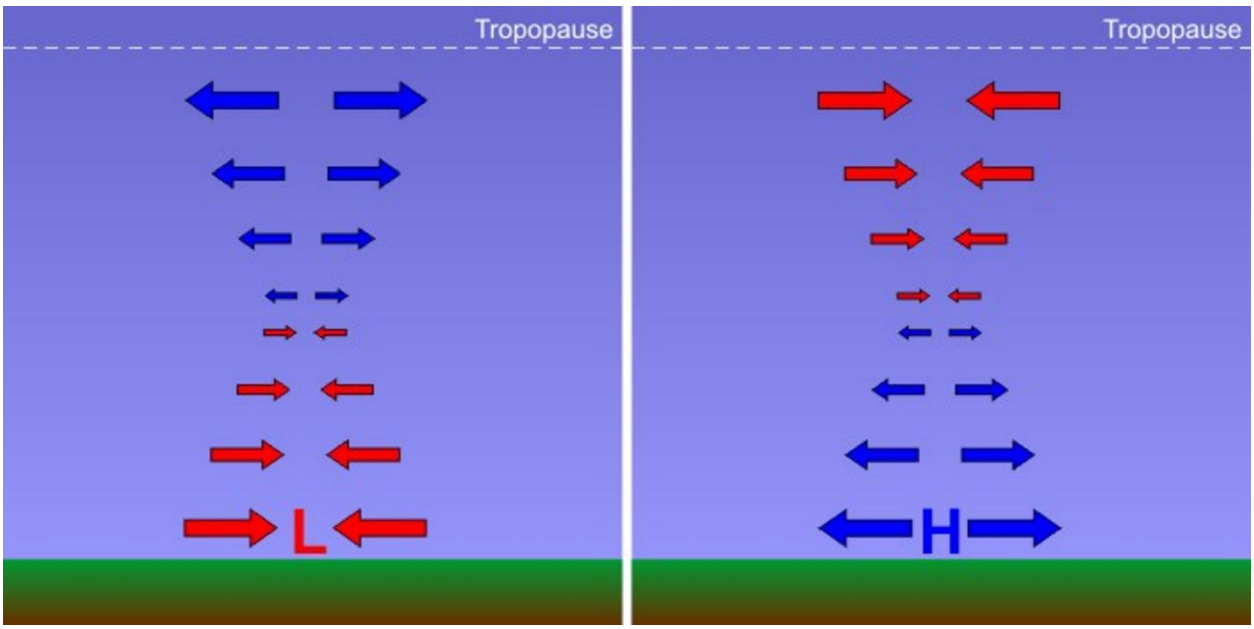

Figure 7-3: Blue arrows represent divergence. Red arrows represent convergence. (left) A surface low pressure has convergence at the surface with divergence aloft. (right) A surface high pressure has divergence at the surface with convergence aloft.

Divergence aloft when a jet stream resides over a stationary front supports the formation of a surface low pressure on that front. The surface low pressure is the beginning of a midlatitude cyclone, and cyclogenesis has begun.

When examining satellite images of the beginning cyclogenesis stage, a kink develops in the cloud pattern. The gray area in Figure 7-4 illustrates this kink in the cloud pattern.

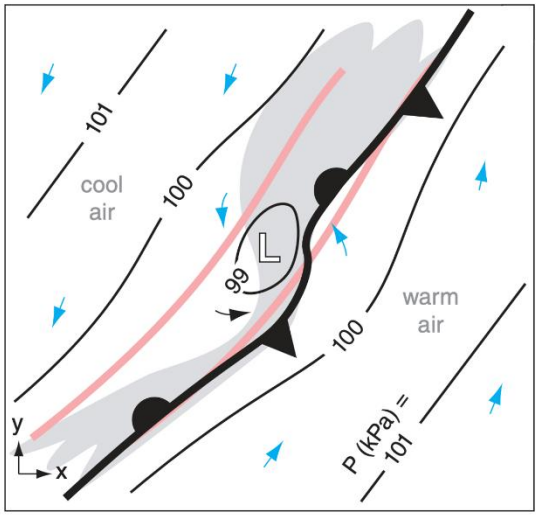

Figure 7-4: The gray area is the cloud pattern near the stationary front. The jet stream location is highlighted in pink. Isobars are the black lines and surface winds are the blue arrows.

During the beginning cyclogenesis stage, satellite imagery indicates that a kink develops in the cloud pattern.

7.1.2 – Vertical Structure of the Mature Cyclone

The next two stages of the Norwegian Cyclone Model (section 6.5.6) are the intensification and mature stages. With divergence aloft and a surface low pressure in place, a midlatitude cyclone can intensify. The next step at the surface is for a cold front and warm front to form. Air continues to rise from the surface low pressure center as it deepens and the surface pressure decreases. Winds rotate around the cyclone in a counterclockwise manner (in the Northern Hemisphere). The atmosphere aloft over this intensification is important for these developments to occur. Figure 7-5 illustrates the vertical structure of a mature midlatitude cyclone with three levels: 250 mb, 500 mb, and the surface.

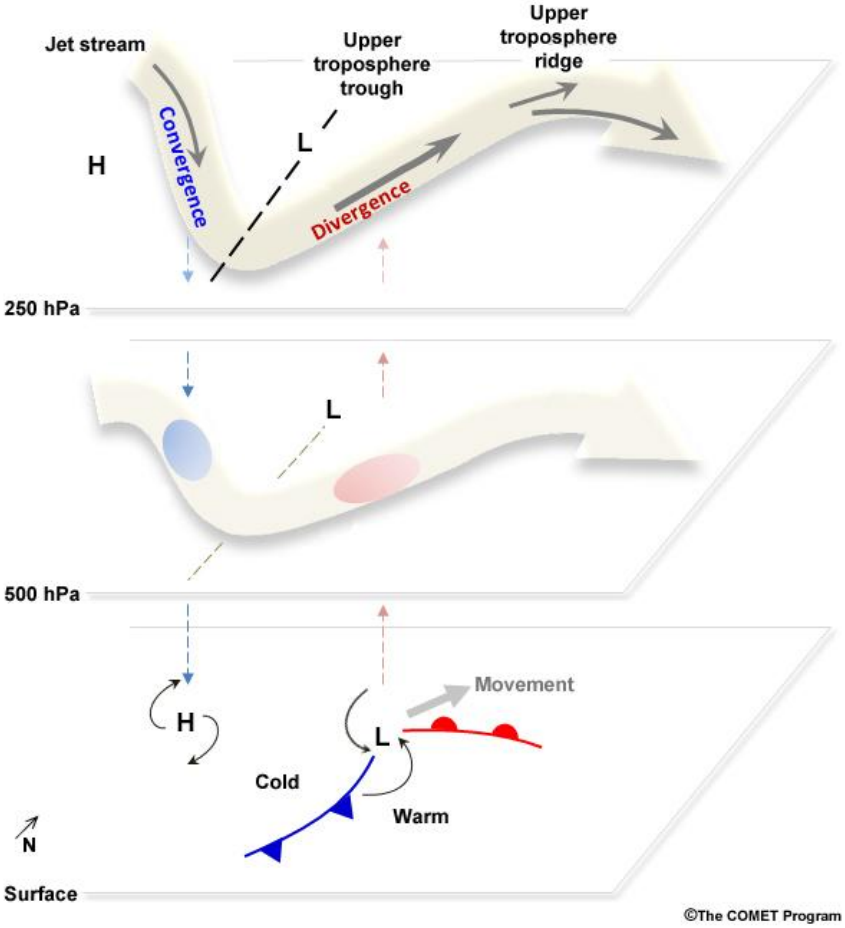

Figure 7-5: Vertical structure of a mature midlatitude cyclone. Top figure is at 250 mb, middle figure is at 500 mb and the bottom figure is on the surface.

Notice in Figure 7-5 that the surface low pressure center is supported aloft with divergence. The jet stream, indicated by gray arrows at 250 mb, resides over the cold front and surface low. Rossby longwaves aloft are now present in this diagram at 250 and 500mb. Convergence occurs at 250 mb which causes downward motion over the surface high pressure. The 250 mb and 500 mb troughs designated by the dashed gray line and "L" are west of the surface low pressure.

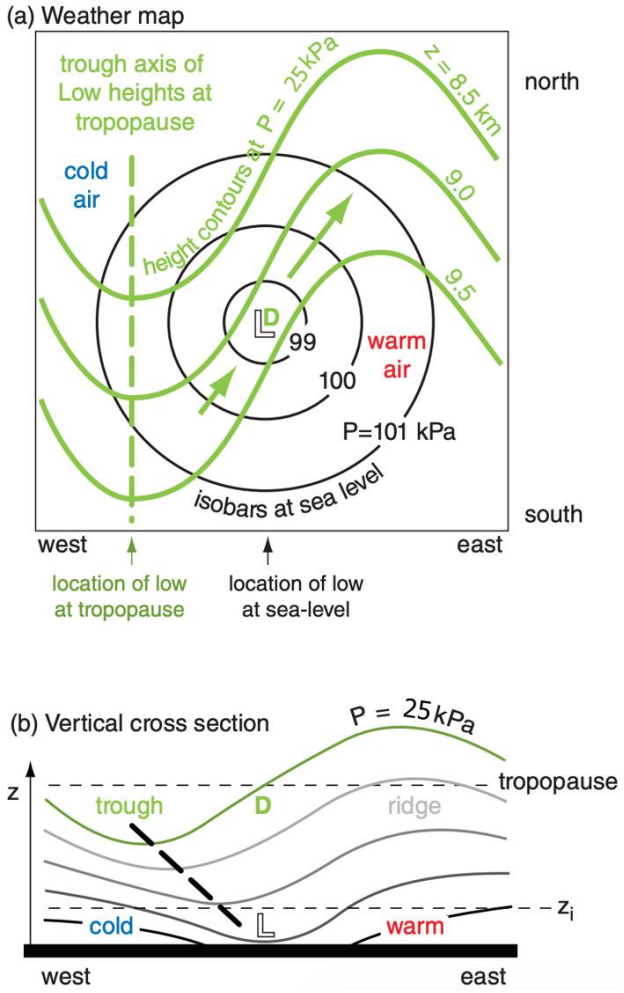

Figure 7-6: The top diagram (1) is a view of a mature midlatitude cyclone from above. The bottom diagram (b) is a cross section of the same cyclone.

The diagrams in Figure 7-6 contain similar information to Figure 7-5, although are different ways to visualize how these features fit together. The top portion (a) is looking at everything from above as in a weather map view. Notice the divergence "D" aloft is over the surface low pressure and upper level trough (green lines) is to the west of the surface system. The bottom portion (b) is a cross section which clearly depicts the upper level trough tilted to the west. The divergence aloft "D" is again over the surface low pressure in the cross section.

Clouds associated with a mature midlatitude cyclone have a comma shape as illustrated in Figure 7-7. This figure depicts the clouds associated with an intensifying (left) and mature cyclone (right).

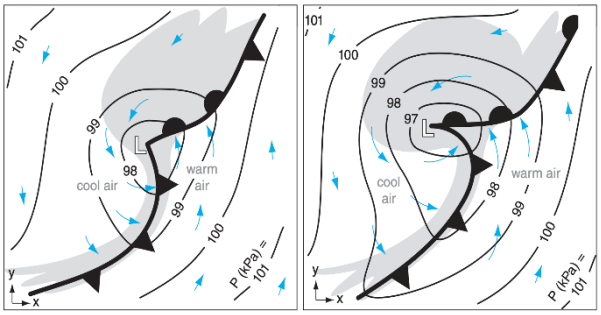

Figure 7-7: Illustrations of the comma clouds (gray area) associated with an intensifying (left) and mature (right) midlatitude cyclone.

A cyclone has the lowest surface pressure and strongest winds at the point when the occluded front forms. An occluded front is the first indication the storm is about to enter the dissipation stage. The cold, dry air (commonly a cP air mass) behind the cold front begins to wrap into the low pressure. The cloud pattern associated with this phase is illustrated in Figure 7-8. Many times, this drier air can be seen wrapping into the cyclone on satellite imagery. When the drier air reaches the top (northern portion) of the cyclone rotation, the dissipation stage is about to begin.

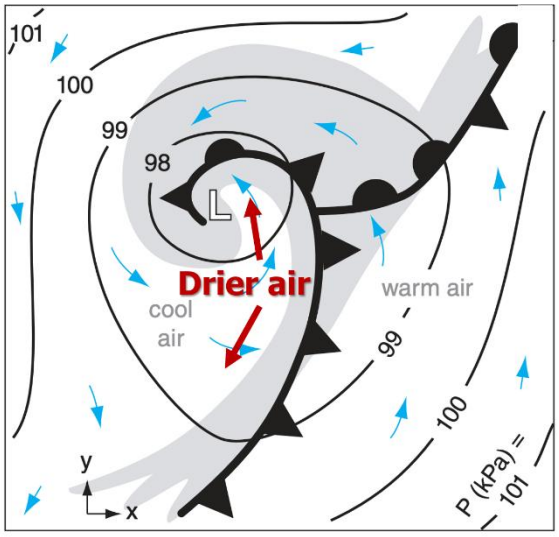

Figure 7-8: A mature midlatitude cyclone about to enter the dissipation stage with dry air wrapping into the low pressure. The gray area represents clouds.

7.1.3 – Vertical Structure for Occlusion and Decay Stage

In the dissipation stage, the cyclone occlusion grows and the low center becomes surrounded by cool, dry air. Clouds during this stage spiral around the center of the low. This spiral signature can easily be seen in animated satellite images. The jet stream moves east of the surface low center to remain over the weakening surface warm and cold fronts, which are becoming more stationary. Thus, the surface low center loses its upper level divergence support.

Without support from the jet stream, the surface low pressure center begins to fill. The central pressure starts to rise and the winds slow. The surface low pressure center drifts slowly poleward. The spiral of clouds dissipates into scattered clouds and precipitation diminishes. A stationary front remains, which may totally dissipate or aid in the formation of a future midlatitude cyclone. Figure 7-9 illustrates the continued occlusion and dissipation of the cyclone.

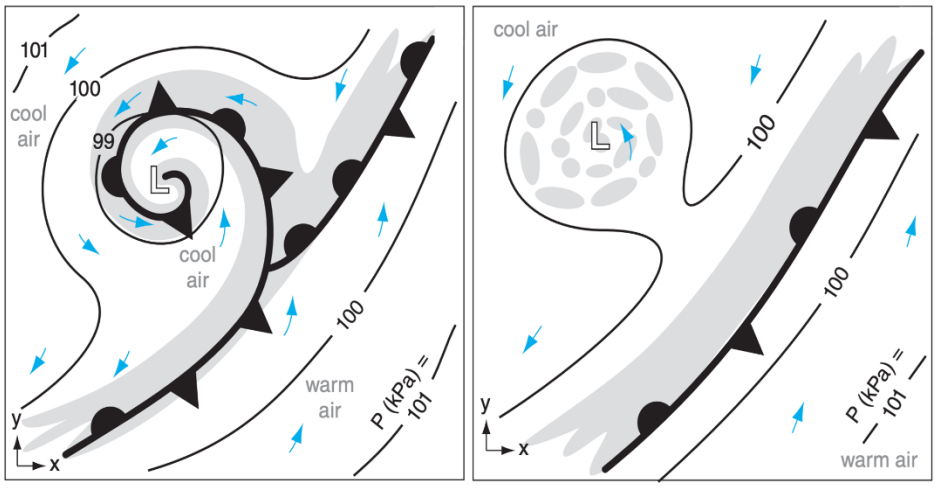

Figure 7-9: Dissipation stage of a midlatitude cyclone. (left) The occlusion grows as drier air spirals into the low center. (right) After fully dissipated, a stationary front remains. The gray area represents the cloud pattern.

When the jet stream moves east, the upper level trough aligns vertically to be closer or on top of the surface low. The vertical low pressure structure has gone from a tilted configuration in the mature stage to a stacked configuration as it decays. The upper level low is directly above or close to the surface low pressure center.

Dry air can frequently be seen on satellite imagery wrapping into a midlatitude cyclone as the occlusion expands. This condition is indicative of the decaying storm. The water vapor satellite image in Figure 7-10 shows the dry air wrapping into the low center near the Aleutian Islands. The yellow and dark blues are drier air. The white and green are moister air. Notice the large comma shaped moisture pattern associated with this cyclone.

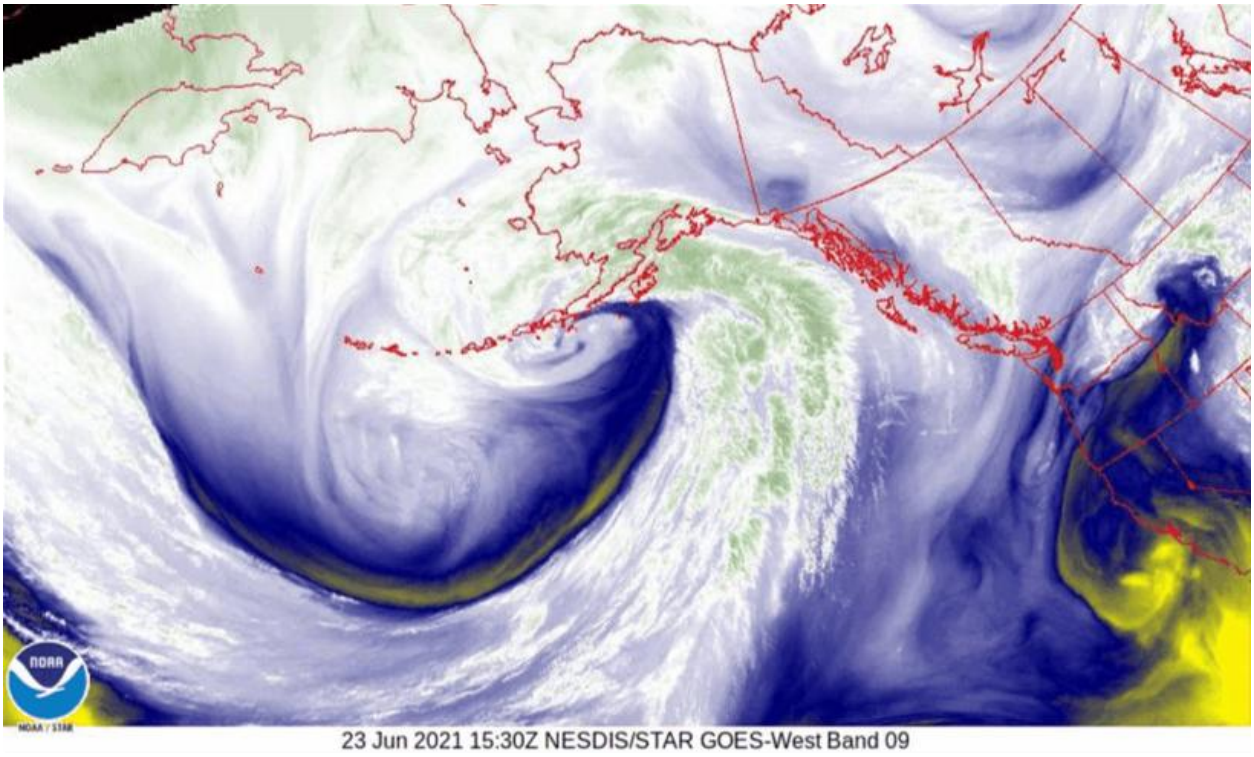

Figure 7-10: A water vapor satellite image showing dry air (yellow and dark blue) wrapping into a dissipating midlatitude cyclone near the Aleutian Islands. Notice the moister air (white and green) has a large comma cloud associated with this low pressure.

7.1.4 – Conveyor Belt Conceptual Model

Another more recently developed conceptual model of midlatitude cyclones is called the conveyor belt model. The conveyor belt model focuses on the three-dimensional wind structure of a midlatitude cyclone, rather than air masses and fronts. Figure 7-11 depicts the conveyor belt model.

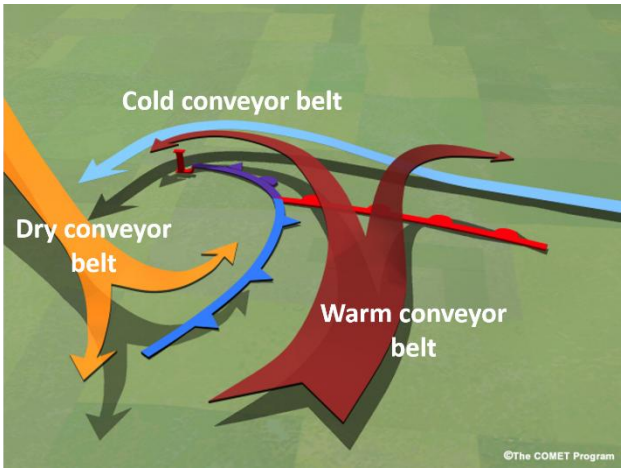

Figure 7-11: Conveyor belt midlatitude cyclone model, which consists of three wind regimes (cold, dry, and warm).

Three major wind regimes or belts are present in this model: (1) the warm conveyor belt, shown as the burgundy in Figure 7-11, (2) the cold conveyor belt shown as the light blue, and (3) the dry conveyor belt shown as the yellow or orange.

The warm conveyor belt is associated with the warm, moist air moving poleward. As the warm conveyor belt encounters cooler air, it is lifted and rises as high as 30,000 feet. At these heights, this belt encounters the westerly flow and turns eastward. Additionally, this warm air can get wrapped into the surface low pressure. The satellite images in Figure 7-12 depict the clouds and moisture associated with a warm conveyor belt. Both of these images are water vapor, which captures this moisture laden air well.

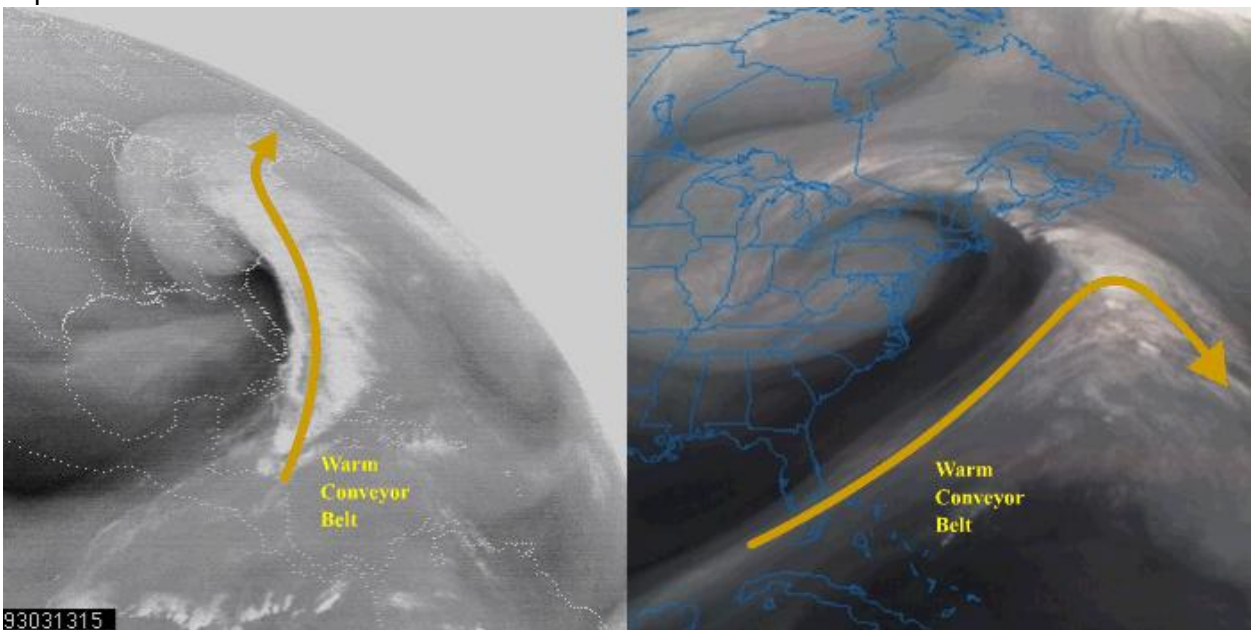

Figure 7-12: Water vapor satellite images depicting the warm conveyor belt.

The cold conveyor belt is the cooler air that lifts the warm, moist air associated with the warm conveyor belt. This cold belt is responsible for creating the comma cloud pattern indicative of a mature midlatitude cyclone. Likewise, this cooler air get wrapped into the surface low pressure center too. The diagrams in Figure 7-13 illustrate the cold conveyor belt of a mature midlatitude cyclone.

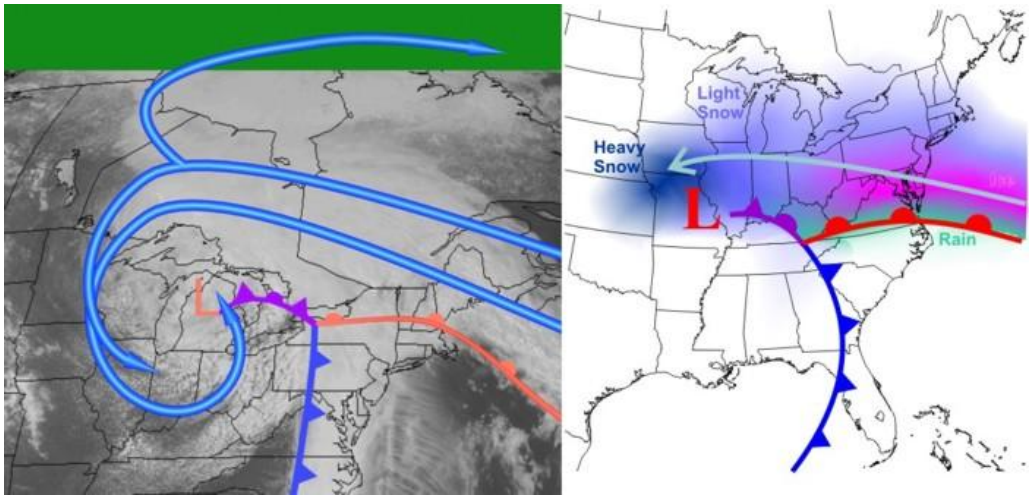

Figure 7-13: Illustrations of the cold conveyor belt associated with a mature midlatitude cyclone. The blue arrows represent this wind regime.

The dry conveyor belt is associate with cold, dry air originating from the mid-troposphere. This air creates the inside of the comma cloud pattern since it lacks moisture. Many people mistake the cold conveyor belt as the cold air behind the cold front, which is not true. The naming convention in this model has the air behind the cold front as dry conveyor belt. This dry air can create a cloud free area behind the cold front called a dry slot. Additionally, as this dry air wraps into the low center, its orientation can be a direct indication of when a cyclone is passing from a mature to a dissipation phase. The satellite images in Figure 7-14 depict a dry slot associated with a dry conveyor belt. The image on the left is visible data and the image on right is water vapor.

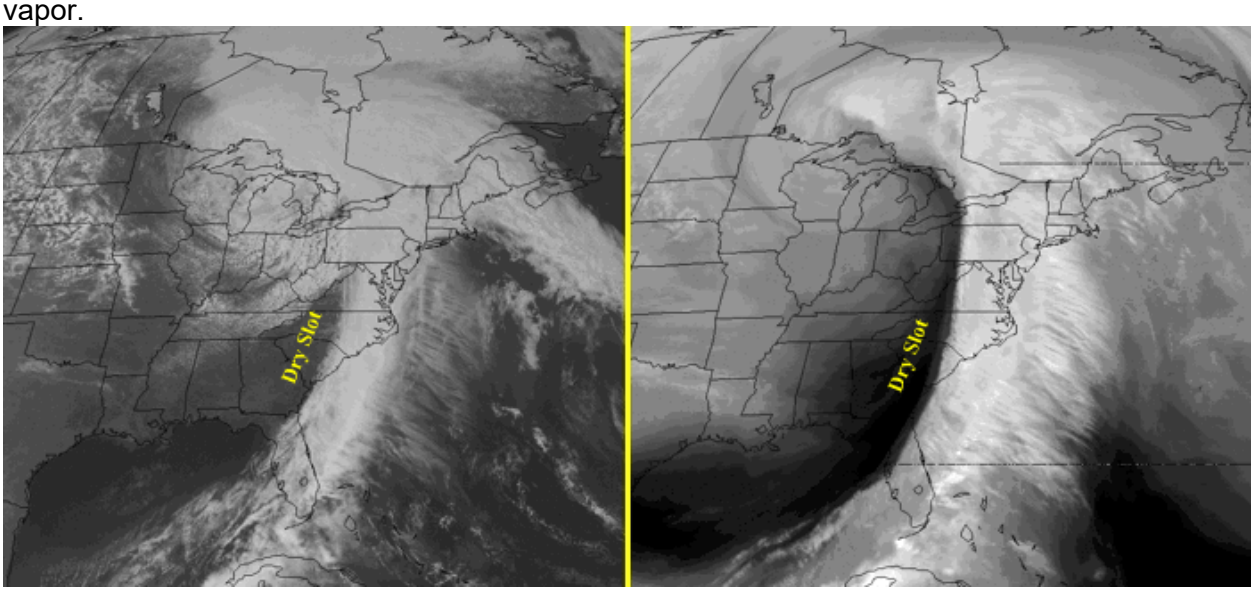

Figure 7-14: Two satellite images of the same storm system depicting the dry slot associated with the dry conveyor belt. The image on the left is visible. The image on the right is water vapor.

Figure 7-15 contains a water vapor satellite image with a low pressure off the southern California and Mexico coasts. All three conveyor belts are highlighted in this image. Since the dry air (yellow arrow) has reached the top of the low pressure circulation, this midlatitude cyclone just entered the dissipation stage. The cold conveyor (blue arrow) belt is underneath the warm conveyor belt (red arrow) and wraps into the low center.

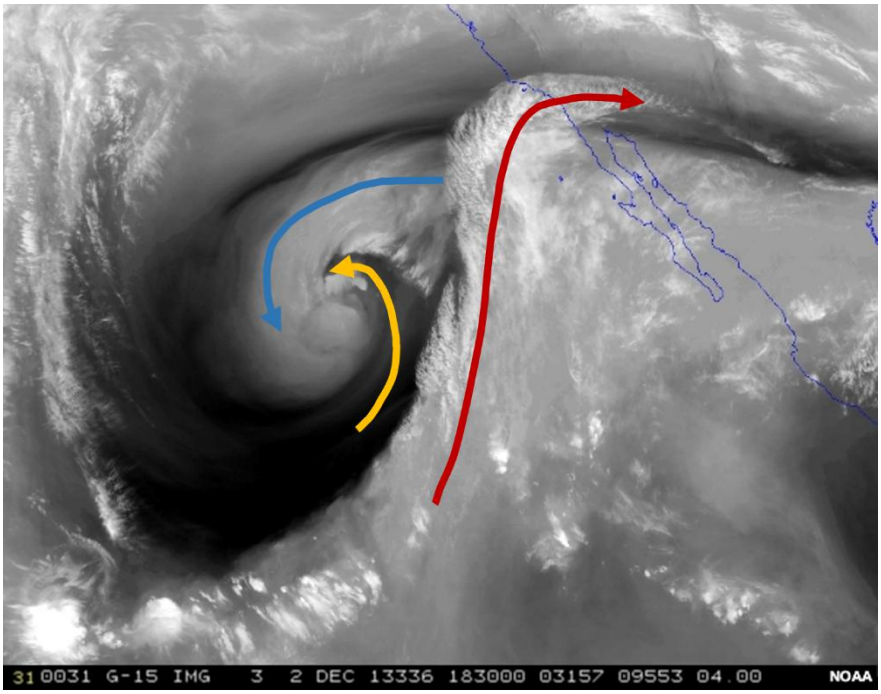

Figure 7-15: A midlatitude cyclone off the southern California and Mexico coasts. All three conveyor belts are highlighted.

7.1.5 – Storm (Midlatitude Cyclone) Tracks

Two geographic conditions highlighted earlier in this chapter favor cyclogenesis, and they were: (a) east of mountain ranges where the terrain slopes downhill under the jet stream, and (b) where cold air moves over warm water such as the Gulf Stream (increases the instability).

The two conditions so frequently cause midlatitude cyclone cyclogenesis in North America, that storms originating from these areas have been given names. These names are:

1. Alberta Clipper – Forms in the Canadian Province of Alberta and moves across southern Canada.
2. Nevada Low – Forms on the lee side of the Sierra Nevada Mountains and moves through Utah into Colorado. These storms frequently undergo cyclogenesis again in Colorado.
3. Colorado Low – Forms on the lee side of the Rocky Mountains and tracks across the Great Lakes.
4. Gulf Low – Forms over the warm water in the Gulf of Mexico and tracks to the west of Appalachian Mountains or up the east coast of the U.S. following the Gulf Stream.
5. Hatteras Low – Forms off the Carolinas and follows the Gulf Low track.
6. Bahamas Low – Forms near the Bahamas and tracks up the east coast of the U.S.
7. Nor'easter – Undergoes cyclogenesis off New England and travels up the east coast of Canada.

The map in Figure 7-16 shows these favored locations for cyclogenesis and the storm movement. The Alberta Clipper, Nevada Low and Colorado Low form on the east side of mountain ranges. The remaining storm tracks are associated with the cyclogenesis favored by cold air moving over warm water (the Gulf of Mexico and Gulf Stream).

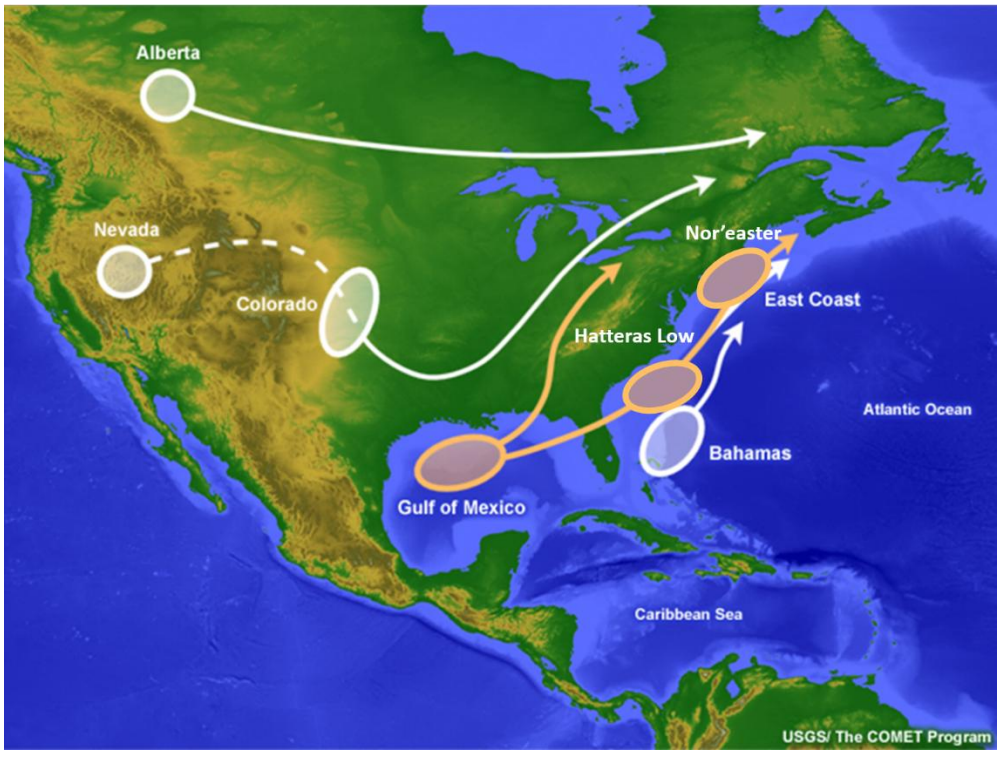

Figure 7-16: A map of the storm tracks over North America.

7.1.6 – Lake Effect Snow

Lake effect snow is a localized band of snow that occurs on the lee side of a lake as cold air passes over the lake. These conditions are most prominent in the late fall and early winter when lake water is warmest, and are associated with the passage of a midlatitude cyclone. The snow bands occur in the coldest air behind the cold front. The circumstances associated with these snow bands is illustrated in Figure 7-17. Cold air moves over warmer lake water picking up moisture. This moist air creates a band of snow which is deposited on the lee side of the lake.

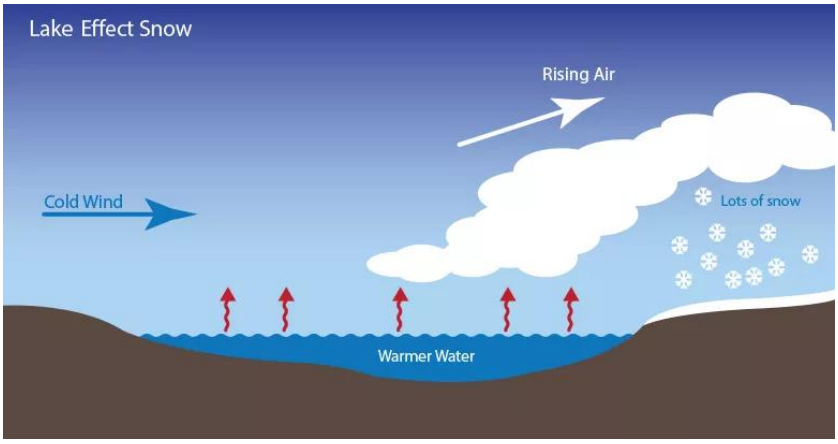

Figure 7-17: The circumstances associated with lake effect snow. Cold air moves over a warm lake entraining moisture. This moisture laden air creates a snow band depositing copious amounts of snow as the air rises off the lake.

The snow bands in these situations can be very narrow. Heavy snow and treacherous driving conditions can occur in one area, while several miles away sunny skies prevail. Lake effect snow can occur with any lake. In the United States, these conditions are most commonly associated with the Great Lakes. Every year areas around the Great Lakes experience lake effect snow. Figure 7-18 provides a satellite image (left) and snow depth (right) from an early winter storm on November 29, 2023. The windward side of the lake has cloudless conditions associated with the cold air. As this cold air moves over the warmer water entraining moisture, skies become cloudy and precipitation forms. Buffalo, New York experiences these increased snow amounts every winter. During the episode depicted in Figure 7-18, Buffalo got between 18 and 24 inches of snow.

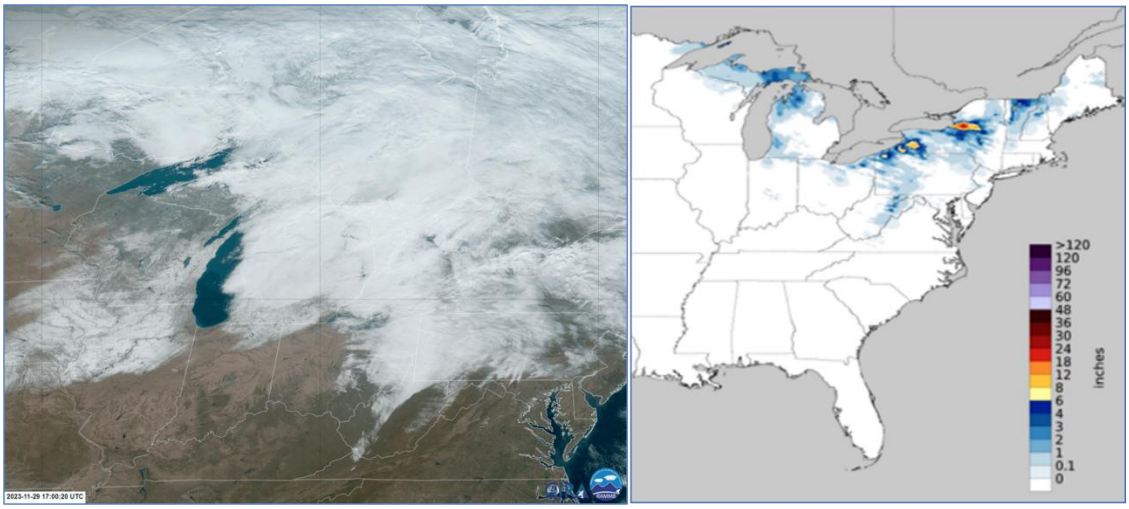

Figure 7-18: A visible satellite image (left) and snow amounts (right) associated with a lake effect snow event on November 29, 2023.

7.2 – Concept of Vorticity

Vorticity is a measure of the rotation in a fluid, like air. In the atmosphere, vorticity can be correlated with surface low pressure development and upward vertical motion. Hence, vorticity is a topic of interest to us.

To begin the study of vorticity, dividing it into three components is beneficial. The first component is Earth's vorticity, which is due to the Earth's rotation. Earth vorticity is dependent on latitude, and is associated with the Coriolis force. Earth's vorticity is zero at the equator and highest at the poles.

The second component is relative vorticity, which is rotation relative to the Earth's surface. Relative vorticity is what is observed from the Earth's surface. If you see rotation in clouds when viewing the sky, you are seeing the relative vorticity of those clouds. The last component is absolute vorticity. Absolute vorticity is the sum of the Earth's vorticity and relative vorticity.

Rotation in a counterclockwise manner is called positive vorticity. Rotation in a clockwise manner is called negative vorticity. Why is this positive and negative notation used? Positive vorticity complements or adds to the Earth's vorticity. Negative vorticity diminishes or subtracts from the Earth's vorticity. Figure 7-19 illustrates this concept with the wind pattern around a high a low pressure.

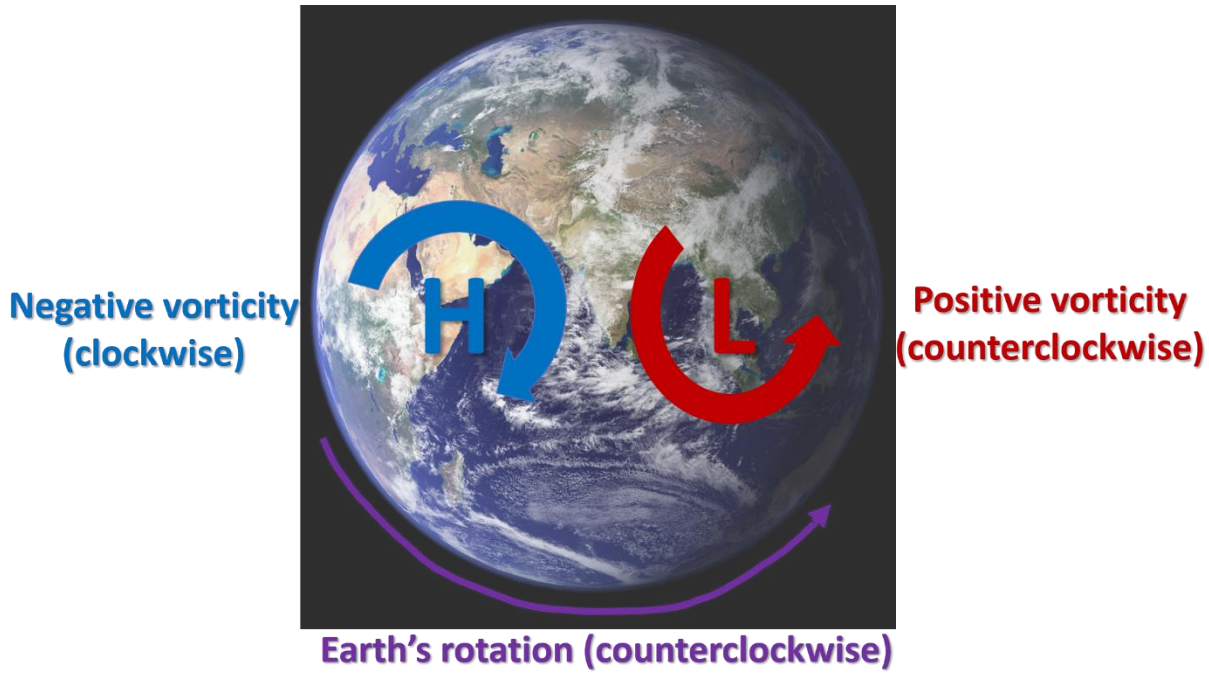

Figure 7-19: Negative vorticity (clockwise) diminishes the Earth's vorticity associated with its rotation (purple arrow). Positive vorticity (counterclockwise) adds to the Earth's vorticity.

The wind pattern associated with a high and low pressure has rotation and hence relative vorticity. Applying these concepts to an upper level height chart shows that positive relative vorticity exists at the bottom of an upper level trough, because the wind rotates in a

counterclockwise manner. Along the sides of a trough, relative vorticity is absent because the wind direction does not change. Figure 7-20 highlights the positive relative vorticity in a trough.

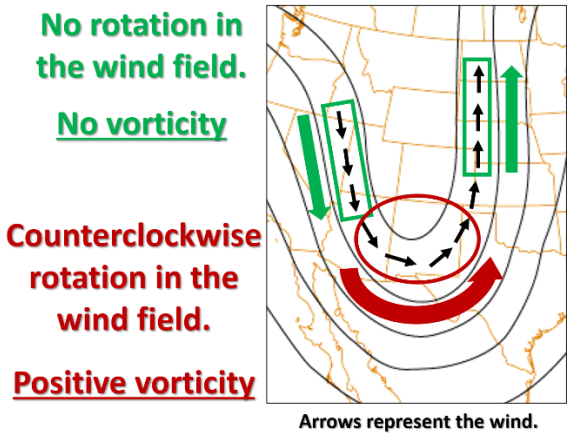

Figure 7-20: Positive relative vorticity occurs at the bottom of an upper level trough.

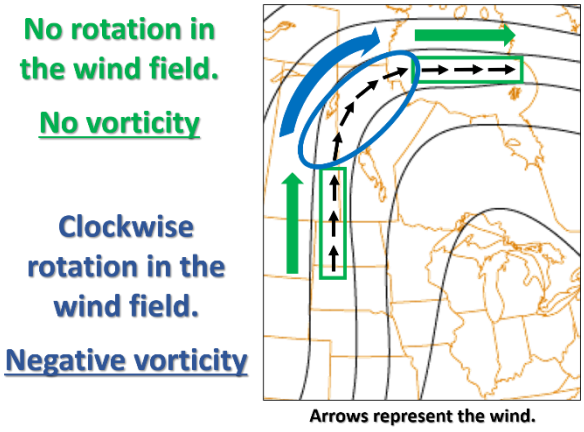

Figure 7-21: Negative relative vorticity occurs at the top of an upper level ridge.

A similar situation is present in an upper level ridge, except with negative relative vorticity being present. The sides of the ridge lack relative vorticity, since the wind does not change direction. The top of the ridge has the wind rotating in a clockwise manner for an area of negative relative vorticity, as depicted in Figure 7-21.

7.2.1 – How Vorticity Supports Midlatitude Cyclones

Examining the absolute vorticity associated with longwaves indicates a maximum value at the bottom of a trough and a minimum value at the top of a ridge. The maximum absolute vorticity resides in the trough because Earth's vorticity is added to the relative vorticity. Adding two positive vorticities together gives a maximum of absolute vorticity. Likewise, the minimum absolute vorticity associated with a ridge is because the relative vorticity is negative. Adding Earth's vorticity to a negative number reduces the absolute vorticity. Figure 7-22 depicts these areas using the same height field as shown in the previous section.

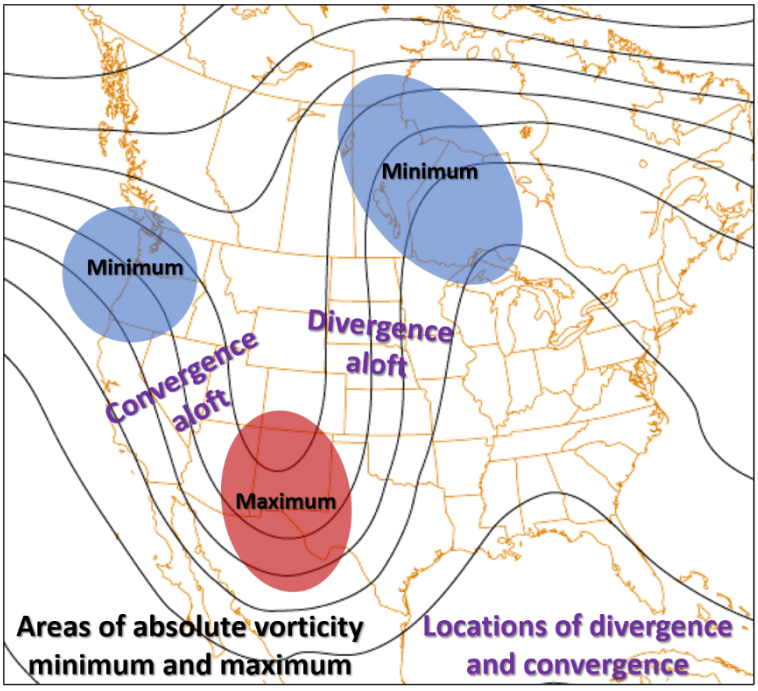

Figure 7-22: Areas of minimum and maximum absolute vorticity associate with an upper level trough and ridges. Notice the convergence and divergence aloft between these areas which support the surface pressure systems.

Locations downstream of maximum absolute vorticity areas experience rising motion.

Rising motions in the troposphere result in divergence aloft as this air encounters the tropopause. This principle agrees with the vertical structure of a midlatitude cyclone. Thus, the placement of an absolute vorticity maxima and its divergence aloft agrees with the conceptual model of a midlatitude cyclone. A midlatitude cyclone has rising air over the surface low pressure center with divergence aloft. This area of divergence aloft is in the same location whether using the surface low pressure center or the maximum absolute vorticity to find it. All these physical principles agree with each other.

Locations downstream of minimum absolute vorticity areas experience sinking motion. This sinking motion occurs over the surface high pressure center. Again all these physical principles in the conceptual models agree with each other.

7.2.2 – Examining Relative Vorticity in More Detail

One source of relative vorticity is due to the curvature of the wind flow. Relative vorticity resulting from curvature was described previously as the wind changes direction when flowing around a longwave ridge or trough. Another source of relative vorticity is due to the variations in the speed of the flow. These variations in wind speed are called shear. Hence, relative vorticity has two sources from a wind field due to its (1) curvature and (2) shear.

Shear is best described with an imaginary paddle wheel. If wind speeds increase with height from the surface up into the atmosphere, vertical wind shear is present. Placing a paddle wheel into these wind conditions would cause the paddle wheel to rotate. The wind at the top of the paddle wheel is stronger than the wind at the bottom. Figure 7-23 illustrates vertical wind shear with the rotation of a paddle wheel.

Since the paddle wheel is rotating, the vertical wind shear is creating vorticity. In Figure 7-23 the rotation is clockwise and negative relative vorticity is present. Negative vorticity can also be referred to as anticyclonic vorticity, and positive vorticity as cyclonic vorticity. Anticyclonic and cyclonic terminology is valid in both the Northern and Southern Hemispheres. The negative and positive vorticity terminology used in this course is only valid for the Northern Hemisphere.

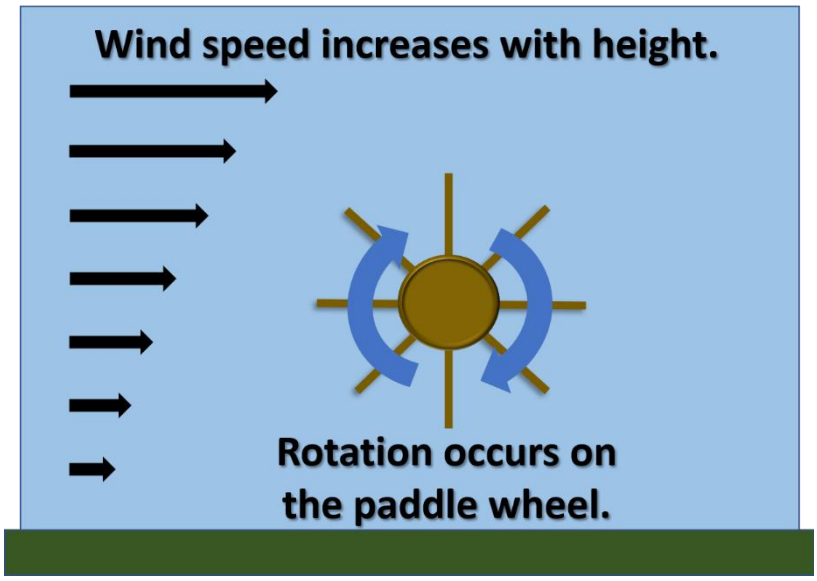

Figure 7-23: Wind speed increasing with height (wind shear) creates relative vorticity as illustrated by a rotating paddle wheel.

Shear vorticity can be created from any change in the wind speed whether that change occurs in the vertical or the horizontal direction. These two components of relative vorticity are extremely important in understanding thunderstorm development, and will be used in an upcoming chapter.

7.3 – Local Wind Systems - Sea Breeze

So far, everything covered in this book has been either of the global or synoptic scales. The sea breeze is a local coastal wind that blows from the sea toward the land during the day and reverses at night. These breezes are a mesoscale phenomenon caused by the temperature differences between the sea surface and the adjacent land mass. Sea and land breezes are thermally driven circulations.

The specific heat of water is much higher than land. This difference causes the land to heat up and cool down much faster than the adjacent body of water. In the absence of other synoptic scale features, such as a front, these temperature differences cause a local circulation to develop which is diurnal in nature. The breeze goes one way during the day (onshore) and the other direction at night (offshore).

Sea and land breezes are strongest during the summer when the temperature contrast between the water and land is greatest. In the wintertime, the land may not get warm enough to cause a breeze. The eight illustrations in Figures 24 and 25 depict the details of sea and land breezes throughout a 24 hour period.

During the early morning hours, a weak offshore flow (wind from the land to the sea) may be present or the wind may be calm (Figure 7-24a). As mid-morning approaches, air begins to rise over the land (Figure 7-24b). This motion is caused by the Sun heating the land surface heating, which in turn warms the air next to the surface. This warmer air becomes buoyant and rises and the physical process of convection occurs. As this air rises, it must be replaced and a breeze starts to move inland from the ocean. The temperature differences between the ocean and land air are substantial enough that a transition zone or front is created as the sea breeze comes onshore. This sea breeze front is very shallow in depth.

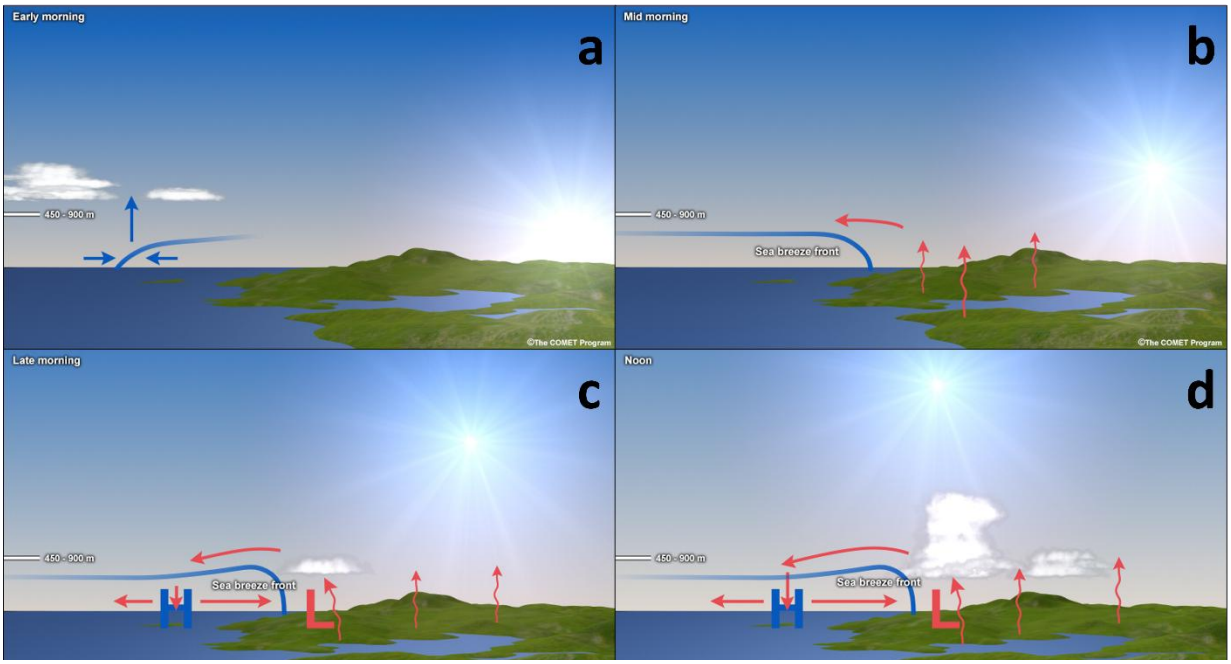

Figure 7-24: The sea and land breeze from early morning to noon. (a) In the early morning a weak offshore flow is present. (b) By mid-morning, the land is heating causing rising air and the sea breeze comes on shore. (c) In late morning the sea breeze front has strengthened with high and low pressures forming. (d) By noon everything has strengthen with clouds forming along the sea breeze front.

By late morning (Figure 7-24c), the sea breeze front has strengthened as a lower pressure forms over the land and a higher pressure over the water. These low and high pressures are caused by the differences in temperature between the water and land. Notice small cumulus clouds may form along the sea breeze front. At noon (Figure 7-24d) everything has strengthened from the late morning. The clouds near the sea breeze front may experience some vertical development. The rising thermals caused by the warm land surface may also create some clouds.

By early afternoon (Figure 7-25e), the sea breeze front has pushed inland. The low pressure over land is well established with rising air. The high pressure over the water is well established with descending air.

The location of the sea breeze front can be determined by the cloud boundary. Clouds occur ahead of and on the front, with generally cloud free conditions behind the front. Depending on atmospheric stability, a cumulonimbus or thunderstorm may develop along the sea breeze front. These early afternoon conditions last into the peak heating of the late afternoon when the sea breeze is strongest.

By early evening (Figure 7-25f), the Sun angle is lower and the peak heating during the day has subsided. Everything begins to weaken. The low pressure over land diminishes along with the rising air. The clouds over land decrease in vertical and areal extent. The sea breeze front is becoming diffuse. As the Sun sets (Figure 7-25g), the temperature contrast between water and land has equalized. Winds have subsided. Cloud free skies predominate. Slightly cooler air may reside over the water, but the temperature difference is not enough to create wind. However, the land will continue to cool into the night while the air temperature over the water remains relatively constant.

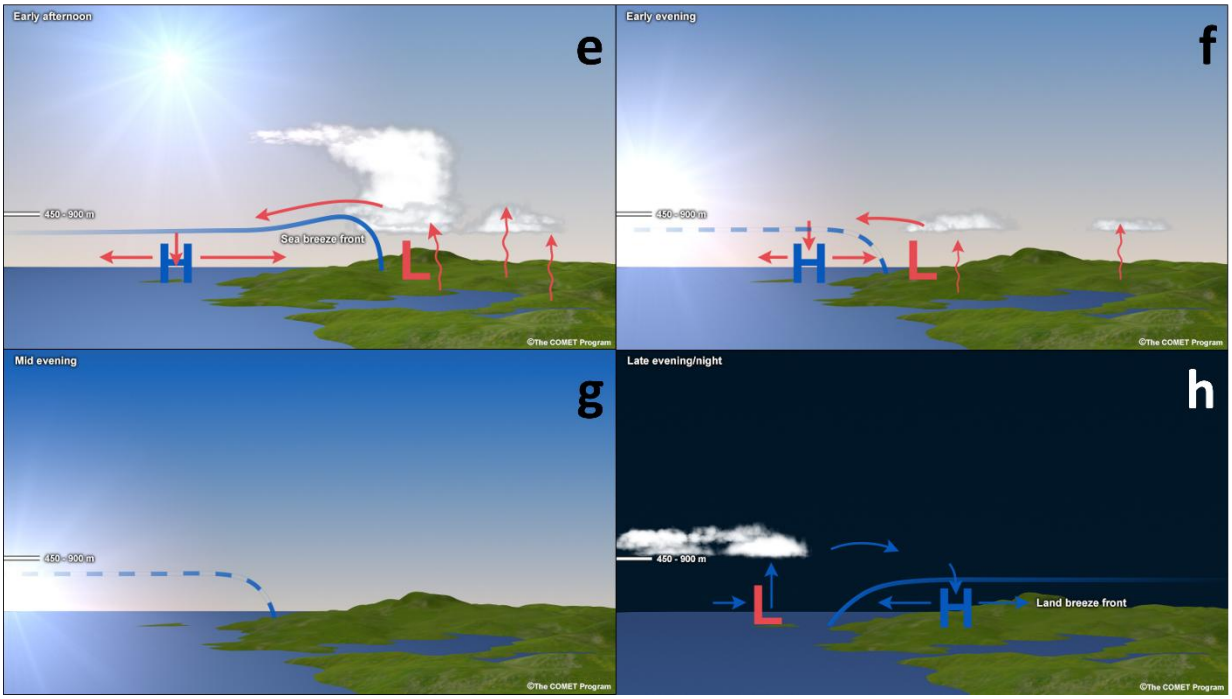

Figure 7-25: The sea and land breeze from early afternoon to night. (e) Everything is strongest in the afternoon. (f) By early evening, peak heating is past and everything begins to subside. (g) In the mid-evening winds have subsided and skies become clear. (h) During the night, flow is offshore with a few clouds over the water.

By late evening and into the night, the land continues to cool. This creates a temperature gradient again. A weak high pressure forms over the land and a weak low pressure over the water (Figure 7-25h). These pressure and temperature differences enable a land breeze (wind blowing from the land out to sea) to establish itself. Some low clouds may form over the water. By early morning this entire thermally driven process starts over again.

7.3.1 – Local Wind Systems - Mountain/Valley Breezes

Mountain and valley breezes occur due to a physical process similar to sea-land breezes. All these wind patterns are thermally forced and have a diurnal nature. Heating of a land surface during the day causes rising air. Cooling of the land surface at night causes descending air.

When the Sun rises in the morning, the east and south facing slopes of a mountain heat faster than the surrounding area. This condition causes warm air to travel up these slopes (upslope flow) toward the mountain top as shown in Figure 7-26. Slopes not receiving sunshine yet would have a weaker downslope wind from the previous night.

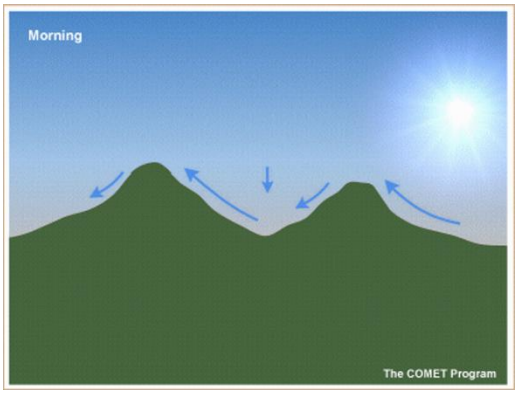

Figure 7-26: Mountain breezes are upslope in the morning as the Sun warms the land.

As the Sun approaches solar noon (the highest Sun angle), the entire mountain receives sunshine with all the wind flow traveling upslope. This flow pattern creates convergence at the mountain top and rising air over the mountain. Clouds form first on the top of the mountain associated with this convergence (Figure 7-27). If the atmosphere is conditionally unstable, a thunderstorm could form on the mountain top as temperatures rise. If the prevailing wind aloft is strong enough, this thunderstorm may get pushed off the mountain top into nearby valleys.

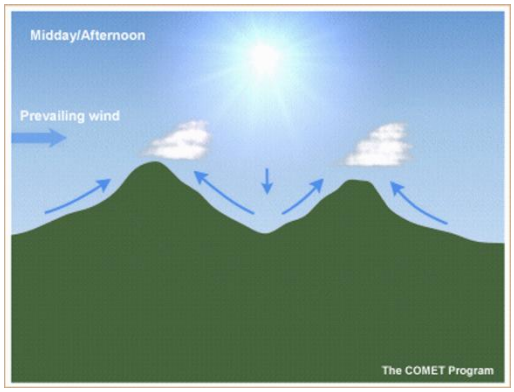

Figure 7-27: Mountain breeze upslope flow is strongest in the afternoon with clouds forming over the mountains.

As the Sun begins to set, the air over the mountain cools rapidly due to its higher elevation (Figure 7-28). A higher elevation location has less atmosphere to go through when radiating heat to space. As the mountain elevations cool, the air becomes denser and begins to sink. This sinking air moves down the slope of the mountains (downslope flow). Any clouds over the mountains tend to dissipate, since the previously rising air is replaced with descending air.

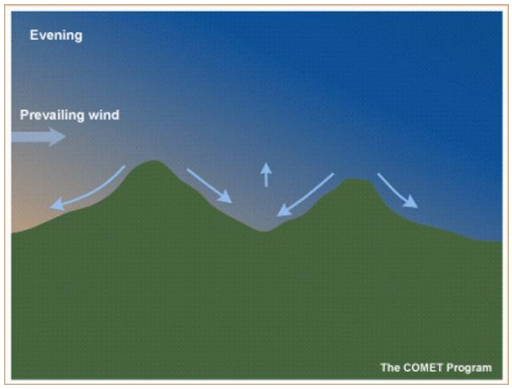

Figure 7-28: Mountains breezes are downslope in the evening.

As you might expect, this thermally driven mountain breeze affects the wind in a nearby valley. When the mountain slopes warm, air is eventually pulled from a nearby valley to replace the air rising up the mountain. This condition creates both an upslope wind on the mountain and a wind up the valley. As the Sun sets and

winds turn downslope on the mountain, this denser eventually makes it into a nearby valley. Since the air is channeled within the terrain, down valley winds can be as strong as 15 mph in the late evening and into the night. When the Sun rises the next day, this entire process repeats itself. Figure 7-29 shows these up valley and down valley wind patterns.

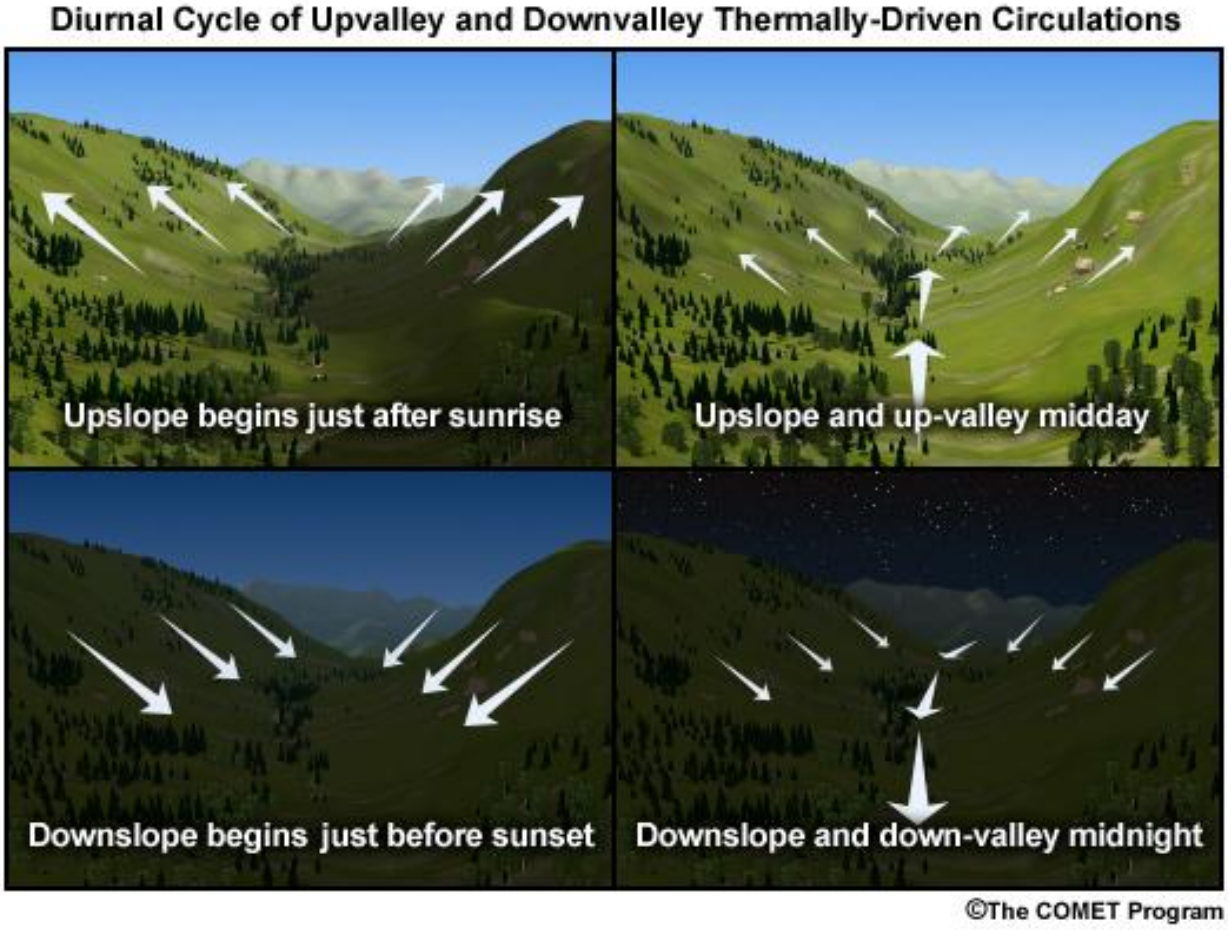

Figure 7-29: Thermally driven circulations are up-valley during the day and down-valley at night.

7.3.2 – Wind Systems in the Western U.S.

As you know, the pressure gradient force causes wind to blow from high to low pressure. When surface wind encounters mountainous terrain, it must move around these barriers as it travels towards lower pressure. These conditions can create strong winds in localized areas, even though the weather pattern driving these winds is on the synoptic scale. Since the winds occur in a local area, people in those areas frequently give them names. The map in Figure 7-30 lists the local names given these wind patterns.

Figure 7-30: The names of pressure gradient driven winds in the western U.S.

The western United States is not unique in experiencing local wind patterns due to terrain. The map in Figure 7-31 depicts areas across the globe where strong winds have been documented. Wherever mountainous terrain is present, these winds may develop. Hence, this global map likely does not represent all the places where they have occurred.

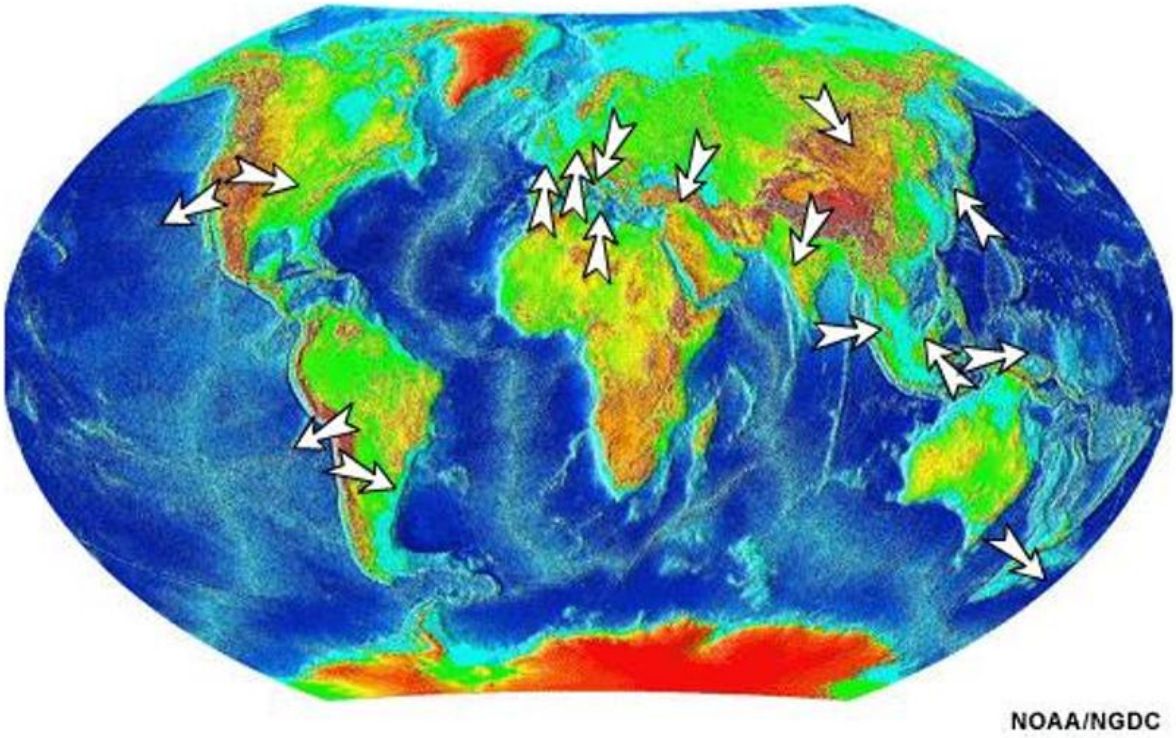

Figure 7-31: Global locations where local wind patterns due to terrain have been documented.

7.4 – Monsoons – Asian Monsoon

Monsoon is a seasonal wind pattern. The word “monsoon” is derived from the Arabic word “mausin” which means a season. A monsoon occurs due to the thermal differences between land masses and large bodies of water. A monsoon can be thought of as a sea-land breeze on a large scale; the synoptic scale. During the summer, the land mass continues to heat and temperatures increase. The surrounding ocean water warms too, but not nearly as much. This persist rising air over land eventually creates a synoptic scale thermal circulation. The rising air over land pulls in moist, cooler air from the ocean. Adding moisture to an already conditionally unstable air mass can create strong thunderstorms and heavy precipitation. This entire process takes months to establish itself. Hence, the reason the monsoon definition has the word “season” in it.

Thermally driven monsoons have prevailing winds from one direction much of the year and another direction in the summer. The most well-known monsoon is the Asian Monsoon which moves moist air and precipitation into southern Asia during the summer. Figure 7-32 indicates that these seasonal wind patterns occur at many locations around the globe.

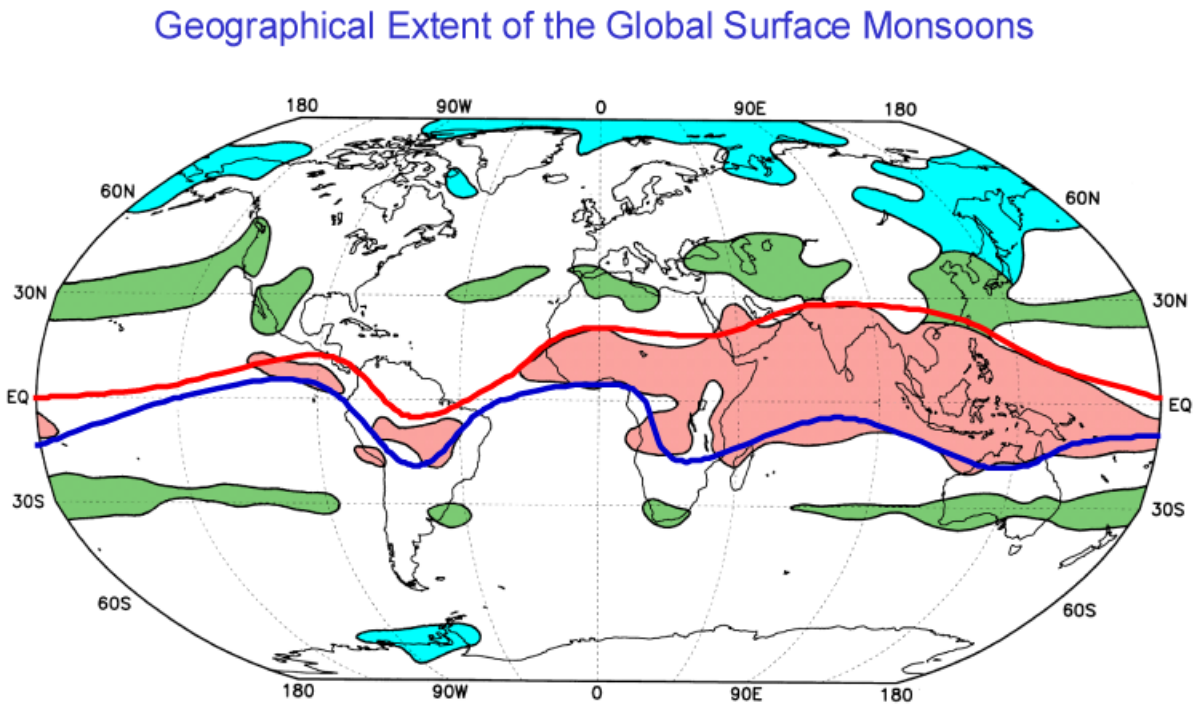

Figure 7-32: A global map of monsoon locations. The red and blue lines are the ITCZ seasonal locations.

The Asian Monsoon has northeasterly trade winds going from the land into the Indian Ocean during the winter and spring. In the summer, the ITCZ (intertropical convergence zone) moves northward up to the Himalayan Mountains. Along with this ITCZ shift, the winds shift to the southwest and now travel from the Indian Ocean onto land. The summertime shift in the ITCZ causes the weather over the southern areas of Asia to go from hot and dry to torrential rain.

This video provides details on the Asian Monsoon and is from the United Kingdom Met Office. The video explains the physical process causing the Asian Monsoon, along with the progression and retreat of rains over India. It briefly mentions El Niño and La Niña oscillations, which is a topic covered in a future chapter.

The video is from NASA's Global Precipitation Measurement (GPM) group, looks at the detailed wind flow over southern Asia along with a brief look at monsoon circulations elsewhere. This video is best viewed in HD or 4K.

7.4.1 – North American Monsoon

The North American Monsoon affects the western portion of Mexico, New Mexico and Arizona. Moisture and precipitation can also move into southern California, Nevada, Utah and Colorado during an active monsoon. Like the Asian monsoon, the North American monsoon is driven by

intense surface heating of the land, resulting in rising air. A thermal circulation develops which pulls moisture in from the Gulf of California, eastern Pacific Ocean, and the Gulf of Mexico. The map in Figure 7-33 illustrates with green arrows where the low-level moisture originates.

Figure 7-33: A map of northern Mexico and the southwest U.S. showing low-level moisture sources as green arrows during the North American Monsoon. The cold fronts depicted are common locations of weak temperature boundaries during the monsoon.

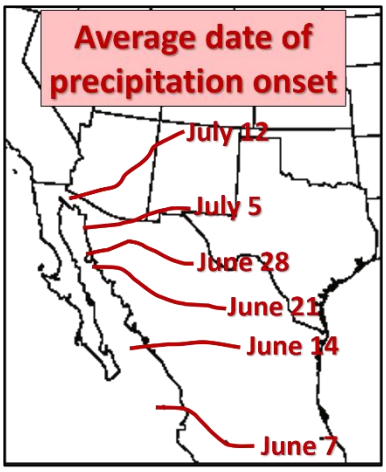

Figure 7-34: Average date of precipitation onset associated with the North American Monsoon.

Precipitation starts in early June in Mexico and advances up the western portion of Mexico through the month. The Sierra Madres Mountains in the western portion of Mexico act as a boundary between the various moisture sources feeding into the desert areas. Figure 7-34 shows the progression of monsoon precipitation through Mexico into Arizona and New Mexico.

By definition, a monsoon should have a seasonal change in its wind pattern. Does the North American Monsoon fit this definition? Examining the average June 500 mb flow (left side of Figure 7-35) for this area shows a westerly flow over northern Mexico and the United States. This westerly flow is common across the midlatitudes throughout most of the year. The subtropical ridge centered over Mexico supports easterly flow and precipitation in southern Mexico, but not elsewhere.

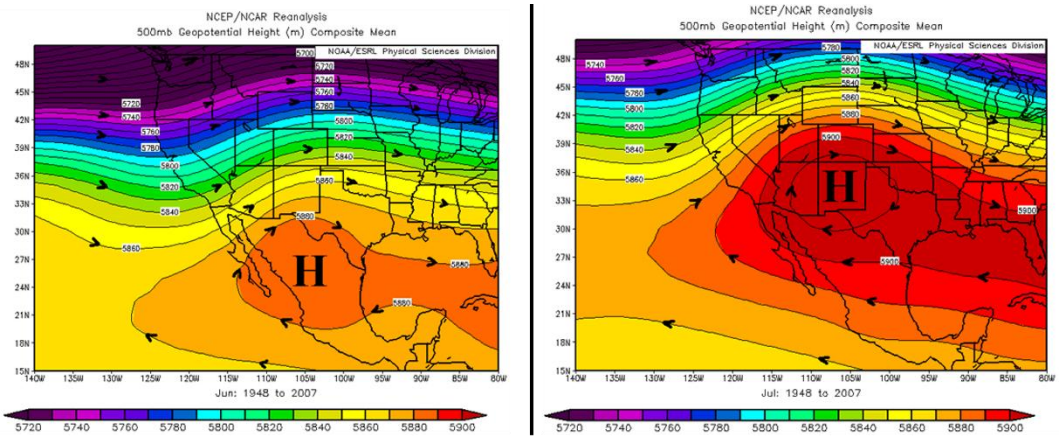

Figure 7-35: The 500 mb height maps for June (left) and July (right) showing the seasonal wind change over Mexico and large portions of Arizona and New Mexico.

Comparing this June flow to the average July 500 mb (right side of Figure 7-35) shows significant changes have occurred. The subtropical ridge has moved further north. This location causes easterly flow across all of Mexico, large portions of Texas, southern New Mexico, and southern Arizona. Thus, the flow switched from westerly to easterly over much of the area affected by the North American Monsoon. This reversal of wind direction is not as widespread as the Asian monsoon, but the changes fit the definition of a monsoon.

The North American Monsoon is a significant source of precipitation for the area affected by it. The monsoon provides much needed precipitation for agricultural industries, and tends to dampen the wildfire season which occurs in the hot, dry weather proceeding the monsoon. Areas in southern Arizona and New Mexico get about half of their annual precipitation from the monsoon. The bar graph in Figure 7-36 depicts the average monthly precipitation received at Tucson in southern Arizona. Tucson receives about 12 inches of precipitation annually; about 6 inches of that total is received from July through September during the monsoon.

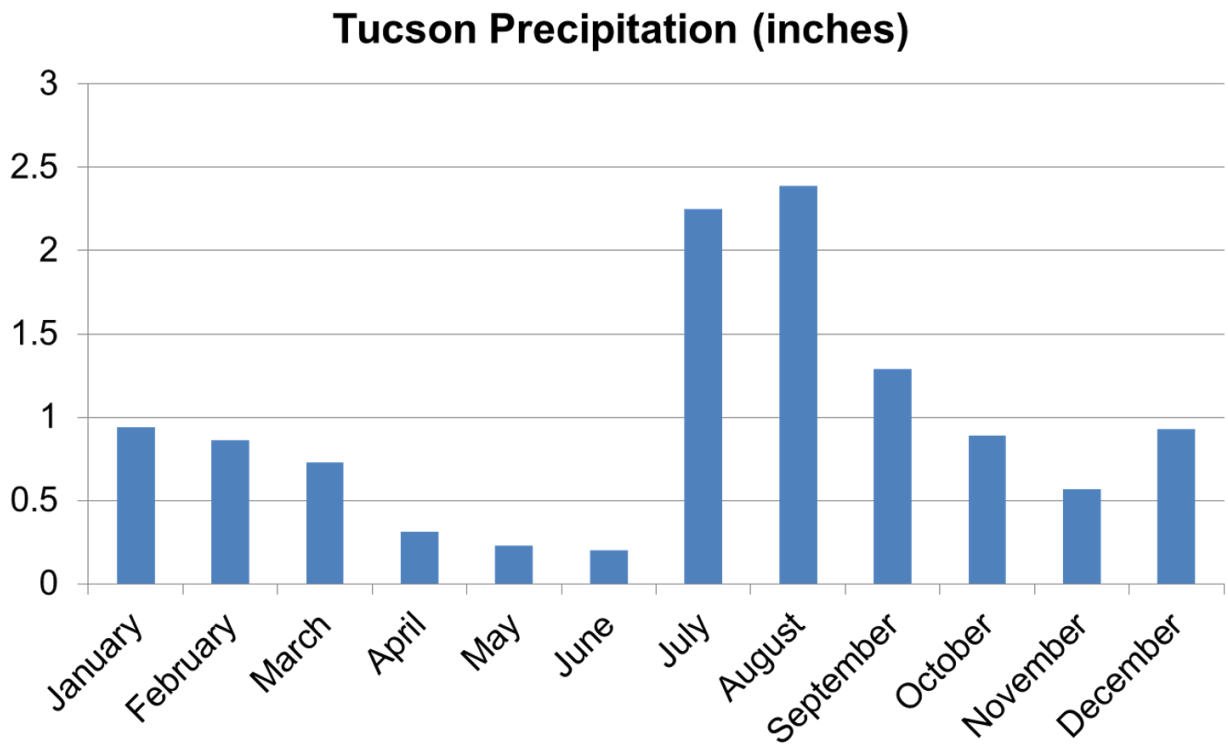

Figure 7-36: A bar graph with the monthly precipitation amounts for Tucson, Arizona.

Chapter 7 Review Questions

1. What conditions encourage cyclogenesis to occur?
2. Describe the dissipation stage of a midlatitude cyclone.
3. When does the lowest surface pressure occur in a midlatitude cyclone? Another way to ask this question is: When is a midlatitude cyclone strongest?
4. Where does the polar jet stream reside as an initial condition for cyclogenesis to occur?
5. Name the wind regimes associated with the conveyor belt conceptual model.
6. Describe where each wind regime is located in the conveyor belt conceptual model.
7. What is the name given a midlatitude cyclone that forms in the lee of the Rocky Mountains and generally tracks across the Great Lakes?
8. What term describes the rotation of a fluid?
9. What are two sources of relative vorticity?
10. At what time of day is a sea breeze the strongest?
11. Around noon on a sunny day, what direction is the wind near a mountain?
12. During a sunny day in the mountains with a conditionally unstable atmosphere, where will clouds and storms first form?
13. What is a monsoon?
14. Describe the seasonal wind direction changes over India associated with the Asian Monsoon.
15. Describe the seasonal wind direction changes over northern Mexico associated with the North American Monsoon.

Chapter 8 – Lightning and Thunderstorms

Overview

This chapter starts by exploring lightning. The types of lightning, the method for monitoring lightning strikes, the process for a lightning strike to occur and lightning safety. Lightning can be extremely dangerous, and staying safe while outside requires a situational awareness that lightning may be in your vicinity.

Thunderstorms and lightning happen together. Hence, this chapter examines the three different types of thunderstorms, the structure of a thunderstorm, features which distinguish basic thunderstorms from extremely strong thunderstorms, and methods to recognize these types of thunderstorms using weather radar observations. Weather radar is the primary method for monitoring and forecasting the short-term development of thunderstorms. Further, this chapter examines how a weather radar works, the basic types of radar data which are available, and techniques for determining the quality of weather radar data.

Chapter objectives:

1. Describe the sequence involved in the formation of lightning.
2. Describe the types of thunderstorms and the differences between them.
3. Explain how a weather radar operates.
4. Describe the limitations of radar observations and factors that may affect data quality.

8.1 - Lightning

Lightning has been seen in volcanic eruptions, intense forest fires, surface nuclear detonations, heavy snowstorms, and in hurricanes. However, it is most often seen in thunderstorms. Lightning, and the resulting thunder, is why a storm is called a thunderstorm.

At any given moment, there can be as many as 2,000 thunderstorms occurring across the globe. This translates to more than 14.5 million storms each year. NASA satellite research indicated these storms produce lightning flashes about 40 times a second worldwide. We live on an electrified planet as is shown in this lightning frequency map (Figure 8-1). As you can see, lightning prefers land rather than the oceans and the tropics rather than higher latitudes.

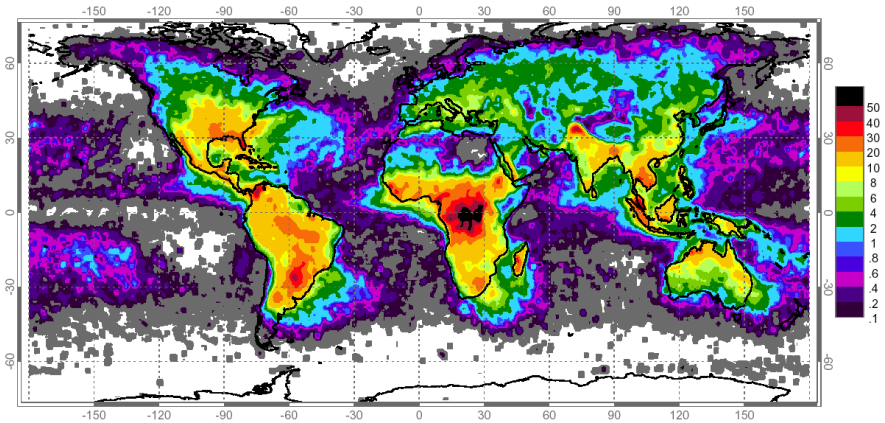

Figure 8-1: Global lightning map. The scale is flashes/km2/year.

Lightning is a transfer of electricity from one part of a cloud to somewhere else. Where the lightning goes is used to classify the types of lightning:

- In-cloud (IC) – Occurs within a cloud and lights up the cloud.
- Cloud-to-cloud (CC) – Lightning goes from one cloud to a different cloud.
- Cloud-to-air (CA) – Lightning goes from a cloud out to the air around the cloud.
- Cloud-to-ground (CG) – Lightning travels from the cloud to the ground

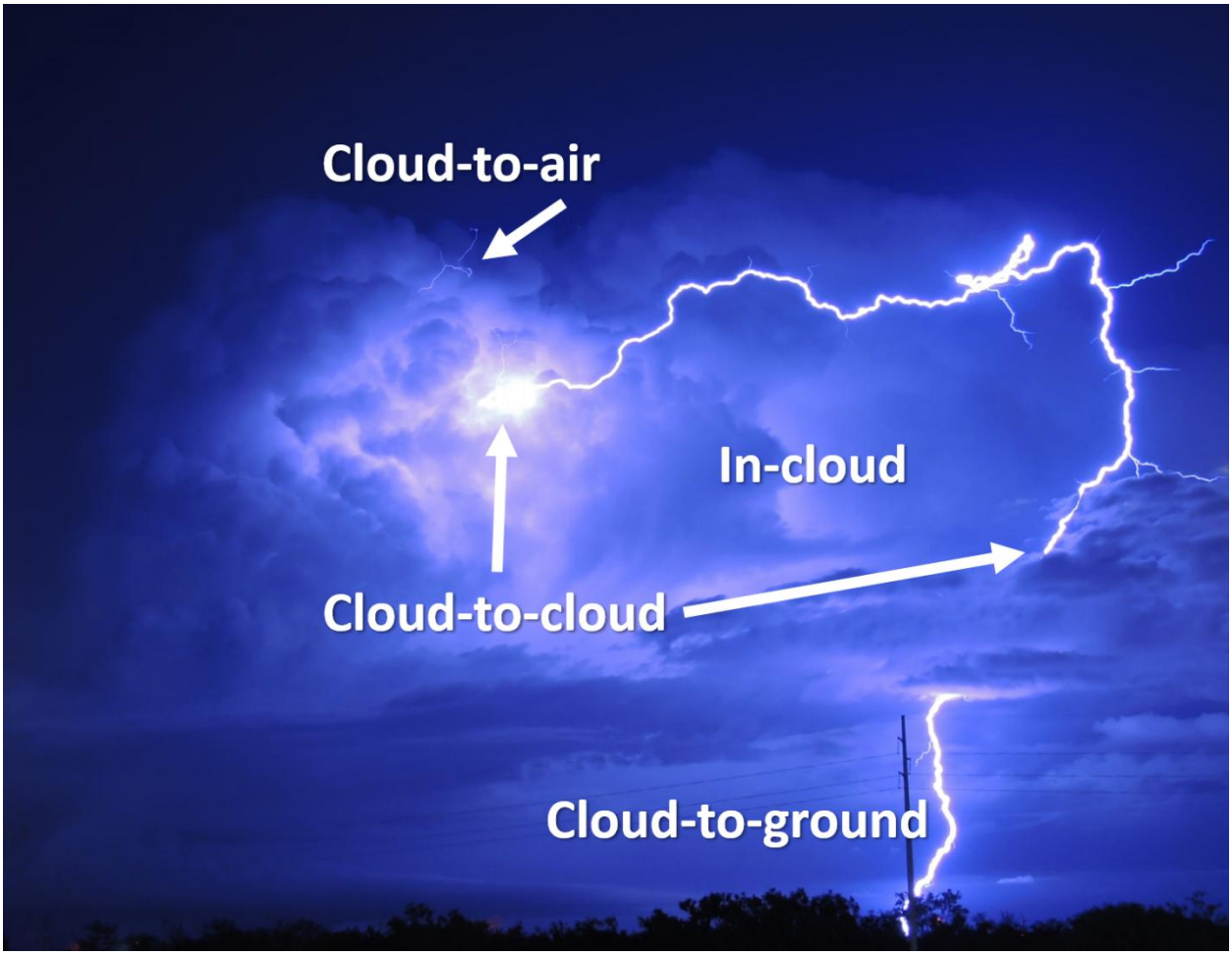

Figure 8-2: Photo with the four different types of lightning.

Most lightning that occurs is cloud-to-cloud and in-cloud (about 80%). Several lightning detection networks exist across the United States for tracking activity. Ground-based networks work by detecting radio waves emitted by the fast electrical currents in lightning. Cloud-to-ground strikes have the most electrical current and are the easiest to detect. These radio waves need to be detected by three or more ground stations to determine the location and time of the lightning. Individual flashes are then plotted on a map. A typical ground sensor looks like the photo in Figure 8-3. The lightning itself is definitely more exciting than the sensor to detect it.

Figure 8-3: Ground-based lightning detection sensor.

Another type of sensor is located on the geostationary weather satellites (GOES) and is called the Geostationary Lightning Mapper (GLM). This sensor monitors the optical emission of lightning which reaches the satellite. The GLM cannot distinguish what type of lightning occurred, only that lightning occurred. Figure 8-4 contains two examples of GLM data near Florida. The left side of this figure contains only the lightning data. The right side has a visible satellite image overlaid with GLM data. Studies have shown that GLM data is slightly more accurate at detecting lightning than ground-based networks.

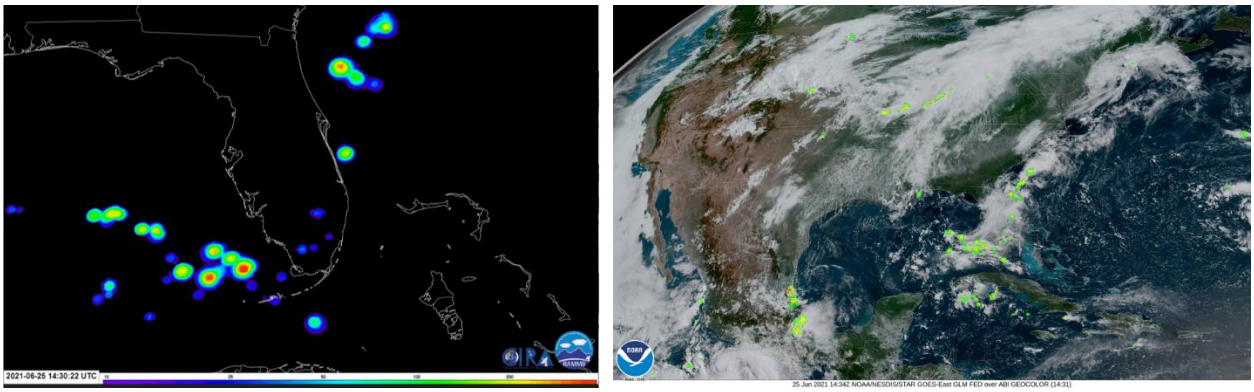

Figure 8-4: Examples of GLM data. Left side is just the lightning data. Blue colors are 25 flashes per 5 minutes. Red colors are over 200 flashes per 5 minutes. Right side is GLM data overlaid on a visible satellite image.

8.1.1 - Steps in Lightning Formation

Thunderstorms are very turbulent environments with strong winds going up (updrafts) and down (downdrafts). The updrafts transport small liquid water droplets from the lower regions of the storm to heights between 35,000 and 70,000 feet. These heights are miles above the freezing level. Meanwhile, downdrafts transport hail and ice from the frozen upper regions of the storm downward. These particles collide within the turbulence and electrons move from the ascending to the descending particles. The result is a cloud with a negatively charged base or middle and a positively charged top as illustrated in Figure 8-5.

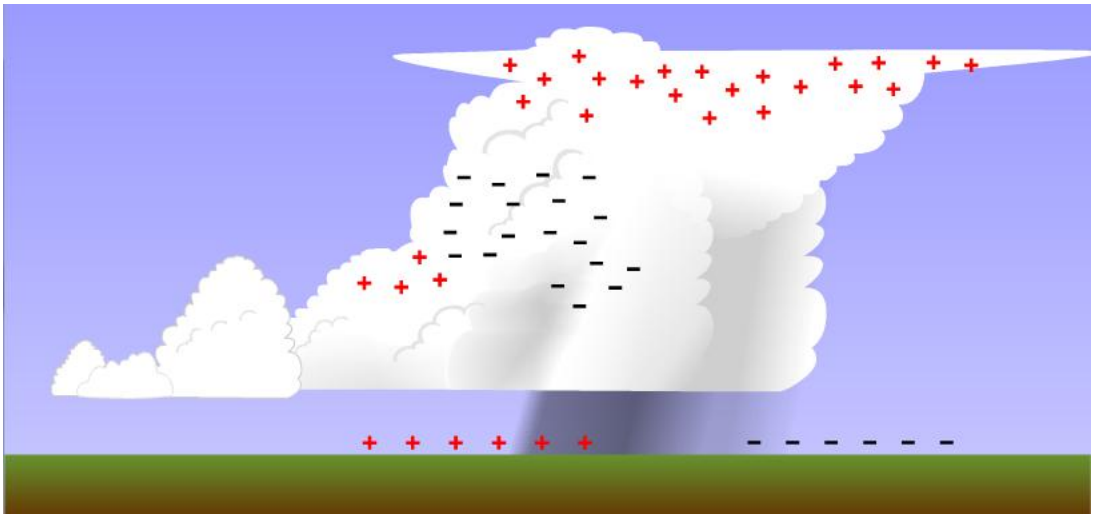

Figure 8-5: Illustration of the charge distribution within a thunderstorm.

In the world of electricity, opposites attract. Further separation of these charges into pools of positive and negative regions results in a strengthening of the electric field. However, the atmosphere is a good insulator that inhibits electric flow, so a tremendous amount of charge must build up before lightning can occur. When that charge threshold is reached, the strength of the electric field overpowers the atmosphere's insulation properties and lightning results.

The electric field within the storm is not the only one that develops. Below the negatively charged storm base, positive charge begins to pool within the surface of the Earth. This positive charge will shadow the storm wherever it goes, and is responsible for cloud-to-ground (CG) lightning. The electric field within the storm is much stronger than the one between the storm base and the Earth's surface, so most lightning occurs aloft (CC, IC, and CA).

With the development of high-speed photography and video, scientists can view the steps in the formation of lightning. All types of lightning more or less have the same steps, but cloud-to-ground is visually the most interesting. Thus, we will examine the steps in the formation of a cloud-to-ground strike.

Step 1

A CG lightning strike originates inside the storm. Under the influences of the electric field between the cloud and the ground, a very faint, negatively charged channel called a **stepped leader** emerges from the storm base and propagates toward the ground in a series of steps about 160 feet (50 meters) in length and 1 microsecond (0.000001 seconds) in duration (Figure 8-6). The stepped leader usually branches out in many directions as it approaches the ground. Between each step there is a pause of about 50 microseconds, during which the stepped leader "looks" around for an object to strike. If none is "seen", it takes another step, and repeats the process until it "finds" a target. The stepped leader takes about 50 milliseconds (1/20th of a second) to reach its full length, though this number varies depending on the length of its path. Studies of individual strikes have shown that a single leader can be comprised of more than 10,000 steps!

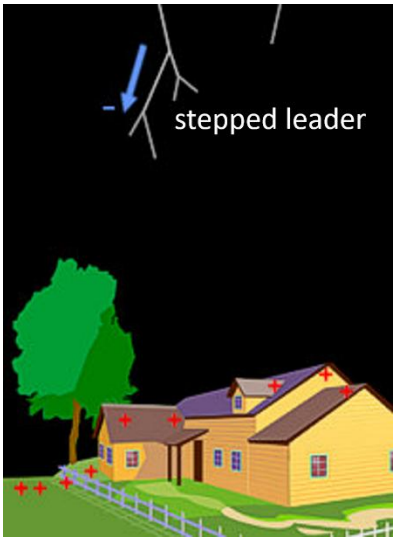

Figure 8-6: Step 1 is a stepped leader emerging from the storm base.

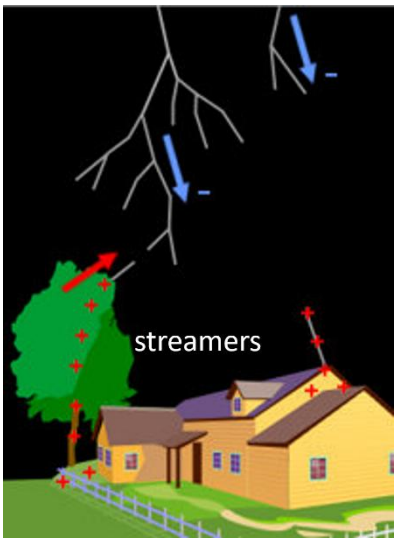

Step 2

As the stepped leader approaches the ground, its strong, negative charge repels all negative charge within the immediate strike zone of the Earth's surface, while attracting vast amounts of positive charge. The influx of positive charge into the strike zone is so strong that the stepped leader induces electric channels up from the ground called **streamers**. See Figure 8-7.

When one of these positively charged streamers connects with a negatively charged stepped leader (anywhere from 100 to 300 feet (30 to 100 meters) above the surface of the earth), the remaining steps (3 to 5) occur in less than 100 microseconds.

Figure 8-7: Step 2 involves streamers rising from the ground.

Step 3

The stepped leader and streamer form a connection for current to flow (left side of Figure 8-8).

Step 4

Electric current shoots up the channel producing a brilliant pulse called a **return stroke** (middle of Figure 8-8). The return stroke takes about 1 microsecond to reach its peak value, which averages about 30,000 amperes.

This step produces more than 99% of a lightning bolt's luminosity and is what we see as lightning. The stroke travels from the ground into the cloud, but because the strike takes place so quickly, it appears the opposite is true.

Step 5

After the return stroke ceases flowing up the channel, there is a pause of 20 to 50 milliseconds. If enough charge remains within the cloud, another leader can propagate down to the ground and the channel lights up again. This leader is called a **dart leader** because it uses the channel already established by the stepped leader and therefore has a continuous path.

Dart leaders and their return strokes do not necessarily have to use the same cloud-to-ground channel that was burned by the initial stepped leader. If a dart leader takes a different path to the ground, the lightning will appear to dance from one spot to another. This is known as forked lightning.

The combination of each leader (stepped and dart) and their subsequent return strokes is known collectively as a stroke. All strokes that use the same channel constitute a single flash. A flash can be made up of a single stroke, or tens of strokes. The highest number of strokes ever recorded in a single cloud-to-ground flash is 47.

The photo on the right of Figure 8-8 captures most of these steps in lightning formation. The stepped leader on the left has not been able to connect to the ground. The streamers coming out of the tree and a nearby light pole were not able to connect to a stepped leader. Obviously, the tree helped a streamer connect to a stepped leader for the return stroke to occur.

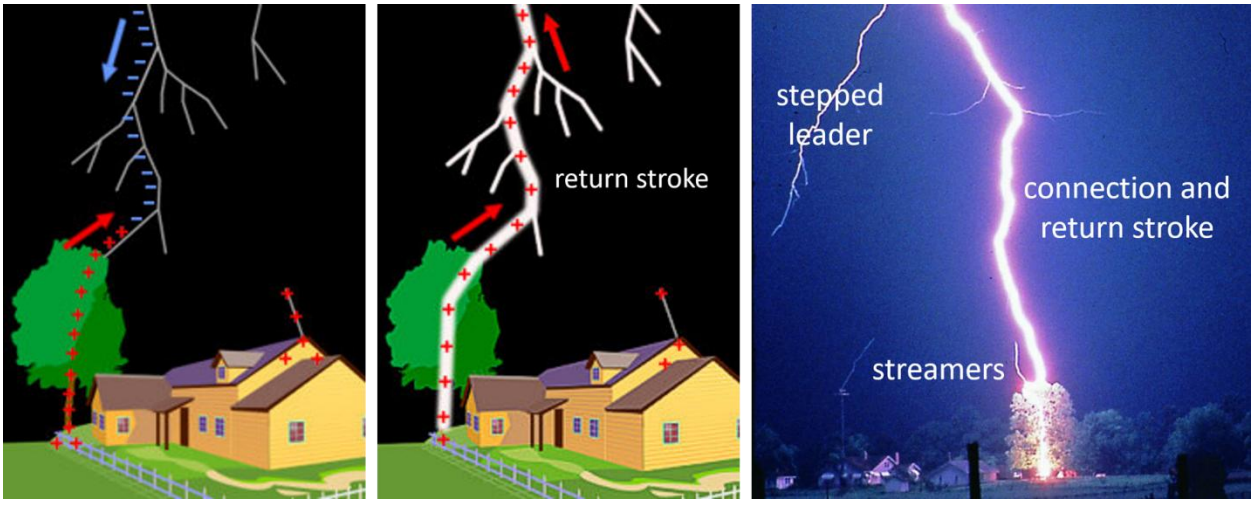

Figure 8-8: (left) Step 3 forms the channel. (middle) Step 4 with a return stroke. (right) A photo with these steps.

This short video has high speed photography of a lightning strike played in slow motion. All the steps in lightning formation can be seen. The pulsing of the channel towards the end of the video is associated with step 5.

8.1.2 - Characteristics of Lightning and Thunder

Once a lightning channel has formed and a return stroke occurs, the electric current heats the air to about 54,000ºF (30,000ºC). This temperature is five times hotter than the surface of the Sun. The air heats to these temperatures in a fraction of a second, and a phenomenon known as explosive expansion occurs. The air expands faster than the speed of sound and it compresses the other air molecules around it. This explosive expansion forms a shock wave and creates a sonic boom. Exploding fireworks produce a similar result.

Thunder from a nearby lightning strike will have a very sharp crack or bang, whereas thunder from a distant strike will have a continuous rumble. The primary reason for this rumble is the sound wave modifies as it passes through the atmosphere, and the sound may be bounding off nearby objects such as tall buildings or mountains.

Sound travels roughly at 0.2 miles / second, whereas light travels at about 186,000 miles / second. This difference causes the visual aspect of lightning to essentially be instantaneous. Counting the number of seconds between a lightning flash and the time the thunder is heard provides an estimated distance to the lightning. Every 5 seconds equals 1 mile. Therefore, thunder which is heard 10 seconds after seeing the lightning flash is 2 miles away. Background noise can obscure thunder from being heard, so lightning with no thunder may be closer than expected in a noisy environment. Generally, thunder is not heard when the lightning is over 10 miles away.

Large thunderstorms can produce other kinds of electrical phenomena called transient luminous events (TLEs) that occur high in the atmosphere. See Figure 8-9. They are rarely observed visually and not well understood. Documented photos of TLEs requires low light cameras or video. The most common TLEs are red sprites, blue jets, and elves.

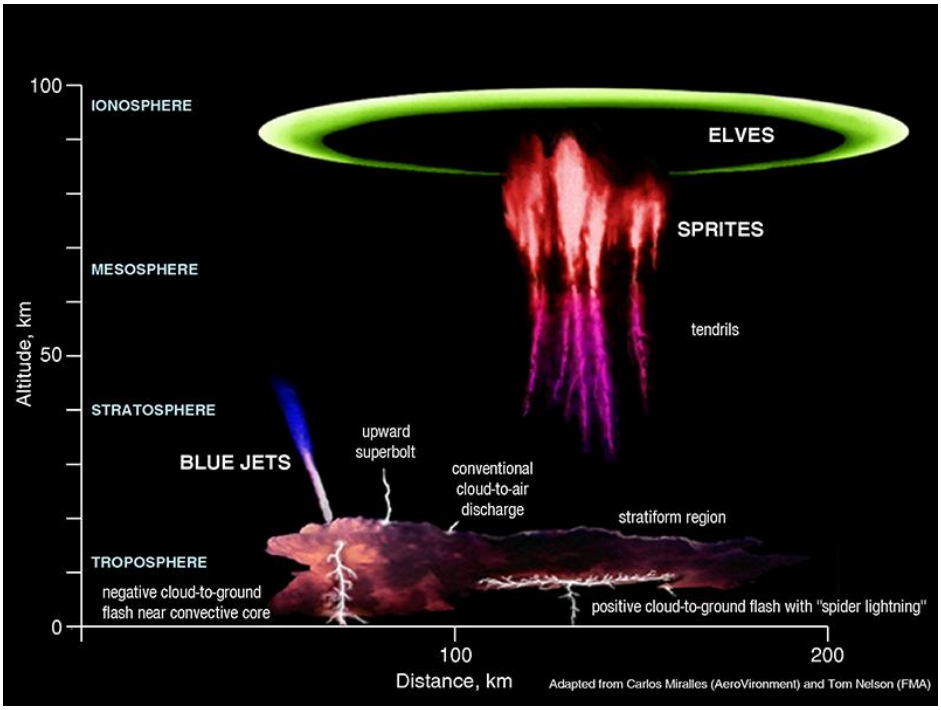

Figure 8-9: Illustration of transient luminous events or TLEs (red sprites, blue jets, and elves).

Sprites can appear directly above an active thunderstorm

as a large but weak discharge. They usually happen at the same time as powerful positive CG lightning strokes, and may extend up to 60 miles from the cloud top. Sprites are mostly red and usually last no more than a few seconds. Their shapes are described as resembling jellyfish, carrots, or columns. Figure 8-10 is a photo from the International Space Station over Central America and depicts red sprites. The moon and airglow from the atmosphere are visible in this picture too.

Figure 8-10: Photo of red sprites over South America from the International Space Station.

Blue jets emerge from the top of a thunderstorm, but are not associated directly with cloud-to-ground lightning. Blue jets last a fraction of a second and have been witnessed by pilots. Figure 8-11 is a photo of a blue jet and red sprites from the National Optical-Infrared Astronomy Research Laboratory on Mauna Kea, Hawaii.

Figure 8-11: Photo of blue jet and red sprites over Hawaii.

Elves are rapidly expanding disk-shaped regions of glowing molecules that can be up to 300 miles across. They last less than a thousandth of a second, and occur above areas of active cloud-to-ground lightning. Elves result when an energetic electromagnetic pulse extends up into the ionosphere, and were first discovered on a Space Shuttle flight in 1992.

8.1.3 - Lightning Safety

In the United States, lightning routinely kills more people each year than tornadoes or hurricanes. Tornadoes, hail, and wind gusts get the most attention, but only lightning can strike outside the storm itself. Lightning is the first thunderstorm hazard to arrive and the last to leave. Lightning can strike up to 10 miles away from where rain is occurring. No place outside is safe when thunderstorms are in the area.

The safest location during a thunderstorm is inside a large, enclosed structure with plumbing and electrical wiring. These include shopping centers, schools, office buildings, and private residences. If lightning strikes the building, the plumbing and wiring will conduct the electricity more efficiently than a human body. If no buildings are available, then an enclosed metal vehicle

such as an automobile, van, or school bus makes a decent alternative. When thunder roars, go indoors, and stay there until 30 minutes after the last clap of thunder.

Studies have shown that most people struck by lightning are struck not at the height of a thunderstorm, but before and after the storm has peaked. Most are unaware of how far lightning can strike from a thunderstorm. Figure 8-12 has bar graphs and pie charts containing interesting statistics on lightning fatalities in the United States.

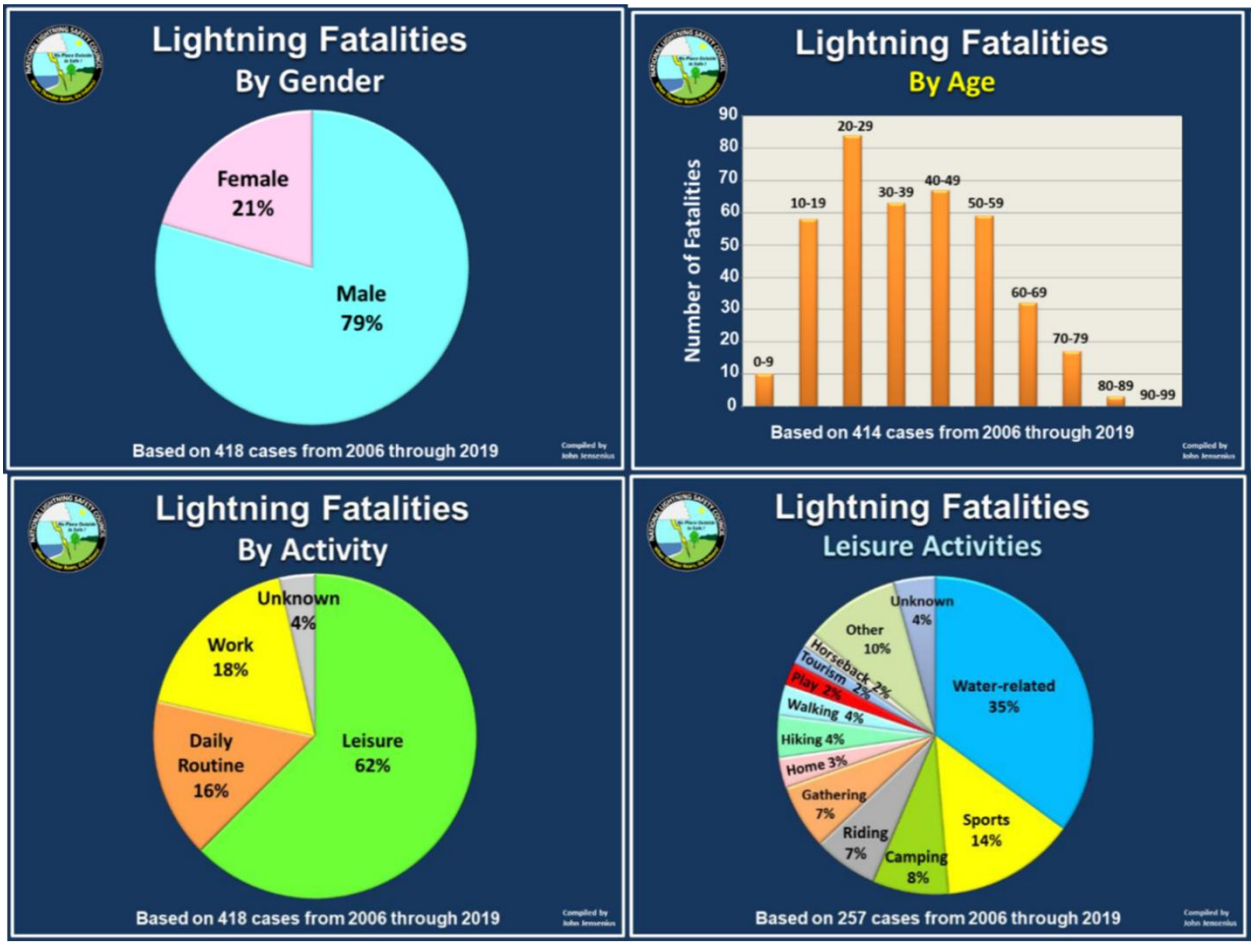

Figure 8-12: Lightning safety pie charts and graphs by gender, age, activity, and leisure activities.

As you can see, lightning fatalities has a gender bias. More men are killed by lightning than women. The most susceptible age group is 20 to 29, and most fatalities occur during outside leisure activities. The number one fatal leisure activity is water-related such as boating, fishing, or swimming. Water more easily builds a charge when compared to soil. During a thunderstorm, being near water is always the most dangerous location. Lightning prefers striking taller objects. A boat on a lake is by default one of the tallest objects around.

The safest place to be when lightning threatens is in an enclosed building with plumbing and electrical wiring. If a building is not accessible, a metal topped vehicle will keep a person safe. While in the vehicle be sure to avoid touching the sides. When lightning strikes a vehicle, the electricity flows around the vehicle into the ground. A lightning myth is that the tires protect a vehicle, which is not true.

This lightning safety video from the National Weather Service covers the details for staying safe in a thunderstorm.

8.2 - Thunderstorms

Three ingredients are needed for thunderstorms to develop:

1. Moisture
2. Atmospheric instability
3. A lifting mechanism

We have already studied all these aspects in this book. We know warm air can hold more water vapor than cold air. Thus, warmer temperatures are much better for thunderstorms. We know about atmospheric instability. A conditionally unstable atmosphere is needed for clouds to develop vertically and produce a thunderstorm. Four lifting mechanisms also have been discussed associated with condensation, cloud formation and precipitation: (1) orographic lifting, (2) convergence at the surface, (3) frontal lifting and (4) convection due to surface heating. These lifting mechanisms can produce thunderstorms.

Figure 8-13 shows the average number of thunderstorm days each year. A thunderstorm day is defined as two lightning flashing within a 10 nautical mile radius. Florida has the highest number of thunderstorm days due to being surrounded by moist, warm air much of the year.

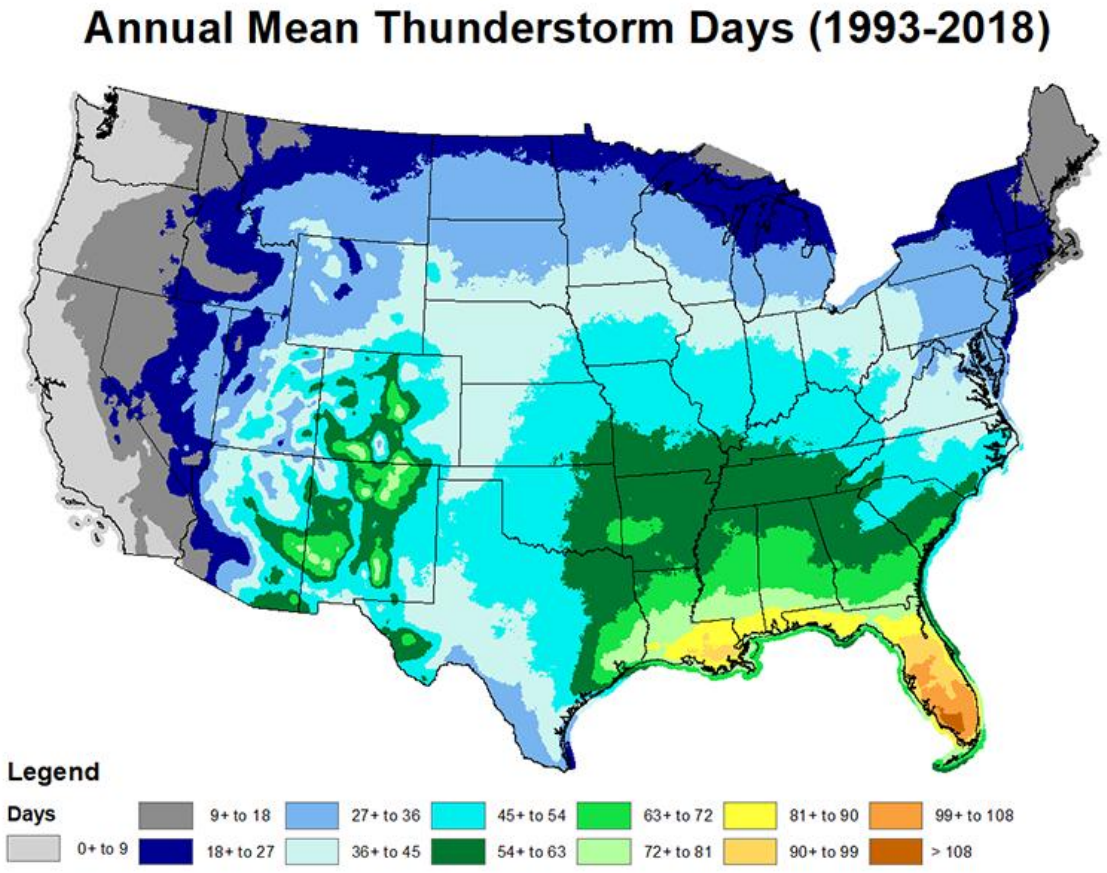

Figure 8-13: Average number of thunderstorms in a year. Florida has the most annually.

Not all thunderstorms are equal. Thunderstorms can be divided into three categories:

1. Basic or air mass thunderstorms
2. Multi-cell thunderstorms
3. Supercell thunderstorms

The environment in which a thunderstorm forms determines the type of thunderstorm. Atmospheric stability and winds are the two key factors for determining the type of storm. Environments with more relative vorticity (wind shear) produce stronger storms. The next three sections discuss these categories of thunderstorms and their characteristics.

8.2.1 - Basic or Air Mass Thunderstorms

Basic or air mass thunderstorms consist of one cell. A thunderstorm cell consists of one updraft (winds moving vertically up) and one downdraft (winds moving vertically down) and lasts 30 to 60 minutes. Basic thunderstorms are sometimes called air mass thunderstorms, since a warm, moist, and conditionally unstable air mass encourages their development. Due to their short duration, basic thunderstorms have the common name of pulse thunderstorms. They pop up, produce precipitation, gusty winds, and possibly small hail, and then dissipate. Basic thunderstorms do not produce much damage, although the lightning is always dangerous.

Basic thunderstorms have three stages in their development: (1) towering cumulus, (2) mature, and (3) dissipating. The first stage is a towering cumulus cloud as shown in Figure 8-14. A cumulus cloud begins to grow vertically, perhaps to a height of 20,000 feet. Air within the cloud is dominated by an updraft with some turbulent eddies around the edges. Precipitation and winds at the surface are generally absent.

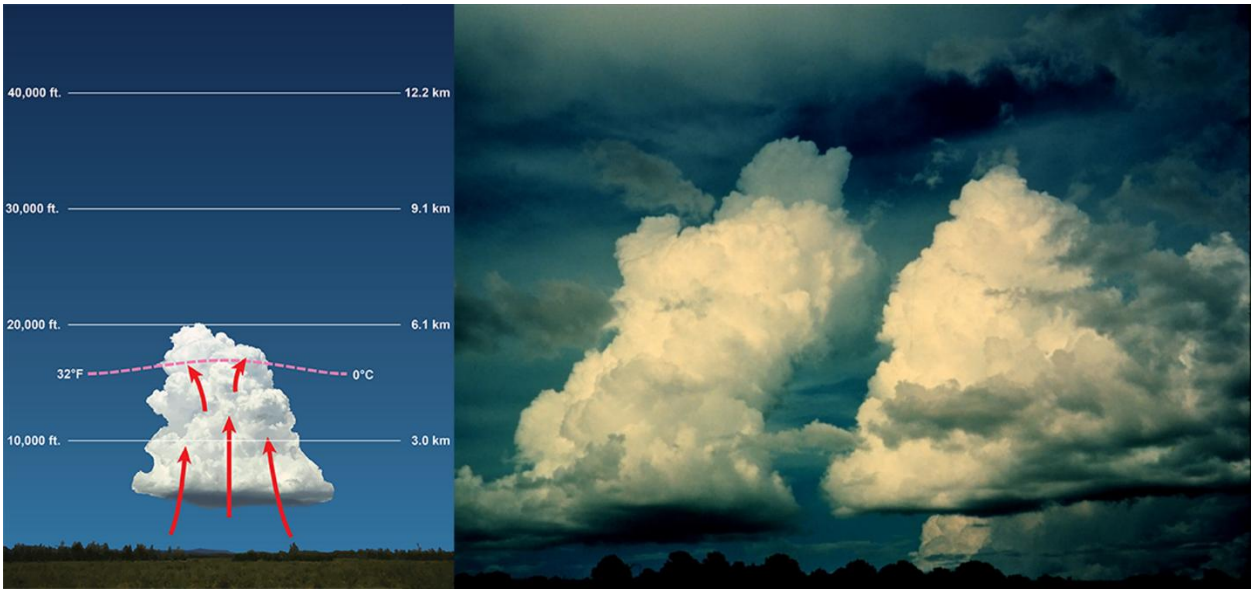

Figure 8-14: (left) Illustration showing the air motion associated with the formation of a towering cumulus cloud. (right) Photo of two tower cumulus clouds.

The mature stage of an air mass thunderstorm has strong a updraft and downdraft. Lightning and thunder are occurring. The cloud height is 40,000 to 60,000 feet. The top of the cloud may reach the tropopause and start to flatten out. This top, flatter portion of the cloud is called an **anvil**. Precipitation is occurring and possibly small hail. Noticeable surface winds are occurring

associated with the downdraft in Figure 8-15. The downdraft has cooler air associated with it and its boundary is frequently denoted by a cold front symbol. A basic thunderstorm, like all thunderstorms, is strongest in the mature stage.

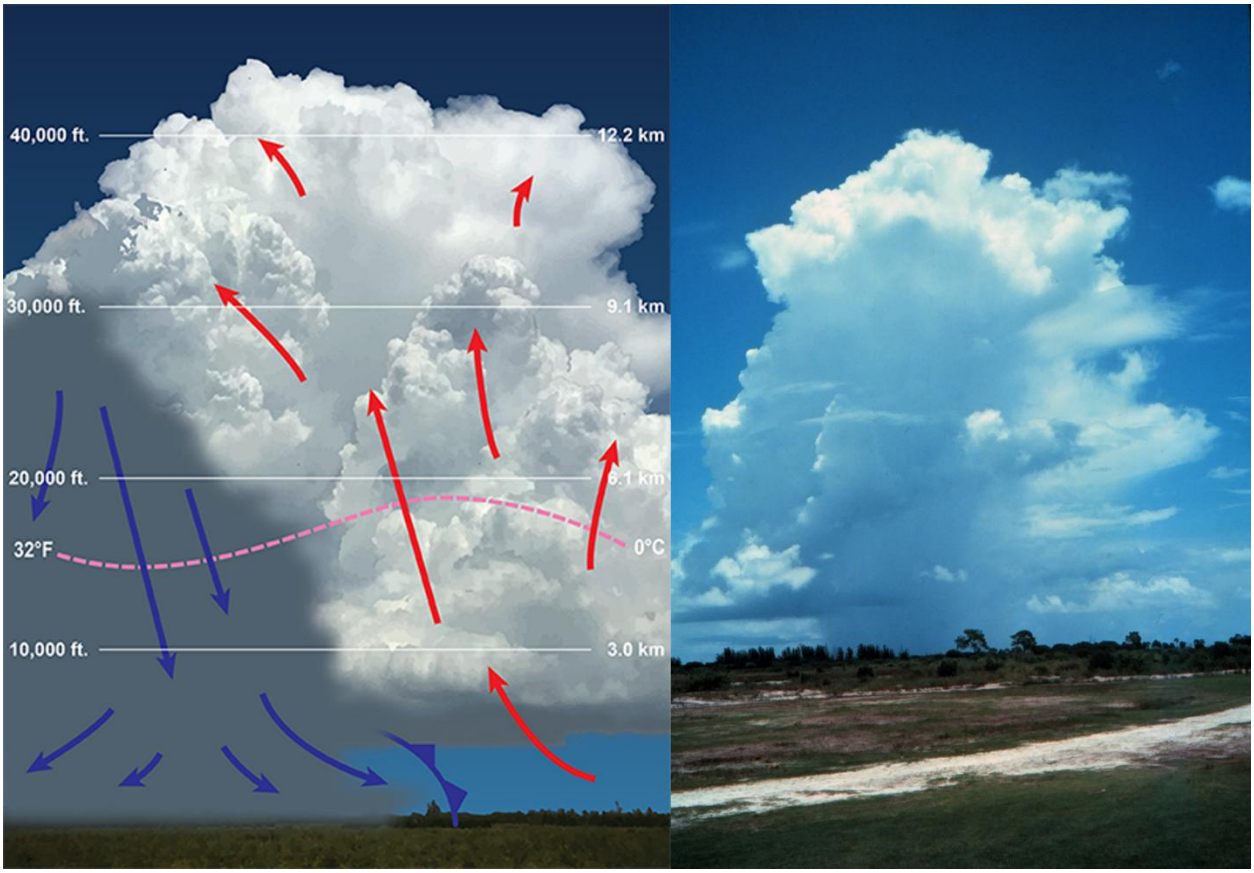

Figure 8-15: (left) Illustration showing the updraft (red arrows) and downdraft (blue arrows) of a mature basic thunderstorm. (right) Photo of a mature basic thunderstorm.

Figure 8-16 contains two illustrations of a basic mature thunderstorm. The left side is a vertical cross section through the storm, and the right side is a top-down view. The precipitation is in green and red, with the red being heavier precipitation. The downdraft is associated with the precipitation area and the transition zone between these cooler winds and the warmer

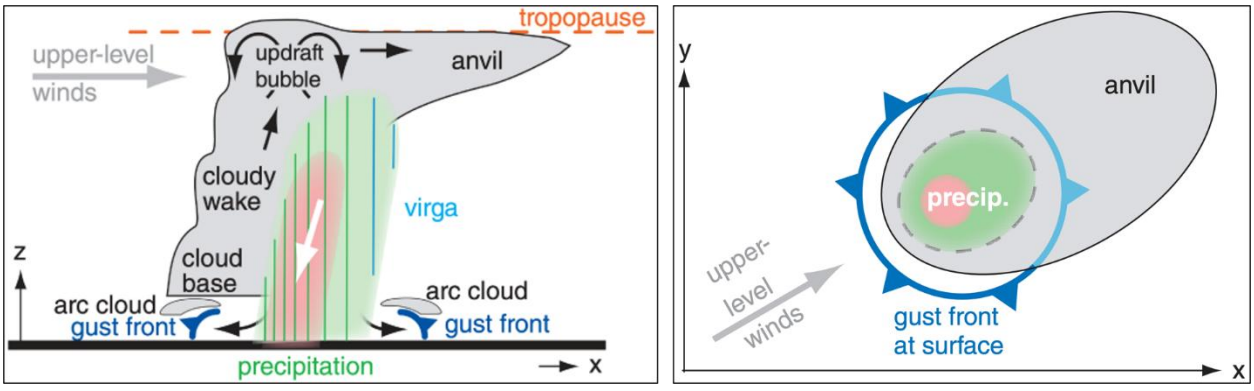

Figure 8-16: (left) A cross section through a thunderstorm. (right) A top-down view of the same thunderstorm. Notice the gust front associated with the cooler downdraft air, and the anvil forming against the tropopause.

surrounding air is called a **gust front**. Many times, clouds can form on a gust front as it moves away from a storm. The updraft resides in the non-precipitation area. The anvil is blown off in the direction of the prevailing winds.

The left side of Figure 8-17 illustrates the life cycle of a basic thunderstorm as viewed by a weather radar. The blue, green and red areas are precipitation. The red is heavier rain and hail. The top series of images is a vertical slice through the storm. The middle images are a horizontal slice through the middle at about 6 km off the surface. The bottom images are 0.5 km off the surface; a low radar slice through the thunderstorm. Internally the storm cell is strongest at 20 minutes before the precipitation core starts descending. As the precipitation descends near 25 minutes, the gust front at the surface is strengthened and the thunderstorm starts to dissipate.

The right side of Figure 8-17 shows basic thunderstorms in an actual radar product in Arizona on a summer day. They appear as red circular dots, like what is shown on the left side in the horizontal slices.

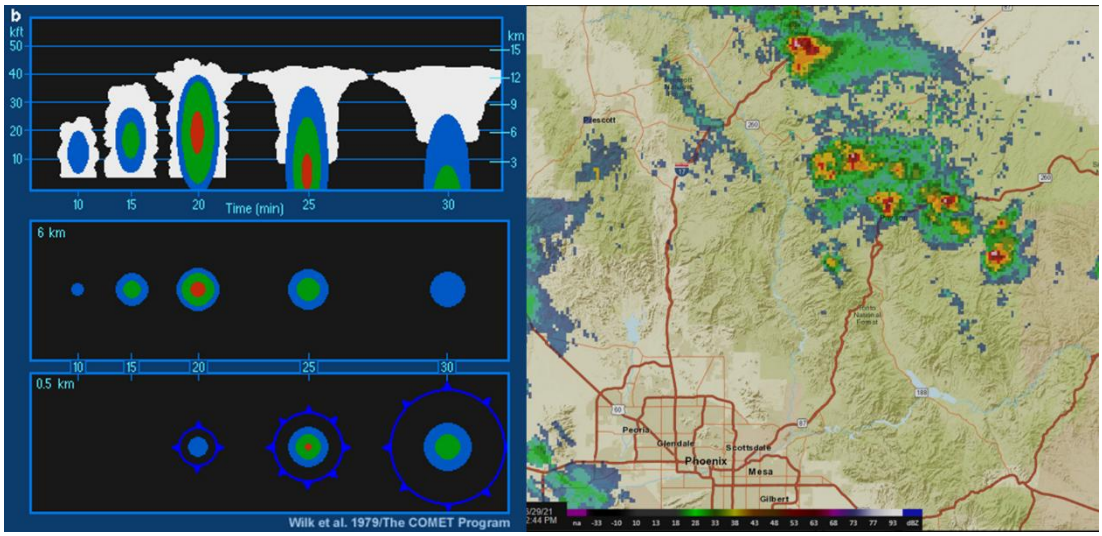

Figure 8-17: (left) Three views over the life time of a basic thunderstorm. The top view is a cross section. The two lower views are horizontal slices at 6 and 0.5 km. (right) A weather radar observation of basic thunderstorms.

In the dissipating stage, the downdraft cuts off the updraft. The storm no longer has a supply of warm, moist air to maintain itself and therefore it dissipates. Light rain and weak outflow winds may remain for a while during this stage. After dissipating, the storm remnant is just an anvil top.

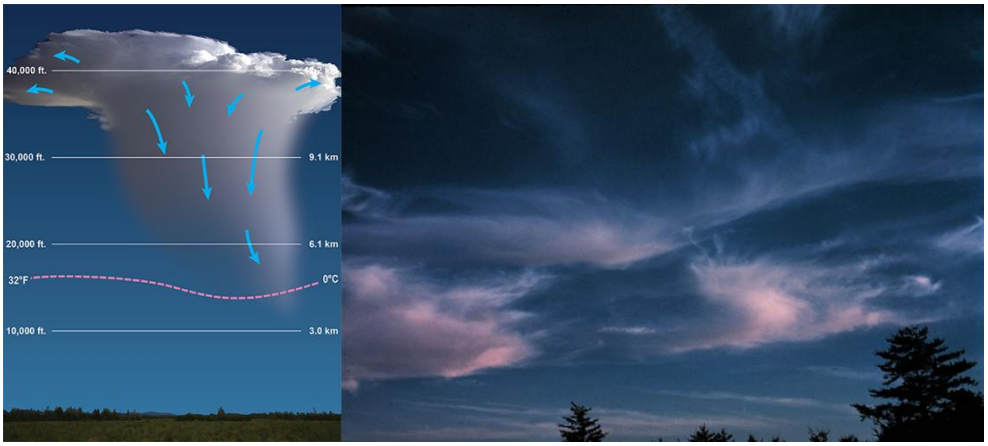

Figure 8-18: (left) Dissipating stage illustration with all downward air motion. (right) Photo of remaining anvils from dissipated thunderstorms.

The anvil of the thunderstorm is composed of ice crystals, which cannot dissipate easily. Hence, thick patches of cirrus remain after the thunderstorm is gone.

8.2.2 - Multi-cell Thunderstorms

Multi-cell thunderstorms are clusters of thunderstorms in close proximity to each other. These organized groups of thunderstorms are also referred to as mesoscale convective systems. Multi-cell thunderstorms fall into two categories: (1) squall lines and (2) mesoscale convective complexes. A **squall line** is a line of thunderstorms. A **mesoscale convective complex** (MCC) is a circular cluster of thunderstorms.

Squall lines are accompanied by high wind and heavy rain. They tend to pass quickly and are less prone to produce tornadoes than supercells. Squall lines can be hundreds of miles long, but only 10 to 20 miles wide. Squall lines frequently move ahead of a cold front and need either vertical or direction wind shear. Directional wind shear is when the wind changes direction with height. Direction shear in the vertical is similar to the vorticity created by the wind curvature on a horizontal surface. The radar image in Figure 8-19 depicts a squall line. The red areas contain the thunderstorms associated with the squall line.

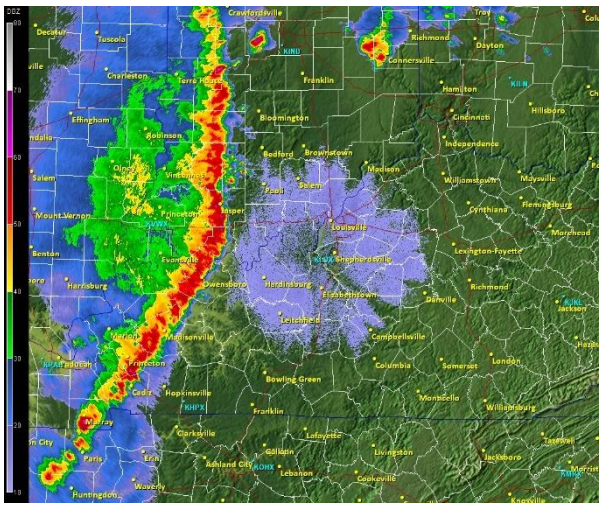

Figure 8-19: Radar reflectivity image of a squall line.

The wind shear environment allows thunderstorms to develop in front of each other, which creates the squall line and propagates it. Figure 8-20 illustrates how the thunderstorms propagate forward. The cold pool of air associated with a downdraft moves out from a thunderstorm. This downdraft eventually dissipates the storm producing it, but other air moves over this cold pool and generates thunderstorms in front of and on top of it. These new storms eventually mature creating precipitation, winds and maintain the squall line's movement forward.

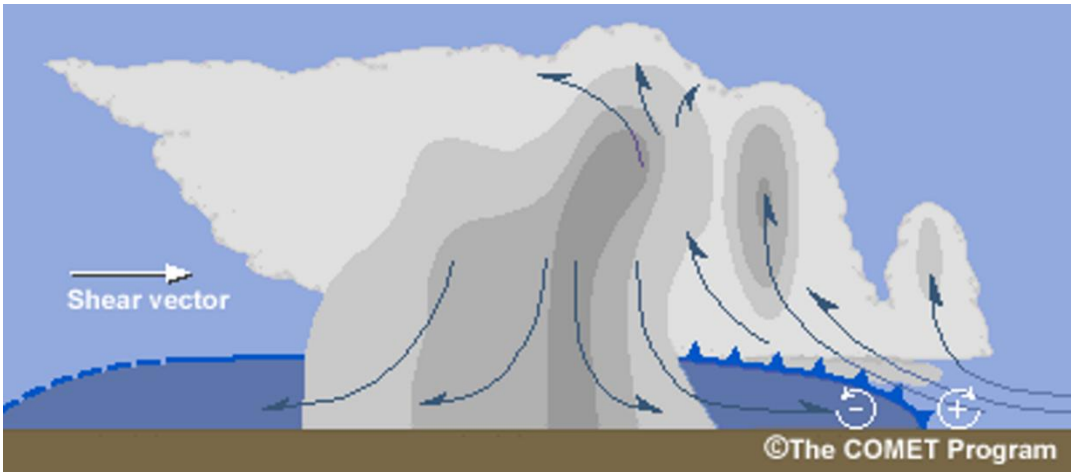

Figure 8-20: Diagram illustrating how the thunderstorms propagate forward in a squall line. The cold air associated with a downdraft generates a new thunderstorm ahead of an existing one.

A mesoscale convective complex is associated with strong wind, hail, heavy precipitation and brief tornados. An MCC can spread across an entire state and last more than 12 hours. They are identified by cloud top temperature and size through satellite imagery. An MCC will form during the late night and early morning hours (around midnight) rather than during the peak heating of late afternoon. The MCC in Figure 8-21 occurred over Arizona on July 7, 2017, and produced damaging winds of over 50 mph across the Phoenix Metropolitan area.

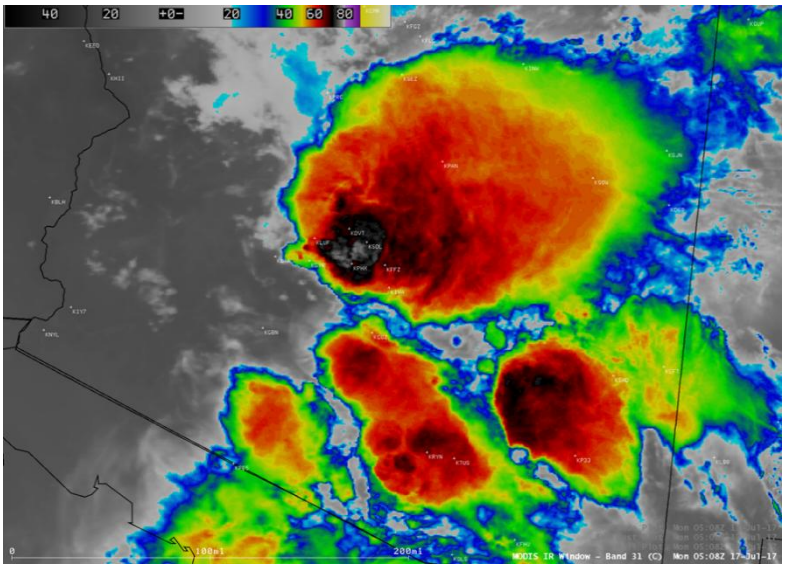

Figure 8-21: A mesoscale convective complex (MCC) over Phoenix, Arizona which caused damaging winds across the area.

8.2.3 - Supercell Thunderstorms

Supercell thunderstorms are exceptionally strong single cell storms that can persist for many hours. When compared to a basic thunderstorm, everything is stronger. Updrafts have some rotation and can attain wind speeds over 100 mph. These updraft speeds can cause hail of an inch or more in diameter. Downdraft winds speeds can be over 100 mph, which can snap trees and wood power poles in half. Most of the tornadoes in the United States are generated by supercell thunderstorms.

The development stages for a supercell are similar to the basic thunderstorm. However, the mature stage lasts longer and exhibits additional characteristics. Figure 8-22 is an artist rendition of a supercell and illustrates some of those characteristics. Whenever a basic thunderstorm starts exhibiting any supercell characteristic, it has become a supercell. Visually a person can see the cloud development along a flanking line, the large size of the thunderstorm and maybe a tornado if one forms. Unfortunately, tornadoes can be "hidden" in precipitation which makes them even more dangerous. The overshooting top is caused by a strong updraft traveling through the entire storm and pushing past the tropopause into the stratosphere. The anvil obscures being able to see an overshooting top from the ground, and is usually only visible on satellite imagery.

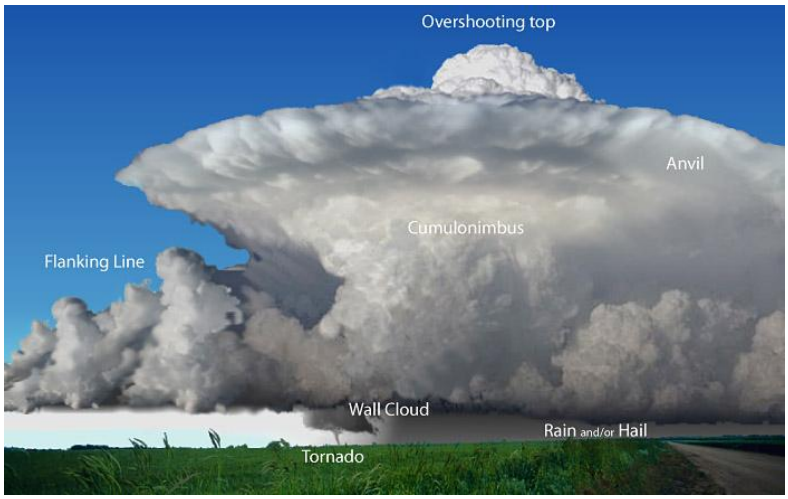

Figure 8-22: Artist rendition of a classic supercell thunderstorm. The visual characteristics of a supercell are labeled.

A horizontal cross section (Figure 8-23) through a supercell shows more details on the characteristics of this thunderstorm. The biggest difference between a supercell and a basic thunderstorm is the gust front from the downdraft does not cut off the updraft. This structure extends the mature stage and allows the thunderstorm to continue growing. Notice the inflow boundary-layer winds shown with light brown arrows in Figure 8-23, has an entry into the storm cell even though it is surrounded by downdrafts. The storm continues to build while strong winds maintain the updraft and downdraft.

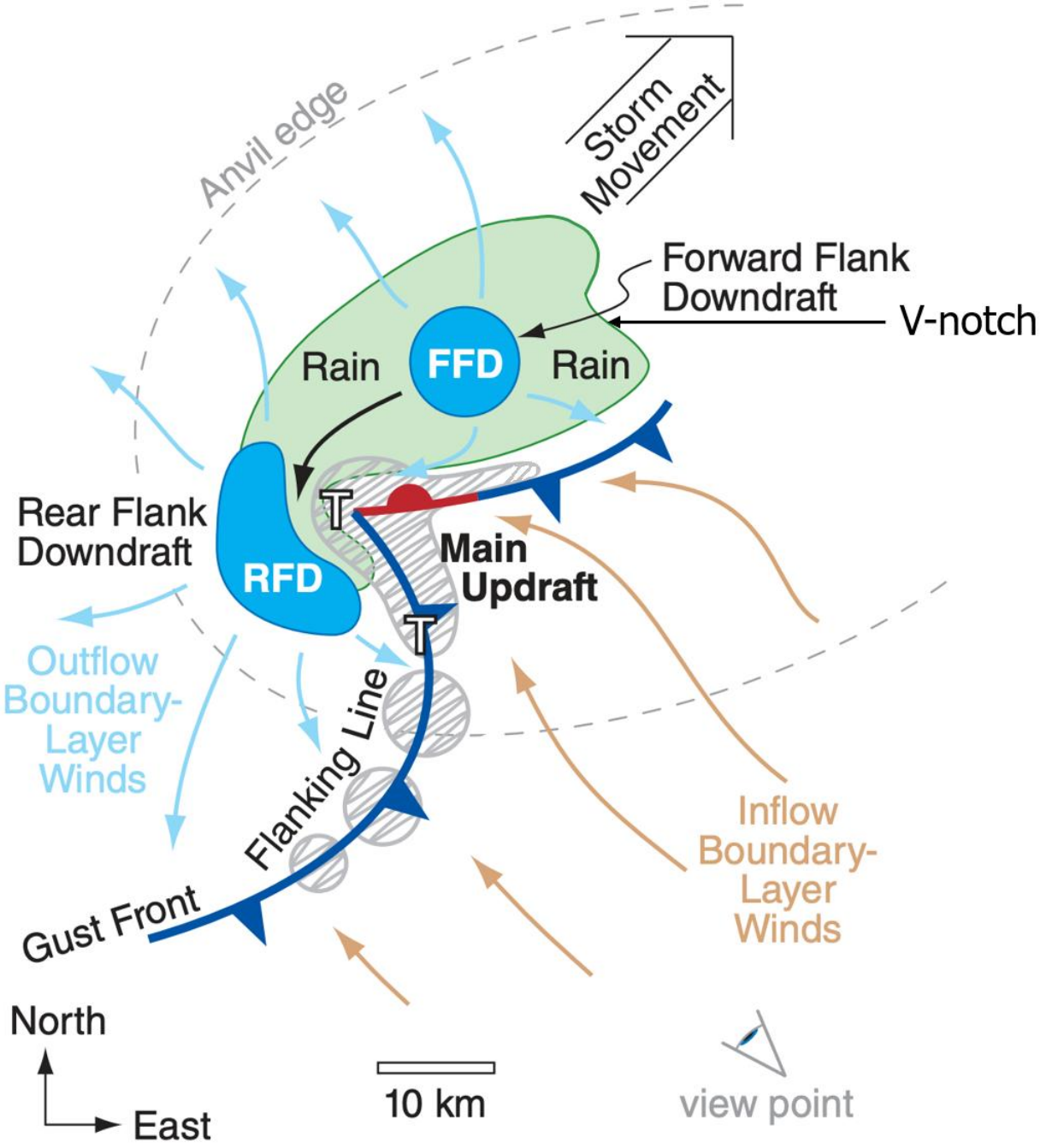

Figure 8-23: A horizontal cross section of a supercell thunderstorm. The outflow downdraft winds do not cutoff the inflow winds, which allows a supercell to get stronger than a basic thunderstorm.

This supercell structure is possible because the storm environment has wind shear. This wind shear is similar to what causes squall lines, in that the winds change direction or speed with height. A directional shear allows the updraft and downdraft to rotate around each other and work in tandem. Hence, supercell thunderstorms continue building, whereas a basic thunderstorm has the downdraft disrupting the updraft which causes the storm to dissipate.

The strongest downdraft areas are in two locations. One towards the back of the storm called the rear flank downdraft (RFD in blue in Figure 8-23), and towards the front called the forward flank downdraft (FFD in blue). The updraft is between these two downdraft locations. These updrafts and downdrafts tend to wrap around each other vertically in the storm.

The flanking line is the boundary between the inflow and outflow of the supercell. Warm, moist air from the inflow is lifted on the flanking line and towering cumulus build on this boundary. The "T"s in Figure 8-23 represent favored locations for tornadoes to form. The precipitation given in green tends to wrap around the updraft and forms a hook shape. When viewing a supercell on weather radar, this hook shape is identifiable and called a **weak echo region (WER)**. The common name used for a weak echo region is a hook echo. Figure 8-24 is an example of a weak echo region with a tornado occurring. The red area in this figure is heavy precipitation and hail.

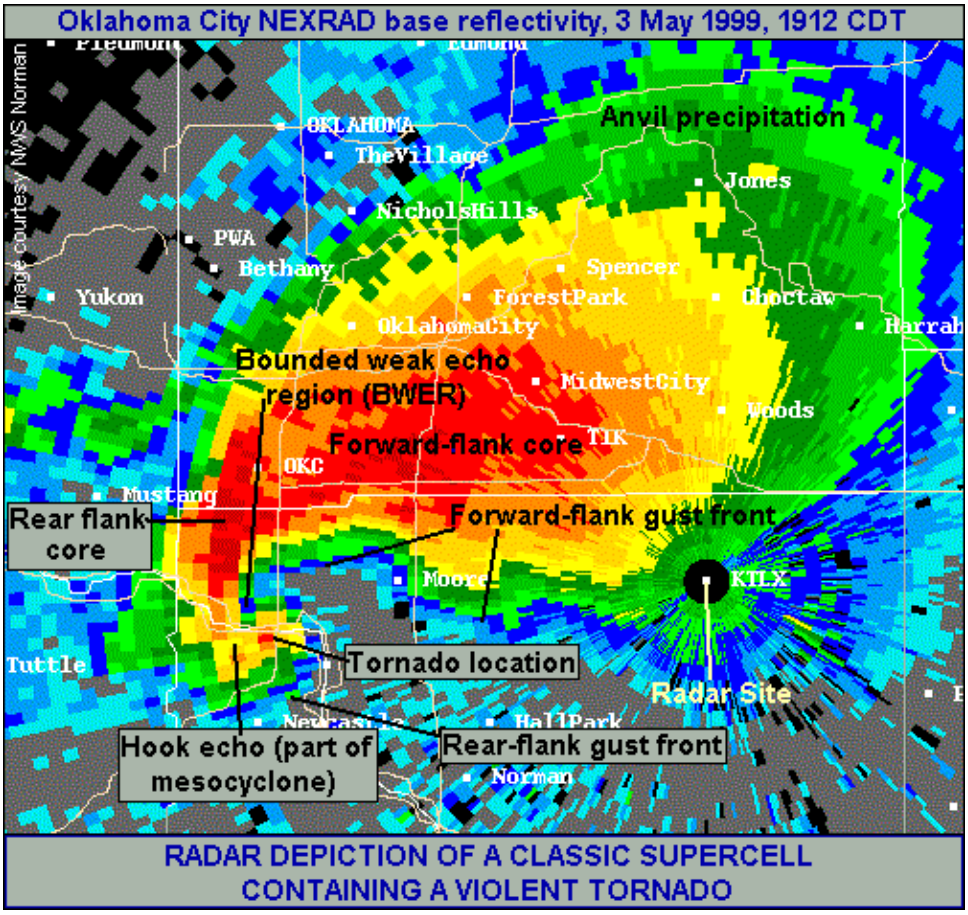

Figure 8-24: Weather radar image of a weak echo region (WER) in a supercell thunderstorm. A common name for a WER is a hook echo, which is frequently associated with a tornado as in this image.

Large hail forms when an updraft carries particles well above the freezing level multiple times. The strong vertical wind allow the hail to be suspended inside the storm and grow. Figure 8-25 illustrates the formation of hail in a thunderstorm. The rain-free region is produced by the updraft and is what suspends rain and hail aloft producing the strong radar echo. This rain free region coincides with the weak echo region (WER). The hail formation process in more detail is:

1. The hail nucleus, buoyed by the updraft is carried aloft by the updraft and begins to grow in size as it collides with supercooled raindrops and other small pieces of hail.
2. Sometimes the hailstone is blown out of the main updraft and begins to fall to the Earth.
3. If the updraft is strong enough it will move the hailstone back into the cloud where it once again collides with water and ice, and grows. This process may be repeated several times.
4. In all cases, when the hailstone can no longer be supported by the updraft it falls to the Earth. The stronger the updraft, the larger the hailstones that can be produced by the thunderstorm.

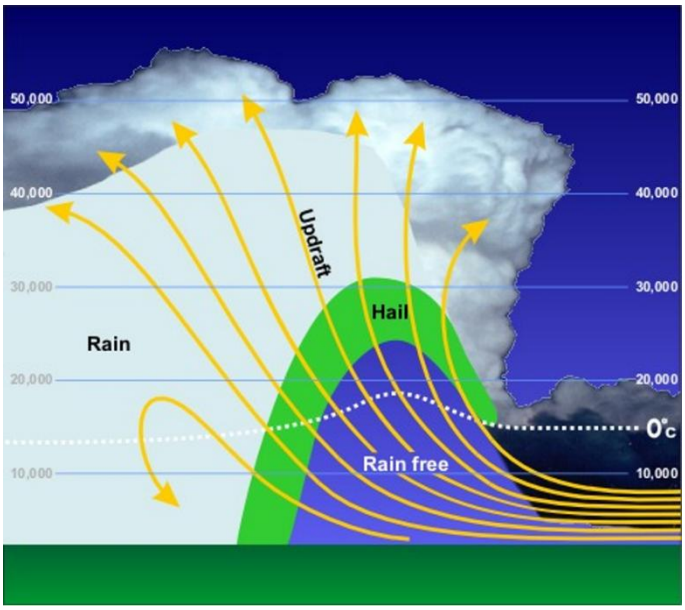

Figure 8-25: A simple diagram illustrating the formation of hail in a thunderstorm.

All other types of thunderstorms may produce hail, but the largest hail comes from a supercell. The sustained updraft in supercell thunderstorms support large hail formation by repeatedly lifting the hailstones into the very cold air at the top of the thunderstorm cloud. The size of the hail provides an estimate of the updraft speed as is shown in this table.

Hailstone size	Measurement		Updraft Speed	
	in.	cm.	mph	km/h
bb	< 1/4	< 0.64	< 24	< 39
pea	1/4	0.64	24	39
marble	1/2	1.3	35	56
dime	7/10	1.8	38	61
penny	3/4	1.9	40	64
nickel	7/8	2.2	46	74
quarter	1	2.5	49	79
half dollar	1 1/4	3.2	54	87
walnut	1 1/2	3.8	60	97
golf ball	1 3/4	4.4	64	103
hen egg	2	5.1	69	111
tennis ball	2 1/2	6.4	77	124
baseball	2 3/4	7.0	81	130
teacup	3	7.6	84	135
grapefruit	4	10.1	98	158
softball	4 1/2	11.4	103	166

The V-notch forms in a strong supercell at the front end of the storm. This notch is indicative of strong forward flank downdraft, and is a characteristic depicted only in weather radar observations. Figure 8-26 shows a supercell thunderstorm with the V-notch, weak echo region (WER), and flanking

line highlighted. A supercell with a V-notch and WER will cause extensive damage over a metropolitan area.

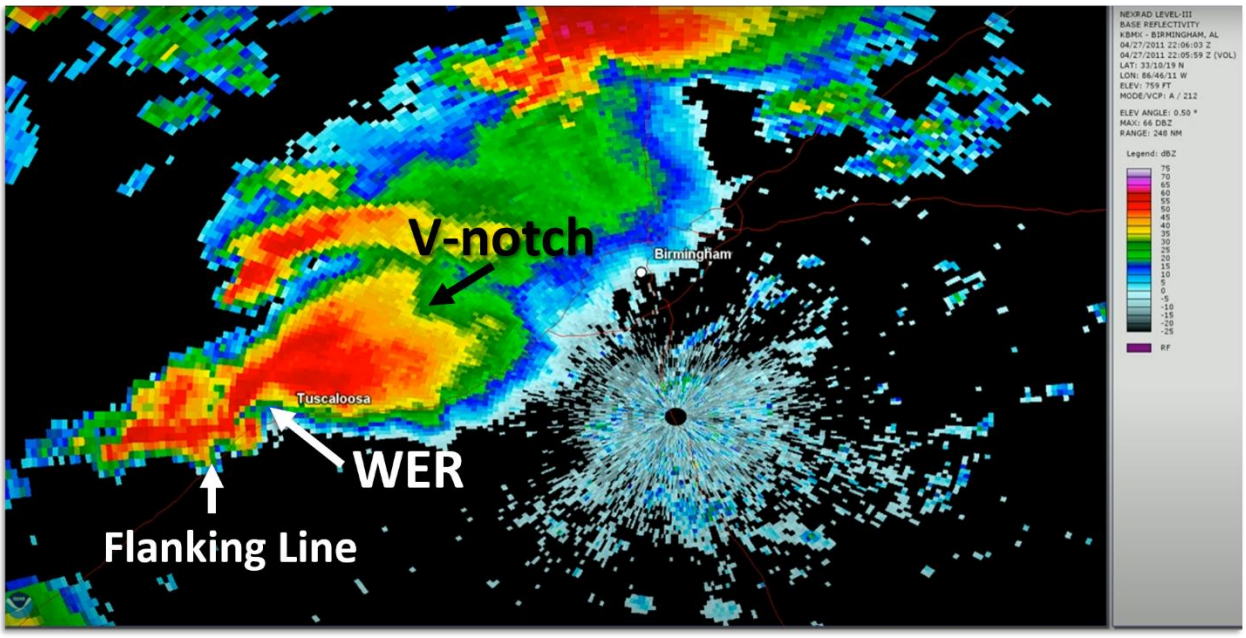

Figure 8-26: A radar image of a supercell thunderstorm with the flanking line, weak echo region (WER), and V-notch highlighted.

8.2.4 - Outflow Boundaries, Derechos and Downbursts

Outflow boundaries are the same as gust fronts. They result from the cooler air in the downburst hitting the ground and spreading outward. Gust fronts can cause cumulus clouds to form as they move outward. They can be visible from the surface, satellite imagery and radar observations. Depending on atmosphere stability, gusts fronts can run into each other and spawn new thunderstorms. Figure 8-27 contains a weather radar image from Hastings, Nebraska and shows a gust front about 50 miles in diameter. Most gust fronts are not this large nor well-defined, but all gust fronts have a similar circular appearance when captured on weather radar.

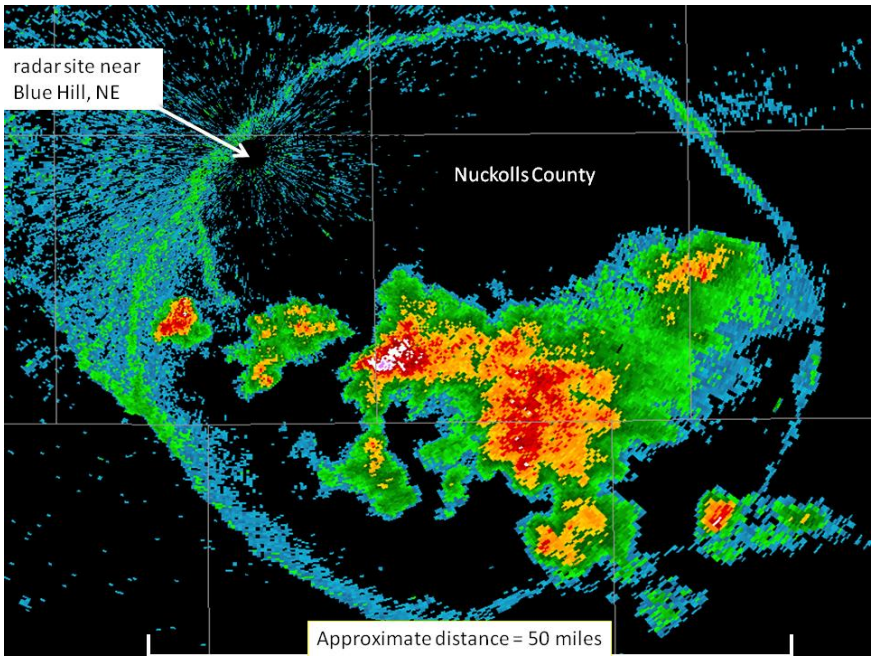

Figure 8-27: A weather radar image from Hastings, Nebraska. The large circular ring is composed of cumulus clouds being generated from the downdraft outflow of the thunderstorm in the middle (white and red area).

A **derecho** is a widespread, long-lived windstorm that is associated with a band of rapidly moving showers or thunderstorms. Although a derecho can produce destruction similar to that of tornadoes, the damage typically is directed in one direction along a relatively straight swath. As a result, the term “straight-line wind damage” may be used to describe derecho damage. By definition, a derecho wind damage swath must extend more than 240 miles. A historic derecho occurred on June 29, 2012, and traveled more than 700 miles across multiple states in 12 hours. Figure 8-28 contains a radar composite of the area affected. The wind speeds are given in mph. The average wind speed of the derecho motion was 60 mph.

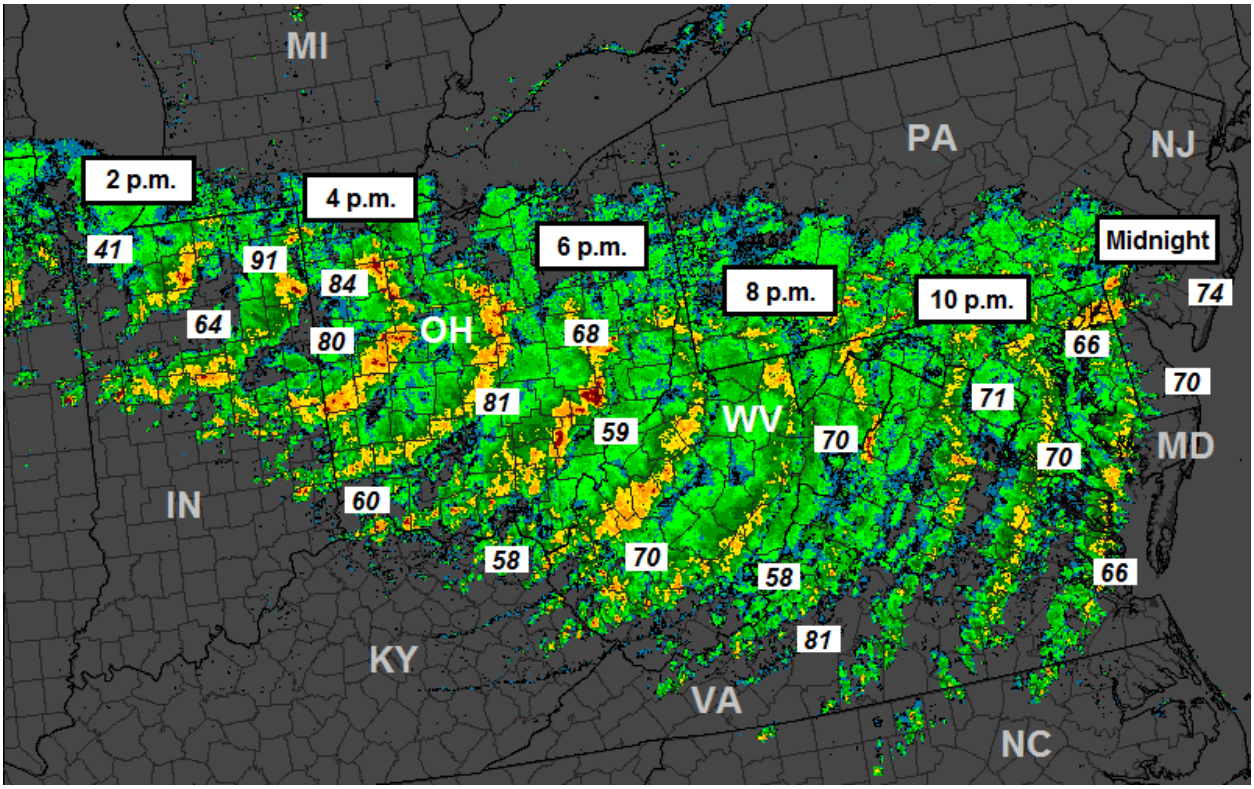

Figure 8-28: Composite radar images of a derecho that moved through 12 states. The times and wind speeds in mph are given in the white boxes.

Downbursts are defined as strong winds produced by a downdraft. A **microburst** is a small downburst. Microbursts are less than 2½ miles (4 km), but can have wind speeds over 100 mph. Winds in these events travel in a straight path and as such are called straight-line winds. Tornadoes on the other hand have wind and debris patterns that curve, which is associated with the rotation of the tornado. We will explore tornadoes in Chapter 9.

Figure 8-29 illustrates a microburst hitting the ground. As the air hits the ground, curls are created on the boundaries. These curls are indicative of strong winds and can be seen visually if dust or rain is carried within the wind. Microbursts only last for 2-5 minutes, but can cause considerable damage.

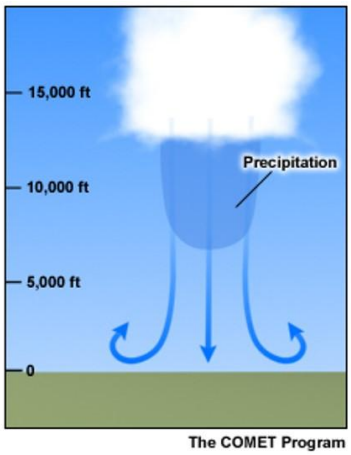

Figure 8-29: Illustration of a dry microburst where the precipitation does not reach the ground.

Microbursts create hazardous conditions for aircraft and have been responsible for several disasters. Figure 8-30 illustrates this dangerous hazard for an airplane.

1. As aircraft descend into the airport, they follow an imagery line called the "glide slope" (solid light blue line) to the runway.
2. Upon entering the microburst, the plane encounters a "headwind", an increase in wind speed over the aircraft. The stronger wind creates additional lift causing the plane to rise above the glide slope. To return the plane to the proper position, the pilot lowers the throttle to decrease the plane's speed thereby causing the plane to descend.
3. As the plane flies through to the other side of the microburst, the wind direction shifts and is now a "tailwind" as it is from behind the aircraft. This decreases the wind over the wing reducing lift. The plane sinks below the glide slope.
4. However, the "tailwind" remains strong and even with the pilot applying full throttle trying to increase lift again, there may be little, if any, room to recover from the rapid descent causing the plane to crash short of the runway.

Since the discovery of this effect in the early to mid-1980's, pilots are now trained to recognize this event and take appropriate actions to prevent accidents. Also, many airports are now equipped with equipment to detect microbursts and warn aircraft of their occurrences.

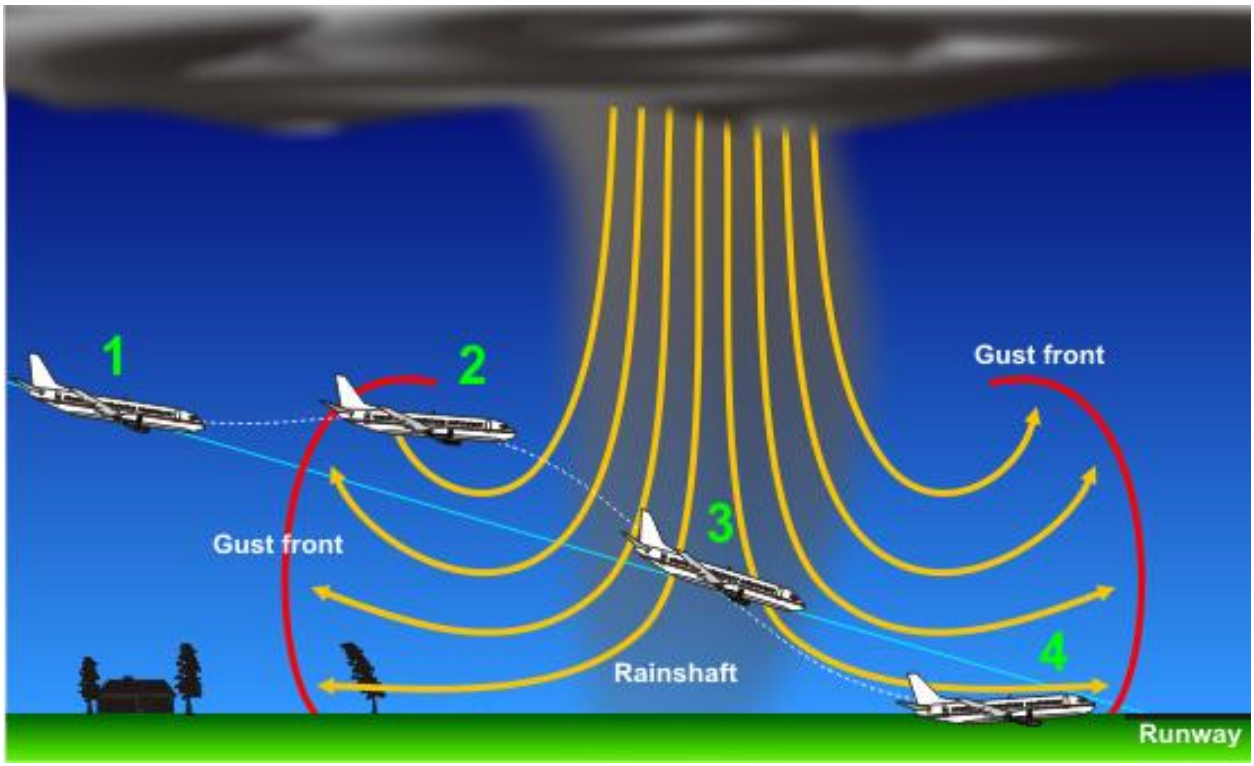

Figure 8-30: Illustration showing the dangers of a microburst as an aircraft crashes short of the runway.

8.3 - How a Weather Radar Works

During and after World War II, radar was used to track precipitation and thunderstorms. By the end of the war, technology had advanced considerably and surplus radars were used exclusively to monitor the weather. Given the short duration and small scale (mesoscale)

characteristics associated with thunderstorms and tornadoes, weather radars are now the primary method used to monitor and track these storms. The word “radar” is actually an acronym which stands for RAdio Detection And Ranging.

A weather radar works by emitting pulses of electromagnetic energy at microwave frequencies into the atmosphere. As this energy encounters objects, some of the energy is reflected back toward the radar. This principle is where the term “reflectivity” originates.

The larger the object, the greater the amount of energy that is returned to the radar. This returned energy gives radar the ability to detect rain, hail and snow in the atmosphere. In addition, the time it takes for the beam of energy to be transmitted and returned to the radar provides the distance to that object. Figure 8-31 describes the sequence of (a) pulse emission, (b) encountering an object and reflecting energy, and (c) the reflected energy traveling back to the radar.

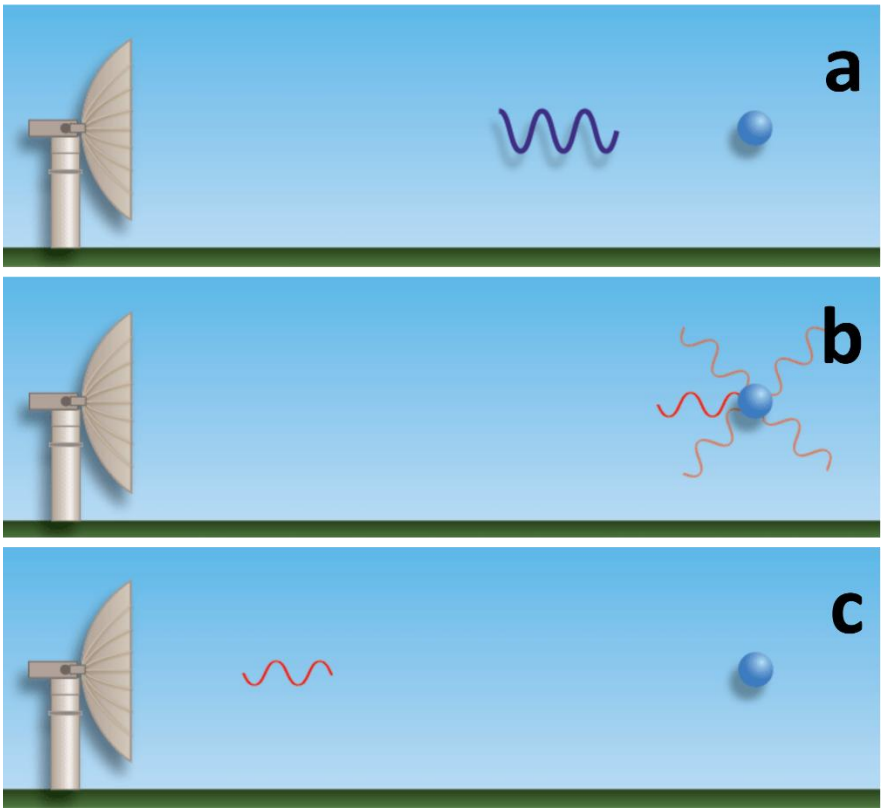

Figure 8-31: Illustration showing (a) the radar pulse emission, (b) the pulse encountering an object and reflecting energy, and (c) the reflected energy traveling back to the radar.

All the federal government weather radars in the United States are Doppler radar systems. These systems can provide information regarding the movement of targets as well as their position. When the radar transmits microwave pulses, the system keeps track of the phase (shape, position, and form) of those pulses.

By measuring the change in phase between a transmitted pulse and a received echo, the target's movement directly toward or away from the radar is calculated. This technique provides a velocity along the direction the radar is pointing, and is called a radial velocity. A positive phase shift implies motion toward the radar, and a negative shift indicates motion away from the radar.

This phase shift is similar to the "Doppler shift" observed with sound waves. With the "Doppler shift", the sound pitch of an object moving toward your location is higher due to compression of sound waves resulting in a higher frequency. As an object moves away from your location, sound waves are stretched resulting in a lower frequency. You have probably heard this effect from an emergency vehicle or train. As the vehicle or train passes your location, the siren or whistle's pitch lowers as the object passes by.

A Doppler weather radar transmits a pulse and then listens for a returning echo. The pulse lasts 0.00000157 seconds. In one hour of operation, the radar is transmitting for 7 seconds and listening for 59 minutes and 53 seconds. Most of the time, a weather radar is listening for information to be returned.

Figure 8-32 contains two photos of the outside and inside of a Doppler weather radar. The dish or antenna inside the dome is about 28 feet in diameter. The dish scans 360º around the horizon and has up to 14 different elevations angles or tilts to view the atmosphere near the radar. All the horizontal and vertical sampling takes less than 5 minutes to complete. When operating, the radar dish is spinning very fast! More on these sampling techniques known as scan strategies in the next section.

Figure 8-32: Photos of the outside and inside of a Doppler weather radar.

8.3.1 - Radar Scan Strategies

A weather radar can transmit a 1º degree pulse of energy. To cover the entire horizon around the radar, the radar dish needs to rotate 360º around a circle and transmit 360 pulses. This rotation provides a horizontal slice of the atmosphere. To observe a volume of the atmosphere, the radar dish needs to tilt up and down while it is scanning a horizonal slice.

When the radar is operating, it starts at the lowest tilt angle and goes to the next higher tilt angle with each revolution. After the radar antenna reaches the highest tilt angle, it drops to the lowest tilt angle and starts over again. A diagram depicting the 14 common tilt angles used for a weather radar observation is given in Figure 8-33. The number and angle of each tilt in a scan can be optimized based on the surrounding weather. For example, 14 tilts are used with vertical developing thunderstorms and a different combination can be used with light precipitation.

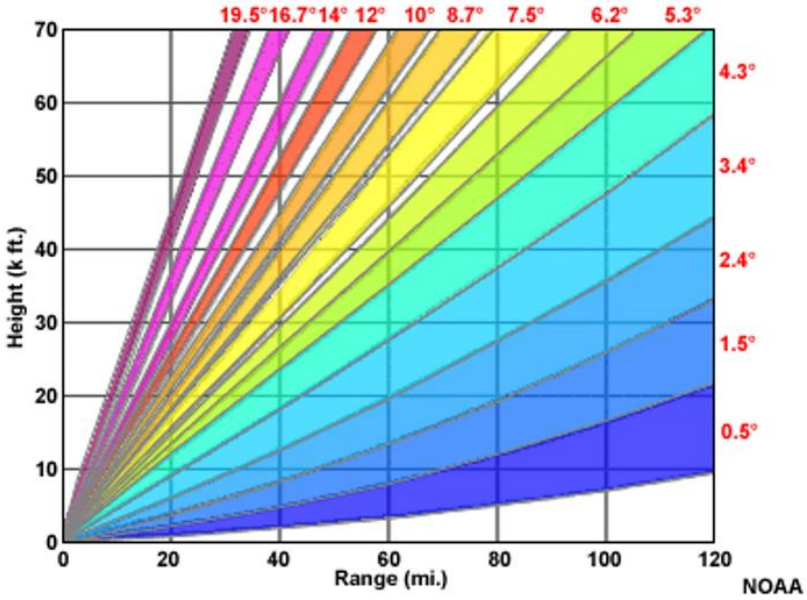

Figure 8-33: The vertical tilt angles associated with a weather radar observation. These angles change depending upon the type of weather near the radar. For example, the tilt angles for observing vertically developed thunderstorms are different than for lower level nimbostratus precipitation.

This process of horizontal and vertical scanning used to take a weather radar observation is called a **volume coverage pattern** (VCP). Multiple VCPs are automatically programmed into the radar system, which allows a meteorologist to quickly switch VCPs depending on the weather which is occurring. Notice in Figure 8-33 that the lower atmosphere at 120 miles and directly over the radar is not observed. However, most of the atmosphere in the vicinity of the radar is observed well.

An addition to the National Weather Service radars in the 2000s was the dual-polarization of the radar pulse. A dual-polarization radar can transmit and receive pulses in both a horizontal and vertical orientation as shown in Figure 8-34. A conventional Doppler radar just transmits a horizontal pulse.

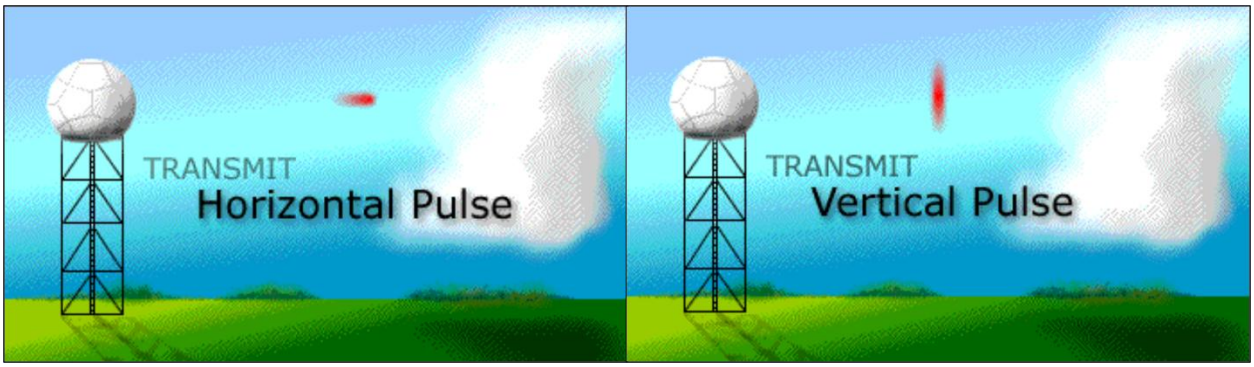

Figure 8-34: The horizontal and vertical pulse orientation of a dual-polarization radar.

A dual-polarization weather radar provides more details on the particles reflecting energy back to the radar, such as identifying areas of rain, hail, snow, the freezing level, ice pellets, blowing dust and other features.

8.4 - Radar Reflectivity Observations

Reflectivity images contain the amount of energy reflected back to the radar. This energy returned from particles is measured in decibels (dBZ). The scale in a reflectivity image usually ranges from 0 to 75 dBZ. Heavy rain with hail can be as high as 10^7 dBZ. However, the radar system truncates these extremely high values and they are never displayed. This approach avoids losing important details from the lower value returns,

Two types of reflectivity are generally available on the web or in weather apps. **Base reflectivity** which is taken from the lowest elevation scan (usually 0.5°), and **composite reflectivity** which are the highest dBZ values from all scan elevations compiled into one image. The reflectivity image in Figure 8-35 is an example of base reflectivity. The radar is located in the middle of the image.

The dBZ scale on the right varies slightly depending on what type of software a person is using to view the data. Typical reflectivity colors are:

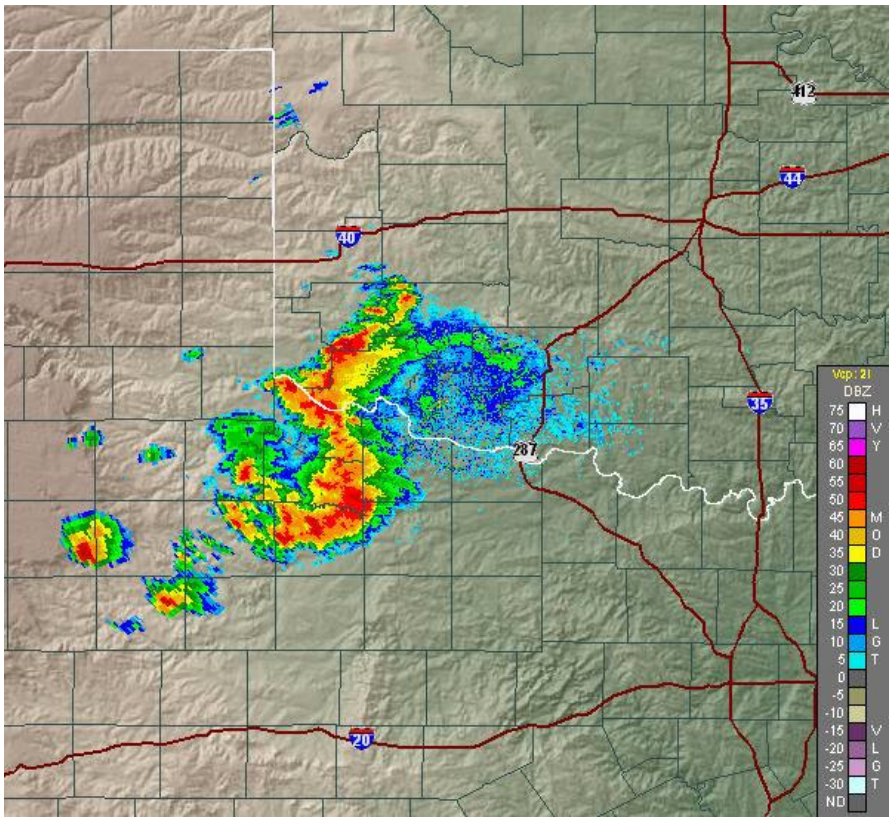

Figure 8-35: Base reflectivity image at the lowest elevation scan of 0.5 degrees.

- Blues and greens – light precipitation
- Yellows, oranges and reds – heavier precipitation
- Above 45 dBZ (reds) – usually precipitation originating from convection (cumulonimbus cloud)
- Above 60 dBZ (magenta and purple) – usually hail

A composite reflectivity image requires all of the elevation scans to be completed prior to creating it. This requirement makes a composite reflectivity product about 5 minutes older than a base reflectivity one. Figure 8-36 is an example of a composite reflectivity around the same time as the base reflectivity product In Figure 8-35.

Notice in Figure 8-36 that the blue and green reflectivity values cover a larger area, and a noticeable area of 65 dBZ is now present in the northern portion. This additional reflectivity information is from the additional scan angles above the base reflectivity angle (0.5°).

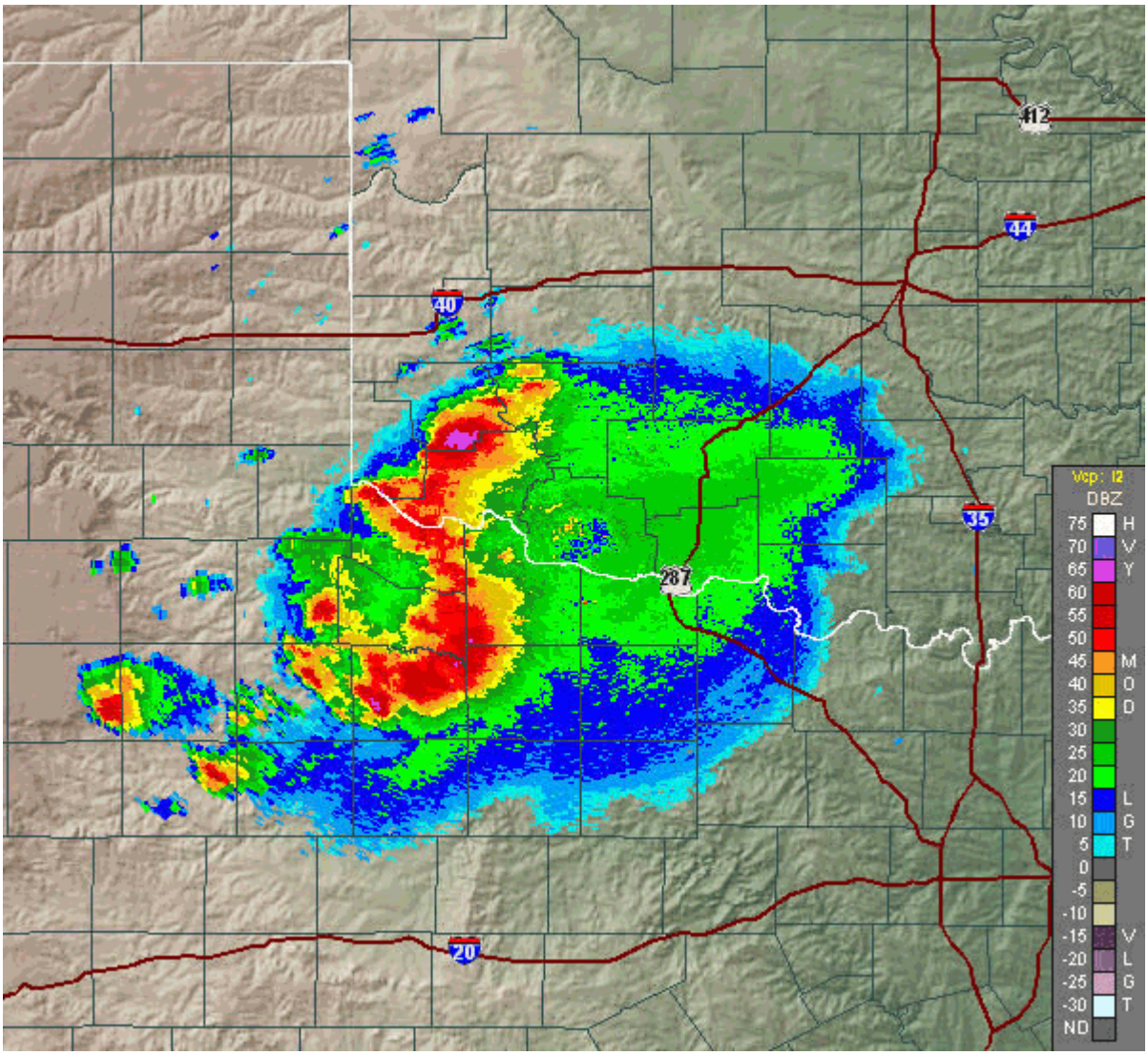

Figure 8-36: Composite reflectivity product containing the highest dBZ from all elevation scans. This product is at the same time as the base reflectivity in Figure 8-35.

8.4.1 - Radar Velocity Observations

Weather Doppler radar has the ability to detect the motion of the particle reflecting energy. However, this motion is not the direction of the wind, but rather the portion of the wind's motion that is moving either toward or away from the radar. A particle's motion either towards or away from the radar is called **radial velocity**.

Velocity fields are difficult to use, but are presented in this textbook for completeness. Additionally, velocity fields are a critical data set in identifying tornadoes, strong winds from downbursts and the speed of fronts.

The motion of the wind, relative to the radar, is broken down into two components:

- the motion perpendicular to the radar beam and
- the motion along that radial (either directly toward or away from the radar).

In Figure 8-37, the wind is moving from south to north (indicated by the black arrows). North of the radar (red shading) the wind is moving away from the radar. As the radar sweeps from position 1 to position 2, the beam becomes more and more in line with the overall wind flow. The blue arrow lengths represent the speed the radar “sees” along that direction. As it does, the radar "sees" an increase in the radial velocity away from the radar. At position 2, the radial velocity (blue arrow) is the same as the overall wind speed (black arrow). Then, as the radar sweeps to position 3 the radial velocity begins to decrease.

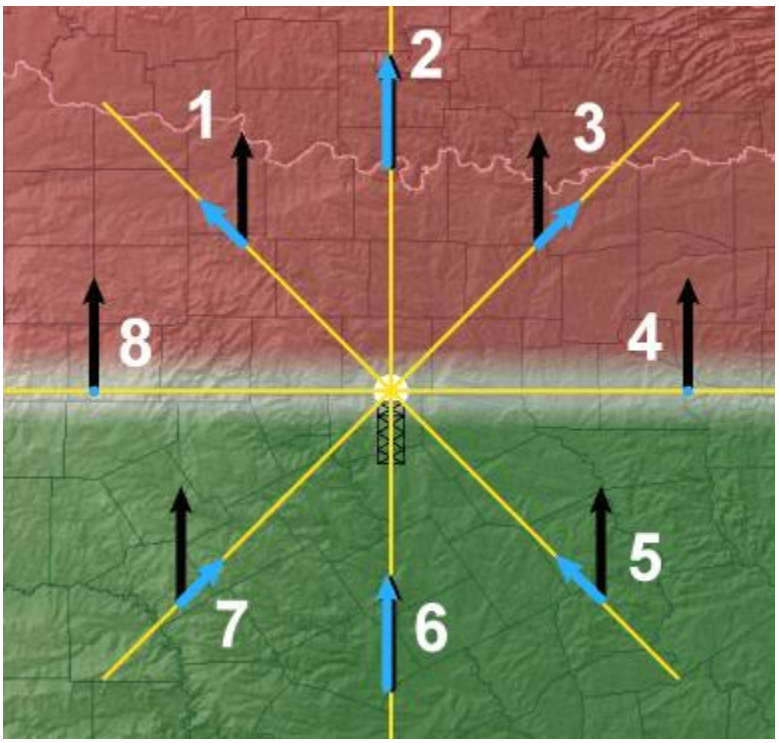

Figure 8-37: A radar map with a south wind indicated by the black arrows. The radar is located in the center. The radial velocities are indicated by the blue arrows. Notice the radial velocity equals the actual wind when parallel to the radar beam at 2 and 6. The radial velocity equals zero when perpendicular to the actual wind at 4 and 8.

On this map radial velocities toward the radar are green (5, 6, and 7). Radial velocities away from the radar are red (1, 2, and 3).

At position 4 and 8, the wind is blowing perpendicular to the radar beam. Since there is no motion toward or away from the radar, it "sees" zero motion. However, the wind is not calm at these points as it is still blowing from the south. This is just the area of zero radial velocity.

Positions 5, 6, and 7, in the green shading, are like 1, 2, and 3 in the red shading except the wind is moving toward the radar. The greatest radial velocity is at position 6 where the wind is blowing directly at the radar.

These observed radial motions are vectors, meaning that the length of the arrows indicates the speed of the wind; the longer the arrow, the faster the speed. The Doppler radar calculates velocity based on the length of these vectors. In velocity graphics, red colors indicate wind moving away from the radar and green colors indicate wind moving toward the radar. The brighter the reds and greens, the greater the radial velocity and a better representation of the true wind speed.

Base velocity, like base reflectivity, is taken from the lowest elevation scan (usually 0.5^{o}). Base velocity is the primary product you will see when encountering this data set. For a radar to determine a radial velocity, particles must be present to reflect energy back. Figure 8-38 shows

a comparison between base velocity and base reflectivity. Notice most velocity information resides within the areas with reflectivity values. The wind direction in this velocity product is coming from the southwest, which is determined by taking a line perpendicular to zero radial velocity. The zero radial velocity is the gray stripe between the red and green colors.

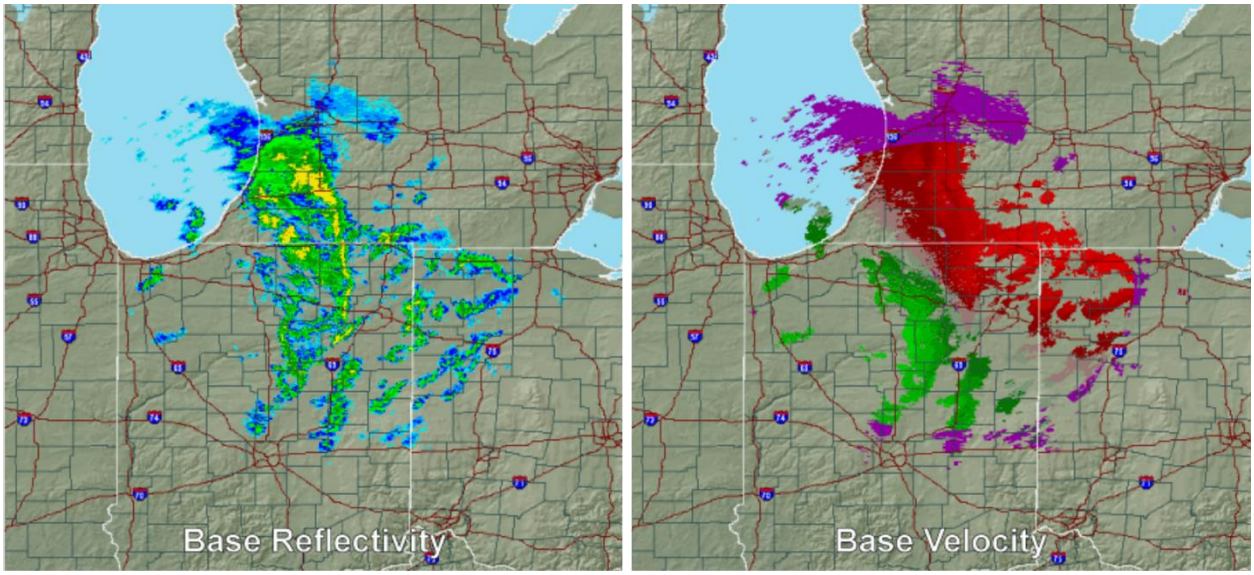

Figure 8-38: Comparison of base reflectivity and velocity products. The wind over this area is from the southwest. The zero radial velocity (gray) is between the green and red velocity colors. The wind direction is perpendicular to the zero radial velocity or from the southwest.

8.4.2 - Beam Spreading and Observation Quality

While often depicted as a cone with distinct edges, the radar beam is better visualized with an ordinary flashlight. In a darkened room, take a flashlight and while standing 10 feet away shine it on a wall. The bright area around the center of the beam is seen, but you will also notice light that fades from the beam's center point. Additionally, the width of the beam changes as the flashlight moves toward or away from the wall.

The beam of energy transmitted from the Doppler radar is no different. A conical shaped beam is formed as the energy moves away from the radar. Near the center of the beam is where most of the energy is located with the energy decreasing away from the centerline.

By convention we define the width of the beam as the distance between the two half power points - the point where there is a 50% reduction in the radar's transmitted energy. All the radar imagery used in this book has the angle between the two half power points as one degree. Outside of the half power points, the energy rapidly decreases.

Figure 8-39 shows the actual physical width of the radar beam, and that it depends upon the distance to the radar. The width of the beam expands at a rate of almost 1,000 feet for every 10 miles away from the radar.

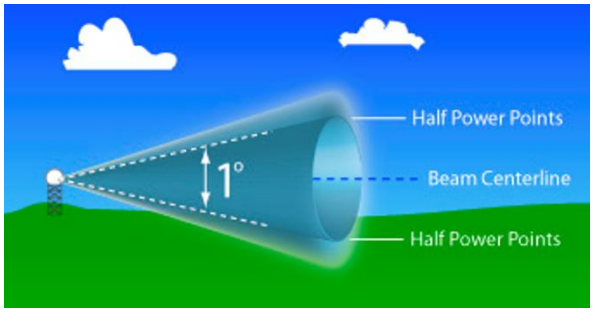

Figure 8-39: Illustration of a one degree radar beam with most of the energy between the half power points.

Thirty miles from the radar, the beam is approximately 3,000 feet wide. At 60 miles, the beam is about 6,000 feet wide. At 120 miles the beam is nearly 12,000 feet or over two miles wide. This beam width spreading affects the resolution capability of the radar. Small features, which can be seen close to the radar, are often obscured when viewed at great distances (Figure 8-40).

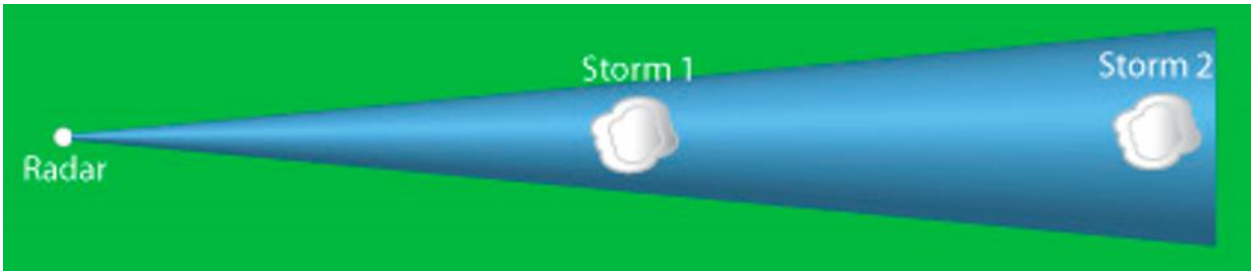

Figure 8-40: Illustration of beam spreading for two identical storms. The storm closest to the radar be observed at a higher resolution.

Therefore, the distance from the radar determines the quality of the observation at a location. Figure 8-41 illustrates observation quality versus distance. Notice convective precipitation from vertically developed clouds has the highest quality at the longest range. Flat, layered clouds like nimbostratus need to be closer to the radar for a better observation quality. The distance from the radar to the weather being observed is the most important factor in determining the quality of a radar observation.

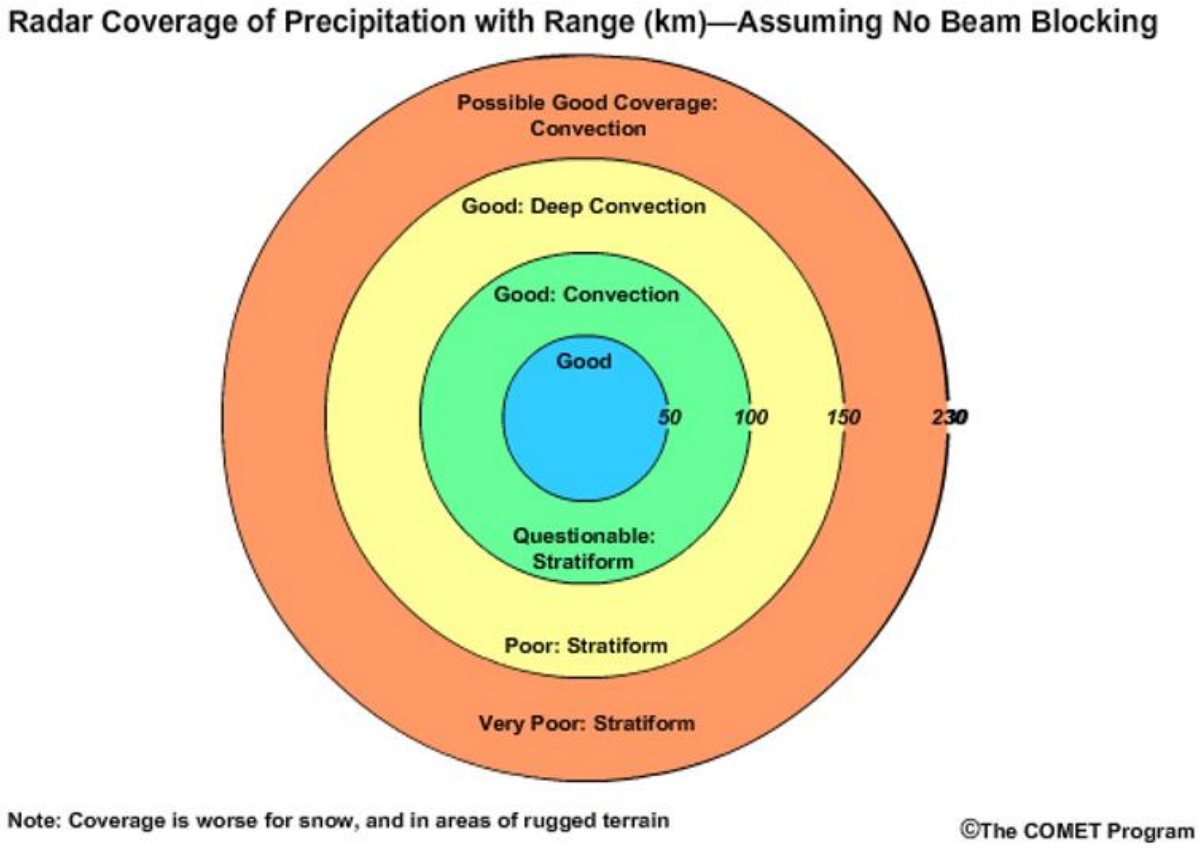

Figure 8-41: A diagram describing the quality of a radar observation based on the distance from the radar.

8.4.3 - Beam Refraction

As a radar beam propagates away from a radar, it increases in height. Much in the same manner as the beam spreading with distance, this increase in height reduces the quality of an observation at long distances as illustrated in Figure 8-42. The further the distance from the radar, the greater the area underneath the beam where details can be missed.

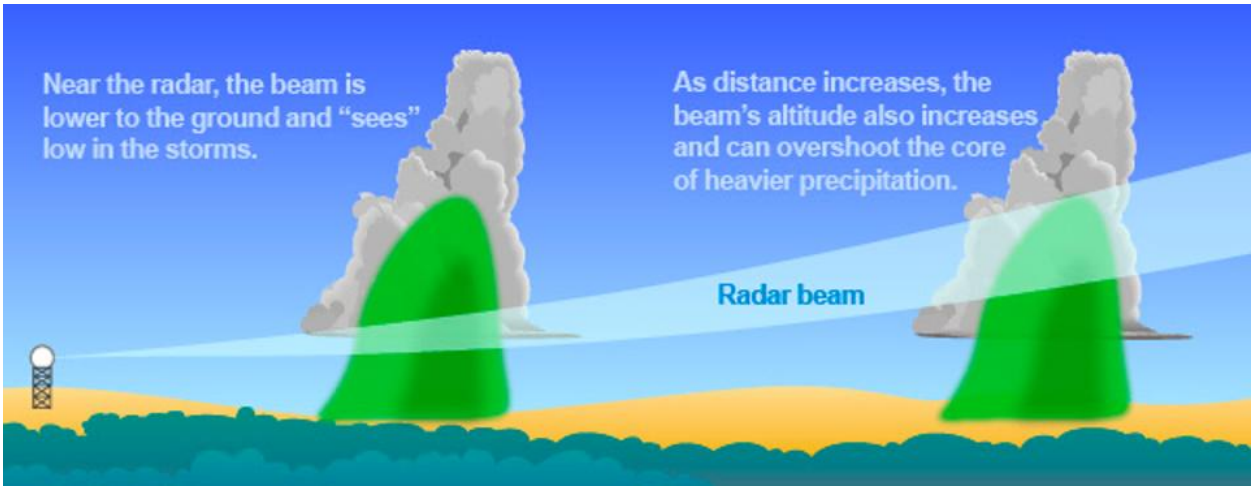

Figure 8-42: A radar beam increases in height the further it travels from the radar. At long distances, important details near the surface may be missed. In this illustration, the area of heavy precipitation (green) in identical storms is missed in the distant storm.

To better understand radar beam propagation, a new term needs to be introduced. **Refraction** is defined as the bending of electromagnetic radiation as it passes through different mediums. The different mediums have different densities, which is what causes the radiation to bend. The most common application of refraction are eyeglasses. The light passes from air through the lens into a person's eye, the light is bent so that a person can see clearly.

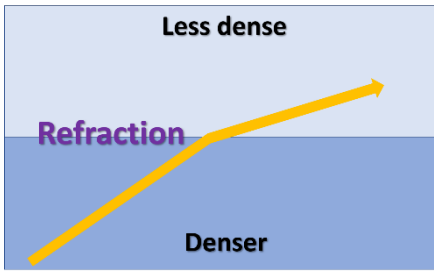

Figure 8-43: The bending of electromagnetic radiation as it passes between different mediums is called refraction.

Applying refraction to the atmosphere, lower portions of the atmosphere are slightly denser than higher altitudes. This change in density causes the radar beam to bend towards the Earth. However, you likely noticed in the first diagram that the radar beam increases with height. The reason the beam increases with height is because the lowest elevation of the radar dish is 0.5°. If the tilt angle was set to zero, the radar beam would frequently hit the Earth and return no useful observations of the atmosphere.

Figure 8-44 depicts beam refraction for a standard atmosphere for the lowest tilt angle. A radar beam's curvature is slightly less than the Earth's curvature, and the beam height increases with distance from the radar. A standard atmosphere assumes a uniform decrease in temperature with height.

Figure 8-44: Radar beam refraction in a standard (normal) atmosphere.

When the atmosphere is **warmer** than a standard atmosphere, the refraction of the beam is less. This causes

the radar beam to increase even more with height the further from the radar. This condition is called subrefraction. The subrefraction occurs in a warmer atmosphere and overshoots distance storms making them appear shorter. The left side of Figure 8-45 illustrates subrefraction.

The opposite condition of subrefraction is called superrefraction, and occurs in a **colder** atmosphere. A colder atmosphere causes the beam to be bent more towards the Earth. Superrefraction will cause distant storms to appear taller, and ground clutter may increase. Ground clutter is energy returned from objects on the ground, and is explained in the next section.

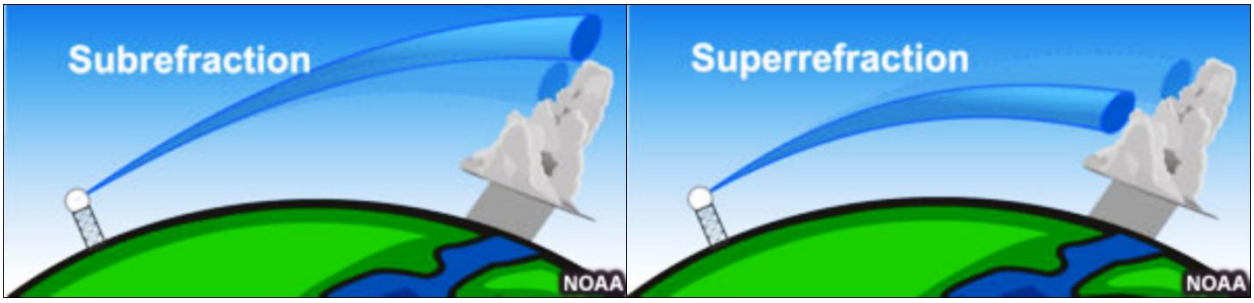

Figure 8-45: (left) Subrefraction occurs in a warmer than normal atmosphere, which causes the beam to increase more with height. (right) Superrefraction occurs in a cooler than normal atmosphere, which causes the beam to bend more towards the Earth.

The assumption is that a standard atmosphere is present and normal refraction is occurring. This assumption is valid most of the time. Determining the actual refraction which may be occurring is difficult. However, a person should remember that errors in the data are associated with these refraction issues. Most of these errors are at longer distances from the radar, which comes back to the data quality versus distance diagram in the previous section. Remembering that the further from the radar makes the observation less accurate is beneficial in interpreting radar data.

8.4.4 - Ground Clutter and Beam Blockage

Ground clutter is energy received by the radar from trees, buildings, or other objects on the ground. Mountains also result in ground clutter problems and do not need to be near the radar. Figure 8-46 contains a base reflectivity image from Phoenix, Arizona and illustrates ground clutter. The Phoenix radar is located at the Phoenix-Mesa Gateway Airport in Mesa, Arizona and has persistent ground clutter visible on most days. None of the reflectivity values in this figure are associated with clouds or precipitation.

Ground clutter is relatively easy to identify in animated radar images because it does not move. Clouds and precipitation move.

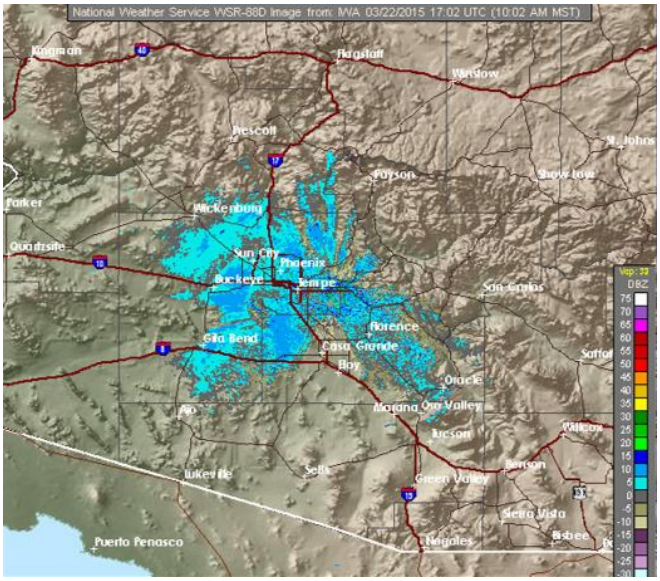

Figure 8-46: Ground clutter on the Phoenix, Arizona radar.

Hence, any reflectivity value that does not move when the imagery is animated is usually associated with ground clutter.

Beam blockage is when higher terrain, like a mountain, stops the propagation of the radar beam. A weather radar cannot "see" behind a mountain. All weather radars located in mountainous terrain have this type of problem.

Beam blockage is most noticeable in the base (lowest scan angle) reflectivity or velocity products. An indication of beam blockage in a product is frequently a pie-shaped data void area. The left side of Figure 8-47 illustrates a mountain blocking a radar beam. The right side is a reflectivity image with two areas of beam blockage highlighted; notice the pie shaped area.

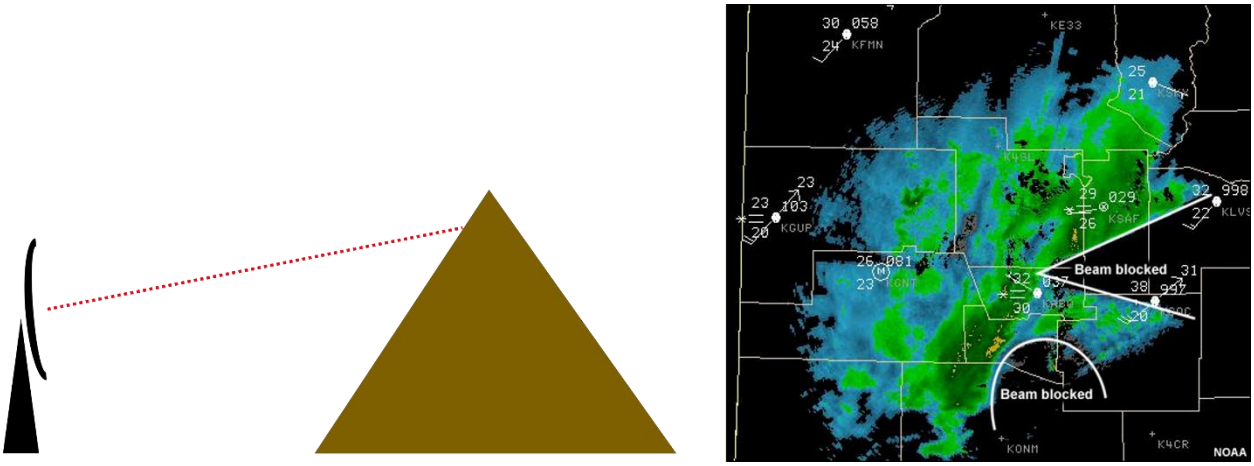

Figure 8-47: (left) Beam blockage occurs when the radar beam encounters a large physical object such as a mountain. (right) A reflectivity image with two areas of beam blockage highlighted.

8.4.5 - Bright Bands

A **bright band** is a spike in returned energy when water and ice co-exist. Water coated ice is very efficient at reflecting energy. This condition occurs slightly below the freezing level in the atmosphere. Ice by itself has lower reflectivity values than rain. As ice falls through the freezing level, it starts to melt and becomes water coated ice. This mixed phase of particles allows them to stick together, which is called aggregation. Aggregation is most efficient at 0º. Thus, the water coated ice particles grow in size as aggregation occurs, and reflect even more energy. As the water-ice particles continue to fall, they fully melt and become rain. Figure 8-48 illustrates the change in phase of the precipitation and the approximate changes in reflectivity values.

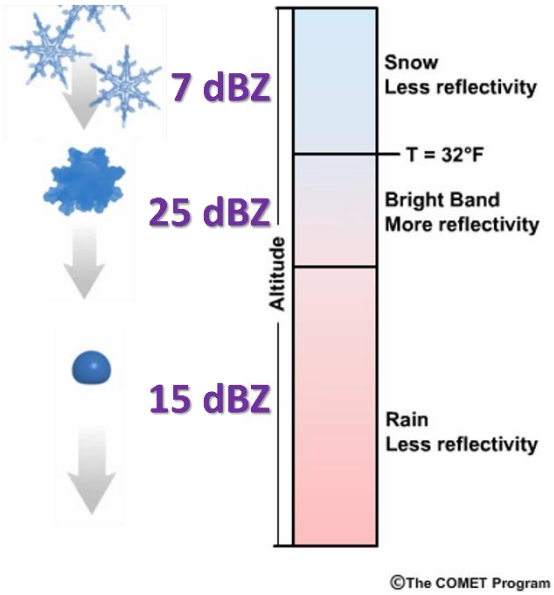

Figure 8-48: : Illustration of a bright band as ice crystals (snow) fall below the freezing level and begin to melt. The dBZ values are approximate changes in reflectivity.

Figure 8-49 illustrates a bright band associated with a layer of precipitation (nimbostratus). If no frozen precipitation was present, no bright band would be present and the yellows and oranges would have been green values. In this example, uniform precipitation is likely occurring across the entire area. A person looking at this data could interpret the data as heavier precipitation at a set distance from the radar. However, if this person was aware of a bright band occurring, they would recognize the data was contaminated.

In convective situations with vertically developed thunderstorms, a bright band is inherent in the radar observation. However, due to the turbulence within a thunderstorm, finding a bright band is difficult. These conditions cause most people to ignore the possibility of bright band reflectivities in convection. Detecting a bright band in layer cloud precipitation (nimbostratus) is easier and appropriate data interpretation adjustments can occur.

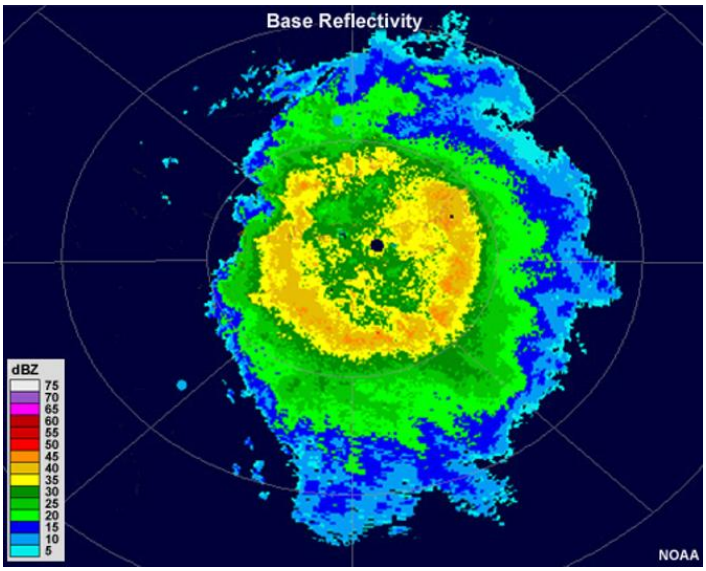

Figure 8-49: A radar reflectivity image containing bright band contamination.

Chapter 8 Review Questions

1. Which state in the U.S. has the highest annual lightning flash rate?
2. What is the annual lightning flash rate where you live?
3. Which continent receives the most lightning in a year?
4. What type of lightning occurs the most?
5. If 15 seconds occurs between a lightning flash and the time thunder is heard, how far away was the lightning?
6. What are the first three steps for a cloud-to-ground strike to occur?
7. What is the safest location when lightning is nearby?
8. What are three ingredients for a thunderstorm to develop?
9. What are the three stages of development in a basic thunderstorm?
10. Describe the differences between a supercell and basic thunderstorm.
11. Name four characteristics that can be associated with a supercell thunderstorm.
12. What is the updraft wind speed when quarter size hail occurs with a thunderstorm.
13. What is the transition zone between the cooler downdraft air and the warming surrounding air in a thunderstorm called?
14. Name two types of multi-cell thunderstorms.
15. What is the process of horizontal and vertical scanning used by a weather radar to take an observation called?
16. What type of wind field is contained in a base velocity product from a Doppler weather radar?
17. What causes a bright band in a weather radar reflectivity image?
18. What is the most important factor in determining the quality of a radar observation?
19. Describe what causes radar ground clutter.
20. What do radar reflectivity values over 60 dBZ usually represent?

Chapter 9 – Tornadoes and Hurricanes

Overview

This chapter examines tornadoes. Tornadoes occur in thunderstorms, so tornadoes are an appropriate topic after Chapter 8. We will look at two types of processes for tornadoes to form: (1) within supercells and (2) non-supercell formation. The strongest tornadoes occur within supercell thunderstorms.

Hurricanes will then be covered. Hurricanes are the largest storms on our planet. They originate in the tropics and subtropics during the summer and fall months. We will explore their formation, structure, classification, decay, and the hazards associated with them. Hurricanes can wreak widespread devastation over multiple days.

Chapter Objectives:

1. Understand how supercell and non-supercell tornadoes form.
2. Describe the tornado damage scale.
3. Describe the steps in the formation of hurricanes.
4. Describe the hurricane damage scale.
5. Describe how hurricanes cause destruction and fatalities.

9.1 – Tornadoes

Figure 9-1: Photograph of a tornado picking up debris.

A **tornado** is a rapidly rotating column extending from a cumulus type cloud to the ground. A **funnel cloud** is a rapidly rotating column extending from the cloud but not touching the ground. A tornado not touching the ground is a funnel cloud. As soon as a funnel cloud touches the ground, it becomes a tornado. Frequently a tornado picks up debris when in contact with the ground, as shown in Figure 9-1. The debris ball is caused by airborne dust, leaves, branches, vehicles, or pieces of damaged buildings.

A low pressure resides inside a tornado, which causes condensation to occur within the rotating column. Thus, many tornadoes are the same color as the surrounding clouds, but not all tornadoes have a cloud inside them. Tornadoes without condensation in the column can be mistaken for funnel clouds. However, when debris becomes visible underneath a funnel, then a tornado has touched the ground.

Tornadoes are most prevalent in the spring and early summer (April through June) with more occurring in the central U.S. than any other place in the world. They occur in this region because moist Gulf of Mexico air (mT) meets cold, dry air from Canada and the Rocky Mountains (cP). The differences between these two air masses are most intense in the spring and early summer, and support tornado development. The map in Figure 9-2 depicts the peak probability of a tornado occurring on May 20. The highest probability is 1.4%, so most people can live in this area for years before seeing a tornado. However, you are much more likely to see a tornado in the central U.S. than in the West.

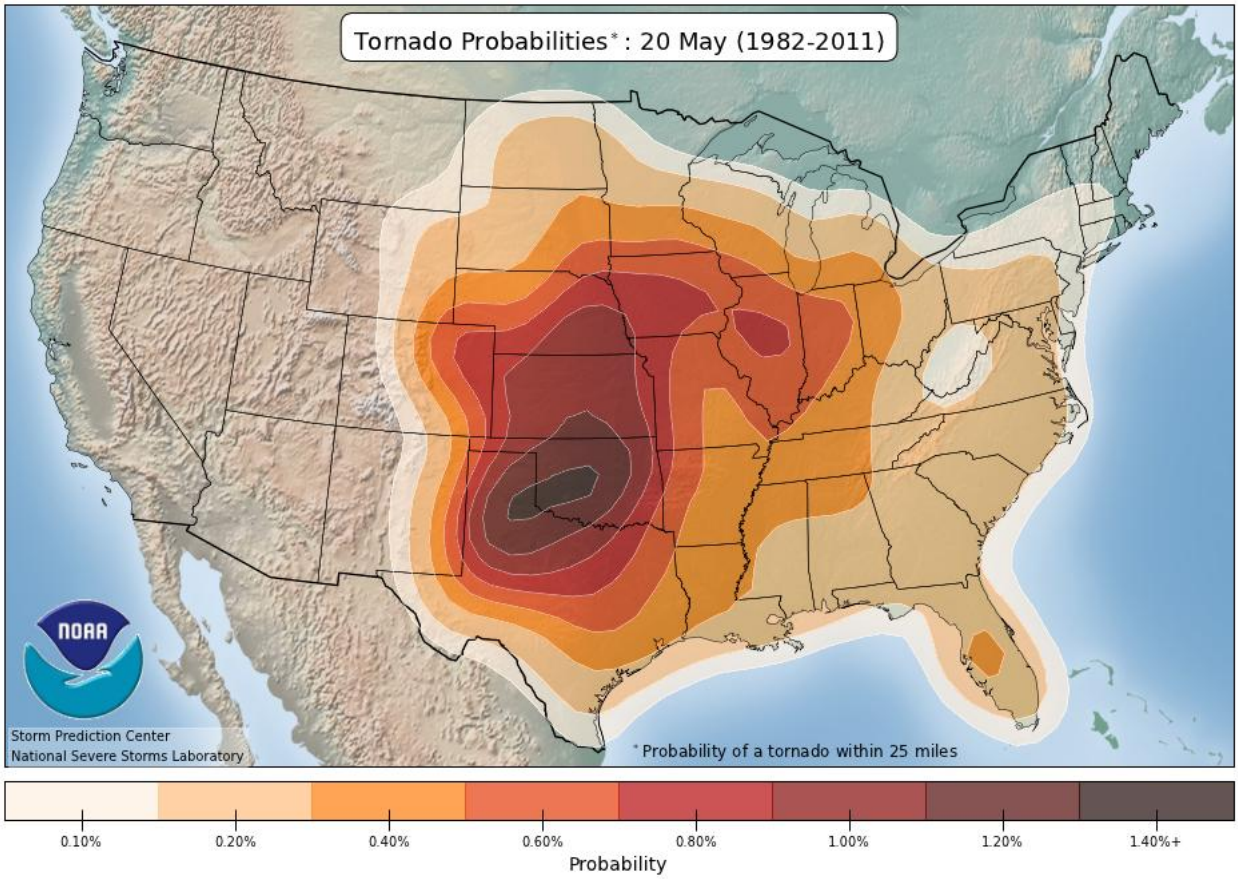

Figure 9-2: Tornado probability map for the 20th of May.

In a typical year about 1200 tornadoes strike the United States. The map in Figure 9-3 depicts the average number of tornadoes by state. Larger states, like Texas, have more tornadoes partially because they encompass more land on which a tornado can form.

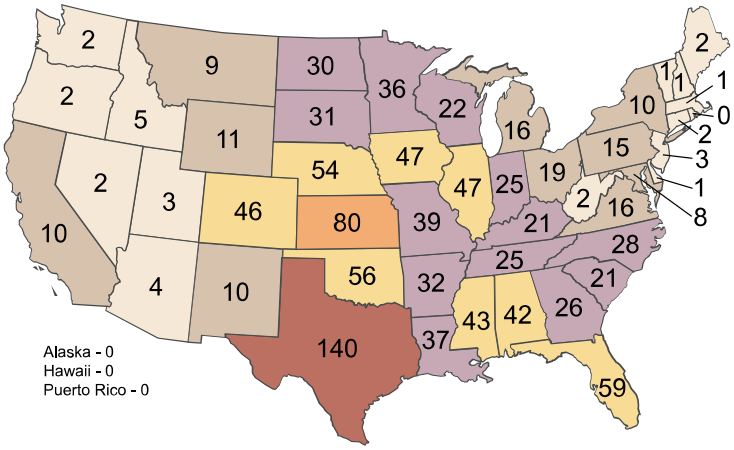

Figure 9-3: Annual number of tornadoes occurring in each state.

Tornadoes can last from several seconds to more than an hour. Most last less than 10 minutes. As a tornado gradually loses intensity, the rotating column decreases and becomes tilted with height. The tornado can take on a contorted, rope-like appearance before it completely dissipates. Tornadoes come in many sizes and shapes as seen in Figure 9-4. The size and shape does not determine its intensity.

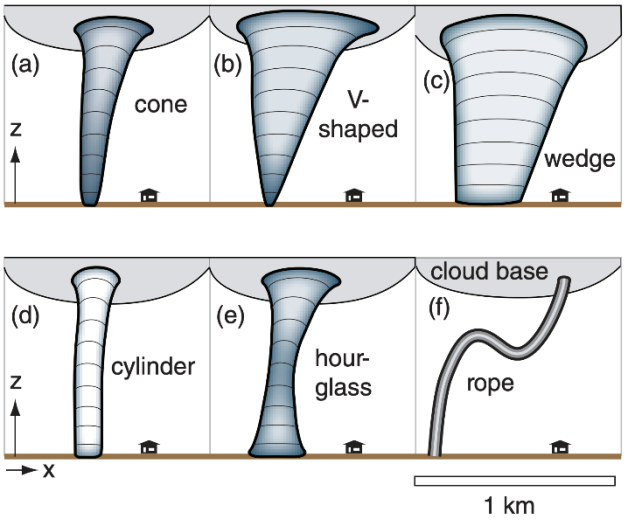

Most tornadoes originate from supercell thunderstorms, but only about 20% of supercells create tornadoes. When examining tornado formation, dividing them into two categories is helpful: (1) supercell tornadoes and (2) non-supercell tornadoes is helpful.

Figure 9-4: The various shapes of tornadoes. Tornado shape does not determine its intensity.

Module 9.1.1 – Supercell Tornadoes

Supercell thunderstorms are characterized by a persistent rotating updraft and form in environments of strong vertical wind shear. Wind shear is the change in wind speed and direction with height. Wind shear was explained in Chapter 8, and the diagrams in Figure 9-5 are a review of directional and speed wind shear.

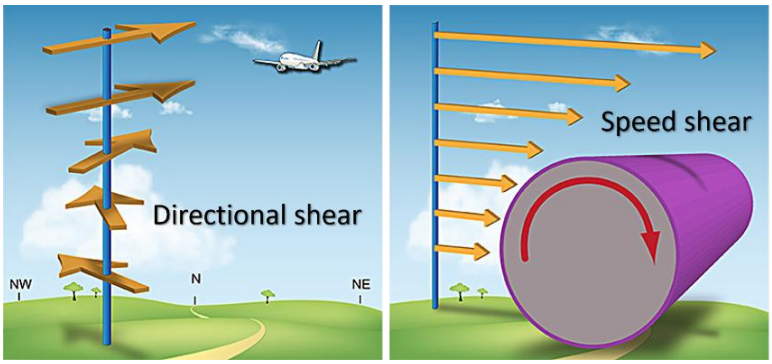

Figure 9-5: (left side) Diagram describing directional wind shear. (right side) Describes speed wind shear.

This wind shear is a key component in creating a rotating updraft within a supercell, and in increasing this rotation within the thunderstorm. How does wind shear do this? The environment in which a supercell develops has horizontal rotation or vorticity inherent in the wind field due to speed shear. In a developing thunderstorm, this horizontal rotation is entrained into the storm through the updraft, as is illustrated on the left side of Figure 9-6.

The directional wind shear amplifies any rotation within the supercell; both speed and directional wind shear are important to create a supercell with strong rotation. Once the rotation within the supercell reaches certain levels it is called a mesocyclone. A **mesocyclone** is a supercell thunderstorm with a strong rotation. However, not all supercells contain a mesocyclone.

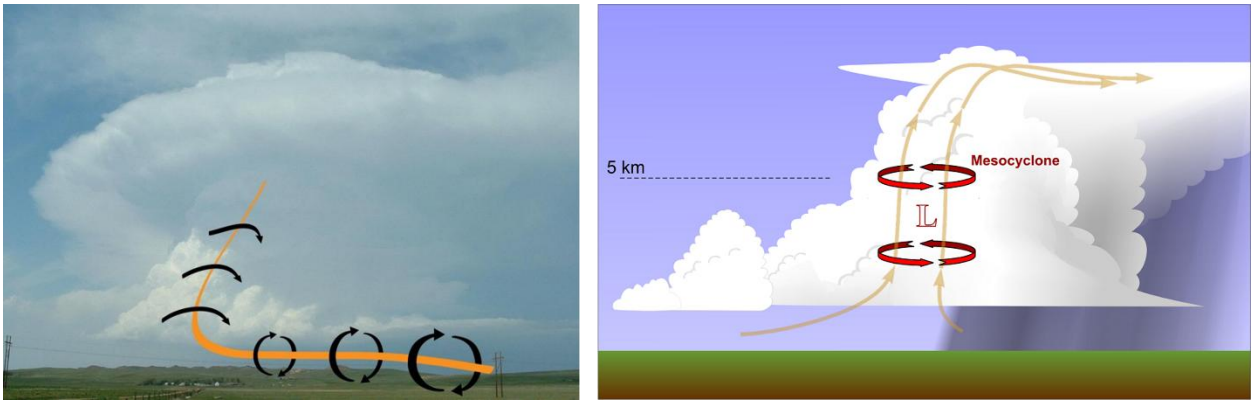

Figure 9-6: (left side) Speed shear near the surface creates horizontal rotation which is entrained into a thunderstorm through its updraft. (right side) Rotation inside the storm is maintained.

If the rotation continues increasing within the mid-levels of the mesocyclone, a funnel cloud may form in the lower portion of the supercell and descend from the base of the storm. If the rotation does not increase, no tornado will form. Forecasters will examine these rotations within the mesocyclone to determine if a tornado will or will not form. Figure 9-7 shows a top view of the mesocyclone with this rotation highlighted. Notice how the mesocyclone rotation aligns with the weak echo region or hook echo.

About 20 to 30% of mesocyclones produce tornadoes. The exact processes for the formation of a funnel and subsequent tornado are not fully known, and more research is needed to fully understand tornadoes.

This short video from the United Kingdom Met Office explains how supercell tornadoes form.

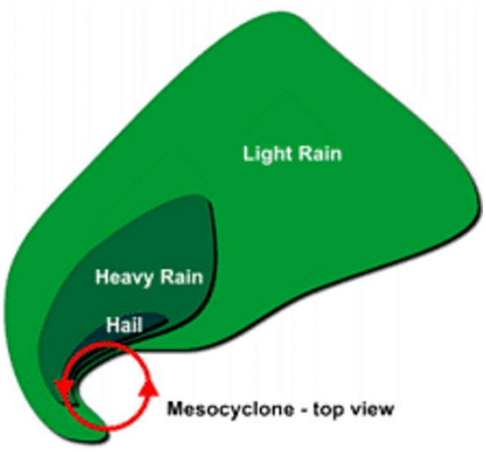

Figure 9-7: Top view of the rotation in a supercell thunderstorm. This rotating storm is referred to as a mesocyclone.

9.1.2 – Non-supercell Tornadoes

Not all tornadoes come from supercell thunderstorms. These non-supercell tornadoes can originate from (1) multi-cell squall lines, and (2) updrafts in a developing cumulus cloud.

Nearly 20% of all tornadoes are associated with squall lines that occur during the late night and early morning hours. These types of squall lines have been given the specific name of "quasi-linear convective systems" (QLCS), but for simplicity we will just refer to them as squall lines. The tornadoes in these squall lines tend to be weaker and shorter-lived on average than those associated with supercell thunderstorms. Figure 9-8 depicts a squall line with embedded tornadoes in it. Distinguishing the atmospheric conditions which favor a tornadic squall line versus a non-tornadic one is another active area of research.

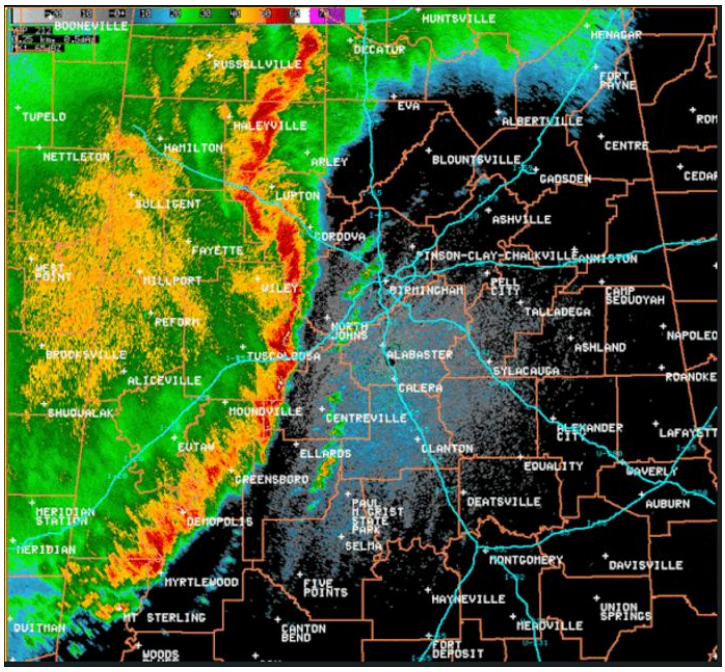

Figure 9-8: Reflectivity product of a quasi-linear convective system.

Other non-supercell tornadoes arise from low level circulations that are entrained into an updraft of a developing cumulus cloud. A weak convergence zone exists in the winds at the surface. This convergence zone creates weak rotations along the boundary. Likewise, the convergence zone leads to rising air which can form cumulus clouds. When the updraft of a cumulus cloud aligns with one of these weak rotations, the rotation is stretched as it enters the updraft. This stretching greatly increases its spin and the strength of the updraft. This situation is similar to an ice skater going into a spin and pulling their arms close to their body. This action greatly increases their spin speed.

These non-supercell tornadoes that originate from the lower levels up into a cumulus cloud are called **landspouts**. Landspouts are generally weaker tornadoes, and appear as a narrow, rope-like condensation funnel. They form while the cumulus cloud is still growing and no rotating updraft is present. After a landspout forms, its rotation may cause a rotation to occur in the updraft which could then develop into a supercell thunderstorm. Hence, the landspout aids in developing a supercell thunderstorm. The landspout tornado occurs before the thunderstorm matures. This situation is the exact opposite of a supercell tornado which requires the thunderstorm first. Landspouts are the most common tornado to occur in southern Arizona. The left side of Figure 9-9 illustrates how landspouts form. The blue line is the convergence zone at the surface with weak rotations. These rotations align with the updraft of a developing cumulus cloud.

When a landspout forms over water, it is called a waterspout. The physical process for a waterspout to form is similar to a landspout. Rotation exists at the surface which is then pulled

into a developing cumulus cloud. The right side of Figure 9-9 illustrates the formation of a waterspout. Waterspouts are generally weaker tornadic rotations too.

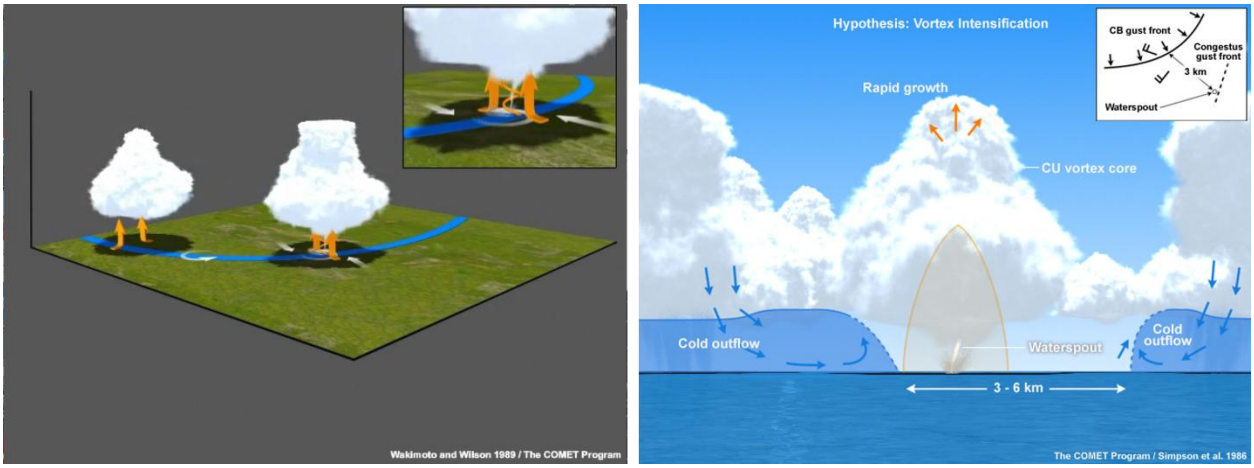

Figure 9-9: Left side is an illustration of landspout formation. Right side is a similar illustration for waterspout formation.

A **dust devil** is a small, vigorous whirlwind in shown in Figure 9-10. Dust devils are visible because of dust, sand and debris picked up from the ground. Dust devils are not tornadoes because no cumulus-type cloud is inherent in their formation. Dust devils are not associated with thunderstorms. Remember the definition of a tornado has a rotating column extending from the cloud to the ground. Hence, by definition a dust devil is not a tornado since no cloud is present.

Figure 9-10: Photo of a dust devil.

Dust devils may be strong enough to cause damage similar to the weakest tornadoes. Diameters range from 10 to 300 feet and their average height is about 600 feet. They develop during hot, dry, calm days with clear skies and intense surface heating. Once the ground heats up enough, a localized pocket of air will quickly rise through the cooler air above it. Hot air rushes in to replace the rising air at the bottom of the developing vortex, intensifying the spinning effect. Once formed, the dust devil is a funnel-like chimney through which hot air moves both upwardly and circularly. If a steady supply of hot, unstable air is available, the dust devil will continue to move across the ground. However, once that supply is depleted or the rotation is broken in some other way, the dust devil will dissipate.

9.1.3 – EF Scale and tornado forecasts

A tornado damage scale was developed in 1971 by T. Theodore Fujita at the University of Chicago, and was called the F-Scale. In 2007, this scale was revised into the Enhanced Fujita

scale or EF Scale. The EF Scaled uses observed structural damage to estimate tornado wind speeds. A tornado is assigned an EF number based on these observations. The EF Scale is used across North America, and has specific, required procedures before assigning an EF number to a tornado.

A damage survey occurs after a tornado strikes. This survey examines the types of structures, what damage occurred and known relationships on wind speeds capable of causing the damage observed. Based on the results of this survey an EF number is assigned to a tornado. Tornadoes can change in intensity while causing damage. Hence, the highest EF number found in the tornado path is assigned. The following table contains a description of the EF Scale.

EF Number	3-second wind gust (mph)	Damage description (from the original F-Scale)
0	65-85	**Light** – Some damage to chimneys; branches broken off trees, shallow-rooted trees uprooted; sign boards damaged.
1	86-110	**Moderate** - Roof surfaces peeled off; mobile homes pushed off foundations or overturned; moving autos pushed off road.
2	111-135	**Considerable** - Roofs torn from frame houses; mobile homes demolished; boxcars pushed over; large trees snapped or uprooted; light objects become projectiles.
3	136-165	**Severe** - Roofs and some walls torn from well-constructed houses; trains overturned; most trees in forested area uprooted; heavy cars lifted and thrown.
4	166-200	**Devastating** - Well-constructed houses leveled; structures with weak foundation blown some distance; cars thrown; large missiles generated.
5	Over 200	**Incredible** - Strong frame houses lifted off foundations, and blown downwind; steel-reinforced concrete structures badly damaged; auto-sized airborne missiles generated.

At times, damage from a tornado may be so incredible that obtaining a wind speed estimate is difficult. For example, if a strong structure is destroyed at 210 mph wind gusts, then the possibility exists that a wind gust of 250 mph could have occurred. Due to this situation, the EF-5 category has wind speeds set at “over 200 mph” to account for these conditions.

A tornado outbreak is when 10 or more tornadoes occur within a specific synoptic-scale system, such as a midlatitude cyclone. In other words, conditions are favorable for tornadoes across a large area and on multiple days. An outbreak can include hundreds of tornadoes across multiple states. When an outbreak occurs, each tornado is surveyed and assigned an appropriate EF scale rating.

As science improves, forecasts associated with tornadoes have improved. The mission of the National Weather Service (NWS) in the United States is the protection of life and property. To fulfill this mission, the NWS has two categories of products to alert people to dangerous weather. These product categories are: (1) watches and (2) warnings. A **watch** is when atmospheric conditions are conducive for severe weather to occur. The philosophy behind a watch is to alert people of possible dangerous weather and for them to stay alert.

A **warning** is when dangerous weather is eminent or occurring. The philosophy behind a warning is that people need to act. For a person to act correctly in a dangerous situation, they should plan ahead of time on what to do. The average lead time for a tornado warning is 13 minutes. If a tornado action plan is in place, a person can act within minutes to move themselves and loved ones to a safer location, such as interior rooms, a basement or a storm shelter.

The Storm Prediction Center (SPC) of the National Weather Service is responsible for issuing severe thunderstorm and tornado watches for the United States. Local NWS offices are responsible for issuing the warnings. The Storm Prediction Center issues convective outlooks several times a day alerting people of where thunderstorms may occur. Figure 9-11 is an example of an SPC convective outlook.

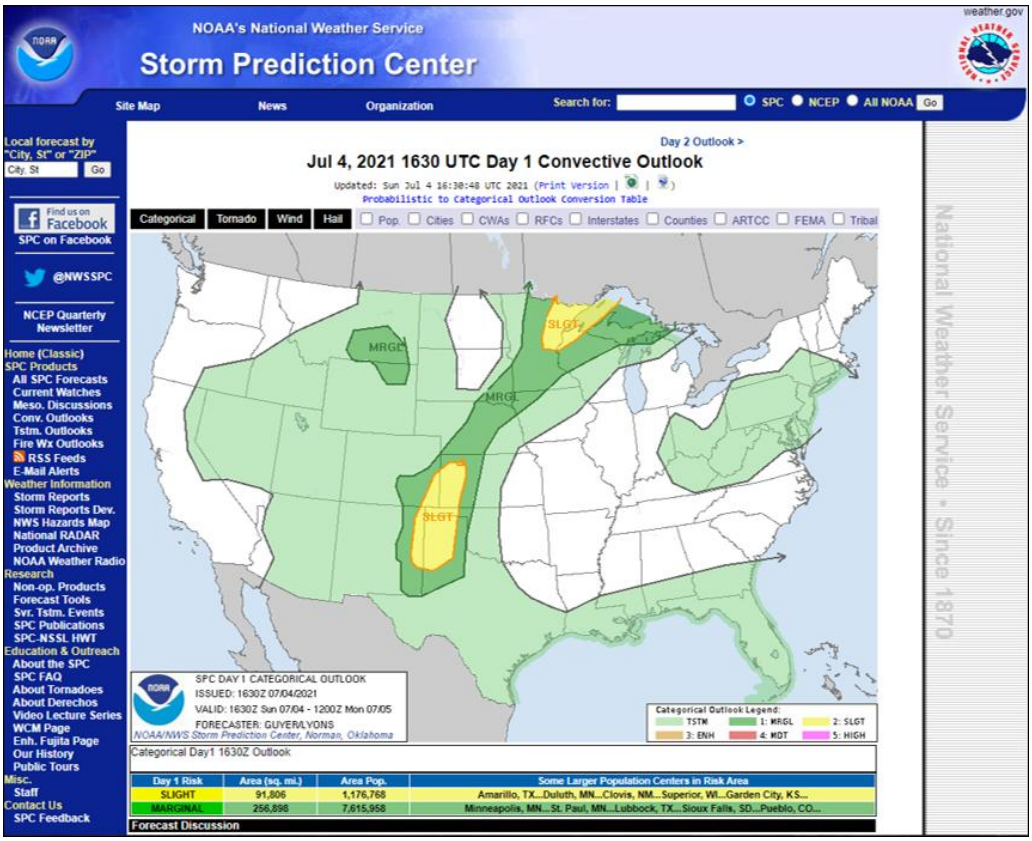

Figure 9-11: A convective outlook issued by the Storm Prediction Center for July 4, 2021.

The light green area indicates 10% or more areal coverage of basic thunderstorms. The other categories (marginal, slight, enhanced, moderate, and high) indicate increased potential for thunderstorms becoming severe. A severe thunderstorm is defined as 1 inch hail or wind greater than 50 knots (about 60 mph). This convection outlook includes a forecast for the probability of tornadoes occurring in these thunderstorms. A current convective outlook can be found at this link.

9.1.4 – Tornado Vortex Signature (TVS)

With the implementation of Doppler weather radars, Doppler velocity patterns associated with tornadoes have been discovered. A **tornado vortex signature (TVS)** is a radar velocity pattern

that indicates a region of intense concentrated rotation. A TVS may appear several kilometers above the ground before a tornado touches down.

Doppler weather radar velocity fields indicate whether a particle is moving towards or away from the radar. When a Doppler radar views a tornado rotation, a radar beam will detect fast particles moving towards the radar on one side of the tornado. The adjacent beam will detect fast particles moving away from the radar. This couplet of adjacent beams with opposite motions to each other is a tornado vortex signature. The left side of Figure 9-12 illustrates the TVS pattern in a base velocity product. The right side of this figure is the corresponding base reflectivity product.

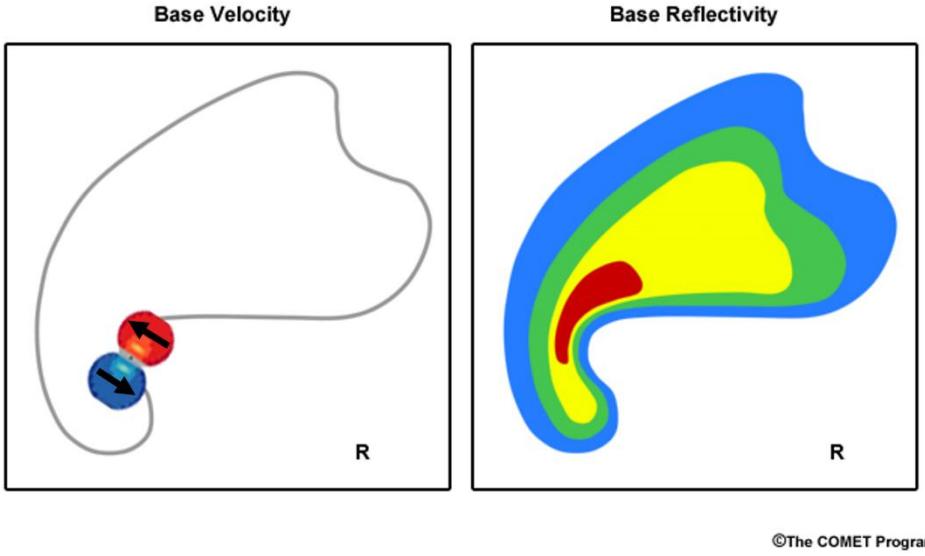

Figure 9-12: A base velocity and reflectivity illustration with a tornado vortex signature (TVS) pattern. The black arrows in the velocity product indicate the wind direction as seen by the radar. The radar is located at the "R".

The base reflectivity in Figure 9-12 has a weak echo region or hook echo associated with the tornado rotation. A TVS is much smaller and concentrated when compared to the overall rotation of a mesocyclone. A TVS does not guarantee a tornado, but its presence strongly increases the probability of a tornado occurring.

The base velocity and reflectivity products in Figure 9-13 illustrate an actual tornado and its associated TVS. The radar in these images is located towards the southwest (lower left) of the white circles. Knowing the location of the radar is important to ensure adjacent radar beams have opposing velocity values.

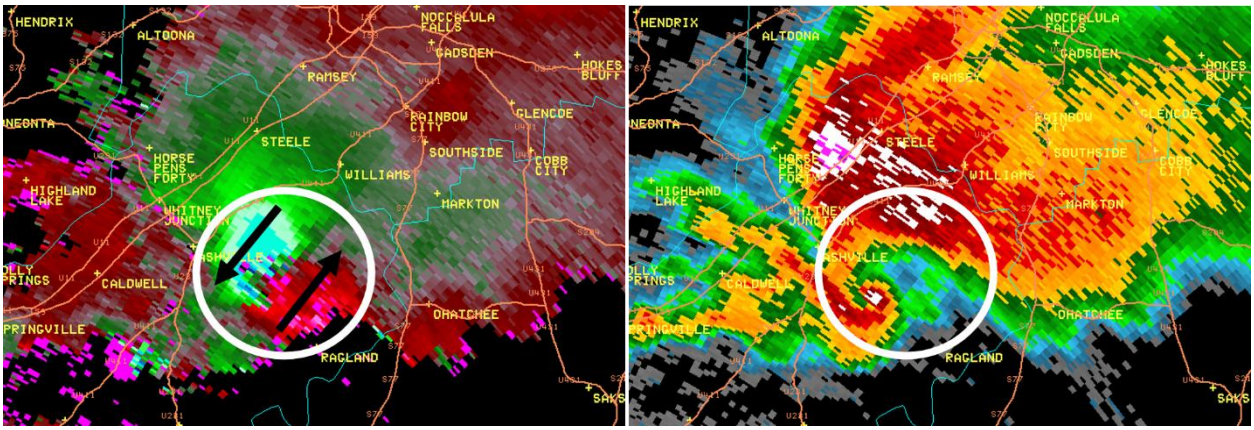

Figure 9-13: Base velocity (left) and reflectivity (right) products which contain a TVS and hook echo. The black arrows in the velocity product indicate the wind direction as seen by the radar.

9.1.5 – Tornado Trends

One of the difficulties with tornado records is that a tornado, or evidence of a tornado, must be observed to be recorded. Unlike rainfall or temperature, which may be measured by a fixed instrument, tornadoes are short-lived and very unpredictable. In the past, if a tornado occurred in a place with few or no people, it was likely not documented.

Today, nearly the entire United States is reasonably well populated and covered by Doppler weather radars. Even if a tornado is not observed by a person, modern assessments can determine if a tornado caused the damage and how strong it was. This disparity between past tornado records and more recent ones contributes a great deal of uncertainty when examining tornado trends. For example, improved tornado observation practices have led to an increase in the number of weaker tornadoes. EF-0 tornadoes are more prevalent now than in the past.

With increased Doppler radar coverage starting in the 1990s, increasing population, and greater attention to tornado reporting, there has been an increase in the number of tornado reports over the past several decades. This situation creates a misleading appearance of an increasing trend in tornado frequency. To better understand the variability and trend in tornado frequency in the United States, the total number of EF-1 and stronger, as well as strong to violent tornadoes (EF-3 to EF-5) should be analyzed. These violent tornadoes would likely have been reported even before Doppler radar use became widespread. The bar charts in Figures 9-14 and 9-15 indicate little or no trend in the frequency of stronger tornadoes over the past 55 years.

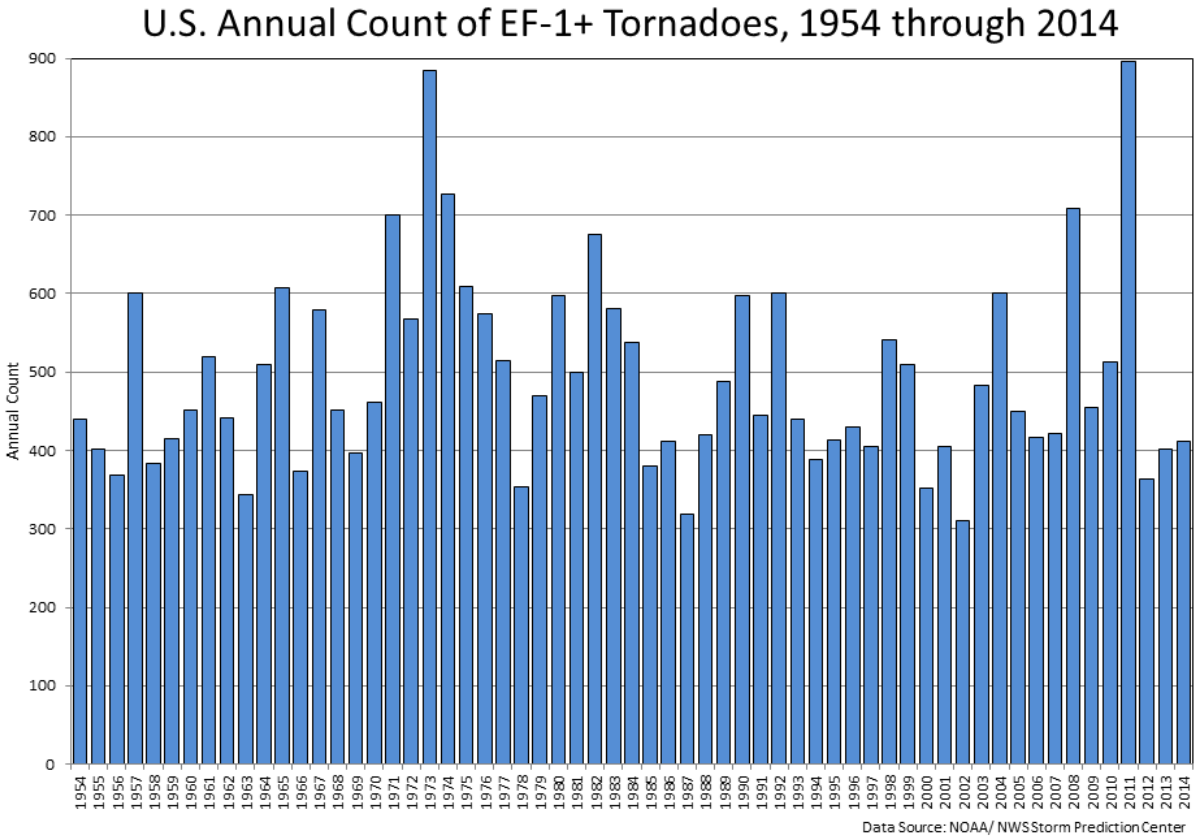

Figure 9-14: Annual count of U.S. tornadoes of EF-1 and stronger from 1954 through 2014.

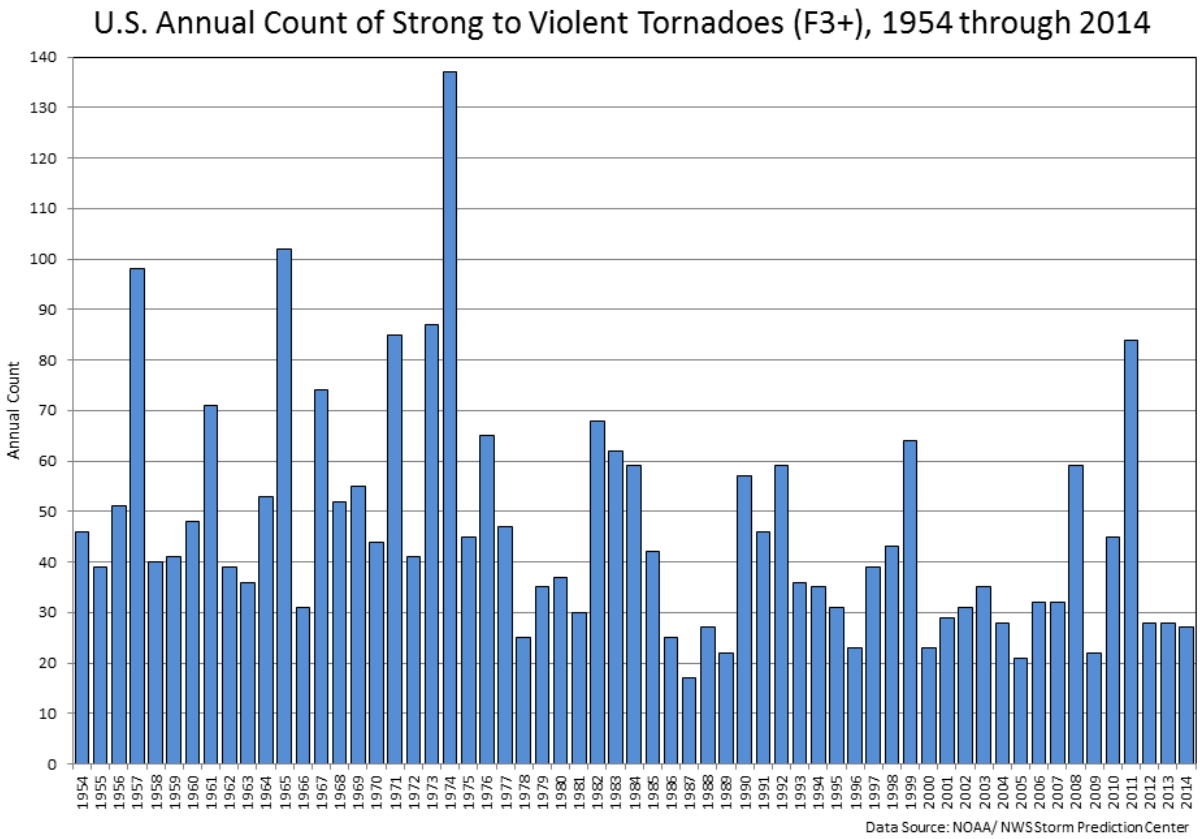

Figure 9-15: Annual account of U.S. tornadoes of strength EF-3 and higher from 1954 to 2014.

Most tornadoes are related to the strength of a thunderstorm. Thunderstorms are normally strongest in the afternoon and early evening due to the rising air associated with solar heating. Therefore, most tornadoes occur in the afternoon and evening hours. A minimum frequency occurs around sunrise when temperatures are lowest. However, tornadoes have occurred at all hours of the day. This bar chart in Figure 9-16 depicts the time of day when tornadoes occur. The peak of occurrence is 5 to 6 pm.

In addition, tornadoes occur throughout the year. Like with the diurnal pattern during a day, the months in which tornadoes are most likely corresponds to the time of year with increased solar heating and strong frontal systems. Regionally, the frequency of tornadoes in the United States is closely tied with the progression of the warm season when moist warm (mT) and cold dry air masses (cP) often clash. Most of the early spring tornadoes in the United States tend to occur in the Southeast and South Central regions. Gulf States, such as Mississippi and Louisiana, are the frequent recipients of tornadoes from February to April. Late spring tornadoes

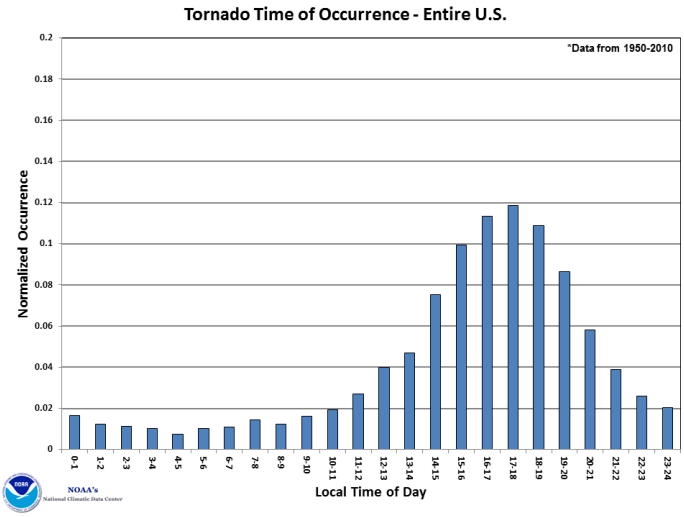

Figure 9-16: Tornado time of occurrence during a day, which peaks from 5 pm to 6 pm.

generally spread a bit farther north, often into Kansas, Nebraska, and the Tennessee Valley region. By midsummer, tornadoes may occur throughout the United States. Late summer tends to bring some of the stronger tornadoes into the upper Midwest and Ohio valleys, and the pattern shifts back southward into the late autumn. The fewest tornadoes are documented during the winter months. Figure 9-17 gives the U.S. tornado averages by month.

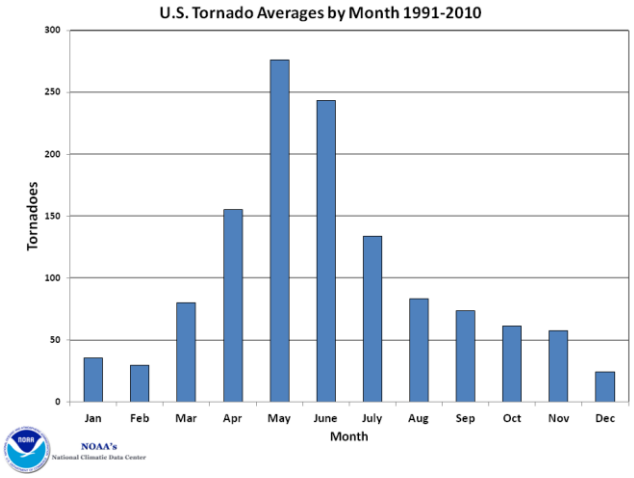

Figure 9-17: Tornado averages by month. Most tornadoes occur during May and June in the U.S.

This last graph in Figure 9-18 shows the fatalities associated with tornadoes in the United States from 1875 to 2012. This graph is normalized per million people. As the population of the U.S. increases, the expectation would be for the fatalities to increase. Normalizing the data analysis removes the change in population to directly determine whether fatalities are changing with time. This graph shows a significant decline in fatalities due to tornadoes. This decline can be attributed to better detection of tornadoes before they occur, better warnings to alert people of danger, increased understanding in the population of what to do when tornadoes are present, and most importantly improvements in building techniques to withstand high winds.

In Figure 9-18, the purple points are the annual death rates; the red line is simply a smoothed version of the purple points; the green line is the long-term trend for two groups of years (1875 to 1925 and 1925 to 2000).

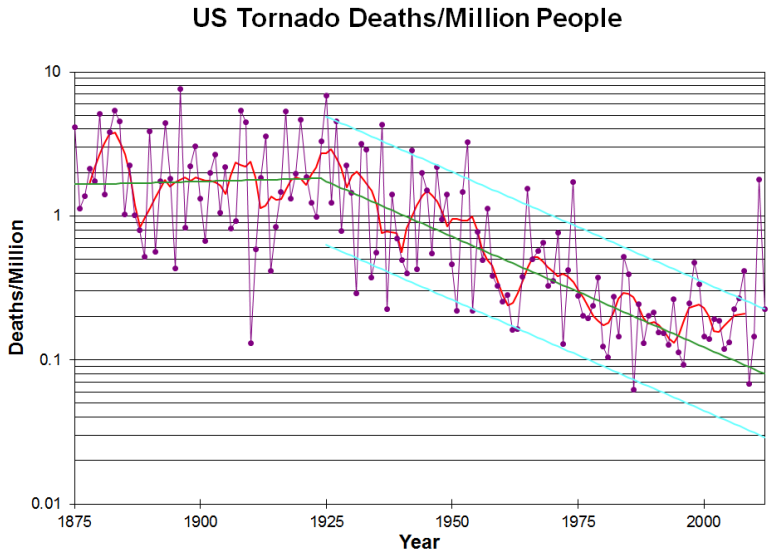

Figure 9-18: U.S. tornado fatalities from 1875 to 2012. A decreasing trend in fatalities has been observed since 1925 .

9.2 – Tropical Storms and Hurricanes

A **tropical cyclone** is a warm-core low pressure system that develops over tropical or subtropical waters. In contrast, a midlatitude cyclone (extratropical cyclone) is a cold-core low pressure system. Tropical cyclones do not have fronts and they can last much longer than a midlatitude cyclone. These storms have seven basins where they form (Figure 9-19).

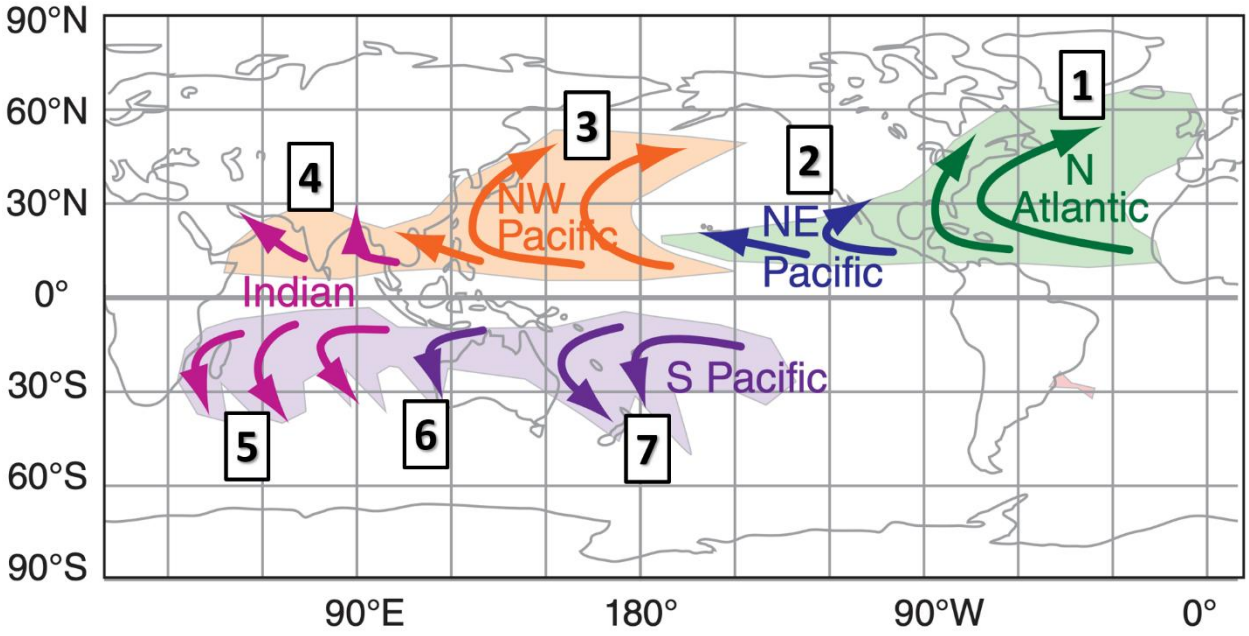

Figure 9-19: The seven ocean basins where tropical storms form.

These basins are:

1. Atlantic basin which includes the North Atlantic Ocean, Gulf of Mexico, and the Caribbean Sea.
2. Northeast Pacific basin from Mexico to about the dateline (180º)
3. Northwest Pacific basin from the dateline to Asia including the South China Sea
4. North Indian basin, including the Bay of Bengal and the Arabian Sea
5. Southwest Indian basin from Africa to about 100E
6. Southeast Indian/Australian basin (100E to 142E)
7. Australian/Southwest Pacific basin (142E to about 120W)

Tropical cyclones are essentially steered from the east to the west by the global circulation, which are the trade winds at lower latitudes. As they grow bigger, their track is more influenced by monsoon circulations or the midlatitude westerlies depending on the time of year. Most hurricanes form in the late summer and early fall when ocean waters are warmest. Approximately 69 percent occur in the Northern Hemisphere, and 31 percent in the Southern Hemisphere. Approximately 57 percent occur in the Pacific Ocean, mostly because the Pacific is the largest ocean, 31 percent in the Indian Ocean and the remaining 12 percent in the Atlantic Ocean.

Tropical cyclones are called hurricanes in the Atlantic and eastern Pacific Oceans (around North America), typhoons in the western Pacific Ocean (near Japan), and cyclones in the Indian Ocean and near Australia. Tropical cyclones are defined by their sustained wind speeds. A **hurricane** is defined as a tropical storm with wind speeds at or greater than 64 knots or 74 mph.

Hurricanes are the most powerful of all storms due to their size and duration. Tornadoes have stronger winds but are small and quick in comparison to a hurricane. Figure 9-20 illustrates the largest and smallest tropical cyclones on record.

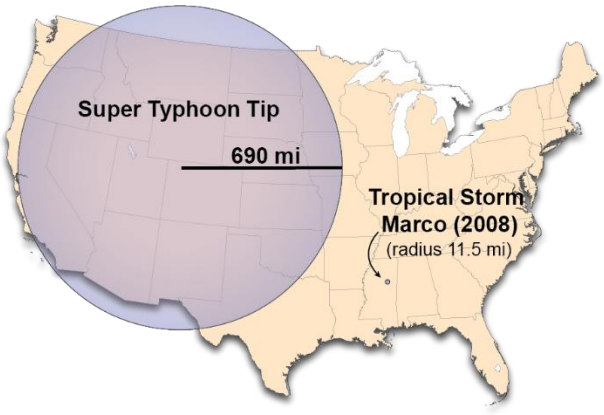

Figure 9-20: Illustration showing the largest and smallest tropical cyclones on record.

Warm water is an important ingredient in the formation of a hurricane. This warm water creates water vapor that rises off the ocean; as it rises it cools.

This cooling causes the water vapor to condense into liquid droplets and clouds form. The latent heat of condensation is released, which makes the air warmer and even more buoyant as it continues to rise. As the air rises further, surrounding air moves in near the surface to take its place. This vertical air motion creates a convergence area at the surface and a corresponding surface low pressure. In summary, tropical cyclones are fueled by rising warm, moist air that releases the latent heat of condensation. This simple explanation for how a hurricane forms is illustrated in Figure 9-21.

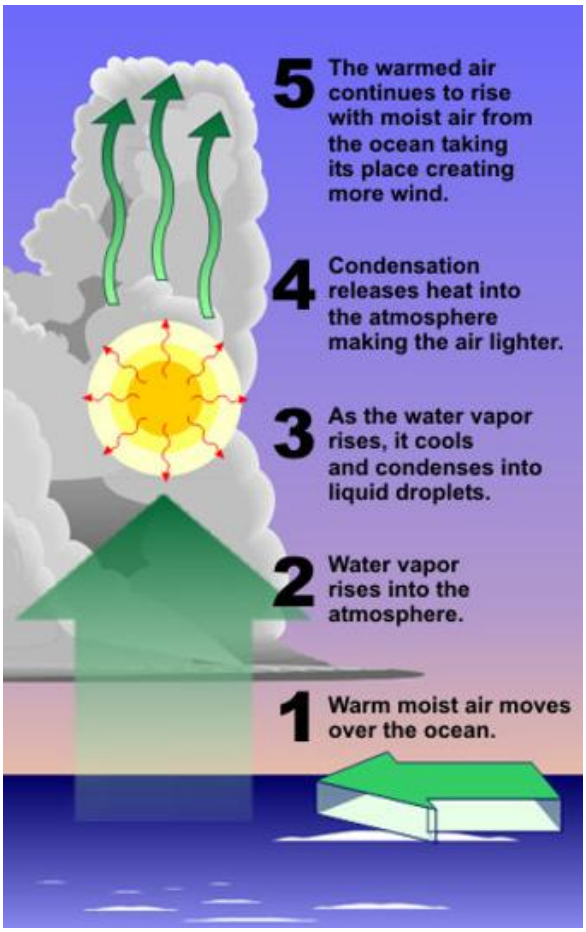

Figure 9-21: A simple diagram showing how warm, moist ocean water fuels a hurricane.

These two short videos describe hurricane formation and have the titles of “How Does A Hurricane Form?” Part 1 and Part 2.

9.2.1 – Conditions for Hurricane Formation

The five specific conditions necessary for a hurricane to form are:

- Warm ocean surface temperatures greater than 80°F (26.5°C).
- Very moist air (high humidity) through the lower and middle troposphere.
- Coriolis force to maintain the hurricane structure (greater than 5° latitude).
- Light winds with minimal wind shear.
- A disturbance or easterly wave to start the formation.

All these conditions are required. If one of these conditions is missing, a hurricane will not form. Sometimes a sixth condition is cited; the need for a conditionally unstable atmosphere. The warm ocean surface temperatures and very moist air conditions imply a conditionally unstable air mass, so these five conditions adequately describe the environment needed. Remembering 5 conditions is easier than remembering 6 too.

The map in Figure 9-22 depicts the monthly average ocean temperatures for September. The areas in orange are greater than 80°F. Obviously, this warm water is present only in the tropics and subtropics, and is most prevalent from summer into fall (June through November) in the Northern Hemisphere. The depth of this warm water should be at least 50 meters. In other words, a lot of warm water is needed as a condition for formation.

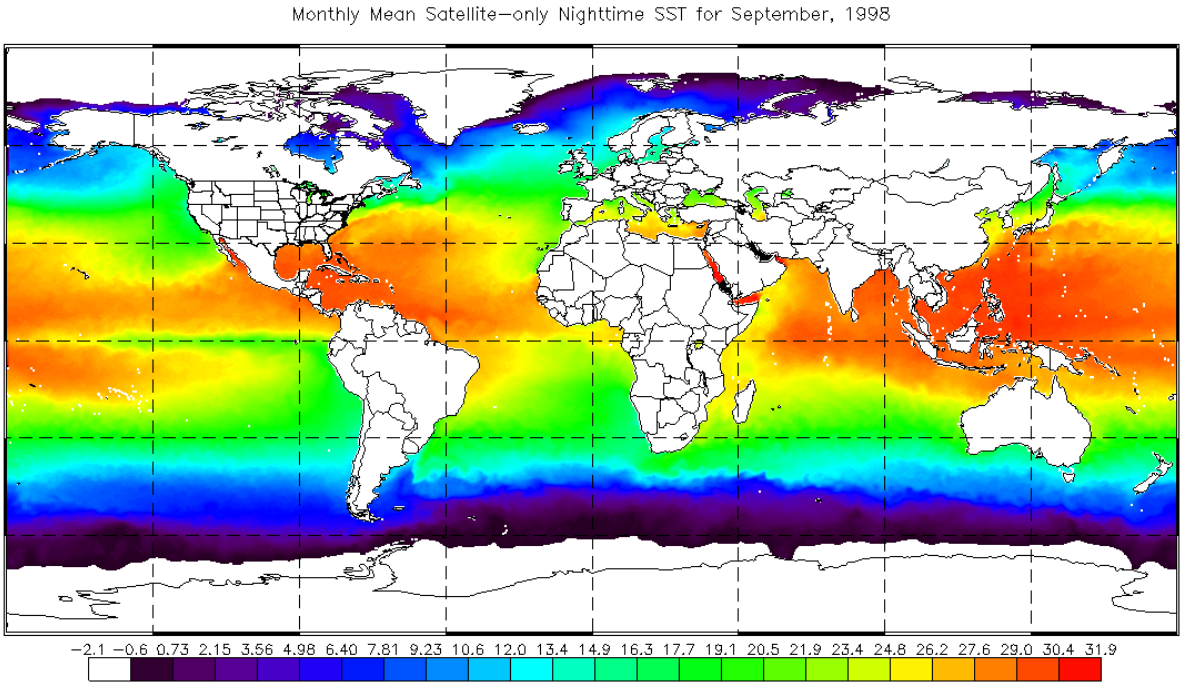

Figure 9-22: A map with the mean sea surface temperatures for September 1998.

Once these warm ocean waters are present, evaporation supplies the humidity to the lower portion of the troposphere, which eventually mixes up to the middle layers. Hence conditions one and two are closely linked.

Another condition, the Coriolis force, is needed to maintain the internal structure of the hurricane as it forms. The Coriolis force deflects winds to the right in the Northern Hemisphere and the left

in the Southern Hemisphere. This deflection or curving of the wind causes the air to spiral into a hurricane surface low pressure center. Without this spiral organization of the wind, a hurricane would not form. Since the Coriolis force is zero at the equator, hurricanes do not form at the equator. Since the Coriolis force deflects winds differently in each hemisphere, a hurricane cannot form in one hemisphere and move into the other hemisphere.

The condition of light winds or rather a lack of wind shear allows the Coriolis force to create the spiral structure of a hurricane. If stronger winds are present, the spiral structure cannot be maintained and physically the hurricane would be blown apart. Additionally, hurricanes contain thunderstorms in this spiral structure. If wind shear is present, these thunderstorms would become stronger and move out of the organized hurricane causing the hurricane to decay.

The last condition is a disturbance in the tropical waters to get the formation of a hurricane started. Since the easterly trade winds are the prevailing winds in the tropics, these disturbances are referred to as easterly waves. **Easterly waves** are ripples in the normal trade wind pattern. Figure 9-23 depicts an easterly wave. In this figure, the dashed black lines are isobars; the red lines with arrows indicate the wind over the area. This representation of the wind is called a streamline analysis.

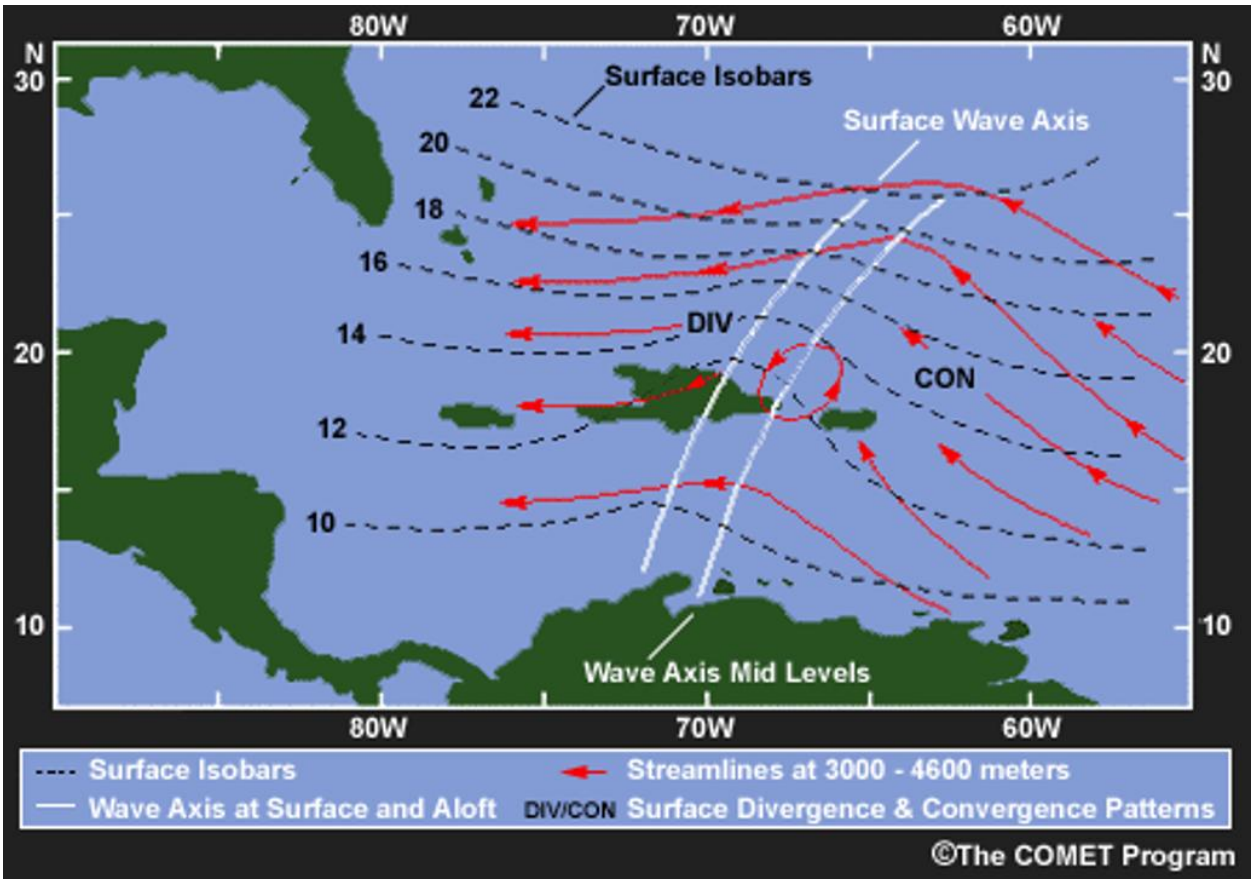

Figure 9-23: A map of the Caribbean with isobars and winds that highlight an easterly wave. The trough axis of this easterly wave is denoted by the white lines.

Pressure fields in the tropics are relatively flat and pressure gradients are generally weak. Hence light winds are common in tropical locations. Since winds are light, a streamline analysis provides an early indication of a ripple developing. Notice in Figure 9-23 how the streamline

analysis shows a distinct circulation occurring, while the pressure (isobar) analysis just has a curve to the lines. This small circulation is an easterly wave and the beginning of a surface low pressure. As soon as an extremely weak surface low pressure develops, rising air occurs over the area. The rising air causes condensation with an enormous release of latent heat. This latent heat causes the air to rise further and the process for a hurricane to form has begun.

These disturbances appear as patches of clouds or small thunderstorms when they are present. For the Atlantic Ocean, a source of easterly waves is the West African Monsoon. During the summer, the ITCZ moves northward over Africa and multi-cell thunderstorms develop. These convective systems move with the trade winds into the Atlantic Ocean where they spawn hurricanes which can impact the U.S. This satellite image in Figure 9-24 illustrates these easterly waves moving from West Africa into the Atlantic Ocean.

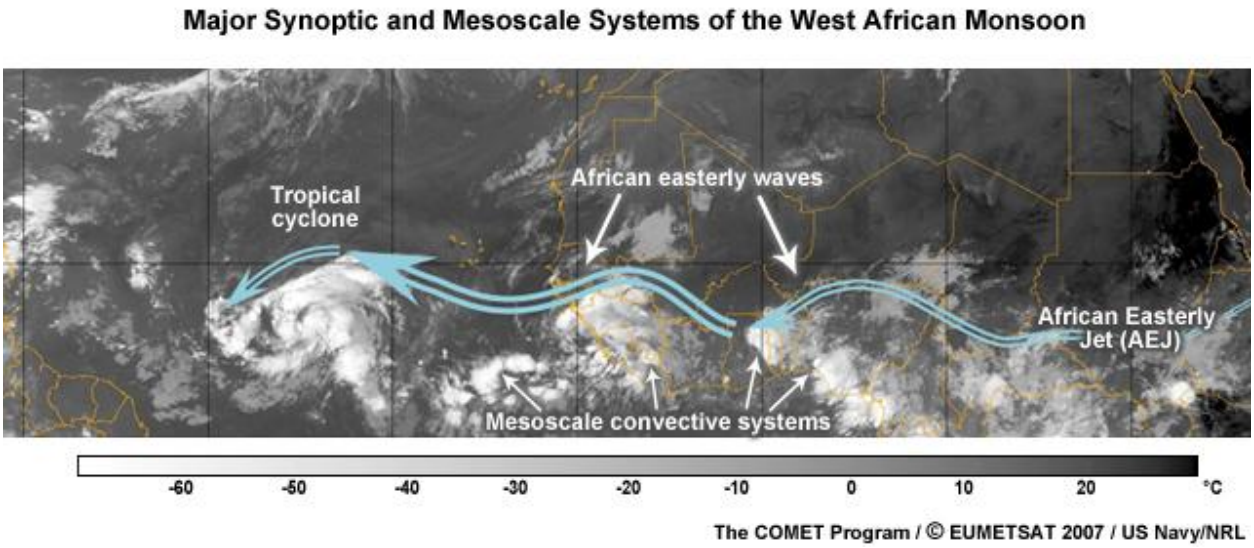

Figure 9-24: Satellite image of the easterly waves created by the West African Monsoon.

9.2.2 – Hurricane Structure

Once the conditions for the formation of a hurricane are present, any hurricane that forms has a unique structure. The main parts of a hurricane are the rainbands, the eye, and the eyewall. Air spirals in toward the surface center in a counterclockwise pattern in the Northern Hemisphere, and out the top in the opposite direction. This air motion is a result of the Coriolis force. Figure 9-25 illustrates the main features of a hurricane.

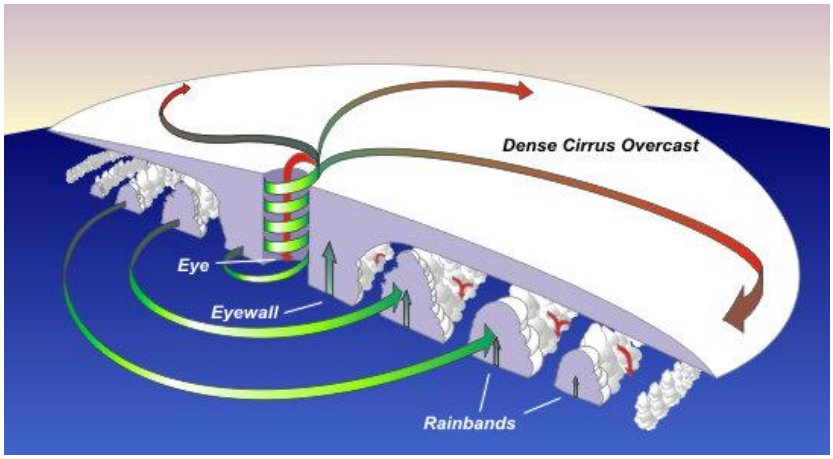

Figure 9-25: The main features of a hurricane: rainbands, eye, and eyewall. A cirrus cloud shield covers everything at upper levels.

In the very center of the storm air sinks forming an eye that is mostly cloud-free. The **eye** is a region of relatively clear skies, light wind, and slowly descending air. An eye will usually develop when the sustained wind speeds go above 74 mph. Many times, ocean water can be seen through the eye of a hurricane when viewed from above.

Next to the eye resides the eyewall. The **eyewall** consists of a ring of tall thunderstorms with heavy rains and usually the strongest winds. Whereas the eye is relatively clear and calm, the eyewall contains the most intense storm activity in the hurricane. Rainfall rates under the eyewall can be up to 100 inches per day.

Hot towers are localized portions of an eyewall that rise to great heights. These hot towers are strong updrafts in the eyewall thunderstorms, and are indicative of an intensification occurring within 6 hours. A graphic reproduction of a hot tower is shown in Figure 9-26.

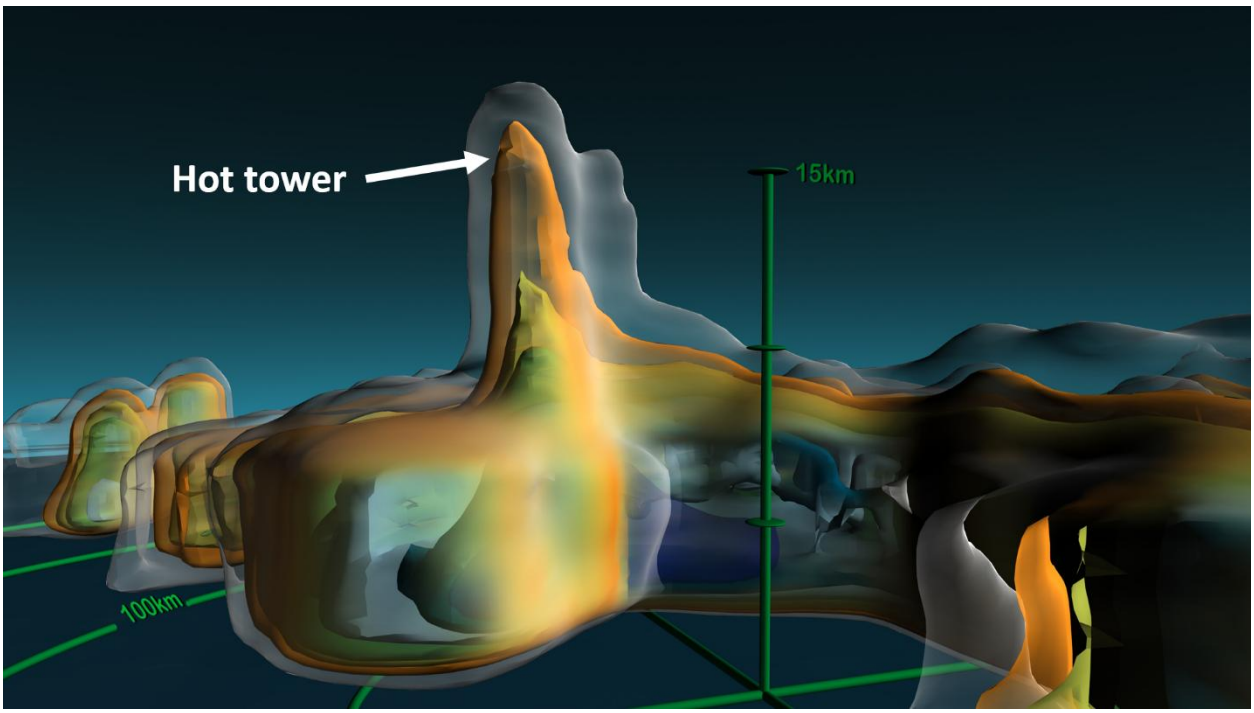

Figure 9-26: A graphic reproduction of a hot tower, which are associated with strong thunderstorm updrafts in the eyewall. The presence of a hot tower indicates a hurricane is intensifying.

Rainbands are curved bands of clouds and thunderstorms that trail away from the eye wall in a spiral fashion. These bands are most intense near the eyewall and decrease in intensity further from the center. If one were to travel between the outer edge of a hurricane to its center, one would experience breezy winds with rain, dry conditions and light wind, then back to increasingly stronger wind and heavier rain, then drier conditions over and over again. Each period of rain and wind being more intense and lasting longer the closer one got to the center.

The cirrus cloud shield (see Figure 9-25) over the top of a hurricane is a result of the thunderstorms. Much like a basic thunderstorm anvil, this cloud shield is caused by multiple thunderstorms generating cirrus clouds.

The vertical pressure structure of a hurricane is much different than a midlatitude cyclone. In a midlatitude, the surface low pressure is supported by an upper level low pressure usually tilted

to the west. In a hurricane, the surface low pressure is supported by an upper level high pressure directly above the surface low as is shown in Figure 9-27.

Notice in Figure 9-27 that the wind motion in a tropical cyclone is cyclonic (counterclockwise) at the surface and anticyclone (clockwise) aloft. The pressure inside a hurricane is about equal to the atmosphere outside the hurricane at about 400 mb. From the surface to 400 mb, the pressure is lower than the surrounding atmosphere. From 400 mb through the rest of the troposphere the pressure is higher than the surrounding atmosphere. Tropical cyclones are much different than midlatitude storms due to being driven by warm, moist air.

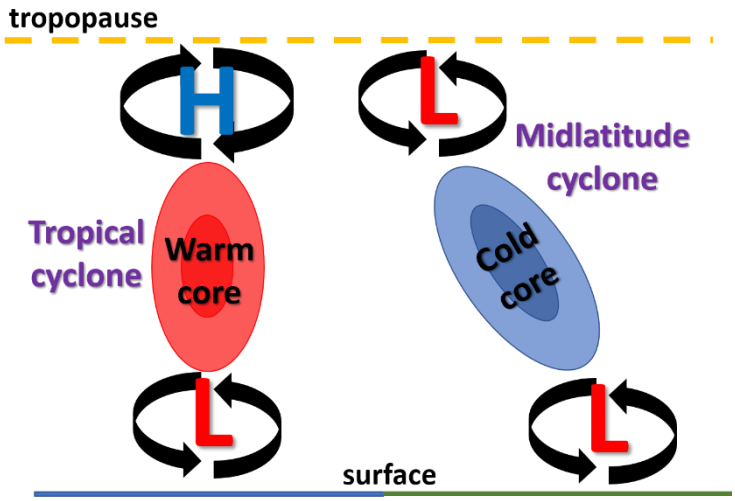

Figure 9-27: Vertical structure of a tropical cyclone as compared to a midlatitude cyclone.

9.2.3 – Classification and the Saffir-Simpson Hurricane Wind Scale

While a hurricane is defined as a tropical cyclone with wind speeds greater than 64 knots or 74 mph, they do not instantly become this strong. Like most storms, hurricanes have developmental stages as shown in this table.

Designation	Wind speed	Features
Tropical disturbance	Light	Patches of cloud (100 to 300 nmi in diameter) which maintain their identity for more than 24 hours.
Tropical depression	Up to 38 mph	Organizing circulation with light to moderate rain.
Tropical storm	39 to 73 mph	Storm is assigned a name; closed isobars with circular organization and heavy rain
Hurricane	74 mph and higher	Well-defined surface low pressure with organized deep convection.

Wind speeds are the determining factor in the designation of a tropical cyclone. Once the tropical storm category is reach, the storm is assigned a name. This occurs because most (over 50%) tropical storms increase in intensity and become hurricanes.

Once a tropical storm is designated as a hurricane, the Saffir-Simpson Hurricane Wind Scale assigns a 1 to 5 category based on the wind speeds. This table describes the Saffir-Simpson Wind Scale.

Category	Wind speed	Damage
1	74 to 95 mph	Very dangerous winds will produce some damage.
2	96 to 110 mph	Extremely dangerous winds will cause extensive damage.
3 (major)	111 to 129 mph	Devastating damage will occur.
4 (major)	130 to 156 mph	Catastrophic damage will occur.
5 (major)	greater than 156 mph	Catastrophic damage will occur.

Major hurricanes can cause devastating to catastrophic wind damage and significant loss of life simply due to the strength of their winds. Hurricanes of all categories can produce deadly storm surges, rain-induced floods, and tornadoes. These hazards require people to take protective action, including evacuation from areas vulnerable to a storm surge. Note that in the western North Pacific, the term "super typhoon" is used for tropical cyclones with sustained winds exceeding 150 mph. In North America the same tropical cyclone would be referred to as a category 5 hurricane.

Once a tropical cyclone reaches hurricane status, its category within the Saffir-Simpson scale can change as the wind speed changes. One indication of a change in hurricane intensity is the condition of the eye and eyewall. If the eye begins to fill in, the hurricane weakens. If the eye reforms the hurricane is intensifying. These fluctuations in the eye and eyewall are called an eyewall replacement. The reformation of an eyewall is associated with a convective burst of energy and the release of heat into the hurricane. This situation occurred with Hurricane Wilma in October 2005 as seen in Figure 9-28.

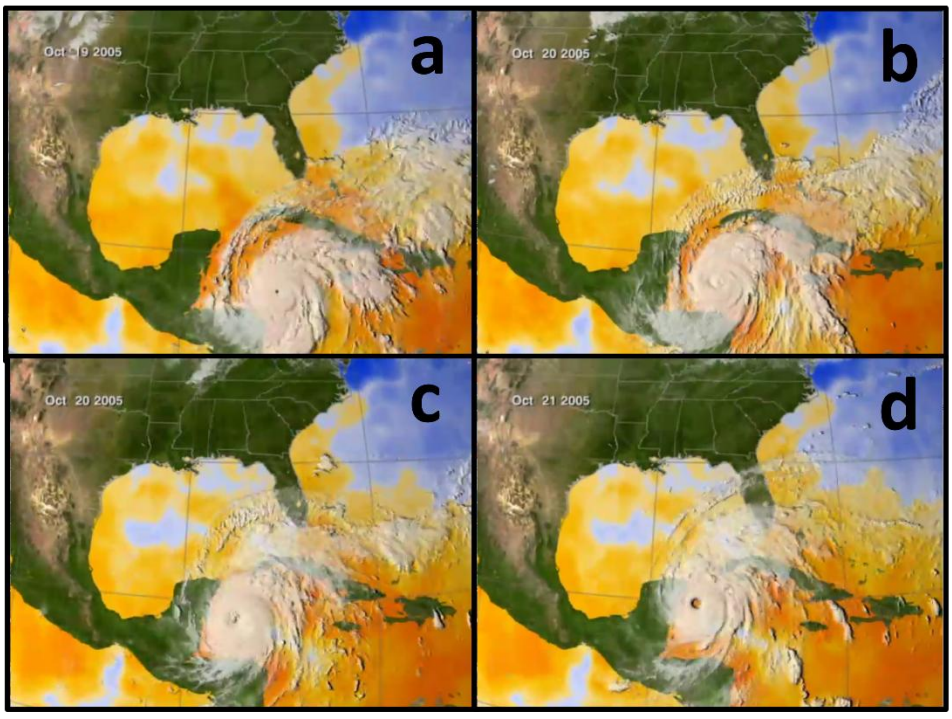

Figure 9-28: Hurricane Wilma in the Gulf of Mexico on October 19 through 21, 2005 as an eyewall replacement occurs. (a) October 19 with a well-defined eye. (b) Early in October 20 as the eye fills and is no longer visible. (c) Later in October 20 as a convective burst occurs in the hurricane center. (d) October 21 as a large eye has formed associated with the hurricane intensification.

9.2.4 – Hurricane Movement

As mentioned previously, tropical cyclones tend to follow the general circulation patterns. In the tropics, this involves the Hadley cell circulation and surface trade winds. Tropical disturbances and depressions are guided by the trade winds and move from east to west. As they become tropical storms and hurricanes, they are guided more by upper-level winds and the pressure patterns interacting with the storm. Tropical storms and hurricanes tend to move poleward at some point, which moves them into the westerlies. Once a hurricane is influenced by the westerlies, they begin to move eastward again. The graphic in Figure 9-29 contains all the hurricane tracks in the Atlantic and eastern Pacific Oceans. Notice that the movement is westward at lower latitudes and eastward at higher latitudes in the Atlantic Ocean.

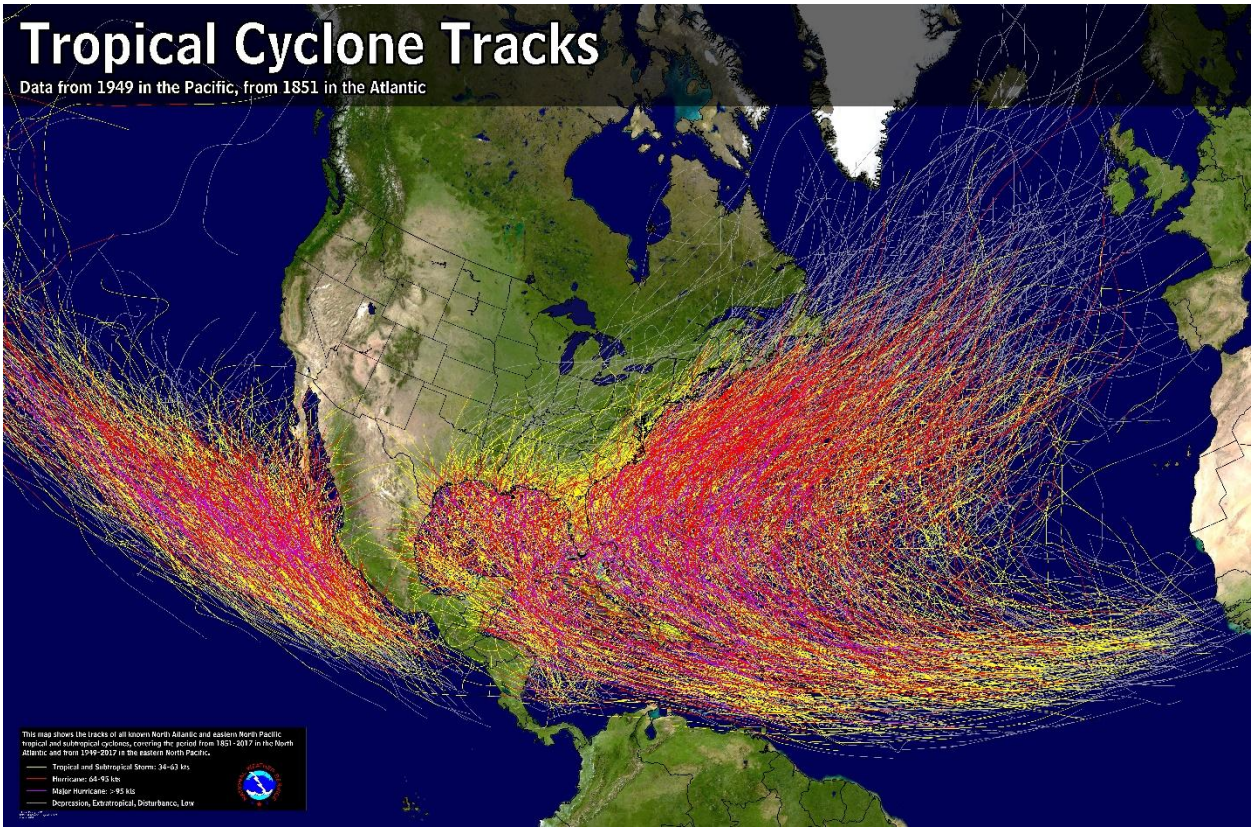

Figure 9-29: A map of Tropical Cyclone tracks in the Atlantic Ocean and eastern Pacific Ocean from 1851 to 2017. Notice the westward track at lower latitudes as the tropical storms are steered by the trade winds. As storms move further north, they begin moving eastward when entrained in the westerlies.

Hurricane tracks change depending on the month and season. Figure 9-30 has a map for each month from June through November. The blue areas contain the likely track a hurricane will move. The green area is more likely and the orange area is most likely. September is the winner for having the largest area where hurricanes may track.

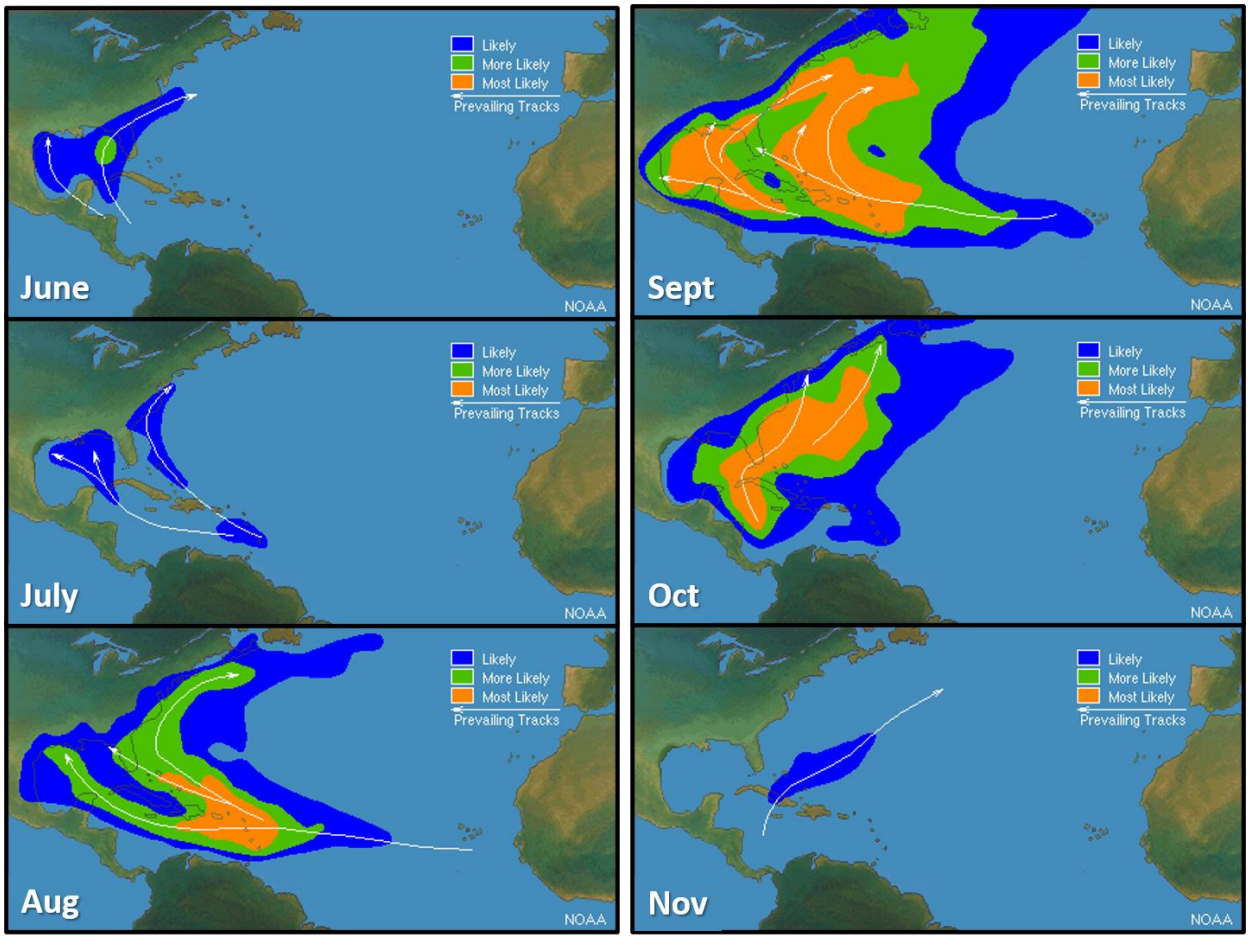

Figure 9-30: Maps of monthly hurricane tracks from June through November. Blue is the likely area for a tropical cyclone to move through. Green is more likely and orange is the most likely area.

9.2.5 – Hurricane Decay

The conditions which help form a hurricane are required to maintain it. Thus, when one of these conditions no longer exists, the hurricane starts to decay. The decay of a hurricane can be caused by:

1. Moving over land;
2. Moving over cooler water;
3. Encountering vertical wind shear.

When a hurricane moves over land, the water vapor fueling it through the latent heat of condensation is lost. Land does not have as much evaporation as an ocean, and is a drier environment. Additionally, the increase in surface friction over land disrupts the hurricane's circulation. The graph in Figure 9-31 shows how fast a hurricane's winds decrease when it makes landfall.

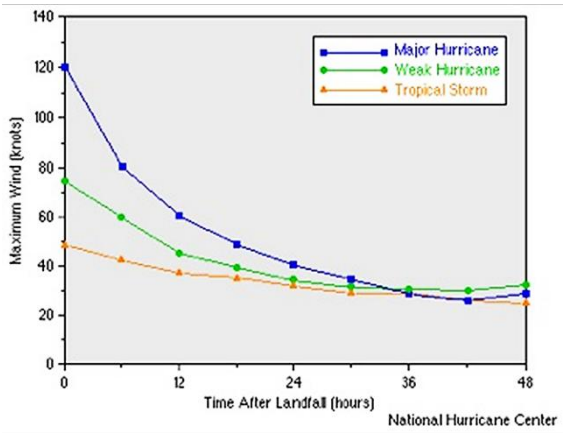

Figure 9-31: A hurricane's wind speed (y-axis) decreases quickly after making landfall (x-axis).

Within 12 hours of making landfall, a major hurricane with 120 kts of wind has decreased to 60 kts (half). The loss of moist air and an increase in surface friction rapidly decreases the winds in a hurricane. However, much of the destructive potential remains.

Moving into colder water also removes the moist air fuel needed for a hurricane. When a hurricane moves higher than 25º latitude, the chances of it encountering colder water increases. Warm ocean currents, like the Gulf Stream, which moves up the east coast, permit a hurricane to move further north while maintaining their strength. Figure 9-32 depicts the location of the Gulf Stream and the warm water it transports northward from the Gulf of Mexico. The northern edge of the Gulf Stream (dark orange) in this image is about 38ºN.

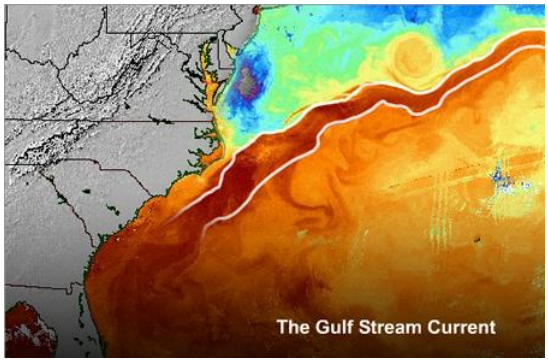

Figure 9-32: The location of the Gulf Stream along the east coast of the U.S.

Vertical wind shear disrupts the circulation within a hurricane and it decays rapidly. This type of shear can be encountered if a hurricane approaches the subtropical jet stream. An example of a hurricane which encountered wind shear is seen in Figure 9-33, which contains a satellite image off the coast of Africa. The cirrus cloud shield on top of the hurricane is dispersed as the thunderstorms within the rainbands die.

Figure 9-33: A visible satellite of a decaying hurricane as it encounters wind shear off the west coast of Africa. The dense cirrus cloud shield dissipates as the thunderstorms within these rainbands decay.

9.2.6 - Hurricane Names

Tropical cyclones can last for a week or more. Therefore, more than one cyclone can exist at a time. Weather forecasters give each tropical cyclone a name to avoid confusion. In general, tropical cyclones are named according to the rules associated with an ocean basin. In the Atlantic and in the Southern hemisphere, tropical cyclones receive names in alphabetical order, and women and men's names are alternated. Nations near the Northern Indian ocean began using neutral gender names in 2000. These tropical cyclone name lists are proposed by World Meteorological Organization (WMO) members for a specific region, and approved internationally. The WMO is a United Nations organization with most countries being a member. Other than coordinating tropical cyclone names, the WMO promotes common data exchange formats, which allows atmospheric data to be shared internationally by all countries.

The practice of naming tropical cyclones began years ago to allow for the quick identification of storms in warning messages. Hurricane names are easier to remember than numbers or technical terms. Naming hurricanes makes it easier for the media to report on tropical cyclones, heightens interest in warnings and increases community preparedness.

Experience shows that the use of short, distinctive names in written and spoken communications is quicker and less subject to error than a cumbersome latitude-longitude identification or numbering methods. These advantages are especially important in exchanging detailed storm information between hundreds of widely scattered stations, coastal bases, and ships at sea.

In the beginning, storms were named arbitrarily. An Atlantic tropical cyclone that ripped off the mast of a boat named Antje became known as Antje's hurricane. Then the mid-1900's saw the start of the practice of using feminine names for storms.

In the pursuit of a more organized and efficient naming system, meteorologists later decided to identify storms using names from a list arranged alphabetically. Thus, a storm with a name which begins with A, like Anne, would be the first storm to occur in the year.

Since 1953, Atlantic tropical storms have been named from lists originated by the National Hurricane Center. They are now maintained and updated by an international committee of the World Meteorological Organization. The original name lists featured only women's names. In 1979, men's names were introduced and they alternate with the women's names. Six lists are used in rotation. Thus, the 2024 list will be used again in 2030.

The only time that there is a change in the list is if a storm is so deadly or costly that the future use of its name would be inappropriate for sensitivity reasons. The offending name is stricken from the list and another name is selected to replace it. Infamous storm names such as Mangkhut (Philippines, 2018), Irma and Maria (Caribbean, 2017), Haiyan (Philippines, 2013), Sandy (USA, 2012), Katrina (USA, 2005), Mitch (Honduras, 1998) and Tracy (Darwin, 1974) are examples of names that will no longer be used.

Hurricanes names for all of the ocean basins can be found at this WMO link.

9.3 – Hurricane Hazards

Since hurricanes are the largest storms on our planet, they can wreak wide swaths of damage. The damage can be divided into groups determined by the specific type of weather causing the damage:

- Wind and squall lines
- Tornadoes
- Storm surges and associated flooding
- Heavy rain and associated flooding

Hurricanes are known for their damaging wind. They are rated in strength by their wind speed. However, when the NWS's National Hurricane Center issues a statement concerning the wind and its category, that value is for sustained wind only. The Saffir-Simpson Scale does not include gusts or squalls.

Gusts are short bursts in wind speed. As a hurricane makes landfall, wind gusts are primarily caused by turbulence over land mixing faster air aloft to the surface. Squall lines, on the other hand, are longer periods of increased wind speeds. They are generally associated with the bands of thunderstorms which make up the spiral bands around the hurricane.

A tropical cyclone's wind damages and destroys structures in two ways. First, many homes are damaged or destroyed when the high wind simply lifts the roof off of the dwellings. Once lifted, the roof acts as a sail and is blown clear of the dwelling. With the roof gone, the walls are much easier to be blown down by the hurricane's wind.

The second way the wind destroys buildings is by hurling debris towards them. The wind picks up the debris (building construction wood, metal siding, outdoor furniture, trash cans or tree branches) and sends them hurling at high speeds into other structures. Based on observations made during damage investigations, researchers realized that much of the damage in windstorms is caused by flying debris. These two photos in Figure 9-34 are from wind damage associated with Hurricane Andrew in 1992. No tornadoes were confirmed to occur in Florida with Hurricane Andrew, so the damage in these photos is purely from strong winds.

Figure 9-34: Two photos of Hurricane Andrew wind damage in 1992. (left) A piece of plywood is embedded in the center of a palm tree. (right) A neighborhood with multiple houses completely destroyed.

9.3.1 – Right-front Quadrant and Tornadoes

As a hurricane makes landfall, the surface winds encounter an increase in friction from trees, buildings and other vegetation. This friction slows the surface wind speed, but the winds aloft are initially unaffected. This situation causes a significant increase in the vertical wind shear. We know wind shear is an important ingredient for tornadoes to form. Thus, many hurricanes have clusters of tornadoes as they make landfall. This tornado hazard is greatest in the right-front quadrant of the hurricane. The right-front quadrant is determined by the direction of motion of the hurricane as illustrated in Figure 9-35.

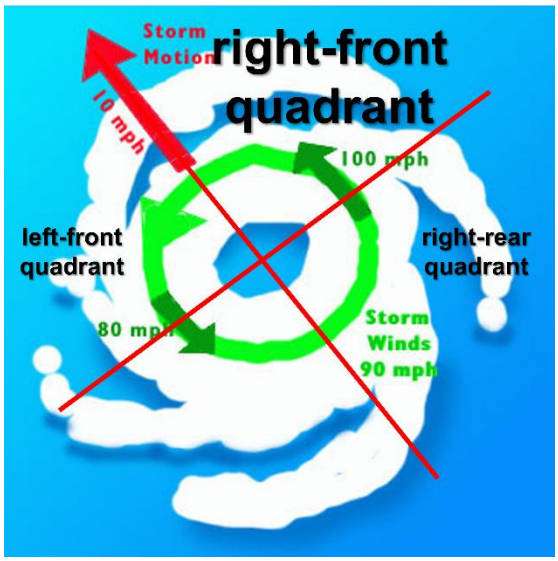

Figure 9-35: Illustration of the right-front quadrant of a hurricane.

The reason the right-front quadrant has the most tornadoes is because the strongest winds occur there. If the internal winds of a hurricane are 90 mph and it is moving north at 10 mph, the winds in the right-front quadrant would be 100 mph. These stronger winds create more wind shear.

These tornadoes most often occur in the thunderstorms embedded in the rain bands away from the hurricane center. However, tornadoes can occur near the eyewall. Tornadoes produced by tropical cyclones are generally weak and short lived, but are still a significant hazard. The map in Figure 9-36 depicts the tornadoes associated with Hurricane Katrina (2005) as landfall occurred. The center of Hurricane Katrina as it moved inland is indicated by the shaded red area. Notice that the tornados occurred in the right-front quadrant.

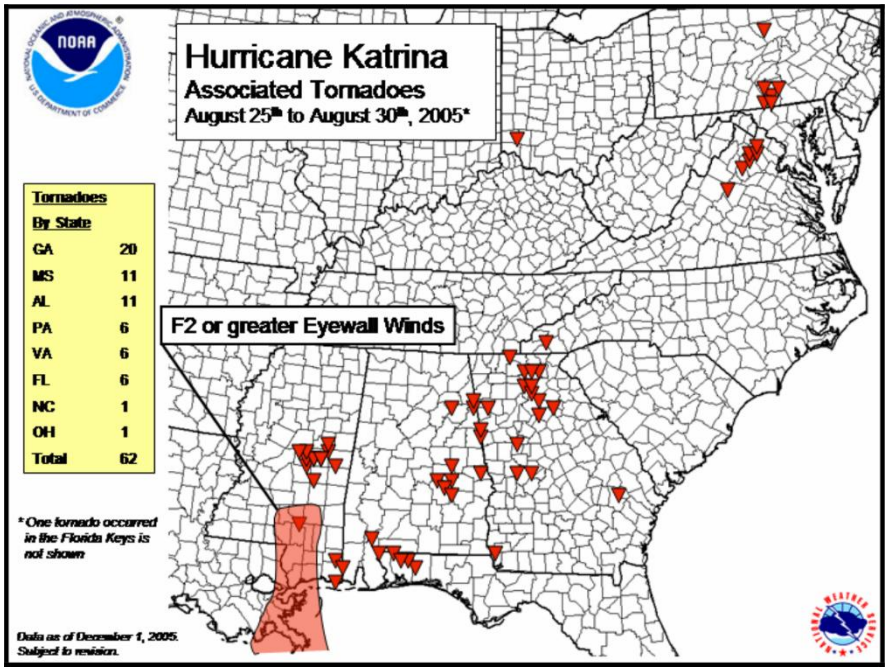

Figure 9-36: Tornadoes associated with Hurricane Katrina from August 25-30, 2005. The shaded red area is the center of the hurricane as it moved inland.

Some tropical cyclones seem to produce no tornadoes, while others develop multiple ones. Studies have shown that more than half of the landfalling hurricanes produce at least one tornado; Hurricane Buelah (1967) spawned 141 according to one study.

When associated with hurricanes, tornadoes are usually not accompanied by hail nor a lot of lightning. They can occur for days after landfall when the tropical cyclone remnants maintain an identifiable low-pressure circulation. They can also develop at any time of the day or night during landfall. However, 12 hours after landfall tornadoes tend to occur mainly during daytime hours.

9.3.2 – Storm Surges and Associated Flooding

A **storm surge** is ocean water pushed on to the shore by the wind. This advancing surge combines with the normal tides to create the hurricane storm tide, which can increase the average water level 15 feet (4.5 m) or more. In addition, wind driven waves are superimposed on this storm tide. This rise in water level can cause severe flooding in coastal areas, particularly when the storm tide coincides with the normal high tides. The highest winds with a hurricane making landfall are in the right-front quadrant. Thus, storm surges are usually worse in the right-front quadrant of the hurricane. Figure 9-37 shows the changing water levels associated with a storm surge.

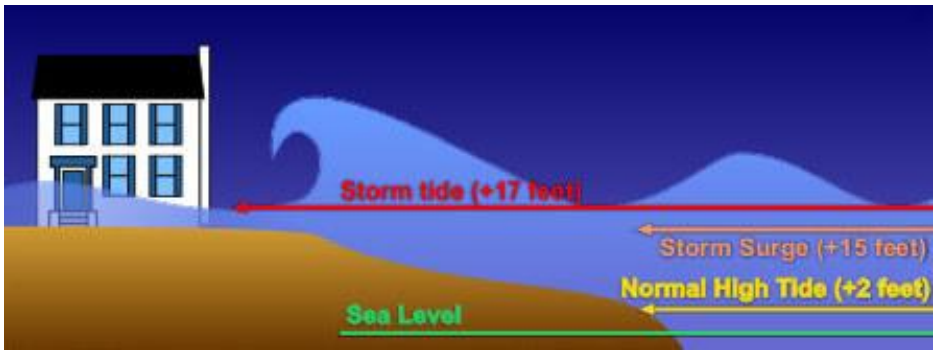

Figure 9-37: Water levels associated with the normal tide and a storm surge.

The level of surge in a particular area is determined by the slope of the continental shelf. A shallow slope off the coast will allow a greater surge to inundate coastal communities. Communities with a steeper continental shelf will not see as much surge inundation, although large breaking waves can still present major problems. Additionally, storm tides, waves, and currents in confined harbors can severely damage ships, marinas, and recreational boats. Because much of the United States' densely populated Atlantic and Gulf Coast coastlines lie less than 10 feet above sea level, the danger from storm tides is tremendous.

About half of the direct fatalities from Atlantic hurricanes are from storm surges as seen in Figure 9-38. Adding in the fatalities associated with heavy rain (flooding), surf, and offshore, means 88% of direct hurricane fatalities are water related.

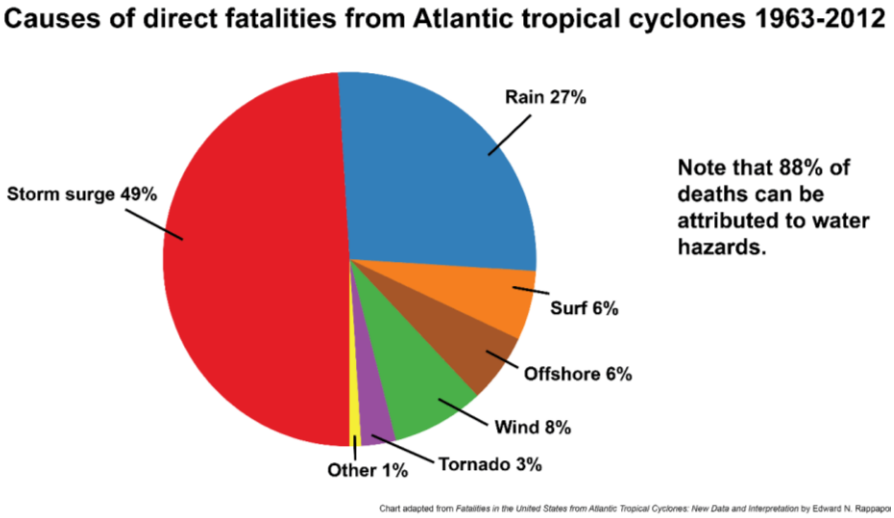

Figure 9-38: The causes of direct fatalities from Atlantic tropical cyclones.

Despite this section highlighting the death and destruction associated with storm surges, proper building techniques can withstand the strongest hurricanes. The photo in Figure 9-39 was taken in the aftermath of Hurricane Ike (2008) and illustrates these building techniques. Reports were that this house was built to withstand a Category 5 hurricane after it was previously destroyed by Hurricane Rita in 2005. Hurricane Ike was a Category 4 hurricane. This house withstood the storm surge, the wind and the torrential rain. The nearby structures and bridge did not survive as well.

Figure 9-39: Photo of a beach front house which survived Hurricane Ike in 2008. The surrounding structures were not as fortunate.

9.3.3 – Heavy Rain and Associated Flooding

As a hurricane progresses inland, the winds subside but the moisture remains. Since 1970, nearly 60% of the 600 deaths due to floods associated with tropical cyclones occurred inland from the storm's landfall. Additionally, over three-fourths (78%) of children killed by tropical cyclones drowned in freshwater floods. Most of these fatalities occur because people underestimate the power of moving water and purposely walk or drive into flooding conditions.

If this tropical moisture encounters a midlatitude cyclone, the combination of these two storm systems will create torrential rains over a widespread area. As Hurricane Katrina moved up the east side of Appalachian mountains in 2005, rainfall exceeding 5 inches occurred in many states. The map in Figure 9-40 shows the rainfall associated with Hurricane Katrina; her track is given by the yellow line.

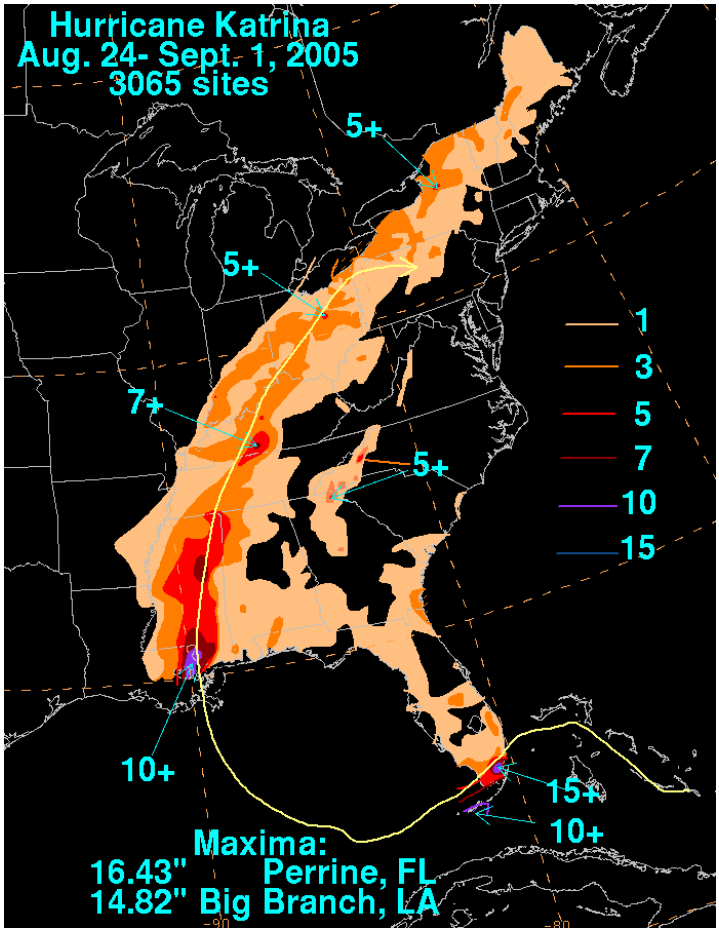

Figure 9-40: The precipitation associate with Hurricane Katrina in 2005. The yellow line is the track of the hurricane center as it moved over land.

The interaction of a midlatitude cyclone with a decaying hurricane can occur at many locations. In 1983 the remnants of Tropical Storm Octave brought abundant moisture over the State of Arizona as a midlatitude cyclone moved into the area. This combination caused locations in southern Arizona to get over 10 inches of rain in less than a week, which caused record flooding. After this event, officials in the area began a riverbank reinforcement program (levies) which continues today. The left side of Figure 9-41 is map illustrates the positioning of an upper-level trough associated with a midlatitude cyclone that enables tropical cyclone remnants to cause widespread rain and possibly flooding over much of Arizona. The right side of Figure 9-41 depicts the rainfall amounts associated with Tropical Storm Octave.

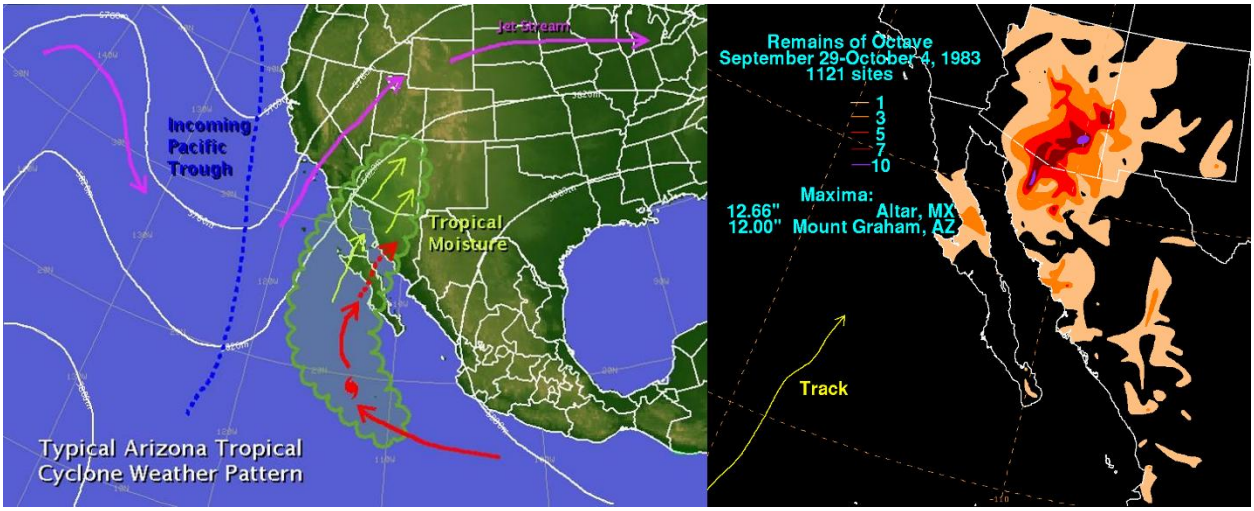

Figure 9-41: Left side depict the location of a midlatitude cyclone which can interaction with hurricane remnants. Right side is the precipitation amounts associate with Tropical Storm Octave in 1983.

Hurricanes can cause several types of flooding:

- Flash flooding
- Urban area floods
- River flooding

Flash floods are rapid occurring events. This type of flood can begin within a few minutes or hours of excessive rainfall. The rapidly rising water can reach heights of 30 feet or more and can roll boulders, rip trees from the ground, and destroy buildings and bridges.

Urban/area floods are also rapid events, although not quite as severe as a flash flood. Streets can become swift-moving rivers and basements can become death traps as they fill with water. The primary cause is due to the conversion of fields or woodlands to roads and parking lots. Infiltration is decreased and runoff is increased.

River floods are longer term events and occur when the runoff from torrential rains, brought on by decaying hurricanes or tropical storms, reach the rivers. A lot of the excessive water in river floods may have begun as flash floods. River floods can occur within hours of landfall and last a week or longer.

9.3.4 – Hurricane Forecasting and Trends

The National Hurricane Center located in Miami, Florida is responsible for predicting and tracking Atlantic and east Pacific Ocean hurricanes. The Hurricane Center is part of the National Weather Service. Therefore, hurricane forecasts follow the standard watch and warning format used throughout the National Weather Service. The photo in Figure 9-43 shows the National Hurricane Center building. Since Miami could be affected by a Category 5 hurricane, the building is constructed to survive and continue operating during such an event.

Figure 9-42: Photo of the National Hurricane Center located in Miami, Florida.

The National Hurricane Center issues tropical storm and hurricane watches about 48 hours prior to the predicted onset of conditions in an area. Tropical storm and hurricane warnings are issued 36 hours prior to onset. A hurricane watch is for when sustained winds of 74 mph or

higher are possible in a specified area. A hurricane warning is when sustained winds of 74 mph or higher are expected in a specified area. Tropical storm watches and warnings have the same definition except the wind speeds are 39 to 73 mph.

Associated with these products is a map depicting the forecast path of the storm and the expected strength. Figure 9-43 is an example of the forecast for Hurricane Earl in 2010.

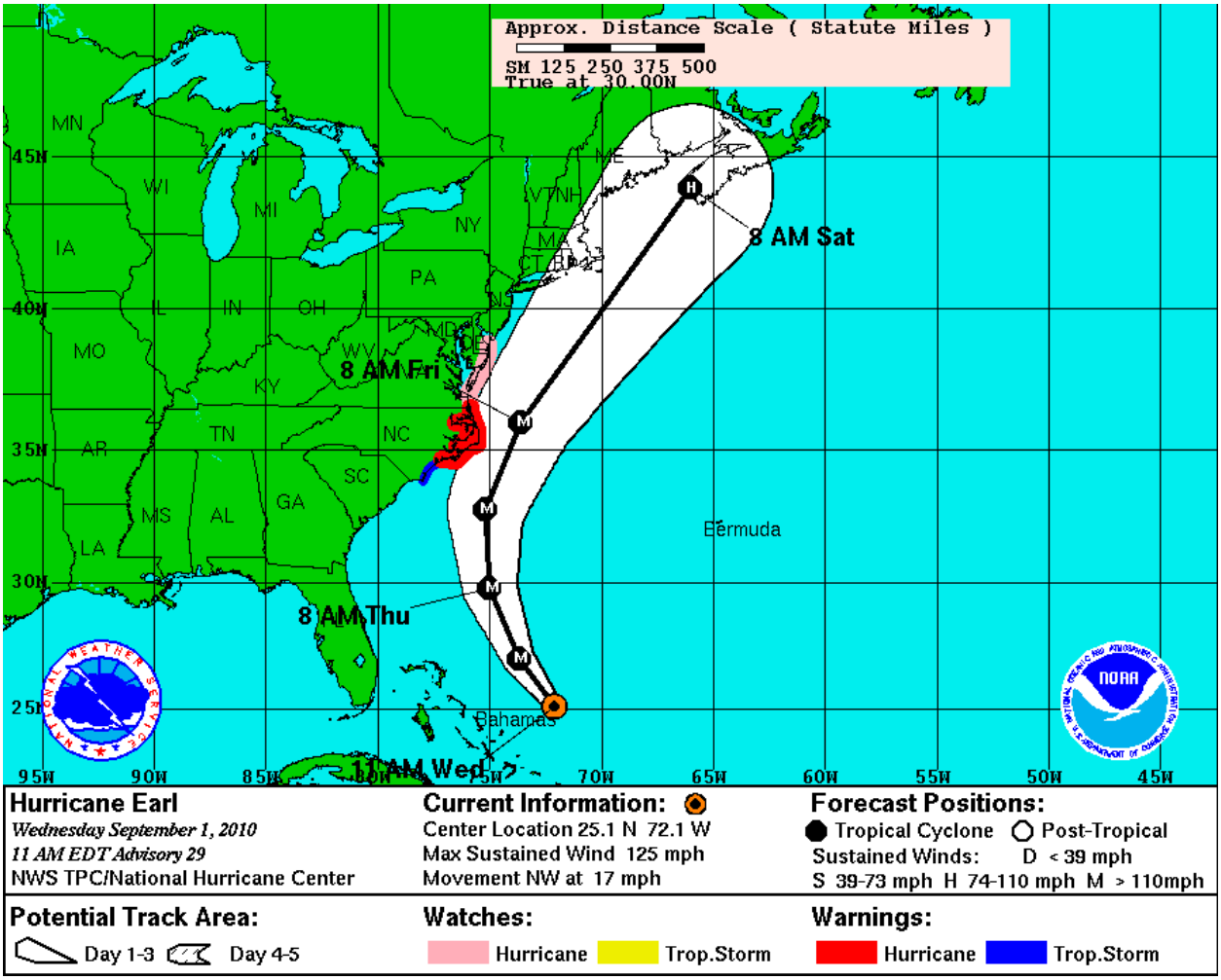

Figure 9-43: The forecast for Hurricane Earl on September 1, 2010.

The coastal areas affected by watches and warnings are highlighted in difference colors. The most probable track is given by the black line along with the expected dates at that location. The intensity of the storm is given by an “S”, “H” or “M” at each forecast location. The white area surrounding the black track line is called a cone of uncertainty or uncertainty cone. Forecasting the exact track of a tropical storm is difficult. Therefore, the cone of uncertainty provides a boundary for where the actual storm track may occur.

Tropical cyclone forecasts are updated every 6 hours. Many times, these forecast graphics are used directly by the media to inform those affected. These forecasts are available on the web and can be found at this link. Select the “Central Pacific”, “Eastern Pacific” or “Atlantic” tab depending on your interest.

Intensity and frequency trends associated with hurricanes are always a question. Are hurricanes getting stronger? Are more hurricanes occurring? This topic is an active research area associated with a changing climate. The graph in Figure 9-44 contains the number of tropical storms and hurricanes occurring in the Atlantic Basin along with the count of major hurricanes that occurred from 1850 through 2015. This graph shows the number of hurricanes in the Atlantic basin has not changed much. Other studies have examined the intensity of hurricanes in the Atlantic basin and tend to indicate hurricanes may have more intensity than in the past. However, Figure 9-44 does not show any well-defined trend in intensity for the Atlantic Ocean.

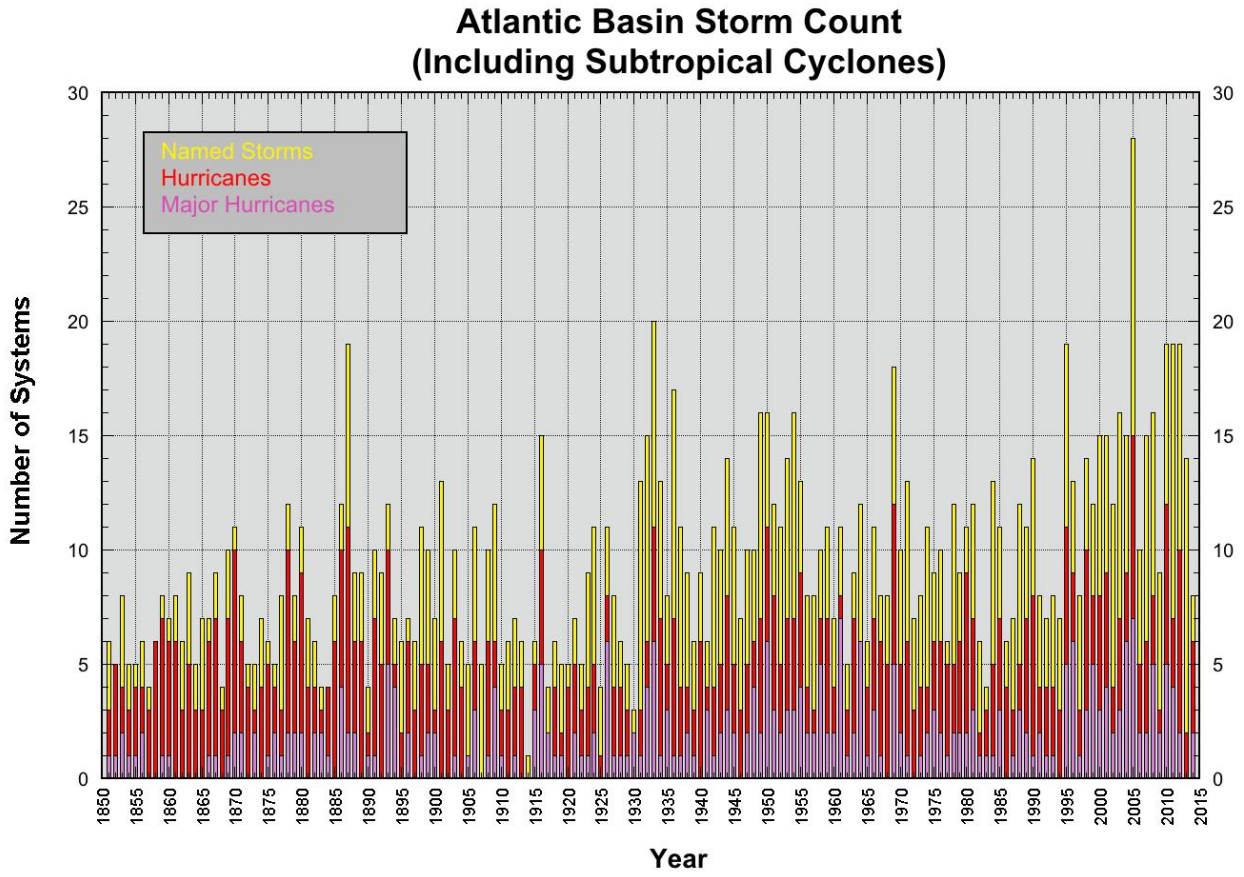

Figure 9-44: The number and strength of tropical cyclones in the Atlantic Ocean from 1850 through 2015.

Figure 9-45 shows the Central Pacific Ocean from 1970 to 2013. Tropical cyclones in the Central Pacific Ocean may affect Hawaii. This graph does not indicate any definite trend either.

Other studies examining the Pacific Basin find no change in intensity or frequency of hurricanes in the Pacific Ocean, even though most hurricanes occur there. More details on how a changing climate may affects hurricanes will be covered in Chapter 15.

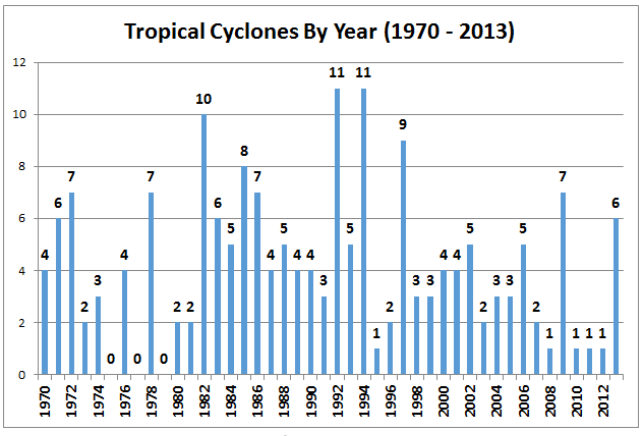

Figure 9-45: The count of tropical cyclones in the central Pacific Ocean from 1970 through 2013.

Chapter 9 Review Questions

1. Why is vertical wind shear important for the development of a supercell tornado?
2. What does a tornado warning mean?
3. Why are tornadoes most prevalent in the spring and early summer?
4. What is a region of intense rotation seen by a Doppler weather radar velocity image called?
5. What are the reasons for tornado fatalities decreasing in the U.S.?
6. What is the primary criteria for determining the EF-scale of a tornado?
7. What is a tropical cyclone?
8. Why do hurricanes not form at the equator?
9. What are the conditions necessary for a hurricane to form?
10. Why do hurricanes weaken when they make landfall?
11. When in the eye of hurricane, what is a person most likely to observe?
12. When is a tropical cyclone given a name?
13. When will a tropical storm be classified as a hurricane?
14. Place these labels on this cross section of a hurricane.
    - rainbands
    - low pressure
    - eye
    - eyewall
    - high pressure

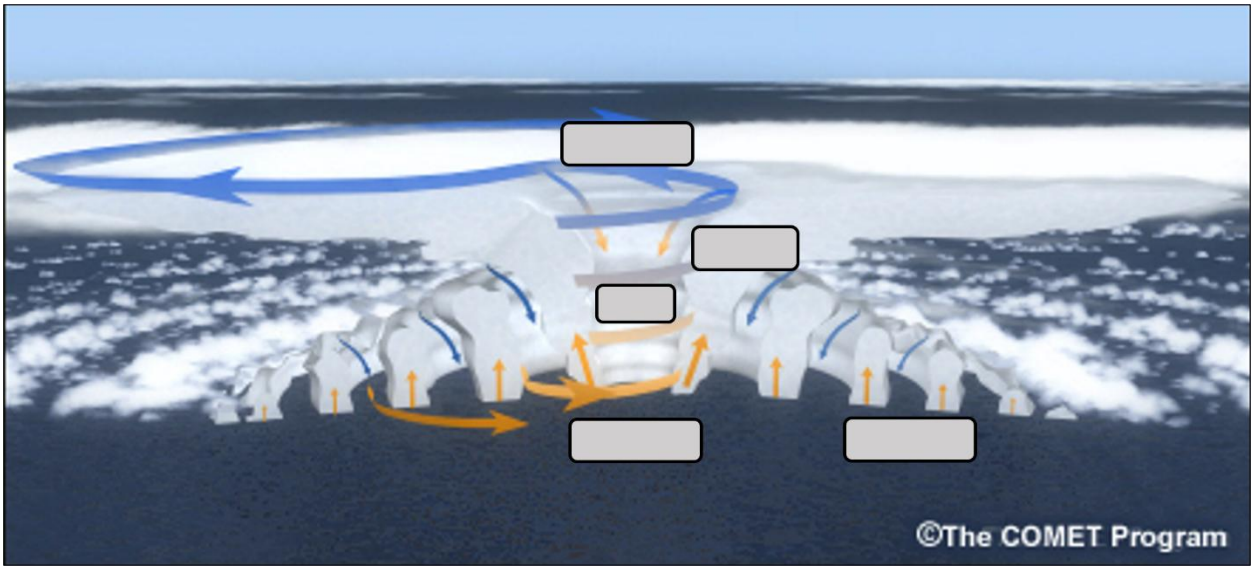

15. Where are tornadoes likely to occur when a hurricane makes landfall in the U.S.?
16. When a hurricane make landfall, where is the storm surge most likely to be the worst?
17. As a hurricane progresses inland, the winds subside but the moisture remains. What is a possible scenario for these hurricane remnants to cause torrential rains and flooding?
18. What percentage of hurricane fatalities are directly attributed to water hazards?
19. What is the trend in the number of hurricanes occurring in the Atlantic and central Pacific Oceans?
20. What does a hurricane warning mean?

Chapter 10 – Optical Phenomena and Weather Forecasting

Overview

This chapter examines optical phenomena that occur in the atmosphere. The displays of light explored are rainbows, inferior mirage, superior mirage, green flash, corona, glory, halos, sundogs, Sun pillars, and a couple of other "surprises".

Additionally, weather forecasting is included in this chapter. Four weather forecast methodologies are available. One of the methodologies is numerical weather prediction, also known as computer models. Numerical weather prediction is the most widely used and generally the most accurate. This chapter discusses the details of each methodology, although numerical weather prediction is examined the most.

Weather forecasts become less accurate the further they go out in time. After about 10 days, weather forecasts will be incorrect as often as they are correct. To get a seasonal outlook a different approach is needed. The details for how seasonal outlooks are created and interpreted is the last topic in this chapter.

Chapter Objectives:

1. Explain the reflection, refraction, and diffraction of light and the resulting optical effects.
2. Describe the four methods of weather forecasting.
3. Describe the phases of numerical weather prediction.
4. Interpret a seasonal outlook.

10.1 – Atmospheric optics

Light can be viewed as both photon particles and electromagnetic radiation that travels along paths called rays. For the most part light rays travel in straight lines. However, when light strikes particles in the air, the ray can be reflected, refracted, scattered, or diffracted. The word "diffracted" is new, but the others have been used in this book previously. Since this section uses these concepts to explain atmospheric optics, such as a rainbow, a short review may be helpful.

Reflection occurs when light strikes an object and is redirected away from it. **Refraction** is the bending of light as it passes through different mediums. **Scattering** is the dispersion of light in multiple directions when it strikes an object. Light travels in a straight line until it strikes an object, and then in a straight line after it leaves the object. The geometry of reflection and refraction can be determined as shown in Figure 10-1.

Diffraction is the slight bending of light as it passes around an object. Diffraction is sometimes called an optical “edge effect” and has similarities to scattering. The amount of bending depends on the relative size of the wavelength of light to the size of the opening. If the opening is much larger than the light's wavelength, the bending will be almost unnoticeable. However, if the two are closer in size or equal, the amount of bending is considerable, and easily seen with the naked eye.

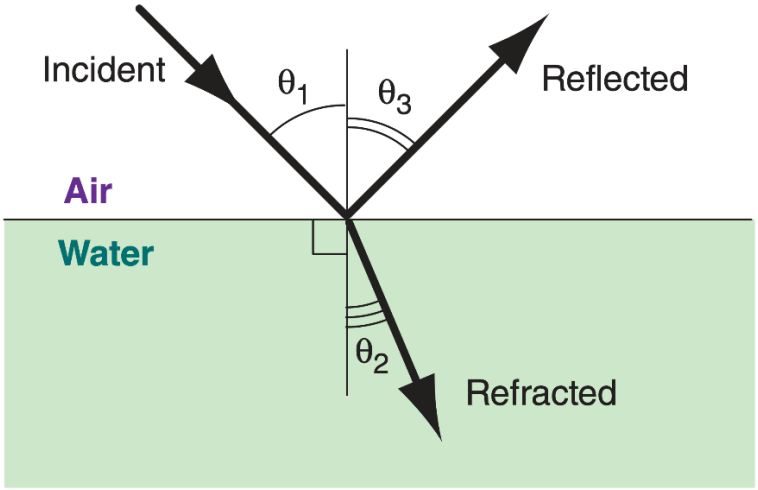

Figure 10-1: Illustration of reflection and refraction of a light ray. The angles θ_1 and θ_3 are equal; θ_2 is a different angle and depends on the refractive index on the medium.

In the atmosphere, diffracted light is usually bent around tiny water droplets found in clouds. Diffracted light can produce fringes of light, and dark or colored bands. An optical effect that results from the diffraction of light is the bright glow sometimes found around the edges of clouds or coronas surrounding the Sun or Moon. The left side of Figure 10-2 shows how light is bent around small droplets in a cloud. The right side of Figure 10-2 is a photo showing a corona around the Moon due to diffraction. Small water droplets in the atmosphere are causing this diffraction. If the droplets vary in size, faint colors can be seen in the rings.

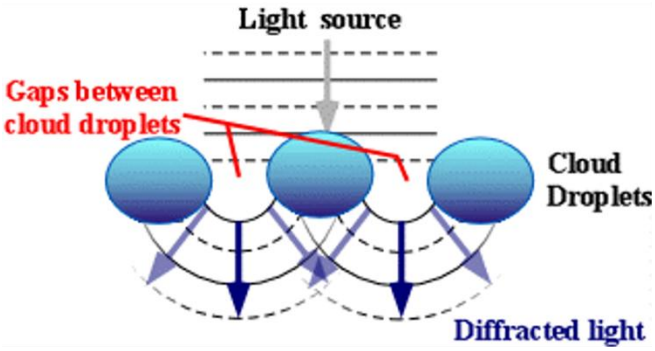

Figure 10-2: Left side is an illustration of diffraction occurring with cloud droplets. The light bends around the droplets. Right side is a photo of this diffraction effect around the moon due to water droplets.

Another type of diffraction occurs in what is called a glory. A glory is small, colored rings of light around a shadow when looking at cloud water droplets from above. The photo in Figure 10-3 shows a glory. The shadow is not important, but exists because the light source is behind the person. Glories are observed primarily from aircraft, and appear when droplets have a radius smaller than 25 microns. Both diffraction and reflection occur in a glory.

The amount of refraction (bending) which occurs with light is wavelength dependent. Light is composed of multiple wavelengths, and each wavelength is a different color. Shorter wavelengths are the violet and blue colors, and longer wavelengths are the reds. Figure 10-4 shows the wavelengths of each color in nanometers.

Figure 10-3: A glory as seen from a plane. Both diffraction and reflection are occurring.

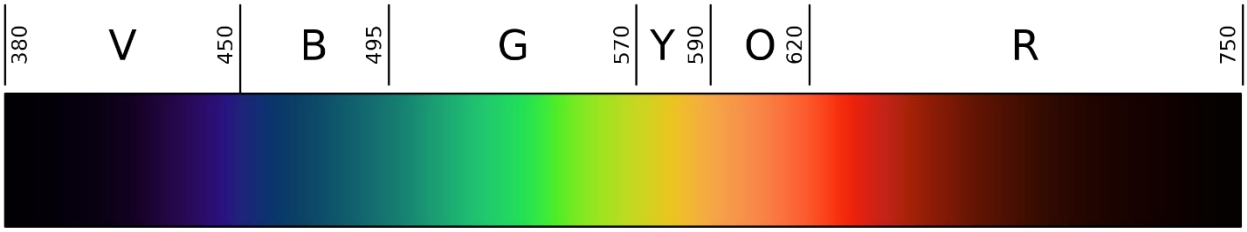

Figure 10-4: The wavelengths of light in nanometers. Violets and blues are shorter wavelengths; oranges and reds are longer.

10.1.1 – Mirages

The density of the atmosphere decreases with height, and the density at a specific altitude is largely dependent on temperature. When examining the optical properties of the atmosphere, the refractive index of air depends primarily on the number of air molecules at a particular altitude. Thus, the refractive property of the atmosphere depends upon temperature. These changes in temperature (density) within the atmosphere cause the light rays to curve rather than follow a straight line.

When the Sun is low on the horizon, the refraction of the light from the Sun is greatest because the light travels through more atmosphere. Under normal circumstances when temperature decreases with height in the troposphere, light is bent towards the surface of the Earth. At sunset, the refraction is great enough to see the Sun's rays even though the Sun has passed below the horizon as illustrated in Figure 10-5. This refraction effect of the atmosphere gives several extra minutes of sunlight each day. The exact amount of additional daylight depends on the season and a person's latitude.

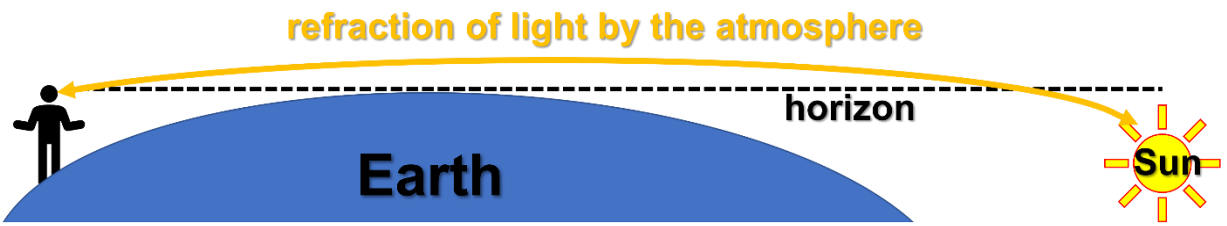

Figure 10-5: Illustration depicting the additional daylight from atmospheric refraction at sunrise (and sunset).

When the atmosphere temperature profile is not normal, such as unusually cold or hot air near the surface, the atmosphere acts like a lens. A **mirage** is the image formed when the atmosphere behaves like a lens. Two types of mirages are commonly seen: (1) an inferior mirage and (2) a superior mirage.

Inferior mirages occur with intense surface heating and the image is displaced downward from the position of the object. In other words, the viewer sees an inverted image of an object. The most common inferior mirage seen is when the Sun shines on an asphalt road, as seen in the left side of Figure 10-6.

The hot air over the road is much less dense than the rest of the atmosphere. Looking at the road a person will see light rays refracted from the sky, giving the road a wet appearance and an inverted image below the object on the road. Photos of inferior mirages frequently have wavy lines or shimmer because of the turbulence associated with the hot air rising off the surface. The right side of Figure 10-6 shows how the light refracts to create an inferior mirage.

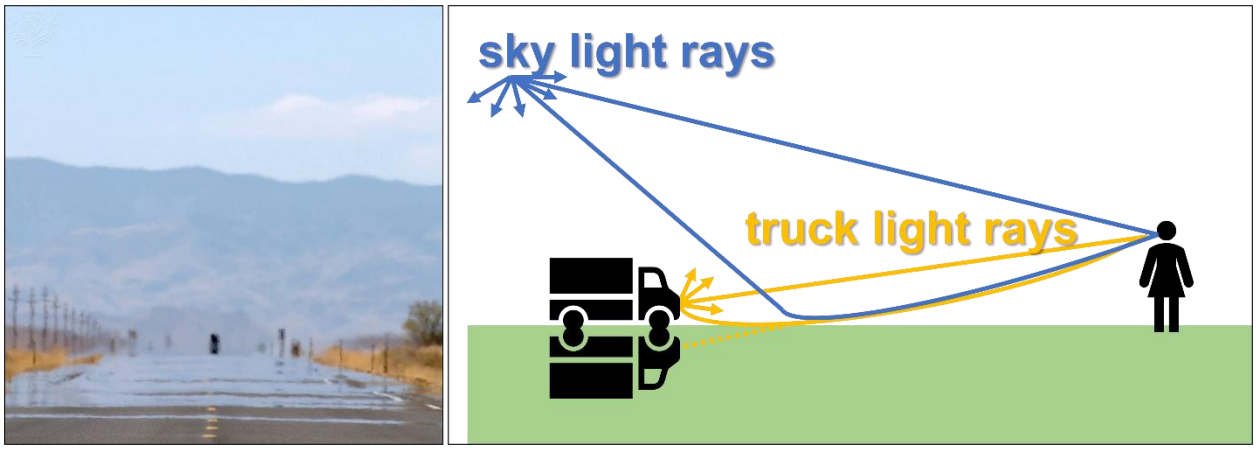

Figure 10-6: (left side) Photo of an inferior mirage. (right side) Path light rays take to create an inferior mirage. Intense surface heating causes the rays to bend abruptly near the surface.

The green flash of a rising or setting Sun is a mirage. A green flash is a flash of green light on the upper rim of the Sun. The upper edge of a low angle Sun normally has a thin green rim that is too narrow to be seen by the naked eye. If the rest of the sun is obstructed, say by the horizon, it can be seen briefly. The more remarkable flashes seem to involve multiple and magnified images of the green rim. Indeed, the presence of such multiple images of a small portion of the Sun is a good indicator of a forthcoming flash. The optical signature of multiple images is a serrated edge to the Sun. The refraction that allows a low angle Sun to be seen favors the shorter wavelengths. This leads to a red rim on the bottom of the Sun and a blue or green rim on the top as is illustrated in Figure 10-7.

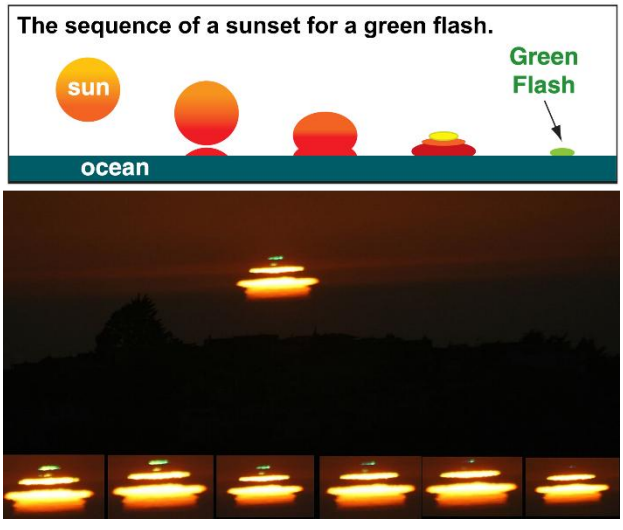

Figure 10-7: (top) Diagram depicting a green flash with a setting Sun. (bottom) Photo of a green flash which matches the top diagram.

Frequently green flashes are seen over the ocean because an unobstructed view is available. The temperature differences between ocean water and atmosphere help establish the appropriate refraction environment for a green flash too. The green flash photo in Figure 10-7 was taken from the San Francisco, California area. Caution should be used if visually trying to see a green flash because a low angle Sun can still damage a person's eyes.

Superior mirages occur with cold air at the surface, and the image is displaced upward from the position of the object. In other words, the object is made higher or taller. Superior mirages occur when temperature increases with height (an inversion is present). The exact image depends on the location of the viewer, the number of inversions which may be present, and the altitude of the inversions. As you might anticipate, photos of superior mirages can look a bit strange.

The superior mirage is most striking when it exhibits three or more images. The upper and lower images are always erect, while a single middle image will be inverted. The top portion of Figure 10-8 illustrates a superior mirage with two images. The bottom portion is a photo of a superior mirage that matches the top diagram.

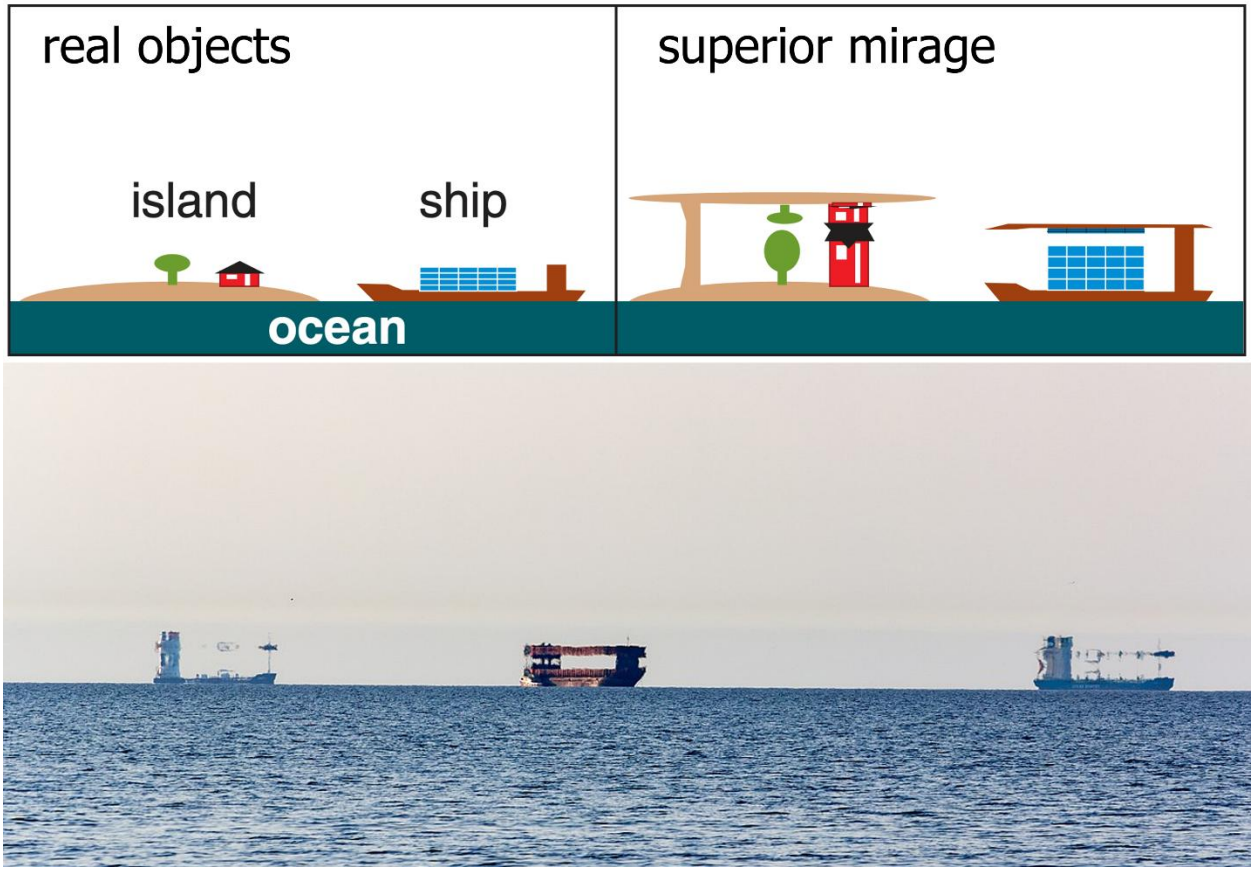

Figure 10-8: (top) Diagram illustrating a superior mirage. (bottom) Photo of a superior mirage.

10.1.2 – Rainbows

Rainbows are associated with water droplet optics. They form through both the reflection and refraction of light as it enters a water droplet. For a person to see a rainbow, the Sun must be

behind them. Hence, rainbows are most common in the early morning or early evening. During midday, the Sun has a higher angle and is above a person. Since many thunderstorms occur in the late afternoon or early evening, they are frequently associated with rainbows.

Rainbows are a portion of a circle or an arc. The center of the arc corresponds to an imaginary line from the Sun through the observer. This imaginary line is in the center of the rainbow and is called the antisolar point. Figure 10-9, while not to scale, illustrates this rainbow geometry.

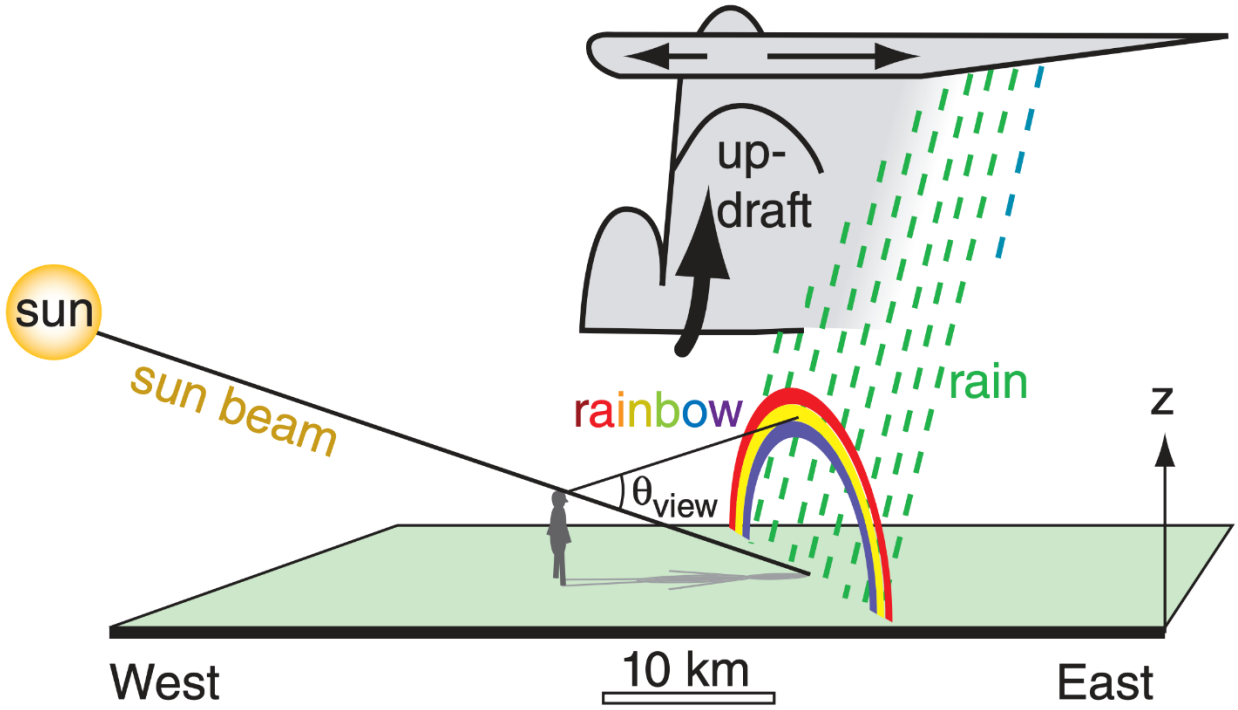

Figure 10-9: Rainbows occur with the Sun is behind a person. The center of a rainbow arc is an imaginary line from the Sun through the observer. The viewing angle θ is 40-42° with the colors dispersed over 2 degrees.

The primary rainbows have red on the outside of the arc and violet on the inside. The viewing angle θ is 40 to 42 degrees since the colors are dispersed over 2 degrees. At any one time, different observers see different rainbows. Each person is seeing light interacting with different droplets as illustrated in Figure 10-10.

As the Sun's rays enter a water droplet, the light is refracted as it leaves the air and enters the water. As the light hits the back of the droplet a reflection occurs. The light is refracted again as it exits the droplet going from water to air. Figure 10-11 shows how refraction and reflection occur within the droplet.

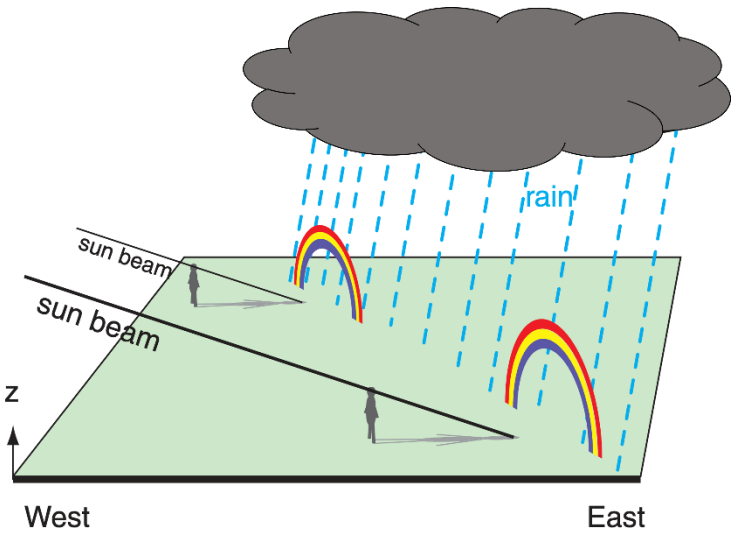

Figure 10-10: Two people observing a rainbow are actually seeing two difference rainbows.

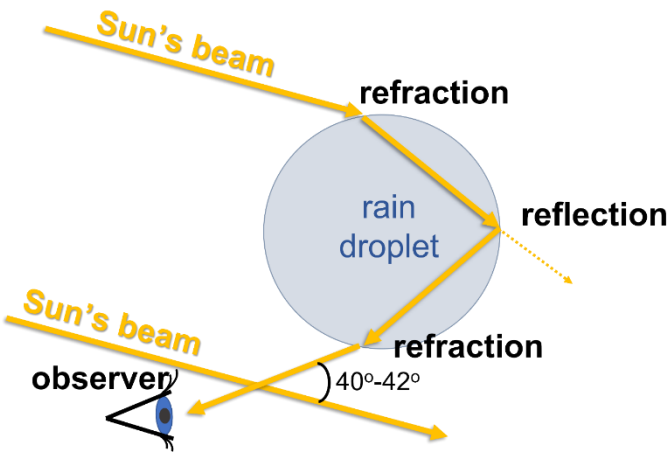

Figure 10-11: The refraction and reflection of light within a water droplet.

As the refraction occurs, the different wavelengths (colors) of the light are bent at different angles. This difference separates out the colors to an observer. The reds are bent less and appear on the outside of the rainbow. Violets are bent more and appear on the inside of a rainbow. One droplet will allow the observer to only see one color of the many colors in a rainbow. Thus, an abundance of droplets are required for the observer to see the full color spectrum and arc of a rainbow. Figure 10-12 illustrates how a person sees all the colors.

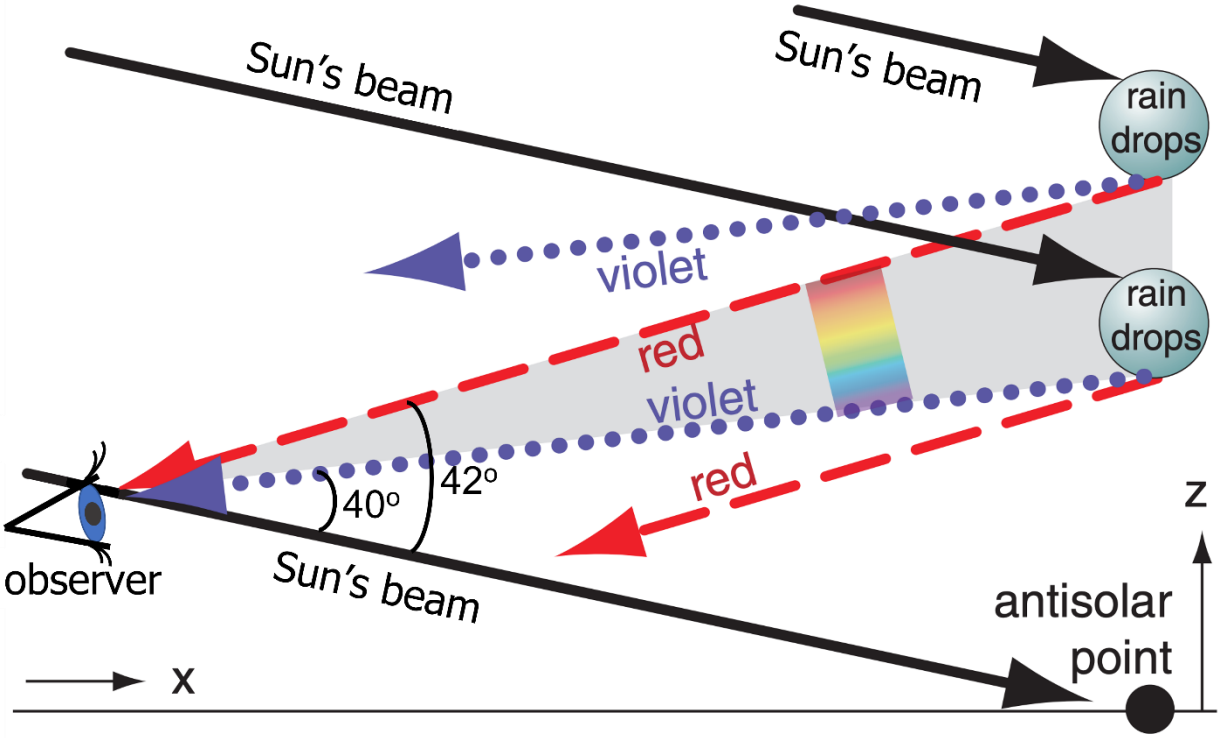

Figure 10-12: Illustration for creating the colors in a rainbow. Multiple droplets are required to create all the colors. The antisolar point is at the center of the rainbow arc.

At times, a secondary rainbow may appear above the primary rainbow. The secondary rainbow is a result of two reflections inside the droplet. The extra reflection reverses the colors putting the red on the inside of the arc and the violet on the outside. A little light is lost each time it reflects inside the droplet. Hence, a secondary rainbow is always less intense than the primary rainbow. The left side of Figure 10-13 illustrates two reflections inside a rain droplet to create a secondary rainbow. The right side of Figure 10-13 is a photo of a secondary rainbow. Two additional aspects to notice in this photo is the dark area between the two rainbows, and the brighter area underneath the primary rainbow.

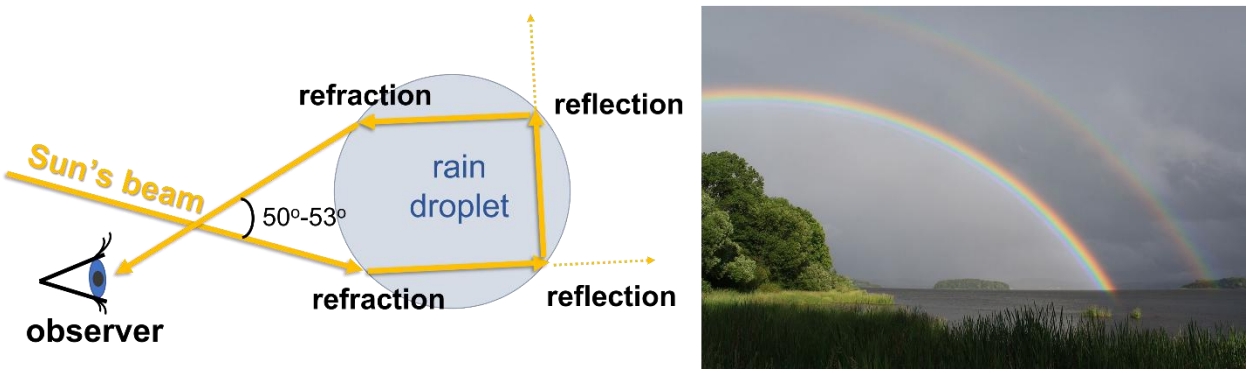

Figure 10-13: (left side) The multiple refractions and reflections within a rain droplet to create a secondary rainbow. (right side) A photo of a primary and secondary rainbow.

Sunlight strikes the entire surface of a spherical rain droplet. Some of this light is reflected back from the front of the droplet before passing into it. An observer will see this reflected light off the front of the droplet from 0° to 42° making the area underneath the primary rainbow brighter. From 42° to 51° the light reflected off the front is diminished as most enters the droplet to create the rainbows. This lack of reflected light causes the dark area between the primary and secondary rainbows. This area is called Alexander's dark band, after the Greek philosopher Alexander of Aphrodisias who described it during the third century A.D.

Depending on the number of reflections inside the droplet, tertiary, quaternary and high orders of rainbows are possible. Each additional rainbow is less bright than the previous one. Many of these higher order rainbows are only visible through enhanced digital photography, and cannot be seen with the naked eye.

This video from the United Kingdom Met Office describes the important features of rainbows and how they form.

10.1.3 – Other Phenomena (Halos, Sundogs and Sun Pillars)

All the optical phenomena examined in section 10.1.3 are created from ice crystals. Ice crystals can have many shapes, as we saw in the module on precipitation processes. Two ice crystal shapes commonly used in understanding atmospheric optics are the column and plate. A plate can be thought of as a short column as shown in Figure 10-14.

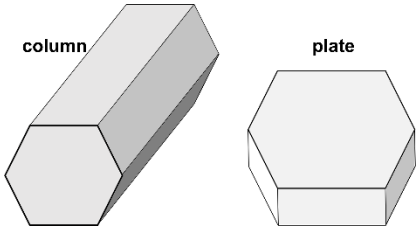

Figure 10-14: The shape of a column and plate ice crystal.

Small ice crystals are free to tumble in all directions, and light can be reflected and refracted in all directions. Determining the optics for ice crystals is not simple. However, the optical phenomena they exhibit are routinely seen. Halos are frequently seen, and an example is the photograph on the left side of Figure 10-15.

Cirrostratus clouds produce halos. The angle between the Sun or Moon and the halo is usually either 22° or 46°, although halos of 9°, 18° to 24°, 35° and 46° have been photographed. All these different halo angles depend on the ice crystal orientation with respect to the light source. As you can see from the diagram on the right side of Figure 10-15, the orientation of the crystal

and light beams can get complicated. Amazingly halos are a common occurrence when cirrostratus covers the sky.

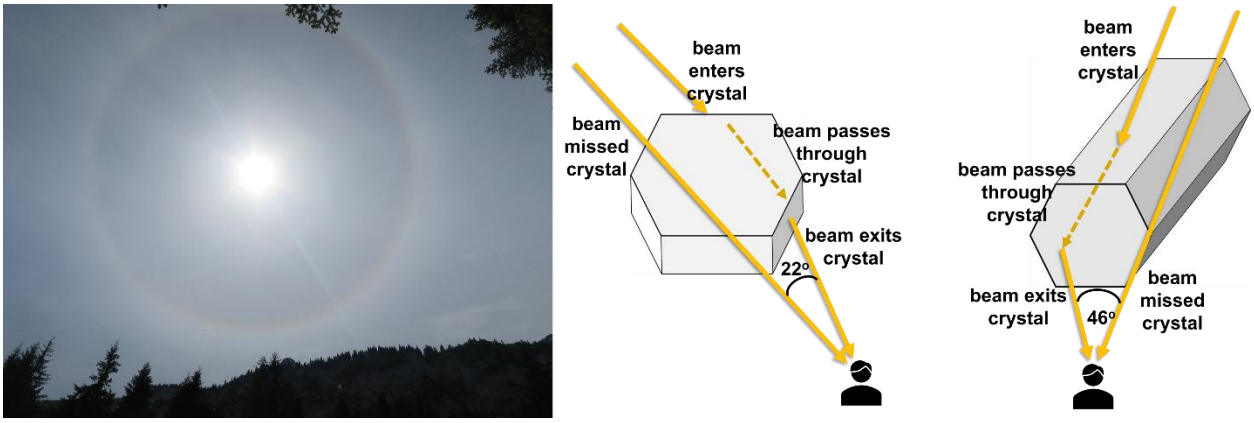

Figure 10-15: (left side) Photograph of a 22° halo. (right) Diagram of light rays when passing through ice crystals to create 22° and 46° halos.

The easiest method to determine the angle of a halo is to use your hand. If you extend your arm fully and open your hand as widely as possible. Place your thumb on the Sun or Moon and your smallest finger on the halo as shown in Figure 10-16. The angle across your open hand is about 22°. This works for people of different sizes, because hand size and arm length are often proportional. Remember to protect your eyes and avoid looking at the Sun. Moon halos are much easier to enjoy because of the lower light intensity.

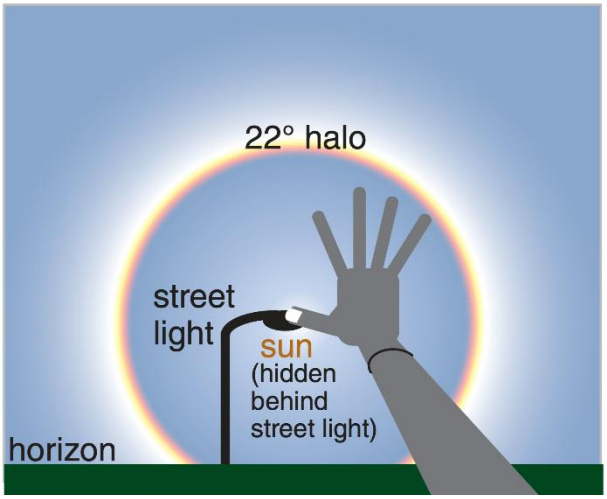

Figure 10-16: Method for determining the size of a halo. A 22° degree halo is most common.

Sundogs (also called a parhelia) are colored spots at about 22° on either side of the Sun. The photo in Figure 10-17 depicts sundogs. They are given the name "sundog" because they follow the Sun like a dog follows its owner.

Sundogs can be explained by the refraction of light in plate crystals that are oriented horizontally with respect to the ground. Light passes through the crystal to the viewer. If the Sun is higher in the sky, the angle between the sundogs will move further apart. In many respects, sundogs are a partial halo. Sometimes a full halo is visible with the sundogs and a sun pillar.

Figure 10-17: A photograph of sundogs.

A sun pillar is a vertical column of light that aligns itself with the Sun. Sun pillars are caused by light reflecting off the outside of the crystals, rather than passing through the crystal. The left side of Figure 10-18 depicts a sun pillar.

The diagram on the right side of Figure 10-18 illustrates how the sun light reflects off the surface of the crystal to the observer. As you can see, not all the ice crystals align properly. However, enough are oriented correctly to create the vertical column of light.

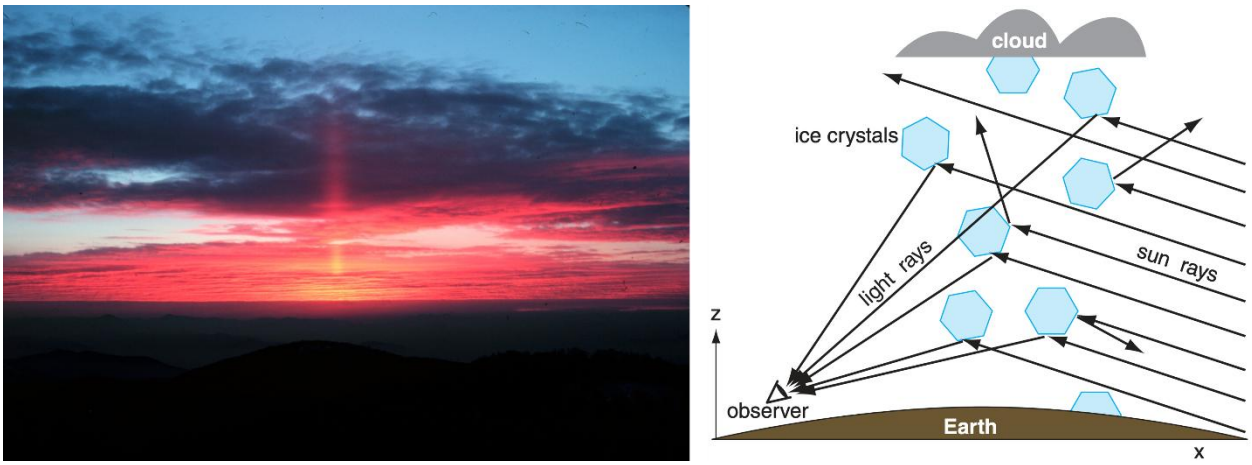

Figure 10-18: (left side) A photograph of a sun pillar. (right side) A diagram demonstrating the reflection of light off ice crystals to create a sun pillar.

Figure 10-19: Photo from the South Pole Station containing a halo, sundog and sun pillar.

Figure 10-19 is a photo from the South Pole Station, and contains all the ice crystal optical phenomena discussed. Can you find the halo, sundog and sun pillar? The light at the top of the halo is called an upper tangent arc. An upper tangent arc has a disk shape associated with it, and is not as common as the others. All these ice crystal optical phenomena are more frequent in winter and at higher latitudes when crystals in the atmosphere are most abundant.

This United Kingdon Met Office video looks at sundogs (parhelia), crepuscular rays (sun beams), circumzenithal arc, haloes, and an aurora. Auroras were covered previously in Chapter 3 and are glowing ions rather than light passing through atmospheric particles. All the other phenomena in this video are associated with atmospheric optics. The circumzenithal arcs mentioned were not covered in this section, and are rare at lower latitudes due to the higher Sun angles.

10.2 – Weather Forecasting

Today people have numerous ways to access weather information and forecasts. Weather apps are a standard feature with all computer technology, the media reports on weather constantly, and weather is the most frequent topic of small talk. Weather affects everyone. Anyone can talk to another person about the weather, and avoid political or social topics that might otherwise be offensive.

Additionally, weather can turn violent at times and a public safety aspect is inherent in weather forecasting. Due to this public safety aspect, almost all countries have one or more agencies established to organize and disseminate weather information for the safety of their citizens. This list contains a sample of the weather-oriented government organizations.

- United States – National Weather Service (part of NOAA)
- United Kindgom (England) – Met Office
- Mexico - Servicio Meteorológico Nacional
- Canada – Environmental Canada
- European Union – European Centre for Medium-Range Weather Forecasting (ECMWF)
- Japan – Japan Meteorological Agency
- China – China Meteorological Administration

Like many organizations, they all have their own logos (Figure 10-20).

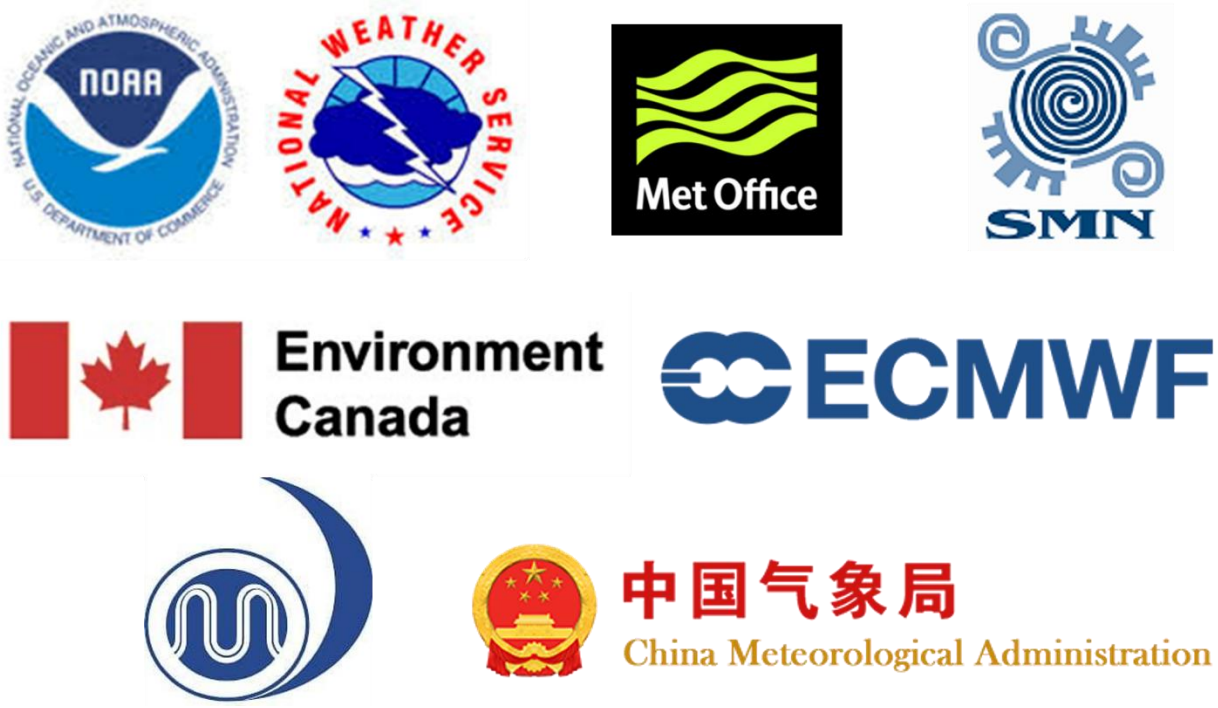

Figure 10-20: A collage of logos from weather-oriented government organizations.

Forecasting the weather is a complex process. Everything presented in this book and more is needed to create a good weather forecast. Prior to the invention of computers, most weather forecasts were based on surface observations because that was the data available. As technology increased, weather balloons provided information aloft and weather radar and

satellites increased the ability to remotely sense the atmosphere from afar. Putting all these data sources into computer models of the atmosphere was a huge step forward in creating a good weather forecast. Due to these circumstances, creating a weather forecast is directly linked to the technology used. As technology improves, weather forecasts improve.

10.2.1 – Examining Forecast Methodologies

With the progression and advancement of technology, four forecast methodologies have been developed. All these methodologies are still in use today, because each has a different aspect of creating a weather forecast. These methodologies are:

1. climatological – based on long-term averages of data.
2. persistence – based on current conditions.
3. analog approach – based on well-studied patterns from the past
4. numerical weather prediction – based on computer models that predict the behavior of the atmosphere.

The **climatological forecast** method takes an average of long-term conditions to determine the most likely conditions for a specific day. Generally, 30 years or more of data are needed for a location to implement this approach. For example, 30 years of surface observation data for the city nearest you can be used. These data would be from the years 1990 to 2020. A surface observation consists of multiple parameters: temperature, dewpoint, relative humidity, wind speed and direction, sea-level pressure, sky conditions and precipitation for each hour of the day. Each hour of every day for 30 years can be summed up and divided by 30. The result is an average temperature, dewpoint, relative humidity, etc. for every hour of every day for the entire year. The high and low temperatures and precipitation for each day can be calculated too. This table illustrates a climatological forecast.

Parameter	Climate conditions (30-year average for this date)	Forecast for today
Maximum temperature	71°	71°
Minimum temperature	46°	46°
Sky conditions	Mostly sunny	Mostly sunny
Precipitation	0.02	0.02

The climatological approach catches the seasonal variations of the weather. Industries affected by the seasons, such as planting crops or moving livestock, have a basis for making economic decisions with a climatological forecast. General weather trends for any location can be discovered. Two examples of trends are (a) Tucson, AZ is coldest in January like many cities in the Northern Hemisphere and wettest in July, and (b) Seattle, WA has cooler and rainy conditions in January with July being the sunniest and driest month. This approach will not catch the day-to-day variations of the weather, but the approximate weather conditions for any day in the future is available.

Now you may be thinking with climate change this approach to making a forecast is archaic history. Those thoughts are incorrect. Climate changes very slowly, so this approach is still valid. If only the last 30 years of data is used for a location, any changes in the climate of the location are inherent in the averages. In other words, the last 30 years of data was recorded in a "changed climate" environment, and automatically accounts for these changes.

The **persistence forecast** method assumes that weather conditions in general change very slowly, and tomorrow's forecast will be similar to yesterday's weather. In the midlatitudes, Rossby waves move slowly and the weather that occurred yesterday will likely be close to what occurs today and tomorrow. The tropics have a similar slow variation of weather from one day to the next. Thus, the persistence methods takes what occurred yesterday and makes it the forecast for today and tomorrow. For example:

Parameter	Conditions yesterday	Forecast for today	Forecast for tomorrow
Maximum temperature	72°	72°	72°
Minimum temperature	48°	48°	48°
Maximum wind speed	12 mph	12 mph	12 mph
Sky conditions	Sunny	Sunny	Sunny
Precipitation	0.0	0.0	0.0

As long as the weather does not change rapidly, a persistence forecast is a reasonable forecast. Both the climatological and persistence forecast methods are referred to as "low skill" methods. Anyone can create a forecast using these approaches and no knowledge about the atmosphere is needed. The only requirement is for past data to be available.

An **analog forecast** is based on the concept that weather patterns tend to repeat themselves. If a particular type of weather occurred once, it will occur again. The creation of an analog forecast requires:

1. Analyses of the conditions surrounding all similar past weather events.
2. Documented weather patterns common to all these similar events. This documentation defines the conditions necessary for this weather event to occur again.
3. When the current conditions indicate patterns similar to these past events, a forecast can be made based on what happened previously.

An example of an analog forecast approach is the tornado vortex signature (TVS) examined in Chapter 9. As Doppler weather radar data became available, the velocity fields were analyzed for when tornadoes occurred. These analyses noted a common pattern of adjacent radial velocities going the opposite directions prior to a tornado being observed. This information was documented for others to use. Now when a pattern of adjacent radial velocities is present, issuing a tornado warning may be warranted based on this analog forecast methodology.

The last forecast method to examine is numerical weather prediction, and is also referred to as numerical weather forecast. The study of the atmosphere is a physical science. Many of the physical sciences lend themselves to being described with mathematical equations. These equations represent the behavior of the system being studied, and can be placed in a computer program. **Numerical weather prediction** is the use of computers to model the atmosphere, and predict how atmospheric motions change with time.

Numerical weather prediction is closely linked to the state of science and the state of computer technology. As the understanding of the atmosphere increases, this new knowledge can be integrated into the computer model. As computer technology advances, the ability to run more sophisticated and larger weather models is made possible. Weather computer models are run on some of the fastest computers in the world, and an improvement in computer technology automatically leads to an improvement in weather forecasts. Today, numerical weather prediction is the dominant method used to create weather forecasts, because it is the most accurate. The photo in Figure 10-21 shows the supercomputer used to produce the National Weather Service forecast models.

Figure 10-21: A photograph of the NOAA Weather and Climate Operational Supercomputing System.

These forecast methodologies are not independent of each and can be combined. An example of this approach is called Model Output Statistics (MOS). MOS is a type of statistical post-processing of numerical weather model output. This statistical processing considers the climatology, past observations, and other details of a location to improve on the weather model forecast. MOS forecasts are available for specific cities as tables of data or graphs, and as maps for larger areas. MOS products are fully automated without oversight from a human forecaster. An example of a MOS forecast for Tucson, Arizona is given in Figure 10-22 in both a tabular and graphical format.

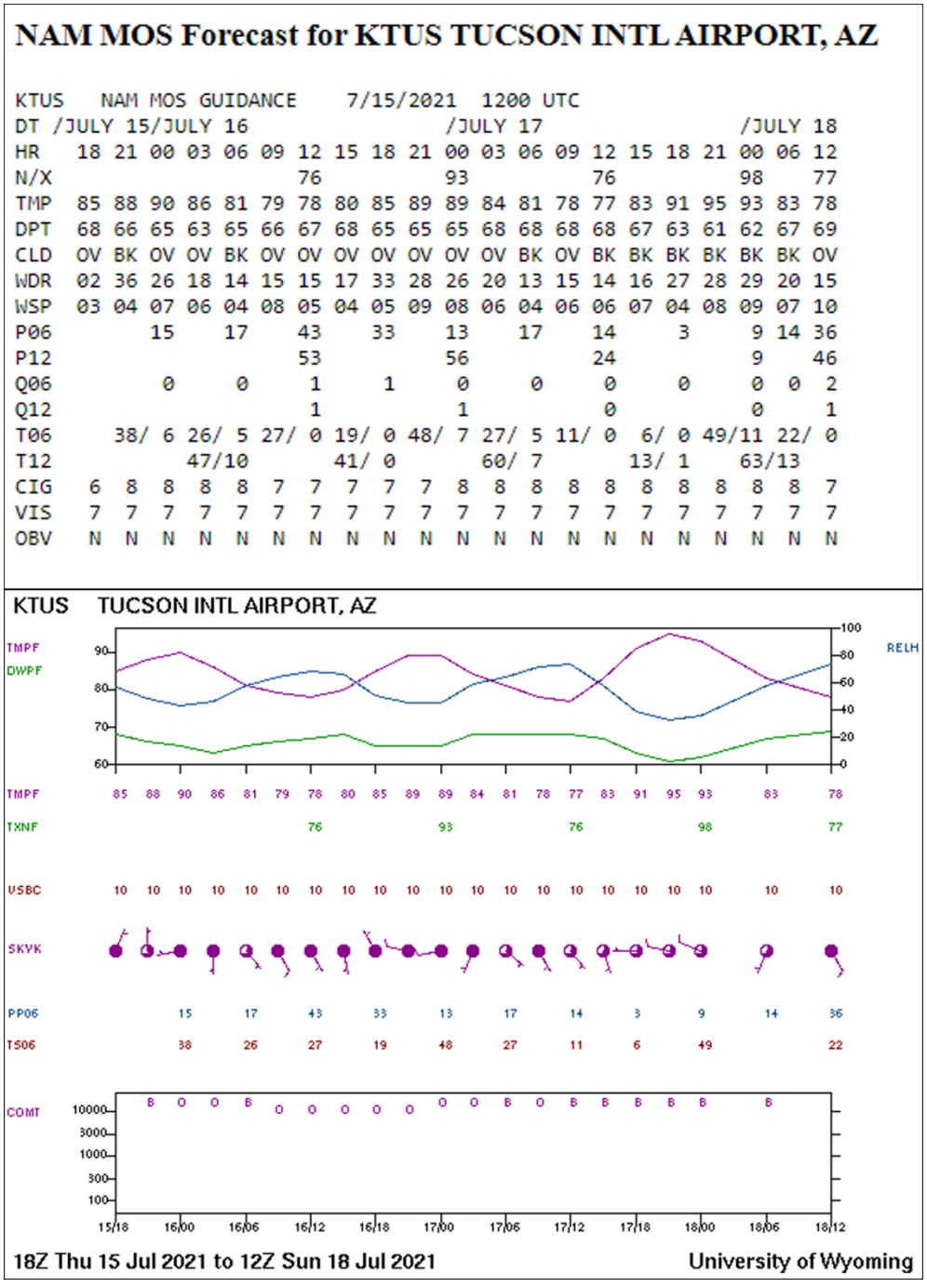

Figure 10-22: Model Output Statistics (MOS) for Tucson Arizona. The top is a tabular format; the bottom is a graphical format.

10.2.2 – More Details on Numerical Weather Prediction

There are two basic sizes of weather models, global (covering the entire Earth) and regional (covering part of the Earth). The area represented inside the model is also referred to as the model domain. Each of these models utilizes a grid system where forecast points are laid out in

a grid over the area they cover. The distance between the centers of these grids, called grid points, vary with scale and design of the model. Naturally, the more grid points there are in a model, the finer the resulting details in the forecast. However, as the number of grid points increases, so does the need for more computing power. For example, a forecast for 6 x 6 grid (36 forecast points) needs four times the computing time as a 3 x 3 grid (9 forecast points) even though the actual physical area remains the same. Forecast precision improves at the cost of four times the number of calculations to produce a forecast for the same physical area. Figure 10-23 illustrates these forecast resolutions and computing resource principles.

Regardless of the grid size, all models must know the initial conditions to begin the computations for making a forecast. A variety of weather data is input into the model from weather balloons, satellites, surface observations over land and sea as well as information from commercial aircraft in a process called initialization. (Figure 10-24, #1)

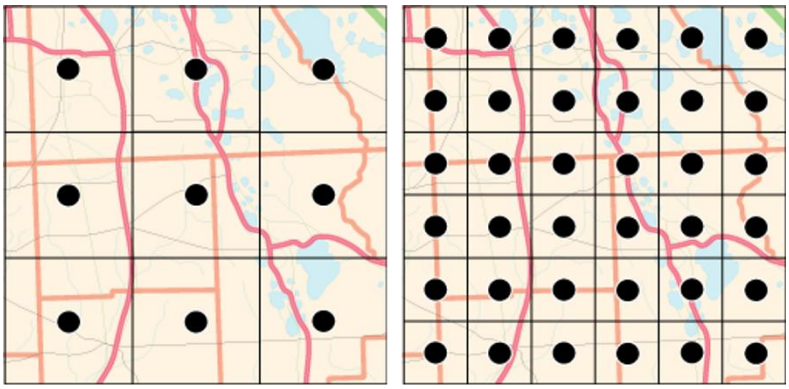

Figure 10-23: Diagrams illustrating that 9 forecast points are present in the 3 x 3 grid and 36 forecast points are in a 6 x 6 grid, although the same area is covered in each forecast grid. A finer grid resolution significantly increases the computing time for a numerical forecast.

Upon the input of this initial data, the computer uses mathematical equations to calculate a future state of the atmosphere in a 'time step'. Depending upon the type of model and aerial coverage, a time step interval can be as short as a few seconds or as long as several minutes. (Figure 10-24, #2)

The resulting state of the atmosphere at the end of the time step (Figure 10-24, #3) then becomes the 'new' initialization input for a repeat of the calculations (Figure 10-24, #4). This output (Figure 10-24, #5) then loops around again for another future state of the atmosphere.

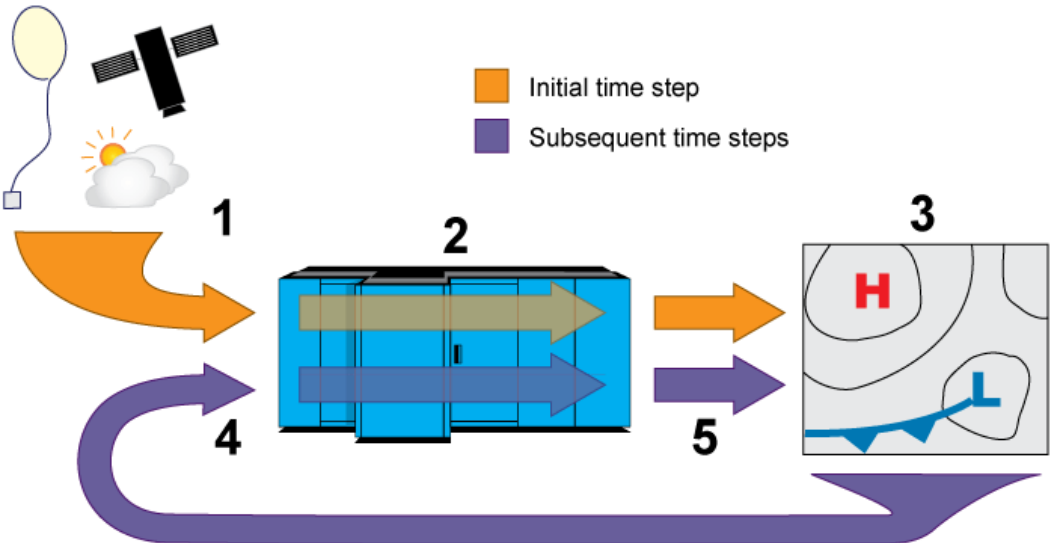

Figure 10-24: Steps in creating a numerical weather forecast. (1) initialization, (2) run the model, (3) get a new state of the atmosphere, (4) and (5) repeat the model run multiple times with the new atmospheric state to go further out in time.

This process, the result of the previous time step becoming the initial input for the next time step, repeats itself until the end of the model run. The length of a time step greatly affects model accuracy.

Smaller time step intervals produce more accurate forecasts as there is less variation in output at the end of each computation. Unfortunately, the cost is that smaller time steps require more computations. Conversely, large time step intervals require less computation time, but introduce larger variations in output.

Therefore, a tradeoff exists between time step interval lengths and grid sizes versus computational power. Supercomputers are used for the trillions of computations needed to produce weather models. A global forecast model makes over 10 quadrillion (10 with 16 zeros) calculations for a complete model forecast and takes about two hours to complete.

All computer weather models have three phases in their execution:

- **Analysis and initialization** – Observations are analyzed and used to create the initial state of the atmosphere for the model. This data assimilation step ensures the observations will not make the model numerical unstable.
- **Prediction** – The computer model is run forward in time.
- **Post-processing** – Data internal to the computer model is processed into graphs and charts suitable for people to view and use.

Every numerical weather model has these three phases. Amazingly the last phase, post-processing, usually takes the longest to run. Internally the equations and coordinate systems used in the initialization and prediction steps are optimized for rapid execution on a supercomputer.

The post-processing produces charts, graphs and tables of data for whatever a person wants to know. Figure 10-25 is an example of the model output, and is a 24 hour forecast for 500mb heights, winds, and relative humidity.

Due to the need for expensive computing resources to execute these numerical prediction models, countries centralize their efforts to minimize cost. The United States' model are developed and run by the National Center for Environmental Prediction (NCEP), which is a branch of the National Weather Service. The European Union, Canada, United Kingdom and China have all taken this approach. Through international agreements, much of the data from these models is shared with other countries.

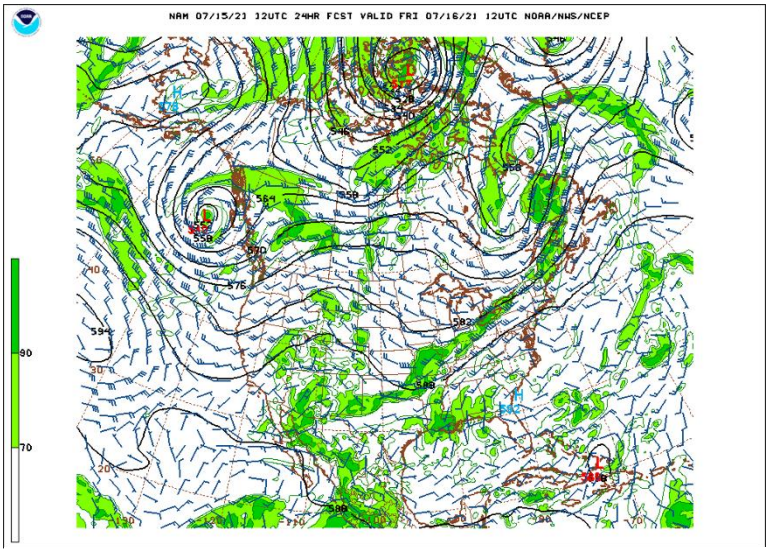

Figure 10-25: A 24 hour forecast for 500 mb heights, winds, and relative humidity (green shading).

10.2.3 – Ensemble Forecasts

All numerical weather prediction forecasts decrease in accuracy the further they go out in time. At some point in the future, say 10 days, a numerical model forecast is less accurate than a low skill forecast method like a climatological forecast. This type of behavior is a result of a property of the atmosphere called chaos. **Chaos** describes a physical system that exhibits erratic behavior such that very small changes in the initial state can lead to unpredictable changes in a future state.

Chaos exists in the atmosphere partially because its initial state cannot be fully observed at any one time. Due to the vastness of the atmosphere, small errors are always present in any data describing its state. These errors amplify with time and the accuracy of the forecast diminishes. Hence, all weather forecasts have some uncertainty associated with them. A method for dealing with this uncertainty is called ensemble forecasts. **Ensemble forecasts** are a collection of different computer model forecasts all valid at the same time. Meteorologists use two basic types of ensembles based on:

- Many different computer models (each with their own unique flaws)
- Many runs of one computer model started with slightly different initialization data.

The ensemble forecasts that meteorologists use fall into one of these two categories, or a combination of the two. Having access to ensemble forecasts from computer models essentially gives forecasters many looks at different possibilities for an upcoming weather situation. If the advantages of seeing many possibilities does not make sense to you initially, imagine you are competing in an archery contest. Would you rather shoot one arrow at a target (Figure 10-26) or increase your chances of hitting the bull's eye by shooting a quiver full of arrows?

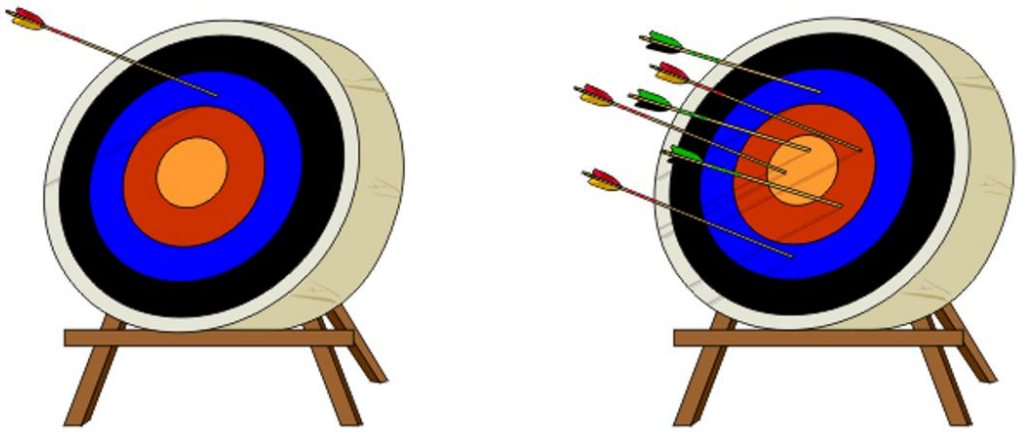

Figure 10-26: The left target with one arrow is analogous to a single numerical model solution. The right target is an ensemble solution with many possibilities. Notice the right one has two arrows in the center.

Having access to only one computer model forecast is like an archery contest that allows a forecaster only one shot at the target. Using the archery contest analogy, an ensemble of forecasts allows a forecaster to shoot a quiver full of arrows at the same target. For a pending forecast fraught with uncertainty, utilizing ensembles gives forecasters a better chance of hitting the target. Ensemble forecasts show meteorologists the probability of various forecast events

happening; essentially a forecast has the bounds of its uncertainty defined. Properly developed ensemble forecasts will have one of its members verify as to what actually occurred.

One method to view ensemble forecasts is to plot all the solutions on one map. These maps have many lines and are referred to as a spaghetti plot or spaghetti diagram. The left side of Figure 10-27 is a 120 hour ensemble forecast for 500 mb heights. This forecast was for 5 days (120 hours) into the future when it was created. Two 500 mb height values are plotted from each member of the ensemble, 5820 meters and 5940 meters. The more uncertain a forecast, the larger variation in the solutions plotted. In a sense, the spaghetti is spread over a larger area. The number of lines across the Atlantic Ocean in this figure illustrates the forecasts in that area have a high degree of uncertainty.

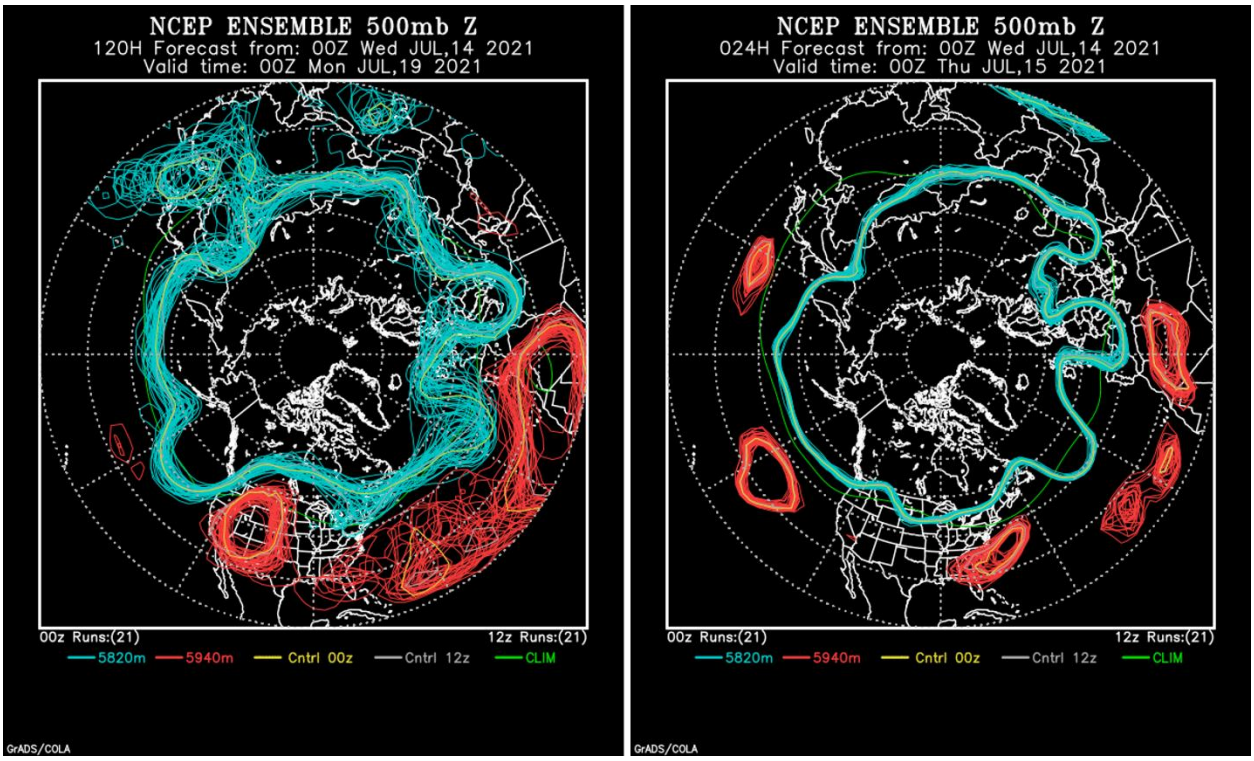

Figure 10-27: (left) A 120 hour ensemble forecast for 500 mb heights at 5820m and5940m. The large variation in height lines over the Atlantic Ocean indicates a high degree of uncertainty. (right) A similar ensemble forecast for 24 hours. The closeness of the height lines indicates less uncertainty.

Comparing a 120 hour to a 24 hour forecast on the right side of Figure 10-27 shows a substantial reduction in the uncertainty. Notice how all the solutions are close to each other in the 24 hour forecast. This characteristic emphasizes that shorter-term forecasts have less uncertainty than longer-term ones.

10.2.4 – Forecast Types, Value, and Accuracy

Several different types of forecasts are always available to a person. These types can be divided into three groups: (1) quantitative, (2) qualitative, and (3) probabilistic. Figure 10-28 provides an example from the National Weather Service on these groups.

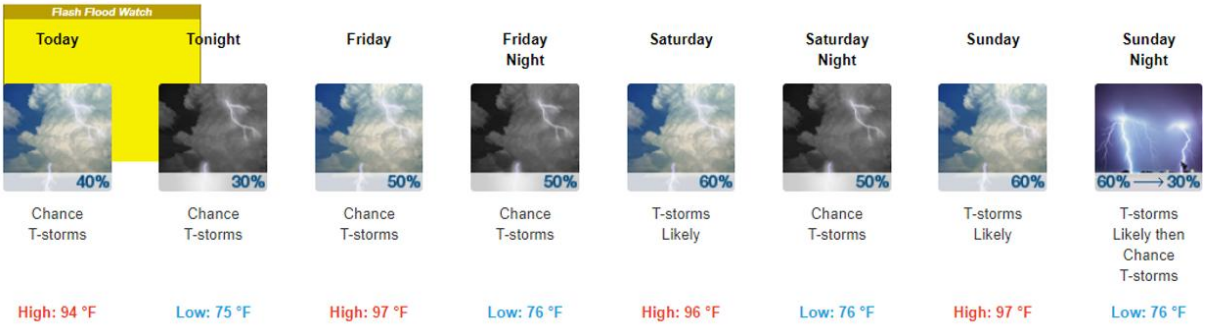

Figure 10-28: Examples of the type of forecast groups. A quantitative forecast is the high and low temperatures for each day. A qualitative forecast is the weather icon associated with each day. A probabilistic forecast is the probability of precipitation number at the bottom of the icons.

In this example, the quantitative forecast would be the exact high and low temperatures forecast for each day and night. The qualitative forecast would be the icons with clouds and lightning (a thunderstorm). The probabilistic forecast would be the number and percentage sign in the bottom left corner of each icon, which is the probability of precipitation occurring. This probabilistic forecast is linked to the text "Chance of T-storms". Notice when the probability is 60% the text changes to "T-storms likely". If precipitation occurs it will come from a thunderstorm. Additionally, a probability of precipitation at 60% implies the probability of no precipitation is at 40%, or 4 out of 10 times an area will stay dry.

Over the "Today" and "Tonight" periods resides a yellow banner with the title "Flash Flood Watch". This banner indicates the National Weather Service has issued a Flash Flood Watch for the location associated with this forecast. Following the watch and warning criteria, a watch means conditions are suitable for flooding to occur over this time period. Even though the probability of precipitation is 40% and 30% during these time periods, conditions are such that the precipitation could cause flooding. Therefore, a person should be aware of possible flooding associated with the thunderstorms as they go about their daily activities.

The value of a weather forecast is determined by how a person uses it. Most people look at a forecast to determine what to wear, or if an umbrella is needed. Depending on a person's activities, the two most valuable pieces of information in the Figure 10-28 example may be the Flash Flood Watch and the forecast of thunderstorms. Being aware that flooding or lightning is forecast could save a person's life.

Every weather forecast has some errors in it. The size of the error can be determined by comparing what occurred to what was forecast. A simple subtraction of the two values will tell exactly the magnitude of the error present. For example, if 94°F was forecast and 96°F was observed the forecast error was 2°F. Overall, most high and low temperature forecasts are reasonably accurate with errors of less than 3 degrees. On the other side of accuracy are precipitation forecasts. Quantitative precipitation forecasts are difficult to make. The computer models have difficulty representing cloud physics and moisture fields. With time the models have improved in making precipitation forecasts; however, these improvements are much less than other weather parameters. Hence, precipitation forecasts are generally expressed in probabilities of it occurring. This approach provides the highest quality information while not misleading people.

Forecast verification data indicate that having a person involved in the forecast process tends to improve the accuracy of the forecast. Many forecasts can be automated by directly using the output from a computer model. Forecasts that provide minute by minute values are definitely automated. When a person is involved in the forecast process, they have the ability to recognize when errors are present and make corrections. Where you get a weather forecast matters and you have many options. If you are getting a forecast from television, the National Weather Service or a major private weather company, chances are the forecast had a person involved in the process.

Determining exactly how a forecast was created can be difficult. If you are not sure exactly where the forecast originated or how it was assembled, keep these thoughts in mind:

- Forecasts with some human input tend to generally be more accurate.
- Forecasts which provide an icon or a couple of pieces of information to describe the weather for a day have omitted a lot of details.
- Forecasts with highly specific details at longer time ranges into the future should be regarded with skepticism. (Remember forecast accuracy decreases further out in time.)

10.2.5 – Seasonal Outlooks

After about 10 days, a numerical weather model has less than a 50% chance of being accurate. The errors internal in the model have amplified enough that the output has little value. This situation implies that a seasonal outlook needs different tools for its creation. Additionally, seasonal outlooks will only be able to provide a couple of parameters like temperature and precipitation. Outlooks for other weather parameters are low quality and not as useful. Seasonal outlooks use a three month period of time as defined below:

- Winter – December, January, and February (DJF)
- Spring – March, April, and May (MAM)
- Summer – June, July, and August (JJA)
- Fall – September, October, and November (SON)

These long-term outlooks use a dynamic and statistical approach. The dynamic approach uses math equations much like numerical weather prediction. However, a climate-oriented dynamic approach focuses more on energy balance and long-term global patterns rather than day-to-day variations in the weather. A statistical approach analyzes global anomaly patterns in temperature, wind, height, etc. to anticipate the global patterns for an upcoming season. With a significant amount of research focusing on climate change, a dynamic approach to a seasonal outlook is becoming more important as the statistic approach diminishes.

The forecasts for a seasonal outlook are expressed as probabilities of what will be observed. Three classes of probability are available for an outlook either (1) above normal, (2) near normal or (3) below normal. As one class of probability goes up or down, the others must be adjusted accordingly. If all classes of probability are equal, the outlook area is labeled as equal chances.

These classes of probability can be thought of as three piles of objects. The total objects in all three piles is always 100 (100%). A normal or median value for a pile is 33.3%. If an object is taken out of one pile, it must be added to another pile. No pile can have all of its objects removed, and the lowest value a pile can go to is 3.3%. No probability in any of the classes can ever go to 0%.

Figures 10-29 through 10-31 illustrate the three classes (piles) for equal chances, 30% above normal, and 50% above normal. The median or normal value for all classes starts at 33.3%. In other words, each class has an equal chance of occurring as shown in Figure 10-29.

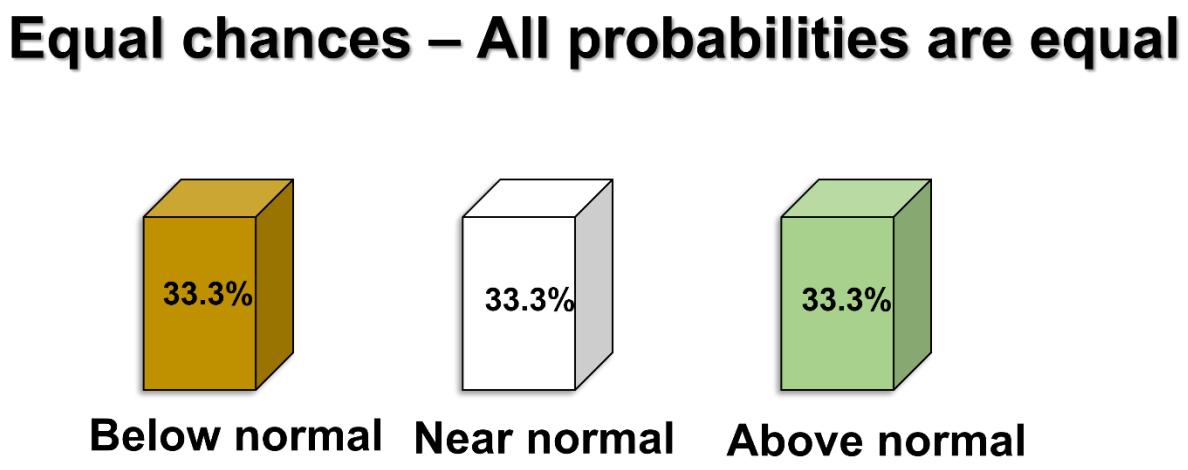

Figure 10-29: Equal chances in that all classes (below normal, near normal, and above normal) are all at 33.3%.

When a class has a 30% greater than normal of occurring, this implies that this class will be 30% over its median of 33.3%. Figure 10-30 illustrates this concept with the above normal class having a 63.3% of occurring whereas the below normal drops to 3.3%. Notice all classes still sum up to 100.

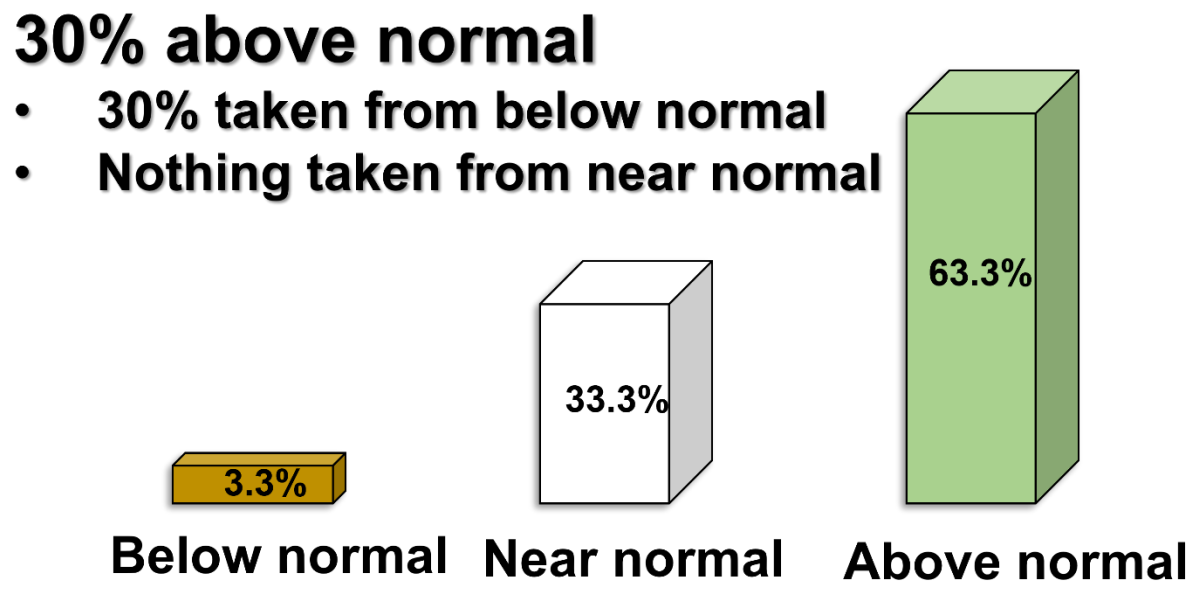

Figure 10-30: The above normal class is 30% above normal and has a 63.3% probability of occurring. This situation reduces the below normal class to 3.3% and the near normal class stays the same.

The 50% above normal example implies that the above normal class will be 50% over its median (normal) of 33.3%. Hence, the above normal class has an 83.3% of occurring whereas the below normal drops to 3.3% and the near normal to 13.3% as shown in Figure 10-31. The highest any class can go is 60% above its median (normal) or 93.3%.

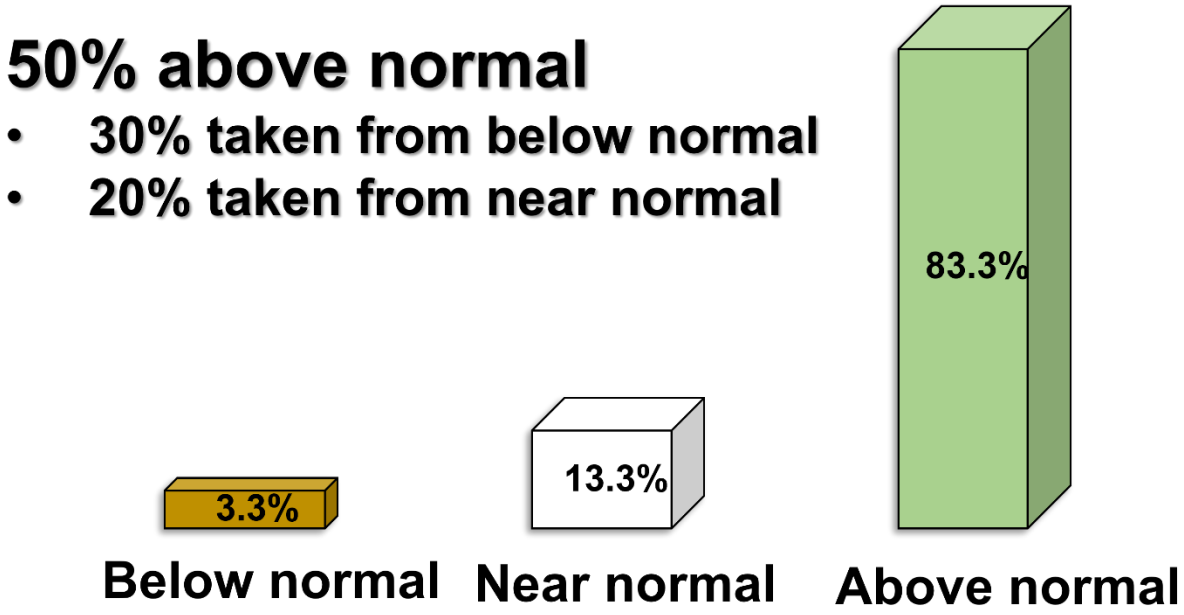

Figure 10-31: The above normal class is 50% above normal and has a 83.3% probability of occurring. This situation reduces the below normal class to 3.3% and the near normal class to 10.3%.

These seasonal outlooks are distributed in a map format. Figure 10-32 contains a winter outlook (DJF) for temperature and precipitation. If you think this approach is rather confusing, most people will likely agree with you. Most people just look at the map and see an above or below normal for their area, and not do the calculations as shown in the above examples.

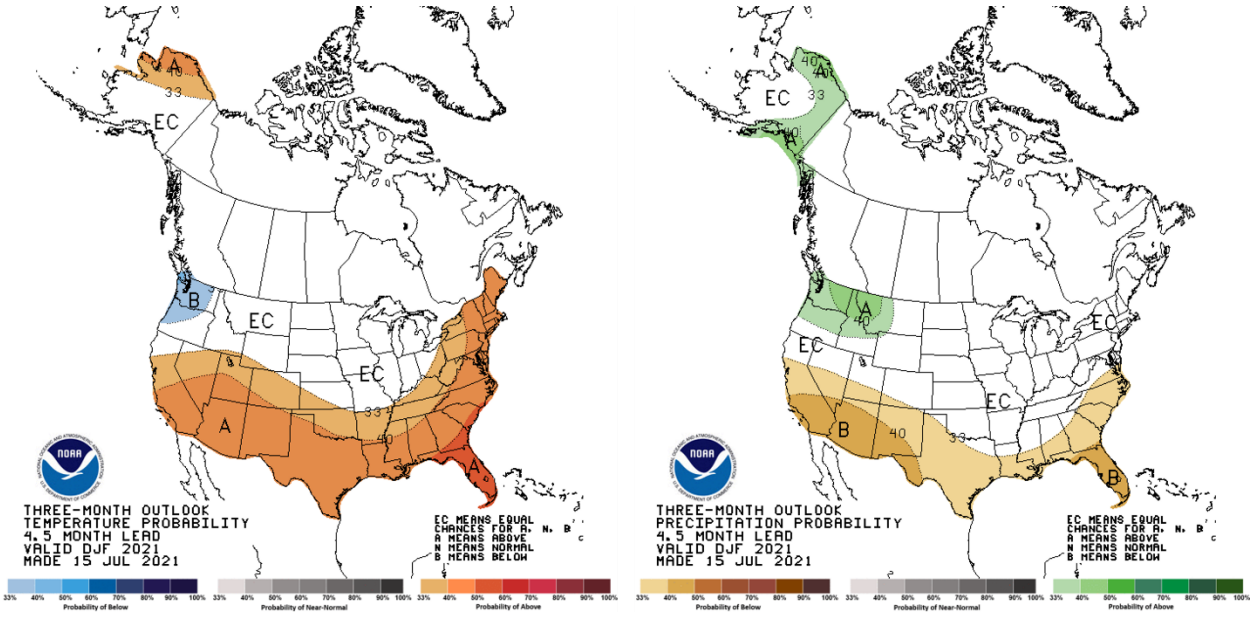

Figure 10-32: A winter outlook for December, January, and February (DJF). The left side is temperature and the right is precipitation.

Chapter 10 Review Questions

1. What is the atmospheric phenomenon that occurs when hot air resides near the ground?
2. Which two behaviors of light cause a rainbow?
3. What is the slight bending of light called as it passes around an object?
4. Where is the Sun when a person sees a rainbow?
5. What atmospheric optical phenomena **<u>are</u>** present in this photo?

6. What atmospheric optical phenomena is occurring in this photo?

7. What two atmospheric optical phenomena occur as a result of diffraction?
8. What is the dark band between a primary and secondary rainbow called?
9. Which forecast methodology predicts rain in April because it has rained every day in past Aprils?
10. Why was numerical weather prediction not used 100 years ago?
11. Which forecast methodology predicts a high temperature of 91 degrees tomorrow because yesterday's high temperature was 91 degrees?
12. What is the numerical weather prediction phase where observations are used to create an initial state of the atmosphere?
13. What is the forecast methodology based on the idea that weather patterns tend to repeat themselves?
14. Why would a weather forecaster use ensemble forecasts?
15. Why are numerical weather prediction models not used to create a seasonal outlook?

Chapter 11 – Earth's Climates

Overview

This chapter starts by exploring the factors that influence temperatures across the globe. Temperature and precipitation are important variables when examining climate classification. Thus, factors that influence temperature also influence climate. Since weather during the day affects the high and low temperatures for that day, we will also examine how weather affects these daily temperatures.

The remaining chapters in this book explore climate and its variability. Before all these climate topics are examined, an important topic to understand is the variables defining a climate, and the classification of different climates. The Köppen-Geiger climate classification system is widely used across the globe and is described in this chapter. Climate by its nature requires a lot of data and analyses. Therefore, this chapter has a lot of graphs and maps.

Chapter Objectives:

1. List the geographic factors that influence temperatures.
2. Describe the effects of weather on high and low temperatures.
3. Identify the main climate groups in the Köppen-Geiger classification system.
4. Identify characteristics associated with a climate group and its subgroups.

11.1 – Temperature and Climate

Climate is the long-term average of daily weather. Another way to look at climate is the statistical properties of the atmosphere-Earth system. Initially the view of climate science was simply the long-term averages of surface observations like temperature and precipitation. As climate science matured, the emphasis shifted to the underlying processes that determine climate and its variability.

The definition of "long-term" for climate is usually 30 years of data or more. The United States uses the 30-year definition with updates every 10 years. For example, a climate normal is defined as data from the years 1990 through 2020. After all the data for the year 2030 is available, the new climate normal will be for the years 2000 through 2030. Every 10 years the average climate values for a location are updated.

Many methods are available to classify regions of the Earth into similar climate zones. Most of these methods are based partially or totally on observed values of temperature and precipitation. Unfortunately, the Earth's surface observation network does not cover every square kilometer of the Earth. Fortunately, vegetation covers most of the Earth's surface, and types of vegetation are influenced by temperature and precipitation. Therefore, weather observation data can be combined with vegetation information to create a robust climate classification system.

Wladimir Köppen (1846-1940), a German climatologist and amateur botanist, divided the world's climates into categories based upon general temperature profiles related to latitude. He

worked with Rudolf Geiger (1891-1981) to modify these categories, which is known today as the Köppen-Geiger climate classification system. An example of their climate classification system for North America is given in Figure 11-1.

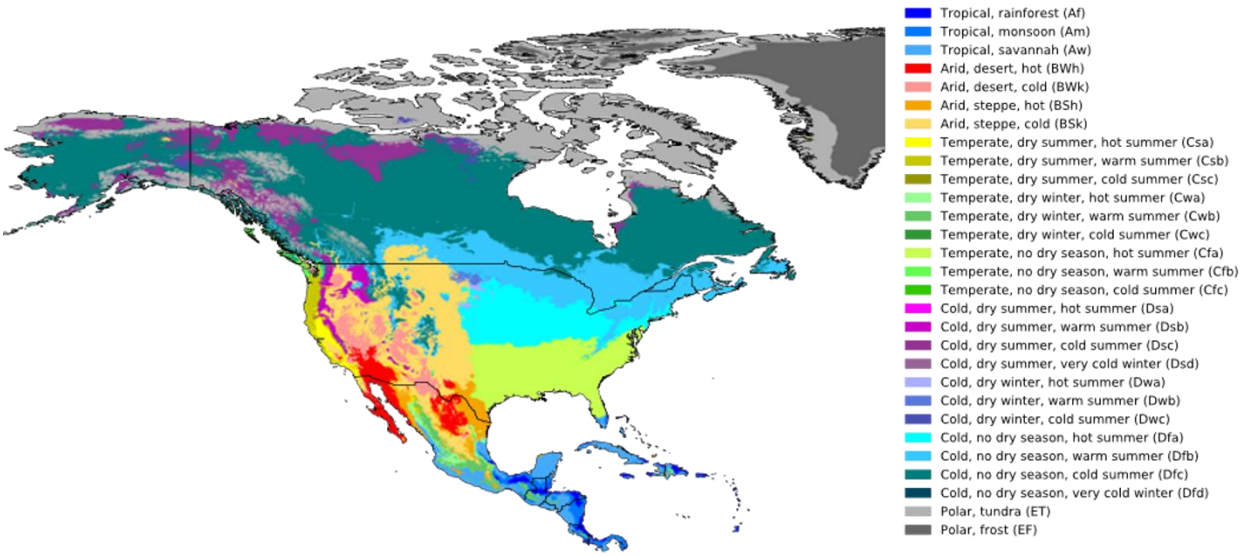

Figure 11-1: A map of the Köppen-Geiger climate classification for North America.

Since temperature is inherent in climate classification systems, examining the influences on temperature across the globe will provide insights on what influences climate. Geographic factors which affect temperature are:

- latitude
- elevation
- global atmospheric circulation patterns
- proximity to an ocean or an interior land location
- ocean circulation patterns

Together, these factors control the range of temperatures and the amount of rain and snow each region receives throughout the year. In other words, these factors control climate, and in turn, climate controls ecology—the types of native plants (flora) and animals (fauna) that live in a region.

11.1.1 – Latitude

The amount of solar radiation received at a location is determined by its latitude. Locations at lower latitudes in the tropics receive about 12 hours of sunshine every day of the year. Locations at higher latitudes vary from no sunshine in the winter to 24 hours in the summer. The Sun angle is always higher at low latitudes, which means the intensity of solar radiation is stronger at lower latitudes than at higher ones. The amount of solar radiation received at a location directly relates to its average annual temperature. Figure 11-2 depicts the annual average temperatures across the globe, and as such depicts the variation in solar radiation due to latitude. As you can see, the tropics are warm and the higher latitudes are cold. The ice

sheets on Greenland and Antarctica are the coldest. These temperatures are directly related to the amount of solar radiation received. Thus, a major factor in climate classification is latitude.

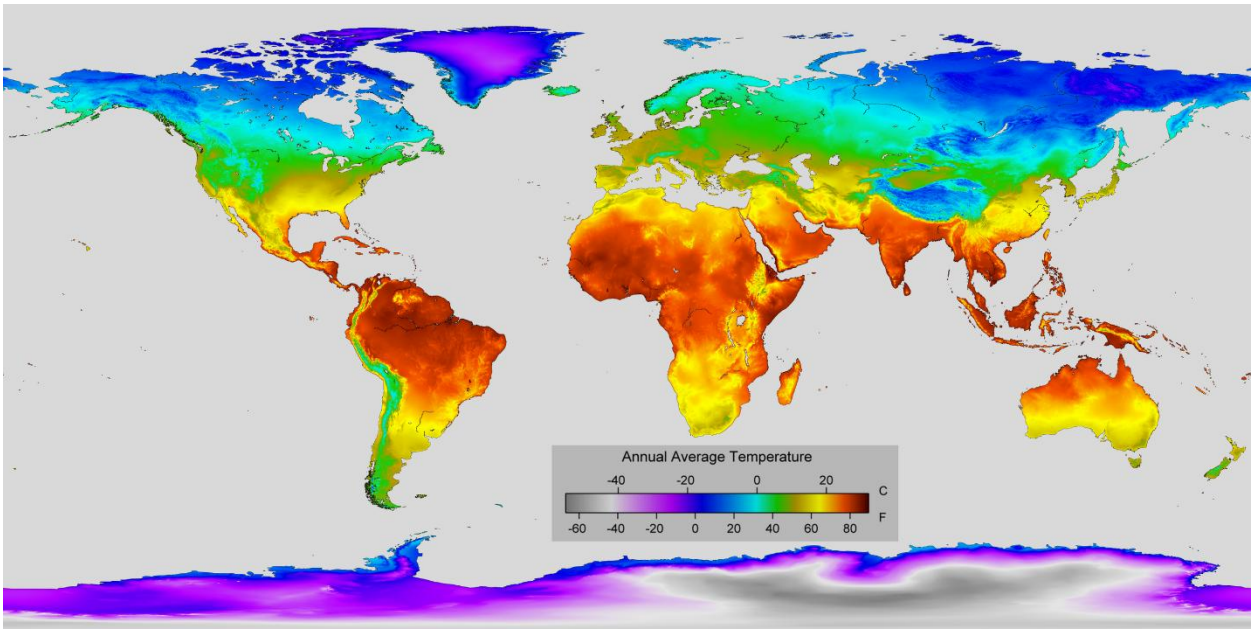

Figure 11-2: A global map depicting the annual average temperature. Temperature at a location is directly related to the latitude of that location.

Since the amount of solar radiation received at higher latitudes varies considerably from winter to summer, the seasonal temperature variation at these higher latitudes should have the largest range. Figure 11-3 depicts the average seasonal temperature range across the globe. As you can see, temperature ranges across northern Canada and Russia are the greatest. The Southern Hemisphere has little land mass at higher latitudes, other than Antarctica, and lacks these large seasonal variations. The tropics have consistent solar radiation throughout the year, and subsequently lack seasonal temperature variations too.

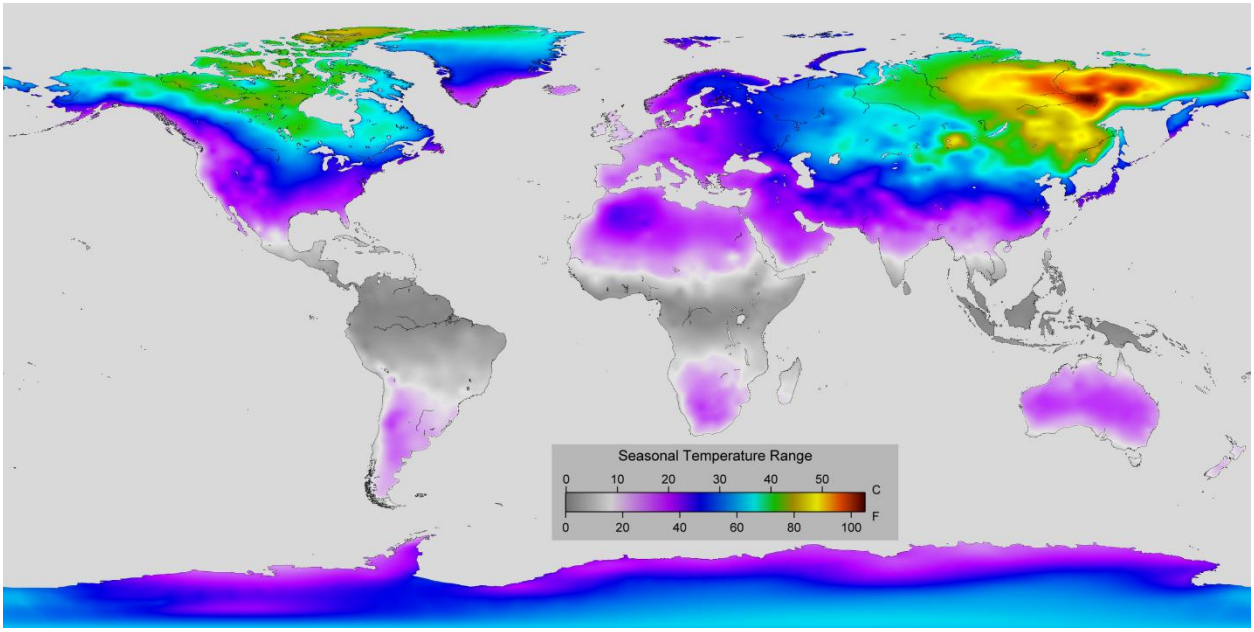

Figure 11-3: A global map of the average seasonal temperature range over a year.

11.1.2 – Elevation

In the troposphere, we know that higher altitudes generally have cooler temperatures; temperatures decrease with height. This temperature profile occurs because the Sun heats the surface which in turn transfers heat to the atmosphere. The air mixes in the troposphere to transfer this heat upward, but the warmest air will always be closest to the surface. The atmosphere captures this heat from the surface before it is radiated to space. Lower elevations have higher air pressure and more air molecules (denser atmosphere) than higher elevations. This variation in density enables lower elevations to capture and retain more heat than higher elevations. In other words, valleys (lower elevations) are warmer than nearby mountains (higher elevations). Figure 11-4 illustrates these elevation differences in heat transfer and retention.

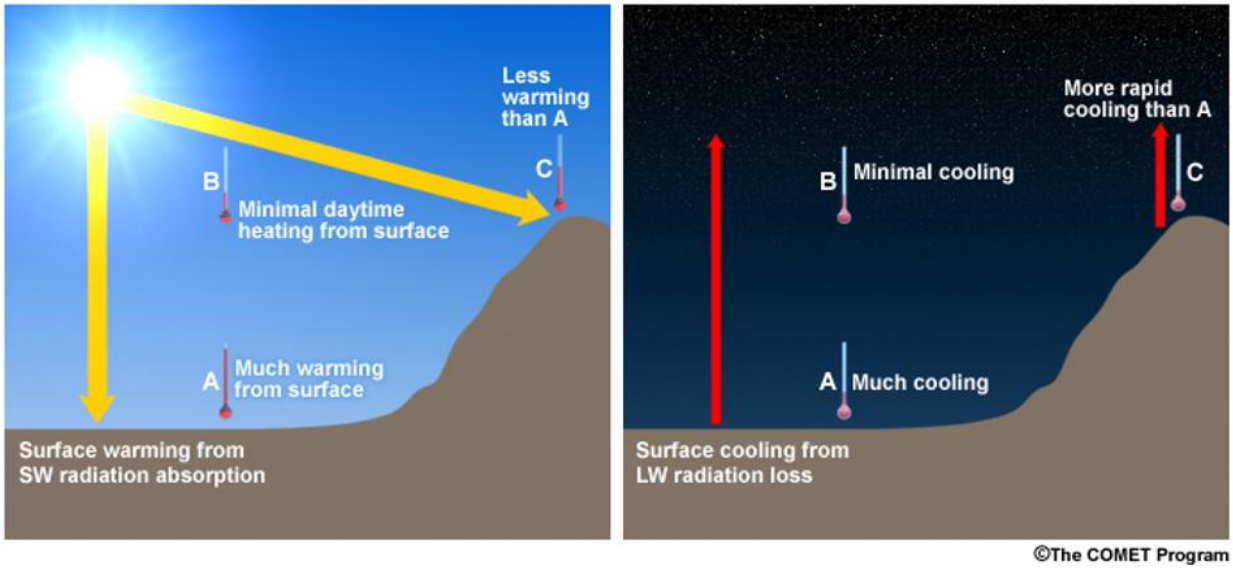

Figure 11-4: A diagram with three thermometers. "A" is located in a valley. "B" and "C" are located at 10,000 feet. "C" is on a mountain whereas "B" is suspended in the atmosphere. The amount of atmosphere and the proximity to the surface determines the temperature variations at these locations over 24 hours.

Figure 11-4 has three thermometers. Location A is in a valley. Locations B and C are at 10,000 feet. While locations B and C are at the same height, location C is near the mountain surface whereas location B is suspended in the atmosphere. The two locations A and B near the surface warm during the day due to surface heating. However, location C is not able to retain the surface heating as much as location A. Mountain location C has less atmosphere surrounding it, and is unable to capture as much heat as location A. Since Location B is not near the surface, the change in temperature at this location is minimal during the day.

At night, the surface emits longwave radiation (heat) to space. Hence, both locations on the surface (A and C) have significant cooling. Again, since the mountain location has less atmosphere to capture heat, it cools rapidly after the Sun sets. If you have been at a higher elevation after sunset, you have likely noticed the air rapidly gets a chill to it. Location A in the valley cools too, but the denser atmosphere at the lower elevation delays this heat from radiating directly to space. Location B has minimal cooling because it is further from the surface where most of the cooling is occurring.

This mountain/valley example illustrates vastly different diurnal temperature variations due to elevations. Likewise, these temperature differences lead to a different climate and different vegetation at mountain versus valley locations.

11.1.3 – Global Atmospheric Circulation Pattern

The global atmospheric circulation pattern refers to the three-cell circulation model previously explored in Chapter 6. Figure 11-5 provides a short review of this model.

The Hadley cell consists of year-round warm tropical air and the inter-tropical convergence zone (ITCZ). This circulation cell greatly influences the climates found in the tropical latitudes. The season variation of the ITCZ location has a tremendous impact on the annual precipitation distribution across southern Asia and Africa.

The subtropical high pressure near 25° latitude creates the hottest temperature areas on the globe. These hot and dry conditions of the global circulation in turn create the dry, desert climates.

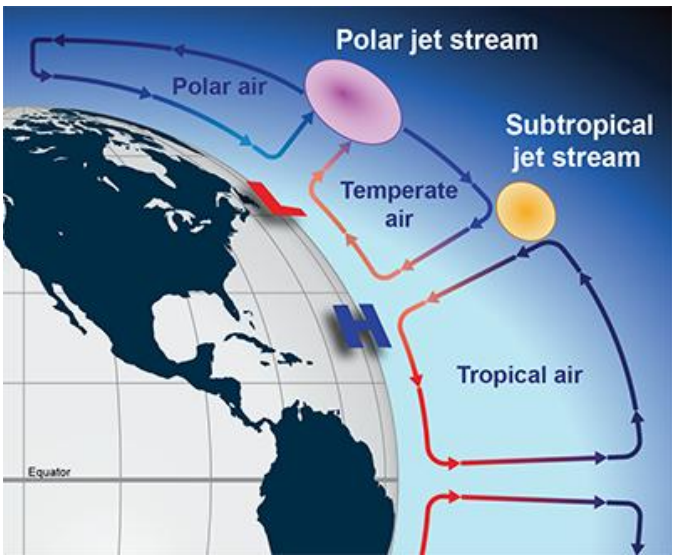

Figure 11-5: An illustration of the three-cell global circulation model.

The polar cell keeps the temperatures at higher latitudes cold year-round. These global circulations affect the temperature and precipitation over large areas, and interact with the other geographic climate factors.

11.1.4 – Proximity to an Ocean or an Interior Land Location

Locations near large bodies of water have their temperatures moderated by the water. This environment near an ocean is referred to as a marine environment. A marine environment reduces the temperature range because:

1. Solar radiation received on water can penetrate tens of meters, whereas the same radiation received on land rapidly warms the upper layer of soil.
2. Water allows the easy mixing of heat to other regions.
3. Any warming of the water surface is considerably reduced by evaporation.
4. The specific heat of water is about five times that of land, so any temperature change occurs slowly.

These moderate temperatures throughout the year make coastal areas a favorite location for people to live. Many of the largest cities in the world reside near an ocean which moderates both the high and low temperatures. The temperature variations between the seasons is reduced, and temperature ranges remain consistent throughout the year.

The opposite of a location near an ocean is a location in the middle of a continent. Continental locations have a much larger temperature range. Diurnal and seasonal temperature variations

are much greater. Winter temperatures are colder and summer temperatures are warmer. This effect of a large land mass is called continentality. Continentality causes a larger seasonal temperature range, which is the exact opposite of a marine environment.

Two climographs in Figure 11-6 illustrate the marine and continental influences on temperature. A **climograph** is a graph of average temperature and precipitation values throughout the year. The climographs used in this textbook will have temperature as a red line, and precipitation as the blue bar graphs. The temperature scale is on the left side of the graph in degrees Celsius. The precipitation scale is on the right side of the graph in millimeters. Every month for the year is labeled at the bottom of the graph. All the values on a climograph are average monthly values.

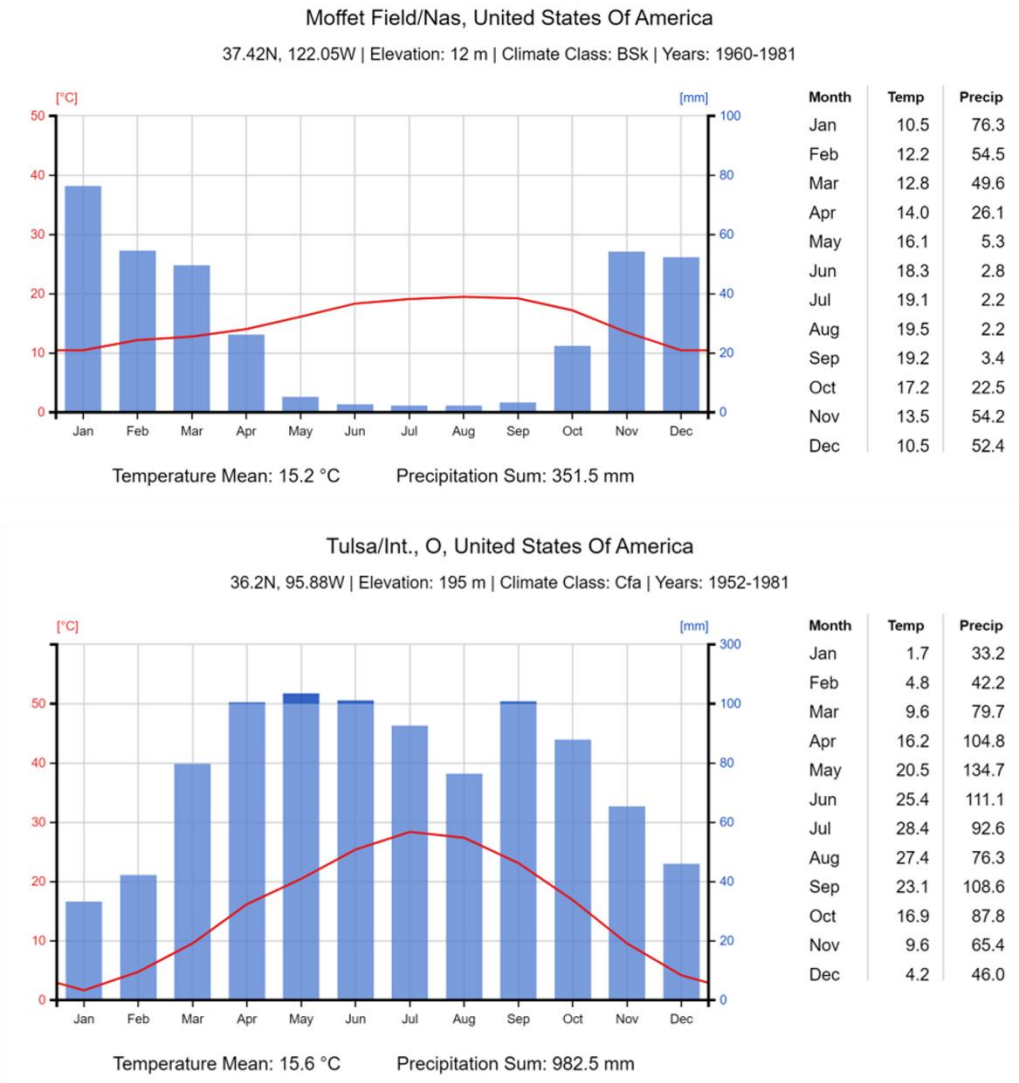

Month	Temp	Precip
Jan	10.5	76.3
Feb	12.2	54.5
Mar	12.8	49.6
Apr	14.0	26.1
May	16.1	5.3
Jun	18.3	2.8
Jul	19.1	2.2
Aug	19.5	2.2
Sep	19.2	3.4
Oct	17.2	22.5
Nov	13.5	54.2
Dec	10.5	52.4

Month	Temp	Precip
Jan	1.7	33.2
Feb	4.8	42.2
Mar	9.6	79.7
Apr	16.2	104.8
May	20.5	134.7
Jun	25.4	111.1
Jul	28.4	92.6
Aug	27.4	76.3
Sep	23.1	108.6
Oct	16.9	87.8
Nov	9.6	65.4
Dec	4.2	46.0

Figure 11-6: Two climographs with average temperature (red line) and precipitation (blue bars). The top is Moffet Field near San Francisco, CA and the bottom is Tulsa, Oklahoma. Both sites are at a similar latitude, although one is near an ocean (top) and the other is in the center of the U.S. (bottom).

Moffet Field (top of Figure 11-6) is near San Francisco and is heavily influenced by the nearby Pacific Ocean and San Francisco Bay. Notice the variation in average temperature is only 9°C

throughout the year. Tulsa, Oklahoma is a location in the middle of the continent (bottom of Figure 11-6). The annual temperature variation at Tulsa is about 25°C or almost three times what is observed near San Francisco. Both locations are at similar latitudes and elevations. The main difference is the influence of the marine environment as compared to an interior continental location.

11.1.5 – Ocean Circulation Patterns

The eastern side of a continent is influenced by warmer ocean currents than the western side. This warmer water originates from the topics and travels up the east side of the continents. The cooler water on the west side of the continents originates from the polar regions. The global map in Figure 11-7 depicts the major surface ocean currents. The warmer currents are in red. The cooler currents are blue. Notice the origin of the warm and cold currents.

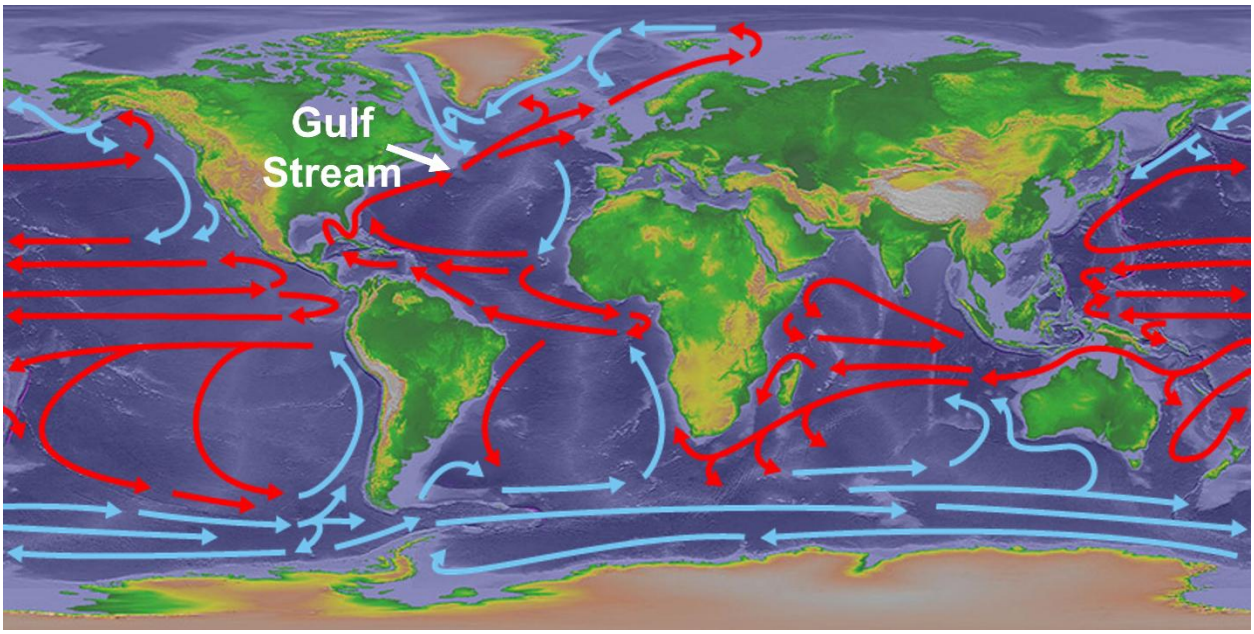

Figure 11-7: A global map of the surface ocean currents. Warmer currents are in red; cooler in blue. The east side of a continent has warmer currents and the west side has cooler currents.

Surface ocean currents are driven by the surface winds. Surface winds are influenced by the Coriolis force which is the reason the east side of a continent has warmer currents. Both the wind and ocean currents are on our rotating Earth, so both are influenced by the Coriolis force.

The larger ocean currents, like the Gulf Stream, can travel across an entire ocean. Notice the Gulf Stream off the eastern coast of the United States carries warm water across the Atlantic towards the United Kingdom and northern Europe (Norway). This warm water significantly impacts the temperatures in these regions, and likewise the climates in these regions

11.1.6 – Temperature Trivia

Are daily mean temperature and daily average temperature the same? The calculation for a daily mean temperature and a daily average temperature are not the same. At first glance a person may think that “daily mean” and “daily average” are the same, but they are not. The

calculations for various temperatures are defined explicitly. This section describes these calculations for completeness.

The temperature graph shown in Figure 11-8 for Tucson, Arizona is typical for a December day without much weather. The graph goes from 5 am December 25 to 5 pm December 26. Christmas Day 2020! The morning starts out with a low temperature of 50°F with a maximum temperature of 70°F occurring at about 3 pm. The temperature drops to a cooler 41°F the next morning. No large temperature changes occur throughout the day. Figure 11-8 depicts a smooth diurnal change of the temperature over this 24-hour period.

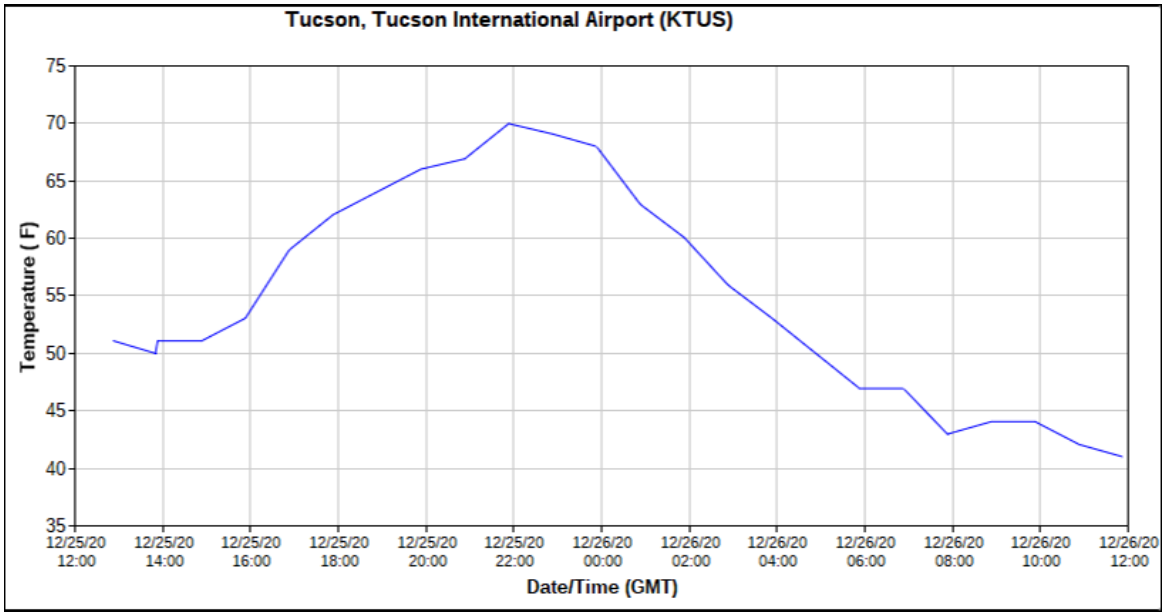

Figure 11-8: A temperature graph for Christmas Day 2020 at Tucson, Arizona.

Using the data in Figure 11-8, let us examine these temperature calculations. The daily mean temperature is the maximum temperature plus the minimum temperature divided by two. Using this graph,

Daily mean temperature = 55.5°F

The daily average temperature is the sum of the hourly temperatures divided by 24. For this December day, most of the hourly temperatures are less than 55 degrees so the daily average temperature is going to be less than the daily mean temperature. Specifically,

Daily average temperature = 54.8°F

Sometimes the daily average temperature uses a midnight-to-midnight time constraint rather than the 5 am to 5 am 24-hour period shown in this graph. The actual 24-hour time period used changes the actual values too. Other temperature calculation definitions are:

- Daily temperature range = maximum temperature – minimum temperature
- Monthly mean temperature = sum of daily mean temperatures / number of days in the month
- Annual mean temperature = highest monthly mean – lowest monthly mean

Now looking at world temperature records, the highest all-time record high temperature was 134ºF recorded at Greenland Ranch in Death Valley on July 10, 1913. Greenland Ranch is now called Furnace Creek Ranch. The photo in Figure 11-9 is of the observation site at this ranch. The thermometer resides in the white box inside the fence.

Figure 11-9: An old photo of the observation site in Death Valley.

The coldest temperature in the world was -129ºF recorded at Vostok Research Station in Antarctica on July 21, 1983. July is winter in the Southern Hemisphere, so outdoor pictures in July tend to be very dark.

11.2 – Weather Factors Affecting Temperature

Day-to-day temperature variations depend on the weather occurring at a location. Three types of conditions can affect these daily temperatures:

- Clouds
- Precipitation
- Wind

Clouds can influence both the high and low temperatures in a day. During the day, clouds reflect solar radiation and reduce the amount of surface heating. This reduction in solar radiation decreases the high temperature. During the night, clouds capture heat radiating off the surface and increase the low temperature. Figure 11-10 illustrates nighttime temperatures with no clouds, partial clouds, and full cloud cover. In summary, when clouds occur the daily temperature range decreases. The high and low temperatures are closer to each other.

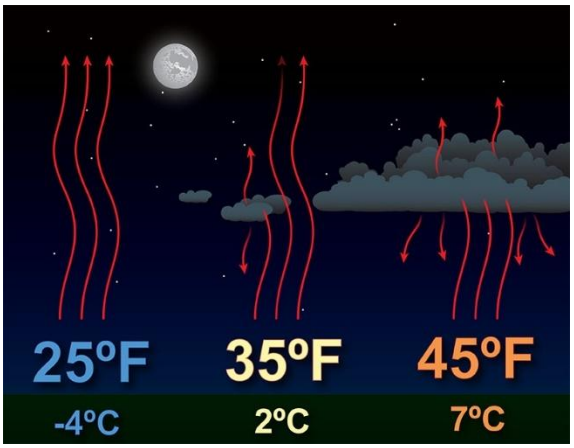

Figure 11-10: Illustration with various amounts of clouds during the night and their effect on minimum temperatures.

Obviously when precipitation is occurring clouds must be present, so precipitation has the same effect as clouds in reducing the daily temperature range. However, precipitation has a more extreme effect on affecting these temperatures. If precipitation occurs throughout an entire day, the high and low temperatures may almost be equal to each other. Figure 11-11 has two temperature graphs for Seattle, Washington to illustrate this principle. The top graph in this Figure is a sunny,

clear July day in Seattle and has a normal diurnal temperature variation. The temperature range is 24 degrees, and illustrates the pleasant summertime temperatures in a marine environment. The bottom graph is for a January day in Seattle when it rained all day. The temperature range on this wet day was 3.5 degrees.

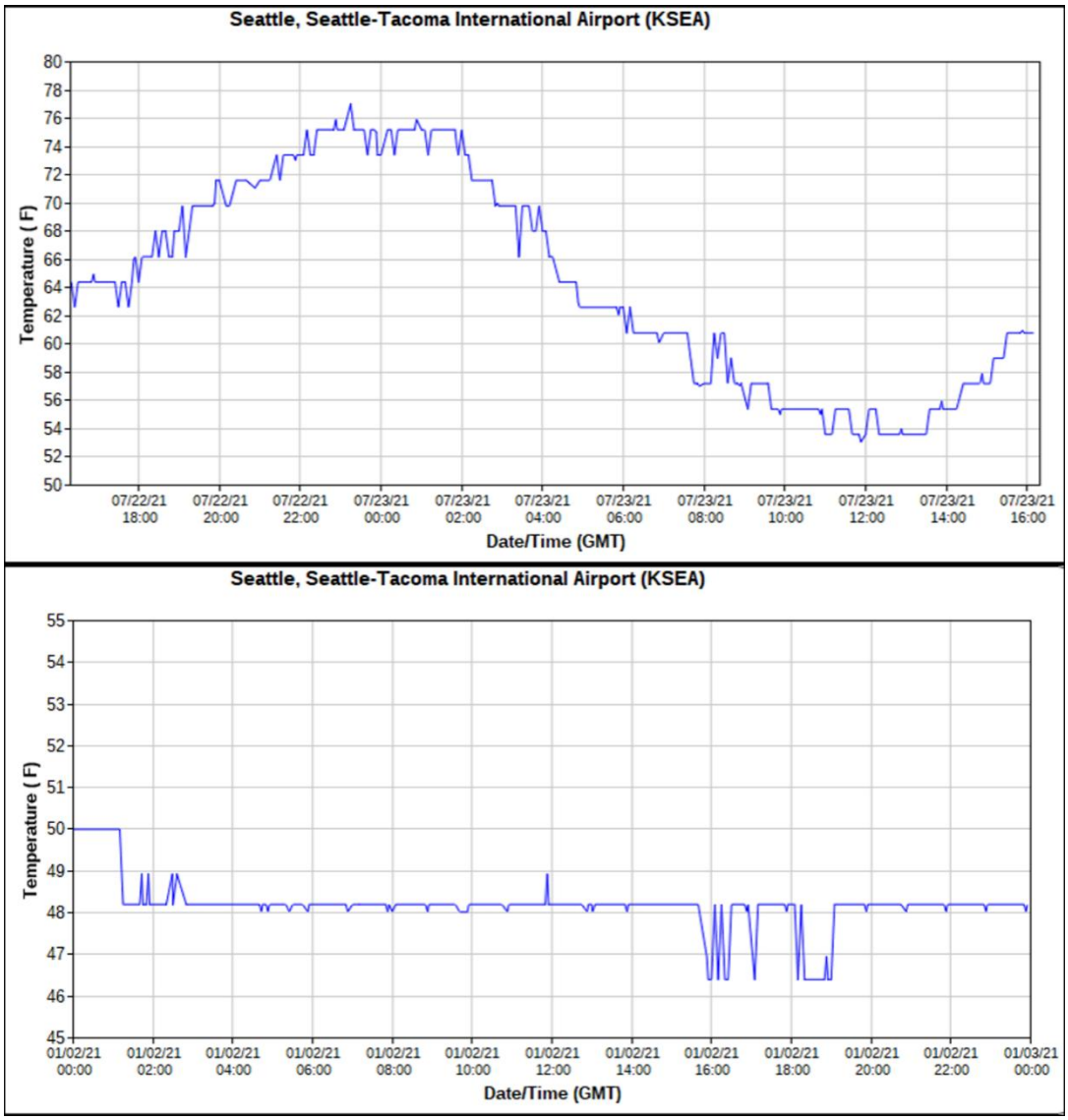

Figure 11-11: Temperature graphs for Seattle, WA. The top is for a sunny day in July. The bottom is for a rainy day in January. Notice the rainy day (bottom) has little temperature variation throughout the day.

Wind has the same effect on temperatures as both clouds and precipitation. If wind is occurring during the day, the heat originating from the surface is distributed through a larger portion of the atmosphere which reduces the high temperature. If wind is occurring during the night, the heat leaving the surface is mixed back down to the surface by the wind. Thus, wind at night increases the low temperature.

Overall, whenever clouds, precipitation or wind are occurring the minimum temperature is increased and the maximum temperature is decreased. The temperature range during a day decreases when these weather conditions are present the entire day.

11.2.1 – Heat and Wind Chill Indexes

Temperature extremes, both hot and cold, can be hazardous to people. Under certain weather conditions, these temperature extremes can be more hazardous than anticipated. During periods of hot weather, a person's ability to cool themselves depends on their perspiration. When humidity is higher, perspiration may not be sufficient to cool a person. This combination of hot temperatures and higher humidity can be deadly.

A Heat Index chart was created to alert people to these dangerous conditions. The word "index" when used in the atmospheric sciences implies two are more values are combined to represent important conditions in a single number or chart. The Heat Index correlates temperature and humidity to represent the heat exposure danger to a person. Heat Index is a measure of how hot it really feels when relative humidity is factored in with the actual air temperature. A Heat Index chart is shown in Figure 11-12.

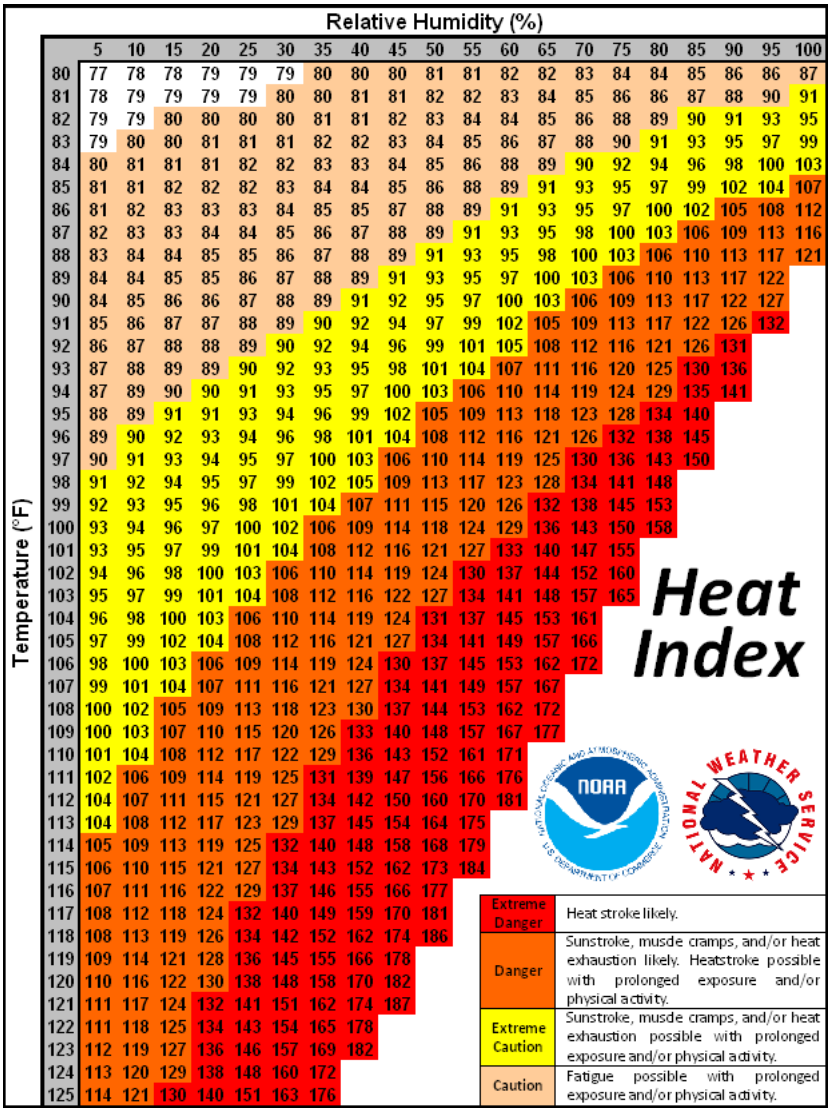

Figure 11-12: Heat Index chart which combines humidity and temperature to provide a better temperature number for how hot it feels.

Figure 11-12 indicates that lower humidity is more efficient for a body to cool itself, and higher humidity is less efficient. As an example, if the air temperature is 96°F and the relative humidity is 65%, the heat index--how hot it feels--is 121°F. These Heat index values were devised for shady, light wind conditions. Exposure to full sunshine can increase the values by up to 15°F over the ambient air temperature. Also, strong winds, particularly with very hot, dry air, can be extremely hazardous. In all hot temperature situations, a person needs to stay hydrated to avoid heat stroke.

Cold temperature conditions can also be hazardous to a person especially when strong winds are present. Wind carries heat away from a body much faster, and frostbite can occur quickly. The Wind Chill Index (Figure 11-13) uses advances in science, technology, and computer modeling to provide an accurate, understandable, and useful formula for calculating the dangers from winter winds and freezing temperatures. This index does the following:

- Calculates wind speed at an average height of 5 feet, the typical height of an adult human face, based on readings from the national standard height of 33 feet, which is the typical height of an anemometer (instrument that measures wind speed).
- Is based on a model of a human face.
- Incorporates heat transfer theory based on heat loss from the body to its surroundings during cold and windy days.
- Assumes these conditions occur at night with no sunshine.

For example, a temperature of 0°F with a 15 mph wind will have a Wind Chill Index – how cold it feels – of minus 19°F. Frostbite will occur within 30 minutes. In other words, unprotected skin will freeze in 30 minutes.

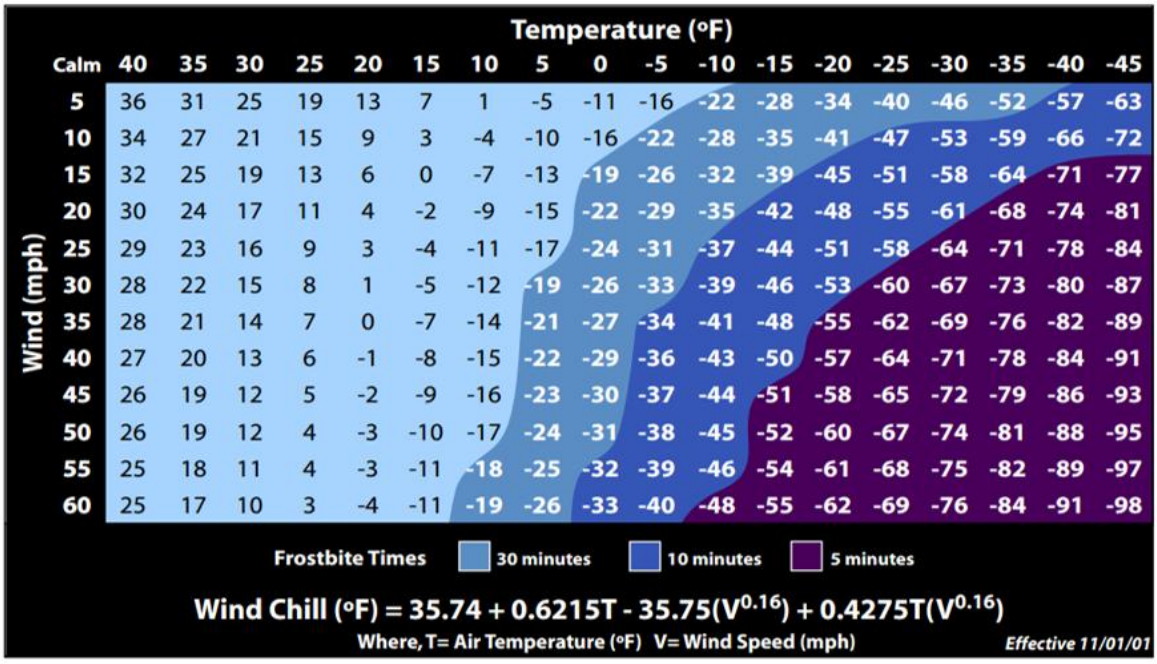

Figure 11-13: Wind Chill chart.

11.3 – Climate Classification

The Köppen-Geiger climate classification system has five main climate groups (A through E) and a highland (H) group:

- **A – Tropical**
- **B – Dry**
- **C – Mild midlatitude**
- **D – Severe midlatitude**
- **E – Polar**
- **H – Highland**

Here is a brief description of each group.

Tropical (A) climates have an average temperature for all months greater than 18°C (64°F) and annual precipitation greater than 1500 mm (59 inches). They extend north and south of the equator to about 15° or 25° latitude. This climate group tends not to have seasons, because the amount of sunshine is relatively consistent throughout the year.

Dry (B) climates have an annual evapotranspiration exceeding precipitation. Transpiration is the movement of water through a plant, which is released into its environment. Evapotranspiration is the total of evaporation and plant transpiration. Thus, dry climates always have a precipitation deficit. More water is released into the atmosphere through evapotranspiration than is received in precipitation. These climates extend from 20° to 35° latitude and in large continental regions of the midlatitudes often surrounded by mountains. Most of the western U.S. resides in the dry climate group. Dry climates cover roughly 30% of the Earth's landmass, which is the largest of any climate group.

Mild midlatitude (C) climates have warm to hot summers with the summer months averaging above 10°C (50°F). The cool winters have a monthly average temperature between -3°C and 18°C (27°F and 64°F). These climates extend from 30° to 50° latitude, and are on the eastern or western borders of most continents. Areas influenced by a marine environment tend to fall into this climate group.

Severe midlatitude (D) climates have warm to cool summers and cold winters. The location of these climates is poleward of the "C" climates. The average temperature of the warmest month is again greater than 10°C (50°F), but the coldest months are less than -3°C (27°F). Winters are severe with snowstorms, strong winds, and bitter cold from continental polar (cP) or Arctic air masses. Snowfall stays on the ground for extended periods of time.

Polar (E) climates have all months with a mean temperature below 10°C (50°F). These climates tend to have bitterly cold winters and cool summers because of the low Sun angle. They are found across the continents that border the Arctic Ocean, Greenland, upper Canada, and Antarctica. Regions with this climate tend to be quite dry, with annual precipitation less than 250 mm (10 inches).

Highland (H) climates are a result of a location's elevation. They occur in mountainous terrain where rapid elevation changes cause rapid climatic changes over short distances. Their higher elevation mimics the latitude dependency present in the other climate groups. Climates typically found at higher latitudes may also be found in other areas of the world at high elevation. The "H" climate group was not included in the original Köppen classification system, and may be omitted in some descriptions of the Köppen system. The highland group is included here for completeness.

Climate groups A, C, D, and E are generally defined by temperature. Climate group B is defined by evapotranspiration and precipitation. All these climate groups (A through E) are strongly influenced by latitude because of their temperature dependency. Climate group H is partially defined by elevation and partially by biomes. A biome is the naturally occurring flora and fauna (plants and animals) occurring in a region. Figure 11-14 depicts the location of these climate groups in the U.S.

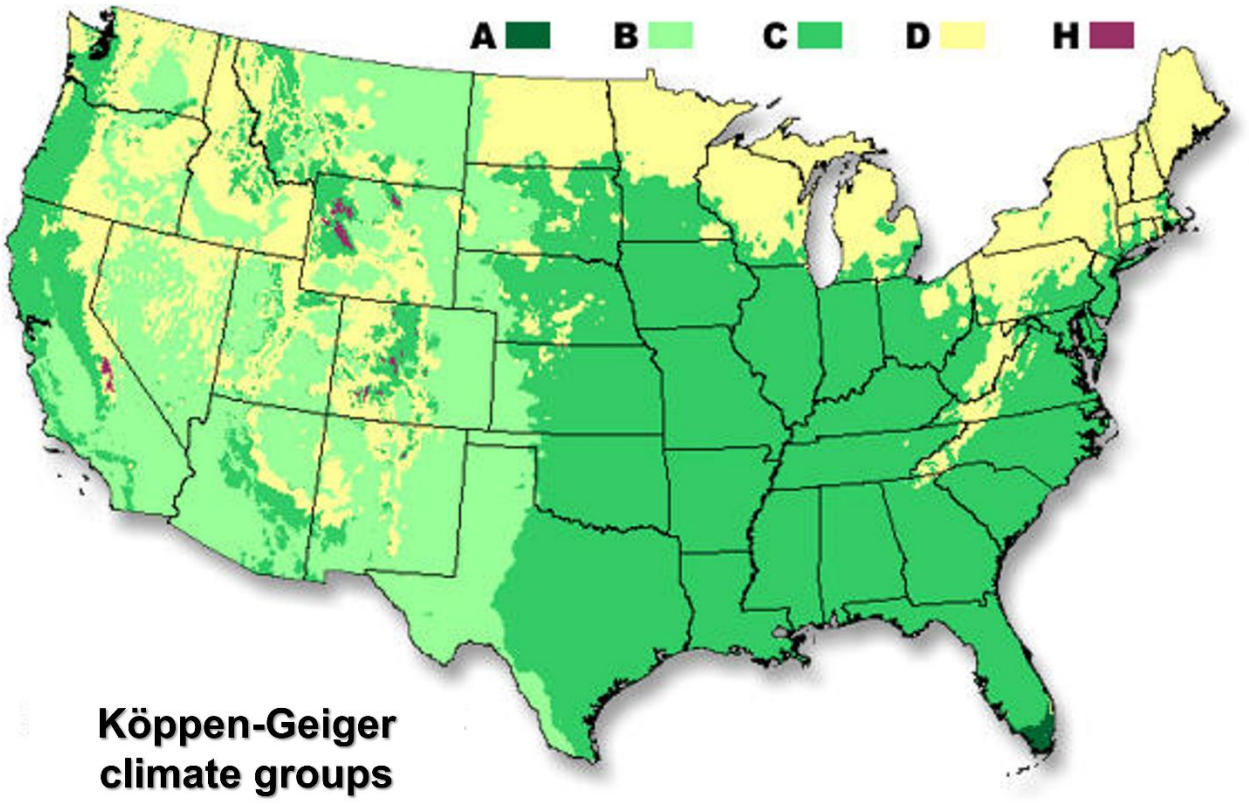

Figure 11-14: Map of the Köppen-Geiger climate groups found in the continental U.S.

Köppen and Geiger further divided each major group (A, B, C, D, E, and H) into smaller categories based on more detailed precipitation and temperature patterns. These subcategories are as follows:

Second letter (lower case) adds divisions based on precipitation patterns.

- f - wet year-round
- s - dry summer season
- w - dry winter season
- m - monsoon

Third letter (lower case) adds divisions based on temperature patterns.

- a - hot summer
- b - warm summer
- c - cool summer
- d - very cold winters

Not all of these subcategories apply to all the major groups. For example, the hot summer (a) subcategory is not applicable in the polar (P) group. The polar group does not have any hot summers.

Figure 11-15 shows the entire Köppen-Geiger climate classification system across the globe. This climate classification system is the dominant method used to classify climate according to weather and biomes. Once a person understands this system, all other similar climate

classifications schemes are easier to interpret. The remaining sections in this chapter examine details associated with these climate subcategories.

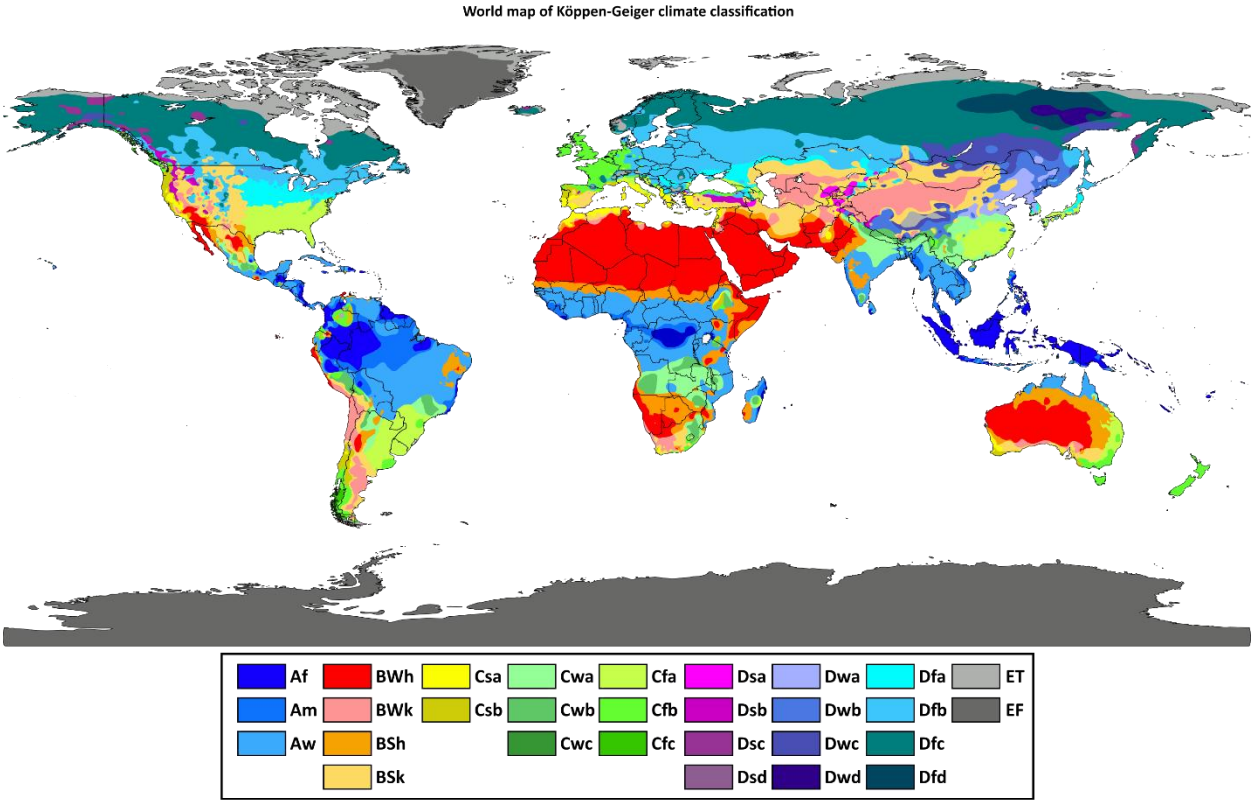

Figure 11-15: A world map of the Köppen-Geiger climate classification system.

11.3.1 – Tropical Group (A)

Figure 11-16 depicts the tropical climate group with the relevant subcategories (Af, Am, and Aw). These three categories are based on precipitation. Tropical wet (Af) rains all the time. Tropical monsoon (Am) has abundant rain for half the year associated with a monsoon flow. The other half of the year is much drier. Tropical wet and dry (Aw) is a transition climate to the dry (B) climates, and has a shorter period of rain compared to the tropical monsoon category. Tropical wet and dry can also be referred to as tropical savanna. Savanna is the type of drought tolerant vegetation that occurs in this climate category. All the tropical climates lack a seasonal variation in the temperature and annual temperature ranges are usually less than 8 degrees Celsius.

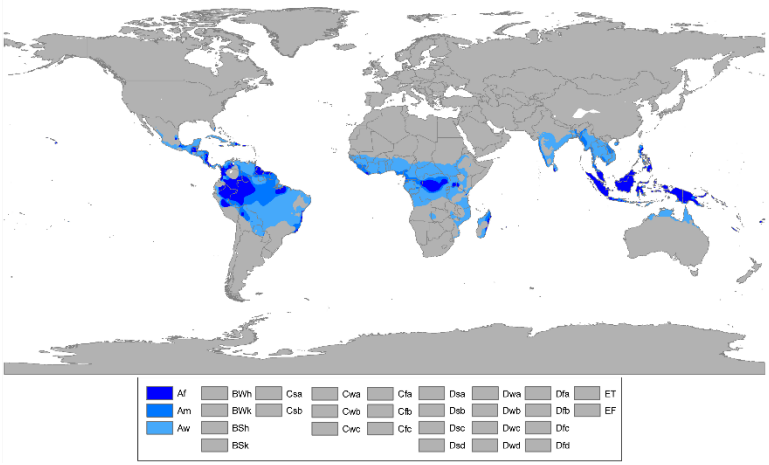

Figure 11-16: World map of the tropical group (A).

Tropical wet (Af) climates have almost no annual temperature variation and tremendous amounts of rainfall year-round, between 1750 to 2500 mm (65 to 100 inches). Although located near the equator, this climate category does not have the hottest temperatures, because of the abundant precipitation and evaporation. These conditions support the tropical rainforest biome, which is densely packed, broadleaf evergreen trees. These regions tend to have the highest number of species or biodiversity of any ecosystem. Figure 11-17 is the location of Manaus, Brazil. Figure 11-18 contains a climograph and photo for Manaus, Brazil (along the Amazon River) and depicts this type of climate.

Figure 11-17: Location of Manaus, Brazil.

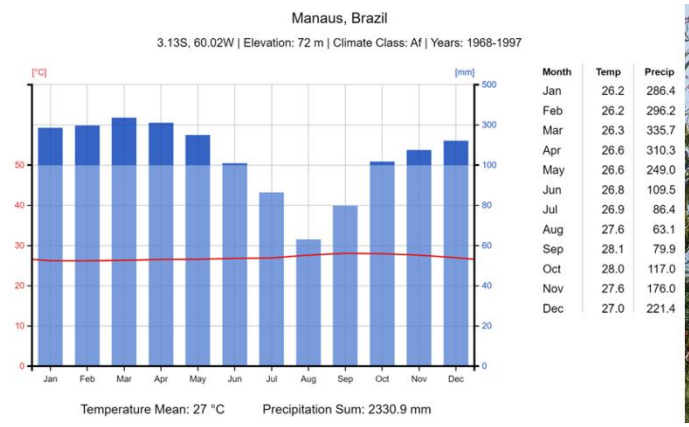

Month	Temp	Precip
Jan	26.2	286.4
Feb	26.2	296.2
Mar	26.3	335.7
Apr	26.6	310.3
May	26.6	249.0
Jun	26.8	109.5
Jul	26.9	86.4
Aug	27.6	63.1
Sep	28.1	79.9
Oct	28.0	117.0
Nov	27.6	176.0
Dec	27.0	221.4

Figure 11-18: Left side is a climograph for Manaus, Brazil. Red line is temperature and blue bars are precipitation. The right side is a photo from Manaus.

Tropical monsoon (Am) climates are defined by seasonal monsoonal wind patterns in southern Asia, northeastern South America, and western Africa. The monsoon tends to be strongest in regions where strong monsoonal winds exist. These climates tend to have incredible amounts of precipitation with a couple drier months during the year. Figure 11-19 is the location of Libreville, Gabon. Figure 11-20 contains a climograph and photo from Gabon, Africa (west Africa near the equator) and illustrates this type of climate.

Figure 11-19: Location of Libreville, Gabon.

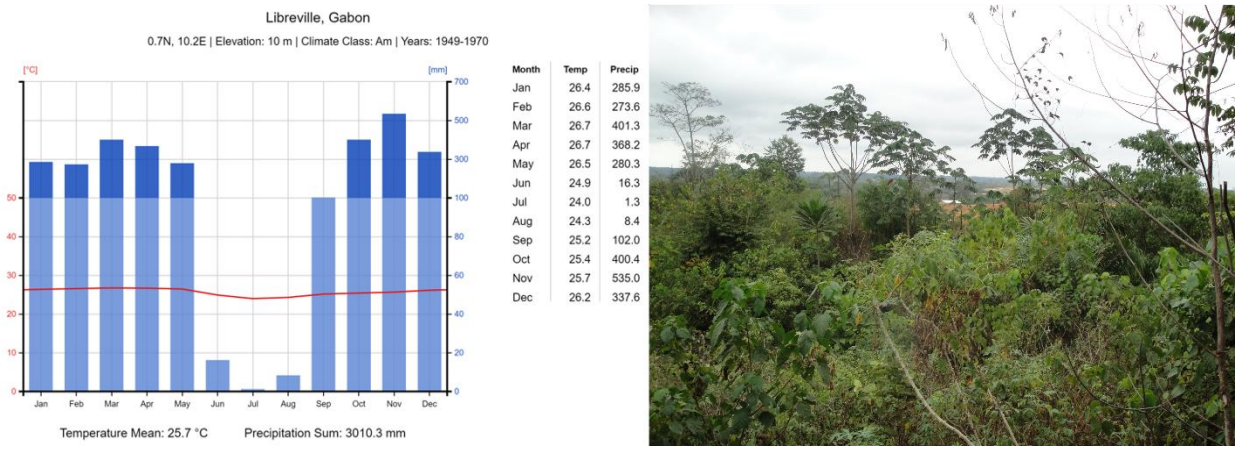

Figure 11-20: Left side is a climograph for Libreville, Gabon. Red line is temperature and blue bars are precipitation. The right side is a photo from Libreville.

Tropical wet and dry (Aw) climates are defined by dry winters and very wet summers. During the summer months, the Intertropical Convergent Zone (ITCZ) migrates into the region, bringing vast quantities of moisture. During the winter months, the ITCZ migrates away from the region bringing arid conditions. The average annual temperature ranges are roughly 3 to 8 degrees Celsius (5 to 15 degrees Fahrenheit). The type of vegetation which occurs in this climate category is referred to as savanna. Savanna vegetation must be drought tolerant, since several months are present with little or no precipitation. Mumbai, India (formally known as Bombay) is an example of this climate category. Figure 11-21 contains the location of Mumbai, India. Figure 11-22 contains a climograph and photograph from Mumbai.

Figure 11-21: Location of Mumbai, India.

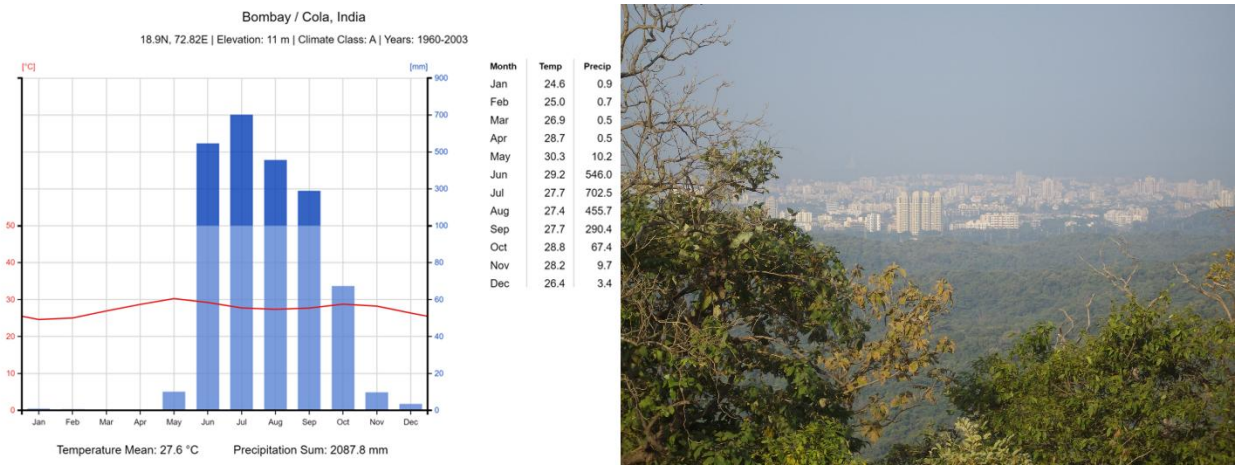

Figure 11-22: Left side is a climograph for Mumbai, India. Red line is temperature and blue bars are precipitation. The right side is a photo from Mumbai.

11.3.2 – Dry Group (B)

Figure 11-23 depicts the dry climate group with the relevant subcategories (Bwh, Bwk, Bsh, and Bsk). The arid desert categories have a “w” (Bwh and Bwk). The steppe categories have an “s” (Bsh and Bsk). The difference between desert and steppe is vegetation, which is determined by the amount of precipitation. The other subcategory letters are an “h” for subtropical and a “k” for midlatitude. In other words, “h” and “k” designate the latitude. For simplicity, we will just examine arid desert (Bw) and semi-arid or steppe (Bs). Since the dry climate group exists at higher latitudes than the tropical group, seasonal temperature variations are present.

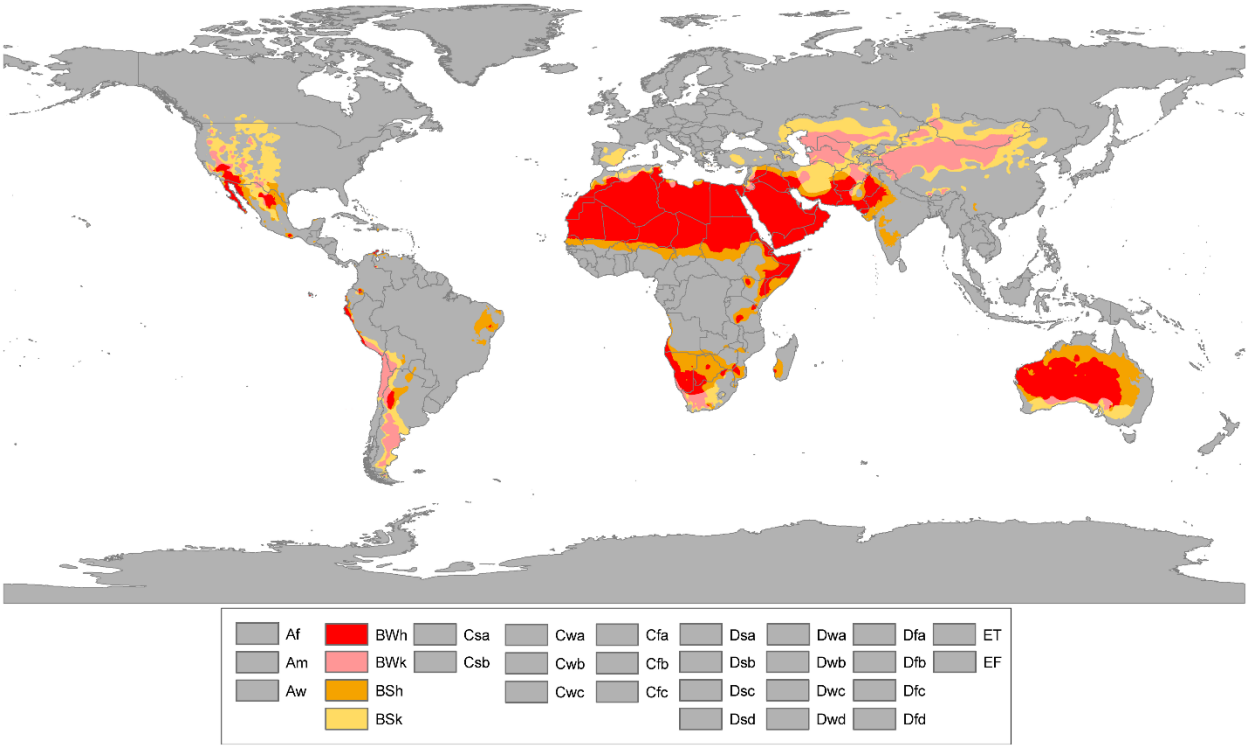

Figure 11-23: World map of the dry group (B).

Arid deserts tend to be found between 15 and 30 degrees latitude, where warm, dry air sinks because of the subtropical high. Vast deserts in this climate group, such as the Sahara or Gobi deserts, make up roughly 12 percent of the Earth’s landmass. The typical weather is sweltering summer days and chilly winter nights. Annual rainfall is less than 250 mm (10 inches), and precipitation tends to fall during two seasons. Yuma, Arizona is a typical example of an arid desert climate. Figure 11-24 shows the location of Yuma. Figure 11-25 contains the climograph and a photograph from Yuma.

Figure 11-24: Location of Yuma, Arizona.

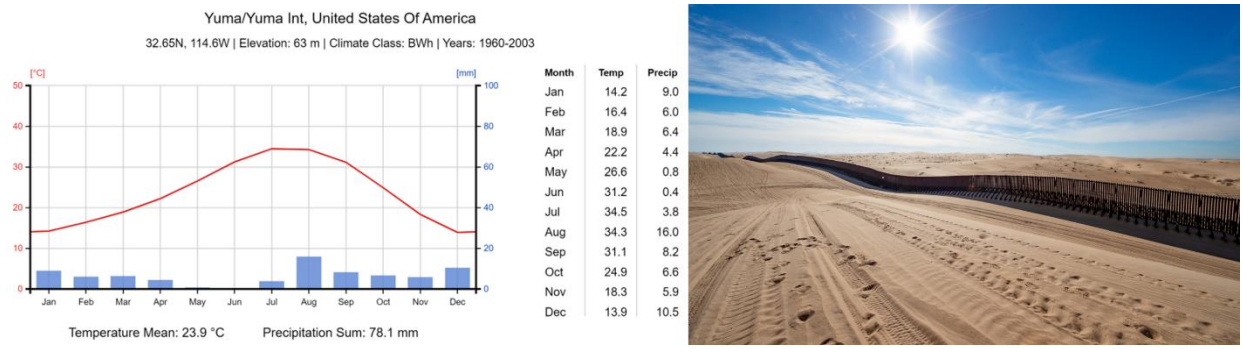

Figure 11-25: Left side is a climograph for Yuma, Arizona. Red line is temperature and blue bars are precipitation. The right side is a photo from Yuma.

Semi-arid deserts, also called steppe, are found in continental interiors. Semi-arid deserts receive between 200 and 400 mm (8 to 16 inches) of rain annually. In the United States, the Great Plains, portions of the southern California coast, and the Great Basin (in Nevada) are semi-arid deserts. Steppe vegetation is composed of grasses and low scrubs. Prescott, Arizona illustrates a semi-arid desert. Figure 11-26 shows the location of Prescott. Figure 11-27 contains the climograph and a photograph from Prescott.

Figure 11-26: Location of Prescott, Arizona.

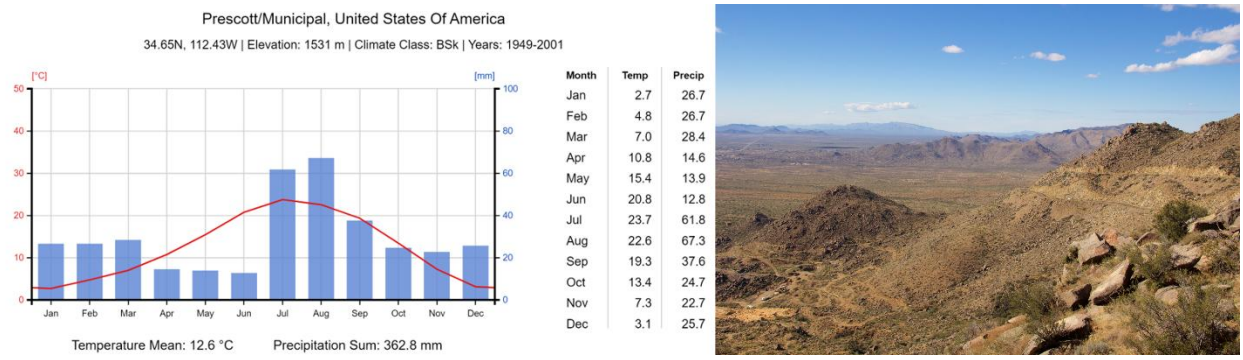

Figure 11-27: Left side is a climograph for Prescott, Arizona. Red line is temperature and blue bars are precipitation. The right side is a photo from Prescott.

11.3.3 – Mild Midlatitude Group (C)

The map in Figure 11-28 shows the mild midlatitude climate group. This group has been described as a transition zone between tropical climates and polar climates. Temperatures are temperate and four well-defined seasons are present. The primary subcategories in this group are Mediterranean (Csa, Csb, and Csc), humid subtropical (Cfa, Cwa, and Cwb), and marine west coast (Cfb and Cfc).

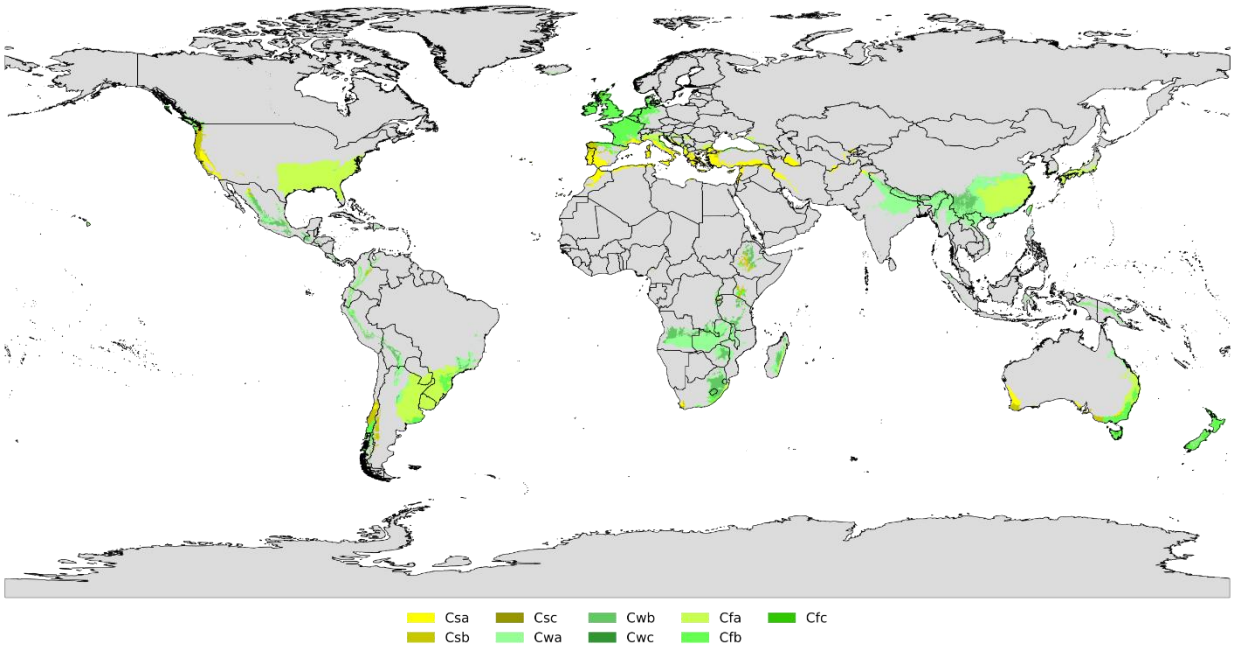

Source: Beck et al.: Present and future Köppen-Geiger climate classification maps at 1-km resolution, Scientific Data 5:180214, doi:10.1038/sdata.2018.214 (2018)

Figure 11-28: World map of the mild midlatitude group (C).

Mediterranean (Cs) climates are primarily found on the western sides of continents between 30 to 45 degrees latitude. Mediterranean climates receive most of their annual precipitation during the winter months with totals of 300 to 900 mm (14 to 35 inches). The summers are hot and dry because of their location near the subtropical high-pressure zones. These climates can have abundant sunshine during the summer. Jerusalem, Israel is an example of this type of climate. Notice the summer (June, July, and August - JJA) is dry on this climograph with most precipitation occurring in winter (December, January, and February - DJF). Figure 11-29 shows the location of Jerusalem, Israel. Figure 11-30 contains the climograph and a photograph from Jerusalem.

Figure 11-29: Location of Jerusalem, Israel.

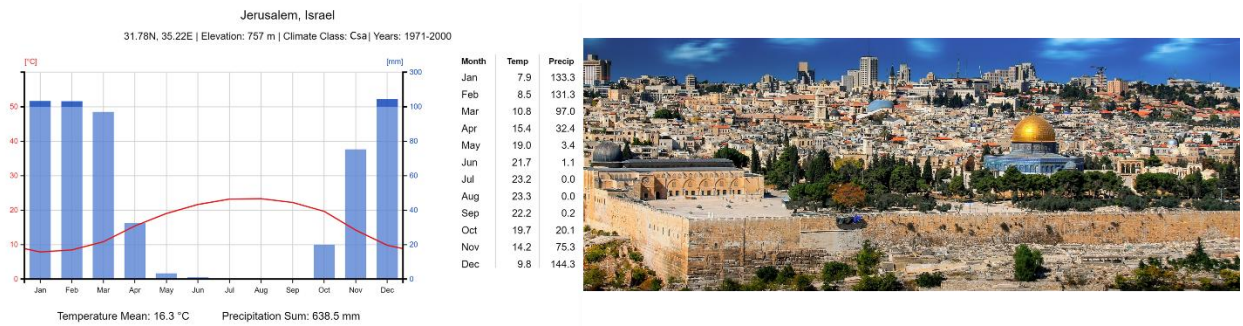

Figure 11-30: Left side is a climograph for Jerusalem, Israel. Right side is a photo of Jerusalem.

Humid subtropical (Cfa, Cwa, and Cwb) climates are found mostly on the eastern sides of continents. Precipitation occurs throughout the year with annual averages between 800 and 1650 mm (31 and 65 inches). Summer days are humid and hot. Summer temperatures range from the lower 30s up to 40°C (mid-80s up to 104°F). Afternoon and evening thunderstorms are frequent as warm tropical air passes over the hot continent. Winters are mild with midlatitude cyclones providing substantial amounts of precipitation. The southeastern United States, like New Orleans, Louisiana with its hot humid summers and mild winters is typical of this climate regime. The location of New Orleans is shown in Figure 11-31. Figure 11-32 contains the climograph and a photo of New Orleans that illustrates this humid subtropical climate category.

Figure 11-31: Location of New Orleans, Louisiana.

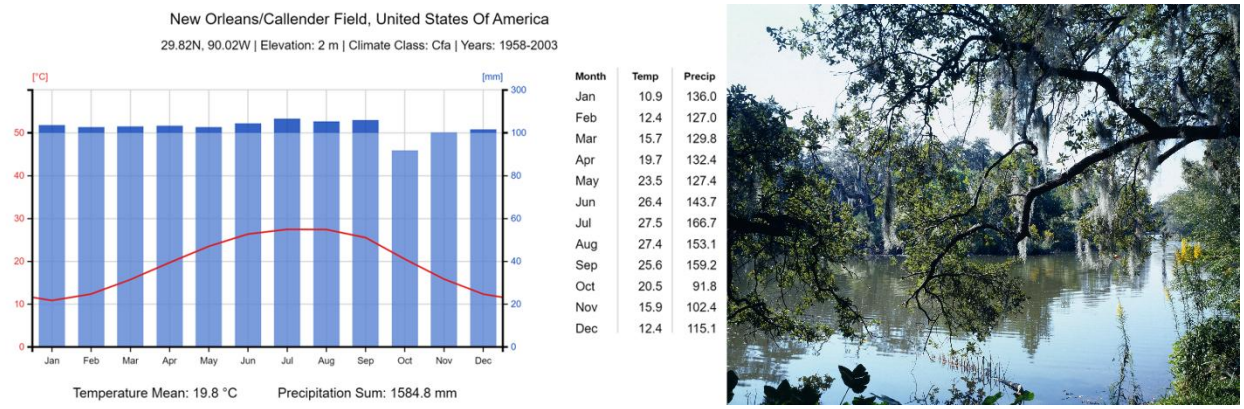

Figure 11-32: Left side is a climograph for New Orleans, Louisiana. Right side is a photo from New Orleans.

Marine west coast (Cfb and Cfc) climates follow the coasts of continents, between 40 degrees and 65 degrees latitude. Common regions with this climate include the west coast of Canada, western and central Europe, New Zealand, and southeast Australia. Ocean winds bring mild winters and cool summers, with daily and annual temperature ranges being relatively small. Precipitation tends to occur year-round, although summers can be drier as the jet stream moves northward. Low clouds, fog, and drizzle are frequent in these locations. Dublin, Ireland is an example of a marine west coast climate category. The location of Dublin is shown in Figure 11-33. Figure 11-34 contains the climograph and photo from Dublin. Notice the moss growing on the trees in this cool, wet climate category.

Figure 11-33: Location of Dublin, Ireland.

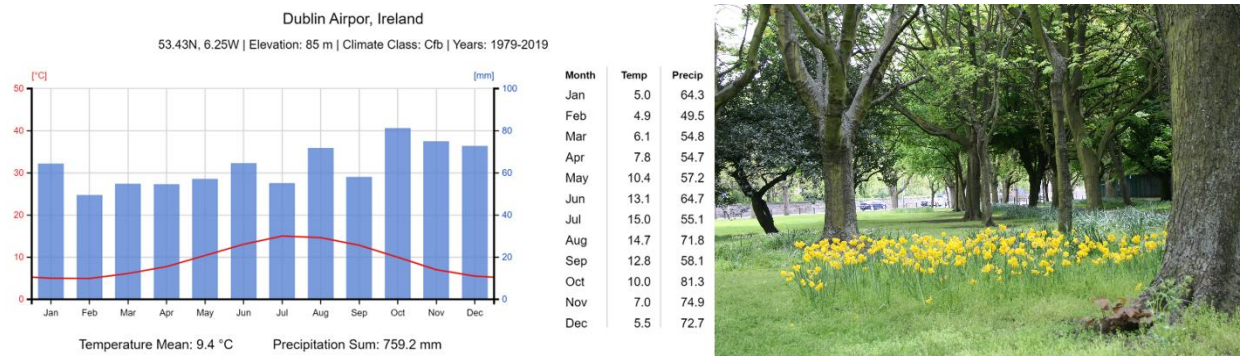

Figure 11-34: Left side is a climograph for Dublin, Ireland. Right side is a photo from Dublin.

11.3.4 – Severe Midlatitude Group (D)

The map in Figure 11-35 depicts the severe midlatitude climate group. This group is only found in the Northern Hemisphere between 40º and 70º. These climates are primarily found in interior continental locations away from an ocean and a marine environment. The "D" group has all four seasons with warm average summer monthly temperatures over 10ºC (50ºF). Winters are cold and stormy with the coldest months below -3ºC (-27ºF).

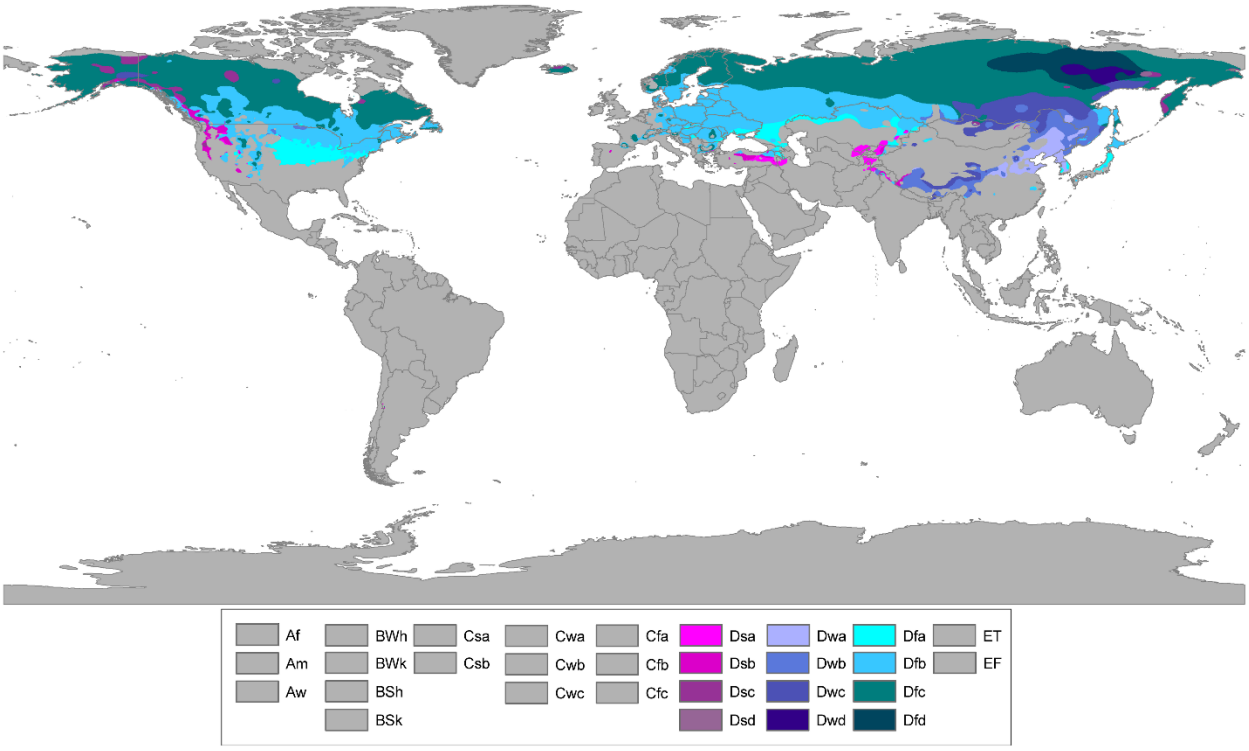

Figure 11-35: World map of the severe midlatitude group (D).

The primary subcategories in the "D" group are the humid continental (Dfa, Dfb, Dwa, Dwb, Dsa, Dsb) and the subarctic (Dfc, Dfd, Dwc, Dwd, Dsc, Dsd) climates. The 12 individual subcategories in the "D" group are defined by marine influences, monsoon influence, seasonal precipitation, number of cold or warm months and other criteria. For simplicity, we will just examine the humid continental and subarctic categories, rather than all 12 categories.

Humid continental climates are affected by the polar front in North America, Europe, and Asia as it seasonally shifts north and south. In the winter, midlatitude cyclones bring chilly temperatures, snow, and prolong this season. In the summer, westerly winds bring warmer temperatures. The average summer temperatures are often above 20ºC (70ºF). This climate region typically has deciduous trees, which lose their leaves in winter. Many large cities like New York, Chicago, and Moscow reside in this climate category. The location of New York City, New York is shown in Figure 11-36. Figure 11-37 contains the climograph and a photograph from New York City.

Figure 11-36: Location of New York City, New York.

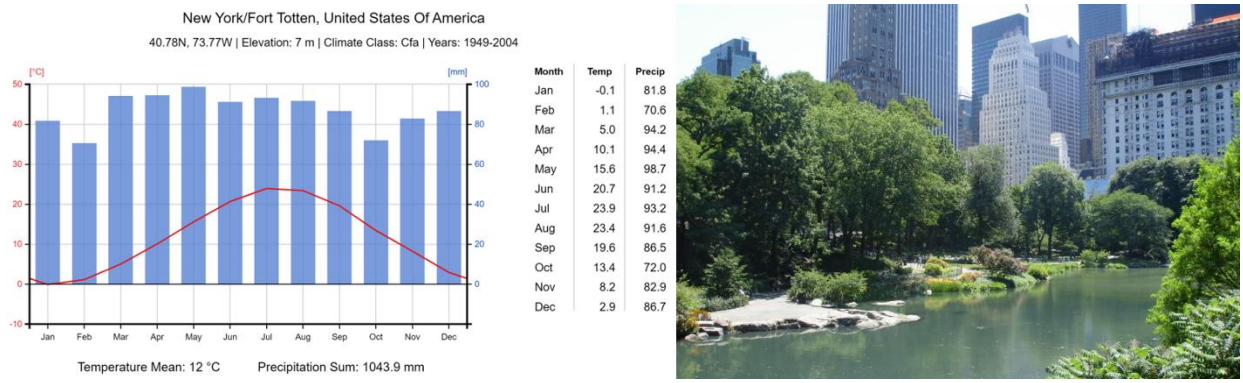

Figure 11-37: Left side is a climograph for New York City, New York. Right side is a photo from New York City.

Subarctic climates are dominated by continental polar (cP) air masses. Snowfall is light, but cold temperatures keep snow on the ground for months. Most of the approximately 500 mm (20 inches) of annual precipitation falls during the summer. The Sun angle is low year-round. These climate regions have a large annual temperature range. Vegetation is dominated by boreal, coniferous forests which are also called taiga. These vast forests stretch across Eurasia and North America. Dawson in the Yukon Territory of Canada has a subarctic climate. Figure 11-38 shows the location of Dawson. Figure 11-39 contains the climograph and a photo from the Dawson region. Notice the annual mean temperature is below freezing, and the annual temperature range is over 40ºC (70ºF).

Figure 11-38: Location of Dawson, Yukon Territory in Canada.

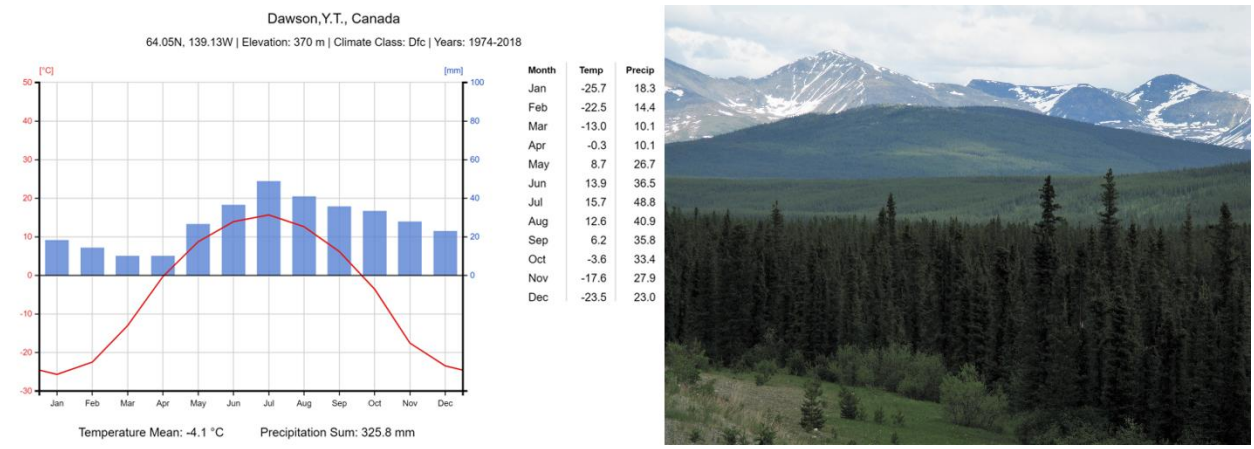

Figure 11-39: Left side is a climograph for Dawson, Yukon Territory in Canada. Right side is a photo from the Dawson region.

11.3.5 – Polar and Highlands Group (E and H)

Polar climates are found across the continents that border the Arctic Ocean, Greenland, and Antarctica. These climates tend to have bitterly cold winters and cool summers because of a low Sun angle in the summer and no sunlight during the winter. The average temperature of the warmest months is less than 10°C (50°F). Regions with this climate tend to be quite dry, with annual precipitation less than 250 mm (10 inches). Most of the meager precipitation in this climate category occurs during the summer months when the air is warm enough to hold moisture for precipitation. This climate group has two categories: (1) tundra – ET and (2) ice cap or frost – EF. Figure 11-40 shows the polar group (E) regions.

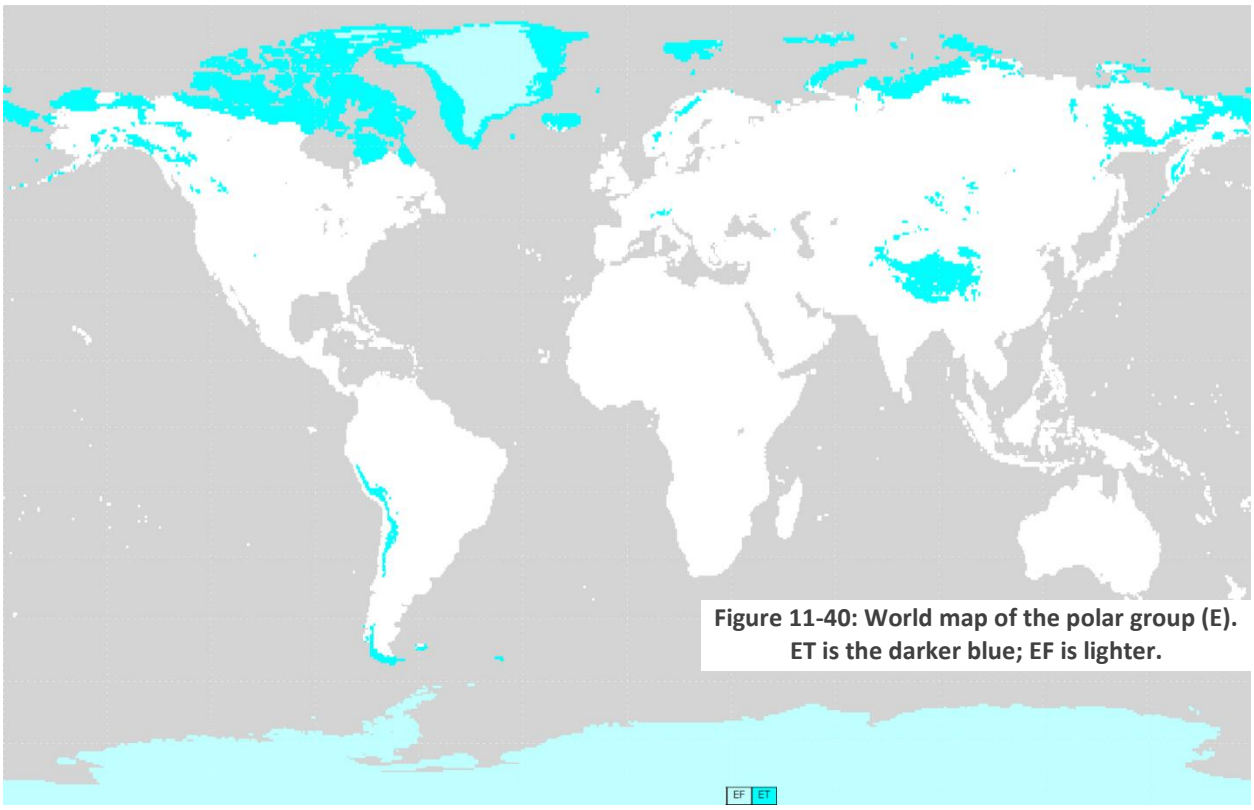

Figure 11-40: World map of the polar group (E). ET is the darker blue; EF is lighter.

Tundra climates were first described by the type of vegetation that grew in the region. The average temperature of the warmest month is below 10°C (50°F). Tundra vegetation consists of short plants that can survive in a short growing season (one month). No scrubs or trees are present. These cold temperatures, lack of sunshine, and persistent snow cover do not allow trees to grow. At higher elevations, the cold temperatures and snow conditions also limit tree growth. Where the trees stop growing on mountain tops is called a tree line. Tundra vegetation occurs at high latitudes and high elevations. These similarities caused the highlands climate category to be created. The highlands (H) and tundra (ET) climates have very similar vegetation and temperature conditions.

Temperatures in tundra climates are so cold that a layer of permanently frozen ground, called **permafrost**, forms below the surface. The average temperature of the warmest months is above freezing, so summer temperatures melt the uppermost part of the permafrost. In winter, permafrost prevents water from draining downward. The northern most city in the United States is Barrow (Utqiagvik), Alaska which is in the tundra climate category, and its location is shown in Figure 11-41.

Figure 11-41: Location of Barrow, Alaska.

Figure 11-42 contains a climograph and a photograph of Barrow (Utqiagvik), Alaska.

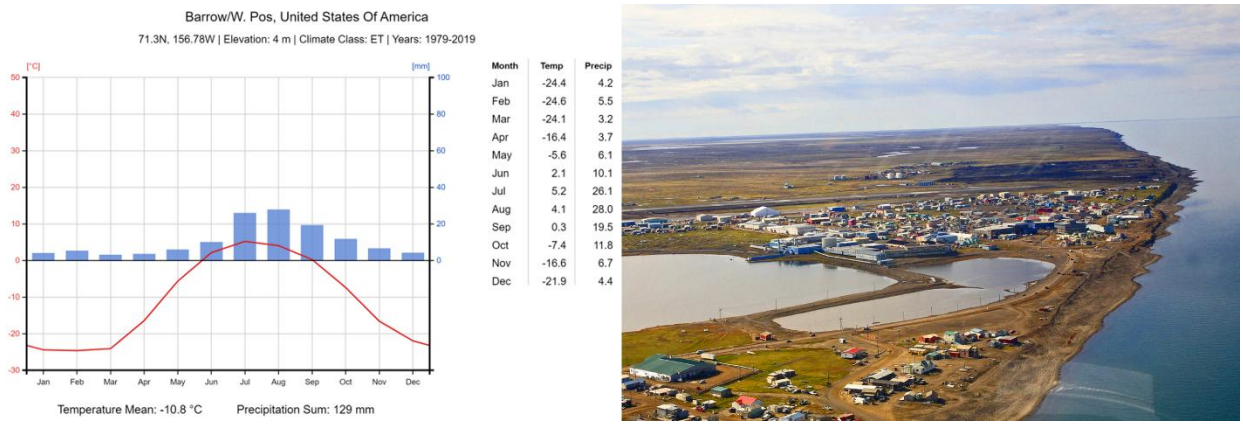

Figure 11-42: Left side is a climograph for Barrow, Alaska. Right side is a photo of Barrow.

The photo in Figure 11-43 is of a mountain top in Colorado, and illustrates the highlands (H) tundra vegetation. Notice the short vegetation in both Barrow and Colorado. Tundra vegetation is dormant most of the year, and only has 4-8 weeks to grow and reproduce. The green tundra shown in the Colorado picture is in the middle of the summer. The yellowing tundra shown in the Barrow picture is likely in early fall as the vegetation goes dormant.

Figure 11-43: Tundra vegetation in Colorado.

Ice cap climates are found mostly on Greenland and Antarctica. Because of their location near the poles, sunshine is limited. These climates have all average monthly temperatures below freezing. Precipitation is extremely low because the air is too cold to hold significant amounts of moisture. The permanent ice cover does not allow any vegetation to grow. The Vostok Research Station on Antarctica is an example of this harsh environment, and its location is shown in Figure 11-44. Figure 11-45 contains the climograph and an overhead photo of this Research Station. Notice the annual precipitation amount at Vostok is even lower than the arid desert climates, and all monthly temperatures are well below freezing. An ice cap climate can be thought of as a frozen desert.

Figure 11-44: Location of the Vostok Research Station in Antarctica.

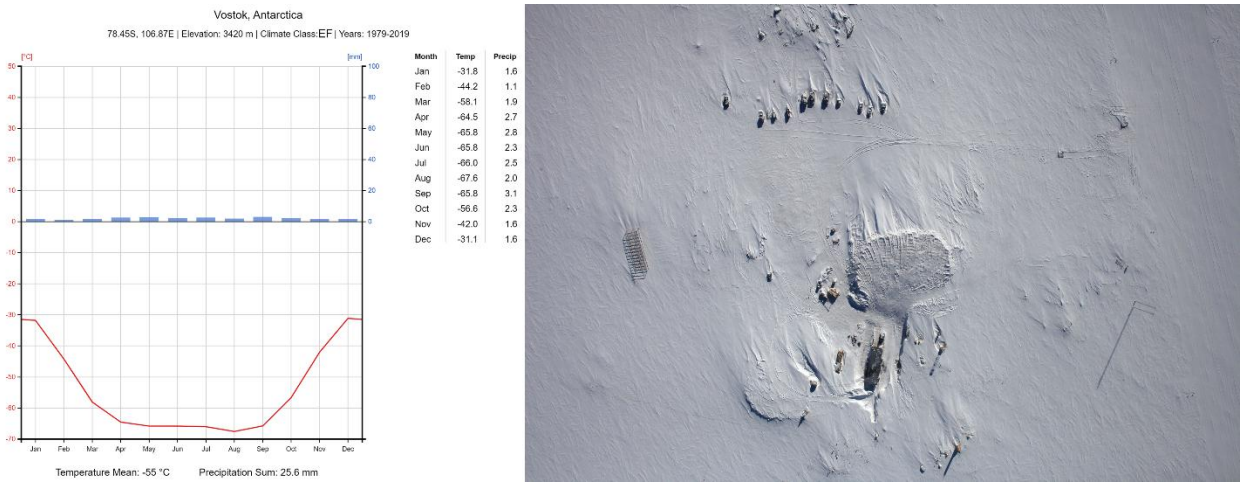

Figure 11-45: Left side is a climograph for the Vostok Research Station in Antarctica. Right side is an overhead photo of Vostok.

11.3.6 – U.S. Climate Trivia

The previous material in this module examined climate groups and categories based on temperature, precipitation, and naturally occurring vegetation. However, from a county, state, regional and federal government standpoint, the map in Figure 11-46 shows the U.S. climate divisions.

There are 344 climate divisions in the continental U.S. For each climate division, monthly station temperature and precipitation values are computed from daily observations. The divisional values are weighted by area to compute statewide values and the statewide values are weighted by area to compute regional values. All states have 10 or less climate divisions, except Alaska. Alaska, being the largest state, has 13 divisions (See Figure 11-47.

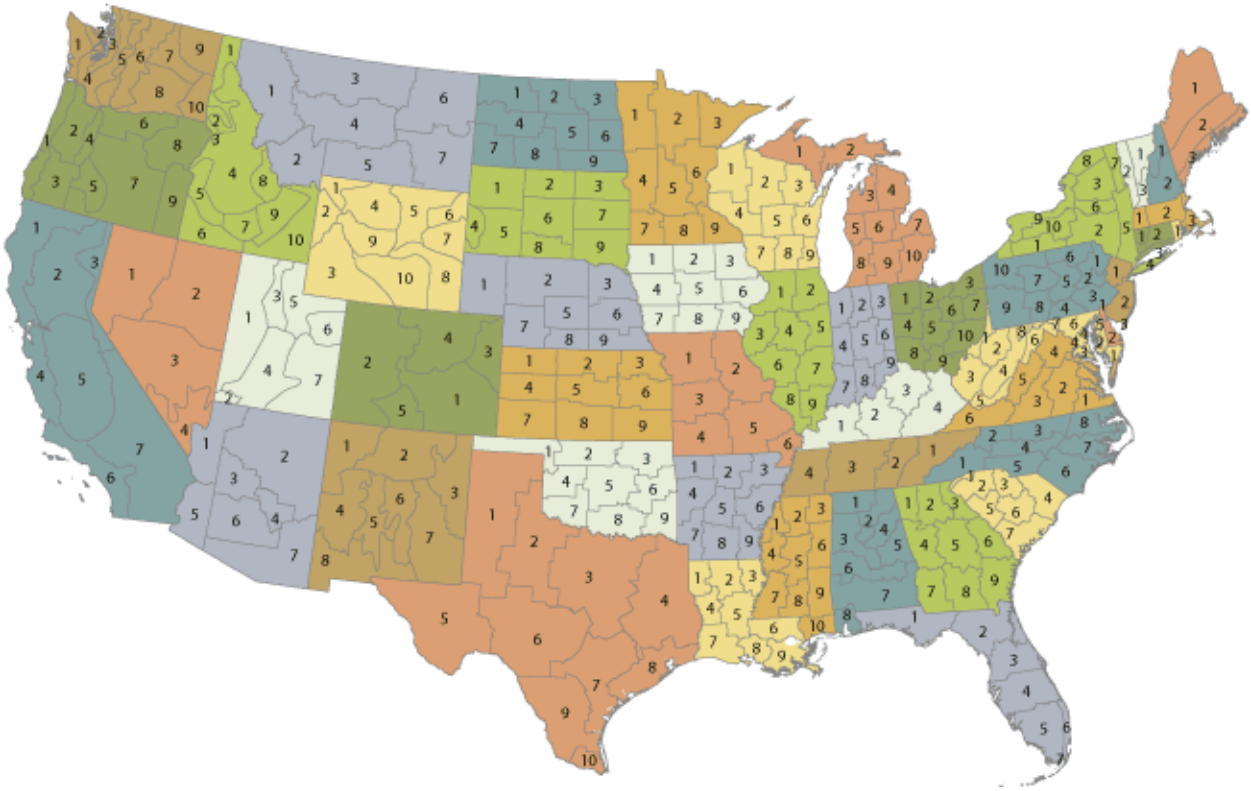

Figure 11-46: Climate Divisions in the continental United States.

Figure 11-47: Climate Divisions in Alaska.

As you can see from Figures 46 and 47, these climate divisions are based on geopolitical boundaries rather than climate science. However, these climate divisions are used to determine drought declarations and other natural disasters. Federal emergency funding can be secured based on what is occurring in these divisions.

Chapter 11 Review Questions

1. How does climate differ from weather?
2. How many years of data are usually needed before examining the climate at a location?
3. What is the most important geographic factor affecting climate classification?
4. Why does a mountain location warm less during the day and cool more rapidly at night than a valley location?
5. What global circulation feature creates the dry, desert climate around the globe?
6. Why do large bodies of water moderate the temperatures of the cities near them?
7. Where are the warmest ocean currents with respect to a continental landmass?
8. What is a climograph?
9. What is the heat index for 95ºF and 80% humidity?
10. How long does it take frostbite to occur with a temperature of -10ºF and 35 mph wind?
11. How does wind affect the minimum temperature during a 24-hour period?
12. What happens to the maximum and minimum temperature when it rains all day?
13. How can clouds affect the maximum and minimum temperatures?
14. Which climate group covers the largest percentage of land on Earth?
15. What are the defining characteristics of a dry climate? Of a polar climate?
16. Label each of the climate groups on this map.

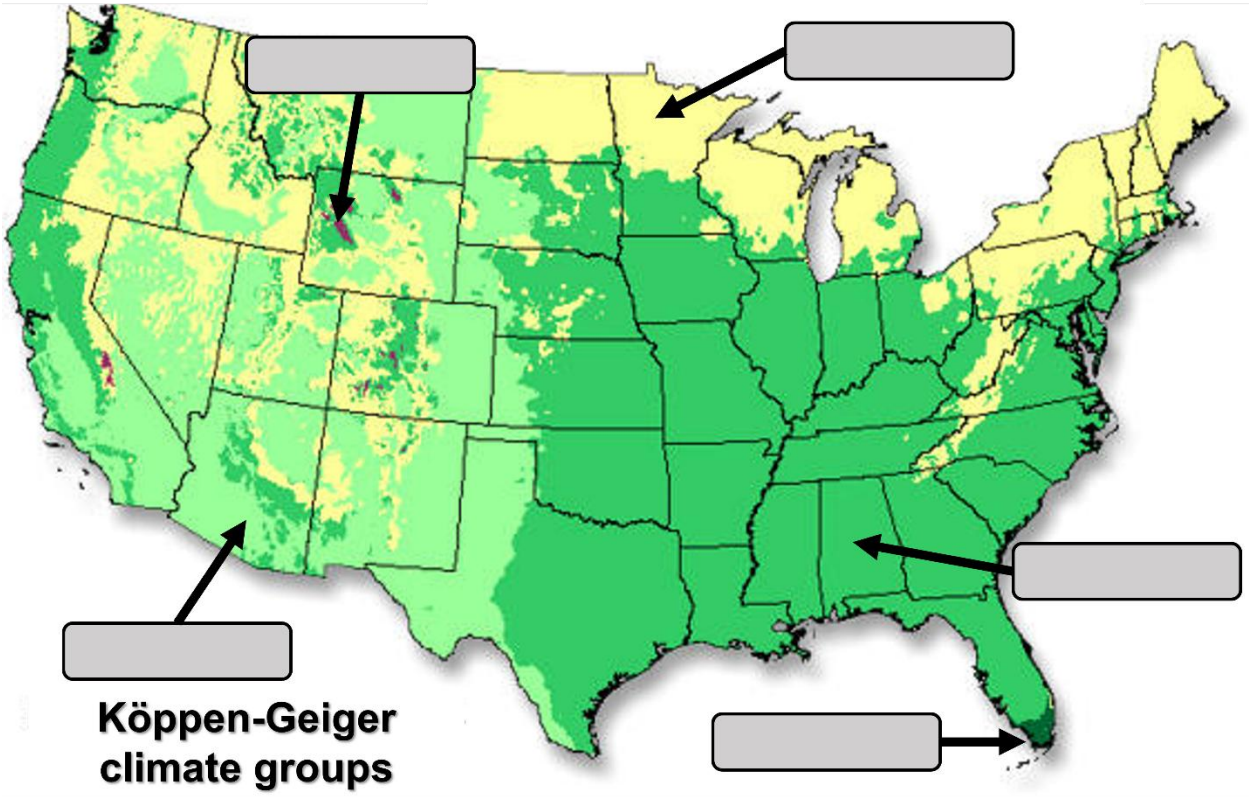

17. Although the wet tropical climate category (Af) is near the equator, why is it not the hottest?
18. The highland (H) climate group is most similar to what other climate group?
19. What are the location examples associated with each climate group?
20. What is a layer of permanently frozen ground called?

Chapter 12 – Human Influences on the Atmosphere

Overview

This chapter examines the influences people have on the atmosphere. These influences are broadly defined as air pollution. However, the gases associated with air pollution also occur in the atmosphere naturally. This chapter does not focus on these natural occurrences, but rather the additional gases human activities put in the air. The gases examined are carbon monoxide (CO), lead (Pb), nitrogen dioxide (NO_2), ozone (O_3), sulfur dioxide (SO_2) , and particulate matter (PM). In the United States, the Clean Air Act created the Environmental Protection Agency (EPA) to monitor and regulate these pollutants. To accomplish this task, the EPA established the Air Quality Index (AQI) for reporting air quality. This chapter will look at data from the EPA associated with the AQI.

As city boundaries grow bigger, temperatures within the city increases. This increase in temperature is due to a reduction in vegetation, and the ability of roads and buildings to capture and retain more heat than a natural environment. This increase in temperature is called an urban heat island. We will examine these heat islands in several cities across the United States.

At this point in this overview, you may be thinking “what about carbon dioxide?” Carbon dioxide is not a pollutant in the sense it is not harmful to people or plants. Carbon dioxide is a greenhouse gas which keeps our planet warm. An increase in carbon dioxide in the atmosphere will make the planet warmer. The last section in this chapter examines the human activities that create the most carbon dioxide. In subsequent chapters, carbon dioxide will be examined in even more detail.

Chapter objectives:

1. Describe the AQI and the types of atmospheric pollutants it measures.
2. Explain the factors that produce urban heat islands.
3. Describe the carbon cycle and its importance in the climate system.
4. Identify renewable and non-renewable energy resources.
5. Describe the human activities that create the most carbon dioxide.

12.1 – Atmospheric Pollutants

Other gases and substances are present in the atmosphere outside of its general composition, such as carbon monoxide, oxides of nitrogen and sulfur, and volatile organic compounds. Many times, these gases and substances occur naturally as when a volcano erupts or lightning causes a wildfire. Other times, human activities cause these contaminants to be released into the atmosphere, and substantially degrade the air quality in a region. These undesirable gases and substances in the atmosphere are referred to as **air pollution**. In this section, we will focus on human caused or anthropogenic air pollution rather than what occurs naturally. Additionally, this section focuses on what occurs in the United States rather than air pollution globally.

Air pollutants can be divided into two categories, primary and secondary. **Primary pollutants** are released directly into the atmosphere. Primary pollutions may also be referred to as direct pollutants. Examples of primary pollutants are carbon monoxide and nitrogen oxide as by-products of combustion, and volatile organic compounds. Volatile organic compounds (VOCs) are chemical organic compounds that evaporate under normal atmospheric conditions. Usually anything that has an odor when drying or evaporating is a volatile organic compound. Examples of VOCs are paint, nail polish, rubbing alcohol, and gasoline.

Secondary pollutants are a result of chemical reactions which occur in the atmosphere. Thus, secondary pollutants are not released directly into the atmosphere. Many times, primary pollutants chemically react with the atmosphere to create these secondary pollutants. For example, VOCs photochemically interact with oxygen in the atmosphere to create ozone. This process makes ozone is a secondary pollutant, while the VOCs which cause the ozone are a primary pollutant. The word “photochemical” is used here because sunlight is required to initiate the chemical reaction.

In 1970, the U.S. Congress passed the Clean Air Act of 1970 and the Environmental Protection Agency (EPA) was established. The EPA sets and enforces the standards associated with air pollution, and regulates six common air pollutants.

1. Carbon monoxide (CO)
2. Lead (Pb)
3. Nitrogen dioxide (NO_2)
4. Sulfur dioxide (SO_2)
5. Ozone (O_3)
6. Particulate matter (PM)

After reading this list of regulated pollutants, you may have noticed that carbon dioxide is absent. The EPA provides information on greenhouse gases (GHGs), their emissions levels, sources, partnership (voluntary programs) to modify emissions, and options for reducing emissions. With respect to climate change, the EPA studies and reports on climate change as it impacts various populations and the natural environment. Thus, the EPA does not regulate the normal atmospheric GHGs (variable gases) directly.

The graph in Figure 12-1 shows the trend of these six common pollutants. The downward kink in gross domestic product, vehicle miles traveled, and energy consumption in 2020 was a result of COVID-19. Notice the aggregate emissions of all six common pollutants has a downward trend since 1980. The EPA is succeeding in their mission.

This video from Harvard University provides an overview of the pollutants we will examine in Chapter 12.

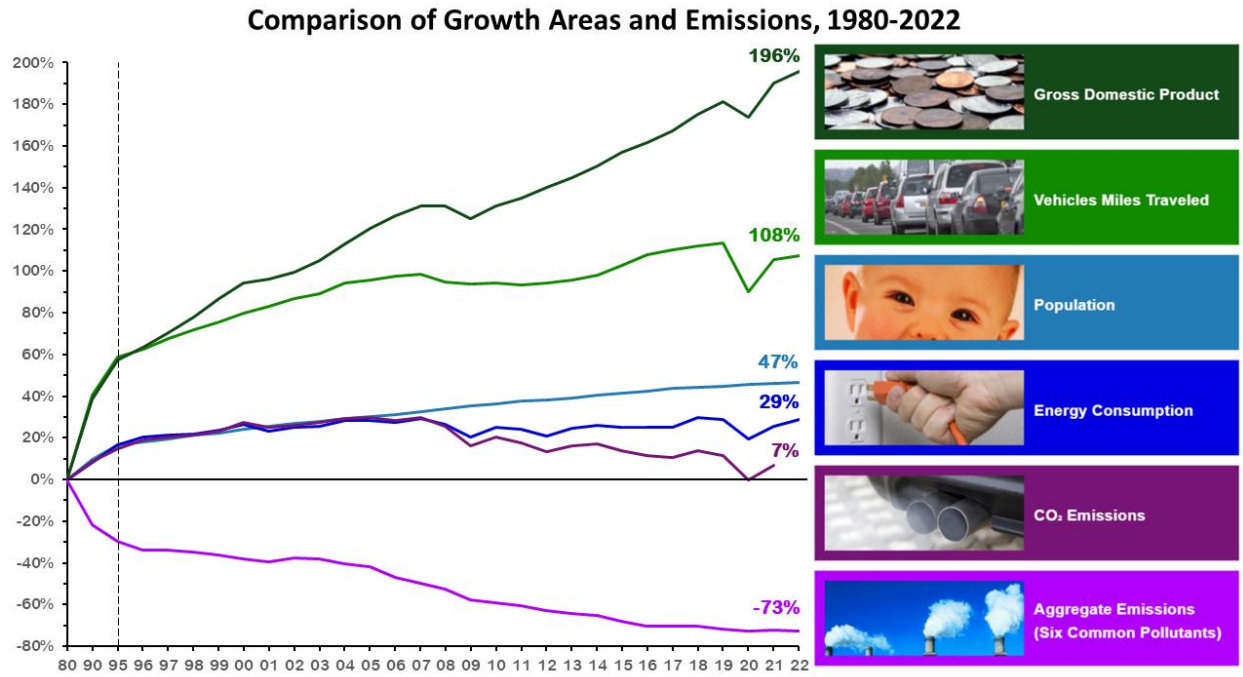

Figure 12-1: Comparison of growth areas in the U.S. and aggregate emissions. Notice emission have decreased in the U.S. since 1980, while the growth areas affecting emissions have increased.

12.1.1 – Carbon Monoxide

Carbon monoxide (CO) is a colorless, odorless gas that can be harmful when inhaled in large amounts. CO is released when something is burned. The greatest sources of outdoor CO are cars, trucks and other vehicles or machinery that burn fossil fuels. A variety of items in a home, such as unvented kerosene and gas space heaters, leaking chimneys and furnaces, and gas stoves, can release CO and affect indoor air quality.

Breathing air with a high concentration of CO reduces the amount of oxygen that can be transported in the blood stream to critical organs like the heart and brain. Hemoglobin is the protein in blood that transports oxygen throughout the body. Unfortunately, hemoglobin has a 200 times greater affinity for attaching to a CO molecule than to an oxygen (O_2) molecule. When carbon monoxide attaches itself to hemoglobin, blood can no longer transport oxygen. A person can suffocate to death even though they are breathing normally. Very high levels of CO, which are possible indoors or in other enclosed environments, can cause dizziness, confusion, unconsciousness and death.

This Centers for Disease Control (CDC) video describes carbon monoxide poisoning, and the steps that can be taken to prevent it in an indoor environment.

Very high levels of CO are not likely to occur outdoors. However, when CO levels are elevated outdoors, they can be of particular concern for people with some types of heart disease. These people already have a reduced ability for getting oxygenated blood to their hearts. They are especially vulnerable to the effects of CO when exercising or under

increased stress. In these situations, short-term exposure to elevated CO may result in reduced oxygen to the heart, resulting in corresponding chest pain. The graph in Figure 12-2 shows the mean CO outdoor levels from 1980 through 2022, and is based on 32 locations. As you can see, the United States is below the established national standards.

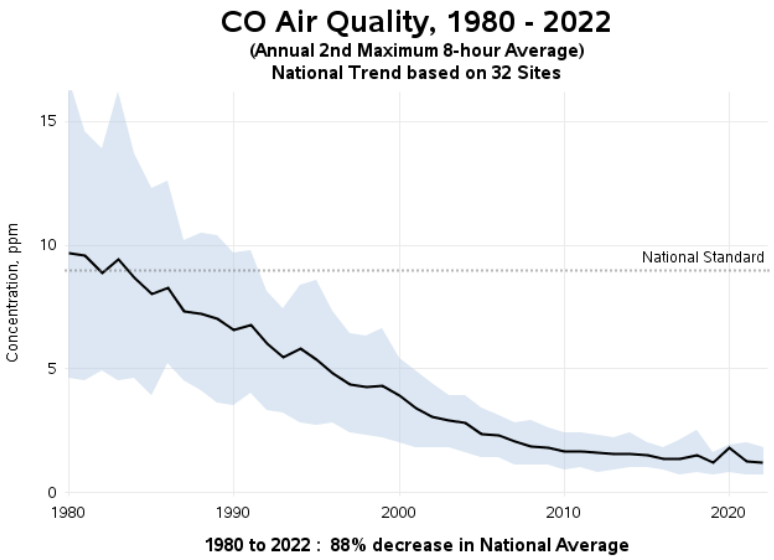

Figure 12-2: Carbon monoxide (CO) air quality, 1980-2022. The blue area defines the range of the individual site measurements. The black line is the average of all sites.

Global CO concentrations can also be monitored by satellite. This image from NASA (Figure 12-3) illustrates this type of satellite product. The higher concentrations of CO in Africa and China are associated with fires.

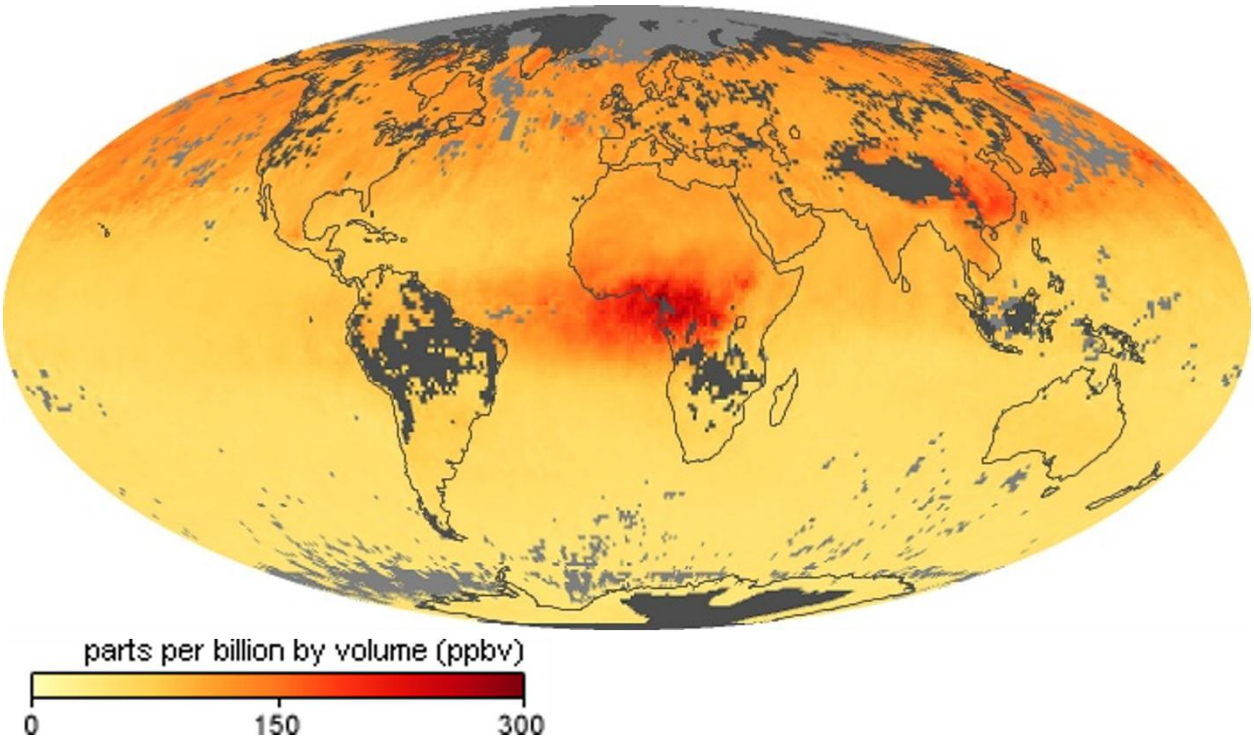

Figure 12-3: A global map of CO levels in February 2017. The higher concentrations in Africa and East Asia are associated with fires.

12.1.2 – Lead

Sources of lead emissions vary from one area to another. At the national level, major sources of lead in the air are ore and metals processing and piston-engine aircraft operating on aviation

fuel with lead additives. Other sources are waste incinerators, utilities, and lead-acid battery manufacturers. The highest air concentrations of lead are usually found near lead smelters. Prior to the Clean Air Act, lead was an additive in vehicle gasoline. Vehicle exhaust put substantial amounts of lead into the atmosphere, which has now been eliminated.

Once taken into the body, lead distributes itself throughout the body and accumulates in the bones. Depending on the level of exposure, lead can adversely affect the nervous system, kidney function, immune system, reproductive and developmental systems and the cardiovascular system. Lead exposure also affects the oxygen carrying capacity of blood. The lead effects most likely to be encountered in current populations are neurological effects in children. Infants and young children are especially sensitive to lead exposures, which may contribute to behavioral problems, learning deficits and lowered IQ.

Lead can be found in all parts of our environment – the air, the soil, the water, and even inside our homes. Much of our exposure comes from human activities including the use of lead additives in gasoline, some types of industrial facilities and past use of lead-based paint in homes. Lead and lead compounds have been used in a wide variety of products found in and around our homes, such as pipes and plumbing materials, batteries, ammunition, ceramics, and cosmetics.

Lead may enter the environment from these past and current uses. Lead can also be emitted into the environment from industrial sources and contaminated sites. While natural levels of lead in soil range between 50 and 400 parts per million, mining, smelting and refining activities have resulted in substantial increases in lead levels in the environment, especially near these industrial sites.

When lead is released into the air from industrial sources or engine aircraft exhaust, it may travel long distances before settling to the ground. Once on the ground, lead usually sticks to soil particles. Lead may move from soil into ground water depending on the type of lead compound and the characteristics of the soil.

Federal and state regulatory standards have helped to reduce the amount of lead in air, drinking water, soil, consumer products, food, and occupational settings. Figure 12-4 shows the lead air quality levels from 2010 to 2022, and is based on 81 locations. As you can see, the United States is below the established national standards.

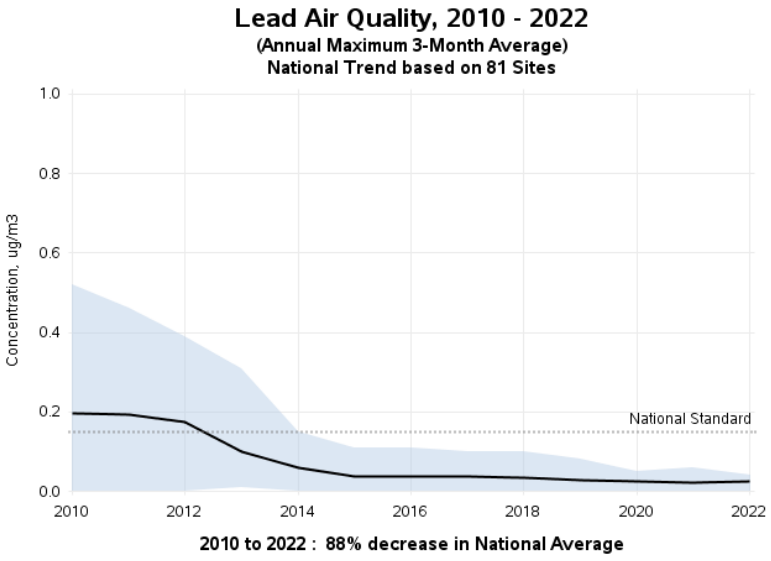

Figure 12-4: Lead air quality, 2010 to 2022, which is currently below the national standard.

12.1.3 – Nitrogen Oxides

Nitrogen Dioxide (NO_2) is one of a group of highly reactive gases known as nitrogen oxides (NO_x). Other nitrogen oxides include nitrous acid and nitric acid. NO_2 is used as the indicator for this entire group of nitrogen oxides. NO_2 primarily gets into the air from the burning of fuel in cars, trucks and buses, power plants, and off-road equipment.

Scientists estimate that nature produces between 20 and 90 million tons of nitrogen oxides each year. Natural sources include volcanoes, oceans, biological decay, and lightning strikes. Human activities add another 24 million tons of nitrogen oxides to our atmosphere annually.

Both NO and NO_2 are formed during high-temperature combustion when oxygen combines with nitrogen from the atmosphere. These exhaust gases are major sources of multiple nitrogen oxides compounds. Automobile exhaust has more NO than NO_2, but once the NO is released into the atmosphere it quickly combines with oxygen in the air to form NO_2.

Nitrogen oxides are at least partially responsible for several types of air pollution. Nitrogen dioxide lends its color to the reddish-brown haze we call smog. Photodissociation of nitrogen dioxide by sunlight produces nitric oxide, ozone, and particulate matter in the troposphere. All these secondary pollutants are also components of smog. If Volatile Organic Compounds (VOCs) are present, chemical reactions can combine them with nitrogen dioxide to produce PAN (Peroxyacytyl nitrate). In summary, nitrogen oxides are a precursor to several undesirable chemicals in the atmosphere.

Figure 12-5 contains an aerial photo of Mexico City, and depicts the reddish-brown haze associated with nitrogen dioxide in the atmosphere. A reddish-brown haze occurs in many large cities with combustion engine vehicles.

Figure 12-5: Aerial photo of the reddish-brown nitrogen dioxide pollution over Mexico City, Mexico

Although nitrogen oxides have gained dubious distinction as pollutants, they are also used beneficially in some industrial processes. Nitric oxide is manufactured on a large scale, and is subsequently used to make nitric acid (HNO_3). To create nitric oxide for industrial uses, chemists combine ammonia (NH_3) with oxygen (O_2), releasing water (H_2O) as a byproduct. Nitrogen compounds derived from nitric acid are used to create chemical fertilizers, explosives, and other useful substances.

Unfortunately, breathing air with a high concentration of NO_2 can irritate airways in the human respiratory system. Such exposures over short periods can aggravate respiratory diseases, particularly asthma, leading to respiratory symptoms (such as coughing, wheezing or difficulty breathing), hospital admissions and visits to emergency rooms. Longer exposures to elevated concentrations of NO_2 may contribute to the development of asthma and potentially increase susceptibility to respiratory infections. People with asthma, as well as children and the elderly are generally at greater risk from the health effects of NO_2.

Nitrogen dioxide concentration in unpolluted air is around 10 parts per billion (ppb). In smog, the concentration rises twenty-fold to about 200 ppb. The graph in Figure 12-6 shows a downward trend of the mean nitrogen dioxide levels from 1980 through 2020, and is based on 20 locations.

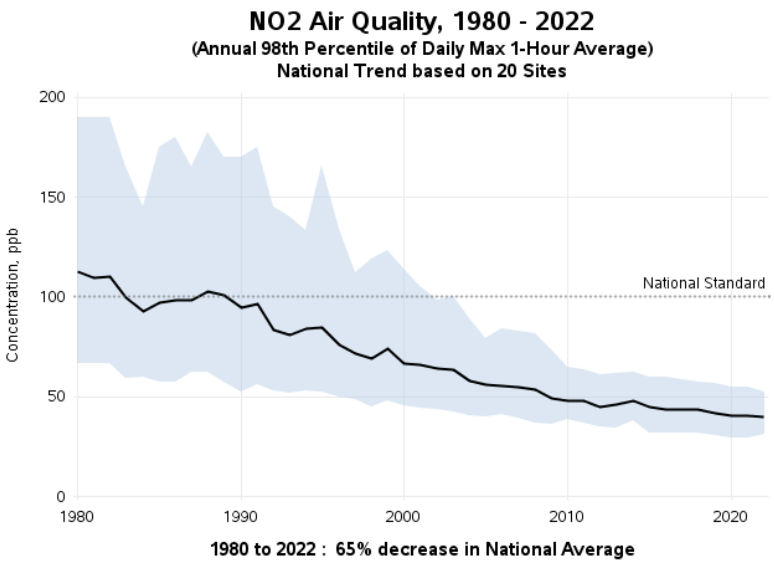

Figure 12-6: A graph of nitrogen dioxide air quality, 1980-2022, which is again currently below the national standard.

12.1.4 – Sulfur Oxides

Sulfur oxides are a group of molecules made of sulfur and oxygen atoms, such as sulfur dioxide (SO_2) and sulfur trioxide (SO_3). Sulfur oxides are pollutants that contribute to the formation of acid rain, as well as particulate pollution. Some are released into Earth's atmosphere by natural sources, but most are the result of human activities.

Some sulfur oxides are gases, and some are liquids or solid particles. Sulfur dioxide is the most dangerous of the sulfur oxides. It is a colorless gas that smells like burnt matches. Sulfur trioxide is often a colorless or white solid that creates white fumes in the air and has strong reactions with water. Both sulfur dioxide and sulfur trioxide react to form sulfuric acid, which is toxic to living tissue and is the main component of acid rain.

Volcanoes are a natural source of sulfur oxides in the atmosphere, but 99% of the sulfur dioxide in the atmosphere comes from human activity, such as burning coal, oil, and gas to make electricity and heat. When coal and oil burn, the sulfur in them combines with oxygen in the air to make the sulfur oxides. Processing mineral ores that contain sulfur and industrial burning of fossil fuels are also sources of sulfur oxides in the atmosphere.

SO_2 emissions that lead to high concentrations of SO_2 in the air generally also lead to the formation of other sulfur oxides (SO_x). SO_x can react with other compounds in the atmosphere to form small particles. These particles contribute to particulate matter (PM) pollution. Small

particles may penetrate deeply into the lungs and in sufficient quantity can contribute to health problems. Short-term exposures to SO_2 can harm the human respiratory system and make breathing difficult. People with asthma, particularly children, are sensitive to these effects of SO_2.

Figure 12-7 shows the sulfur dioxide air quality from 1980 through 2022, and is based on 29 locations. As you can see, the United States' SO_2 emissions have improved considerably over this 40 year time period, and are currently well below the national standard.

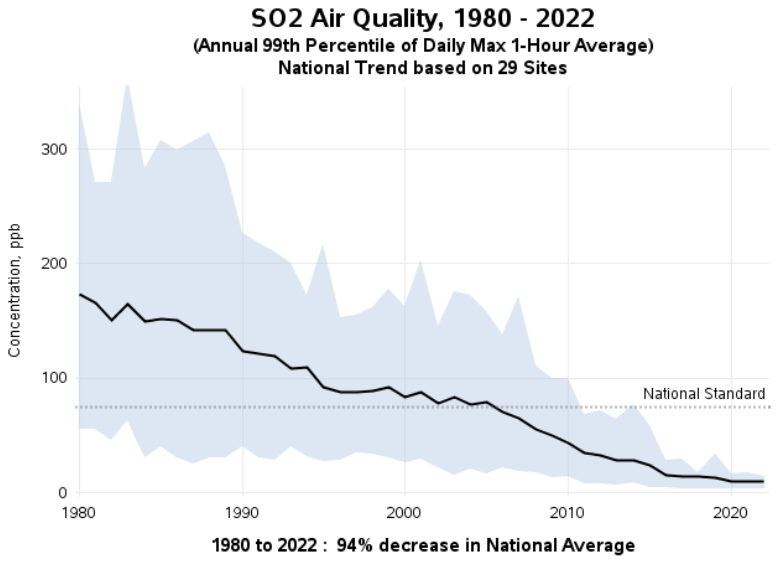

Figure 12-7: A graph of sulfur dioxide air quality, 1980-2022.

This video from Harvard University examines the primary pollutants of lead, nitrogen oxides, sulfur oxides, and carbon monoxide. These pollutants are associated with combustion, and techniques at reducing these combustion by-products are presented.

12.1.5 – Ozone

Ozone is a gas composed of three atoms of oxygen. Ozone occurs both in the Earth's upper atmosphere and at ground level. Ozone can be good or bad, depending on where it is found. "Bad" ozone is found in the troposphere, the layer nearest the ground. Tropospheric ozone is a harmful pollutant which forms when sunlight alters various chemicals emitted by humans.

"Good" ozone forms in the stratosphere, the layer above the troposphere where some jet planes fly. Stratospheric ozone forms naturally and helps shield us from ultraviolet (UV) radiation. Ozone in the stratosphere forms when a photon of ultraviolet radiation from the Sun strikes a normal oxygen molecule, breaking it apart. One of the atoms freed by this photodissociation process attaches itself to another oxygen molecule, converting it into ozone.

Tropospheric, or ground level ozone, is not emitted directly into the air, but is created by chemical reactions between oxides of nitrogen (NOx) and volatile organic compounds (VOC). This happens when pollutants emitted by cars, power plants, industrial boilers, refineries, chemical plants, and other sources chemically react in the presence of sunlight. Ozone in the troposphere is "bad" and is a secondary pollutant. Figure 12-8 illustrates how ozone forms. Nitrogen oxides react with volatile organic compounds (VOCs) in a sunny, hot environment to create ozone.

Typically, ozone levels reach their peak in mid to late afternoon, after exhaust fumes from the morning rush hour have had time to react in sunlight. A hot, sunny, calm day is the perfect

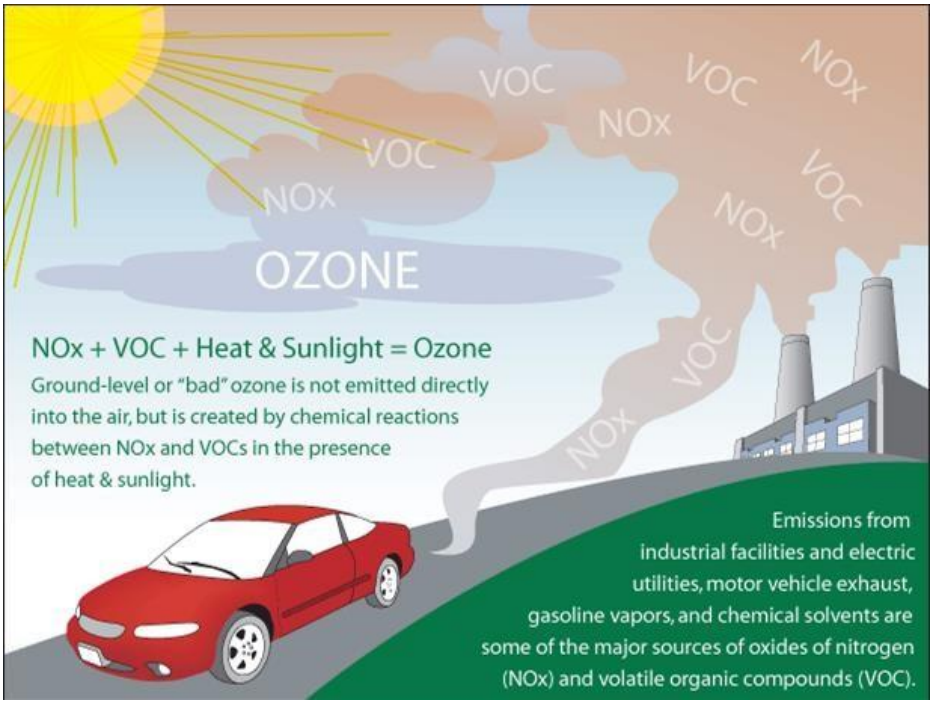

Figure 12-8: Illustration combining oxides of nitrogen with volatile organic compounds and sunlight to create ozone.

environment for the production of ozone pollution. At the end of the day, as the Sun starts to set, the production of ozone begins to subside.

When ozone pollution reaches high levels, pollution alerts are issued urging people with respiratory problems to take extra precautions or to remain indoors. When it's inhaled, ozone can damage lung tissues. Ozone is harmful to all types of cells. It can impair an athlete's performance, create more frequent attacks for individuals with asthma, cause eye irritation, chest pain, coughing, nausea, headaches and chest congestion. It can worsen heart disease, bronchitis, and emphysema. Figure 12-9 shows the ozone air quality from 1980 through 2022, and is based on 132 locations. As you can see, the United States as a whole is just barely below the national standard. The formation of ozone is a complex process involving multiple pathways. Hence, decreasing ozone levels across the entire Nation is not an easy task and is the reason ozone levels are just barely below the national standard.

This third video from Harvard University looks at the complexity associated with ozone formation.

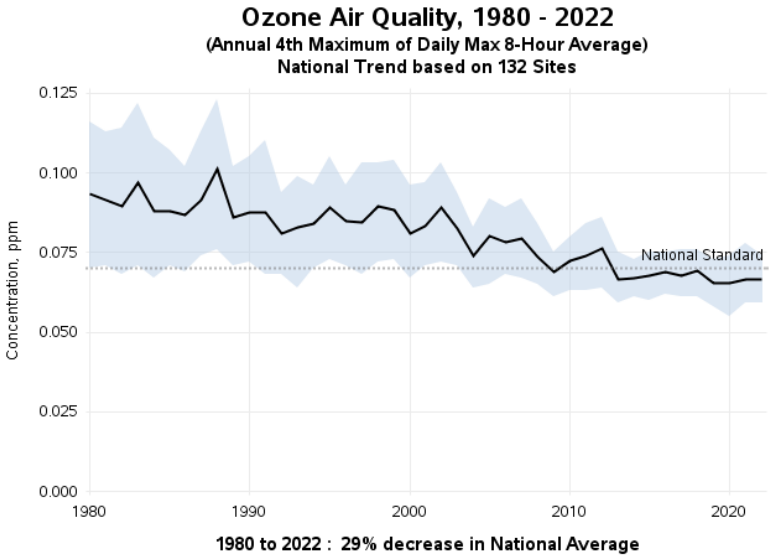

Figure 12-9: A graph of ozone air quality, 1980-2022.

12.1.6 – Particulates (PM 2.5 and PM 10)

Particulate matter (PM) is a mixture of solid particles and liquid droplets found in the air. Some particles, such as dust, dirt, soot, or smoke, are large enough to be seen with the naked eye. Others are so small they can only be detected using an electron microscope.

Particle matter is categorized by their size:

- PM10 : inhalable particles, with diameters that are generally 10 micrometers and smaller; and
- PM2.5 : fine inhalable particles, with diameters that are generally 2.5 micrometers and smaller.

How small is 2.5 micrometers? Think about a single hair. The average human hair is about 70 micrometers in diameter – making it 30 times larger than the largest fine particle. Figure 12-10 illustrates the sizes of PM2.5 and PM10.

Some of these particles are emitted directly from sources, such as construction sites, unpaved roads, fields, smokestacks or fires. Others form in the atmosphere as a result of chemical reactions in the atmosphere involving sulfur dioxide and nitrogen oxides. Therefore, particulate matter is both a primary and secondary pollutant.

Particles less than 10 microns in diameter pose the greatest problems, because they can get deep into a person's lungs, and some may even get into the bloodstream. These small particles are difficult for the body to expel.

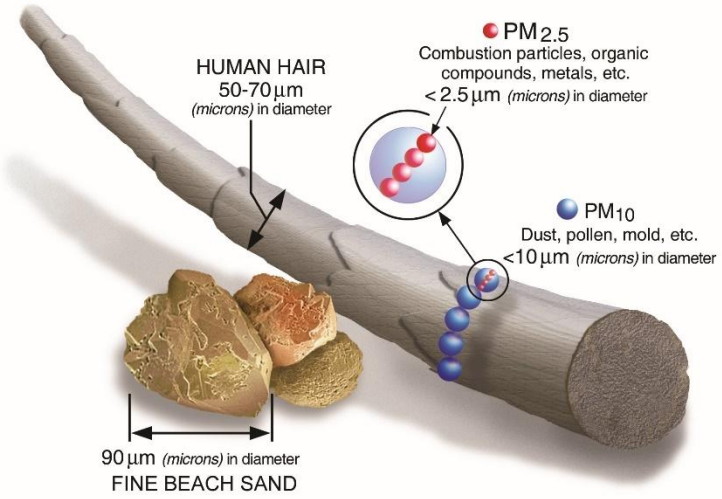

Figure 12-10: Illustration on the size of PM10 (blue) and PM2.5 (red) particles. The comparisons are with fine sand and a human hair.

Exposure to such particles can affect both a person's lungs and heart. Numerous scientific studies have linked particle exposure to a variety of problems, including:

- premature death in people with heart or lung disease
- nonfatal heart attacks
- irregular heartbeat
- aggravated asthma
- decreased lung function
- increased respiratory symptoms, such as irritation of the airways, coughing or difficulty breathing.

Fine particles (PM2.5) are the main cause of reduced visibility (haze) in parts of the United States. All particulate matter settles to the Earth through gravity and precipitation. Particulates

are used as cloud condensation nuclei in the formation of precipitation. Once formed, the precipitation collides with more particles as it falls to the Earth.

Figure 12-11 shows the mean PM2.5 air quality from 2000 through 2022, and is based on 361 sites. Figure 12-12 shows the PM10 air quality from 1990 through 2022, and is based on 83 sites. As you can see, the United States as a whole is below the national standards.

Another video from Harvard University discusses particulate matter and the health effects associated with it. Since particulate matter is both a primary and secondary pollutant, the other pollutants are quickly examined along with the overall efforts of the EPA.

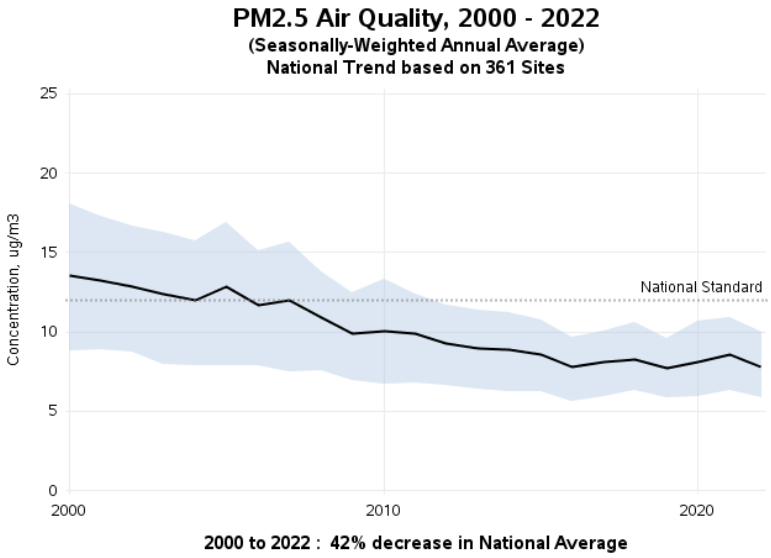

Figure 12-11: A graph of PM2.5 air quality, 2000-2022.

These tiny solid and liquid particles suspended in the atmosphere are also called aerosols. NASA satellites can measure the aerosols in the atmosphere. The NASA aerosol optical thickness is based on the fact that the particles change the way the atmosphere reflects and absorbs visible and infrared light. Figure 12-13 depicts the global aerosol optical thickness. An optical thickness of less than 0.1 (palest yellow) indicates a crystal clear sky with maximum visibility, whereas a value of 1 (reddish brown) indicates very hazy conditions.

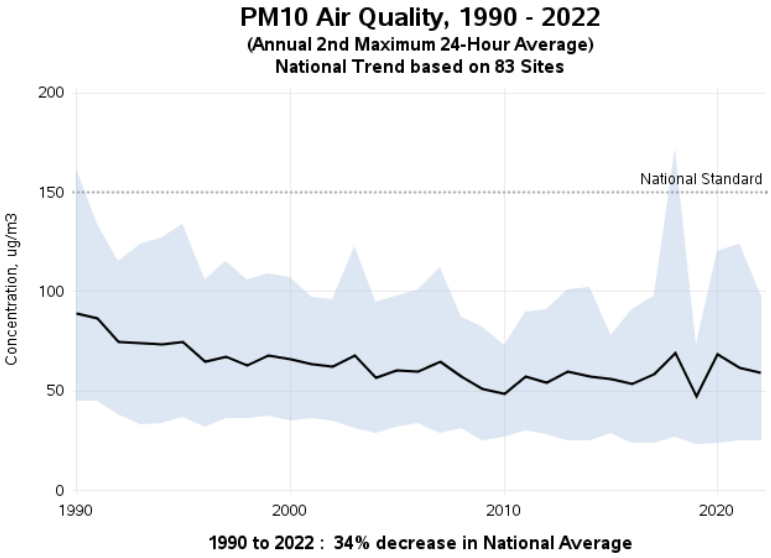

Figure 12-12: A graph of PM10 air quality, 1990-2022.

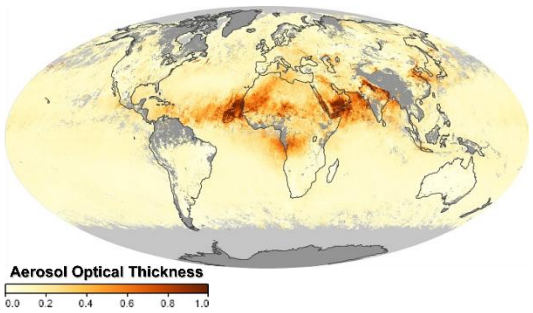

Figure 12-13: A global map of the aerosol optical thickness as measured from a satellite for June 2021. Light yellow are clear skies, and the dark rust colors have very hazy conditions.

12.1.7 – Air Quality Index (AQI)

The EPA established an index for reporting air quality called the **Air Quality Index (AQI)**. The AQI is an indication of the air quality in an area with values ranging from 0 to 500. The higher the AQI value, the greater the level of air pollution and the greater the health concern. For example, an AQI value of 50 or below represents good air quality, while an AQI value over 300 represents hazardous air quality.

For each pollutant, an AQI value of 100 generally corresponds to an ambient air concentration that equals the level of the short-term national ambient air quality standard. AQI values at or below 100 are generally thought of as satisfactory. When AQI values are above 100, air quality is unhealthy for certain sensitive groups of people. As AQI values get higher everyone can be affected.

The AQI is divided into six categories. Each category corresponds to a different level of health concern. Each category also has a specific color. The color makes it easy for people to quickly determine whether air quality is reaching unhealthy levels in their communities. Figure 12-14 chart depicts the AQI.

Daily AQI Color	Levels of Concern	Values of Index	Description of Air Quality
Green	Good	0 to 50	Air quality is satisfactory, and air pollution poses little or no risk.
Yellow	Moderate	51 to 100	Air quality is acceptable. However, there may be a risk for some people, particularly those who are unusually sensitive to air pollution.
Orange	Unhealthy for Sensitive Groups	101 to 150	Members of sensitive groups may experience health effects. The general public is less likely to be affected.
Red	Unhealthy	151 to 200	Some members of the general public may experience health effects; members of sensitive groups may experience more serious health effects.
Purple	Very Unhealthy	201 to 300	Health alert: The risk of health effects is increased for everyone.
Maroon	Hazardous	301 and higher	Health warning of emergency conditions: everyone is more likely to be affected.

Figure 12-14: The EPA Air Quality Index (AQI) described with colors, levels of concern, index values, and a description of the air quality associated with each category.

The AQI is for five major pollutants that are regulated by the Clean Air Act: ozone, particulate matter, carbon monoxide, nitrogen dioxide and sulfur dioxide. The AQI for each pollutant is generally based on the scientific information that supports national ambient air quality standards. The time frame used for the index varies by pollutant. The ozone AQI is an 8-hour index and particulate matter is 24 hours.

This EPA video describes the AQI, and how air quality measurements are used to inform people about their local conditions.

AQI forecasts are issued by state and local air quality forecasts across the country. These forecasts are usually issued in the afternoon for the next day. The forecasters use a number of tools – including weather forecast models, satellite images, air monitoring data, and computer models that estimate pollution movement in the atmosphere. Forecasters also use their knowledge and experience on pollution characteristics in certain communities to issue the air quality forecast for the next day.

The current and forecast air quality conditions for any place in the United States can found by entering your location at this link.

12.2 – The Interactions Between Weather and Pollution

Weather can have a significant impact on air quality, since weather affects the air where pollution is produced or resides. Sunshine, rain, higher temperatures, wind speed, and atmospheric stability all affect pollutant concentrations. This list describes how these weather conditions affect pollution levels:

- Sunshine can cause some pollutants to undergo chemical reactions, resulting in the development of smog.
- Higher air temperatures can speed up chemical reactions in the air.
- Precipitation typically results in less pollution, since it washes away particulate matter and can also wash out pollutants that are dissolvable.
- Wind speed and air turbulence affect how pollutants disperse, or spread out from an area.
- Atmospheric stability affects the mixing depth (volume of atmosphere) where the pollution resides.

Some pollution, such as ground-level ozone, is more easily created in sunny, hot weather. The reactions that create harmful ozone in our atmosphere require sunlight. In the summer, ozone concentrations often reach dangerous levels in cities and nearby rural areas.

The extreme heat and stagnant air during a heat wave increases both the amount of ozone and particulate pollution. Additionally, drought conditions can occur during a heat wave. Droughts favor very dry soil and vegetation, which supports an increase in wildfires. In addition to elevated ozone levels during a heat wave, wildfires will add carbon monoxide and particulate matter to the atmosphere.

Precipitation tends to cleanse the atmosphere of pollutants by collecting them and depositing them on the surface. As the precipitation falls to the Earth, it collect additional pollutants by colliding with them. This collection process is called scavenging.

Wind speed disperses air pollution throughout an area. As the wind speed increases, the dispersion of pollution increases which improves the air quality. Figure 12-15 shows the effect of wind speed on pollution concentrations. As the wind speed doubles, the amount of pollution decreases by half.

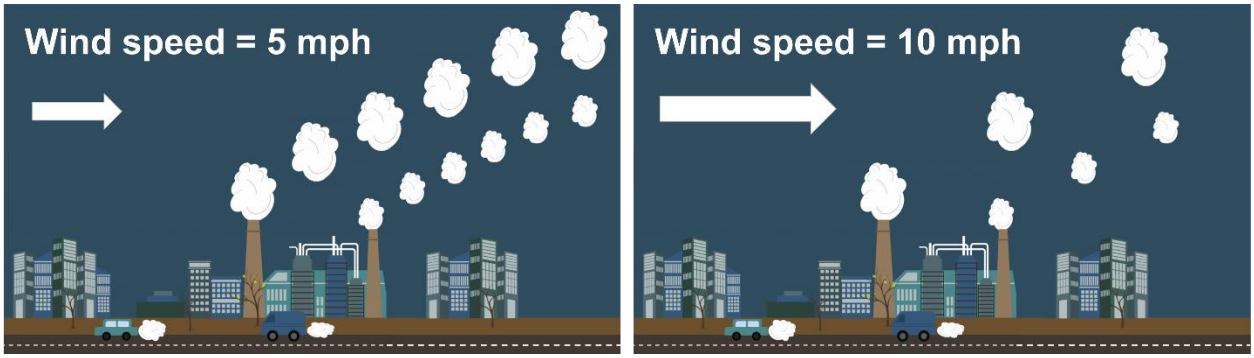

Figure 12-15: A doubling of the wind speed decreases the pollution by half. As the wind speed increases, the pollution is dispersed out of the area faster.

When warm air is present aloft, the atmosphere is stable. Hence, air rising from the surface loses buoyancy and stops. When air pollution is present, an inversion prohibits polluted air from leaving an area. An inversion traps pollution by not allowing it to mix into the atmosphere. Thus, an inversion dramatically degrades air quality.

Figure 12-16 illustrates how an inversion decreases air quality. Rising, warm surface air helps disperse pollution in a normal situation (left). When a temperature inversion is present, the warm air cannot rise, trapping pollution at the surface (right). An inversion essentially acts as a lid over an area to trap pollution.

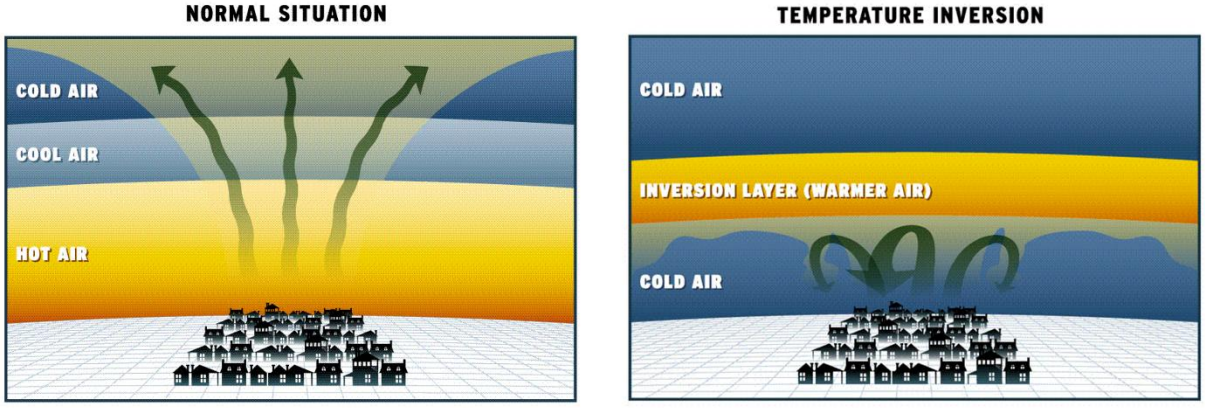

Figure 12-16: (left side) Normal atmosphere where warm air at the surface can rise into the atmosphere. (right side) A temperature inversion halts rising air from the surface to increase pollution levels.

12.2.1 – Acid Rain

Acid rain results when sulfur dioxide (SO_2) and nitrogen oxides (NO_x) are emitted into the atmosphere and transported by wind and air currents. The SO_2 and NO_x react with water, oxygen and other chemicals to form sulfuric and nitric acids. These then mix with water and other materials before falling to the ground.

Figure 12-17 illustrates the pathway for acid rain in our environment: (1) Emissions of SO_2 and NO_x are released into the air, where (2) the pollutants are transformed into acid particles that may be transported long distances. (3) These acid particles then fall to the earth as dust, rain or snow, and (4) may cause harmful effects on soil, forests, streams, and lakes.

Figure 12-17: The pathway for creating acid rain.

1. Emissions of SO2 and NOx are released into the air.
2. The pollutants are transformed into acid particles that may be transported long distances.
3. These acid particles then fall to the earth as dust, rain or snow.
4. This fallout may cause harmful effects on soil, forests, streams, and lakes.

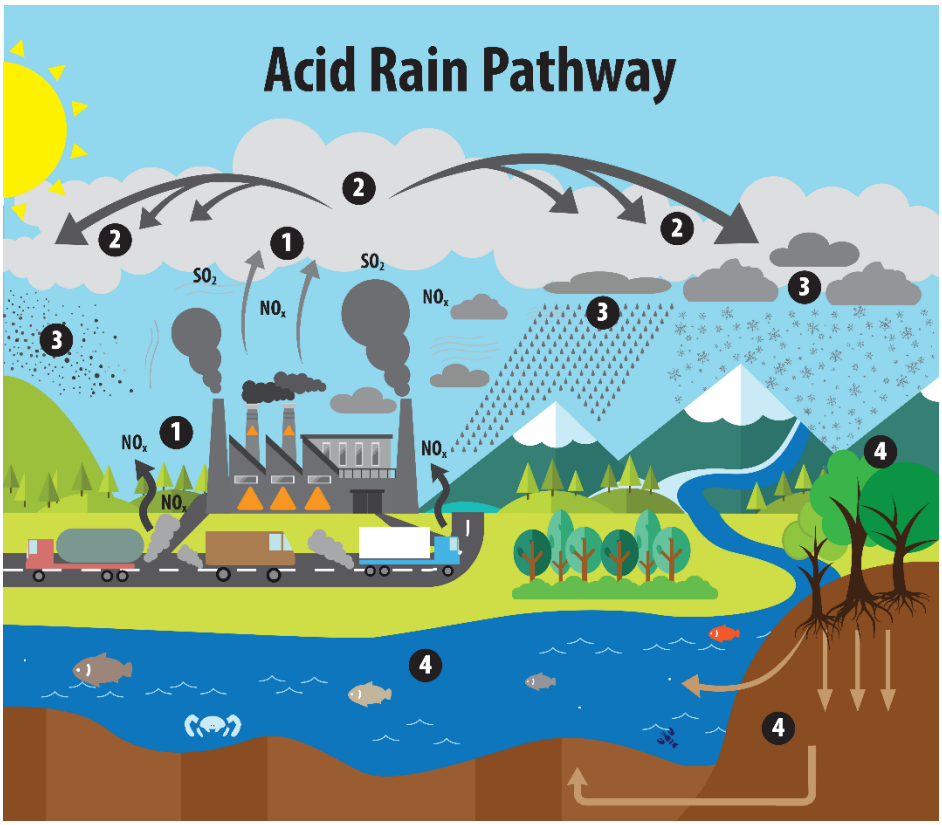

The major sources of SO_2 and NO_x in the atmosphere are:

- Burning of fossil fuels to generate electricity. Two thirds of SO_2 and one fourth of NO_x in the atmosphere come from electric power generators.
- Vehicles and heavy equipment exhaust.
- Manufacturing, oil refineries and other industries.

Winds can blow SO_2 and NO_x over long distances and across borders making acid rain a problem for everyone; not just those living close to these sources.

Acidity and alkalinity are measured using a pH scale for which 7.0 is neutral. The lower a substance's pH (less than 7), the more acidic it is. The higher a substance's pH (greater than 7), the more alkaline it is. Normal rain has a pH of about 5.6. Rain is slightly acidic because carbon dioxide (CO_2) from the atmosphere dissolves into it forming weak carbonic acid. Acid rain usually has a pH between 4.2 and 4.4. This pH scale is depicted in Figure 12-18.

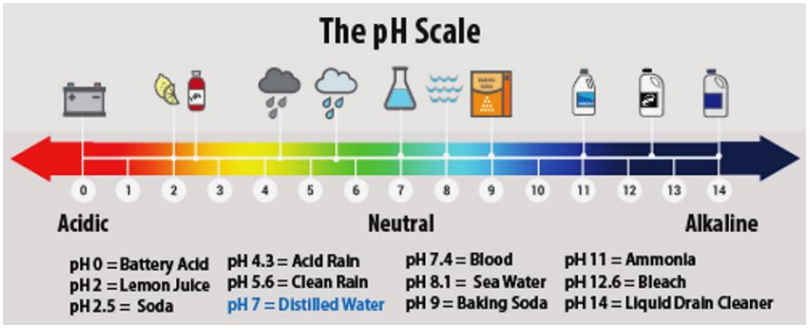

Figure 12-18: The pH scale. Acid rain has a pH of about 4.3.

Figure 12-19 contains two map with the change in the pH of precipitation from 1989 to 2017-2019. These maps indicate the reduction in SO_2 and NO_x pollutants has significantly reduced the occurrence of acidic precipitation in the United States.

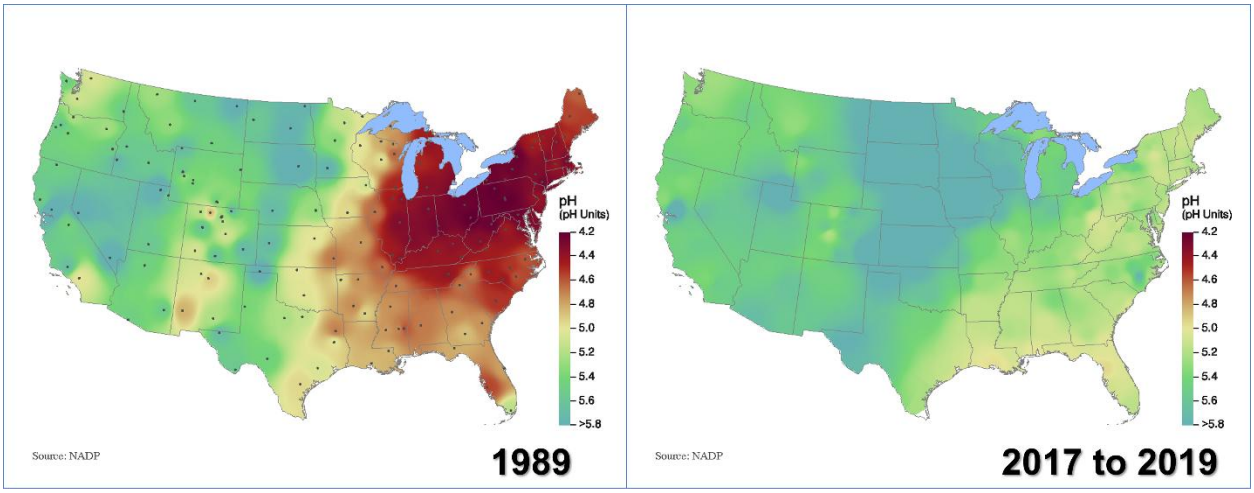

Figure 12-19: The change in precipitation pH from 1989 (left) to 2017-2019 (right). Acid rain are the reddish colors, which are not present in the later time period.

The ecological effects of acid rain are most clearly seen in aquatic environments, such as streams, lakes, and marshes where it can be harmful to fish and other wildlife. As water flows through the soil, acidic rainwater can leach aluminum from soil clay particles and then flow into streams and lakes. The more acid that is introduced to the ecosystem, the more aluminum is released.

Some types of plants and animals are able to tolerate acidic waters and moderate amounts of aluminum. Others, however, are acid-sensitive and will be lost as the pH declines. Generally, the young of most species are more sensitive to environmental conditions than adults. At pH 5, most fish eggs cannot hatch. At lower pH levels, some adult fish die. Some acidic lakes have no fish. Even if a species of fish or animal can tolerate moderately acidic water, the animals or plants it eats might not. For example, frogs have a critical pH around 4, but the mayflies they eat are more sensitive and may not survive pH values below 5.5.

This National Geographic video describes the formation of acid rain and the damage that may result.

12.3 – Heat Islands

Heat islands are urbanized areas that experience higher temperatures than outlying areas. Structures such as buildings, roads, and other infrastructure absorb and re-emit the sun's heat more than natural landscapes such as forests and water bodies. Urban areas, where these structures are highly concentrated and greenery is limited, become "islands" of higher temperatures relative to outlying areas.

The "island" analogy derives from the similarity between the pattern of isotherms and the height contour pattern of an island on a topographic map. Heat islands commonly possess a temperature gradient at the urban–rural fringe, and a maximum value in the most built-up core

of the city. The annual mean temperature of a large city (say a million people) may be 1° to 2°C warmer than before development, and on individual calm, clear nights may be up to 12°C warmer. Nighttime temperatures are most affected by the heat island effect. This warmth extends vertically to form an urban heat dome under light wind conditions.

Figure 12-20 contains a conceptual map of isotherms over a city, and illustrates a heat island. Lights winds across a city tend to shift the heat island isotherms, as shown in Figure 12-20.

Figure 12-20: A conceptual map of a heat island associated with a city. The red dashed line is the center of the city. In this example, a light west wind shifts the heat island slightly to the east.

These warmer temperatures vary inside the city itself. Some areas are hotter than others due to the uneven distribution of heat-absorbing buildings and pavements, while other spaces remain cooler as a result of trees and greenery.

Figure 12-21 contains graphs that depict the day and night surface and air temperatures over a city. Urban parks, ponds, and residential areas are cooler than the downtown areas. Downtown areas are generally the hottest during the day and at night.

Surface temperatures vary more than air temperatures aloft during the day, but they are generally similar at night. The dips and spikes in surface temperatures over the pond area (Figure 12-21) show how water maintains a nearly constant temperature day and night because of its higher specific heat. The pond can be thought of as a small scale marine environment. Parks, open land, and bodies of water can create cooler areas within a city. Temperatures are typically lower at suburban-rural borders than in the central downtown areas.

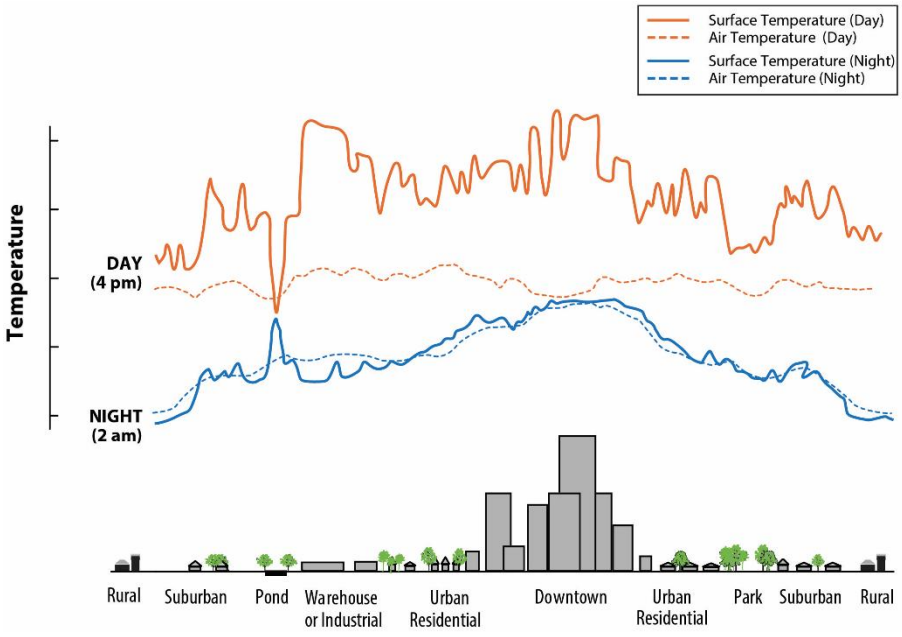

Figure 12-21: The variation of surface and air temperatures across an urban environment. Orange are day time values and blue are during the night. The solid lines are surface temperatures, and the dashed lines are air temperatures.

This short video from National Public Radio (NPR) provides an overview of heat islands.

12.3.1 – Urban Heat Island Examples

Providence, Rhode Island has a noticeable heat island with about 83% of the city being densely developed. Providence is approximately 12°C warmer than its surroundings. Figure 12-22 is a satellite image depicting the temperatures in Providence and the surrounding area. The white line delineates the Providence city limits. The dark purple are cooler temperatures and the yellowish colors are warmer. The area surrounding Providence tends to be dense forest. Heat islands are more pronounced when forests surrounds a city.

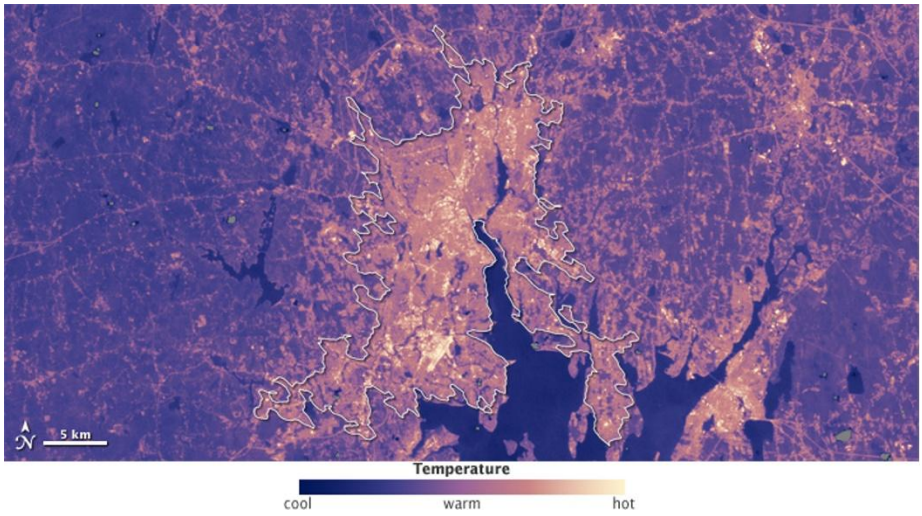

Figure 12-22: Satellite picture depicting the temperatures in Providence, Rhode Island. The white line is the Providence city limits.

As a city grows the heat island associated with it expands. The Phoenix Metropolitan Area in Arizona has grown considerably over the past 100 years. Figure 12-23 illustrates the changes in land use from 1912 to 2000. The green areas are land used for agricultural purposes. The orange/brown areas are land which is urbanized. The gray areas are the native desert landscape. As shown, the Phoenix Metropolitan Area has grown considerably over time by expanding into the surrounding agriculture and desert areas.

Figure 12-24 diagram shows the monthly mean minimum temperatures in June from 1990 to 2004 over the Phoenix area; a 15 year period. Each map represents a 5-year period of time. The overall increase in June mean

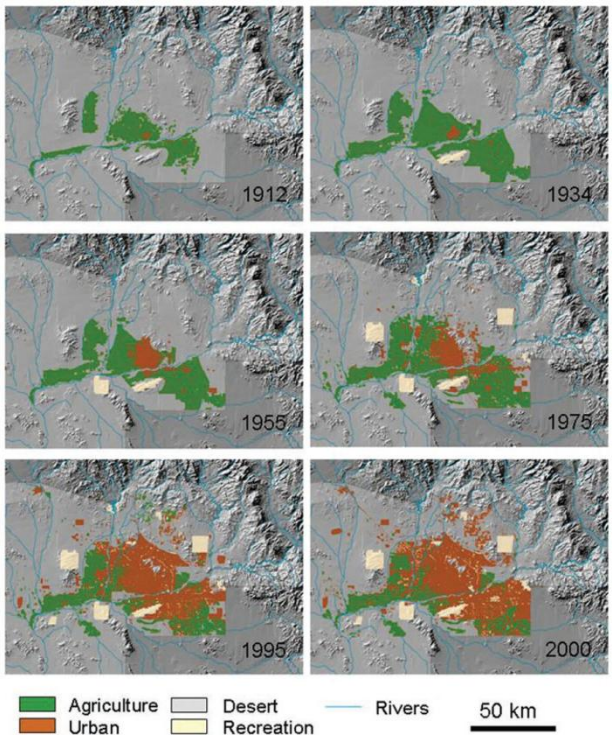

Figure 12-23: Land use changes over the Phoenix, Arizona metropolitan area from 1912 to 2000.

minimum temperatures has been 2°C or higher across the city. This temperature change is a result of the expansion of the urban areas and a contraction of the agricultural areas. Changes in vegetation within a city can have a significant impact on its heat island.

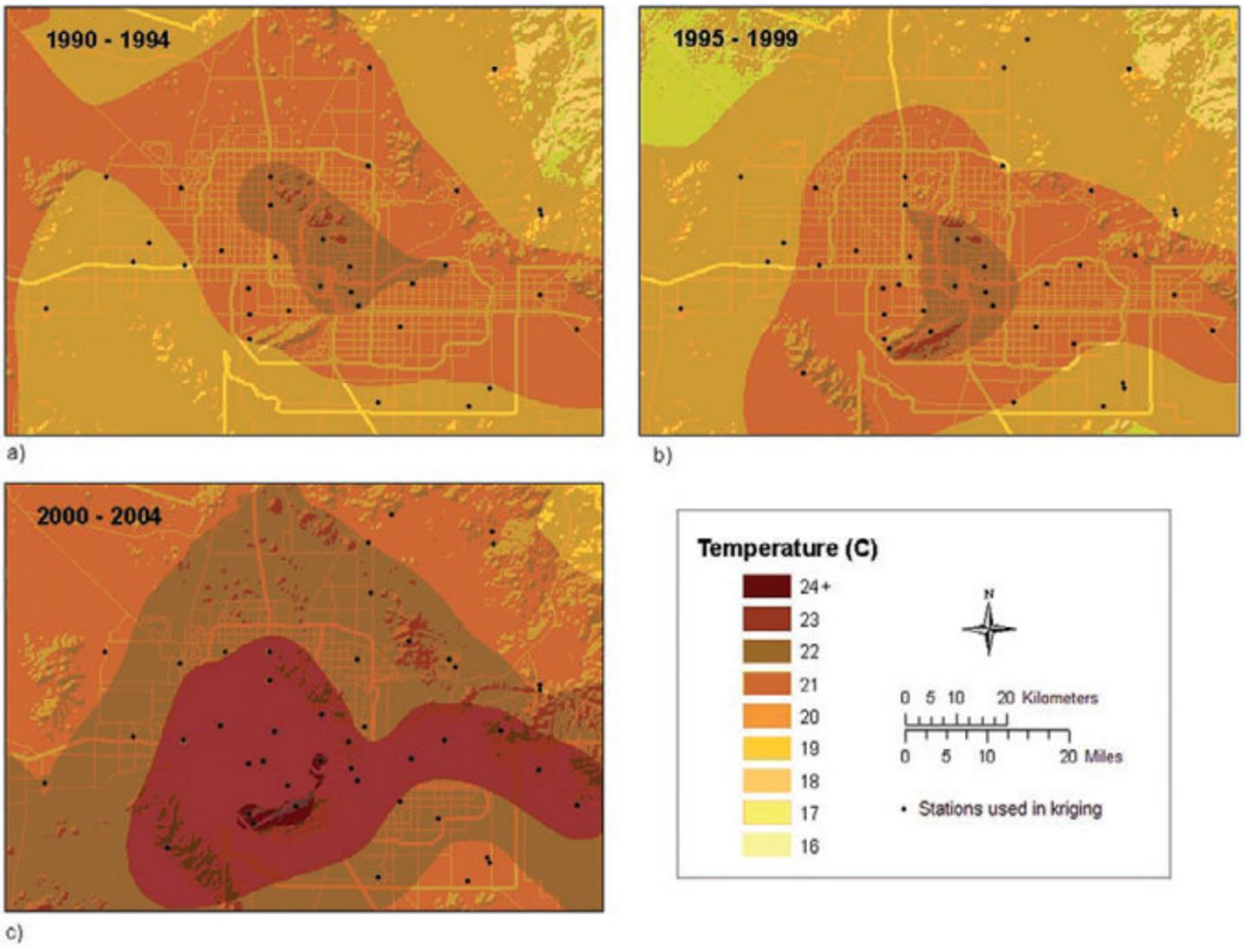

Figure 12-24: Mean June temperature changes over the Phoenix, Arizona metropolitan area in 5 year increments from 1990 to 2004. Large areas of the city rose 2°C or higher in 15 years.

12.3.2 – Heat Islands and Vegetation

Figure 12-25 contains images from NASA that show the cooling effects of plants on New York City's heat island. On the left side of this figure depicts vegetation with the darker green indicating more vegetation. The right side depicts the surface temperatures of the same area; dark purple colors represent cooler temperatures and yellowish colors represent warmer. Notice how the regions of dark green (more vegetation) match up with the areas of dark purple (cooler temperatures). Likewise, areas with little vegetation are hotter.

From Chapter 2 on Earth's Energy Balance, we know that both latent and sensible heat are transferred from the surface to the atmosphere. Latent heat is the energy required to change the phase of water. Sensible heat is the transfer of heat that results in a temperature change.

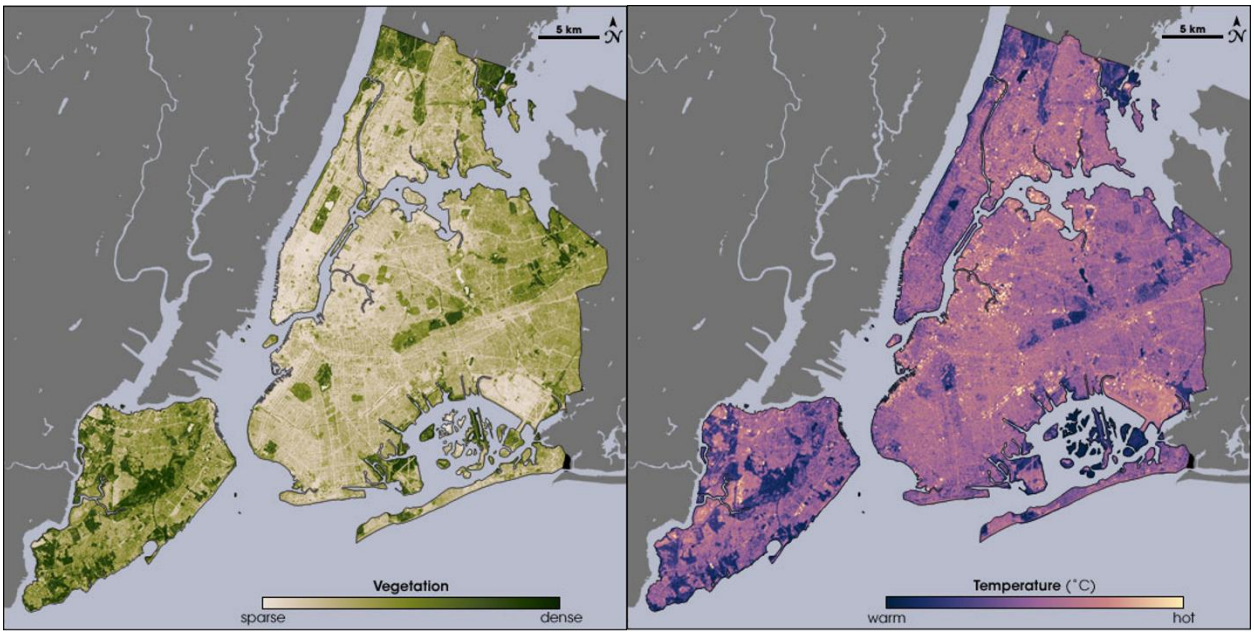

Figure 12-25: Satellite images depicting the vegetation in New York City (left) and the surface temperatures of the same area (right). Areas with more vegetation (dark green) are cooler (dark purple).

In an urban environment, vegetation has been reduced and surfaces such as roads are impervious to precipitation. In other words, when precipitation occurs the water tends to runoff rather than infiltrating into the soil. Both of these conditions greatly reduce the latent heat which is released from the surface. Impervious surfaces have no water to evaporate for cooling. The reduction in plants in an urban area reduces the cooling from transpiration. In a suburban and rural environment, vegetation has increased and more land is available for precipitation to infiltrate into the soil. These two changes allow for more significant cooling to occur through latent heat.

Sensible heat cooling dominates downtown areas. The urbanized downtown area has higher temperatures already with latent heat transfer limited, so sensible heat is the primary mechanism available. For an environment with more vegetation, sensible heat is secondary to the latent heat cooling process. Figure 12-26 illustrates these concepts of latent and sensible.

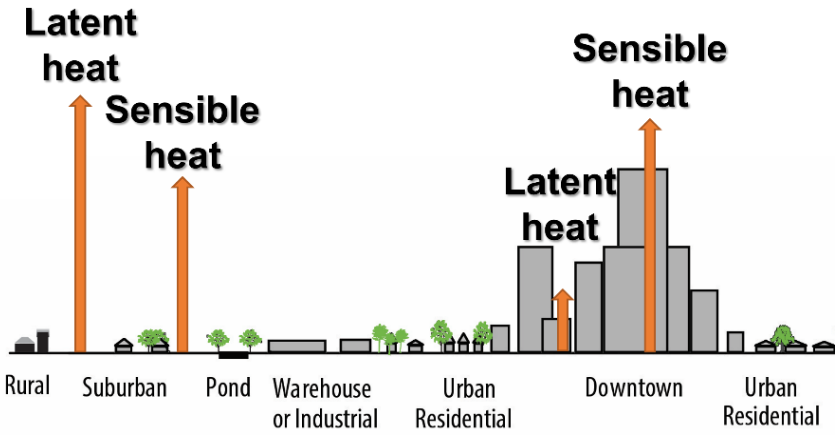

Figure 12-26: Diagram illustrating the differences between latent and sensible heat in rural/suburban and downtown areas. The reduced latent heat transfer in cities supports the formation of a heat island.

Using data from multiple satellites, NASA researchers modeled urban areas and their surroundings. The researchers found that areas covered in part by impervious surfaces had an

average summer temperature 1.9°C higher than the surrounding rural areas. In winter, the temperature difference was 1.5°C higher. Figure 12-27 shows the results of their study.

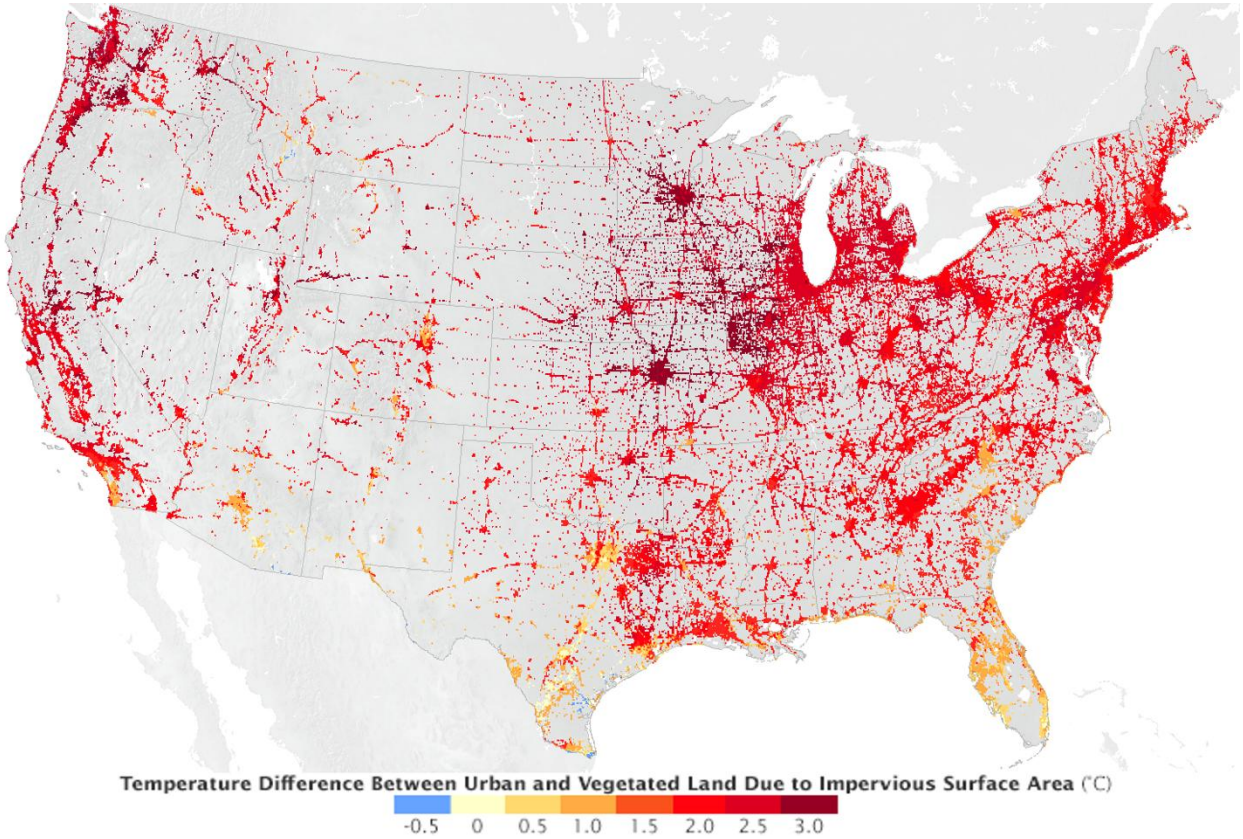

Figure 12-27: Temperature difference between urban and vegetated land due to impervious surface area. Essentially, all cities exhibit a heat island.

Given this knowledge of what influences heat islands, many communities are taking action using these strategies:

- Increasing tree and vegetative cover.
- Installing green roofs (vegetation growing on a roof).
- Installing reflective roofs.
- Using cooler pavements (either reflective or permeable).
- Keeping more open space in new developments.

This video from NASA discusses urban heat islands and what causes them.

12.4 – Earth's Climate System

Earth's climate system consists of these interacting components.

The atmosphere is the air and weather above the Earth's surface.
The ocean which covers almost 70% of the Earth's surface, and is often referred to as the hydrosphere.
The cryosphere contains Earth's snow and ice, which includes sea ice, glaciers and the ice sheets.
The biosphere contains all living things on the land and in the seas, especially plants.
The lithosphere contains rocks and the Earth's mantle.

When trying to understand how climate varies and changes on long (millennial and longer) time scales, knowledge about all these components is needed. The remainder of this book will examine specific pieces of these components as they affect our climate system. A change in one component usually affects the other components, since they are all related.

Due to the importance of CO_2 as a greenhouse gas, the carbon cycle is a critical part of the climate system. Carbon is one of the most important elements on Earth. It is the principal building block for the organic compounds that make up life. Carbon occurs in many forms and places on Earth. It is a major constituent of limestone, occurring as calcium carbonate. It is dissolved in ocean water and fresh water. It is present in the atmosphere as carbon dioxide.

The flow of carbon through the climate system components is complex, and is called the **carbon cycle**. The carbon cycle is a topic of great interest because human activities are altering it. Determining the exact transfer of carbon through this cycle is an active topic of research. These two short videos describe the carbon cycle. The first video is from the National Oceanic and Atmospheric Administration. The second video is from the University of Toledo. These videos provide a basic understanding of the carbon cycle.

Most of Earth's carbon—about 65,500 billion metric tons—is stored in rocks. The rest is in the ocean, atmosphere, plants, soil, and fossil fuels. Figure 12-28 gives more details on this carbon cycle and its interactions within the Earth climate system. The numbers are in gigatons of carbon per year.

A gigaton is a billion metric tons or 10^{15} grams, which is a lot of carbon. The yellow numbers are natural fluxes. The red numbers are human contributions. White numbers indicate stored carbon, which is referred to as a carbon reservoir. The exact numbers representing carbon movements in any global carbon cycle diagram vary depending on the references used by its author. These variations in numbers are a consequence of scientists' incomplete understanding of the carbon cycle. Additionally, new numbers become available as the state of the science progresses.

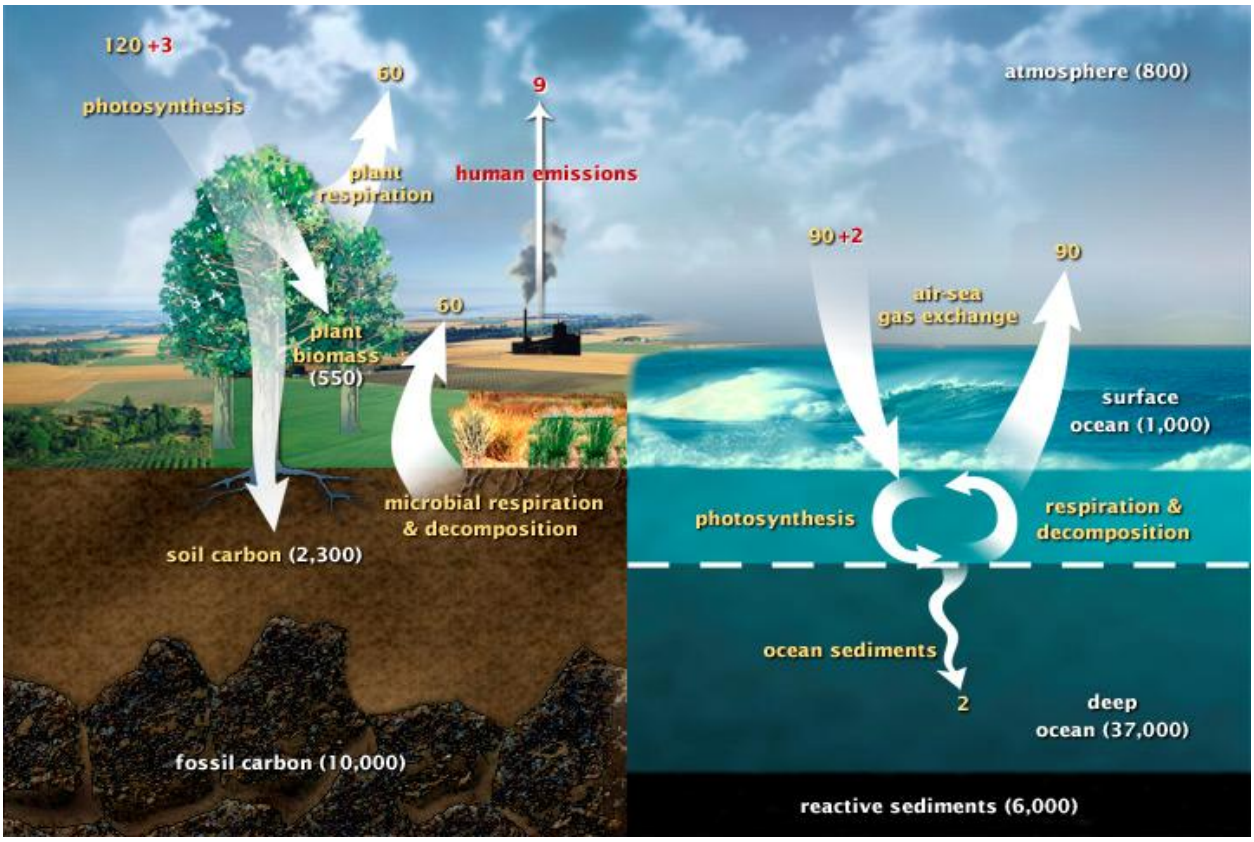

Figure 12-28: A diagram depicting Earth's carbon cycle. Yellow numbers are naturally occurring fluxes. Red numbers are human contributions and white indicate stored carbon, referred to as carbon reservoirs.

The left side of Figure 12-28 depicts the terrestrial processes of carbon flow. The right side of this figure depicts the oceanic processes of carbon flow. Carbon is removed from the atmosphere by plant photosynthesis and the air-sea gas exchange (down arrows). Carbon is put into the atmosphere by plant respiration, microbial respiration and decomposition, human emissions, and the air-sea-gas exchange (up arrows). The arrows below the surface are how the carbon moves once it is out of the atmosphere.

To understand the carbon cycle better, some of the individual components of the cycle need to be examined. The remaining sections in 12.4 examine these components in more detail.

12.4.1 – Plant Photosynthesis and Respiration (Natural)

Photosynthesis is the process by which plants use sunlight, carbon dioxide, and water to create carbohydrates (sugar) and oxygen. Carbon dioxide is taken from the atmosphere, and oxygen is put out into the atmosphere. Photosynthesis occurs during the day and can be expressed as the chemical equation shown below. Chemical equations are similar to math equations in that the number of elements on each side of the equation must be equal. Notice the six carbon atoms on the left side are the same as on the right.

$$6CO_2 + 6H_2O + \text{light} \rightarrow C_6H_{12}O_6 + 6O_2$$

Respiration converts oxygen and carbohydrates into water, carbon dioxide, and produces heat. Respiration is the exact opposite of photosynthesis and occurs at night. The equation below depicts respiration.

$$C_6H_{12}O_6 + 6O_2 \rightarrow 6CO_2 + 6H_2O + \text{heat}$$

Figure 12-29 shows how plants interact with the atmosphere to accomplish photosynthesis and respiration. During the day, plants take in carbon dioxide and put out oxygen. During the night, respiration takes in oxygen and puts out carbon dioxide. Water generally comes in through the vascular structure of the plant.

Photosynthesis and respiration do not balance each other. For a plant to grow, some of the carbohydrates must be stored. The difference between photosynthesis and respiration is called net photosynthesis. The growth of a plant depends on net photosynthesis, and this growth creates its biomass.

Experiments on a variety of plants indicate that the ratio of photosynthesis to respiration is about 2 to 1. When plants are young and growing rapidly, but with not much biomass to maintain, this ratio is even higher. In older, larger plants this ratio is lower, since more carbon needs to go towards maintenance.

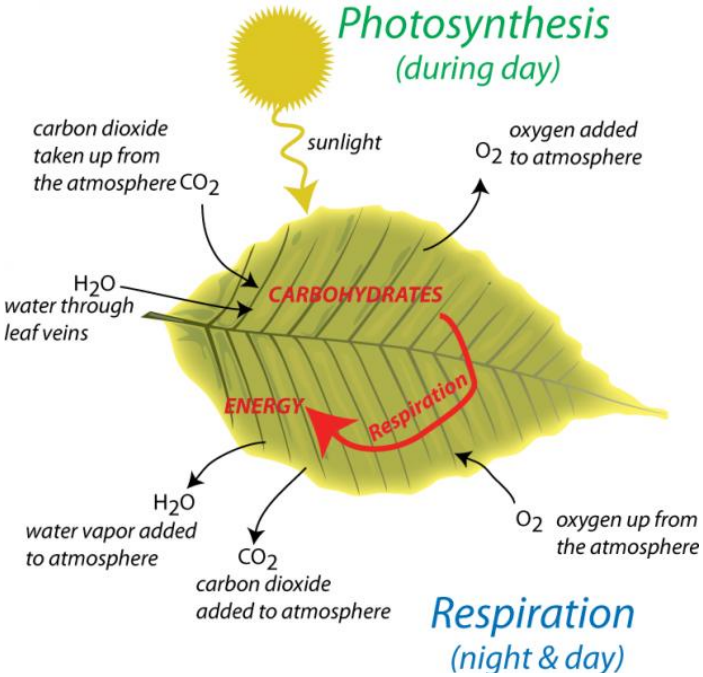

Figure 12-29: An illustration of photosynthesis (top) and respiration (bottom) in a plant. Photosynthesis and respiration are not balanced, which allows a plant to grow.

Trees are amazing carbon storage experts. Depending on the species, approximately 50 to 80% of a tree's weight is made of carbon. This carbon comes from the atmosphere as CO_2. Figure 12-30 shows the carbon cycle of a tree. Each leaf on a tree must operate on the production side of photosynthesis. If sufficient photosynthesis is not occurring, the tree will release the leaf and let it fall to the ground. This carbon is then transferred into the soil.

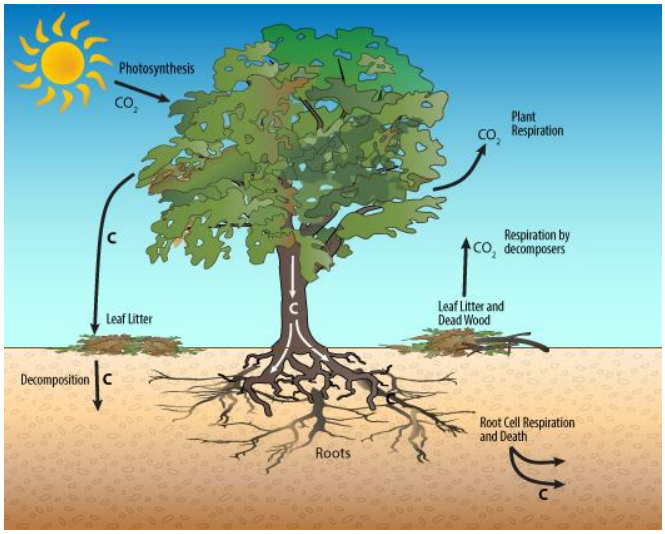

Figure 12-30: The carbon cycle of a tree. From 50% to 80% of a tree's weight is made of carbon, which comes from the atmosphere.

The terrestrial carbon flow explored in this section are circled in black in Figure 12-31. The human contribution red numbers will be explored in section 12.4.5. Note that photosynthesis in this figure has the highest removal of carbon from the atmosphere. The plant biomass number accounts for vegetation that resides on the Earth for many years, such as trees. Since trees can live for hundreds of years, they are a carbon reservoir and are displayed as white numbers.

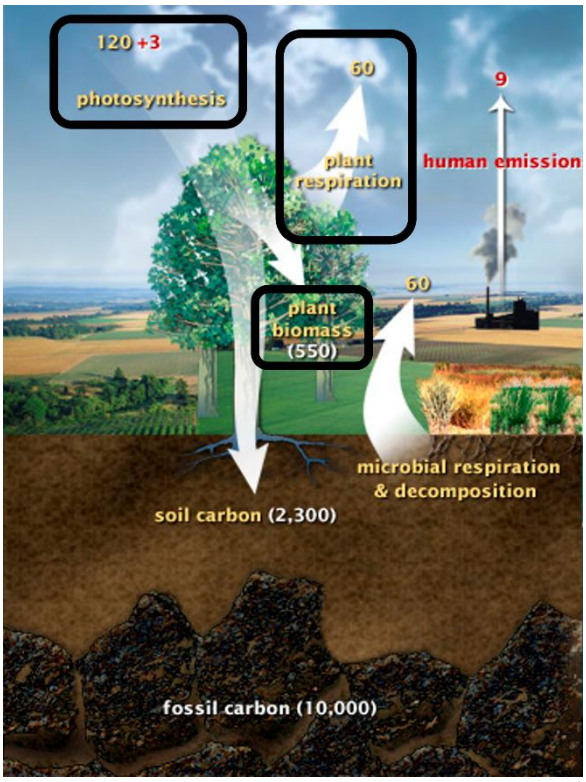

Figure 12-31: Diagram highlighting the plant carbon aspects of the carbon cycle. Photosynthesis is the process that removes the most carbon from the atmosphere.

12.4.2 – Soil Carbon and Decomposition (Natural)

Carbon enters the soil by two paths: (1) dead plant material falls to the ground as litter, and (2) plant roots contribute carbon from their roots. The relative importance of these two pathways into the soil varies according to the plant, but measurements suggest that the two paths are about equal. This situation may seem surprising, since we do not see the loss of organic carbon from the root system. We do see the change in a plant above the ground. For example, we see the leaves that fall off a tree, but see nothing about the roots that are changing below the ground.

Decay (also called respiration) occurs within the soil, as microorganisms consume the dead plant material. In terms of a chemical formula, this process is the same as described previously or plant respiration. The microbes living withing the soil are the keys by which nutrients such as carbon and nitrogen cycle through the soil system. A great diversity of microorganisms live in the soil and can consume tremendous quantities of organic material. This decay releases CO_2 back into the atmosphere. The tree diagram in Figure 12-30 illustrates these additional aspects of the plant carbon cycle well.

Soil microbes causing the decomposition to occur require oxygen. As leaf litter and roots move further into the soil, oxygen becomes scarce and decomposition halts. This carbon stored in the soil becomes a reservoir and remains until the soil is disturbed. Bringing these partially decayed items back into contact with the atmosphere will restart the decomposition process.

In recent years, increasing attention has been directed at permafrost soil carbon since the polar regions are warming. As the permafrost melts, partially decomposed carbon residing in the soil

starts decomposing and releasing CO_2 into the atmosphere. Given that most of the permafrost is still frozen, this source of carbon in the atmosphere is not being observed yet.

The terrestrial carbon flow explored in this section are circled in black in Figure 12-31. Notice that the microbial respiration and decomposition carbon (60) and the plant respiration carbon (60) being released into the atmosphere balances the photosynthesis carbon (120) being removed. The large number for soil carbon represents a carbon reservoir of partially decomposed plant material. After residing in the Earth for several hundred million years, soil carbon can become fossil carbon (fuel).

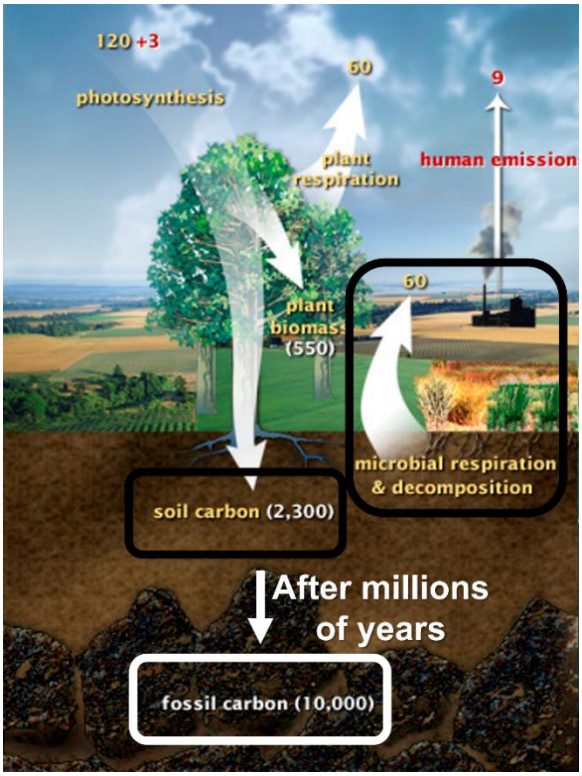

Figure 12-32: Diagram illustrating the soil carbon aspects of the carbon cycle. Much of the soil carbon resides in the Earth for many years and as such is a long-term carbon (fossil) reservoir.

12.4.3 – Ocean-atmosphere Exchange (Natural)

Having explored the terrestrial processes of the carbon cycle, let us now examine the processes occurring in the oceans. Carbon cycling through the oceans is tremendously important. Figure 12-33 contains the air-sea exchange highlighted with the black boxes. Carbon dioxide is always present in the ocean, much in the same manner that it is always present in the atmosphere. The atmosphere and the oceans are constantly exchanging carbon with each other. Much like with photosynthesis and respiration in the terrestrial aspects (Figures 12-30 and 12-31), this exchange of carbon is balanced. Additionally, the ocean surface always has a reservoir of carbon. The surface ocean reservoir is similar to the plant biomass reservoir on the terrestrial side.

Carbon dioxide can be dissolved in seawater, just as it can be dissolved in a can of soda. Carbon dioxide can also be released from seawater, again similar to a can of soda. This transfer of gas back and forth between a liquid and the atmosphere is an extremely important process in the global carbon cycle.

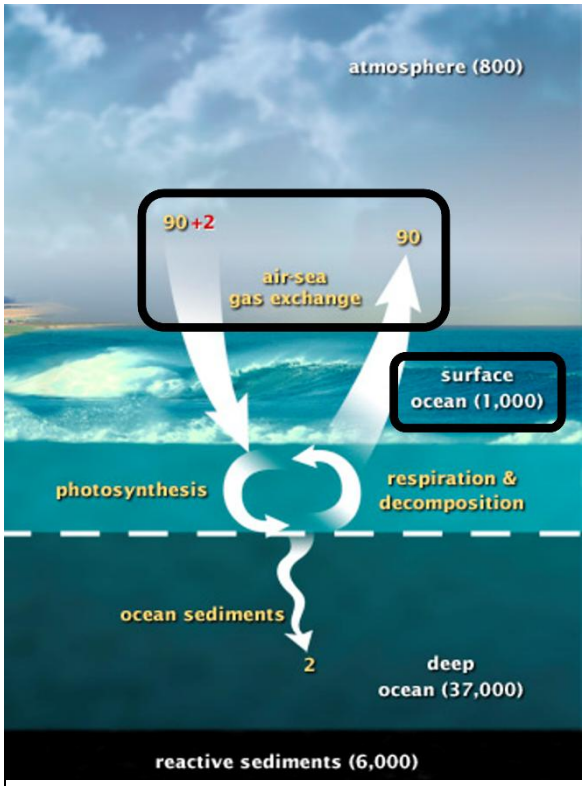

Figure 12-33: Diagram illustrating the air-sea gas exchange between the atmosphere and ocean.

The exchange of a gas, like CO_2 between the air and seawater, is governed by the differences in concentrations (pCO_2) as shown in Figure 12-34. The solid red line represents the concentration in the air and in the ocean before changes occur. The dashed red line indicates what the concentration might look like after the exchange of CO_2 occurs — lower concentration in the atmosphere, and higher in the oceans. Note that the change in concentration is less in the ocean than in the atmosphere, which is a result of carbon chemistry occurring in the water.

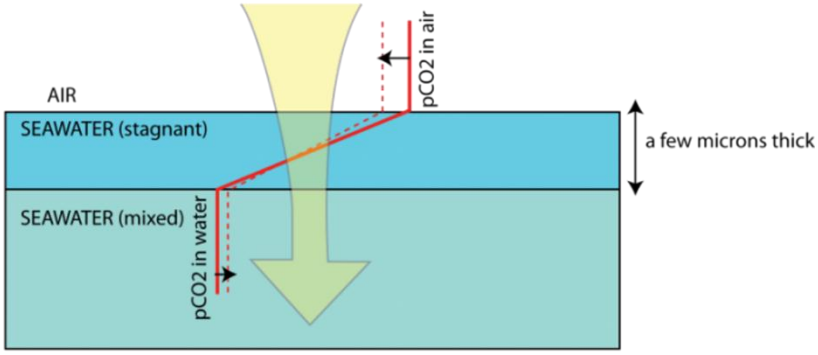

Figure 12-34: Details of the air-sea carbon dioxide exchange. The solid red line is the carbon dioxide concentration (pCO_2) before the exchange. The dashed red line is the concentration after the exchange. The atmosphere concentration decreases, and the seawater concentration increases.

In general, this exchange depends on the concentration of CO_2 in the atmosphere and the oceans, but it gets a little complicated because the concentration of CO_2 in seawater depends on a number of other factors. To understand this process, and to see why the atmosphere's concentration changes more than the ocean, we need to have a sense of what happens to CO_2 once it gets dissolved in seawater.

When CO_2 from the atmosphere comes into contact with seawater, it dissolves directly into the water. Once in the water, it undergoes chemical reactions to form a series of products, such as:

1. CO_2 (dissolved gas) + $H_2O \leftrightarrow H_2CO_3$ (carbonic acid)
2. H_2CO_3 (carbonic acid) $\leftrightarrow H^+ + HCO_3^-$ (hydrogen ion + bicarbonate)
3. $HCO_3^- \leftrightarrow H^+ + CO_3^{-2}$ (hydrogen ion + carbonate)

The amount of CO_2 as dissolved gas is what controls the concentration of CO_2 shown in Figure 12-34. This concentration depends strongly on the temperature. The concentration is lower in cold water and it is higher in warm water. Hence, the colder parts of the ocean absorb CO_2 from the atmosphere and the warm parts of the ocean release CO_2 into the atmosphere.

Due to these chemical reactions, all these different carbon compounds co-exist. In reality bicarbonate (HCO_3^-) is the dominant form of inorganic carbon in seawater; carbonate (CO_3^{2-}) and dissolved CO_2 are important, but secondary.

The important aspect of this seawater chemistry exploration is that CO_2 does not dissolve directly into the oceans and stop as carbonic acid. Other chemical processes are present in the ocean associated with the carbon cycle, which makes the oceanic processes of the carbon cycle rather complex.

12.4.4 – Marine Biome (Natural)

The surface waters of the world's oceans are home to a great number of organisms that include photosynthesizing phytoplankton at the base of the food chain. Phytoplankton, also known as microalgae, are similar to terrestrial plants in that they contain chlorophyll and require sunlight in order to live and grow. Most phytoplankton are buoyant and float in the upper part of the ocean,

where sunlight penetrates the water. Phytoplankton also require inorganic nutrients such as nitrates, phosphates, and sulfur which they convert into proteins, fats, and carbohydrates.

These plants utilize the CO_2 gas dissolved in seawater and turn it into organic matter. Just like land-based plants, phytoplankton perform photosynthesis and respiration, taking and returning CO_2 to the water. Figure 12-35 is an image of phytoplankton.

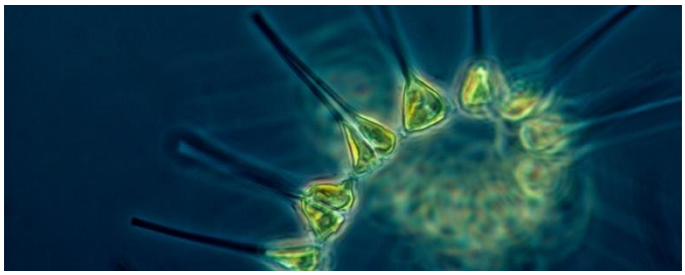

Figure 12-35: An image of phytoplankton.

At the same time, many planktonic organisms extract dissolved carbonate ions from seawater and turn them into $CaCO_3$ (calcium carbonate) shells. When these planktonic organisms die, they decompose and settle into deeper water. This carbon reservoir in the deep ocean exceeds even the amount of carbon estimated to reside in fossil fuels.

Eventually the calcium carbonate shells sink to the bottom of the ocean and become sedimentary rocks. These types of rocks are commonly referred to as limestone. Limestone is present in many places, such as the White Cliffs of Dover found in England (see Figure 12-36). These cliffs were formed from calcium carbonate of planktonic organisms that lived over 100 million years ago.

Figure 12-36: The White Cliffs of Dover, which are calcium carbonate from planktonic organisms that lived over 100 million years ago.

The black box on Figure 12-37 highlights the oceanic processes of the carbon cycle explored in this section. The top portion of the black box is associated with the phytoplankton doing photosynthesis and respiration. The bottom portion is associated with the calcium carbonate of planktonic organisms. Notice that the deep ocean is the largest carbon reservoir in the carbon cycle.

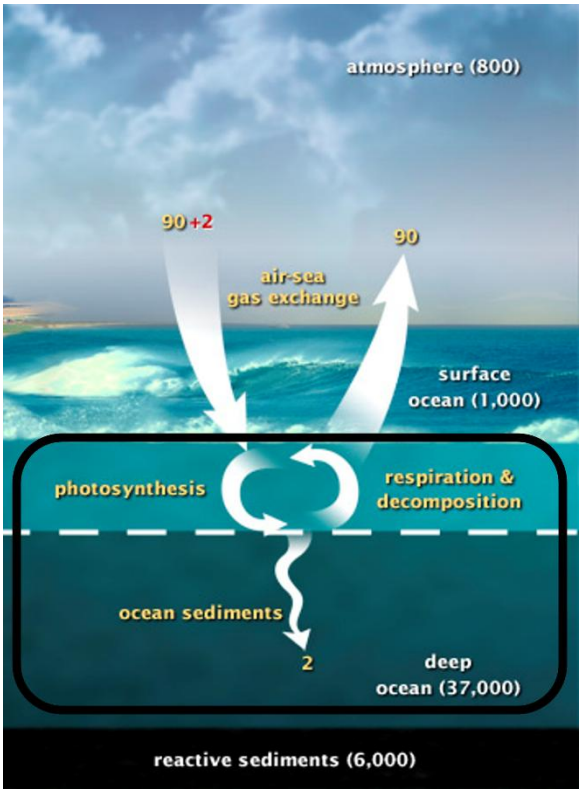

Figure 12-37: Diagram illustrating the marine aspects of the carbon cycle. The largest carbon reservoir is in the deep ocean.

12.4.5 – Human Influences on the Carbon Cycle (Anthropogenic)

This section examines the human influences on the carbon cycle. Specifically, the red numbers in Figure 12-28 will be explored. A pathway for carbon to move into the atmosphere is through the burning of fossil fuels. Fossil fuels are deposited in sedimentary rocks and are essentially the fossilized remains of marine and land plants. The remains took many millions of years to be converted into the oil and coal that are now extracted. Thus, once fossil fuels are used, they will take an equally long time period to be replaced.

Fossil fuels are composed of carbon and hydrogen. The combustion of fossil fuels involves the use of oxygen and the release of carbon dioxide and water. The use of these fossil fuels is currently at about 7.5 gigatons of carbon per year. This carbon enters the atmosphere and influences many facets of the terrestrial and oceanic carbon flows.

Additionally, land-use changes such as deforestation alter the global carbon cycle. When deforestation occurs, most of the plant matter is either left to decompose on the ground or is burned. Burning is a common occurrence, and releases carbon back into the atmosphere immediately. Estimates place this additional CO_2 into the atmosphere at about 1 to 2 gigaton of carbon per year. Adding these two human contributions together totals approximately 9 gigatons of carbon per year.

The map in Figure 12-38 shows the change in forestation from 2000 to 2012. The losses are the red areas. The gains are in purple and blue. Unchanged forests are green. In the tropics, forests are being removed often through fire, and as such release carbon dioxide into the atmosphere.

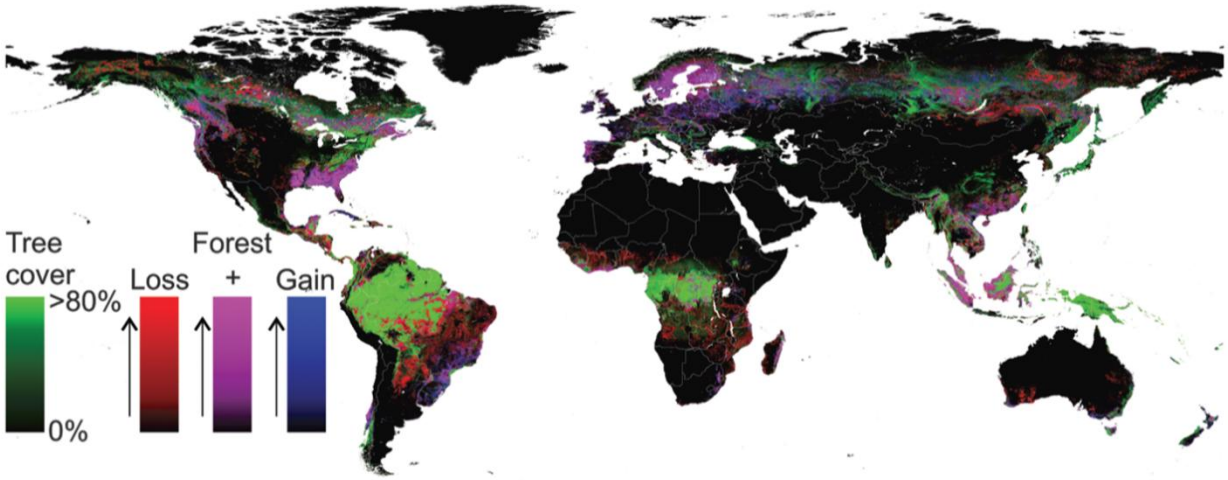

Figure 12-38: Changes in global forestation from 2000 to 2012. Areas experiencing a loss are in red. Blue and purple areas are gains, and green areas are no change.

Increased carbon in the atmosphere will cause changes in the land carbon cycle. Carbon dioxide increases temperatures, extending the growing season and increasing humidity. Both factors have led to additional plant growth. Plants have taken up approximately 30 percent of the carbon dioxide that humans put into the atmosphere. The amount of carbon that plants take up varies greatly from year to year, but in general, the world's plants have increased the amount of carbon dioxide they absorb since 1960. Hence, photosynthesis takes up about 3 gigatons per year of the carbon produced through human activities. This increase in growing season length and plant growth supports improved food production.

With a higher concentration of carbon dioxide in the atmosphere, the oceans take up about 2 gigatons per year of the carbon produced through human activities, or about 25% of the carbon humans put into the atmosphere. All these numbers and percentages are constantly changing as our knowledge about the carbon cycle increases. However, the underlying fact is the atmosphere is receiving the largest portion of the carbon dioxide generated through human activities. Most of the carbon dioxide put into the atmosphere is through the burning of fossil fuels.

12.5 – Energy Resources

Much of the anthropogenic carbon released into the atmosphere is associated with using energy, such as transporting goods or creating electricity. The United States uses and produces many different types and sources of energy. These energy resources can be grouped into two general categories, renewable and nonrenewable. **Renewable** energy is from sources that are naturally replenishing, but may be time limited. Renewable resources are virtually inexhaustible in the long-term, but can be limited to what is available at any given moment. For example, solar energy will remain a renewable resource as long as the Sun exists, which will be for billions of years. However, solar energy is diminished on cloudy days and generates no electricity at night.

The major types of renewable energy sources are:

- Solar energy from the Sun.
- Geothermal energy from heat inside the Earth.

- Wind energy from atmospheric air motions (weather).
- Biomass from plants.
- Hydropower from flowing water.

Nonrenewable resources are limited to the amounts that can be extracted from the Earth. Nonrenewable energy sources once used either cannot be replenished, such as uranium in nuclear power, or take many millions of years to replenish, such as petroleum. The types of nonrenewable energy sources are:

- Petroleum from the remains of animals and plants that lived a long time ago.
- Coal from the remains of plants that lived long ago.
- Natural gas and hydrocarbon liquids from the remains of animals and plants that lived long ago.
- Nuclear energy from fission using large atoms like uranium that split apart.

The fossil fuels are petroleum, coal, and natural gas.

The consumption of energy in the United States is shown by the pie chart in Figure 12-39. The British thermal unit (Btu) used in the chart is a measure of the heat content obtained from the energy source. One Btu is approximately equal to the energy released by burning a match.

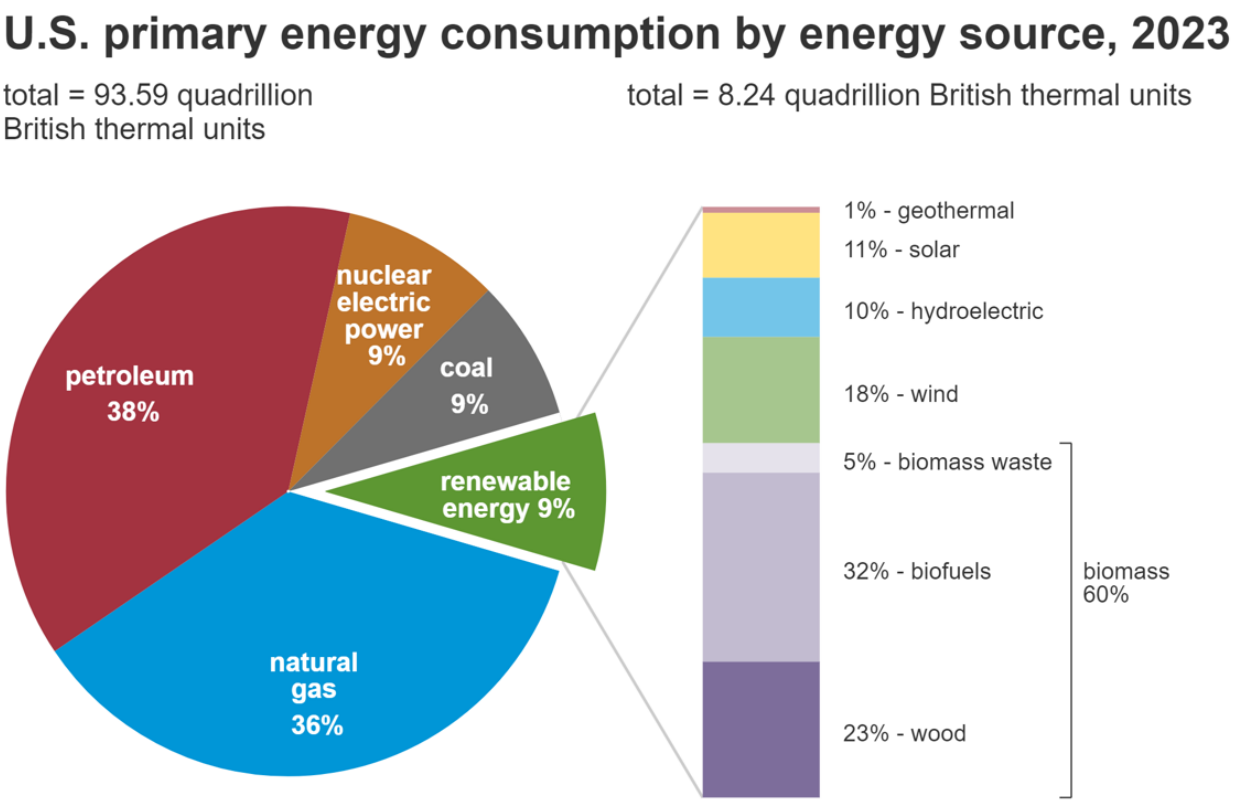

Figure 12-39: U.S. primary energy consumption by energy source for 2023. Fossil fuels were used for 83%, while renewable resources were at 9%.

How are these energy sources in Figure 12-39 then used in the United States? The answer to this question is that there are four end-use sectors that are tracked. The four sectors are:

1. transportation – 37%,
2. industrial for producing goods – 35%,
3. residential – 15%, and
4. commercial such as businesses and non-profit organizations – 13%.

If you are an exceptionally curious person, you may wonder how much and what types of energy resources are used in each of these end-use sectors. Figure 12-40 answers these questions. As shown in this figure, the United States collects a lot of data on what and how energy is used.

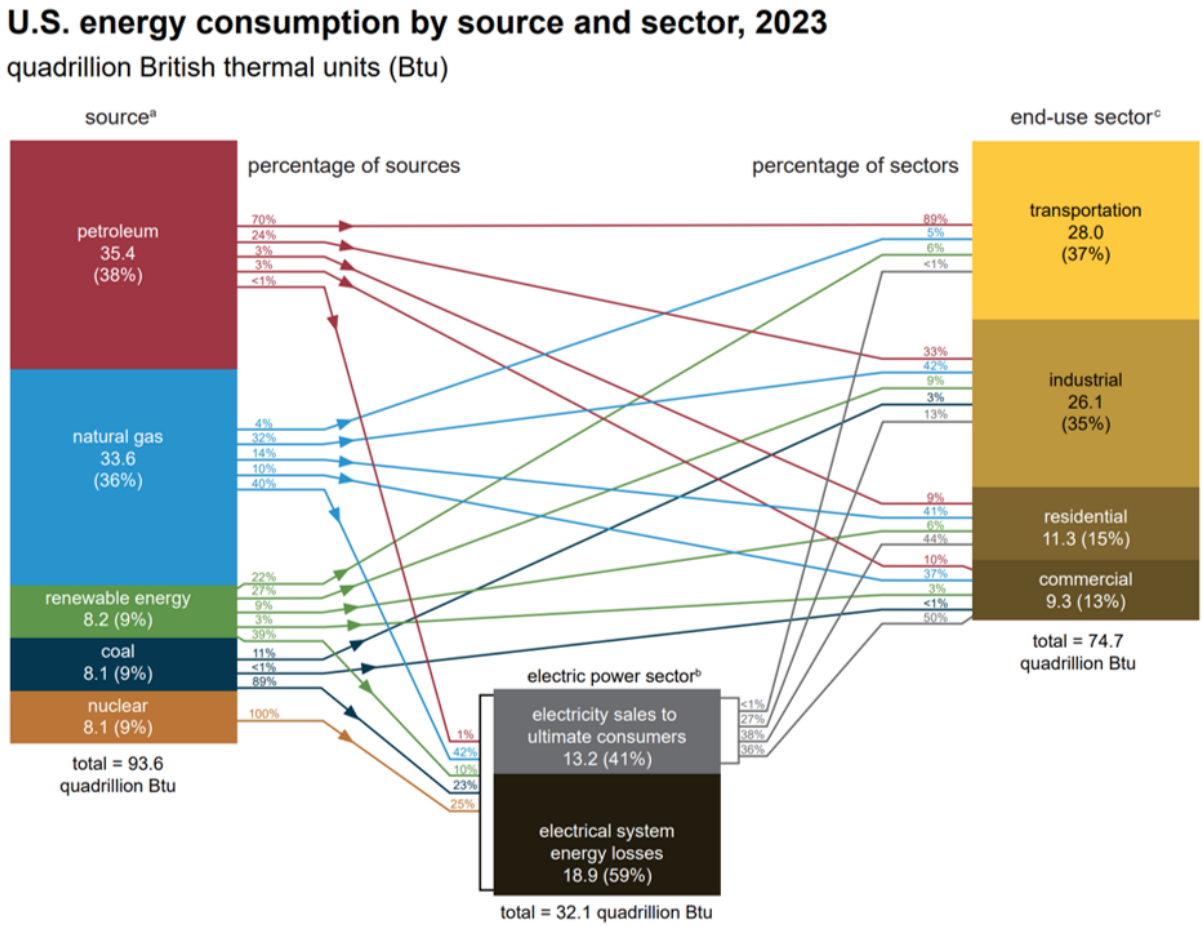

Figure 12-40: U.S. energy consumption by source and end-use sector in 2023. Electrical power generation (in the middle) is an intermediate step before being consumed in an end-use sector.

All the energy related carbon dioxide emissions come from fossil fuels. Nuclear and renewable energy resources do not generate much carbon dioxide. Of all the energy resources used in the United States, petroleum creates the most CO_2 as shown in Figure 12-41.

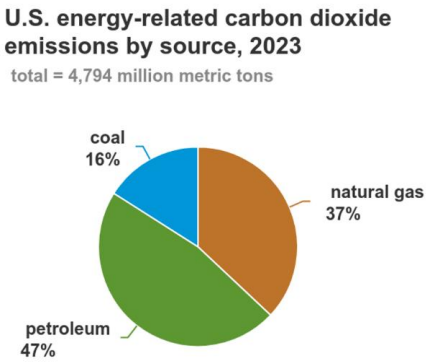

Figure 12-41: U.S. carbon dioxide emissions for each fossil fuel. The use of petroleum creates the most CO_2.

12.5.1 – United States Greenhouse Gas (GHG) Emissions

The use of fossil fuels as energy resources is the biggest generator of greenhouse gas emissions in the United States. However, some non-energy related activities can also create GHGs. For example, the cultivation of rice or raising cattle can generate greenhouse gases, but these activities use minimal energy resources. To monitor the total GHG generation by the U.S., the EPA added an agriculture emissions sector in addition to the four end-use energy sectors discussed in the previous section.

Figure 12-42 displays the percentage of each GHG generated in the U.S. and the emission sectors that generate these GHGs. Transportation and electricity generation create over half of the greenhouse gases in the United States. Transportation is the largest because this emission sector relies heavily on petroleum as its energy source.

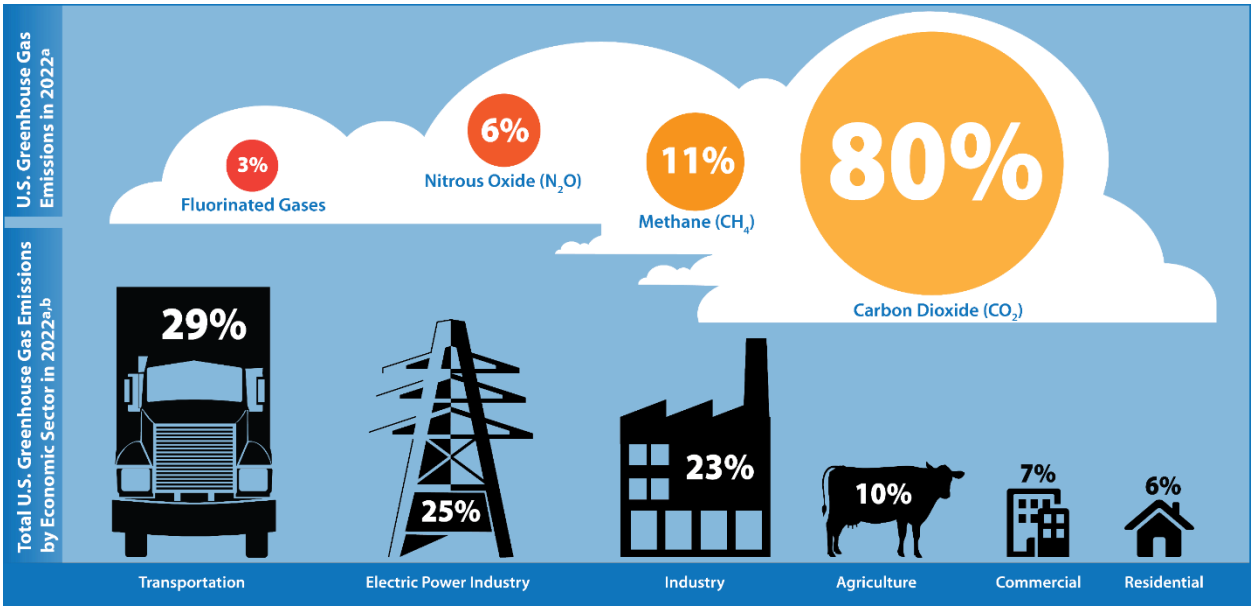

Figure 12-42: An infographic showing the percentage of GHG emissions in the U.S. per economic section and type of the type of GHG emitted. These data are for 2022.

The other greenhouse gases being monitored as a result of human activity are:

- Methane (CH_4), which comes from landfills, coal mines, agriculture, and oil and natural gas operations.
- Nitrous oxide ($N_2$2O), which comes from using nitrogen fertilizers and certain industrial and waste management processes and burning fossil fuels.
- Fluorinated gases, which are human-made industrial gases:
    - Hydrofluorocarbons (HFCs)
    - Perfluorocarbons (PFCs)
    - Sulfur hexafluoride (SF_6)
    - Nitrogen trifluoride (NF_3)

The amount of carbon dioxide (CO_2) that is produced from a fossil fuel weighs more than the fuel itself. During combustion each carbon atom in the fuel combines with two oxygen atoms in the air to make CO_2. The addition of two oxygen atoms (atomic weight of 32) to each carbon atom forms CO_2 and has an atomic weight of 44. This weight is 3.6667 times the atomic weight

of carbon which is 12. Note that 44 / 12 = 3.6667. For example, a gallon of gasoline weighs 6.3 pounds, and is 87% carbon and 13% hydrogen by weight. These numbers can now be used to calculate the weight of CO_2 produced from a gallon of gasoline:

weight of CO_2 = (6.3 pounds x 0.87) x 3.6667 = 20.1 pounds

The combustion of a gallon of gasoline creates about 20 pounds of carbon dioxide.

While CO_2 is the most well-known GHG, do not forget that water vapor is still the most abundant greenhouse gas in the atmosphere.

Chapter 12 Review Questions

1. What is the difference between primary and secondary pollutants?
2. Describe the visual appearance of nitrogen dioxide in the atmosphere.
3. What does the EPA use to publicly report air quality?
4. Since ozone is a secondary pollutant, what is required to create tropospheric ozone?
5. What air pollutant has increased with time in the United States?
6. Which of these particles (combustion particles, fine beach sand, pollen, mold, or dust) is the smallest?
7. How does a heat wave decrease air quality?
8. If the wind speed increases from 11 to 22 mph, what happens to the pollution level?
9. What atmospheric conditions lead to an increase in pollution levels?
10. How does precipitation cleanse the air of pollutants?
11. What causes nighttime temperatures to be higher in an urban area when compared to the surrounding rural areas.
12. Describe the changes in latent and sensible heat from a rural to an urban area.
13. What is net photosynthesis?
14. Where is the largest carbon reservoir on Earth?
15. What two processes remove carbon dioxide from the atmosphere?
16. Which process removes the most carbon dioxide from the atmosphere?
17. What four processes put carbon dioxide into the atmosphere?
18. Which process puts the most carbon dioxide into the atmosphere?
19. Name five renewable energy sources.
20. Name four non-renewable energy sources.
21. What percentage of energy used in the United States is renewable energy?
22. Which energy resource creates the most carbon dioxide in the United States?
23. How much carbon dioxide will the combustion of a gallon of gasoline create?
24. What is the most abundant greenhouse gas in the atmosphere?

Chapter 13 – Paleoclimates and Climate Variability

Overview

To understand changes in climate, knowledge about Earth's past climates is needed. Since weather records from instrumentation only exist for a couple of hundred years, methods were developed which allows a person to infer Earth's past climates. These records become less accurate the further they go back in time. However, they portray significant changes that have occurred on our planet including hot periods with no polar ice, and cold periods with extensive ice sheets. Overall, the past climates on our planet were much warmer than today. This chapter explores Earth's past climates, how these past climates were determined, and what natural variability is present today that influences climate.

Chapter objectives:

1. Explain how scientists determine Earth's past climates.
2. Describe the variations in Earth's past climates.
3. Understand how Milankovich cycles caused Earth's glacial and interglacial periods.
4. Describe ENSO and its influence on seasonal weather conditions.

13.1 – Paleoclimate and Short-term Climate Proxies

Most reliable long-term weather observations only go back about a hundred and fifty years. Measuring instruments, such as thermometers and barometers, were not widely available hundreds of years ago. This length of record is not sufficient to document the natural variability of the climate system. Additionally, any changes in climate are difficult to attribute as to what may have caused them. A paleoclimate approach is used to mitigate this dilemma. **Paleoclimate** is the study of ancient climates prior to the widespread availability of instrumental records.

Similar to the way archeologists study fossils and other physical clues to gain insight into the prehistoric past, paleoclimatologists study different types of environmental evidence to understand what the Earth's past climate was like and why. Over the years, the Earth has kept records of its climate conditions preserved in tree rings, locked in the skeletons of tropical coral reefs, sealed in glaciers and ice caps, and buried in sediments from lakes and the oceans. Scientists can use these environmental recorders to estimate past conditions, extending our understanding of climate back hundreds to millions of years. The preserved physical characteristics of the environment that can be used instead of direct measurements are called **climate proxies**.

If there is one thing that the paleoclimate record shows, it's that the Earth's climate is always changing. Over the past two million years, numerous glacial periods have covered much of the high-latitude northern hemisphere landmasses in ice, dropped sea level as much as 410 feet, and significantly cooled the tropical regions. In the distant past between 145.5 and 65.5 million

years ago (Cretaceous Period), the Earth was significantly warmer than today with less polar ice, higher sea levels, and warm weather organisms thriving at high latitudes.

The study of paleoclimates has been particularly helpful in showing that the Earth's climate system can shift in a matter of years or decades. For example, tree-ring and lake-sediment records from North America show that decadal-scale "megadroughts" occurred multiple times over the last thousand years. During these periods, persistent droughts lasted much longer than any of the droughts we have experienced over the period of instrumental records. Understanding "climate surprises" of the past is critical to avoid being surprised by abrupt climate changes in the future.

The study of past climate change also helps us understand how humans influence the Earth's climate system. The climatic record over the last thousand years clearly shows that global temperatures increased significantly in the 20th century. The paleoclimatic record allows us to examine the causes of past climate change and to help unravel how much may be explained by natural causes, and how much may be explained by human influences.

Most paleoclimate evidence is indirect rather than a direct measure of conditions. This evidence is less precise than measurements with instruments because of uncertainties in the relation between the proxy and the climate variable. For example, pollen found in lake sediments can be used to reconstruct past vegetation cover. Past vegetation can in turn be related to temperature and precipitation conditions. Figure 13-1 shows various types of pollen available for study, and has been colorized for easier identification.

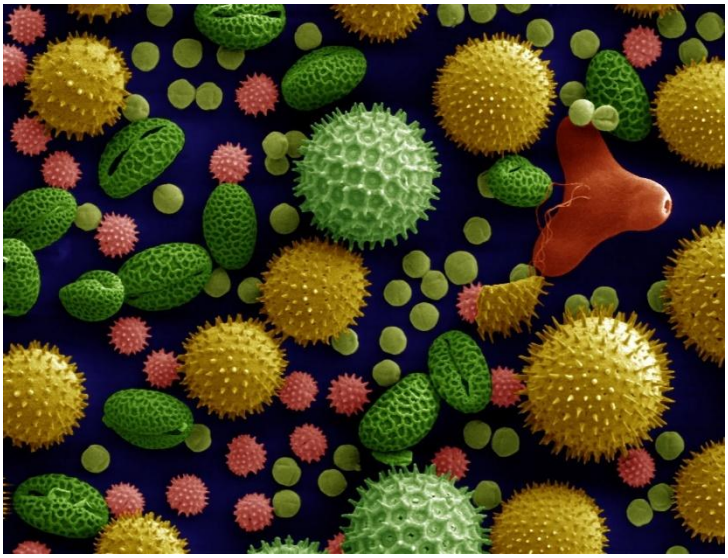

Figure 13-1: A colorized image with different types of pollen.

Similarly, different species of plankton that have a calcium carbonate hard shell prefer different water temperatures. Some live in colder waters, others prefer warmer waters. Their fossil shells accumulate in sediments, and can be retrieved with a coring device employed from a research vessel. Shells deeper in the sediment are older. If shells of cold-loving foraminifera (plankton) are found at a site where currently warm-loving species live, it suggests that near surface temperatures in the past have been colder. Mathematical methods have been developed to quantify the temperature changes from the species composition. The image in Figure 13-2 shows fossil several species of these plankton called planktic foraminifera.

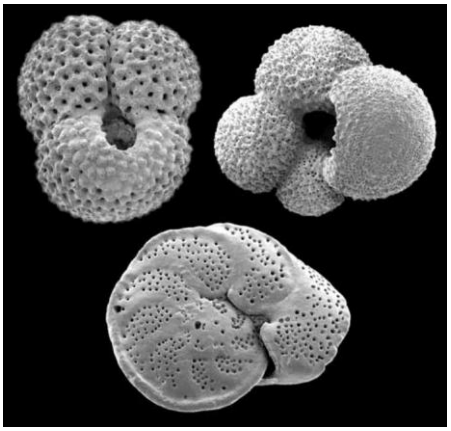

Figure 13-2: An image of hard shell plankton called planktic foraminifera.

Other proxies are chemical in nature. The chemical composition of a fossil or sediment can be related to temperature. For example, isotopes of oxygen or carbon in the calcium carbonate shells of plankton can be used to reconstruct temperature, salinity, ice volume and carbon cycling. An **isotope** is an element which has the normal chemical properties of the element, but a slightly different atom weight. All elements in the periodic table have isotopes. Isotopes are affected by their environment and can be used as climate proxies.

The remainder of this section will examine short-term climate proxies. Short-term for paleoclimate is from 100 to about 50,000 years. Long-term is from 100,000 to millions of years. The words long-term and short-term are useful when examining paleoclimate changes from a chronological standpoint.

13.1.1 – Tree Rings

Dendrochronology is the dating and study of annual rings in trees. Tree-rings are annual layers which can be counted. Thick and thin patterns in a tree can be matched across multiple trees of different ages. Thus, a large number of trees (samples) can be used to create a layer counted chronology. Figure 13-3 is a photo of the rings in pine trees.

Figure 13-3: A photo of the rings in pine trees.

The technique of counting layers can also be used in ice cores and lake sediments. Anything that has changes from one year to the next can be counted to determine a time estimate. Multiple data samples across many years must be available to ensure the accurate dating of each layer.

A large number of tree samples must be used to create a layer count chronology. Figure 13-4 illustrates the approach used to create a layer count chronology. Notice how multiple tree ring samples must all align themselves for a valid timeline to be developed.

Figure 13-4: Illustration of a layer count with multiple tree ring samples, which is then used to develop a timeline.

A layer count approach can be used on tree rings, sea and ocean sediments, speleothems, corals and ice cores. Speleothems are cave formations such as stalactites and stalagmites. The time resolution for each of these data archives differs. Tree rings, corals, and speleothems provide reconstructions at annual to decadal resolution (1 to 10 years), and have the highest temporal resolution. Ice cores typically have decadal to centennial resolution (10s to 100s of years). Antarctica ice can go back almost a million years. Greenland ice cores go back less in time to about 100,000 years. Ocean sediments cover millions of years in the past, but with a low temporal resolution of centennial to millennial timescales (100s to 1000s of years). Figure 13-5 illustrates the various types of layered data archives.

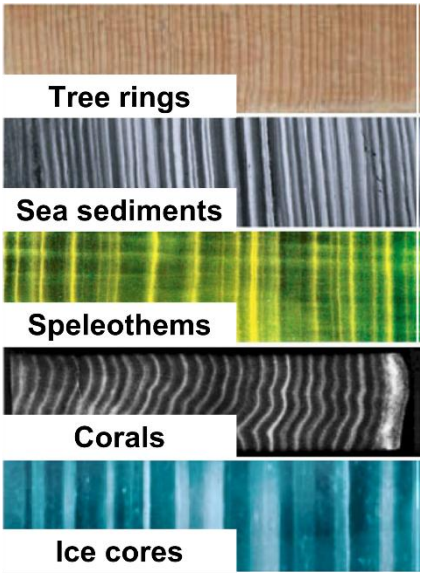

Figure 13-5: Examples of materials useful in creating layer count based timelines.

Tree rings provide information on both temperature and precipitation. Temperature and precipitation determine both the color and size of a ring. Dendrochronology can extend climate records back several thousand years to the exact year.

13.1.2 – Corals

Many coral reefs have existed for millions of years, yet they are extremely sensitive to changes in climate conditions. Corals are affected by ocean warming (sometimes bleaching occurs when temperatures rise or fall), by pollution and runoff, and by changes in the pH of seawater. The pH of seawater decreases as more carbon dioxide enters the ocean, which is a condition known as ocean acidification.

Figure 13-6: Photo of a coral reef with multiple types of living coral.

As corals grow, they form skeletons by making calcium carbonate from the ocean waters. The density of these calcium carbonate skeletons changes as the water temperature, light, and nutrient conditions change. Coral skeletons formed in the summer have a different density than those formed in the winter. These seasonal variations in density produce growth rings similar to those in trees. Scientists can study these rings and other characteristics to determine the climatic conditions during the seasons in which the coral grew. These growth bands also allow scientists to date coral samples to an exact year and season. Figure 13-6 is a photo of a coral reef with multiple types of living coral.

To gather data and information about coral growth bands, scientists dive down to the reefs. Once in position, they use a hollow, diamond-tipped drill bit to gather small core samples from the corals without injuring the animal. Sometimes the banding patterns in these samples are evident by visual inspection alone. At other times, scientists use x-ray imaging to look at the patterns. The scientists then mark the varying layers by year and season. Additionally, samples are extracted from the layers for precise chemical analysis. The photographs in Figure 13-7 show a coral sample being obtained, and the final extracted cores.

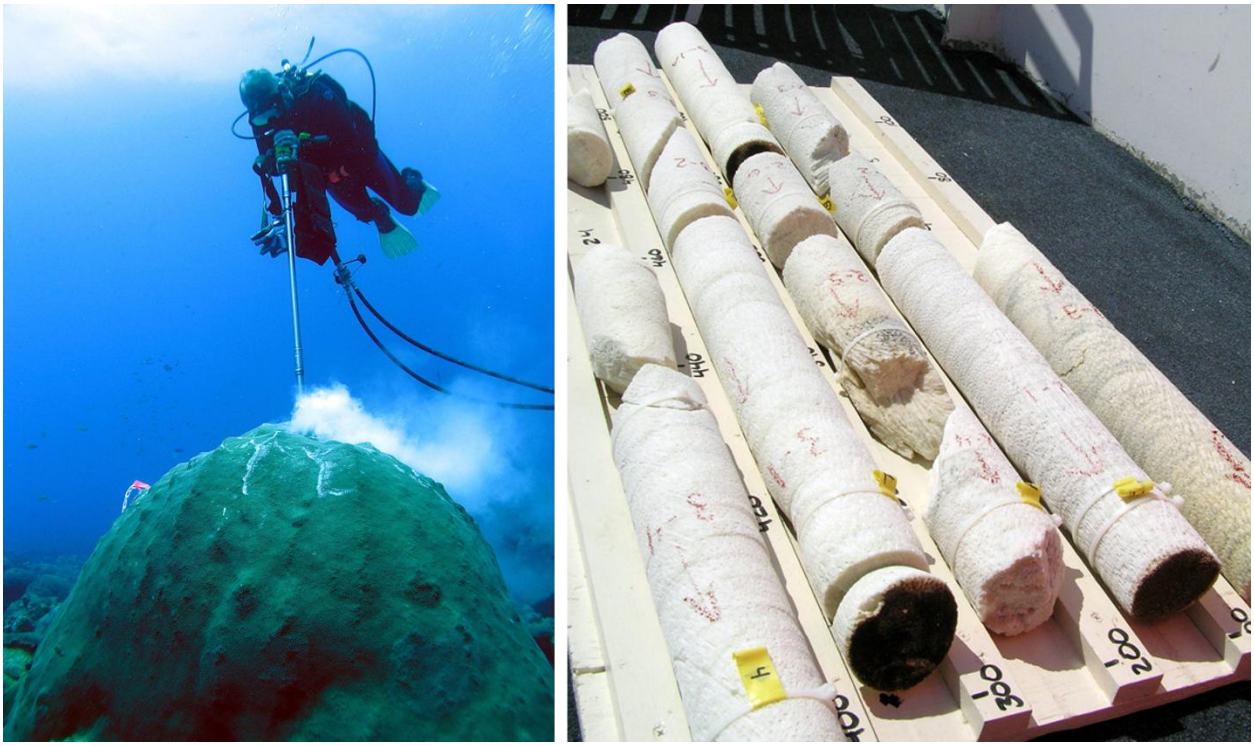

Figure 13-7: Photographs of extracting a coral sample (left) and the final extracted cores (right).

By examining the depth of each growth band, scientists can look back in time to determine when temperatures were warmer or cooler. Larger low-density bands indicate warmer winter temperatures. Slightly darker bands, known as stress bands, indicate periods of environmental stress, such as temperature extremes.

Within each band scientists can evaluate the chemical content to learn more about atmospheric conditions. They examine the oxygen and carbon isotopes to determine specific temperatures during each month of the year. The coral cores shown in the previous photographs (Figure 13-7) contain climate information dating back to the early 1800s.

This short video from the American Museum of Natural History explains how coral samples are used to discover past marine conditions.

13.1.3 – Carbon dating

Carbon, like all elements, has several isotopes. Remember an **isotope** is an element which has the normal chemical properties of the element but a slightly different atom weight. The isotopes for carbon and the percentages of their occurrence are:

- ^{12}C is the most abundant and stable form of carbon (98.89%).
- ^{13}C is another naturally occurring stable isotope (1.11%).
- ^{14}C is a radioactive isotope which slowly decays (~10^{-12}%).

When a plant or animal is alive, the amount of ^{14}C in its body remains constant. When the plant or animal dies, the ^{14}C starts to radioactively decay. The time it takes for ^{14}C to radioactively decay is described by its half-life. ^{14}C has a half-life of 5,730 years. In other words, after 5,730 years, only half of the original amount of ^{14}C remains in the original organic material. After an additional 5,730 years - or 11,460 years total - only a quarter of the ^{14}C remains.

The amount of ^{14}C remaining is used to determine the age of organic materials. After 10 half-lives, or 57,300 years, the amount of ^{14}C remaining (<0.1%) becomes very difficult to detect. Thus, any organic object older than about 50,000 years will have no ^{14}C remaining and cannot be dated. The graph in Figure 13-8 depicts the decay of ^{14}C.

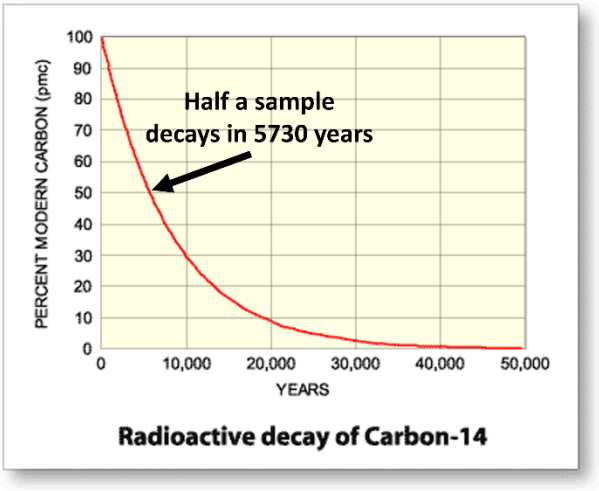

Figure 13-8: A graph showing the decay time for carbon-14.

13.1.4 – Pollen

If you have allergies, you know exactly what the photo of the bee in Figure 13-9 is covered in. It's pollen! Every year around springtime, pollen spores come out and wreak havoc on thousands in the form of itchy watery eyes, runny noses, and uncontrollable sneezing. How can these pesky spores help scientists learn about the past climate?

Figure 13-9: Photograph of a bee covered in pollen.

Pollen grains are the sperm-carrying reproductive bodies of seed plants like conifers, cycads, and flowering plants. Each of these grains has its very own unique shape depending on what plant it comes from. Pollen walls are made of a substance known as sporopollenin, which is chemically stable and strong.

When pollen grains are washed or blown into bodies of water, their tough outer walls allow them to be preserved in sediment layers at the bottoms of ponds, lakes, or oceans. Because of their unique shapes, scientists can then take a core sample of the sediment layers and determine what kinds of plants were growing at the time the sediment was deposited. Knowing what types of plants were growing in the area allows the scientists to make inferences about the climate.

Scientists can isolate the pollen and spores from the core sample. Pollen grains are very small, typically between 10 and 200 microns, and require a microscope for examination. By analyzing pollen from well-dated sediment cores, scientists can obtain records of changes in vegetation going back thousands to millions of years. The vegetation changes in turn can be related to temperature and precipitation changes.

13.2 – Long-term Climate Proxies

This section examines long-term climate proxies, which are 100,000 years to millions of years in the past. The longer a proxy goes into the past, the less accurate it becomes with respect to the exact date something happened. Despite this increase in error, useful knowledge about Earth's past climates can be obtained. These long-term climate proxies indicate that Earth's climate has changed considerably in the past.

Oxygen isotopes are used in several of these long-term proxies. Oxygen has three different isotopes: oxygen 16, oxygen 17 and oxygen 18. These isotopes are all stable and they do not decay radioactively.

- ^{16}O is the most abundant and stable form of oxygen (99.76%).
- ^{17}O is another naturally occurring stable isotope (0.04%).
- ^{18}O is another naturally occurring stable isotope (0.20%).

Both ^{16}O and ^{18}O are abundant enough to be measured. Two additional neutrons are present in ^{18}O, so this oxygen atom weighs more. Their masses are different enough that natural processes, such as temperature and precipitation, can effectively separate where these isotopes are concentrated on the globe. Figure 13-10 illustrates the differences between the two oxygen isotopes. ^{16}O has 8 protons and 8 neutrons. ^{18}O has 8 protons and 10 neutrons.

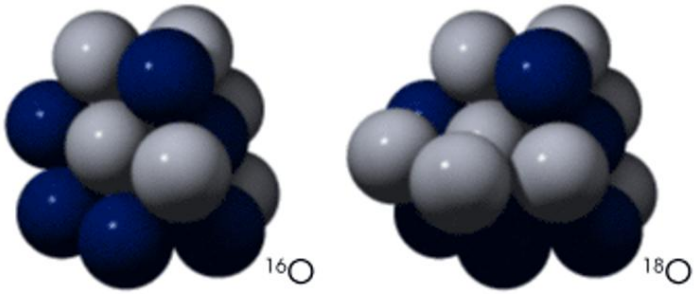

Figure 13-10: Illustrations of ^{16}O and ^{18}O. Protons are in blue and neutrons are white. Oxygen-18 has two more neutrons.

These isotopes are present in water molecules (H_2O – two hydrogen and one oxygen atom) and calcium carbonate ($CaCO_3$ – calcium, carbon, and three oxygen atoms). Calcium carbonate is a common molecule formed in marine organisms from the surrounding water. Thus, the oceans, ice sheets, and fossils offer abundant data samples for oxygen isotope analyses, which can be used to determine Earth's past climates.

Water molecules with heavy oxygen (^{18}O) have 11% more mass than water with light oxygen (^{16}O). This difference in mass affects how readily it can change phase. Thus, evaporation and condensation are affected by whether the water is composed of light or heavy oxygen. The light oxygen (^{16}O) can evaporate more easily, but condensation is more difficult. On the other hand, the heavy oxygen (^{18}O) is the exact opposite. The heavy oxygen (^{18}O) evaporation is more difficult, but it condenses more easily.

The ratio (relative amount) of these two types of oxygen in water changes with the climate. By determining how the ratio of heavy and light oxygen in marine sediments, ice cores, or fossils is different from a universally accepted standard, scientists can learn something about climate changes that have occurred in the past. The standard scientists use for comparison is based on the ratio of oxygen isotopes in ocean water at a depth of 200-500 meters.

During ice ages and cooler temperatures, ocean waters are rich in heavy oxygen. Light oxygen water evaporates more easily and moves towards the poles. Any heavy oxygen water vapor in the atmosphere condenses at lower latitudes, and flows back into the oceans. The light oxygen water vapor condenses at higher latitudes where it falls onto the expanding ice sheets and stays. As global temperatures rise, the melting ice sheets return light oxygen water to the oceans, and the ratio of heavy to light oxygen water becomes more balanced. Figure 13-11 illustrates these concepts associated with heavy and light oxygen, and how temperature affects their location on the globe.

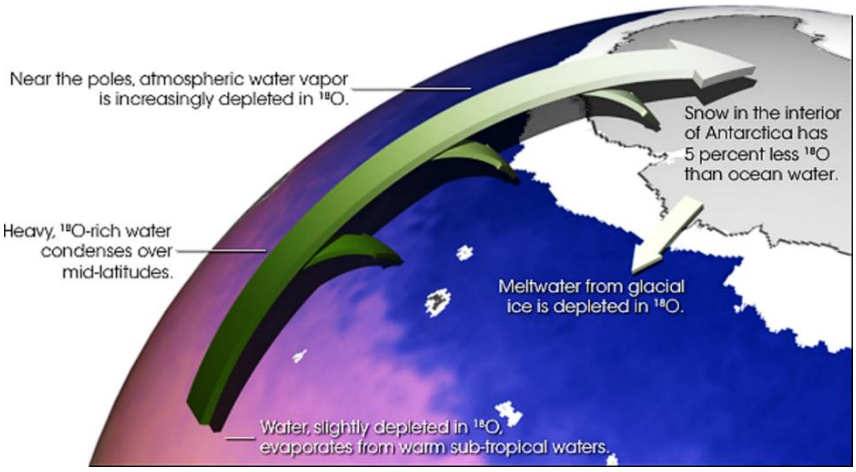

Figure 13-11: The distribution of heavy and light oxygen due to temperature differences across the southern hemisphere.

13.2.1 – Ice Cores

Ice cores provide a unique contribution to our view of past climate, because the bubbles within the ice capture samples of our atmosphere when the ice formed. At the Earth's highest latitudes and altitudes, ice is typically the only environmental data available for scientists to reconstruct the climates of hundreds to thousands of years ago.

Scientists obtain this information by traveling to the ice sheets and use a special drill that bores into the ice to obtain an ice core. Drilling thousands of meters into ice is a feat of technology, endurance, and persistence in an extreme environment. Scientists from Russia, the United States, and France worked together to recover a record of atmospheric carbon dioxide at Vostok Station in Antarctica. The maps in Figure 13-12 show the drilling sites in Antarctica.

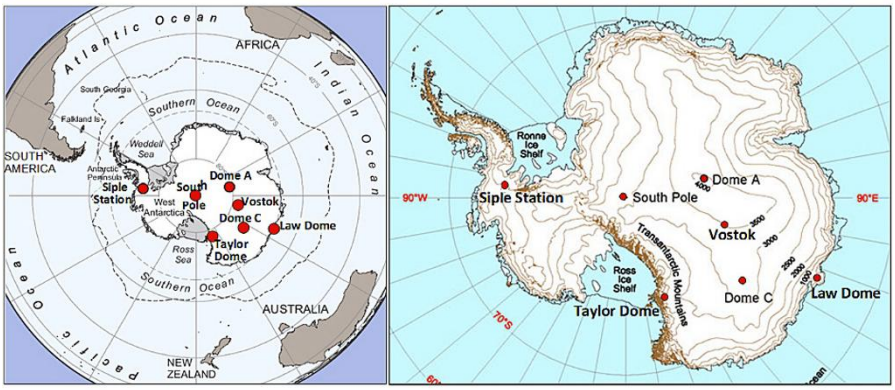

Figure 13-12: Maps of the ice core drilling sites in Antarctica. The right map is an enlarged view of the left.

After scientists procure the cores, they slice them up into various portions each allotted to a specific analytical or archival purpose. Once the samples have been prepared, the scientists run a variety of physical and chemical analyses on the cores. Some of these ice procedures are consumptive, meaning their analysis requires destruction of the ice, while others have no effect on the ice. Scientists study the gas composition of the bubbles in the ice by crushing a sample of the core in a vacuum. These bubbles provide air samples from hundreds of thousands of years ago. Overall, most of the core is reserved for archival purposes, preserving a long record of Earth history for future research. The left side photo in Figure 13-13 shows an ice core with air bubbles entrained in the ice.

Figure 13-13: (left) Photo of an ice with air bubbles entrained in it. (right) A researcher examining ice layers. Each layer is from a different year.

These cores have distinct layers in them that form throughout the years. Every year a layer of snow falls on the ice sheet. Each layer has a different texture and a different chemistry. Winter snow differs from summer snow as well. During the summer, when the Sun is up for 24 hours, the top layer of the snow changes in texture. As winter arrives. it turns cold and dark. New snow falls on top of the summer snow forming a distinct layer. Each of these layers provides scientists with a vast amount of information about the climate each year. The right side photo in Figure 13-13 shows a researcher examining layers from different years.

Ice cores can tell scientists about temperature, precipitation, atmospheric composition, volcanic activity, and even wind patterns. The chemical composition of the snow itself can tell scientists about the temperatures in the area as colder temperatures lead to a higher concentration of the light oxygen isotope in the snow.

Depending on atmospheric conditions, dust from nearby locations can also accumulate in the layers of the ice cores. In addition to seasonal dust, gigantic volcanic eruptions anywhere on the globe can spew enormous quantities of dust into the atmosphere that can accumulate in the ice. The dark band in this ice core photo (see Figure 13-14) is a layer of volcanic ash that settled on the Antarctic ice sheet about 21,000 years ago.

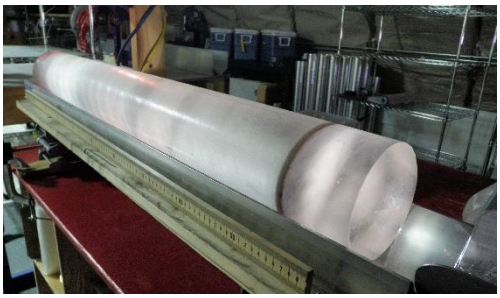

Figure 13-14: Photo of an ice core with a with a volcanic ash layer that settled on the ice sheet about 21,000 years ago.

All the dust layers, combined with the chemical composition of the ice and a flow model that assesses how the ice accumulates over time allow scientists to date the age of the ice cores. The Vostok Station data set goes back 800,000 years. Recent drilling operations in Antarctica have found ice that was formed about 2.7 million years ago.

This video from the National Science Foundation provides an overview of ice cores and how researchers study them.

13.2.2 – Ocean Sediments and Rocks

The climate history preserved within layers of sediments that slowly accumulate on the bottom of lakes and oceans can span hundreds of millions of years. Lake sediment layers provide information about the recent past, and ocean sediments tend towards the distant past. Additionally, rocks on the continents that are from thousands to billions of years old can be used to interpret the distant past.

But where do the sediment layers come from? Sediments in lakes and on the ocean floor near the edge of continents are eroded from the land and carried by rivers. As the moving water slows down, the suspended sediments settle to the bottom, gradually building up layer upon layer. Winds can bring sediments such as volcanic ash and pollen into the water which eventually sink to the bottom. Skeletal remains of plankton and other aquatic life also settle to the bottom, particularly in deep-ocean environments.

The skeletal remains of plankton are composed of calcium carbonate. The oxygen and carbon in the calcium carbonate ($CaCO_3$) were obtained from the water where the plankton lived. Thus, an oxygen and carbon isotope analysis of these remains can be used to reconstruct temperature, salinity, ice volume, and carbon cycling. The pictures in Figure 13-15 show the drilling and extraction of deep ocean sediment cores.

Figure 13-15: Photos of the drilling and extraction of ocean sediment cores.

Deep ocean sediment cores do not have annual layers like ice cores. Hence, deep ocean sediments have the lowest temporal resolution of about 1000 to 5000 years. Cores are sliced in half lengthwise when obtained. One half is used for scientific research and the other half is archived for future studies.

Certain types of sedimentary rocks are, by their very nature, indicative of certain climatic conditions. For example, in the arid subtropical regions, evaporation rates are so high that waters near the margins of the oceans readily evaporate. Once salinities reach certain levels, a sequence of minerals begins to precipitate directly from seawater. These minerals include gypsum ($CaSO_4H_2O$), anhydrite ($CaSO_4$), dolomite ($CaMg(CO_3)2$), halite (NaCl), and sylvite (KCl). This group of minerals is known as evaporites, and when found in the geologic record, are indicative of arid climates. Today the suite of evaporite minerals is being formed in the Persian Gulf. In the past, very thick sequences of evaporites were deposited in the Mediterranean during the late Miocene (6 million years ago), and in Texas and New Mexico during the Permian (250-300 million years ago).

13.2.3 – Earth's Hot Ages

The Earth is approximately 4.5 billion years old. When examining past climates of the Earth, using a geologic column is helpful to capture the entire history of the Earth. Rock formations, developmental biology, ecosystems, climate changes and mass extinctions can be placed on this timeline for a chronological organization of many events in Earth's history. The chart in Figure 13-16 is a geologic column for the Earth. A geologic column has hierarchical divisions for eons, eras, periods, and epochs.

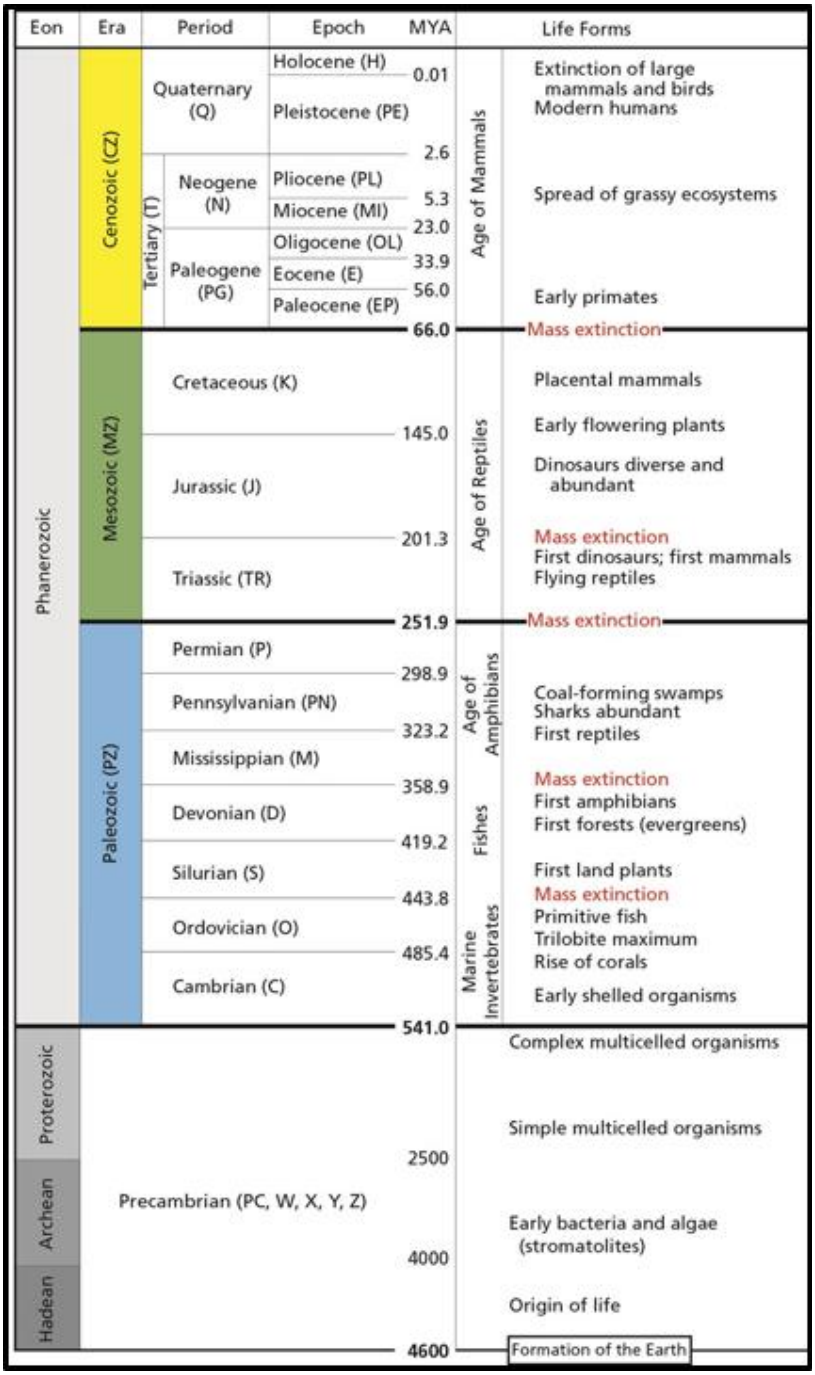

Figure 13-16: A geologic column (or time scale) for Earth. This column has hierarchical divisions.

This 12 minute video describes the creation of the Geologic Column. This video contains a lot more information than is needed in a weather and climate textbook, but it provides a good overview of the past life on our planet and how fossils are used to date rocks.

Using the climate proxies described previously, we find our planet was often much warmer than it is now. One of the warmest times was during the geologic period known as the Proterozoic, between 600 and 800 million years ago. Conditions were also frequently sweltering between 500 million and 250 million years ago. Within the last 100 million years, two major heat spikes occurred: the Cretaceous Hot Greenhouse (about 92 million years ago), and the Paleocene-Eocene Thermal Maximum (about 56 million years ago). The graph in Figure 13-17 shows these hot periods within the last 500 million years. Global temperatures in the red line have no polar ice sheets. The blue line has polar ice caps. The current global average temperature is slightly under 60°F. The Earth is currently in a cold period. Pangea, mentioned in Figure 13-17 around 250 million years, is the unified land mass before the continents drifted apart. Pangea is discussed further in section 13.3.4.

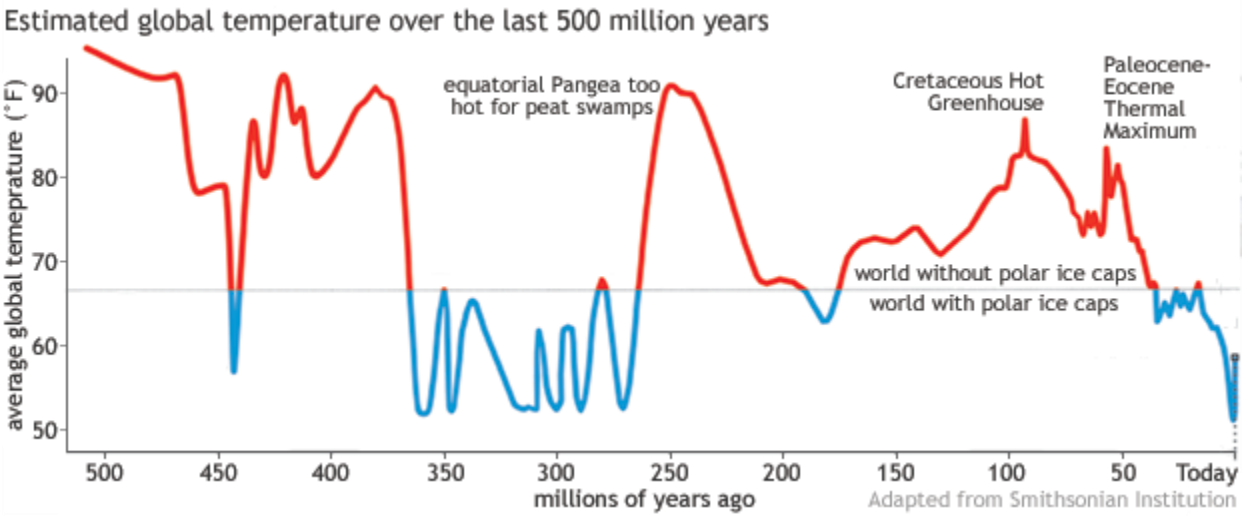

Figure 13-17: A graph of the estimated global temperature over the last 500 million years. The red line is when no polar ice caps were present. The blue line has polar ice caps.

Geologists and paleontologists have found that in the last 100 million years global temperatures have peaked twice. The Cretaceous Hot Greenhouse occurred about 25 million years before Earth's last dinosaurs went extinct. Widespread volcanic activity may have boosted atmospheric carbon dioxide to cause this warm period. Temperatures were so high that Champsosaurus (crocodile-like reptiles) lived as far north as the Canadian Arctic, and warm-temperature forests thrived near the South Pole.

Another hot period was the Paleocene-Eocene Thermal Maximum (PETM). Though not as hot as the Cretaceous Hothouse, the PETM brought rapidly rising temperatures. During much of the Paleocene and early Eocene, the poles were free of ice sheets, and palm trees and crocodiles lived above the Arctic Circle.

During the PETM, the global mean temperature appears to have risen by as much as 5-8°C (9-14°F) to an average temperature as high as 73°F. (Again, today's global average is shy of 60°F.) At roughly the same time, paleoclimate data like fossilized phytoplankton and ocean

sediments record a massive release of carbon dioxide into the atmosphere, at least doubling or possibly even quadrupling the background concentrations. Other research indicates methane, another greenhouse gas, was the cause rather than CO_2. The scientific debate continues with estimated carbon dioxide levels ranging from 700 to 2500 ppm and estimated methane levels also varying widely. The graph in Figure 13-18 shows the changes in temperatures during this time period (PETM) and are inferred from proxies of oxygen isotope ratios of fossil foraminifera (described in section 13.1).

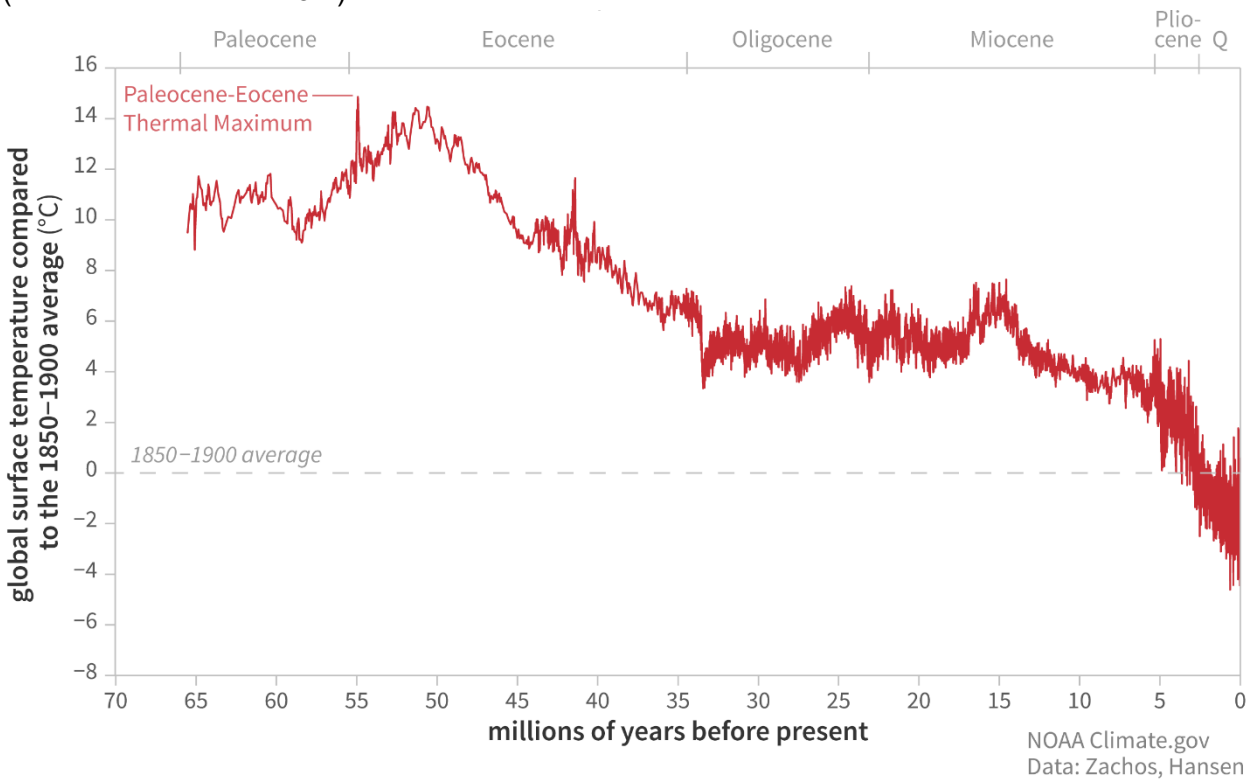

Figure 13-18: Graph of the global average temperature (deviation from a 1850-1900 average) for 70 million years ago to the present. Temperatures are based on oxygen isotope ratios of fossil foraminifera. The Paleocene-Eocene Thermal Maximum (PETM) was the last hot period in Earth's history.

Examining the long-term concentrations of CO_2 going back millions of years indicate levels have risen to over 2500 ppm. The graphs in Figure 13-19 depict these variations in paleoclimate carbon dioxide.

The origin or sequence of events which caused these high carbon dioxide levels is uncertain. Scientists have considered the drying up of large inland seas, volcanic activity, thawing permafrost, release of methane from warming ocean sediments, huge wildfires, and even briefly a comet.

As the graphs in this section show, compared to most of Earth's history temperatures today are unusually cold. This PBS video describes the Paleocene-Eocene Thermal Maximum, which was the last time Earth was very warm. Additionally, the video compares the release of carbon dioxide during the PETM as compared to today.

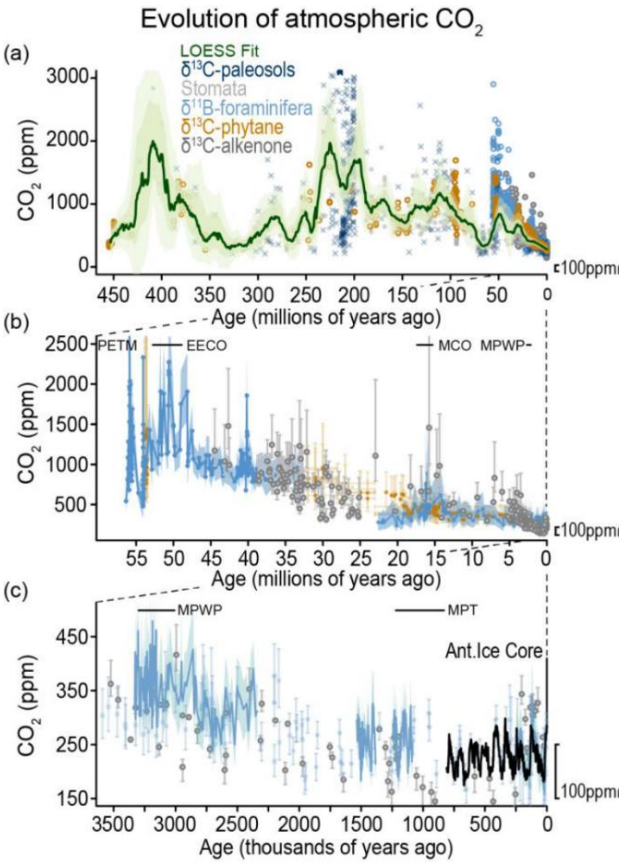

Figure 13-19: Graphs describing the carbon dioxide levels in the atmosphere from 450 million years ago to the present. The left side of each graph depicts the concentration of CO_2 in parts per million (ppm). The top graph (a) is from 450 million years to the present. The middle graph (b) provides more details from about 60 million years ago to today, and includes the PETM. The bottom graph (c) describes CO_2 levels from 3500 thousand years ago to today.

13.2.4 – Earth's Ice Ages and Sea-level

While the Earth's hot periods are long and notable, cold periods have also occurred. During cold periods, ice sheets expand and cover significant portions of the land masses. Currently about 10% of the Earth is covered in ice. During the Last Glacial Maximum (abbreviated as LGM) about 30% of the Earth was covered in ice. The LGM was roughly 20,000 years ago. The Laurentide Ice Sheet covered the North Pole and all of Canada. Figure 13-20 illustrates this ice sheet during the LGM.

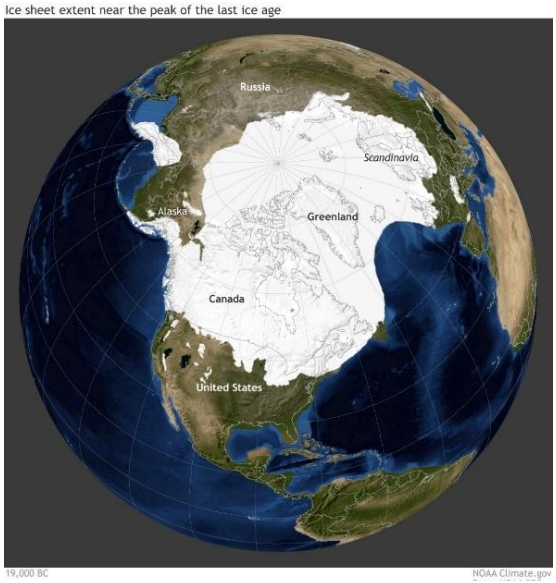

Figure 13-20: Extent of the ice sheet during the last ice age.

Scientists have reconstructed past ice ages by piecing together information derived from studying ice cores, deep sea sediments, fossils, and landforms. Records show that ice ages typically develop slowly, whereas they end more abruptly. The simple graph in Figure 13-21 shows when five major ice ages occurred in the past 2.4 billion years. Notice that the Earth has had cooler and warmer periods throughout its history, and a cooler period is present today.

Examining data from Antarctic ice cores provides more detailed temperature, carbon dioxide and sea level information from 800,000 years ago to the present. Figure 13-22 contains this information on temperature (top), carbon dioxide (middle), and sea level changes (bottom). The time period in Figure 13-22 corresponds to the black graph from Antarctic Ice Core in Figure 13-19c with much more detail.

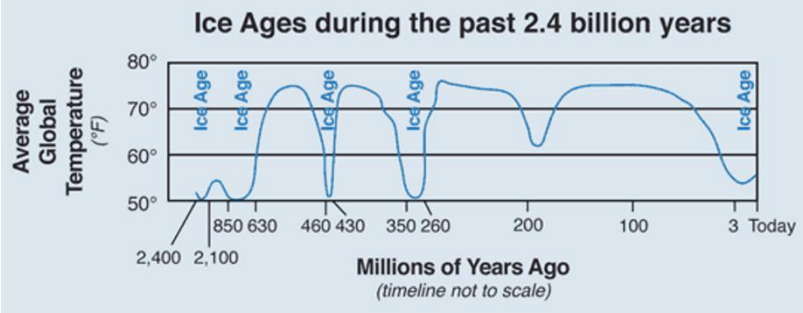

Figure 13-21: Ice ages during the past 2.4 billion years.

The last five interglacial (warmer periods) are highlighted in yellow in Figure 13-22. These shorter interglacial cycles last from about 10,000 to 30,000 years. The longer glacial cycles vary between about 70,000 to 100,000 years in length. Notice in the interglacial periods that the temperatures rise first followed by rises in CO_2 concentrations and sea levels. Changes in carbon dioxide are not the cause of the temperatures increasing at the beginning of an interglacial period. Other factors are causing the temperatures to rise first. Causes of this natural climate variability are explored in the next section 13.3.

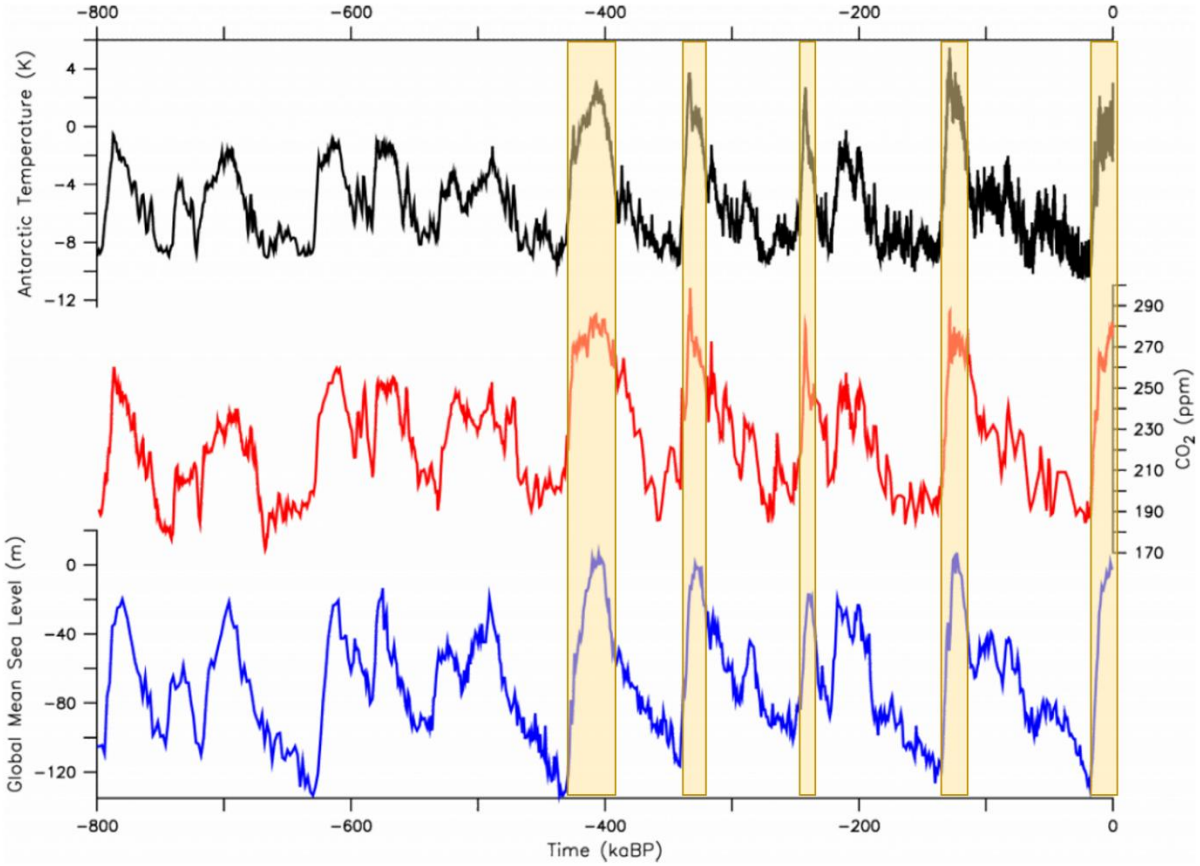

Figure 13-22: Data from Antarctic Ice cores for temperature (black), carbon dioxide levels (red), and sea level (blue). Interglacial (warm) periods are highlighted in yellow. The deviations in temperature and sea level have the base set at the minimum in the interglacial periods. All three parameters are lowest during glacial periods.

As the ice sheets grow during a glacial period, the amount of water in the oceans decreases. Water previously in an ocean gets locked into ice until temperatures warm. As an interglacial period starts, the ice sheets begin to melt and water flows back into the oceans. A glacial period decreases the volume of water in the oceans. An interglacial period increases the volume of water. Additionally, a change in temperature causes thermal expansion or contraction of the ocean water to occur. Warmer water takes up more space. Cooler water takes up less space. Hence, the sea level rises currently being observed are due to (1) an increase in ocean water, and (2) the warmer ocean water is thermally expanding.

13.3 – Natural Climate Variability

Variations in Earth's climates are associated with feedback processes that directly influence the changes. These processes affect what is happening by either increasing the rate of change that is occurring or resisting the change. **Positive feedback** amplifies a change. **Negative feedback** dampens or mutes a change. Whenever changes occur in a natural system, such as climate, both positive and negative feedback mechanisms have an important role in maintaining a stable state.

An example of both positive and negative feedback associated with a changing climate is clouds. A warmer atmosphere can hold more moisture. A moister atmosphere has the ability to create more clouds than previously. More cloud cover reflects more solar radiation from the Sun. If less solar radiation is received at the Earth's surface, the Earth will cool down. This negative feedback aspect of clouds is resisting the change to a warmer climate.

The positive feedback aspect in this same example is water vapor is a greenhouse gas (GHG) which captures heat. Since a warmer atmosphere can hold more water vapor, more of the heat released by the Earth's surface is captured by the atmosphere. Thus, the atmosphere becomes even warmer, which in turn causes it to hold even more water vapor. The cycle of warming is amplified and is positive feedback. The diagrams in Figure 13-23 illustrate the negative and positive feedback mechanisms associated with an increase in clouds and water vapor in a warmer atmosphere.

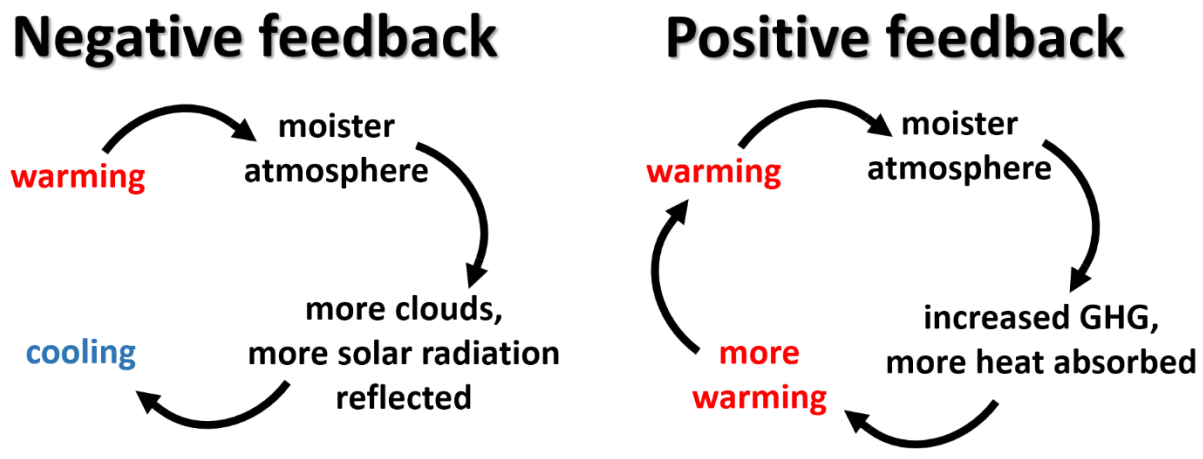

Figure 13-23: Diagrams illustrating negative and positive feedback associated with a moister atmosphere and clouds.

Another feedback mechanism in a warmer or colder Earth is associated with the albedo of snow and ice. Snow and ice are excellent reflectors of insolation and have a high albedo. Reflecting more insolation lowers the temperature of the Earth. As the Earth cools more snow and ice form and last for longer periods of time, which in turn reflects even more insolation. This positive feedback causes a cooling Earth to get even colder.

Similar positive feedback is associated with the albedo of snow and ice in a warming Earth situation. As the Earth warms, the snow and ice covering the Earth is reduced, allowing more insolation to be absorbed by the surface. The warmer surface melts more snow and ice, reducing the albedo and a warming Earth gets even warmer. Thus, the feedback associated with snow and ice (the cryosphere) and any temperature change on the Earth is always positive.

As you can see, the feedback processes inherent in any change associated with Earth's global temperature are complicated. The natural variability of Earth's climate and its causes are examined in the next several sections.

13.3.1 – Volcanoes

The gases and dust particles thrown into the atmosphere during volcanic eruptions have influences on climate. Most of the particles spewed from volcanoes cool the planet by reducing incoming solar radiation. This cooling effect can last for months to years depending on the characteristics of the eruption. Volcanoes have also caused global warming in Earth's history when extreme amounts of volcanism released greenhouse gases into the atmosphere.

Even though volcanoes are in specific places on Earth, their effects are global as gases, dust, and ash get into the atmosphere. Because of atmospheric circulation patterns, eruptions in the tropics can have an effect on the climate in both hemispheres, while eruptions at higher latitudes generally only impact the hemisphere where they happen. Figure 13-24 contains images from NASA depicting the vast amounts of gases and ash that Mount Pinatubo pushed into the stratosphere on June 15, 1991. As you can see, the effects where global and lasted for several years.

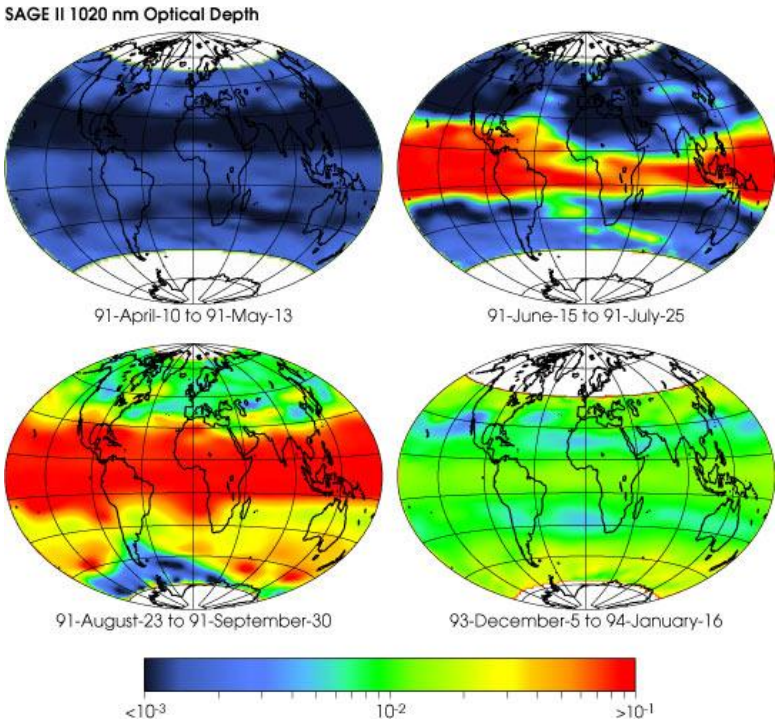

Figure 13-24: Measurements of aerosol particles released into the atmosphere from the eruption of Mount Pinatubo in June 1991. Upper right is prior to the eruption. Lower left is 2½ years after it.

Estimates were that the cooling effects of Mt. Pinatubo lowered temperatures by about 1.6°F by August 1992. This cooling was temporary and the volcanic

particles eventually settled back to the Earth by gravity. Figure 13-25 contains NASA photos of these particulates in the stratosphere before and after the eruption.

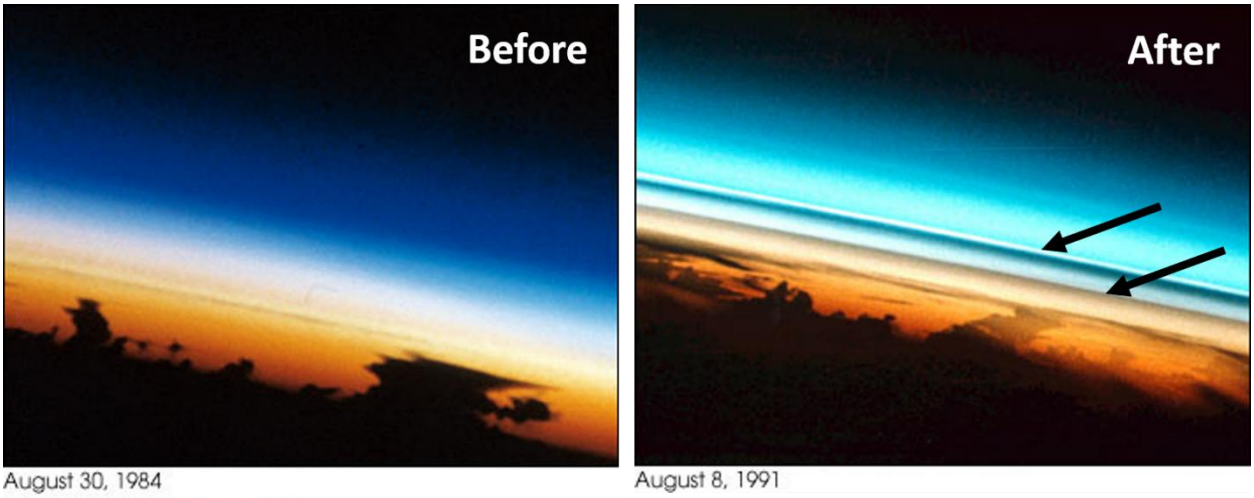

Figure 13-25: NASA photos of the stratosphere before and after the Mount Pinatubo eruption in June 1991. The arrows point to the layers of aerosol particles in the stratosphere from the eruption.

Volcanoes also release large amounts of greenhouse gases such as water vapor and carbon dioxide. The amounts put into the atmosphere from a large eruption (like Mount Pinatubo) does not change the global concentration of these gases much. However, there have been times during Earth's history when intense volcanism has significantly increased the amount of carbon dioxide in the atmosphere, and caused a global increase in temperatures.

13.3.2 – Changes in the Sun's Output

From 1645 to 1715, temperatures across much of the Northern Hemisphere dropped when the Sun entered a quiet phase now called the Maunder Minimum. During this period, very few sunspots appeared on the surface of the Sun, and the overall brightness of the Sun decreased slightly. Already in the midst of a colder-than-average period called the Little Ice Age, Europe and North America went into a deep freeze: alpine glaciers extended over valley farmland; sea ice crept south from the Arctic; and the famous canals in the Netherlands froze regularly—an event that is rare today. Figure 13-26 contains a graph showing the Maunder Minimum in sunspot activity.

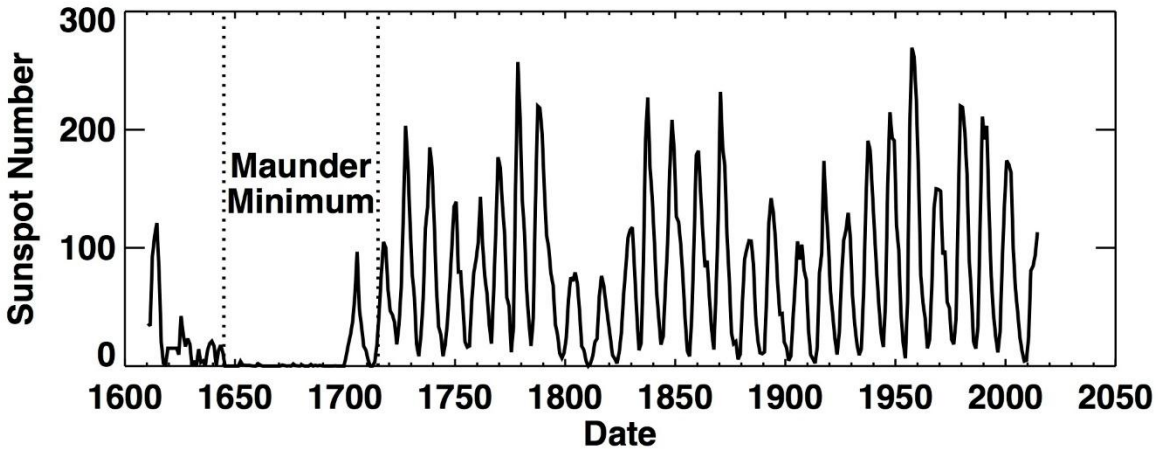

Figure 13-26: A graph of sunspot activity from 1600 through 2000 with Maunder Minimum highlighted.

Figure 13-27 shows the proxy-based global temperature reconstruction for the past 1500 years (back to 500 AD). The Maunder Minimum time period is highlighted. While the temperatures are cooler during this time period, the decrease in the Sun's activity does not cause a dramatic change in the long-term global temperatures.

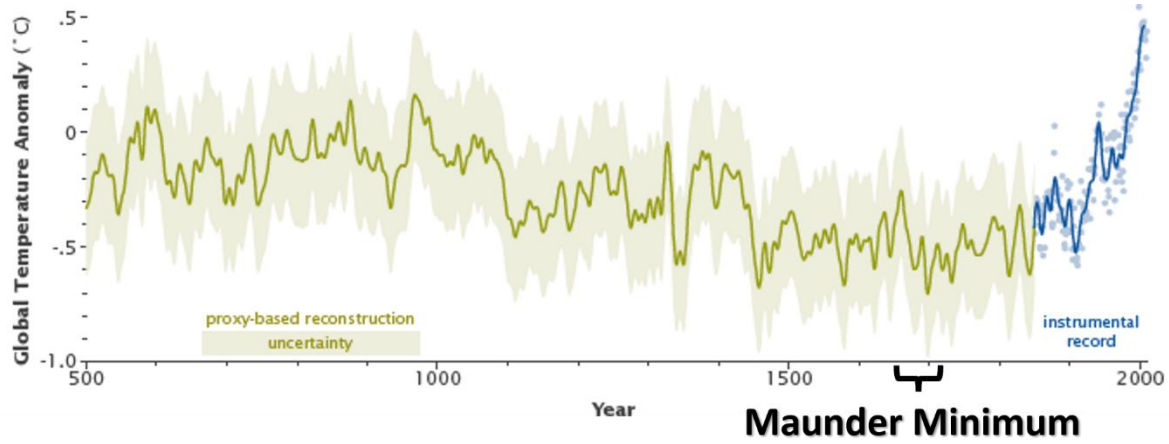

Figure 13-27: Proxy-based global temperature reconstruction for the past 1500 years. The Maunder Minimum is highlighted. While temperatures are lower during this time period, the correlation to sunspot activity is weak.

While solar output can have an effect on the Earth's temperatures, scientists estimate the maximum temperature change would be about -0.3°C if another 'Grand Solar Minimum' were to occur. Figure 13-28 compares global surface temperature changes (red line) and the Sun's energy that Earth receives (yellow line) in watts per square meter from1880 to 2020. The lighter/thinner lines are the yearly levels, while the heavier/thicker lines show the 11-year average trends. The thicker eleven-year averages are used to reduce the year-to-year natural noise in the data, making the underlying trends more obvious.

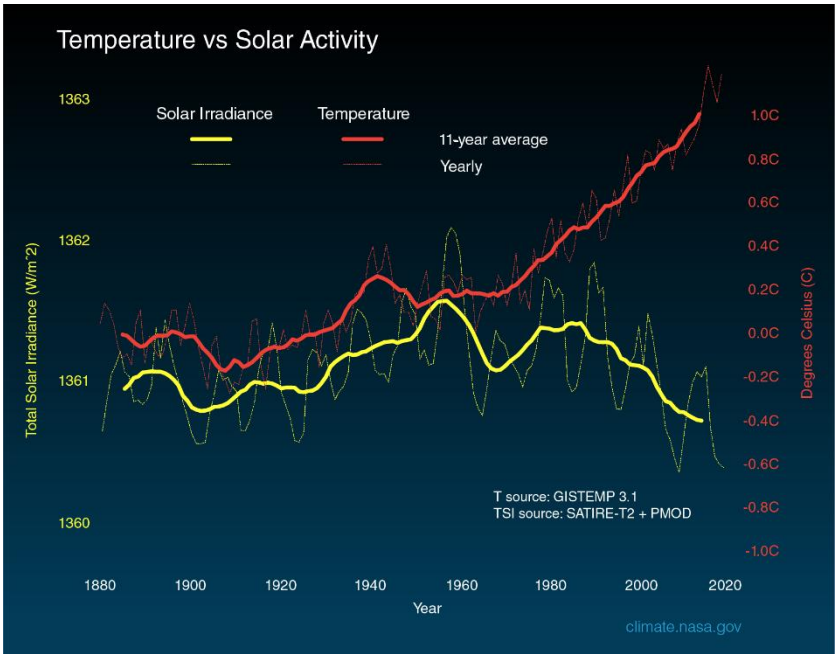

Figure 13-28: Graphs of Earth's temperature in red and solar irradiance (Sun output) in yellow from 1880-2020. The thin lines are the yearly levels and the thick lines are an 11 year average. The warming trend since 1950 is not related to solar activity.

The amount of solar energy that Earth receives has followed the Sun's natural 11-year cycle with small ups and downs and no net increase since the 1950s. Over the same period, the global temperature has risen markedly. Thus, changes in the Sun's output are not the cause of the current warming trend.

13.3.3 – Milankovitch Cycles

We know that the Earth has glacial and interglacial cycles, so what causes them? These cycles are caused by changes in Earth's orbit and orientation with respect to the Sun. This theory was first proposed in 1938 by Serbian astronomer Milutin Milankovitch, who calculated the variations in Earth's orbital parameters and linked those to past ice ages. Earth's orbit can be described by three parameters:

- **Eccentricity** (E) is the deviation from a perfectly circular orbit.
- **Tilt** (T), or obliquity, describes the angle between Earth's axis of rotation and the ecliptic orbit.
- **Precession** (P) is the wobble of Earth's axis, like the wobble of a top.

Figure 13-29 depicts these parameters.

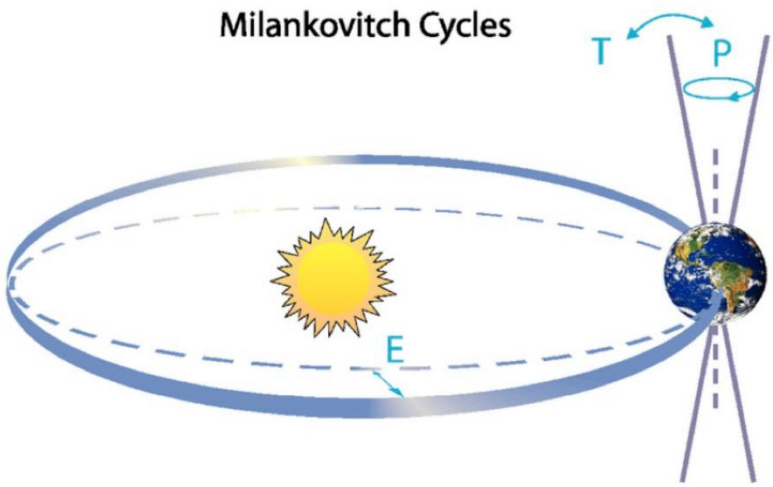

Figure 13-29: A diagram depicting the three parameters associated with Milankovitch Cycles; eccentricity (E), tilt (T), and precession (P).

The Earth's orbit is a slight ellipse, although it is close to circular. This eccentricity (E) varies on approximately 100,000-year cycles between zero and 0.06. Zero is a circular orbit. The axis tilt (T) of the Earth is currently at 23.5°, but it varies between 24.5° and 22.5° on about a 41,000-year cycle. Precession (P) varies on about a 23,000-year cycle and is strongly modulated by eccentricity (E). These variations are caused by gravitational forces from the other planets, particularly Jupiter and Saturn. The graphs in Figure 13-30 show the change in precession, obliquity, and eccentricity back 200,000 years (right side of zero) and into the future 100,000 years (left side of zero). The highlighted yellow areas are the approximate times of the past and current interglacial periods. The Earth is nearing the end of its current interglacial (warm) period.

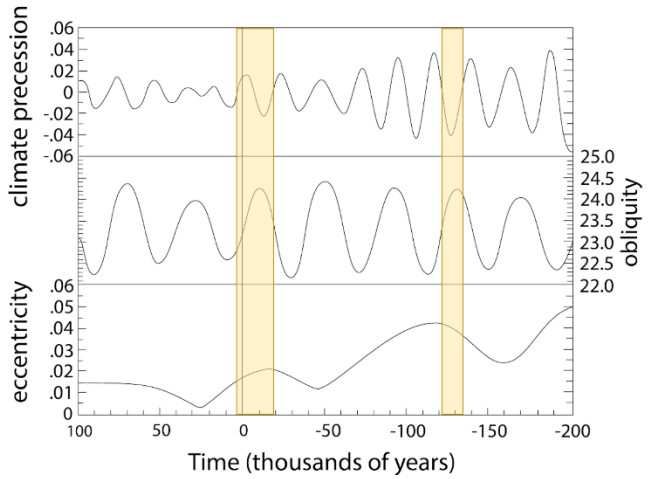

Figure 13-30: Graphs showing changes in Earth's precession, obliquity, and eccentricity. The zero on the time scale is the current time. The right side of zero is 200,000 years into the past and the left side is 100,000 years into the future. The yellow highlighted areas are interglacial (warm) periods, with the remaining being glacial periods.

Milankovitch's theory is that summer insolation in the Northern Hemisphere controls the waxing and waning of the ice sheets. When summer insolation is high, all the snow from the previous winter will melt away. When summer insolation is low, some of the snow survives and during the next winter more snow accumulates. In this way, an ice sheet can grow. The Northern Hemisphere is important because that is where the major land masses are, and where additional ice sheets can grow. The Antarctic ice sheet did not dramatically change during the recent glacial periods.

The Milankovitch theory was essentially confirmed by spectral analysis of deep sea heavy oxygen data, which shows all the predicted periodicities. However, exactly when and why ice ages started and ended remain active topics of research.

This video discusses changes in the Sun's activity, volcanoes and Milankovitch cycles.

13.3.4 – Land Changes

The position of the continents and topography, such as the Rocky Mountains, have not always been in their current locations. The theory is the continents formed one large land mass which is called Pangaea. Pangaea started to break up about 250 million years ago. The theory of plate tectonics states that the Earth's outermost layer is fragmented into a dozen or more large and small plates that are moving relative to one another as they ride atop hotter, more mobile material. Pangaea (meaning "all lands" in Greek) figures prominently in plate tectonics. The maps in Figure 13-31 show the break-up of Pangaea.

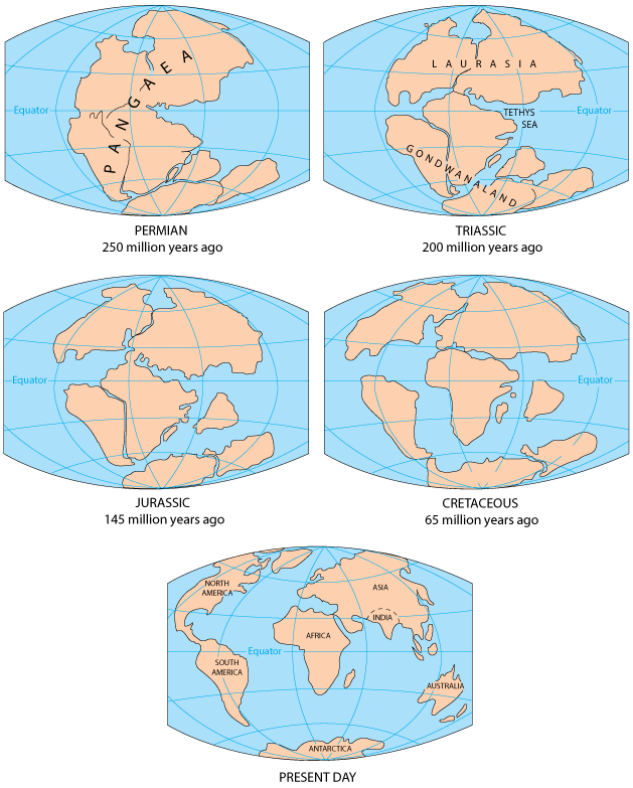

Figure 13-31: The breakup of the single land mass called Pangaea; from 250 million years ago to the present day.

These changes in the configuration of the land masses on our planet have a large effect on regional and global climates:

- When all continents come together to forms supercontinents, the amount of coastal area is decreased and the amount of dry continental interiors is increased.
- If continents are moved to high latitudes, more ice sheets form and sea levels fall.
- The growth of mountain ranges affects atmospheric circulation patterns and the number of alpine glaciers.
- Extreme tectonic activity can cause extreme volcanism which affects the Earth's climate.
- Increased seafloor spreading causes sea level rises, since the newly formed ocean crust will "float" higher on the mantle decreasing the volume of the ocean basins.

The Earth's past climates were significantly affected by these natural land changes.

13.3.5 – Understanding the Arctic Polar Vortex

The term “polar vortex” is frequently mentioned in the news when a cold outbreak occurs in the eastern United States. Climate change sceptics highlight the frigid weather and record breaking cold temperatures as proof the globe is not warming. Climate change activists counter that the warming of the Arctic regions is causing the frigid air to move further south, and these outbreaks are going to occur more often. Both viewpoints lack solid scientific evidence. Since cold outbreaks will continue to occur in the world, the polar vortex will continue to be a topic of discussion. Therefore, this section is devoted to understanding the science associated with the polar vortex.

The Arctic polar vortex is a band of strong westerly winds that forms in the stratosphere above the North Pole every winter. The winds enclose a large pool of extremely cold air. The South Pole has an even stronger polar vortex in its winter. The stronger the winds, the more the air inside is isolated from warmer latitudes and the colder it gets.

Since the polar vortex is located in the stratosphere, it is different than the polar jet stream which is located in the troposphere. When the polar vortex is strong and stable, the polar jet stream stays further north and has fewer troughs (Rossby waves). This pattern keeps the cold air contained over the Arctic and the midlatitudes are warmer than usual.

Every other year or so, the Arctic polar vortex dramatically weakens. The disrupted vortex moves off the pole or splits into two. Sometimes, but not all the time, the polar jet stream may mirror this stratospheric change, becoming weaker with larger amplitude troughs. At the surface, cold air is pushed southward to the midlatitudes and warmer air is drawn into the Arctic. When the polar vortex is disrupted, a spike in polar stratosphere temperatures occurs which is called a sudden stratospheric warming. Figure 13-32 illustrates a stable and disrupted polar vortex.

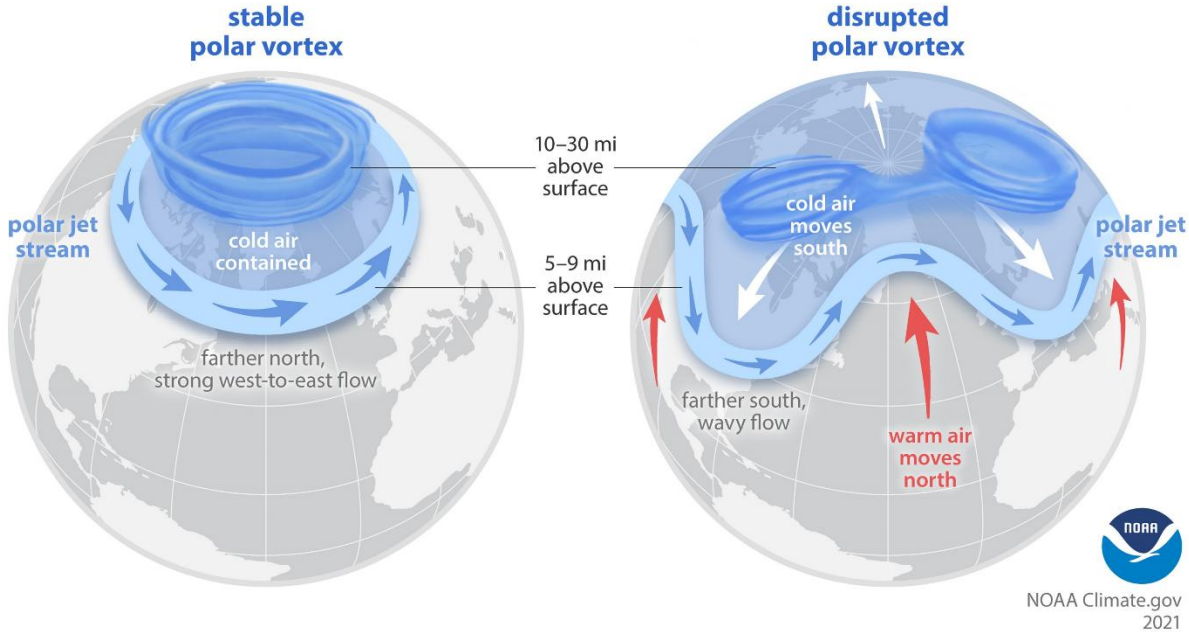

Figure 13-32: Diagrams of a stable polar vortex (left) and a disrupted polar vortex (right). A disrupted polar vortex may amplify the Rossby waves in a hemisphere.

Plenty of Arctic cold air outbreaks happen in a given winter without any help from the polar vortex. Not to mention, sometimes the polar vortex is disrupted and no impacts on the weather occur at the surface. At other times, the polar vortex can be nudged from below by large-scale tropospheric troughs. Rossby waves are always present, and anything that changes their strength could potentially influence the polar vortex. Unfortunately, the exact interactions between the polar jet stream and the polar vortex are not fully understood.

One study indicated that the polar vortex's location may be sensitive to regional variations in sea ice. While the changes in sea ice hypothesis is plausible, any long-term trend in the polar vortex lacks convincing evidence. The records indicate a period in the 1990s when there were no sudden stratospheric warming events observed in the Arctic. In other words, the vortex was strong and stable. Late in the 1990s and over the next decade, sudden stratospheric warmings occurred almost once a year. By the 2010s, a pattern of more disruptions appeared to be happening, but it has not continued. These trends in sudden stratospheric warmings appear to be just natural variability, or a rebound from the quiet 1990s period.

Prior to the polar vortex terminology, an amplification of the Rossby waves over the higher latitudes was referred to as an Arctic Oscillation. Arctic Oscillations are tied closely to surface pressure patterns over the North Atlantic. An Arctic Oscillation can cause unusually cold air to descend southward and lasts about a week, which are similar conditions to a disrupted stratospheric polar vortex.

This video from the United Kingdom Met Office explains the interactions between the polar jet stream, polar vortex, and sudden stratospheric warmings.

13.4 – Natural Ocean Circulations and Oscillations

Since 70% of the Earth's surface is covered by water, the oceans play a huge role in climate. Naturally occurring ocean patterns and circulations interact with the atmosphere, and cause changes in the regional weather patterns from annual to decadal time scales. To explore these atmosphere-ocean interactions, a basic understanding of ocean currents is needed.

The oceans have two distinct currents: (1) surface and (2) deep circulations. The warm surface circulations stir the upper 400 meters of the ocean and are largely driven by the wind. The deep circulation below 400 meters moves along the ocean floor and is all cold water. Figure 13-33 illustrates these currents.

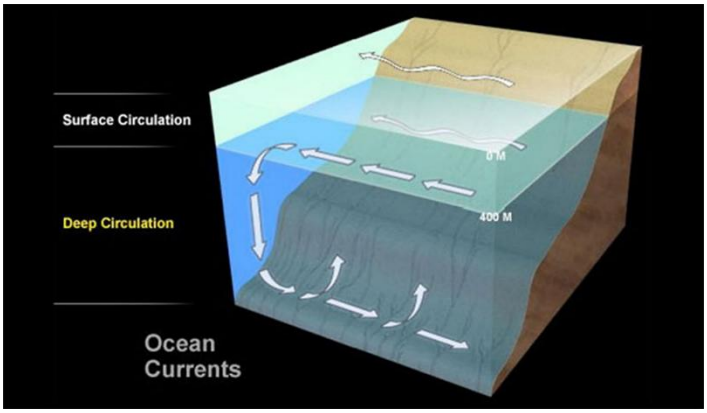

Figure 13-33: Illustration of surface and deep ocean circulations.

Currents may be generated by density differences, such as temperature and salinity, and the influence of gravity. Much like cold air sinks in the atmosphere. Cold (denser) water sinks in the ocean. However, ocean water has salt in it which affects density. Higher salinity in water

makes it denser; thus, water with higher salinity sinks the same as colder water sinks. In summary, three factors affect ocean currents: (1) the surface wind, (2) density differences, and (3) gravity.

A layer within an ocean exists between the warmer surface water and colder deeper water. This transition layer between the warmer and colder water is called a **thermocline**. Bodies of water are made up of layers, determined by temperature, much like the atmosphere. The top surface layer is called the epipelagic zone, and is sometimes referred to as the "sunlight zone." This layer interacts with the wind and waves, which mixes the water and distributes the warmth. At the base of this layer is the thermocline. A thermocline is the transition layer between the warmer mixed water at the surface and the cooler deep water below as shown in Figure 13-34.

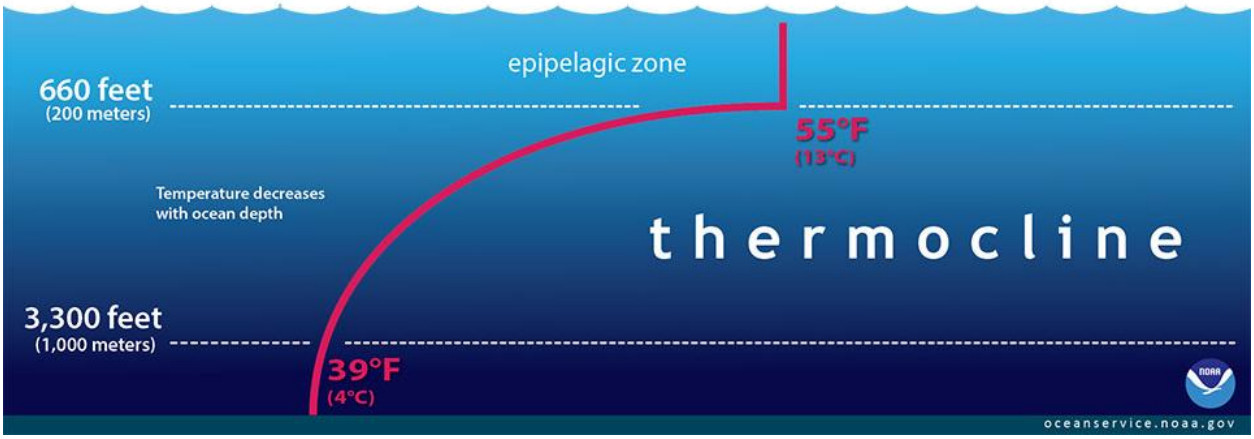

Figure 13-34: A diagram of the thermocline. The thermocline is the transition layer between the warmer surface layer (epipelagic zone) and the cooler deep water.

Global surface winds more over an ocean's surface, causing water to move in the direction the wind is blowing. Just as the Coriolis effect deflects winds to the right in the Northern Hemisphere and to the left in the Southern Hemisphere, the surface ocean currents are affected in the same manner. These spirals of surface ocean currents are called **gyres**. Gyres occur both north and south of the equator, but not at the equator where the Coriolis effect is absent. Figure 13-35 depicts the five major ocean gyres and the surface winds that drive them.

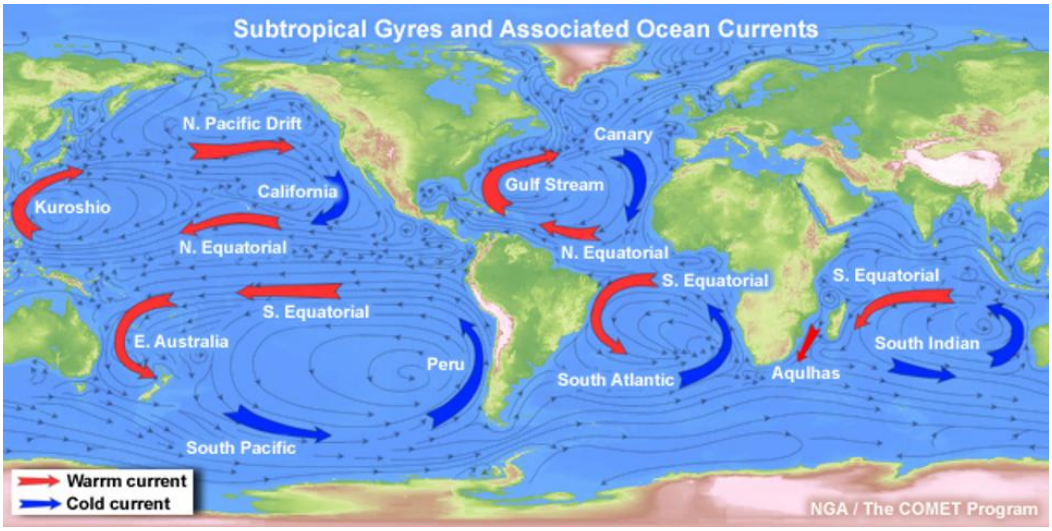

Figure 13-35: A map of the five major ocean gyres and the surface winds that drive them.

Density differences in the ocean are due to temperature (thermo) and salinity (haline). The circulation associated with these density differences is called the **thermohaline circulation**. In the Earth's polar regions, ocean water gets very cold and forms sea ice. When sea ice forms, the salt is left behind and the surrounding seawater gets saltier. As the seawater gets saltier, its density increases, and it starts to sink. Surface water is pulled in to replace the sinking water, which in turn eventually becomes cold and salty enough to sink again. This initiates the deep-ocean currents driving the global thermohaline circulation or the global conveyer belt.

Once water enters the thermohaline circulation, estimates are it takes about 1000 years to complete its path. Figure 13-36 from NASA shows this global conveyor belt of ocean water. The deep-water formation areas are where ice forms to create the denser water that sinks.

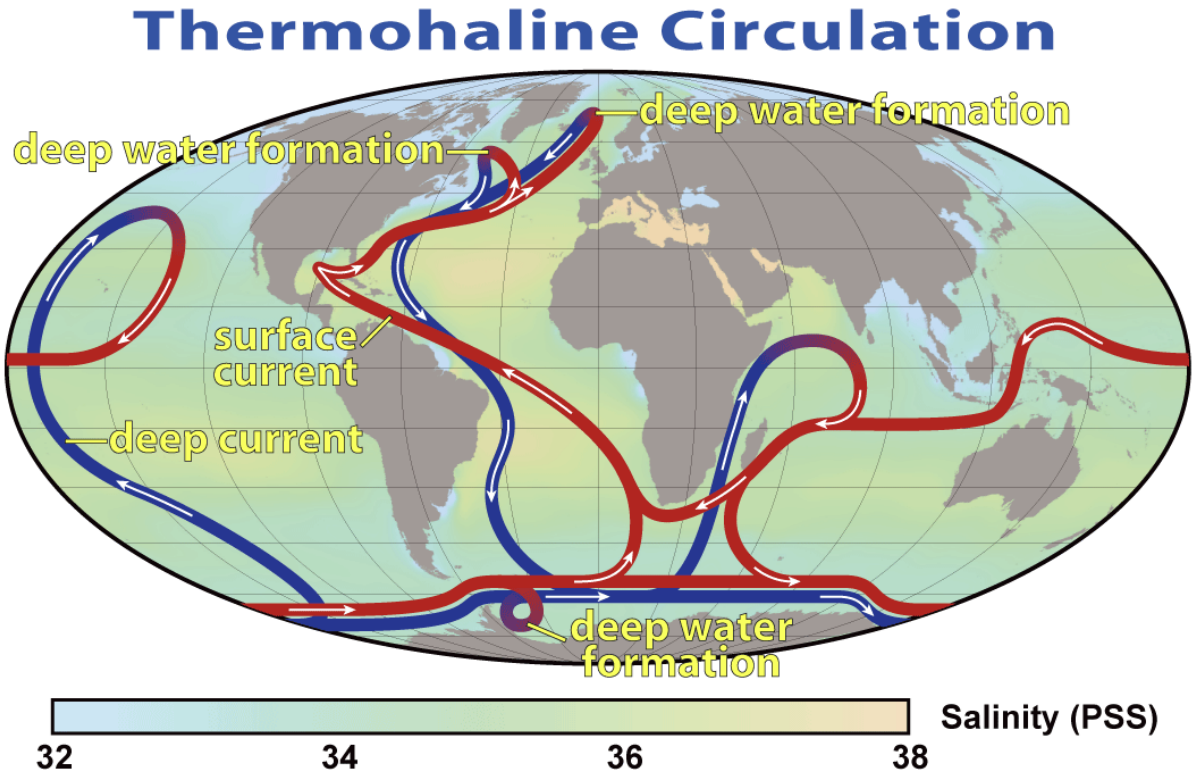

Figure 13-36: A NASA depiction of the global conveyor belt of ocean water. Estimates are that completion of this path takes 1000 years. The deep water formation areas are where ice forms to increase the salinity (density).

This video from NOAA's National Ocean Service discusses tides, surface currents and the thermohaline circulation. While tides are mentioned in the video, they are not discussed in this textbook because they do not directly cause climate variability.

Water's long trip through the ocean depths on the global conveyor belt contributes to the lag time between changes in carbon dioxide concentrations and our planet's reactions to them. Heat and dissolved carbon dioxide are carried to the ocean depths by the thermohaline circulation and remain buried for centuries in the ocean.

13.4.1 – Upwelling and Downwelling

Winds blowing across the ocean surface often push water away from an area or coast. When this occurs, water rises up from beneath to replace the surface water as it moves away. This process is known as upwelling. **Upwelling** draws cooler waters from below to the surface, as is shown in Figure 13-37.

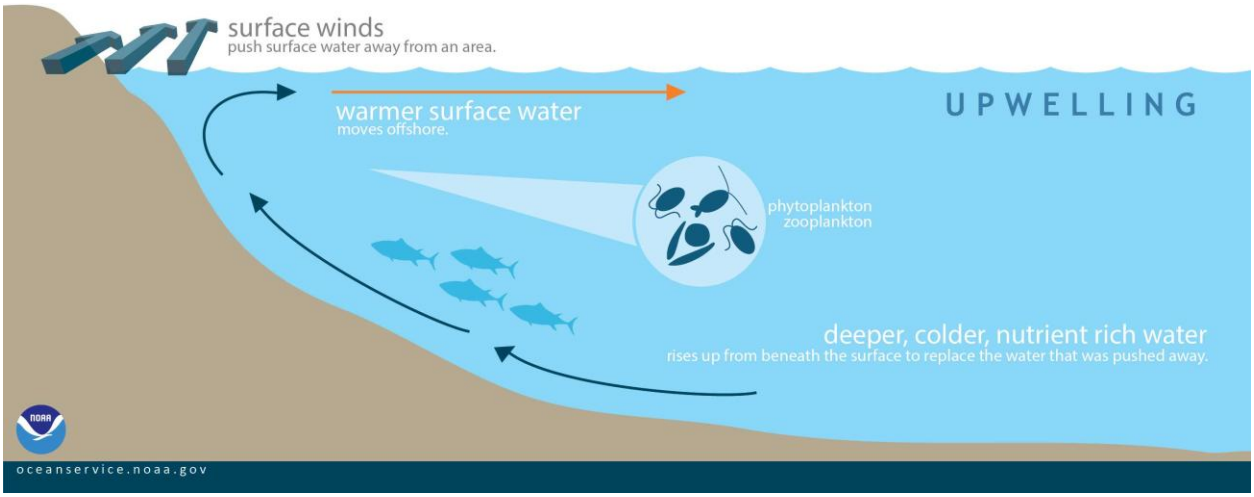

Figure 13-37: Illustration of upwelling near a coastline. Surface winds move water away from the coast causing colder water to rise from the depths to replace it.

Water that rises as a result of upwelling is typically rich in nutrients, such as planktonic organisms. Therefore, good fishing grounds are found where upwelling is common like off the coast of Peru. When upwelling occurs the warmer surface water moves in the direction of the wind further into the ocean.

The exact opposite of upwelling is downwelling. **Downwelling** occurs when warmer surface water sinks to lower depths. Winds in a downwelling situation push water towards a coastline. Water builds up along the coastline and eventually sinks to lower depths through gravity. The formation of sea ice discussed in the previous section is another example of downwelling. Both of these mechanisms for downwelling are a result of gravity pulling water to lower depths.

Figure 13-38 illustrates both upwelling and downwelling across the equatorial (latitude 0°) Pacific Ocean. The top figure depicts the temperatures from the surface to a depth of 500 meters. The bottom figure depicts the departure from a long-term average of temperatures to the same depth of 500 meters. A departure from an average value is called an **anomaly**. Hence, the bottom figure depicts the temperature anomalies for the same date as the top figure. Most of the time, the diagnosis of upwelling or downwelling in an area is easiest by examining the anomaly data. In these illustrations notice the upwelling (colder water moving towards the surface) near South America on the right side. Downwelling (warmer surface water descending) is occurring near Australia on the left side.

Downwelling and upwelling occur at many locations in the oceans. These activities in the Pacific Ocean are of international interest because changes in the world's largest ocean can affect weather conditions in many countries.

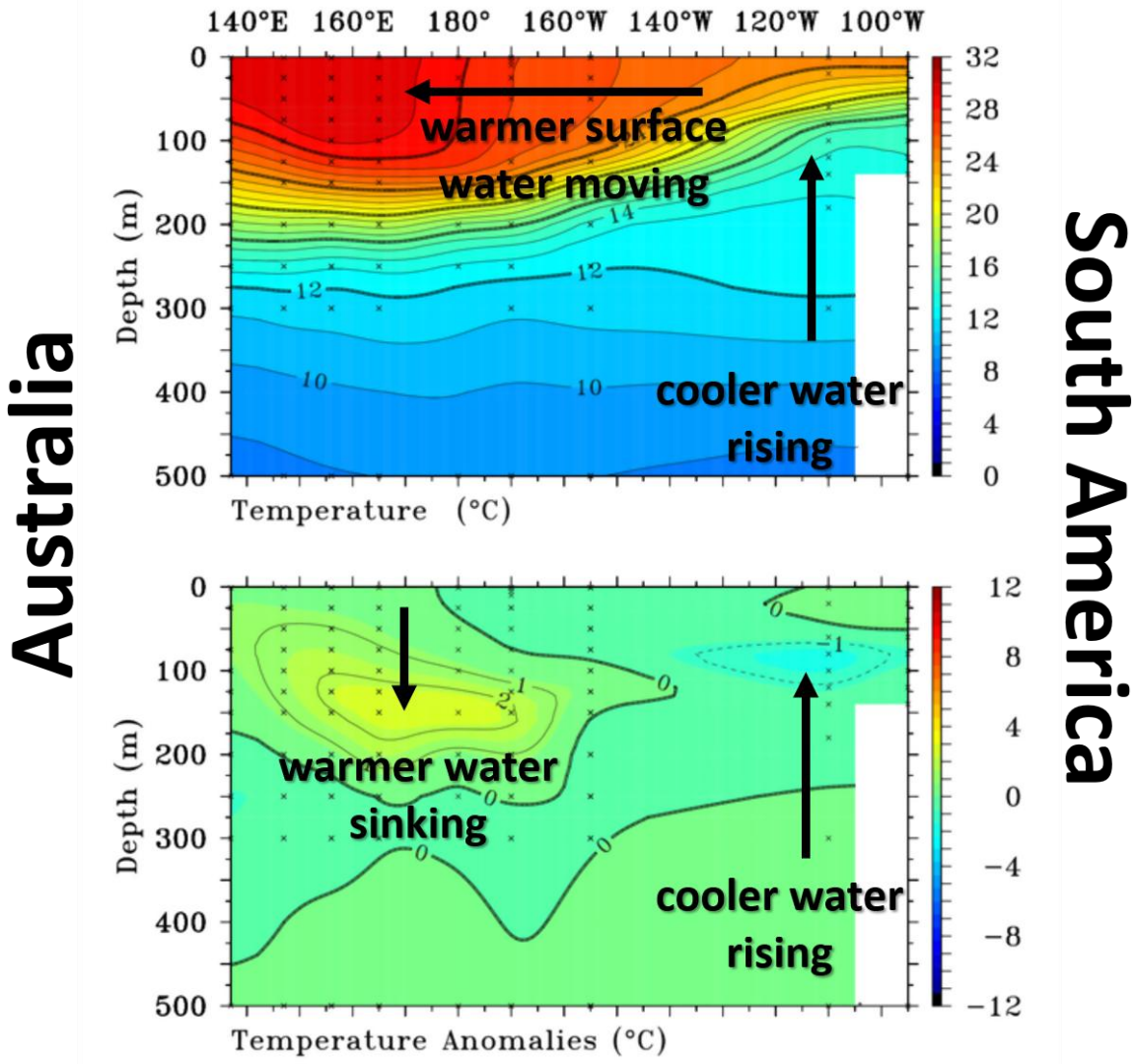

Figure 13-38: Diagram of water temperatures and anomalies in the equatorial Pacific Ocean. South America is on the right side and Australia is on the left. Each image is from the water surface to a depth of 500m. The top image contains the water temperatures, and the bottom image contains the deviation from normal water temperatures or anomalies.

This short, simple video describes upwelling and the fertile fishing grounds it creates. Downwelling, while not mentioned in the video, is the exact opposite. Downwelling in an area causes fish to migrate away from that area due to a decrease in their food supply.

13.4.2 – ENSO (El Niño and La Niña)

As mentioned in previous sections, the oceans strongly interact with the atmosphere and affect climate. Naturally occurring sea surface temperature patterns nudge the weather patterns from annual to decadal time periods. The key word in this last sentence is “nudge”. The oceans do not grab hold of a weather pattern and lock it in place, but rather cause certain weather patterns to be favored. These specific ocean temperature patterns that nudge weather patterns are called **oscillations**. Oscillations are generally diagnosed through sea surface temperature

(SST) anomalies. These SST anomalies are the difference between average SST values and what is currently observed. The most prominent and well-known oscillation is the El Niño-Southern Oscillation (ENSO) which occurs in the equatorial Pacific Ocean.

During normal conditions in the Pacific Ocean, the easterly trade winds blow towards the west along the equator, taking warm water from South America towards Indonesia and Australia. To replace this warm water, cold water rises from the depths (upwelling occurs) near South America. Figure 13-39 illustrates normal conditions in the Pacific Ocean also known as ENSO neutral conditions.

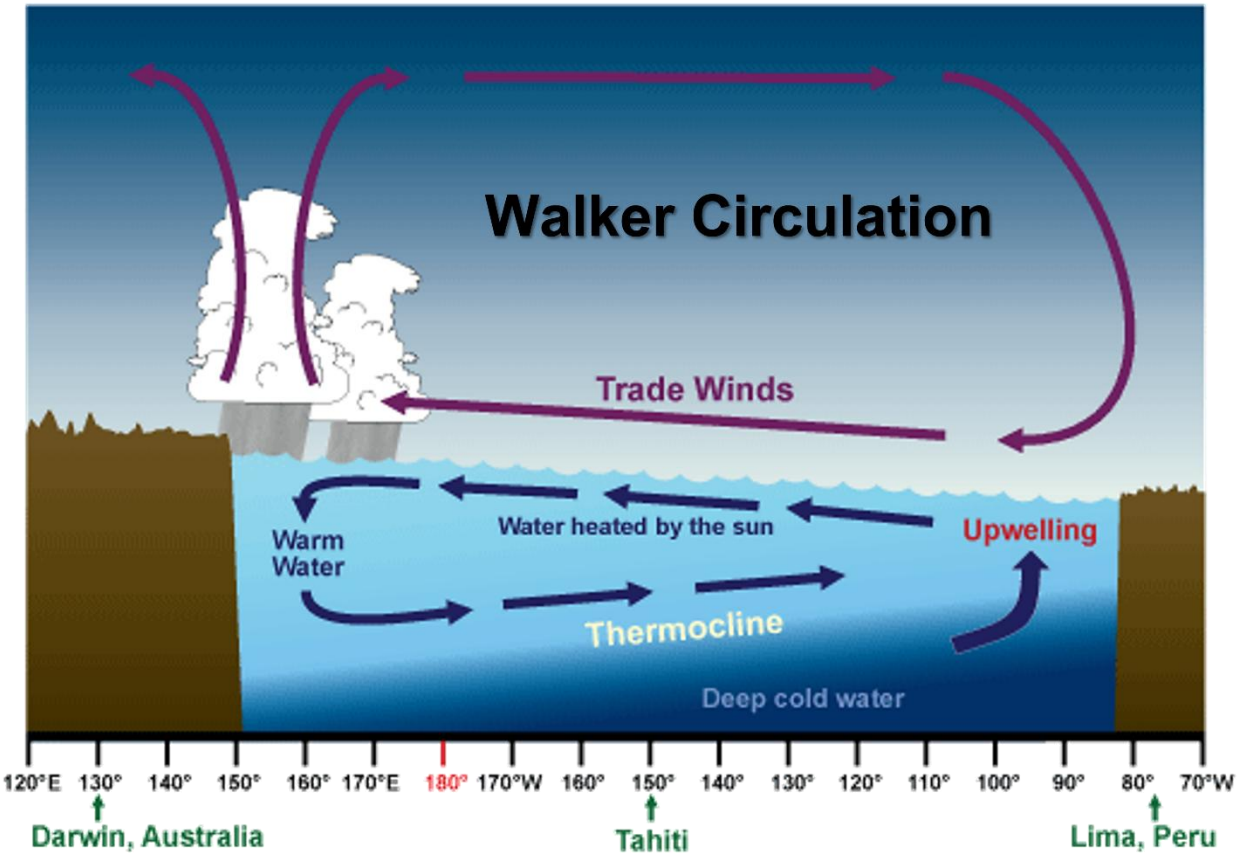

Figure 13-39: A diagram of ENSO neutral conditions with the Trade Winds moving water from South America towards Australia. Upwelling occurs near South America (right side) and downwelling near Australia (right side).

An atmospheric circulation is established across the Pacific Ocean near the equator called the Walker Circulation. The easterly surface winds and abundant warm water near Australia causes a low pressure with convection and precipitation. The South American end of the Walker circulation is drier due to descending air and a high pressure.

When the air pressure patterns in the South Pacific reverse direction (the air pressure at Darwin, Australia is higher than at Tahiti), the trade winds decrease in strength and can reverse direction. This change results in a decrease of water flow away from South America, which pushes the thermocline down and decreases upwelling.

With a deeper thermocline and decreased westward transport of water, the sea surface temperature increases to greater than normal in the Eastern Pacific. This is the warm phase of ENSO, called El Niño.

The net result is a shift of the prevailing rain pattern from the normal Western Pacific to the Central Pacific. The Western Pacific becomes relatively dry, and Australia can experience an increase in wildfires. Figure 13-40 illustrates El Niño conditions.

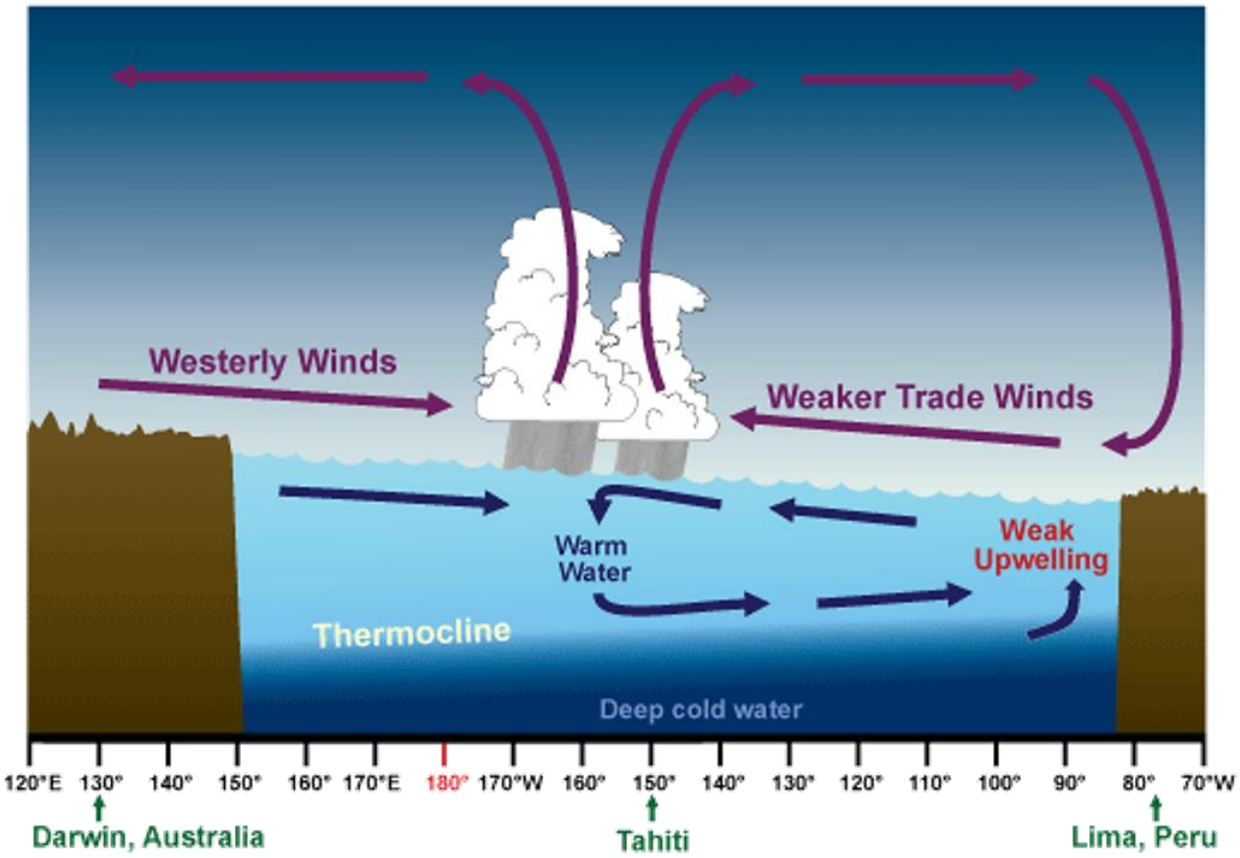

Figure 13-40: A diagram of the warm phase of ENSO, known as El Niño. The Trade Winds have weakened along with a weaker upwelling near South America (right side). Downwelling near Australia (right side) is not occurring and precipitation has moved to the central Pacific Ocean.

At other times, the Walker Circulation is strengthened. An abundance of warm surface water resides near Australia and Indonesia for an increase in precipitation over them. Off the South American coast, cooler waters predominate, since the upwelling has increased. This increase in upwelling coincides with an increase in productivity for the fishing industries. Figure 13-41 illustrates the cool phase of ENSO called La Niña.

El Niño and La Niña are two opposing oscillations that disrupt the normal Walker Circulation. Both oscillations have global impacts on weather, wildfires, ecosystems, and economies. An episode of El Niño or La Niña typically last nine to 12 months, but can sometimes last for several years. El Niño and La Niña conditions occur every two to seven years on average, but they do not have a regular schedule. Generally, El Niño occurs more frequently than La Niña.

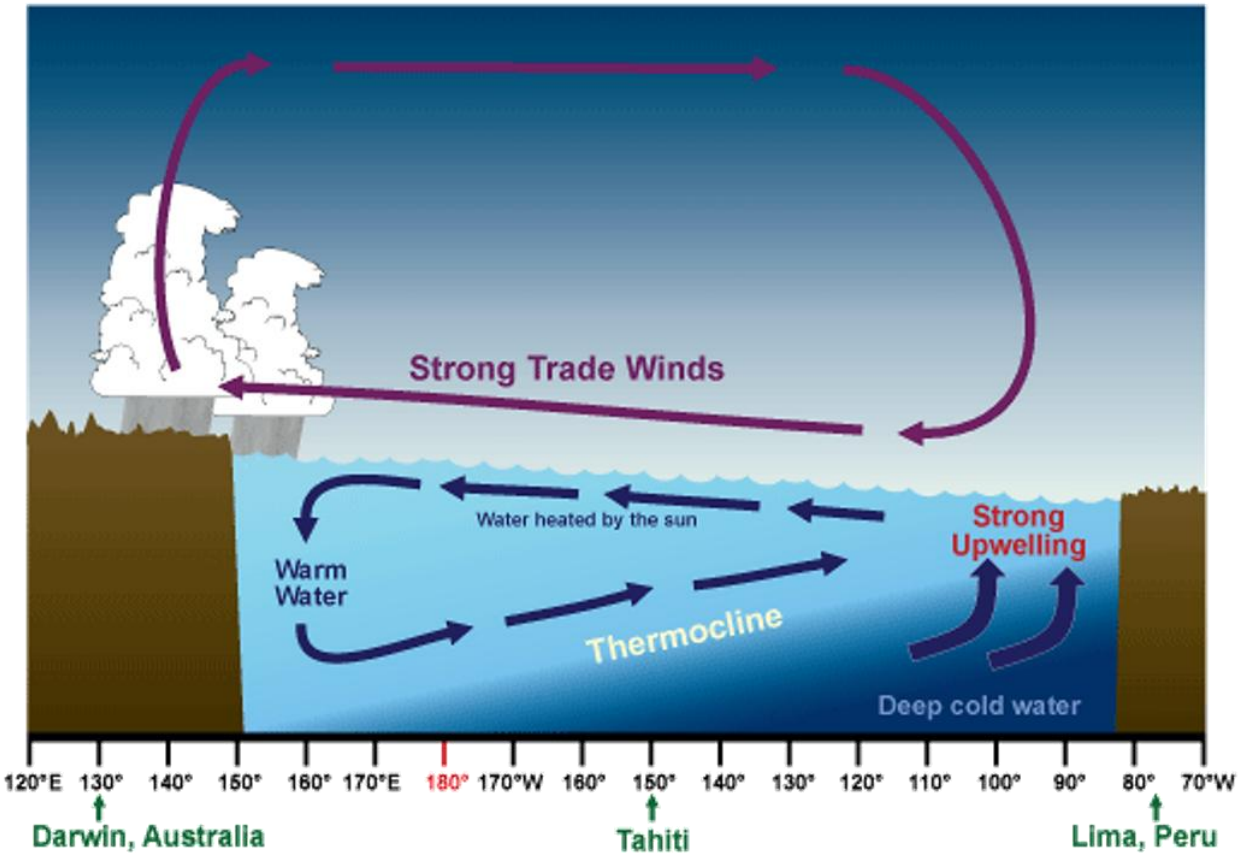

Figure 13-41: A diagram of the cold phase of ENSO, known as La Niña. The Trade winds increase in strength with strong upwelling near South America (right side). Downwelling near Australia and increased precipitation in Indonesia and Australia.

This video from the United Kingdom Met Office describes El Niño and La Niña conditions, and how each occurs.

Sea surface temperature anomalies are used to diagnosis ENSO conditions. The two maps in Figure 13-42 depict the warm phase El Niño and cool phase La Niña. Notice the temperature changes of the water in the central eastern Pacific Ocean. Both of these maps are from strong ENSO episodes.

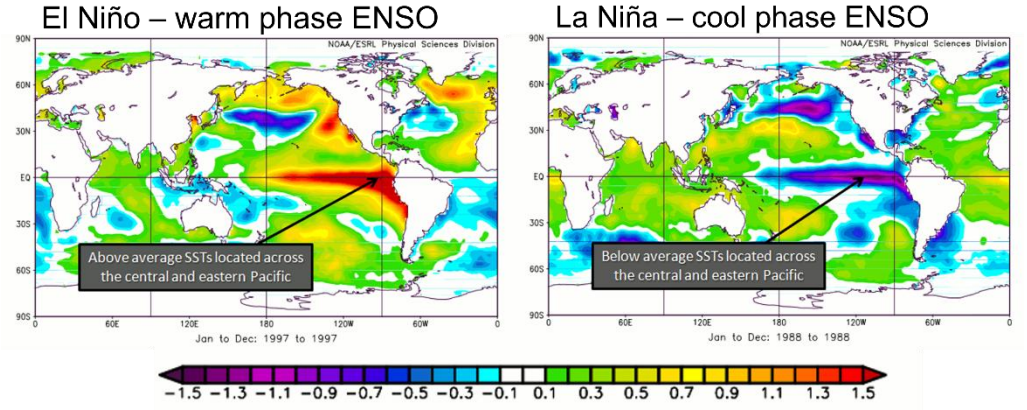

Figure 13-42: Sea-surface temperature anomalies for the warm and cool phases of ENSO.

13.4.3 – ENSO Impacts

As the position of the warm water along the equator shifts back and forth across the Pacific Ocean, the position where the greatest temperature gradient associated with the ocean - atmosphere coupling also shifts. This shift in temperature gradient directly affects the location of the jet stream, which in turn affects the frequency of midlatitude cyclones affecting a region. Increasing the frequency of storms affecting an area can cause flooding, flash flooding, and landslides. The global map in Figure 13-43 depicts the shift in the jet stream over North America for both warm and cool ENSO episodes.

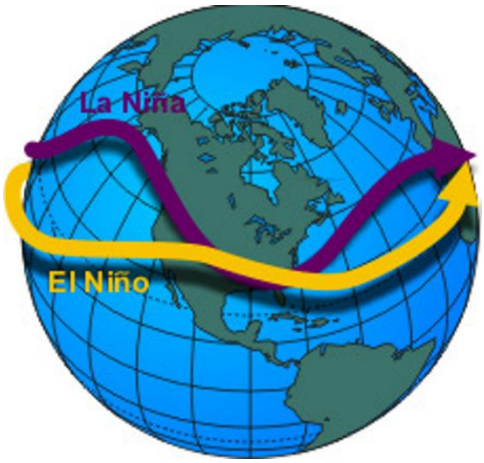

Figure 13-43: Location of the jet stream during La Niña (cool) and El Niño (warm) episodes. These locations favor the frequency of storms affecting an area.

During El Niño (warm phase of ENSO), the jet stream's position shows a dip in the Eastern Pacific. The stronger the El Niño, the farther east in the Eastern Pacific the dip in the jet stream occurs. Conversely, during La Niña this dip in the jet stream shifts west of its normal position toward the Central Pacific.

During the warm episode of ENSO (El Niño) the jet stream moves into California for an increase in the frequency of storms and precipitation in the southwest region of the United States. Rainfall in California can be significantly above normal, leading to flash floods and debris flows. With the storm track shifted south, the Pacific Northwest becomes drier as storms are shunted south of the region.

The effects of ENSO are greatest in the winter months when the jet stream moves towards the equator. The maximum correlation between a strong ENSO episode and the actual weather that occurs in a region is about 80%. Thus, even a strong El Niño or La Niña does not guarantee a seasonal wet/cool or dry/warm forecast. Figure 13-44 depicts the regions affected by a change in precipitation and temperature associated with ENSO conditions. How does a change in ENSO conditions affect the area where you live?

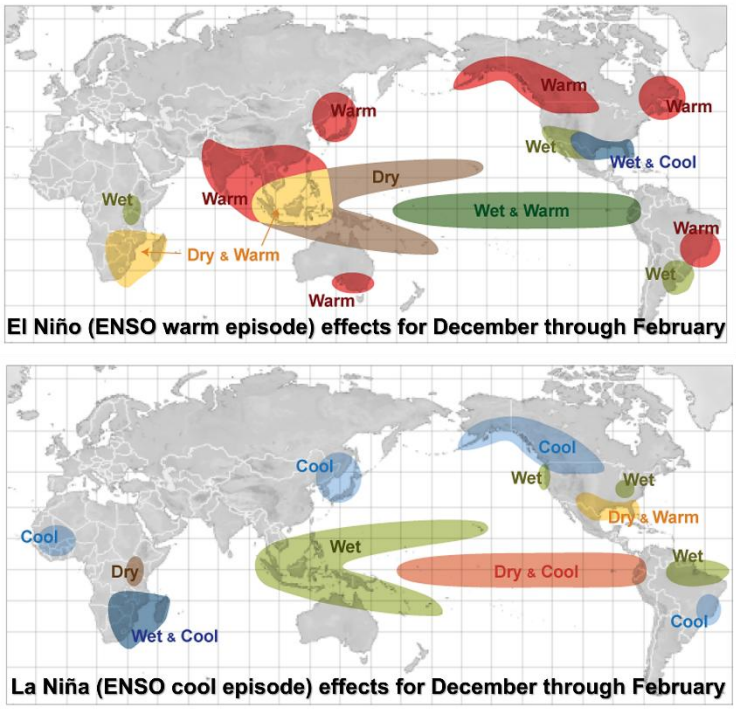

Figure 13-44: Temperature and precipitation impacts associated with warm (top) and cool (bottom) ENSO episodes.

Tropical cyclone activity in the North Atlantic is sensitive to El Niño influences. In years with a moderate to strong El Niño, the North Atlantic basin experiences:

- A substantial reduction in tropical cyclone numbers,
- A 60% reduction in numbers of hurricane days, and
- An overall reduction in hurricane intensity.

This change is likely due to stronger than normal westerly winds that develop in the western North Atlantic and Caribbean region during El Niño years. Likewise, research suggest a subsequent increase in hurricane activity when La Niña conditions are present due to weaker westerly winds.

Warm ENSO episodes cause record warm global temperatures to occur. These record high mean global temperatures are due to the abundance of warm water across the Pacific Ocean, and the methods used for calculating global mean temperatures. Thus, El Niño conditions and record high global temperatures happen together.

The effects of global warming on ENSO are unknown at this time. ENSO is an active research topic, and scientists are working to better understand it, but any links between changes in ENSO and changes in the climate remain uncertain. This short video reviews ENSO warm and cold episode conditions, and their impacts on the United States.

13.4.4 – Pacific Decadal Oscillation (PDO)

The Pacific Decadal Oscillation (PDO) occurs over periods of 20 to 30 years in the Pacific Ocean north of 20°. Due to the long time period in which a PDO occurs, it influences the 30-year climate normals across North America.

The PDO has warm and cool phases, much like ENSO. The climate impacts experienced during a PDO event are strongly correlated with ENSO impacts. If both phenomena are in the same phase, their associated impacts can be amplified. In the opposite phase, the associated impacts on global climate may be muted.

When sea surface temperatures (SSTs) are anomalously cool in the northeast and tropical Pacific and warm along the North America west coast, the PDO has a positive value. When these anomaly patterns are reversed, warm SST anomalies are in the Pacific and cool anomalies are along the west coast, the PDO has a negative value. The global maps in Figure 13-45 show the positive and negative phases of the Pacific Decadal Oscillation.

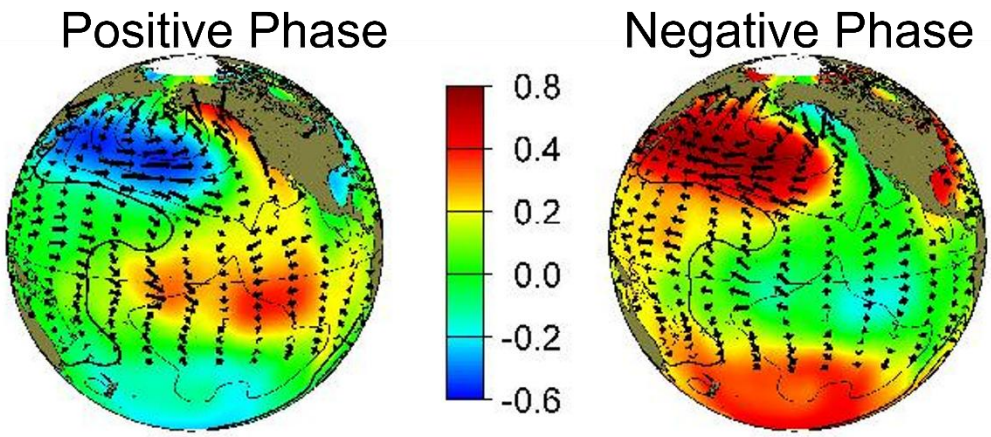

Figure 13-45: The sea surface temperature anomalies associated with the Pacific Decadal Oscillation (PDO). The PDO affects the 30-year climate normals across North America.

Positive PDO values are usually associated with wetter conditions in the Southwestern U.S., while negative PDO values are suggestive of persistent drought. The PDO is also highly correlated with major changes in North Pacific fish populations and marine ecosystems. The causes of the PDO are not known, which limits its predictability; although some climate simulations have produced oscillations that are similar to the PDO. Much like ENSO, the PDO influences the mean global temperature analyses. The graph in Figure 13-46 shows the PDO values from 1960 through 2020.

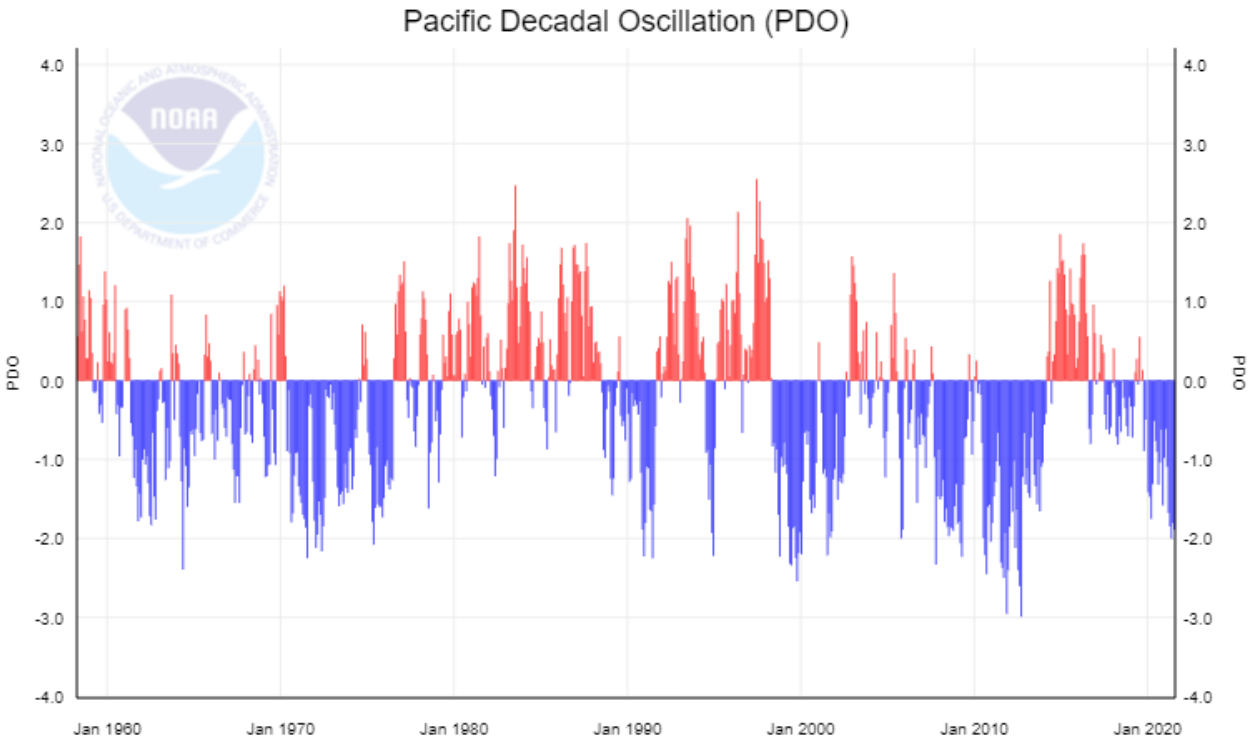

Figure 13-46: Variations in the Pacific Decadal Oscillation from 1960 through 2020.

This short video from the United Kingdom Met Office discusses the Pacific Decadal Oscillation well.

13.4.5 – Atlantic Multidecadal Oscillation (AMO)

The Atlantic Multidecadal Oscillation (AMO) is an ongoing series of long-duration changes in the sea surface temperature of the North Atlantic Ocean. The AMO has cool (negative) and warm (positive) phases that last for 20-40 years with a difference of about 1°F between extremes. These changes are natural and have been occurring for at least the last 1,000 years.

An Atlantic Multidecadal Oscillation (AMO) Index was developed to measure the changes in sea surface temperature and wind shear for large areas of the tropical Atlantic. Figures 13-47 and 13-48 from NASA depicts the sea surface temperature anomalies in the Northern Atlantic during the cool and warm phases of the AMO.

The different phases of the AMO have been associated with a variety of impacts. The positive (warm) phase has been associated with reduced Arctic Sea ice, melting of the Greenland ice sheet, increased hurricane activity in the North Atlantic, decreased rainfall over most of the U.S.

and northeastern South America, and increased rainfall in southern Alaska, northern Europe, west Africa, and the southeastern U.S. Persistent drought across the Midwest U.S., such as the 1930s Dust Bowl, was associated with a positive AMO. As for the cold, negative phase, it has the opposite impacts: cooling at high latitudes, reduced hurricane activity and a switch in rainfall.

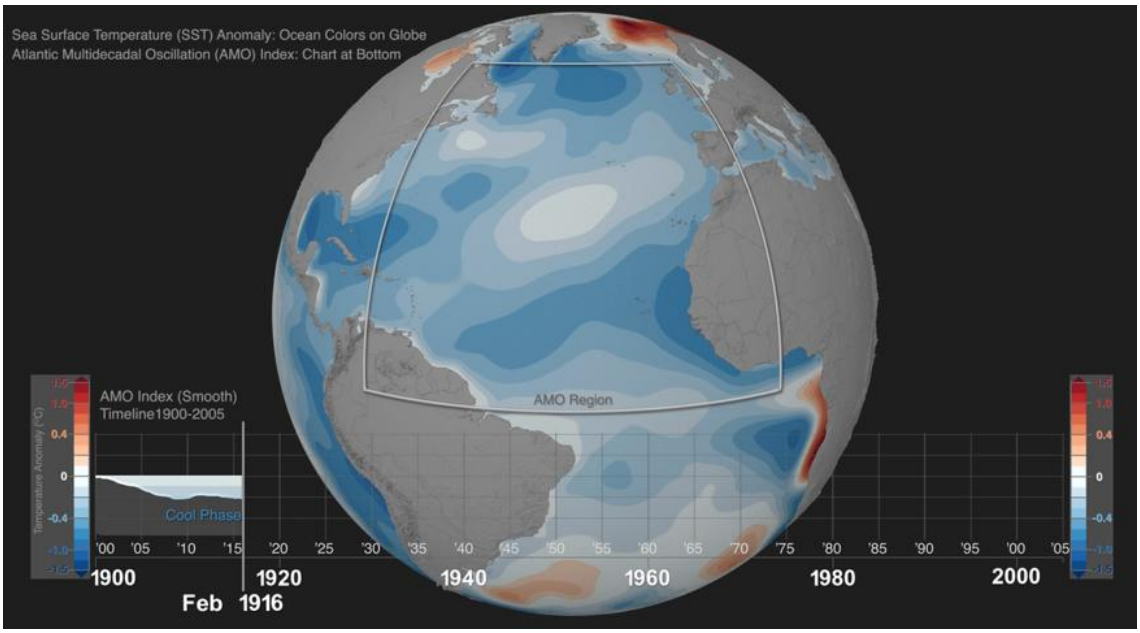

Figure 13-47: Atlantic Multidecadal Oscillation (AMO) cool phase sea surface temperature anomalies for February 1916. A graph of the AMO Index is in the lower left.

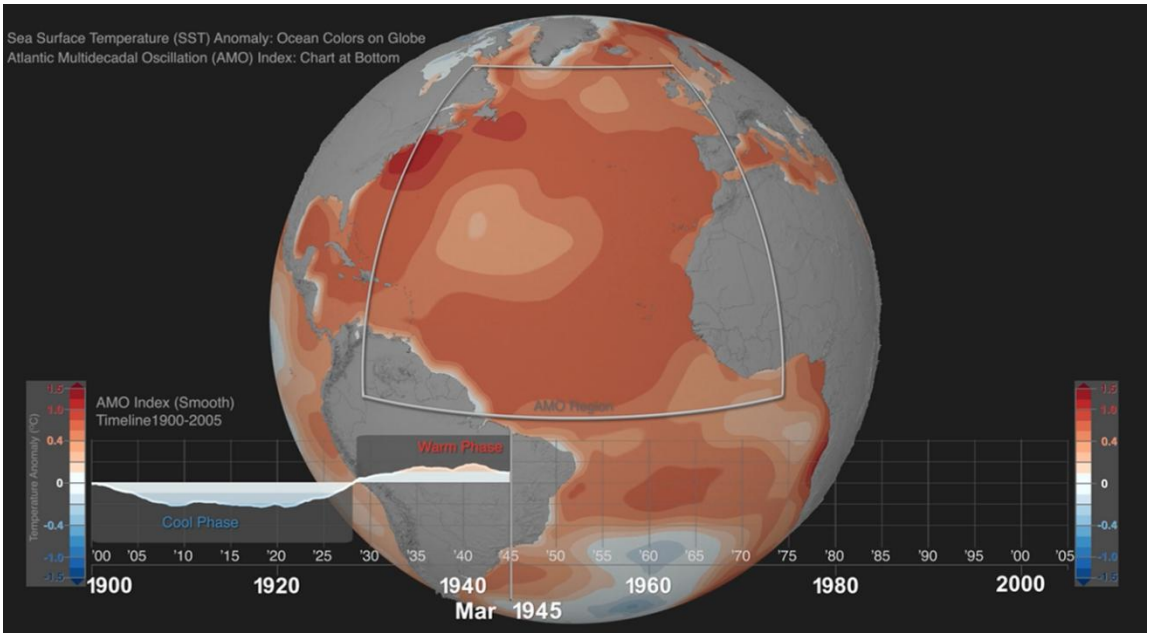

Figure 13-48: Atlantic Multidecadal Oscillation (AMO) warm phase sea surface temperature anomalies for March 1945. A graph of the AMO Index is at the bottom.

This video from the United Kingdom Met Office describes the AMO and the impacts associated with its change in phase.

Chapter 13 Review Questions

1. What is a climate proxy?
2. What is dendrochronology?
3. What type of climate information can be provided by dendrochronology?
4. What is the maximum age an object can be dated using carbon isotope analysis?
5. Does the 11-year sunspot cycle affect climate?
6. Where are light oxygen (^{16}O) and heavy oxygen (^{18}O) concentrated during cold periods?
7. What does each layer of an ice core represent?
8. How long ago was the last ice age (Last Glacial Maximum)?
9. During the Last Glacial Maximum, how much was the Earth covered in ice?
10. Using this graph, answer these questions.
    a. How many glacial periods have occurred in the last 400,000 years?
    b. Which is longer, a glacial or interglacial period?
    c. Are we currently in a glacial or interglacial period?
    d. What is the sea level change during glacial and interglacial periods?
    e. Which changes first, temperature or carbon dioxide?

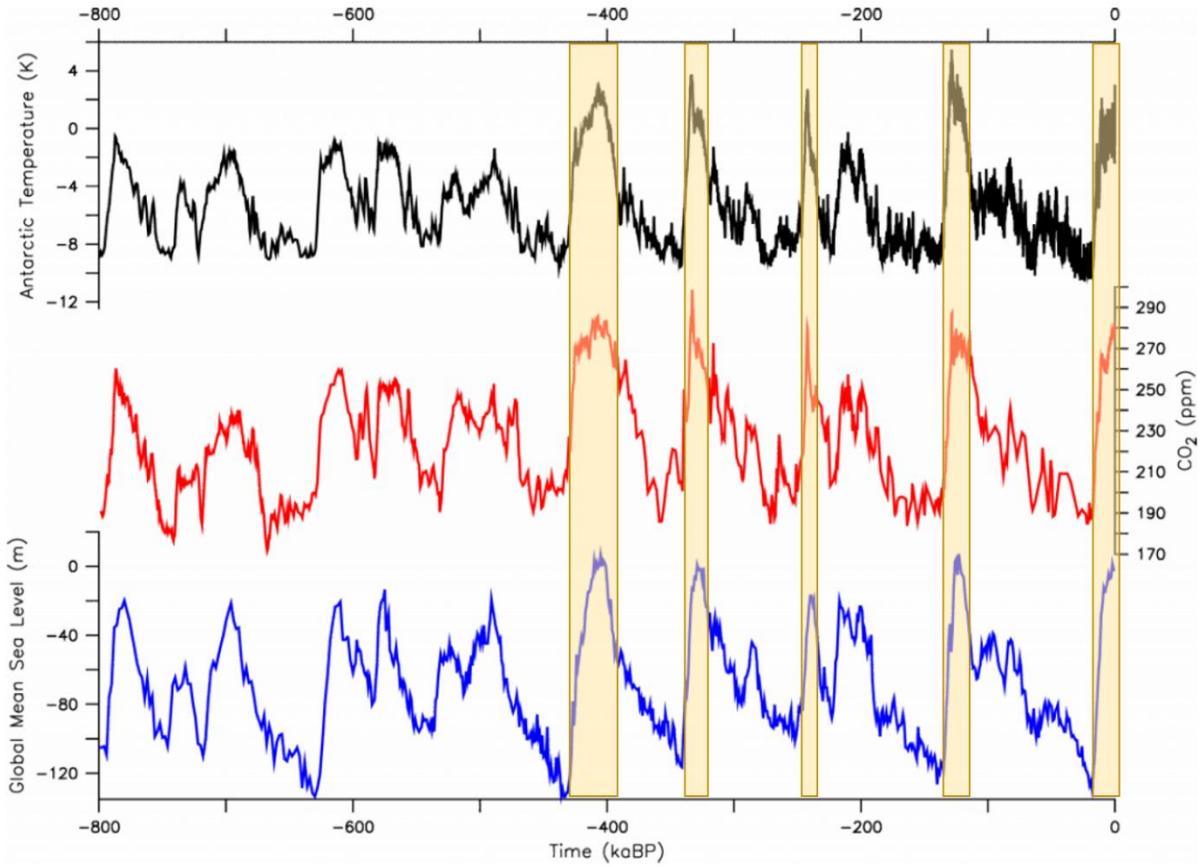

11. What is the current influence from volcanoes on global temperatures?
12. What causes the sea level rise during an interglacial period?
13. What is an example of positive feedback?
14. What is an example of negative feedback?
15. What is the primary cause of glacial and interglacial periods?
16. What is the polar vortex?
17. What drives surface ocean currents?
18. What drives deep ocean currents?
19. How do the oceans affect the natural variability of weather?
20. Describe upwelling in an ocean?
21. Describe downwelling in an ocean?
22. How may a strong El Niño affect your winter weather?
23. How may a strong La Niña affect your winter weather?
24. What types of weather are affected by changes in the Atlantic Multidecadal Oscillation, and where do these changes occur?

Chapter 14 – Anthropogenic Climate Change and Earth's Future Climate

Overview

This chapter explores the observed changes in climate that have been caused by human activities. Examining the observed changes assists scientists in determining the consequences of future changes in climate, and the causes of these past and future changes.

To determine future climates, numerical climate models are used. These climate models focus on the balances in the Earth's climate system, such as greenhouse gas (GHG) changes, the carbon cycle, the hydrologic cycle, and an overall heat/energy balance of the entire Earth system. Projections of future climates out to 2100 are examined based on various scenarios. Since future climate conditions are not always known, scenarios are a method for these climate models to capture a range of possible conditions.

Chapter objectives:

1. Describe the anthropogenic climate changes that are observed.
2. Understand how climate models are evaluated.
3. Understand how scenarios are used to capture the unknowns in a climate projection.
4. Describe how climate models can determine that anthropogenic climate change is occurring.
5. Describe the projected changes in Earth's climate.

14.1 – Observed Anthropogenic Climate Changes

When the topic of anthropogenic climate change is mentioned, most people immediately think about carbon dioxide levels in the atmosphere. While carbon dioxide may be the star of the show, other types of human caused climate change are present. In Chapter 12, urban heat islands were examined. The heat island associated with a metropolitan area is definitely human caused. The temperatures in a metropolitan area are warmer than surrounding rural areas, and many cities have seen increases exceeding the mean global temperature increase (about 2^{o}F) due to these heat islands.

Another land use change is the conversion of land from native vegetation to agricultural land. Land used for agricultural purposes generally has irrigation and plants that transpire more than native vegetation. This land use change increases both soil and atmospheric moisture, which in turn can influence the intensity of storms in that area.

Simulations of the Great Plains in the United States demonstrate this link between land use and storm intensity. The top portion of Figure 14-1 (a) simulates the current vegetation consisting of

a mixture of farmland and native grasses and brushes. A dryline is present between the drier air and moister air over the farmland. Simulations in this environment cause a thunderstorm to occur. The bottom portion of Figure 14-1 (b) has the same initial atmospheric conditions, although the vegetation is just the native grasses and brush. Notice towering cumulus develop but no thunderstorm. This simulation tends to indicate that human activities could be increasing the convective storms in the central U.S.

Figure 14-2 contains maps of the global land use changes from native vegetation to agricultural land from 1500 to 2000. The color key contains the relative fraction of land that was converted. Notice the high percentage of agricultural land in the central United States.

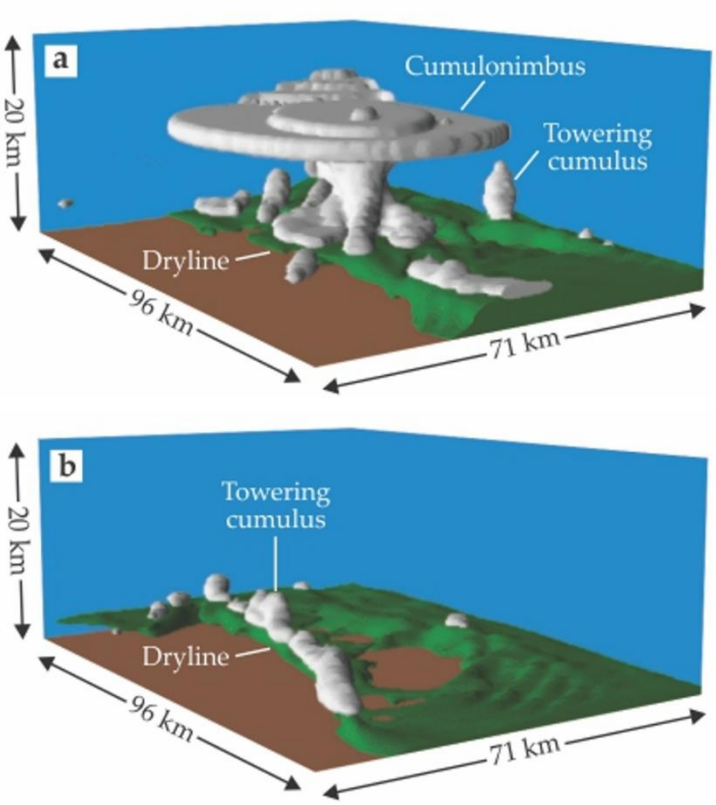

Figure 14-1: Simulations of convective activity on the Great Plains (a) using a mixture of native vegetation and farmland, and (b) with just native vegetation. Notice a thunderstorm develops when considering human modified land use.

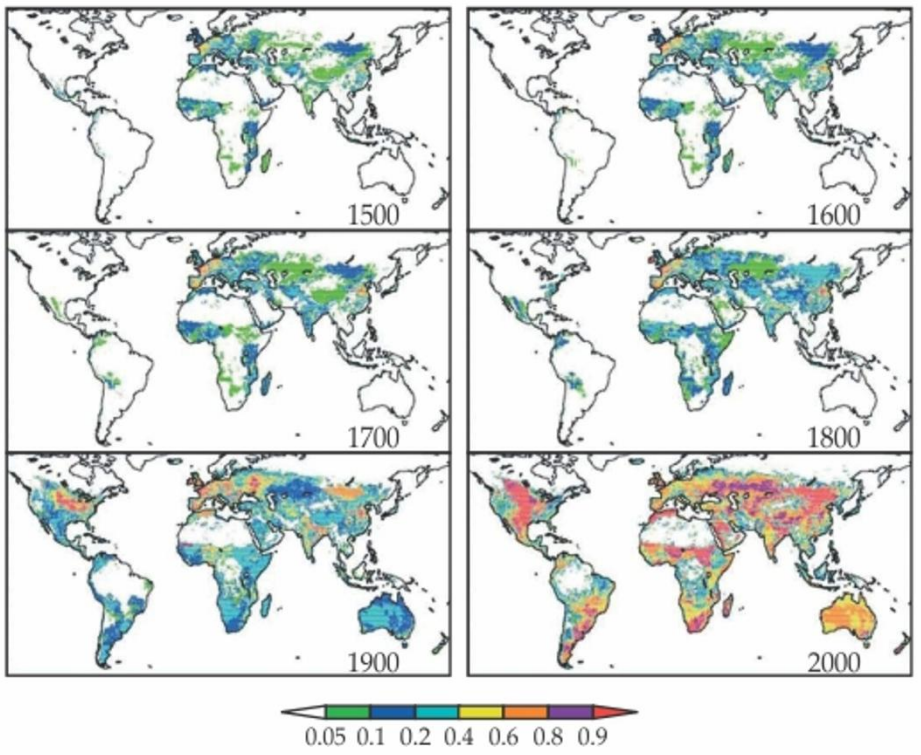

Figure 14-2: Maps depicting the land use changes from native vegetation to agricultural land from 1500 to 2000. Notice the high percentage of agricultural land in the Central U.S.

14.1.1 – Atmosphere Composition Changes

Changes in the composition of the atmosphere are largely attributed to the global increase in the mean temperature. The bar graph in Figure 14-3 highlights the gases and particulates associated with this warming. The black vertical lines associated with each bar indicates the possible error associated with the category or element.

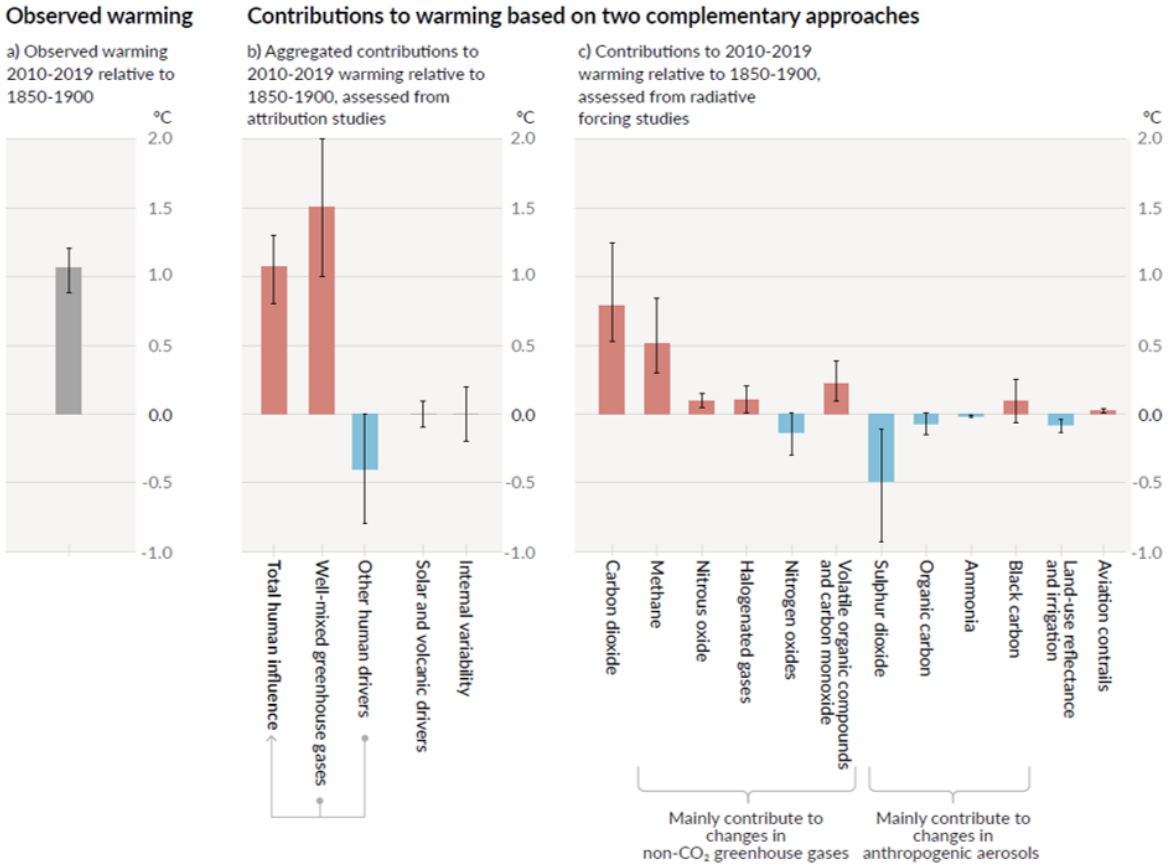

Figure 14-3: Bar graphs containing the details associated with global temperature changes. The total observed warming (left side) is over 1°C. This warming is from human influences (middle graphs). The gases and particulates responsible for these changes (right side).

The total observed warming relative to 1850-1900 is slightly over 1°C (Figure 14-3a - left). This warming is essentially from human influences (Figure 14-3b - middle). The gases causing this warming (Figure 14-3c - right) are carbon dioxide, methane, nitrous oxide, halogenated gases, VOCs and carbon monoxide. These gases should seem familiar since most were discussed in detail in Chapter 12.

Methane is the same as natural gas. Methane is produced by fossil fuel extraction and agricultural activities. While methane contributes less to the total warming than carbon dioxide, as a greenhouse gas, methane is much more efficient at capturing heat. Thus, methane contributes significantly to the warming of the atmosphere, even though its concentration in the atmosphere is much less.

Not all anthropogenic pollutants contribute to warming as is seen by the blue bars. Nitrogen oxides are a byproduct of combustion, and cause a cooling effect. Nitrogen oxides (NO_x) differ

from nitrous oxide (N_2O), which is commonly called laughing gas, and is used in medical procedures. Sulfur dioxide, organic carbon, and ammonia are associated with the generation of particulates or aerosols. Particulates and aerosols lower temperatures due to the reflection of solar radiation, much like what happens after a volcanic eruption.

Figure 14-4 shows the actual change in concentrations of carbon dioxide, methane, and nitrous oxide for the past 2000 years. As this figure indicates, all the concentrations have increased since the industrial revolution.

Aviation contrails (Figure 14-3c) are the condensation trails produced by the combustion of jet fuel. A jet engine puts out warm, moist air. This warm air cools rapidly at high altitudes and condenses creating clouds. The overall impact of these high clouds is a slight warming. However, the effects of clouds and their feedback mechanisms poses a dilemma.

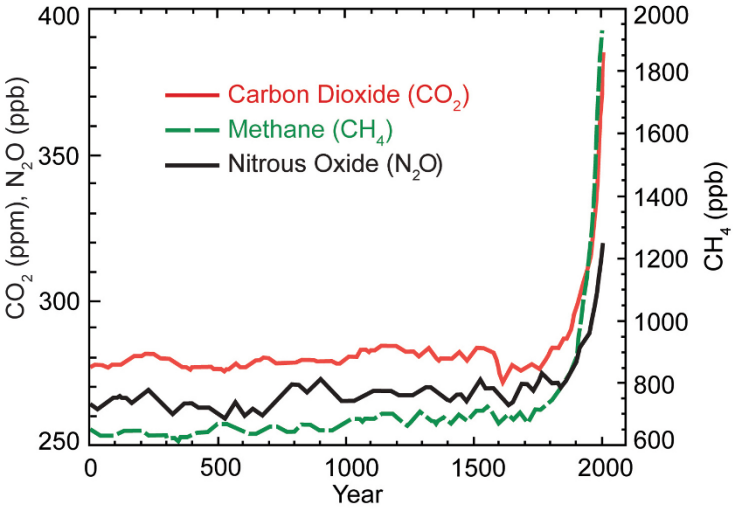

Figure 14-4: The change in concentrations of carbon dioxide, methane, and nitrous oxide for the past 2000 years.

The overall effect of a warmer atmosphere is a moister atmosphere, because more evaporation occurs and warm air can hold more moisture than cold air. Warming will also likely change the amount of cloud cover. However, no clearly understood mechanism has been identified that would make an unambiguous prediction on how clouds would change in a warmer climate. Comprehensive climate models predict a large range of cloud feedbacks. Most of them are positive, but negative feedback cannot be excluded at this point. Cloud feedback is the least well understood and the most uncertain element in climate models. As such, clouds are the source of a large uncertainty in future climate projections. Climate models are a future topic in this chapter as we explore projections of our future climate.

14.1.2 – Global Temperature Changes

Figure 14-5 displays the June global average temperature anomalies from 1850 to 2023. The increase in global temperature is about 2°F.

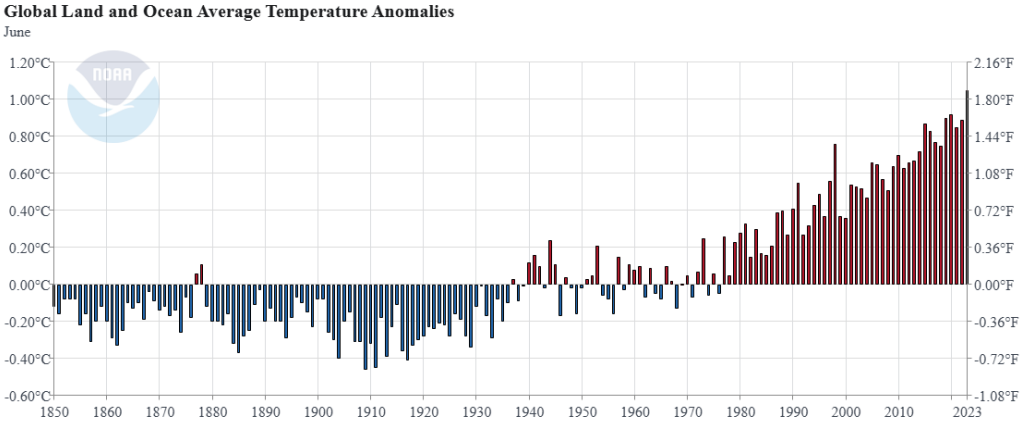

Figure 14-5: Global average June temperature changes from 1850-2023.

Given the size and tremendous heat capacity of the global oceans, it takes a massive amount of heat energy to raise Earth's average yearly surface temperature. The 2-degree Fahrenheit increase in global average surface temperature that has occurred since the pre-industrial era (1850-1900) might seem small, but it required a significant increase in accumulated heat.

This warming has not been uniformly spread across the planet. The upward trend in the globally averaged temperature shows that the higher latitudes in the Northern Hemisphere are warming more than elsewhere. The temperatures over land have changed more than the oceans. The combined land and ocean temperature has increased at an average rate of 0.13 degrees Fahrenheit (0.08 degrees Celsius) per decade since 1880. However, the average rate of increase since 1981 (0.18°C / 0.32°F) has been more than twice that rate.

Figure 14-6 shows the changes in global average surface temperature from 1994-2023. Places that warmed up to 1° Fahrenheit over the past 30 years are in red, places that have cooled up to 1°F are blue.

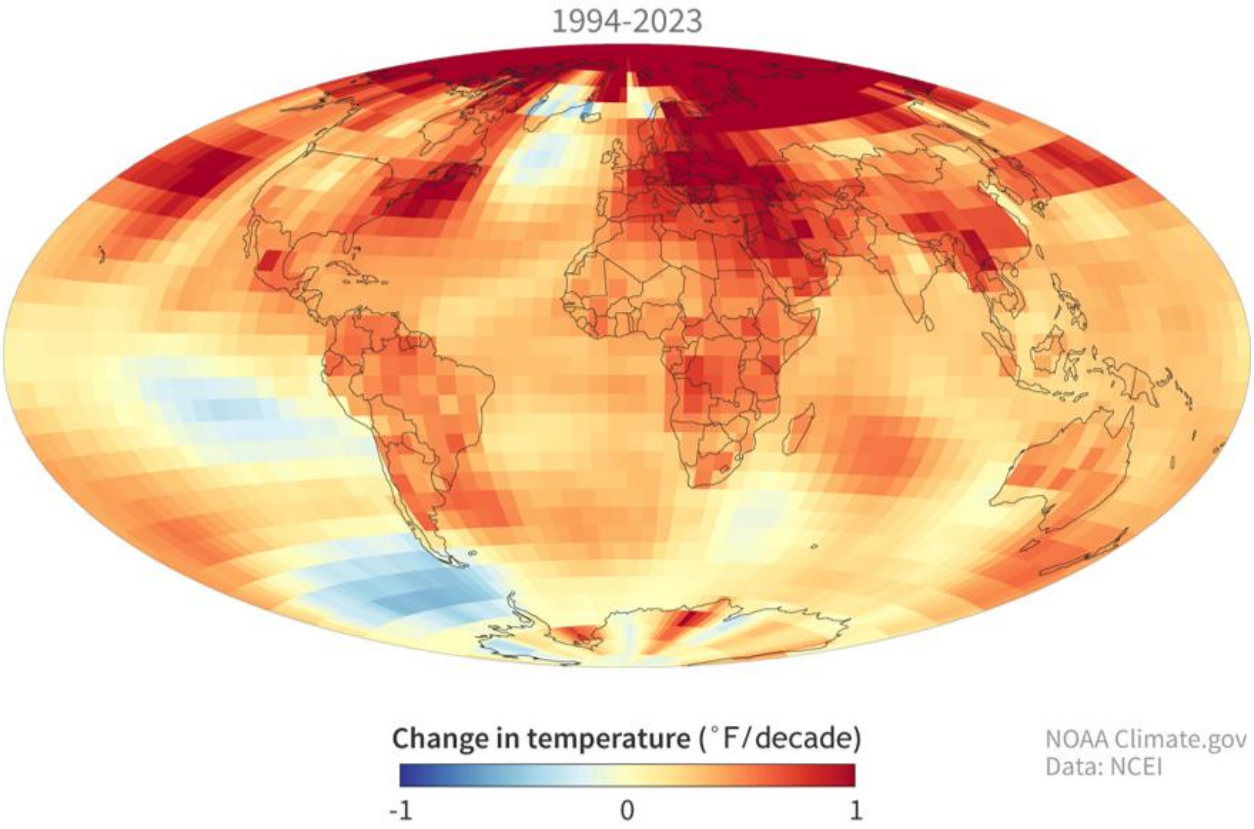

Figure 14-6: Global annual surface temperature changes from 1994 to 2023.

The concept of an average temperature for the entire globe may seem odd. After all, at this very moment, the highest and lowest temperatures on Earth are likely more than 100°F (55°C) apart. Temperatures vary from night to day and between seasonal extremes in the Northern and Southern Hemispheres. This means that some parts of Earth are quite cold while other parts are toasty hot. To speak of the "average" temperature then, may seem like nonsense. However, the concept of a global average temperature is convenient for detecting and tracking changes in Earth's energy budget over time.

To calculate a global average temperature, scientists begin with temperature measurements taken at locations around the globe. Because their goal is to track changes in temperature, measurements are converted from absolute temperature readings to temperature anomalies—the difference between the observed temperature and the long-term average temperature for each location and date. Multiple independent research groups across the world perform their own analysis of the surface temperature data, and they all show a similar upward trend.

Across inaccessible areas that have few measurements, scientists use surrounding temperatures and other information to estimate the missing values. Each value is then used to calculate a global temperature average. This process provides a consistent, reliable method for monitoring changes in Earth's surface temperature over time.

14.1.3 – Ocean Changes

Most of the excess atmospheric heat due to increasing greenhouse gases is absorbed by the oceans. As a result, the upper ocean heat content has increased significantly over the past few decades. Figure 14-7 shows differences from long-term average global ocean heat content (1955-2006) for the top 700 meters of the ocean.

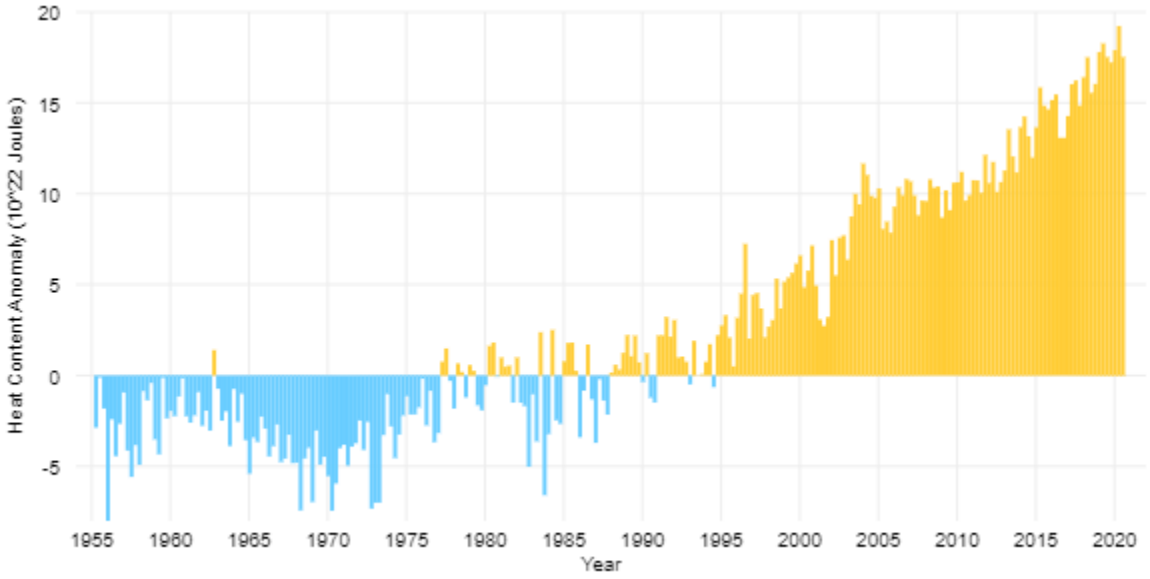

Figure 14-7: Difference in the heat content of the top 700 meters of the ocean with respect to the long-term global average. Data is shown from 1955 to 2021. The long-term average is based on the years 1955 to 2006.

More than 90 percent of the warming that happened on Earth between 1971-2018 occurred in the ocean. The right-side of Figure 14-8 depicts the change in the Earth's energy (heat) content for the oceans, cryosphere, land, and atmosphere. As this figure shows, the oceans have warmed the most on our planet. The atmosphere has warmed the least. The uncertainty in these values is indicated by the red bar.

The map in Figure 14-8 (left side) depicts the change in ocean heat content from 1993 to 2022. Large portions of most ocean basins are gaining heat (orange) and the global average trend is positive. However, some areas have lost heat (blue). Those areas that are gray have shown no significant trend. Hence, the heat is not evenly distributed throughout the oceans.

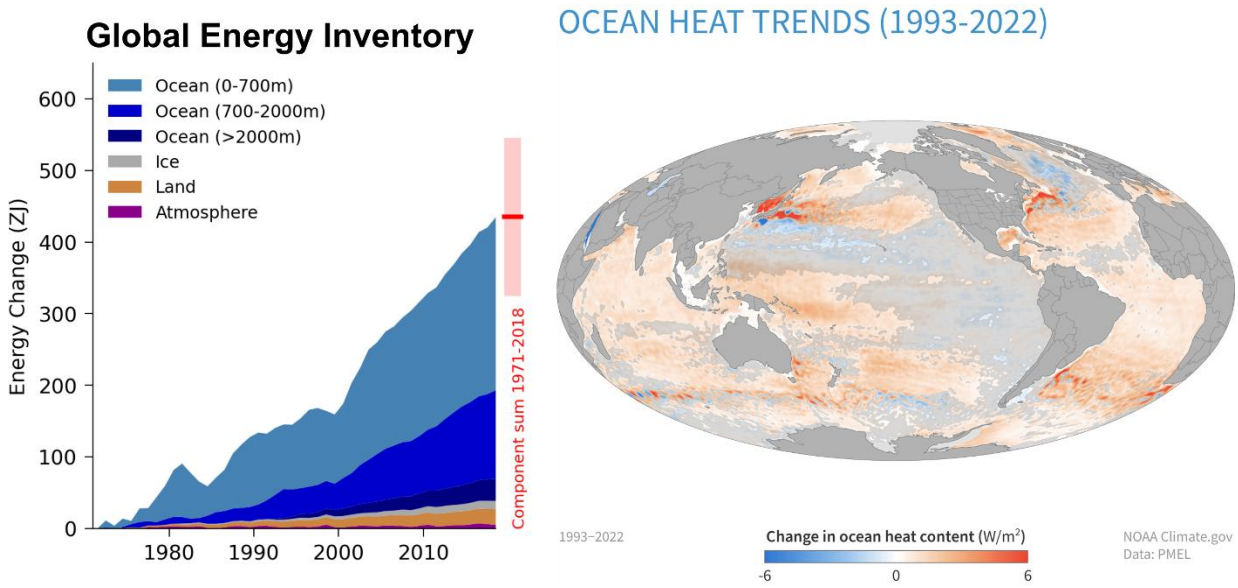

Figure 14-8: (right-side) The change in the Earth's heat content for the oceans, cryosphere, land, and atmosphere. The oceans have warmed the most. The atmosphere has warmed the least. (left-side) The oceans have not warmed uniformly as shown in this global map. Some areas have warmed and others have cooled.

Not only does water cover about 70 percent of our planet's surface, but it can also absorb large amounts of heat without a large increase in temperature. This tremendous ability to store and release heat over long periods of time gives the ocean a central role in stabilizing Earth's climate system. The main source of ocean heat is sunlight. Additionally, clouds, water vapor, and greenhouse gases emit heat that they have absorbed, and some of this heat energy enters the ocean.

Heat absorbed by the ocean moves within it but does not disappear. The heat energy eventually re-enters the rest of the Earth system by melting ice shelves, evaporating water, or directly reheating the atmosphere. Thus, heat energy in the ocean can warm the planet for decades after it was absorbed. If the ocean absorbs more heat than it releases, its heat content increases. Knowing how much heat energy the ocean absorbs and releases is essential for understanding and modeling global climate.

While the oceans are absorbing a lot of heat, they are also absorbing some of the increasing carbon dioxide from the atmosphere. This absorption of carbon dioxide leads to a lower pH and greater acidity. This increase in acidity is called ocean acidification. Ocean acidification changes the chemistry of an ocean. Figure 14-9 shows the changes in ocean acidity. As atmospheric CO_2 increases (red line), the CO_2 concentration in the ocean increases (green line). As additional chemical processes occur, hydrogen ions are liberated which causes the pH to drop (light blue line) and the ocean acidity increases.

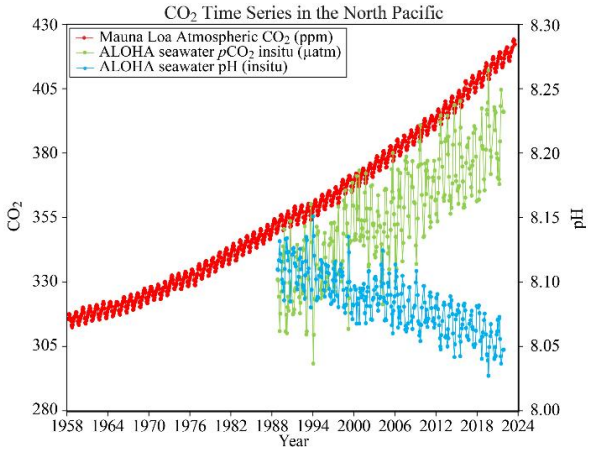

Figure 14-9: Atmospheric CO^2 (red) from Mauna Loa, Hawaii. Ocean CO_2 (green) and the resulting pH (blue).

Water and carbon dioxide combine to form carbonic acid (H_2CO_3), a weak acid that dissociates into hydrogen ions (H^+) and bicarbonate ions (HCO_3^-). As ocean acidification increases, available carbonate ions (CO_3^{2-}) bond with excess hydrogen, resulting in fewer carbonate ions available for calcifying organisms to build and maintain their shells, skeletons, and other calcium carbonate structures. If the pH gets too low (higher acidity), shells and skeletons can begin to dissolve. Figure 14-10 shows this chemical process and changes to a pteropod shell with a lower pH.

The pteropod, or "sea butterfly," is a tiny sea snail about the size of a small pea. Pteropods are an important part of many food webs and are eaten by organisms ranging in size from tiny krill to whales. When pteropod shells were placed in sea water with lower pH, the shells slowly dissolved and the organisms died. The effects of lower pH levels on the health of calcifying organisms in the oceans is a serious concern of biologists.

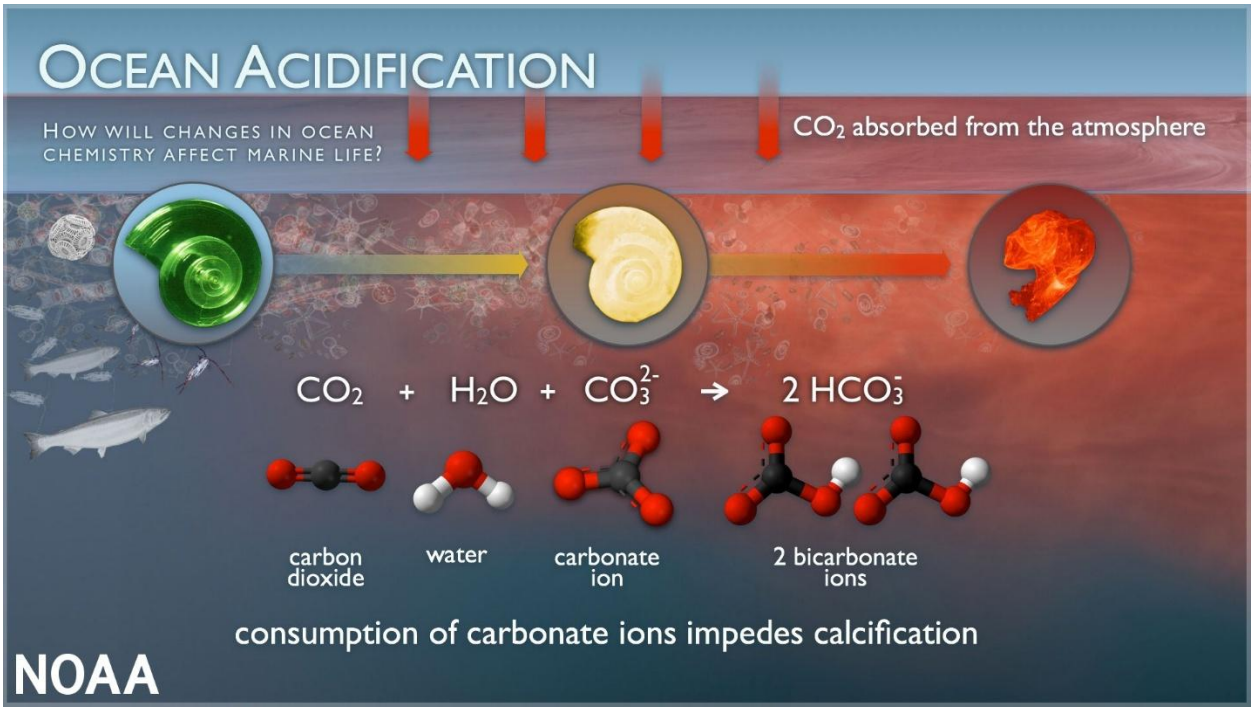

Figure 14-10: The chemical process that creates bicarbonate ions, and changes the ocean pH. These changes affect marine life, as illustrated by the decay of a tiny sea snail (pteropod).

Does the change in ocean heat affect the oscillations associated with natural climate variability? Previously in Chapter 13, ENSO, PDO, AMO, and the AO were examined. All these oscillations show little or no evidence of being changed by anthropogenic forcings at this time.

14.1.4 – Sea Ice Changes

Sea ice is ocean surface water that has frozen. Sea ice grows throughout the fall and winter, and melts during the spring and summer. In the Arctic Ocean, sea ice extent (the area of ocean with at least 15 percent sea ice concentration) typically reaches its maximum in March and its minimum in September.

The maps in Figure 14-11 depict the Arctic sea ice extent in March and September 2020 versus the median extent of the sea ice from 1981 to 2010. The magenta line is the median extent of the ice. Notice the summer sea ice is much less than the median, and the spring (March) ice is close to the median extent.

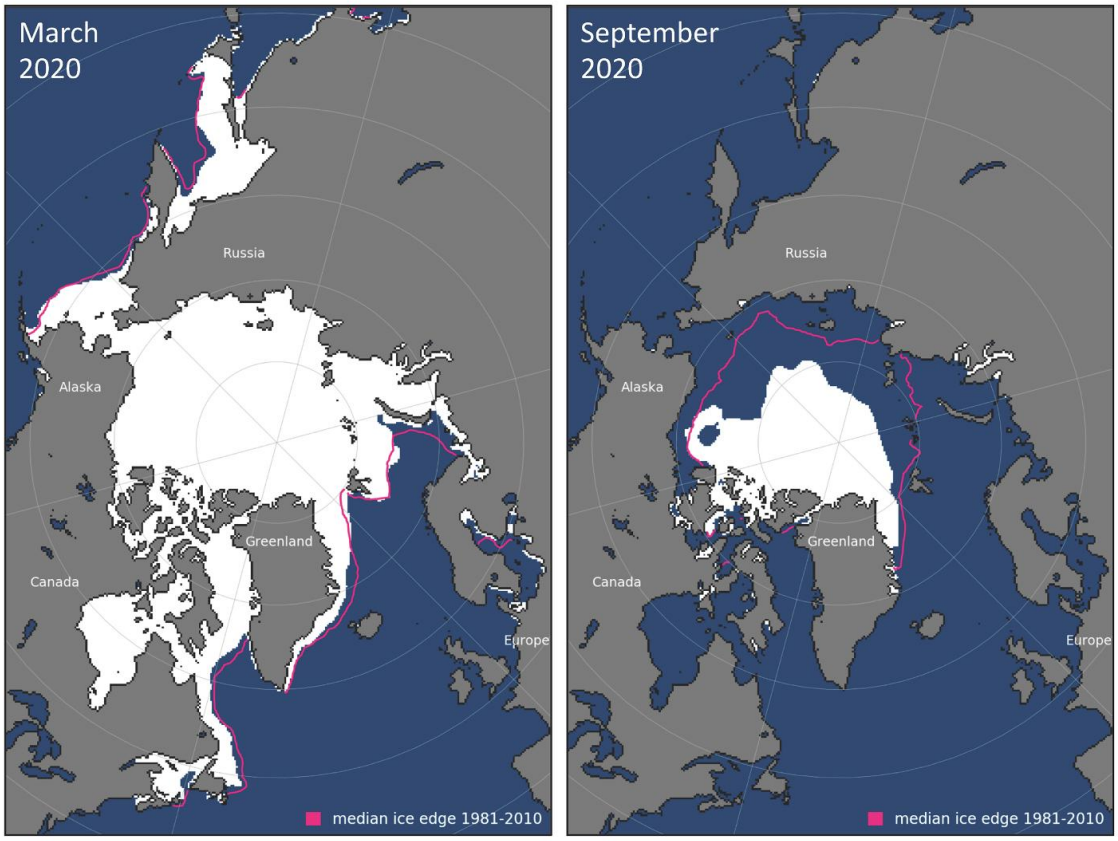

Figure 14-11: Maps of the Arctic sea ice for March (maximum) and September (minimum). The magenta line is the median ice edge from 1981-2010. Both months have decreased in size with September being much smaller.

According to the National Snow and Ice Data Center's (NSIDC) Sea Ice Index, from the start of the satellite record in November 1978 through March 2021, Arctic sea ice showed a declining trend in all months. The smallest declines were in February through May, and the largest declines in August through October. The biggest decline occurred in September. The graph in Figure 14-12 shows the decline in sea ice from 1978 through 2020, with the September decline being the greatest.

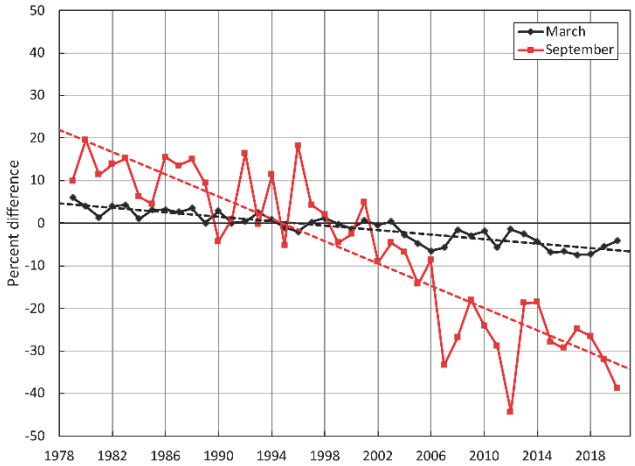

Figure 14-12: Graph with the percent difference in Arctic sea ice decline for March and September from 1978 to 2020. Both months show a decline with the largest changes seen in September.

14.1.5 – Glacier Changes

Glaciers that exist today are remnants of the last ice age, and are continuing to melt in the current interglacial period. Thick ice sheets from the Last Glacial Maximum withdrew to higher latitudes about 10,000 years ago. Continent-scale ice sheets still cover Greenland and Antarctica, along with smaller ice caps and glaciers in the high latitudes and mountains. Figure 14-13 map shows the locations of the world's glaciers.

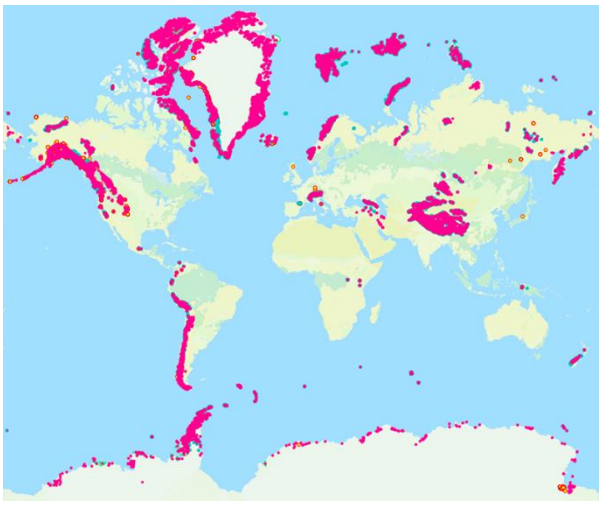

Figure 14-13: A map depicting the world's glaciers.

Glaciers gain mass through snowfall and lose mass through melting and sublimation. Glaciers that terminate in a lake or the ocean also lose mass through iceberg calving. Calving is when the ice breaks off and falls into the water. Negative mass balances (shrinking) were recorded for 16 of the 25 monitored glaciers in the Arctic. Nine registered positive balances (growing) in Arctic Canada and Iceland. Hence, not all glaciers in the Arctic are melting, although most are.

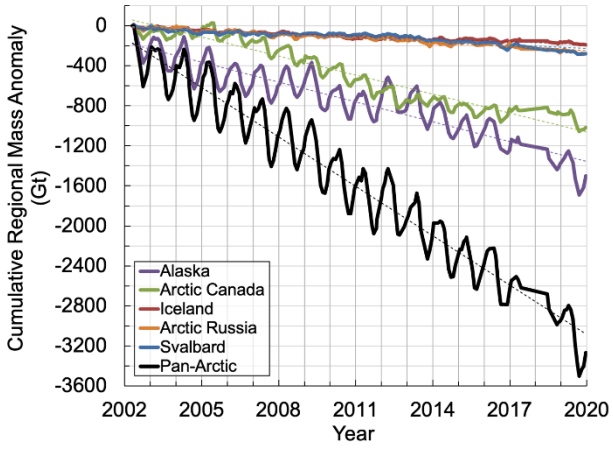

Figure 14-14: Graphs showing the change in Arctic glacier mass from 2002-2020.

The regional total glacier mass balance in the Arctic can be estimated from time series of cumulative regional mass anomalies. For the Arctic glaciers and ice caps as a whole, the overall mass balance was strongly negative during the period 2002 to 2019. This record is dominated by ice mass loss from Arctic Canada and Alaska as is shown by the graphs in Figure 14-14.

Pan-Arctic is the Arctic as a whole or a sum of all the graphs. As shown, the Pan-Arctic has an overall mass loss. Alaska and Canada have the most mass loss in their glaciers. Svalbard is the Norwegian archipelago (group of islands) between mainland Norway and the North Pole, which shows little mass loss along with Iceland and Arctic Russia.

Since glaciers have been melting for 20,000 years, how much of this melt can be attributed to humans? The present day glacial melt is a mix of natural climate variability and anthropogenic forcing. A study in 2014 indicated that about 25% (with an error range of ±35%) of the global mass loss from 1851 to 2010 is attributable to anthropogenic causes. This large error range gives this result a very low confidence of melting being attributed to anthropogenic causes. The anthropogenic signal is detected with a higher confidence for the period 1991 to 2010 with an increase to 69% attributed to human causes. This later time period has an error range of ±24%, which causes the attribution to be from 45% to 93%.

14.1.6 – Ice Sheet Changes

An ice sheet is a mass of glacial land ice extending over more than 50,000 square kilometers (20,000 square miles). The two ice sheets on Earth today cover most of Greenland and Antarctica, as illustrated in Figure 14-15. During the Last Glacial Maximum, ice sheets also covered much of North America and Scandinavia.

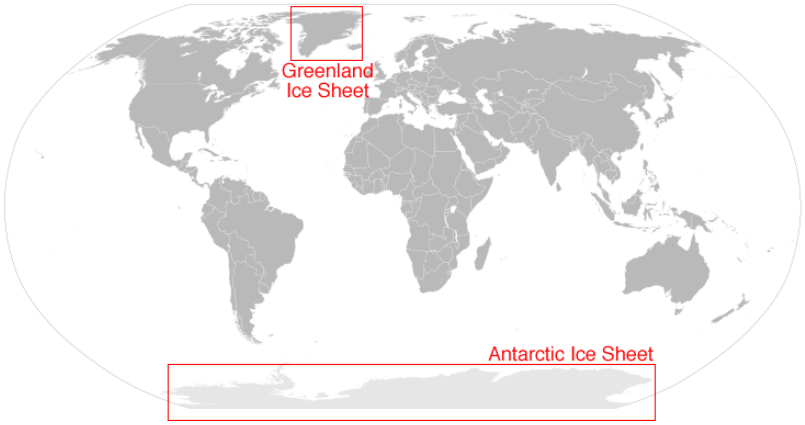

Figure 14-15: Location of the two ice sheets on Earth today.

Together, the Antarctic and Greenland ice sheets contain more than 99 percent of the freshwater ice on Earth. The Antarctic Ice Sheet extends almost 5.4 million square miles, roughly the area of the contiguous United States and Mexico combined. The Antarctic Ice Sheet contains 7.2 million cubic miles of ice. The Greenland Ice Sheet extends about 656,000 square miles, covering most of Greenland, which is three times the size of Texas.

Ice sheets contain enormous quantities of frozen water. If the Greenland Ice Sheet melted, scientists estimate that sea level would rise about 6 meters (20 feet). If the entire Antarctic Ice Sheet melted, sea level would rise by about 60 meters (200 feet).

The mass of ice in the Greenland Ice Sheet has begun to decline. From 1979 to 2006, summer melt on the ice sheet increased by 30 percent, reaching a new record in 2007. At higher elevations, an increase in winter snow accumulation has partially offset the melt. However, the decline continues to outpace accumulation because warmer temperatures have led to increased melt and faster glacier movement to the edges of Greenland.

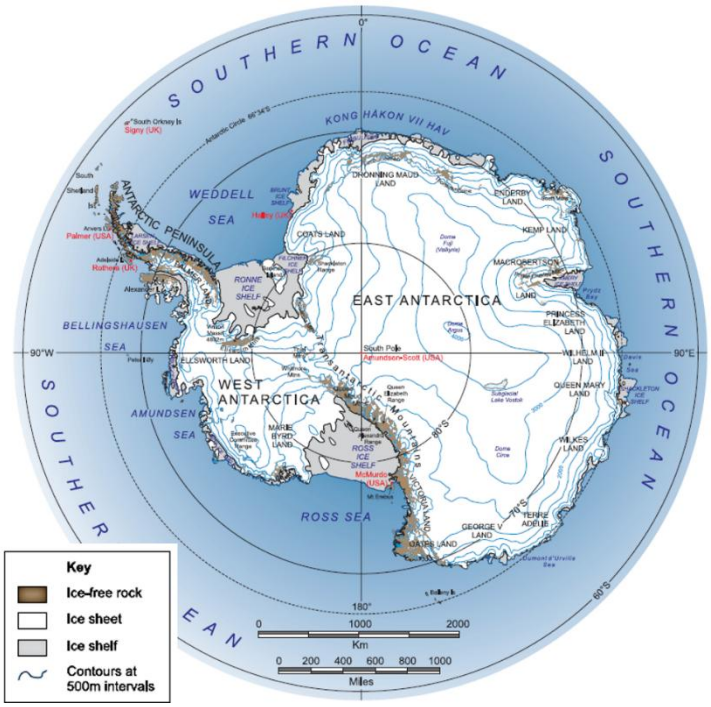

Figure 14-16: Map of Antarctica. Two ice sheets are present in East and West Antarctica. The Antarctic Peninsula has observed the highest warming, since it is surrounded by water.

Most of Antarctica has not experienced warming. However, the Antarctic Peninsula, which juts out into warmer waters north of Antarctica, has warmed 2.5 degrees Celsius (4.5 degrees Fahrenheit) since 1950. See Figure 14-16. A large area of the West Antarctic Ice Sheet is also losing mass, probably because of warmer water deep in the ocean near the Antarctica coast. In East Antarctica, no clear trend has emerged and some

stations appear to be cooling slightly. Overall, scientists believe that Antarctica is starting to lose ice, but the process is not quick and certainly not as widespread as in Greenland.

The East Antarctica ice sheet is roughly 13,000 feet high at its summit. The West Antarctic and the Antarctic Peninsula Ice Sheets are about 8,200 feet high. Most of the ice on Antarctica is in the eastern portion. Overall Antarctica contains about 90% of the world's ice.

14.1.7 – Snow Cover Changes

"Snow cover" refers to the amount of land covered by snow at any given time. Naturally, it is influenced by the amount of precipitation that falls as snow. Air temperature also plays a role because it determines whether precipitation falls as snow or rain, and it affects the rate at which snow on the ground melts. As temperature and precipitation patterns change, so can the overall area covered by snow.

Snow cover is not just something that is affected by climate change; it also exerts an influence on climate. Because snow is white, it absorbs only a small portion of the sunlight that hits it (10 to 20 percent in the case of fresh snow) and reflects the rest back to space. In contrast, darker surfaces such as bare ground and open water absorb the majority of the energy they receive and heat up more quickly. In this way, the overall amount of snow cover affects patterns of heating and cooling over the Earth's surface. More snow means more energy reflects back to space, resulting in cooling, while less snow cover means more energy is absorbed at the Earth's surface, resulting in warming.

On a more local scale, snow cover is important for many plants and animals. For example, some plants and animals rely on a protective blanket of snow to insulate them from sub-freezing winter temperatures. Humans and ecosystems also rely on snowmelt to replenish streams and groundwater. Snow cover keeps the soil moist, so if the snow melts away earlier in the spring, the soil may dry out sooner, which can stress plants and increase the risk of wildfire.

Figure 14-17 shows the annual average area covered by snow, and is based on an analysis of weekly maps. The area is measured in square miles. These data only include North America.

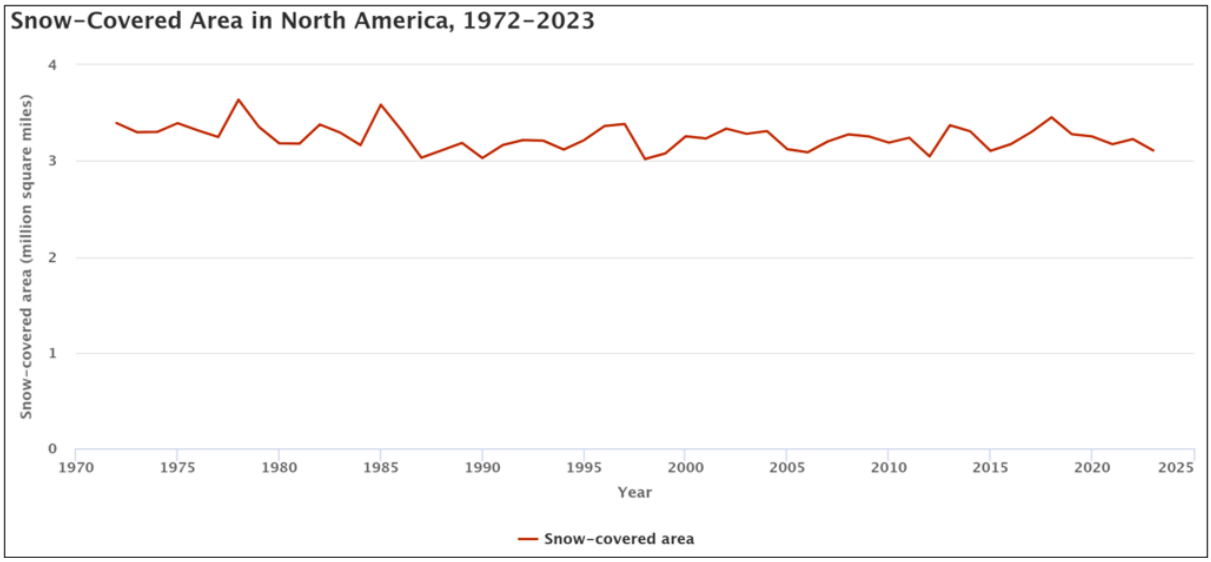

Figure 14-17: The area of snow cover in North America from 1972-2023. A small downward trend of about 3% from the 1972-1981 average is observed in this graph.

Between 1972 and 2023, the average extent of North American snow cover decreased at a rate of about 2083 square miles per year.

Figure 4-18 shows the average area covered by snow during spring (March–May), summer (June–August), fall (September–November), and winter (December–February). Again, the area is measured in square miles, and is just for North America. Decreases in snow cover have largely occurred in spring and summer, whereas winter snow cover has remained fairly steady over the time period studied, and snow cover in the fall months has increased.

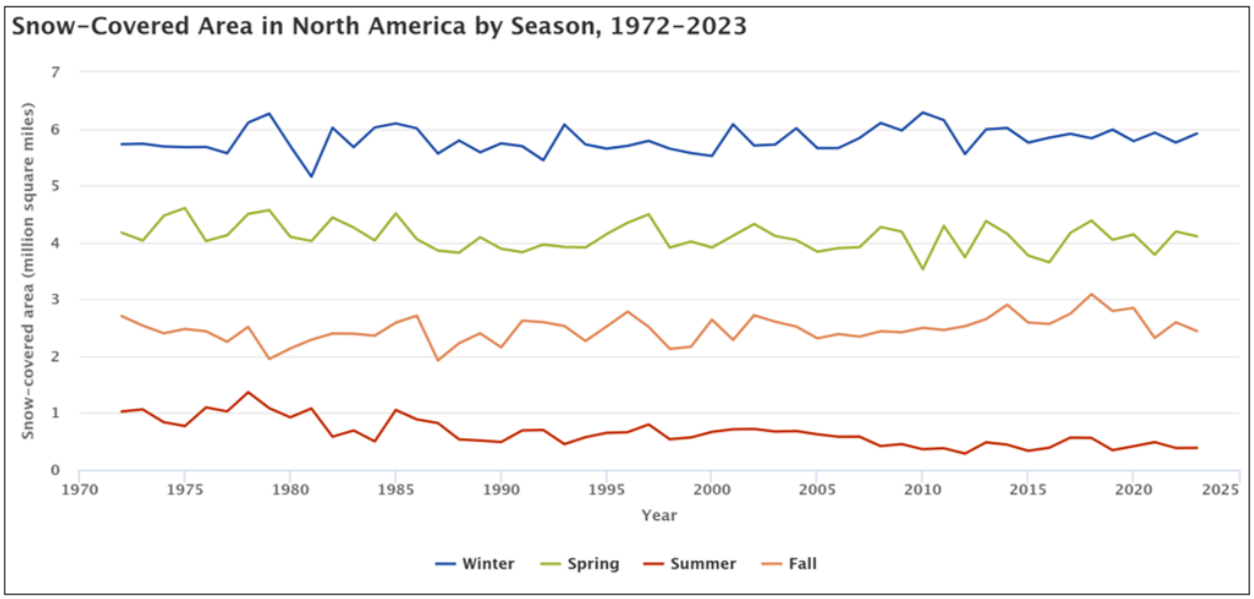

Figure 14-18: Average area covered by snow in North America for each season. Winter snow cover has remained constant. Spring and summer coverage has decreased, and fall coverage has increased.

Figure 14-19 shows the timing of each year's snow cover season in the contiguous 48 states and Alaska, based on an average of all parts of the country that receive snow every year. The shaded band spans from the first date of snow cover until the last date of snow cover. Between 1972 and 2013, the U.S. snow cover season became shorter by nearly two weeks, on average. By far the largest change has taken place in the spring, with the last day of snow shifting earlier by 19 days since 1972. In contrast, the first date of snow cover in the fall has remained relatively unchanged.

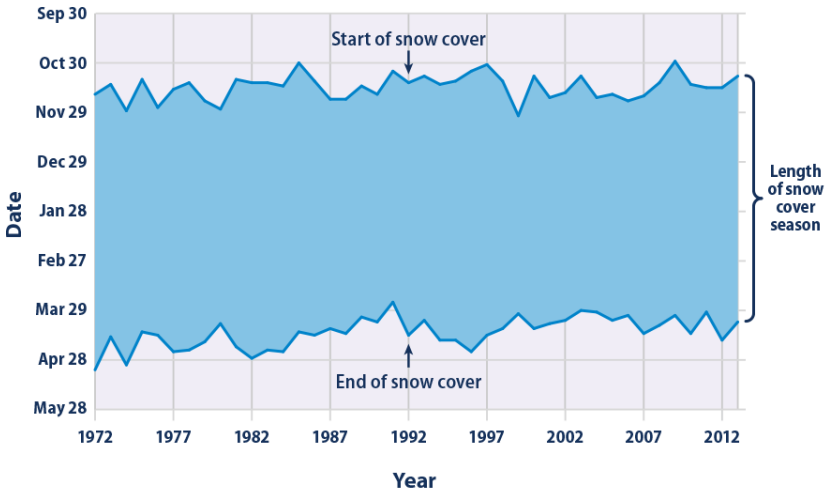

Figure 14-19: Length of the snow cover season for the U.S. from 1972-2013. The start of the season in the fall remains unchanged. The end of the season in the spring is shifting earlier.

Recognizable patterns of climate variability such as the El Niño-Southern Oscillation and the Arctic Oscillation can affect the amount of snow that

falls each year. In different phases of these back-and-forth patterns, some regions receive abnormally large or small amounts of snow. On average, however, despite variations in mid-winter snowfall, Northern Hemisphere snow is melting earlier in the year.

14.1.8 – Sea-level changes

As the temperature of the Earth changes, so does the sea level. Temperature and sea level are linked for two main reasons:

1. Changes in the volume of water and ice on land can increase or decrease the volume of water in the ocean.
2. As water warms, it expands slightly—an effect that is cumulative over the entire depth of the oceans.

Changing sea levels can affect human activities in coastal areas. Rising sea level inundates low-lying wetlands and dry land, erodes shorelines, contributes to coastal flooding, and increases the flow of salt water into estuaries and nearby groundwater aquifers. Higher sea levels also make coastal infrastructure more vulnerable to damage from storms.

The sea level changes that affect coastal systems involve more than just expanding oceans. The Earth's continents can also rise and fall relative to the oceans. Land can rise through processes such as sediment accumulation (the process that built the Mississippi River delta) and geological uplift (for example, as glaciers melt and the land below is no longer weighed down by heavy ice). In other areas, land can sink because of erosion, sediment compaction, natural subsidence (sinking due to geologic changes), groundwater withdrawal, or engineering projects that prevent rivers from naturally depositing sediments along their banks. Changes in ocean currents such as the Gulf Stream can also affect sea levels by pushing more water against some coastlines and pulling it away from others, raising or lowering sea levels accordingly.

Scientists account for these types of changes by measuring sea level change in two different ways. Relative sea level change refers to how the height of the ocean rises or falls relative to the land at a particular location. In contrast, absolute sea level change refers to the height of the ocean surface above the center of the earth, without regard to whether nearby land is rising or falling.

Figure 14-20 depicts the cumulative changes in absolute sea level for the world's oceans since 1880. The graphs in this figure are based on a combination of long-term tide gauge measurements and recent satellite measurements. Satellite data are based solely on measured sea level, while the long-term tide gauge data include a small correction factor because the size and shape of the oceans are changing slowly over time. The shaded band shows the likely range of values, based on the number of measurements collected and the precision of the methods used.

The global mean water level in the ocean rose by 0.14 inches (3.6 millimeters) per year from 2006–2015, which was 2.5 times the average rate of 0.06 inches (1.4 millimeters) per year throughout most of the twentieth century. By the end of the century, global mean sea level is likely to rise at least one foot (0.3 meters) above 2000 levels

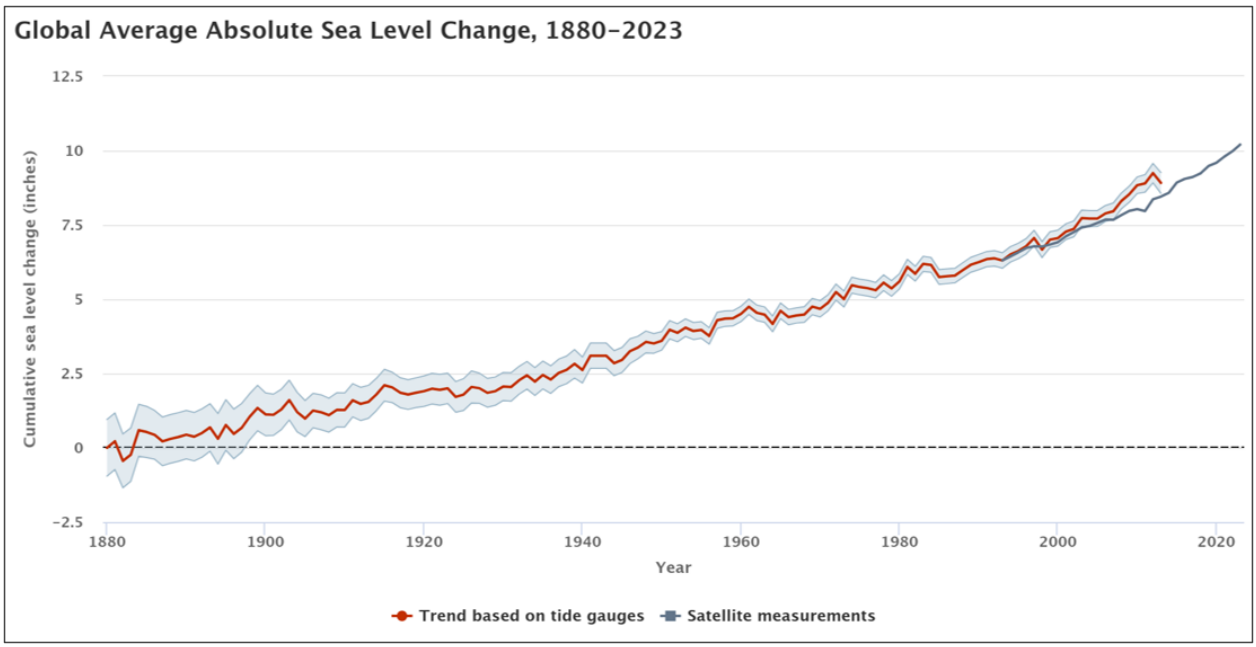

Figure 14-20: Global average absolute sea level change for 1880-2023. The red line is based on tide gauges. The blue line in more recent times is based on satellite measurements. The shaded area represents the precision of the measurements. Overall sea levels are rising.

In some ocean basins, sea level has risen as much as 6-8 inches (15-20 centimeters) since the start of the satellite record. Regional differences exist because of natural variability in the strength of winds and ocean currents. Figure 14-21 indicates mean sea levels have risen across most of the oceans.

Past and future sea level rises at specific locations on land may be more or less than the global average due to local factors previously mentioned. In the United States, the fastest rates of sea level rise are occurring in the mid-Atlantic and the Gulf of Mexico west of the Mississippi River. Only in Alaska and a few places in the Pacific Northwest are sea levels falling as is shown on the map in Figure 14-22.

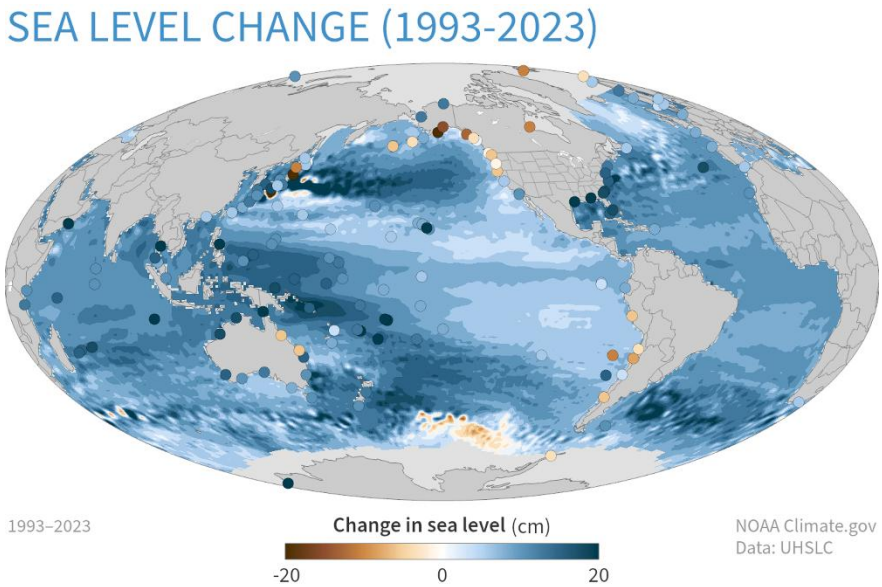

Figure 14-21: Sea level changes across all oceans for 1993-2023. The dots represent rates of local sea level changes, which may be related to ground settling or rebound of land masses due to glacier melt.

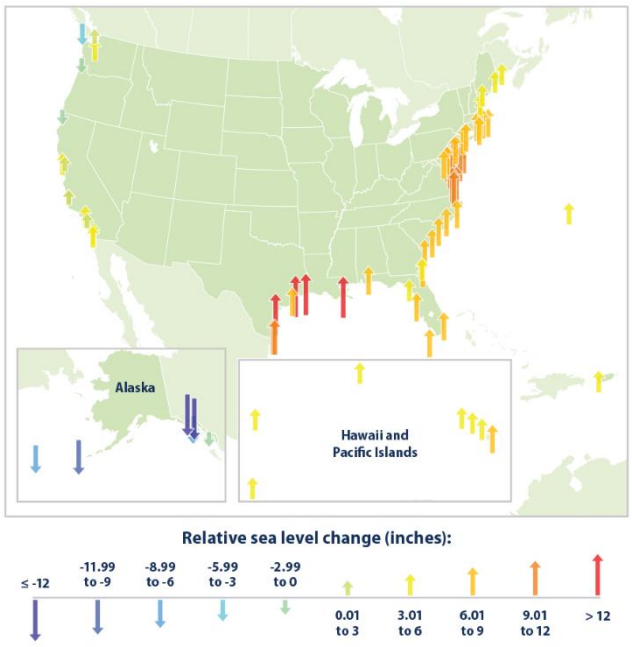

In the United States, almost 40 percent of the population lives near a coastal area, where sea level plays a role in flooding, shoreline erosion, and hazards from storms. Storm surges from hurricanes are expected to push farther inland as sea levels rise. Globally, 8 of the world's 10 largest cities are near the coast, according to the U.N. Atlas of the Oceans.

Figure 14-22: Relative sea level change on the U.S. coasts from 1960-2023.

14.2 – Global Circulation Models (GCMs)

Models help us work through complicated problems and understand complex systems. They also allow us to test theories and solutions. From models as simple as toy cars and kitchens to complex representations, such as flight simulators and virtual globes, we use models throughout our lives to explore and understand how things work.

Climate models are based on well-documented physical processes to simulate the transfer of energy and materials through the climate system. Climate models, also known as general circulation models or GCMs, use mathematical equations to characterize how energy and matter interact in different parts of the ocean, atmosphere, and land. Building and running a climate model is a complex process of identifying and quantifying Earth system processes, representing them with mathematical equations, setting variables to represent initial conditions and subsequent changes in climate forcing, and repeatedly solving the equations using powerful supercomputers.

Climate models separate Earth's surface into a three-dimensional grid of cells. The results of processes modeled in each cell are passed to neighboring cells to model the exchange of matter and energy over time. Grid cell size defines the resolution of the model: the smaller the size of the grid cells, the higher the level of detail in the model. More detailed models have more grid cells, so they need more computing power.

Figure 14-23 shows the concepts used in climate models. Each of the thousands of 3-dimensional grid cells can be represented by mathematical equations that describe the materials in it and the way energy moves through it. The advanced equations are based on the fundamental laws of physics, fluid motion, and chemistry.

To "run" a model, scientists specify the climate forcing (for instance, setting variables to represent the amount of greenhouse gases in the atmosphere) and have powerful computers solve the equations in each cell. Results from each grid cell are passed to neighboring cells, and the equations are solved again. Repeating the process through many time steps represents the passage of time.

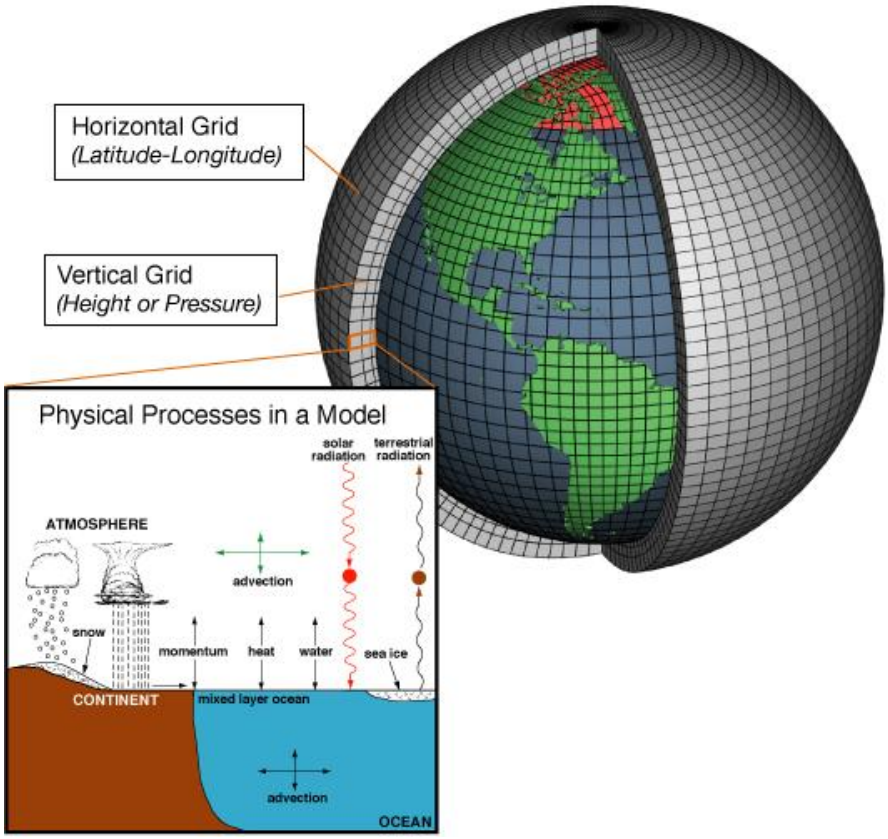

Figure 14-23: Illustration of a General Circulation Model (GCM) containing a 3-D grid of cells. Each cell contains the physical process inherent in the model.

Once a climate model is set up, it can be tested via a process known as "hind-casting." This process runs the model from the present time backwards into the past. The model results are then compared with observed climate and weather conditions to see how well they match. This testing allows scientists to check the accuracy of the models and, if needed, revise their equations. Science teams around the world test and compare their model outputs to observations and results from other models.

Once a climate model can perform well in hind-casting tests, its results for simulating future climate are also assumed to be valid. To project climate into the future, the climate forcing is set to change according to a possible future scenario. Scenarios contain possible stories about how quickly human population will grow, how land will be used, how economies will evolve, and the atmospheric conditions (and therefore, climate forcing) that would result for each storyline.

In 2000, the Intergovernmental Panel on Climate Change (IPCC) issued its Special Report on Emissions Scenarios (SRES), describing four scenario families to describe a range of possible future conditions. Referred to by letter-number combinations such as A1, A2, B1, and B2, each scenario was based on a complex relationship between the socioeconomic forces driving greenhouse gas and aerosol emissions, and the levels to which those emissions would climb during the 21st century. The SRES scenarios have been in use since then, so many climate model results describe their projections using these letter-number combinations.

In 2013, climate scientists agreed upon a new set of scenarios that focused on the level of greenhouse gases in the atmosphere in 2100. Collectively, these scenarios are known as Representative Concentration Pathways or RCPs. Each RCP indicates the amount of climate forcing, expressed in Watts per square meter, that would result from greenhouse gases in the

atmosphere in 2100. The rate and trajectory of the forcing is the pathway. Like their predecessors, these values are used in setting up climate models and are described using the RCP terminology. Figure 14-24 depicts the equivalent atmospheric CO_2 concentrations for both SRES and RCPs.

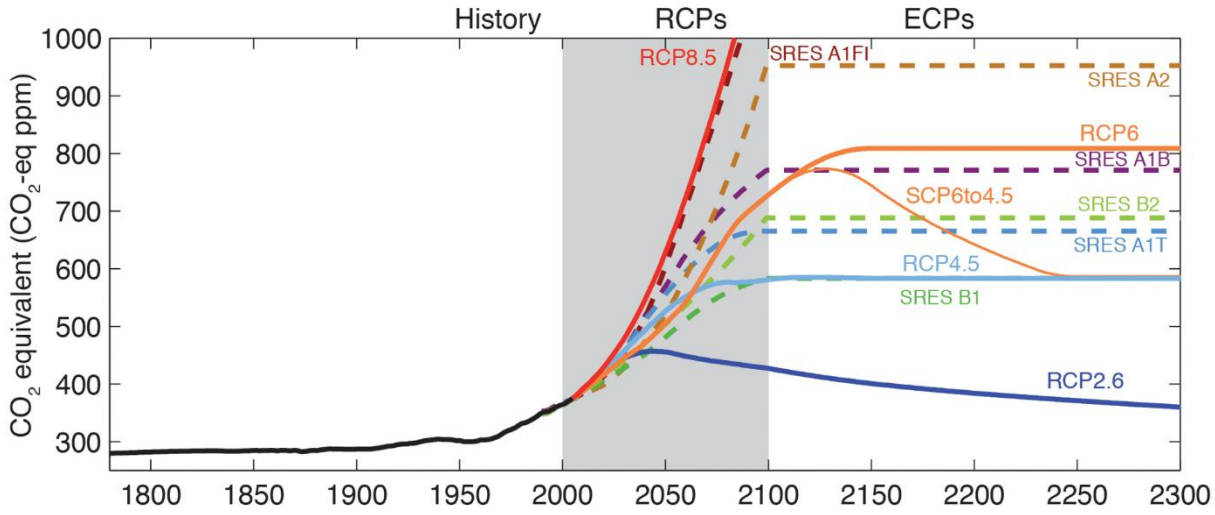

Figure 14-24: Graphs showing the equivalent CO2 concentrations associated with both the SRES and RCP scenarios.

A third set of scenarios has been developed based on how socioeconomic factors may change over the next century. These scenarios are called Shared Socioeconomic Pathways (SSP). Each pathway is an internally consistent, plausible and integrated description of a socio-economic future. However, these socio-economic futures do not account for the effects of climate change, and no new climate policies are assumed. Broadly, the five SSPs represent 'sustainability' (SSP1), a 'middle of the road' path (SSP2), 'regional rivalry' (SSP3), 'inequality' (SSP4), and 'fossil fuel intensive' development (SSP5). The graphs in Figure 14-25 show the concentrations of greenhouse gases and their relationship to SSP1-5. Many scientists believe the RCP8.5 and SSP5-8.5 high carbon dioxide concentrations are not possible, even if humanity tried to exceed the maximum projections given.

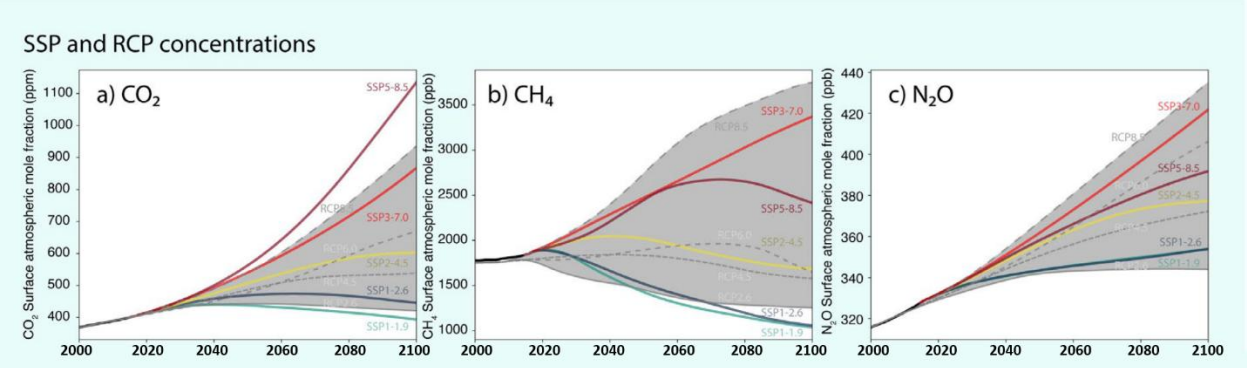

Figure 14-25: Graphs of greenhouse gas concentrations associated with the RCP (gray lines and area) and SSP (colored lines) scenarios.

Unlike weather forecasts, which describe a detailed picture of the expected daily sequence of conditions starting from the present, climate models are probabilistic, indicating areas with higher chances of warmer or cooler and wetter or drier than usual. Climate models are based on

global patterns in the ocean and atmosphere, and indicate the weather that would have occurred under similar patterns in the past.

The terms “forecast”, “prediction”, and “projection” are all similar but different. “Forecast” and “prediction” refer to future conditions with a high probability of verification, like a weather forecast. A climate projection has a lower probability of verifying, and relies on assumptions about future radiative forcing which are unknown, such as anthropogenic emissions or concentrations of greenhouse gases and aerosols. For this reason, they are called climate projections, not forecasts nor predictions. This distinction in terminology is important, and implies the reliability of these different model outputs.

14.2.1 – Coupled Model Intercomparison Project (CMIP)

Around the world, different teams of scientists have built and run models to project future climate conditions under various scenarios into the next century. To coordinate these efforts, the Coupled Model Intercomparison Project (CMIP) was created to assist in the standardization of the future scenarios examined and the different experiments conducted.

The CMIP is a standard experimental framework for studying the output of coupled atmosphere-ocean general circulation models (GCMs). A coupled atmosphere-ocean model includes the interactions between the ocean and atmosphere, which is a more complex GCM than others. This facilitates assessment of the strengths and weaknesses of climate models, which can enhance and focus the development of future models. For example, if the models indicate a wide range of values, then scientists may be able to determine the cause(s) of this uncertainty.

The objective of the Coupled Model Intercomparison Project (CMIP) is to better understand past, present and future climate changes arising from natural, unforced variability or in response to changes in radiative forcing in a multi-model context. This understanding includes assessments of model performance during the historical period and quantifications of the causes of the spread in future projections. Idealized experiments are also used to increase understanding of the model responses. In addition to these long-time scale responses, experiments are performed to investigate the predictability of the climate system on various time and space scales as well as making predictions from observed climate states. Another important goal of CMIP is to make the multi-model output publicly available in a standardized format.

From the inception of CMIP, there has been a focused effort to make the model intercomparison data available to other scientists besides those who run the models. This video provides an overview of CMIP, which coordinates the efforts of numerous climate modeling groups.

Video

14.2.2 – Climate Model Applications

Some of the main applications of climate models are paleoclimate studies, detection and attribution studies, and future projections. Future climate projections will be examined in detail in Section 14.3.

Paleoclimate model studies are not only useful for a better understanding of past climate changes and their impacts, but they can also be used to evaluate the models. For example, model simulations of the Last Glacial Maximum (LGM) are broadly consistent with temperature reconstructions that show global cooling of 4-5°C, polar amplification and larger changes over land than over the ocean. The models reproduce these basic features of the reconstructions, which indicates that they have skill simulating climates different from the present. On the other hand, there are also differences between model results and observations. For example, deep ocean circulation model results and observations do not appear to agree well, which indicates that the model's skills in those aspects are questionable.

Detection and attribution studies attempt to determine which observed climate changes are unusual (detection) and what are its causes (attribution). Climate models driven with only natural forcing show variations from one year to the next due to internal climate variability (for example, ENSO) and short-term cooling in response to large volcanic eruptions. Human-caused forcings include greenhouse gas emissions or atmospheric particulate pollution. Any of these forcings, natural or human caused, could affect internal variability as well as causing a change in the average climate.

Attribution studies attempt to determine the causes of a detected change in observed climate. Over the past century we know that global average temperature has increased, so if the observed change is forced, then the principal forcing must be one that causes warming and not cooling. Formal climate change attribution studies are carried out using controlled experiments with climate models. The model-simulated responses to specific climate forcings are often called the fingerprints of those forcings. A climate model must reliably simulate the fingerprint patterns associated with individual forcings, as well as the patterns of unforced internal variability to yield a meaningful climate change attribution assessment. No model can perfectly reproduce all features of climate, but many detailed studies indicate that simulations using current models are indeed sufficiently reliable to carry out attribution assessments.

Figure 14-26 illustrates part of a fingerprint assessment of global temperature change at the surface during the late 20th century. The observed change in the latter half of the 20th century, shown by the black time series in the left panels, is larger than expected from just internal variability. Simulations driven only by natural forcings (yellow and blue lines in the upper left panel) fail to reproduce late 20th century global warming at the surface with a spatial pattern of change (upper right) completely different from the observed pattern of change (middle right). Simulations including both natural and human-caused forcings provide a much better representation of the time rate of change (lower left) and spatial pattern (lower right) of observed surface temperature change.

Both panels on the left (Figure 14-26) show that computer models reproduce the naturally forced surface cooling observed for a year or two after major volcanic eruptions, such as occurred in 1982 and 1991. Natural forcing simulations capture the short-lived temperature changes following eruptions, but only the natural + human caused forcing simulations simulate the longer warming trend.

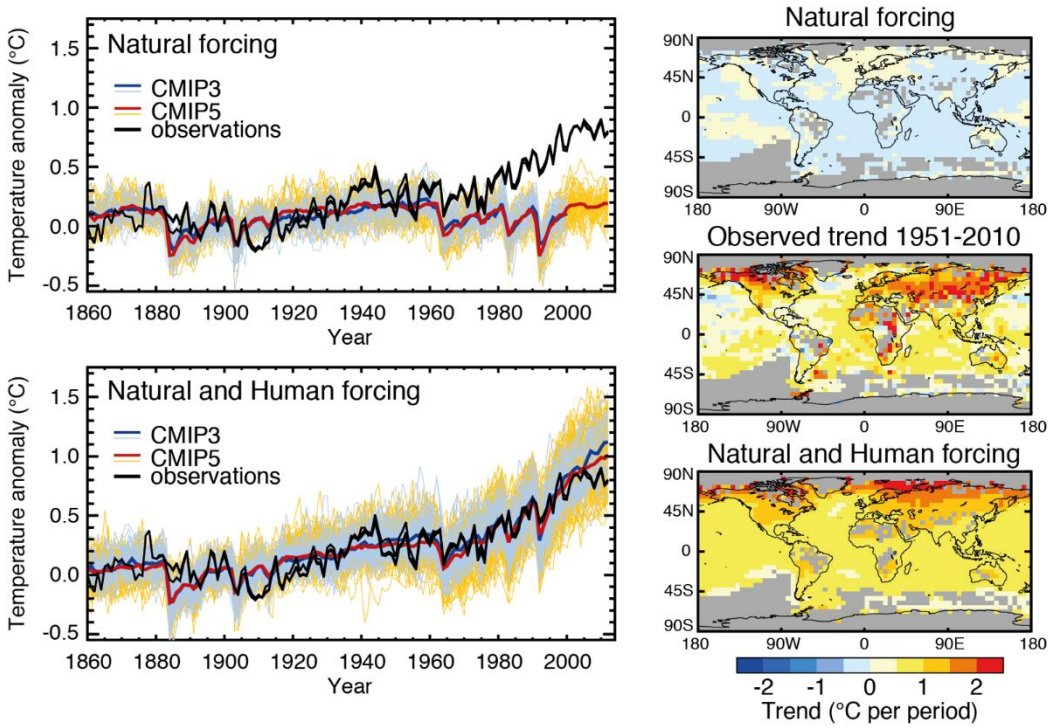

Figure 14-26: Illustration separating the natural and human forcings associated with global temperature. The black line on the left-side graphs is the observed global temperature. The top graph is the temperature associated with natural forcings, and the bottom includes human forcings which better matches the observed temperature changes. The right-side maps depict a similar result.

Models driven with both natural and anthropogenic forcings reproduce both the observed global mean temperature changes, and its spatial distribution such as larger warming at high northern latitudes (polar amplification) and over land (land-sea contrast). These results represent evidence that human activities are the main reason for the observed warming during the past 50-60 years.

14.3 – Climate Projections

The Intergovernmental Panel on Climate Change (IPCC) is the United Nations body for assessing the science related to climate change. The IPCC was created to provide policymakers with regular scientific assessments on climate change, its implications and potential future risks, as well as possible adaptation and mitigation options. This Panel was established in 1988, and the first reports were written in 1990. Climate scientists from all over the world participate in the IPCC. Their Sixth Assessment Report, referred to as AR6, consists of eight reports assembled from 2015 through 2023.

The IPCC reports are a key input into international negotiations associated with climate change. This short video provides background information on the Sixth Assessment Report.

The climate projections used in this section are from the Physical Science Report assembled by Working Group 1 (WG1) of the Sixth Assessment. These projections are from the Coupled Model Intercomparison Project 6 (CMIP6) which consists of about 40 different climate models. Thus, the climate projections represent multiple climate modeling groups from many countries.

Since many unknowns are inherent in climate modeling, such as carbon dioxide concentrations, these projections use the Shared Socioeconomic Pathways (SSP) scenarios for a range of possible solutions. While SSP1 through SSP5 are technical in nature and include many parameters. A simple method of looking at these projections is SSP1 has lower future levels of CO_2 and SSP5 has much higher levels. The middle scenarios SSP2 and SSP3 have the best likelihood of representing what will actually occur in the future.

14.3.1 – Temperature Projections

As expected, climate projections for future temperatures all show warmer conditions. Figure 14-27 graphs the projected mean global temperatures for the various Shared Socioeconomic Pathways (SSPs). SSP1-1.9 has a reduction in greenhouse gases (GHGs) long-term, and exhibits a slight downward temperature trend by 2100. SSP5-8.5 essentially has no reductions in GHGs and unrestricted fossil fuel usage. The lighter shaded colors are the possible range of values (errors) associated with the observations and scenarios. The information in Figure 14-27 can be displayed in a tabular format as shown below.

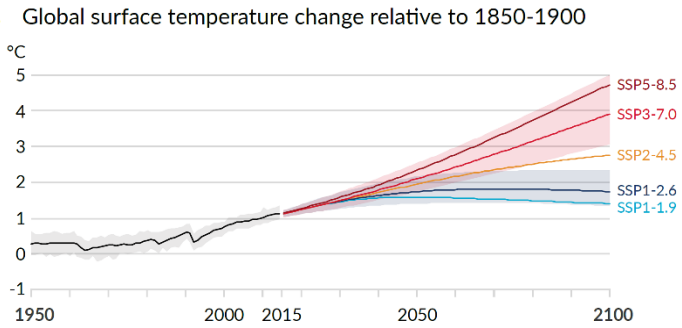

Figure 14-27: Observed global temperature changes (black line) and projections (colored lines) from 1950-2100. The shaded areas are the possible range of values.

	Near term, 2021–2040		Mid-term, 2041–2060		Long term, 2081–2100	
Scenario	Best estimate (°C)	*Very likely* range (°C)	Best estimate (°C)	*Very likely* range (°C)	Best estimate (°C)	*Very likely* range (°C)
SSP1-1.9	1.5	1.2 to 1.7	1.6	1.2 to 2.0	1.4	1.0 to 1.8
SSP1-2.6	1.5	1.2 to 1.8	1.7	1.3 to 2.2	1.8	1.3 to 2.4
SSP2-4.5	1.5	1.2 to 1.8	2.0	1.6 to 2.5	2.7	2.1 to 3.5
SSP3-7.0	1.5	1.2 to 1.8	2.1	1.7 to 2.6	3.6	2.8 to 4.6
SSP5-8.5	1.6	1.3 to 1.9	2.4	1.9 to 3.0	4.4	3.3 to 5.7

However, this warming is not uniform across the whole Earth. The Northern Hemisphere is projected to warm more than the Southern Hemisphere because of its larger land masses. The land warms faster than water. Additionally, higher latitudes are projected to warm more than the tropics. The Arctic is warming the fastest. The maps in Figure 14-28 represent the spatial patterns of these temperature projections.

In Figure 14-28, the number of climate models used to create each map is in the top right. The “robust significant change” or no shading indicates at least 66% of the models show a change greater than the internal variability threshold and at least 80% of the models agree on the sign of the change. In other words, most of the climate models agree with each other. The diagonal lines and crossed line areas represent less or no agreement among the models. This notation (robust, diagonal lines, and crossed lines) is used in all the climate projection maps in this book.

Examining the projected temperature changes in Figure 14-29 for each season, we see that the winter season (DJF) at higher latitudes is warmer than the summer season (JJA). Again, the projected warming is higher for land masses than the oceans in both seasons.

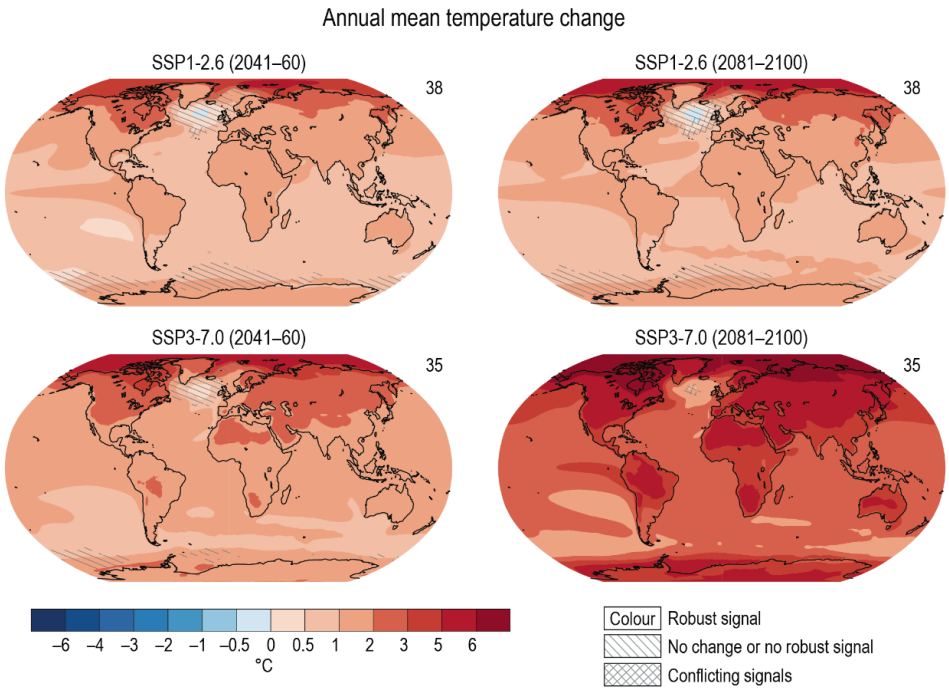

Figure 14-28: Annual mean temperature changes for SSP1-2.6 (top) and SSP3-7.0 (bottom). The time periods are 2041-2160 (right) and 2081-2100 (left) . The Northern Hemisphere is warming the fastest.

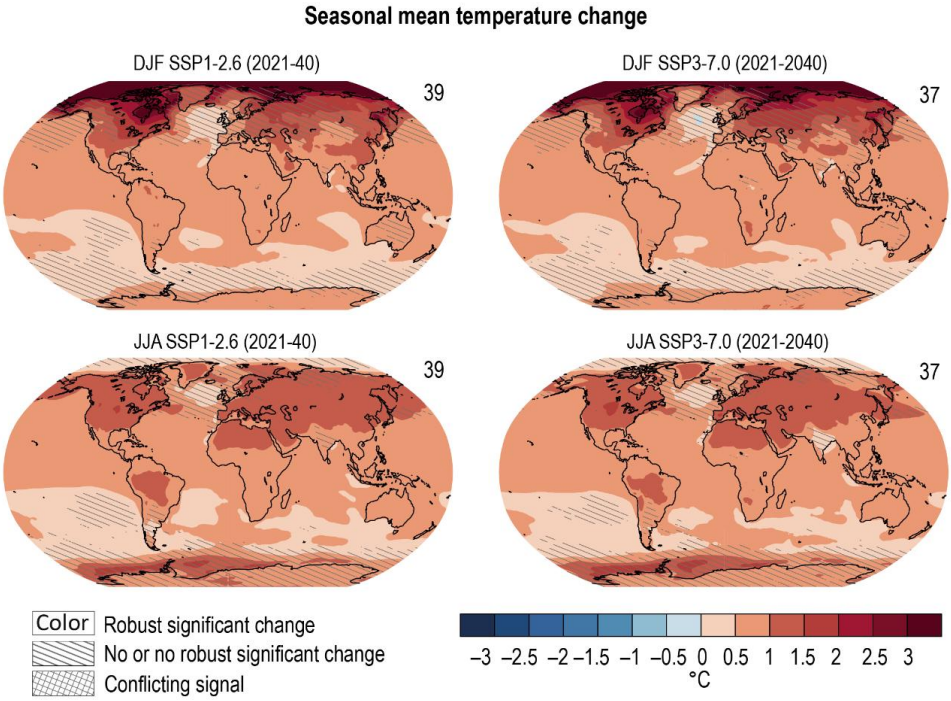

Figure 14-29: Global seasonal mean temperature changes for SSP1-2.6 and SSP3-7.0 from 2021-2040. The winter season (DJF) is warming faster than the summer (JJA).

14.3.2 – Precipitation Projections

Due to a warmer atmosphere and ocean, more evaporation will occur and the atmosphere will hold more moisture. Following this logic, a moister atmosphere should allow for more precipitation. Figure 14-30 contains two sets of maps with the projected seasonal mean precipitation for winter (DJF) and summer (JJA). The top set is near-term for 2021-2040 and the bottom set is long-term 2081-2100.

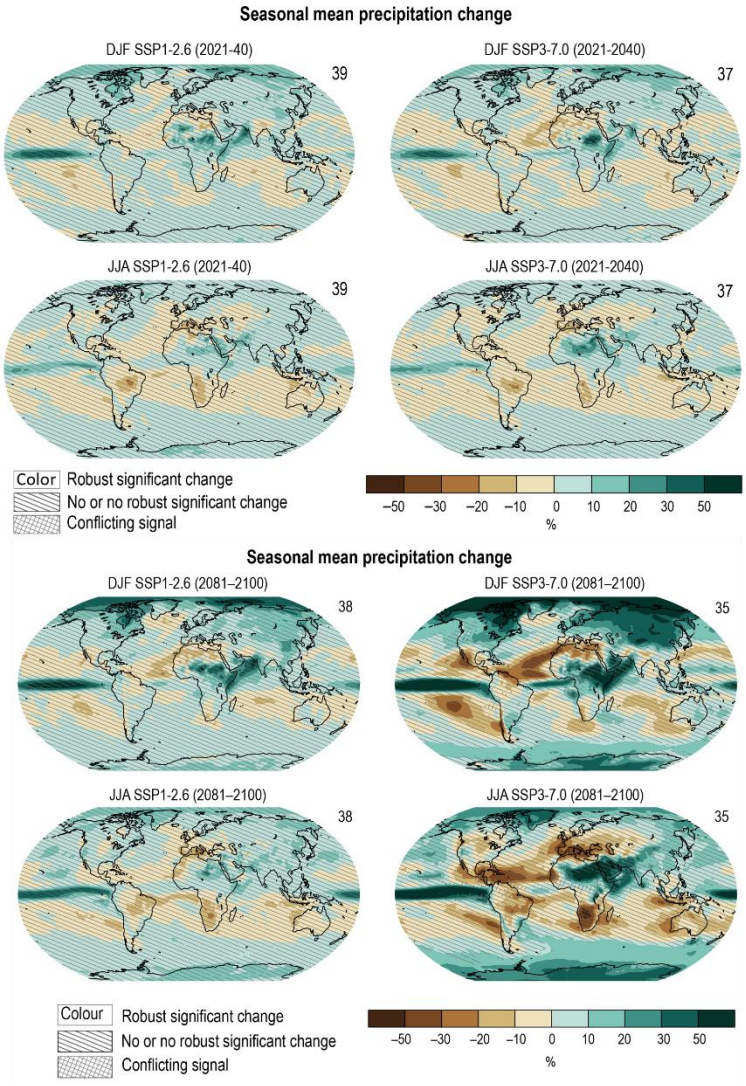

Figure 14-30: : Seasonal precipitation projections for 2021-2040 (top) and 2081-2100 (bottom). The seasons are winter (DJF) and summer (JJA). The left side maps are SSP1-2.6 and the right side are SSP3-7.0. The diagonal lines in all the maps indicate a lower confidence in these projections when compared to the temperature maps (previous figures).

Notice in Figure 14-30 that the green/teal colors predominate and overall coincides with precipitation increasing. The tropics and higher latitudes have a projected increase in precipitation. The subtropics which are already dry have a decrease in precipitation. This wet/dry pattern has been described as the wet areas get wetter and the dry areas get drier.

Notice also that diagonal lines cover the entire globe on all maps. Diagonal lines indicate regions with no change or no significant change, and fewer than 66% of the models show change greater than the internal variability of the model. Whereas temperature projections are in general agreement across the models, the same situation does not apply to precipitation projections. Since the climate model variability is higher in the precipitation projections, the confidence in these projections is less.

These same circumstances associated with precipitation occur in the weather models. Weather temperature forecasts are generally quite accurate and are “easy” for a numerical model to capture correctly. Precipitation forecasts are in the “difficult” category and have more errors. In other words, the climate models have this same dilemma as the weather forecast models with respect to precipitation.

14.3.3 – Sea Ice Projections

Sea ice in the late summer and early fall is projected to decrease. This follows the trend which is currently being observed. The graphs in Figure 14-31 depict the September Arctic sea ice for all SSPs, and illustrates this downward trend in sea ice area continuing. Notice that several of the scenarios in Figure 14-31 have the Arctic Ocean practically ice free in September by 2080. An ice free Arctic Ocean opens a northwest shipping passage between North America and Eurasia, which is desirable for some businesses.

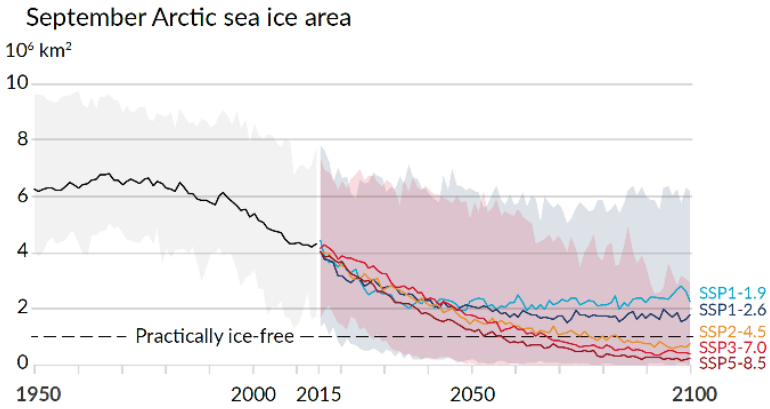

Figure 14-31: The projected decline of September sea ice.

The Arctic Ocean in March is still projected to maintain its ice cover. The maps in Figure 14-32 depict the observed Arctic sea ice from 1979-1988 and 2010-2019 with the change between the two sets of years for both March and September. As stated previously, Arctic sea ice is decreasing in areal coverage. A projection for 2045-2054 is also shown with the white color indicating good agreement between the climate models.

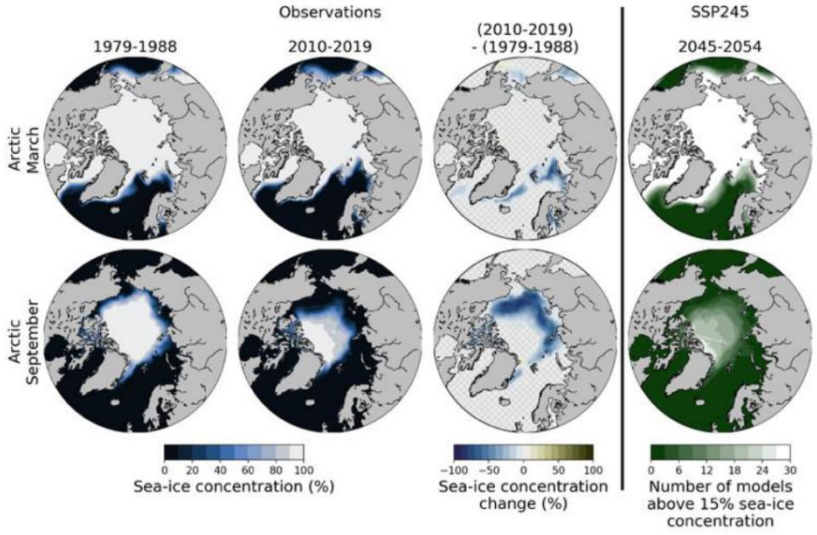

Figure 14-32: The top row contains maps for March. The bottom row contains maps for September. The four left side maps show the observations of Arctic Ocean sea ice.

The next two middle maps have the change from (1979-1988) to (2010-2019). Blue areas have the highest decrease.

The right side maps have the projected sea ice changes for 2045-2054 with white indicating good model agreement on the areal coverage of the ice.

The Antarctic sea ice is projected to not change as much. A significant difference between the Arctic and Antarctic is the North Pole resides in an ocean, while a continent with Earth's largest ice sheet resides at the South Pole. Water can flow under the Arctic ice at the North Pole which is not possible at the South Pole. The maps in Figure 14-33 depict the observed sea ice area and projected areas for 2045-2054 around Antarctica.

Figure 14-33: A set of maps similar to Figure 14-32, except for Antarctica.

Observation of Antarctic sea ice for September and February are the four left side maps.

Change from (1979-1988) to (2010-2019) in the middle.

The right side has the projected sea ice changes for 2045-2054.

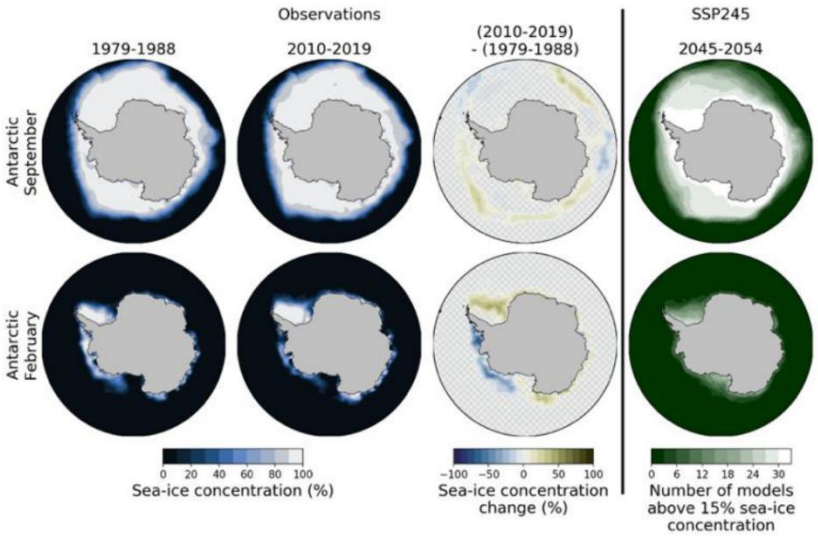

14.3.4 – Ice Sheet and Glacier Mass Projections

Ice sheets have complex motions and mass changes. Therefore, to project the future status of an ice sheet, both ice sheet and climate models need to be coupled together. This unique model is call the Ice Sheet Model Intercomparison Project for CMIP6 (ISMIP6). Ice sheets take hundreds of years to change, which makes future projections more difficult. The maps in Figure 14-34 of Greenland provide the status of the ice sheet during the Mid-Pliocene Warm Period about 4 million years ago, the last interglacial period and the last ice age (Last Glacial Maximum). As indicated in Figure 14-34, Greenland is appearing similar to the previous interglacial period before our current one. However, the ice sheet projection at 2093-2100 may be less than the last interglacial period.

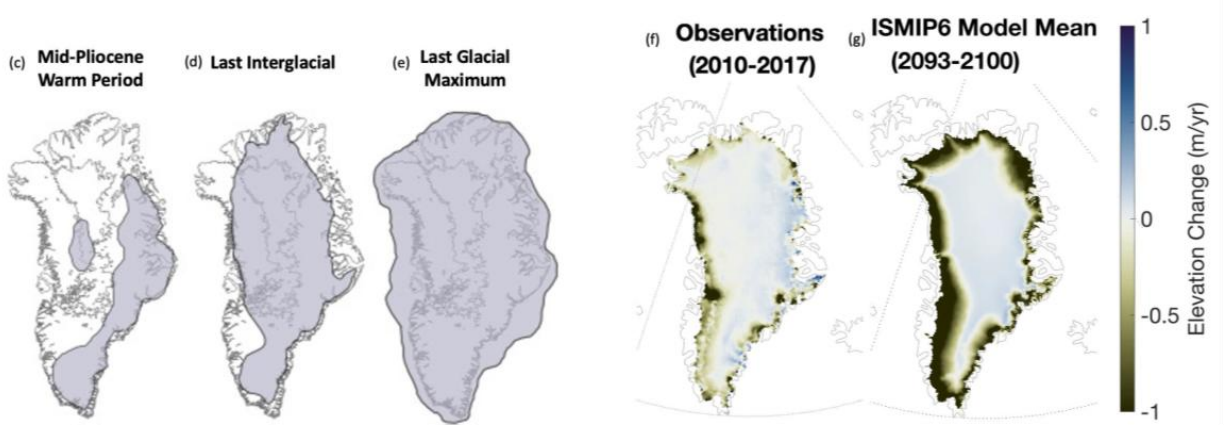

Figure 14-34: Right three maps are the historical ice sheet coverage over Greenland. The observed changes from 2010-2017 and the projected changes at the end of the century on the right side.

The next series of maps in Figure 14-35 are for Antarctica with similar time periods. The Antarctic ice sheet is slower to melt because it is bigger. Notice that ice melted during the last interglacial period appears slightly less than the projection for 2100.

Exploring the glacier mass projections indicates they have been melting since the Last Glacial Maximum about 20,000 years ago. With the increase in global mean temperatures, this melting will continue and accelerate. The loss or gain of ice on the Earth is always a positive feedback

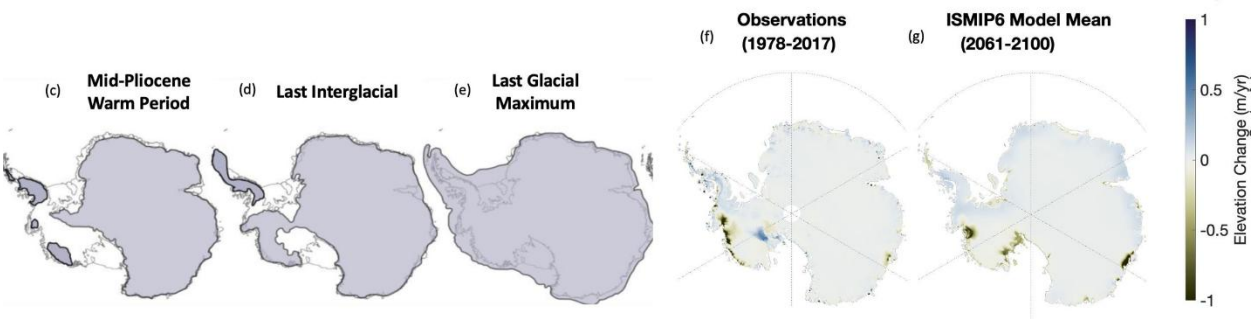

Figure 14-35: Maps similar to Figure 14-34 except for the Antarctica ice sheet.

situation. Thus, the loss of ice promotes warmer temperatures and a continued decrease in ice. The projections from the climate models show this situation in Figure 14-36. The y-axis is the percent of glacier mass relative to 2015. The individual boxes show the change and projected change in glaciers across all regions of the world from 1901 to 2100. Glacier mass is projected to decrease with the slowest changes occurring in the Antarctic.

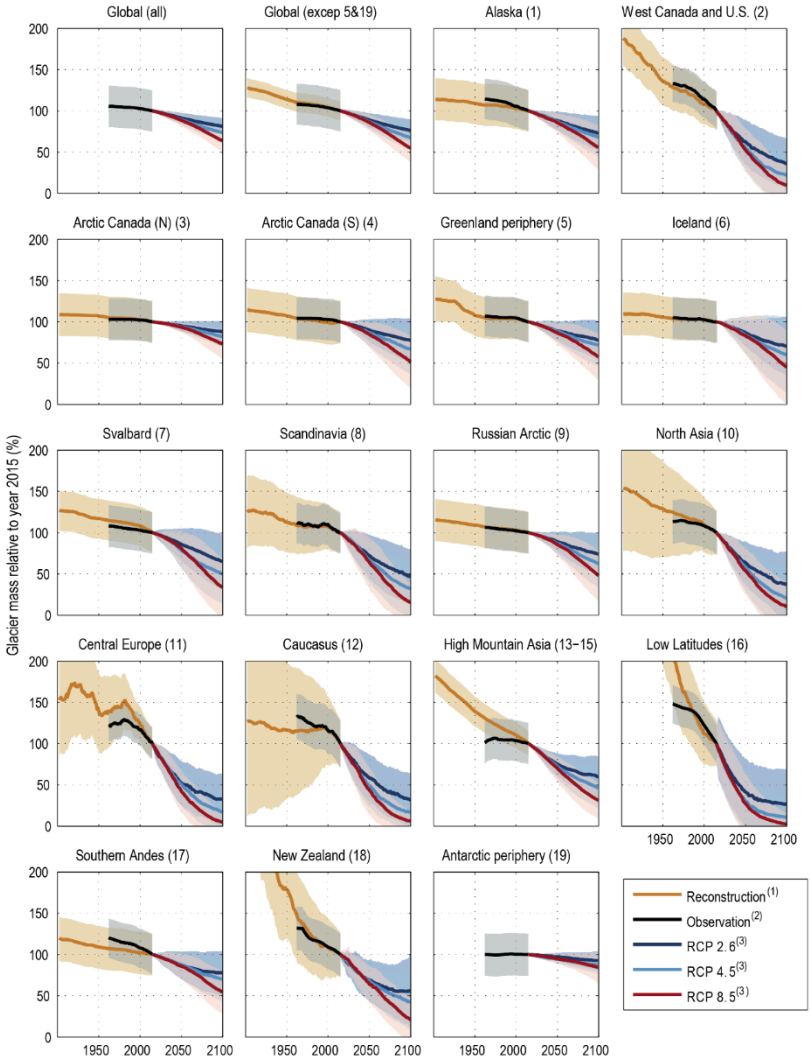

Figure 14-36: Graphs of glacier mass changes from 1901 to 2100. The beige and black lines are reconstructed and observed changes. The colored lines are various RCP scenario projections.

14.3.5 – Sea Level Projections

With glaciers projected to continue melting, sea level is also projected to continue to rise. Figure 14-37 contains the observed and projected global mean sea level change relative to 1900. All SSP scenarios have sea levels rising.

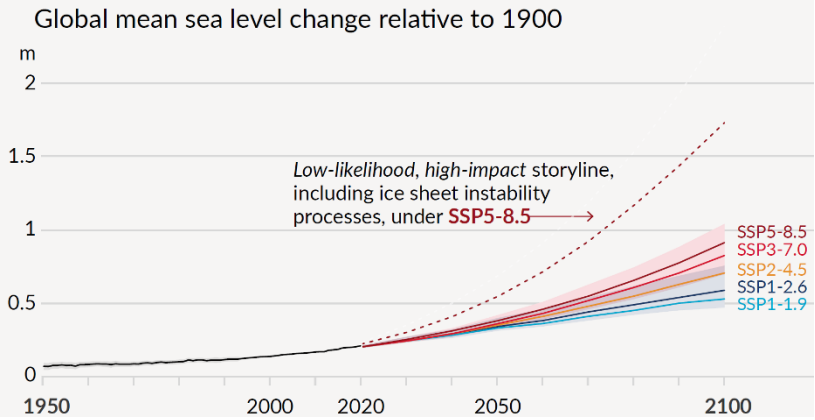

Figure 14-37: Observed (black line) and projected sea level (colored lines) changes.

While in an interglacial period, sea level rises normally occur; however, the anthropogenic warming is increasing them. The dashed line in Figure 14-37 is associated with ice sheet instability, and is a tipping point due to positive feedback that could cause an ice sheet to rapidly melt. This worse scenario has a low probability of occurring.

With the increase of atmospheric carbon dioxide, projections are for ocean acidity to increase. Figure 14-38 shows those projections.

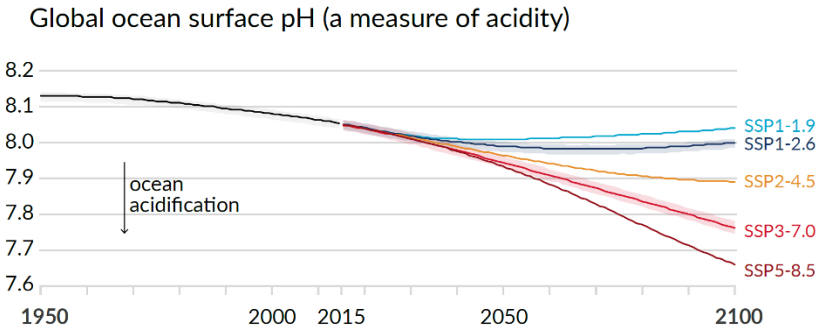

Figure 14-38: Observed (black line) and projected changes to ocean pH (colored lines).

Ocean ecosystems are sensitive to the pH level of the water. Changes to a more acidic ocean will affect these ecosystems, possibly with some surprises scientists cannot anticipate. Additionally, some species of fish appear to be migrating to higher latitudes due to the observed changes in the oceans.

The projected rise in sea levels is not the same at every location. The maps in Figure 14-39 show the projected rises at 2100 for different scenarios. The east coast of the U.S. is projected to have higher sea levels than the west coast. Due to these projected rises, east coast storm surges, like those associated with hurricanes, are anticipated to be worse. The last map (green) in Figure 14-39 is the uncertainty associated with these sea level increases. The uncertainty is quite high in some regions like the northern Pacific Ocean, and lowest in the Southern Hemisphere.

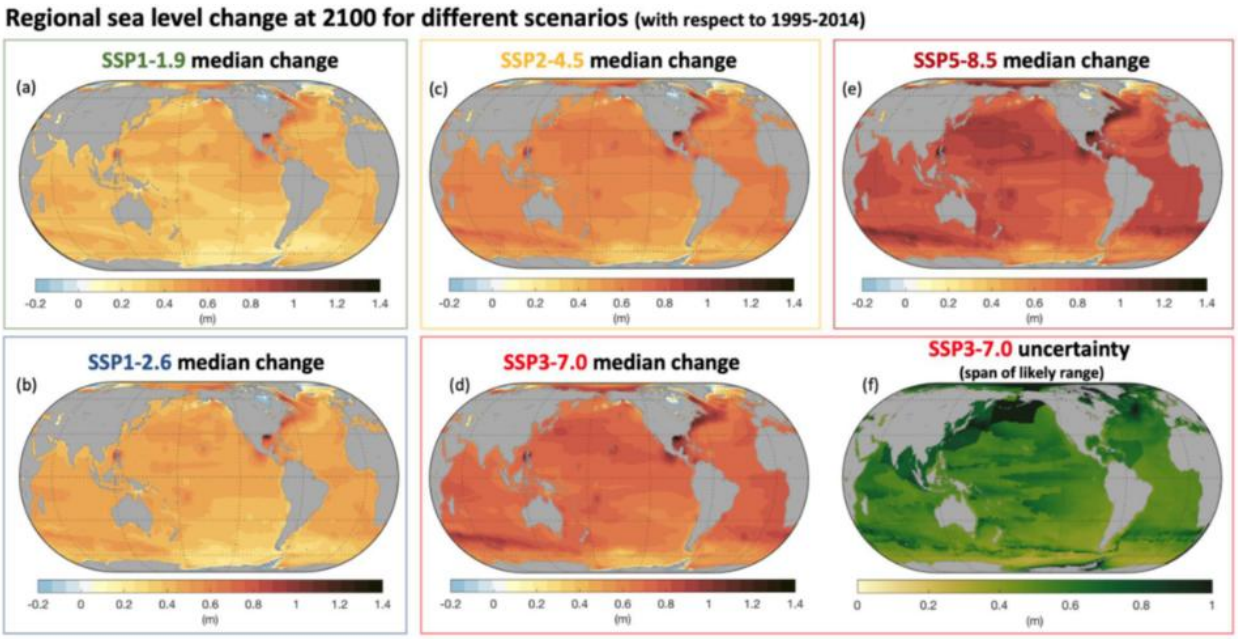

Figure 14-39: Global maps of projected sea level changes at 2100 for various scenarios. The east coast of the U.S. is projected to have noticeable rises. The lower right map is uncertainty associated with these projections. The northern Pacific Ocean is highest, with the Southern Hemisphere having the lowest uncertainty.

Chapter 14 Review Questions

1. What anthropogenic change can cause temperatures in an area to exceed the observed increases in mean global temperature? Explain the cause of this anthropogenic change.
2. List human contributions (pollutants) to the atmosphere that lowers temperatures?
3. What is the latest observed June average global temperature change? Provide this temperature in both the Celsius and Fahrenheit scales.
4. What percentage of the Earth's warming has occurred in the oceans?
5. How does higher pH levels in the ocean (ocean acidification) affect marine organisms?
6. Of the observed glaciers in the Arctic, what percentage are growing?
7. How is the snow cover in North America changing?
8. Describe the sea level changes occurring near the U.S. coasts.
9. How are Global Circulation Models (GCMs) tested or calibrated?
10. Since exact future climate parameters, such as carbon dioxide or human population, and not know, describe the methods climate models use to deals with these uncertainties.
11. What is the difference between the words "forecast" and "projection" in numerical model output?
12. How do GCMs verify that anthropogenic climate change is happening?
13. Why was the Intergovernmental Panel on Climate Change (IPCC) created?
14. Based on climate model temperature projections, which areas are warming the fastest? Which are warming the slowest? Are any areas showing cooling?
15. How does the projected Greenland ice sheet for 2100 compare to the Last Interglacial period?
16. How does the projected Antarctic ice sheet for 2100 compare to the Last Interglacial period?
17. Where are the projected sea level changes along the U.S. coasts supposed to be the highest? Where are they the lowest?

Chapter 15 – Climate Change and Extreme Weather

Overview

Climate change is frequently mentioned in the news and is at times associated with extreme weather events. In a general sense, as climate changes all the weather that occurs in this new climate occurs is affected by it. However, the question is whether the new climate is causing these new extremes in weather events. Attributing a specific weather event as resulting from a new climate normal is difficult. Scientists tackle this problem by looking at types of weather events in general and trying to determine how these events may be influenced by climate changes. This chapter looks at these efforts.

Additionally, the question arises of how do we deal with climate change? The last section in this chapter examines three approaches for dealing with climate change.

Chapter objectives:

1. Understand how extreme weather may be attributed to changes in the climate.
2. Describe any changes to these extreme weather phenomena caused by changes in the climate:
    a. Extreme heat
    b. Extreme cold
    c. Drought
    d. Heavy precipitation
    e. Floods
    f. Tropical cyclones
    g. Extratropical cyclones
    h. Wildfires
    i. Severe convective storms
3. List actions that could be taken to mitigate carbon in the atmosphere.
4. List the pros and cons of adapting to a new climate.
5. List techniques which could be used to manipulate Earth's climate.

15.1 – Attribution of Climate Changes to Weather Events

Long-term changes in climate can directly or indirectly affect many aspects of society in potentially disruptive ways. For example, warmer average temperatures could increase air conditioning costs and affect the spread of diseases, but could also improve conditions for growing crops. More extreme variations in weather are also a threat to society. More frequent and intense extreme heat events can increase illnesses and deaths, especially among vulnerable populations, and damage some crops. While increased precipitation can replenish water supplies and support agriculture, intense storms can damage property, cause loss of life and population displacement, and temporarily disrupt essential services such as transportation, telecommunications, energy, and water supplies.

The extent to which climate change influences an individual weather or climate event is difficult to determine. A weather event involves consideration of natural and anthropogenic factors that combine to produce the specific conditions of an event. By definition, extreme events are rare with only a few examples of past events at any given location. Nonetheless, this relatively new area of science—often called event attribution—is rapidly advancing. The advances have come about for two main reasons: (1) the understanding of the climate and weather mechanisms that produce extreme events is improving, and (2) rapid progress is being made in the methods that are used for event attribution. This emerging area of science also has drawn the interest of the public and strong interest in the media.

The ultimate challenge for the science of event attribution is to estimate how much climate change has affected an individual event's magnitude or probability of occurrence. While some studies now attempt to do this, most studies consider classes of events that are similar to the event that was observed. Irrespective of whether a specific event or a class of events is studied, results remain subject to substantial uncertainty, with greater levels of uncertainty for events that are not directly temperature related. Temperature related events are well simulated in the climate models and well understood. The conclusions drawn from these studies depends on choices made when selecting the events, framing the questions asked about the role of climate change, designing the modeling setup, and selecting statistical tools to quantify the uncertainty.

Event attribution approaches can be generally divided into two classes: (1) those that rely on the observational record to determine the change in probability or magnitude of events, and (2) those that use model simulations to compare the manifestation of an event in a world with human-caused climate change to that in a world without. Most studies use both observations and models to some extent. Modeling studies will use observations to evaluate whether models reproduce the event of interest, and whether the physical mechanisms are implemented correctly. Observational studies may rely on models for attribution of the observed changes. The most reliable event attribution examines three areas or factors. Reliable event attribution:

1. Is based on sound physical principles.
2. Is supported with consistent evidence from observations.
3. Can be replicated with numerical models.

15.2 – Confidence in Attribution Studies

Confidence in attribution findings of anthropogenic influence is greatest for those extreme events that are related to an aspect of temperature. For extreme heat and cold events, changes in long-term mean conditions provide a basis for expecting that there should also be related changes in extreme conditions. Figure 15-1 illustrates these temperature changes as the climate warms.

As the distribution of temperatures shifts to warmer temperatures, the extreme cold events become less cold. Likewise, the previous extreme hot events become more prevalent and the new extreme hot weather conditions becomes hotter.

Heavy precipitation is influenced by a moister atmosphere, which is somewhat directly related to human-induced warming. A warmer atmosphere can hold more moisture. However, a precipitation event is not as directly related to temperature as the actual increase in temperature itself. This indirect temperature relationship to precipitation helps increase the confidence when precipitation changes are linked to climate changes.

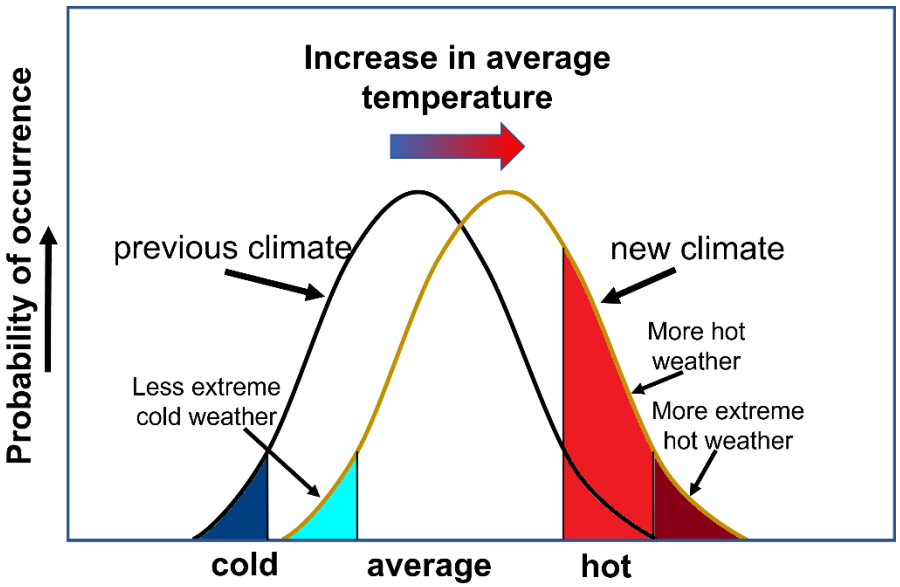

Figure 15-1: Graphs illustrating the increase in temperature from a previous climate to a new climate. Extreme hot events increase and extreme cold events decrease.

The frequencies and intensities of tropical cyclones, midlatitude cyclones, and severe convective storms are related to large-scale climate parameters, whose relationships to climate are understood by varying degrees. Atmospheric circulation and dynamics play some role in the development of an extreme event, which varies by the type of event. Changes in atmospheric circulation and dynamics are generally less directly controlled by temperature, less robustly simulated by climate models, and less well understood. As such, the confidence in whether climate change is influencing these extreme weather events varies considerably. Figure 15-2 catalogs the types of weather events and the confidence that the event could have been influenced by climate change.

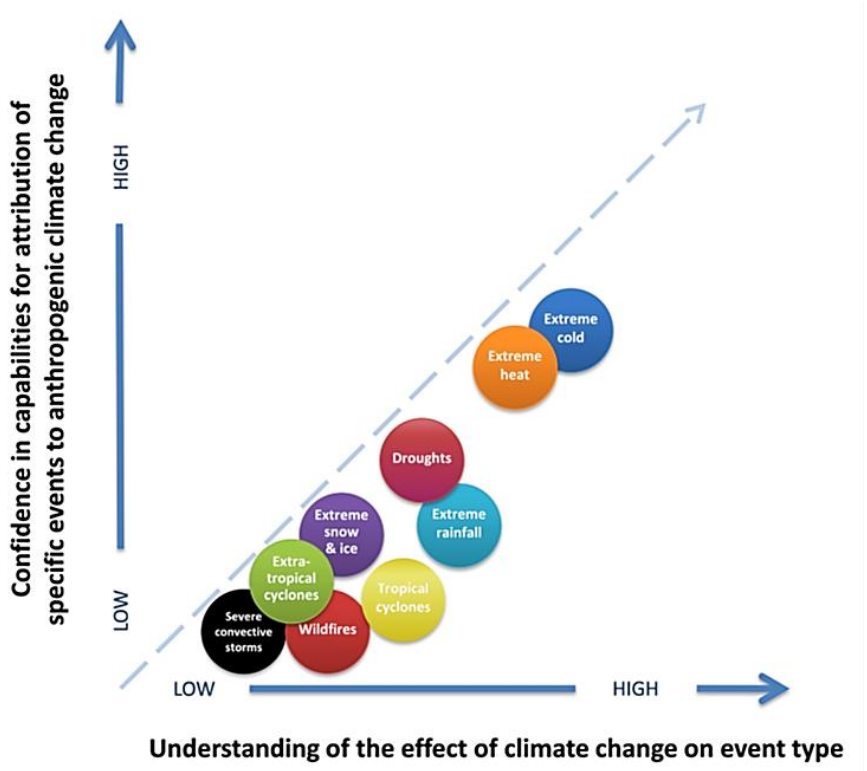

Figure 15-2: Confidence in attributing climate change to specific weather events versus the understanding associated with that event. Extreme heat and cold events have the highest confidence and understanding, while severe convective storms have the lowest.

Examining the three factors associated with reliable event attribution is shown in the following table. Notice only extreme cold and heat events have high confidence in all three factors. Severe convective storms is on the bottom, since these events fail to satisfy the criteria for attribution.

● = high O = medium ○ = low	Capabilities of Climate Models to Simulate Event Type	Quality/Length of the Observational Record	Understanding of Physical Mechanisms That Lead to Changes in Extremes as a Result of Climate Change
Extreme cold events	●	●	●
Extreme heat events	●	●	●
Droughts	O	O	O
Extreme rainfall	O	O	O
Extreme snow and ice storms	O	○	O
Tropical cyclones	○	○	O
Extratropical cyclones	O	○	○
Wildfires	○	O	○
Severe convective storms	○	○	○

15.2.1 – Extreme Heat (Heat Waves)

A series of unusually hot days is referred to as an extreme heat event or a heat wave. Heat waves are more than just uncomfortable. They can lead to illness and death, particularly among older adults, the very young, and other vulnerable populations. Prolonged exposure to excessive heat can lead to other impacts as well. For example, damaging crops, injuring or killing livestock, and increasing the potential for wildfires. Prolonged periods of extreme heat can lead to power outages as heavy demands for air conditioning strain the power grid.

Unusually hot days and multi-day heat waves are a natural part of the day-to-day variation in weather. As the Earth's climate warms, hotter-than-usual days and nights during the summer (June, July, and August) are becoming more common, and heat waves are expected to become more frequent and intense. The graphs in Figure 15-3 show how hot daily highs and lows have varied from 1910 to 2023. The term "hot" is based on the long-term average conditions at each location. The thin lines represent individual years, while the thick lines show a nine-year weighted average. Red lines represent daily highs, while orange lines represent daily lows. Notice how the lows have increased more than the highs in the last several decades.

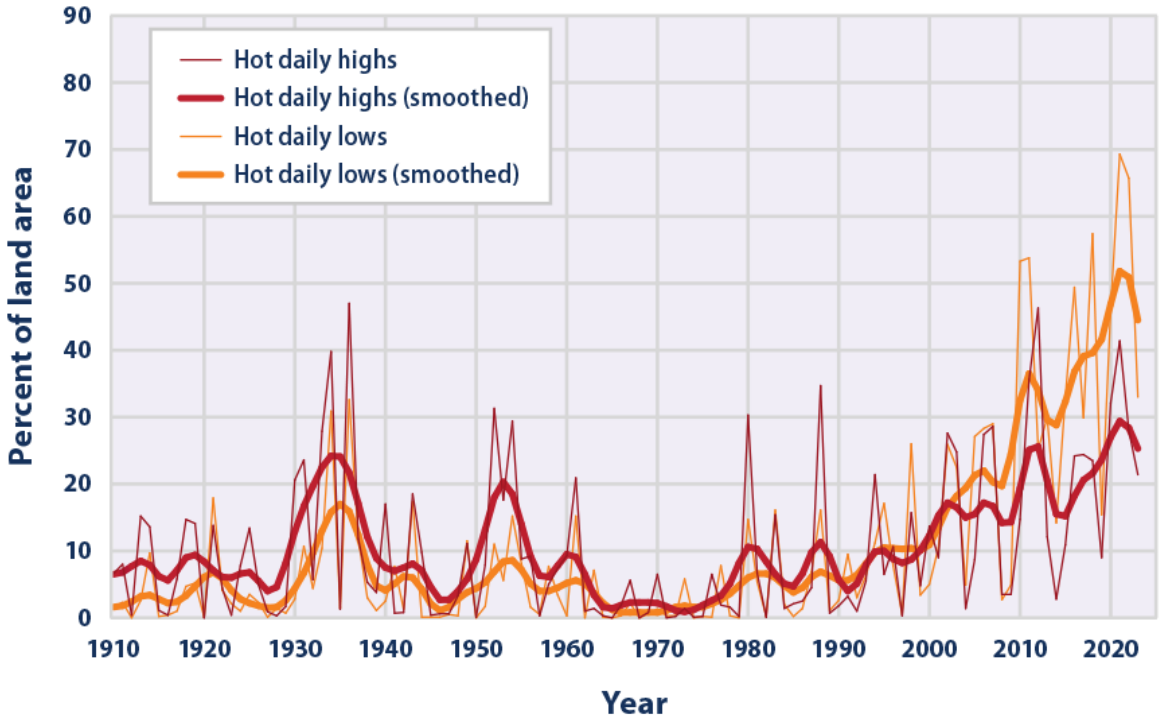

Figure 15-3: the percentage of the land area of the contiguous 48 states with unusually hot daily high and low temperatures during the months of June, July, and August. The thin lines represent individual years, while the thick lines show a nine-year weighted average. Red lines represent daily highs, while orange lines represent daily lows. The term "unusual" in this case is based on the long-term average conditions at each location.

The bar graphs in Figure 15-4 describe the trends in multi-day extreme heat events across the United States.

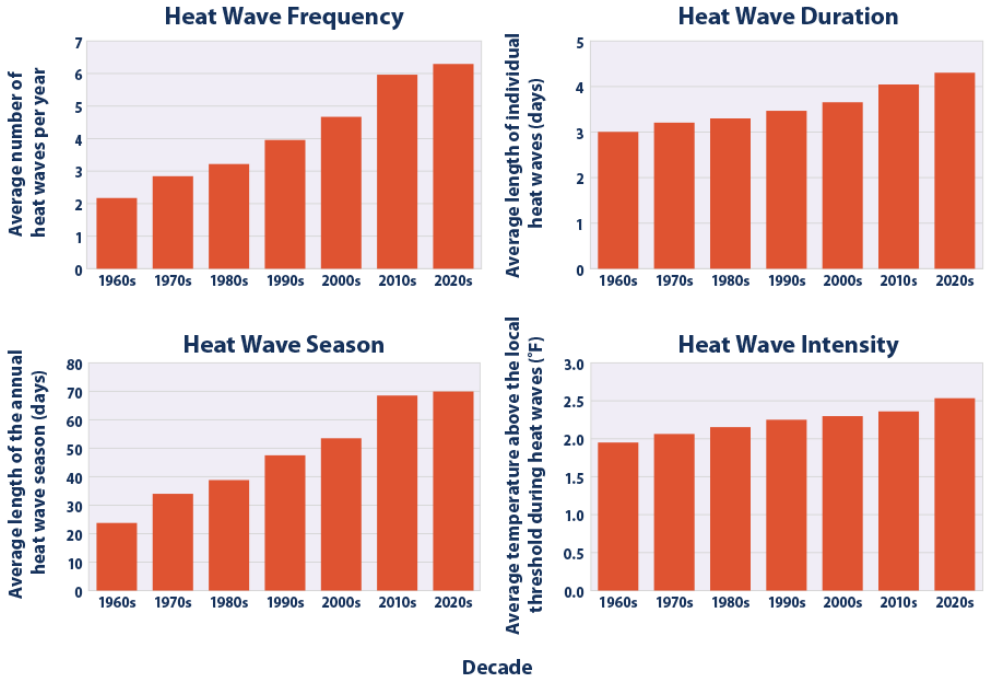

Figure 15-4: Bar graphs showing heat wave frequency, duration, length of season, and intensity from the 1960s into the 2020s.

The key points from the graphs in Figure 15-4 are:

- Heat waves are occurring more often than they used to in major cities across the United States. Their frequency has increased steadily, from an average of two heat waves per year during the 1960s to six per year during the 2010s.

- In recent years, the average heat wave in major U.S. urban areas has been about four days long. This is about a day longer than the average heat wave in the 1960s.

- The average heat wave season across the 50 cities in this indicator is 46 days longer now than it was in the 1960s.

- Heat waves have become more intense over time. In other words, temperatures are higher. During the 1960s, the average heat wave across the U.S. was 2.0°F above the local 85th percentile threshold. The 85th percentile of July and August temperatures equates to the nine hottest days in a typical summer. During the 2020s, the average heat wave has been about 2.5°F above this local threshold.

Despite heat waves increases in the U.S., longer-term records show that heat waves in the 1930s remain the most severe in recorded U.S. history. Figure 15-5 graphs the Heat Wave Index from 1896 to 2021 in the contiguous 48 states. This index defines a heat wave as a period lasting at least four days with an average temperature that would only be expected to occur once every 10 years, based on the historical record. The index value for a given year depends on how often such severe heat waves occur and the size of the area they affect.

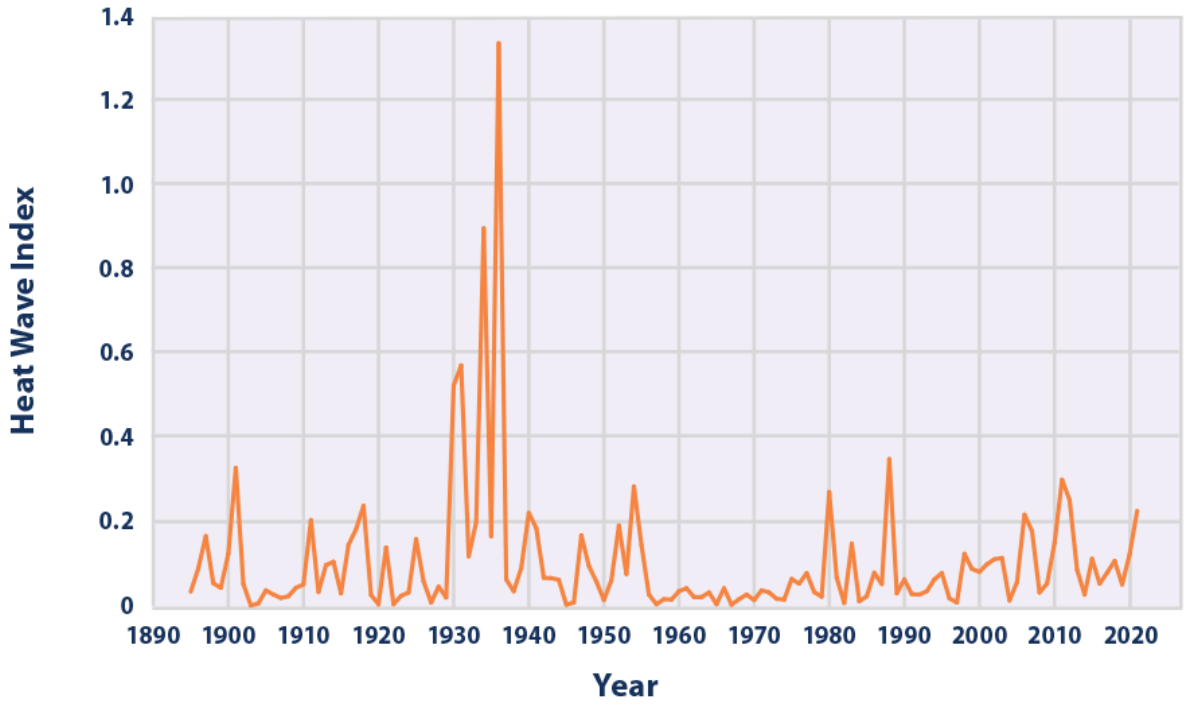

Figure 15-5: Graph of the Heat Wave Index from 1896 to 2021 in the contiguous 48 states. The heat wave during the 1930s "Dust Bowl" is the most severe every recorded.

The spike in Figure 15-5 reflects the extreme, persistent heat waves in the Great Plains region during a period known as the “Dust Bowl.” Poor land use practices and many years of intense drought contributed to these heat waves by depleting soil moisture and reducing the moderating effects of evaporation.

The latest IPCC report states: “It is extremely likely (>95%) that human influence is the main contributor to the observed increase in the intensity and frequency of hot extremes…on the global scale”, and “It is very likely (>90%) that this applies on continental scales as well.”

15.2.2 – Extreme Cold (Cold Waves)

As might be expected, the number of cold spells in the U.S. has decreased. The number of days below freezing has generally decreased throughout the country, particularly in the western United States. The map in Figure 15-6 depicts the changes in the number of days below freezing.

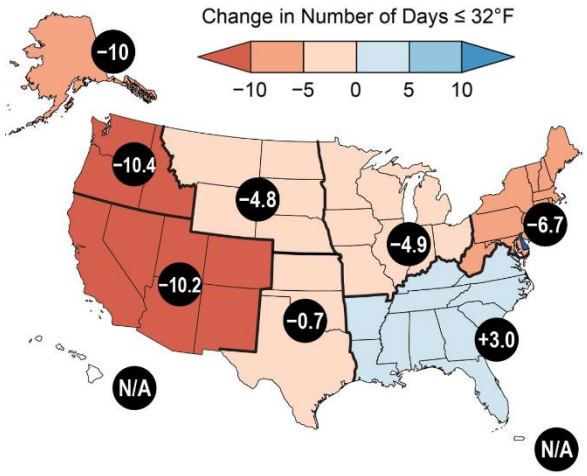

Figure 15-6: The number of days below freezing in each region of the U.S.

This graph in Figure 15-7 shows the percentage of the land area of the contiguous 48 states with unusually cold daily high and low temperatures during the winter months (December, January, and February). The thin lines represent individual years, while the thick lines show a nine-year weighted average. Blue lines represent daily highs, while purple lines represent daily lows. The term “unusual” in this case is based on the long-term average conditions at each location. Notice the size of the areas affected by cold temperatures has decreased in recent decades.

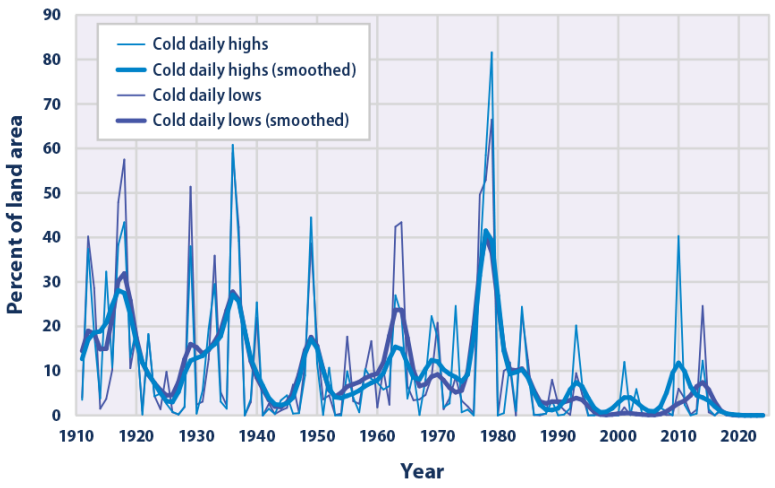

Figure 15-7: Area of the contiguous 48 states with unusually cold winter temperatures from 1911 to 2024.

Cold spells are expected to decrease in the future. In most locations, scientists expect daily minimum temperatures to become warmer at a faster rate than daily maximum temperatures.

The latest IPCC report states: “It is extremely likely (>95%) that human influence is the main contributor to the…observed decrease in the intensity and frequency of cold extremes on the global scale”, and “It is very likely (>90%) that this applies on continental scales as well.”

15.2.3 – Droughts

The word “drought” suggests abnormally dry conditions. However, the meaning of “dry” can be ambiguous and lead to confusion in how drought is defined. Three different definitions of droughts are available, each with different impacts. Meteorological drought describes conditions associated with a precipitation deficit. Agricultural drought describes conditions with a soil moisture deficit. Hydrological drought describes conditions associated with runoff or streamflow deficit. Clearly these three characterizations of drought are related, but are also different descriptions of water shortages with different target audiences and different time scales. Agricultural drought is of concern to producers of food while hydrological drought is of concern to water system managers. Soil moisture is a function of both precipitation and evapotranspiration, and is affected by both meteorological and agricultural droughts.

Due to this multi-faceted nature of drought and who may be affected, several drought indexes have been developed. The most widely known, Palmer Drought Severity Index (PDSI), uses readily available temperature and precipitation data to estimate relative dryness. The PDSI is a standardized index that generally spans -10 (dry) to +10 (wet). The PDSI has been reasonably successful at quantifying long-term drought. The index uses temperature data and a physical water balance model. Additionally, it can capture the basic effect of global warming on drought through changes in potential evapotranspiration.

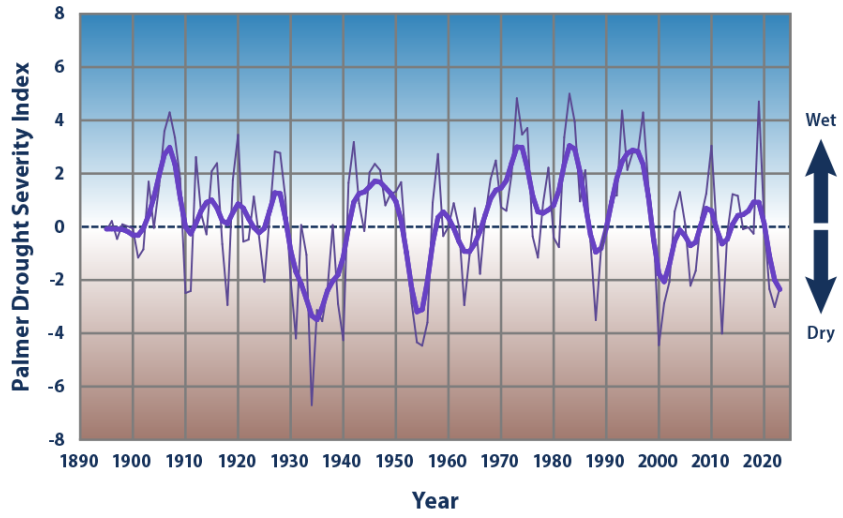

Figure 15-8: Average drought conditions in the contiguous 48 states according to the Palmer Drought Severity Index from 1895 to 2023.

Figure 15-8 shows the annual values of the Palmer Drought Severity Index as the thin line, averaged over the entire area of the contiguous 48 states. Positive values represent wetter-than-average conditions, while negative values represent drier-than-average conditions. A value between -2 and -3 indicates moderate drought, -3 to -4 is severe drought, and -4 or below indicates extreme drought. The thicker line is a nine-year weighted average.

Average drought conditions across the U.S. have varied over time. The 1930s and 1950s saw the most widespread droughts. These dry years dominate the drought record in the United States. The “Dust Bowl” drought of the 1930s is the most significant meteorological and agricultural drought experienced in the United States in terms of its geographic and temporal extent. The 1930s drought happened prior to most of the current global warming. From 1890 to 2020, the PDSI overall trend has been toward wetter conditions.

As average temperatures have risen because of climate change, the Earth’s water cycle has sped up through an increase in the rate of evaporation from soil and transpiration from plants. However, due to its nature the balance within the water cycle is always present. An increase in

evapotranspiration makes more water available in the air for precipitation, but contributes to drying over some land areas, leaving less moisture in the soil. As the climate continues to change, many historically dry areas are likely to experience less precipitation and an increased risk of drought. Since the 1950s, some regions of the world have experienced longer and more intense droughts, particularly in southern Europe and West Africa. Other regions have seen droughts become less frequent, less intense, or shorter (for example, in central North America).

Previous IPCC reports tended to have less than 50% confidence in the detection and attribution of changes in drought over global land areas since the mid-20th century. The latest IPCC report has a medium confidence (50%) that humans have influenced changes in meteorological, hydrological, and agricultural droughts. However, climate projections for "the land area affected by increasing drought frequency and severity expands with increasing global warming" are given a high confidence level (80%). The climate models tend to agree that dry climate areas will expand in coverage.

15.2.4 – Heavy precipitation

Climate change can affect the intensity and frequency of precipitation. Warmer oceans increase the amount of water that evaporates into the air. When more moisture-laden air moves over land or converges into a storm system, it can produce more intense precipitation. For example, heavy rainfall and snowstorms.

Heavy precipitation does not necessarily mean the total amount of precipitation at a location has increased, but that precipitation is occurring in more intense events. However, changes in the intensity of precipitation, when combined with changes in the interval between precipitation events can lead to changes in overall precipitation totals.

Figure 15-9 shows the percentage of the land area of the contiguous 48 states where a much greater than normal portion of total annual precipitation has come from extreme single-day precipitation events. The bars represent individual years, while the line is a nine-year weighted average.

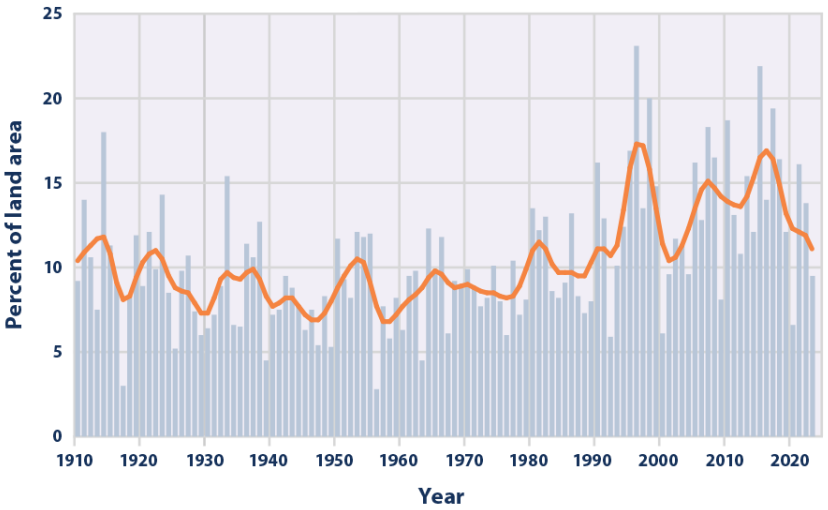

Figure 15-9: Extreme one-day precipitation events in the contiguous 48 states from 1910 to 2023.

In recent years, a larger percentage of precipitation has come in the form of intense single-day events. Nine of the top 10 years for extreme one-day precipitation events have occurred since 1995. The prevalence of extreme single-day precipitation events remained steady between 1910 and the 1980s, but has risen substantially since 1990. Over the entire period from 1910 to 2023, the portion of the country experiencing extreme single-day precipitation events increased at a rate of about half a percentage point per decade.

The map in Figure 15-10 shows the observed changes in the number of one day heavy precipitation events. All regions had increases in heavy one day precipitation with the largest increases in the northeastern U.S. Most of the large increases occurred in the eastern half of the United States with smaller increases in the West.

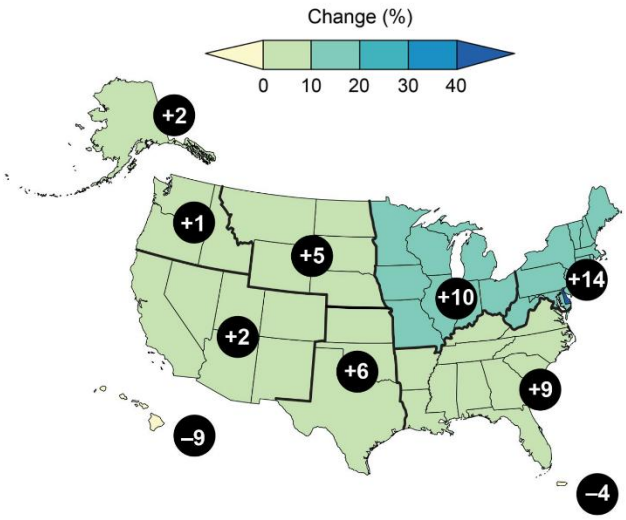

Figure 15-10: The annual heaviest daily precipitation amount observed percent changes over the 1958–2021 period.

The latest IPCC climate projections have high confidence (80%) that global-scale heavy precipitation will be increasing. The intensification of heavy precipitation will follow the rate of increase in the maximum amount of moisture that the atmosphere can hold as it warms. The amount of this increase is about 7% per °C of global warming. For example, a 3.0-inch precipitation event would have about an additional quarter of an inch (0.21 inches) of rain.

15.2.5 – Floods

Flooding damage in the United States can come from flash floods of smaller rivers and creeks, prolonged flooding along major rivers, urban flooding unassociated with proximity to a riverway, coastal flooding from storm surge, and the confluence of coastal storms and inland riverine flooding. Flash flooding is associated with extreme precipitation in an area. Flooding of major rivers in the United States with substantial winter snow accumulations usually occurs in the late winter or spring. In the western coastal states, most flooding occurs in conjunction with extreme precipitation events from atmospheric rivers (section 6.3.3). Hurricanes and tropical storms are an important driver of flooding events in the eastern United States. Changes in streamflow rates depend on many factors, both human and natural, in addition to climate change. Deforestation, urbanization, dams, floodwater management activities, and changes in agricultural practices can all play a role in past and future changes in flood statistics. Projection of future changes is thus a complex multivariate problem.

Rivers and streams experience flooding as a natural result of large rain storms or spring snowmelt that quickly drains into streams and rivers. Although the risk for flooding varies across the United States, most areas are susceptible to floods. The size, or magnitude, of flood events is influenced by how much water enters the waterway upstream and how quickly. Flood frequency largely depends on the frequency of weather events.

Figure 15-11 shows changes in the frequency of flooding events in rivers and streams in the United States between 1965 and 2015. Blue upward-pointing symbols show locations where floods have become more frequent; brown downward-pointing symbols show locations where floods have become less frequent. The larger, solid-color symbols represent stations where the change was statistically significant.

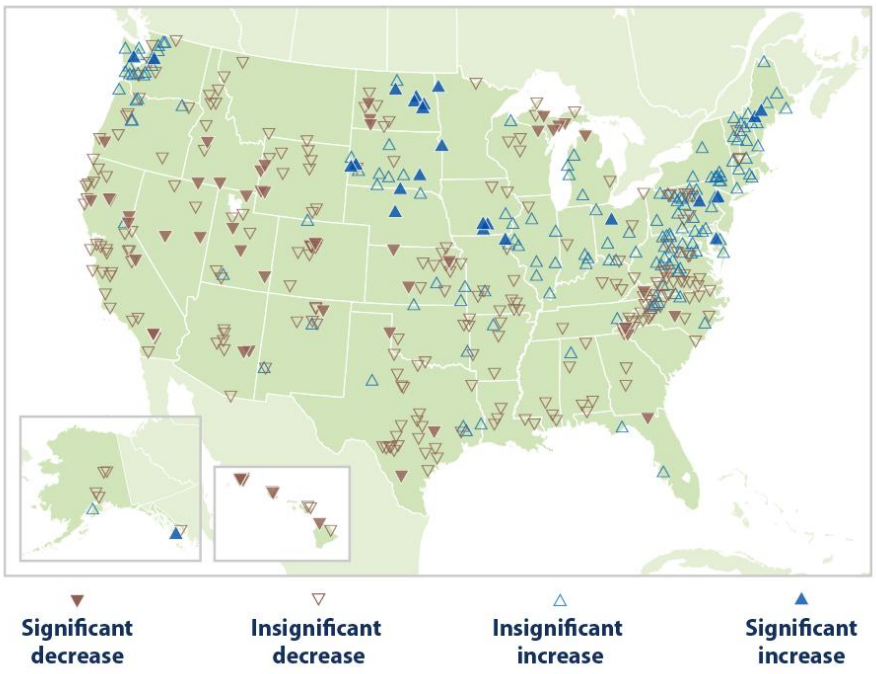

Figure 15-11: Change in the frequency of river flooding in the United States from 1965 to 2015.

Even though the number of heavy precipitation days has increased, the number of floods has not correspondingly increased. This apparent disparity with overall increases in observed extreme precipitation can be partly explained by the seasonality of the two phenomena. Extreme precipitation events in the eastern half of the U.S. are larger in the summer and fall when soil moisture and seasonal streamflow levels are low and less favorable for flooding. By contrast, high streamflow events are often larger in the spring and winter when soil moisture is high and snowmelt and frozen ground can enhance runoff.

In summary the latest IPCC report states “there is low confidence in the human influence on the changes in high river flows on the global scale. Confidence is in general low in attributing changes in the probability or magnitude of flood events to human influence because of a limited number of studies and differences in the results of these studies, and large modelling uncertainties.”

15.2.6 – Tropical Cyclones (Hurricanes and Tropical Storms)

Detection and attribution of past changes in tropical cyclone behavior remain a challenge due to the quality of the historical data. The observations are diverse in both time and content from the various regions that collect and analyze them. While there are ongoing efforts to reanalyze and homogenize the data, there remains low confidence that any reported long-term (multidecadal to centennial) increases in tropical cyclone activity are of sufficient quality to make a conclusion. This conclusion is not meant to imply that no changes have occurred, but rather that the observational data are not of high enough quality to determine any changes with confidence. Furthermore, it has been argued that within the period of highest data quality (1980 to the present), the globally observed changes in the environment do not support a detectable trend in tropical cyclone intensity. That is, the trend signal has not had time to rise above the background variability of natural processes.

However, both physical principles and numerical modeling simulations indicate an increase in tropical cyclone intensity should occur in a warmer world. The climate models generally show an increase in the number of intense tropical cyclones, although the exact rate of intensification per

degree of global warming remains uncertain. The global frequency of tropical cyclone formation is projected to decrease. For the Atlantic hurricanes overall, there will likely be fewer hurricanes and wind speeds for the ones that form will be about 4% stronger for every 1°C increase in sea surface temperatures, as is seen in Figure 15-12.

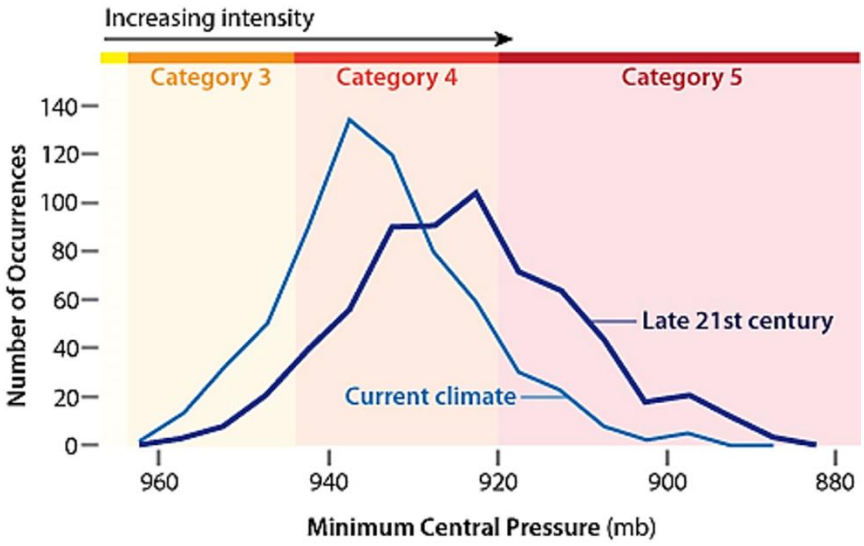

Figure 15-12: Observed (thin line) and projected (thick line) hurricane frequency (occurrences) and intensity (pressure) changes. Hurricane projections are for less frequent, but stronger storms.

Precipitation in tropical cyclones is expected to increase, because of the increased water vapor content in the atmosphere. According to climate model projections, tropical cyclone rain rates within 62 miles of the storm's center are likely to increase by 20% over the next century. Figure 15-13 illustrates this increase in precipitation rates between the present climate and a warmer climate.

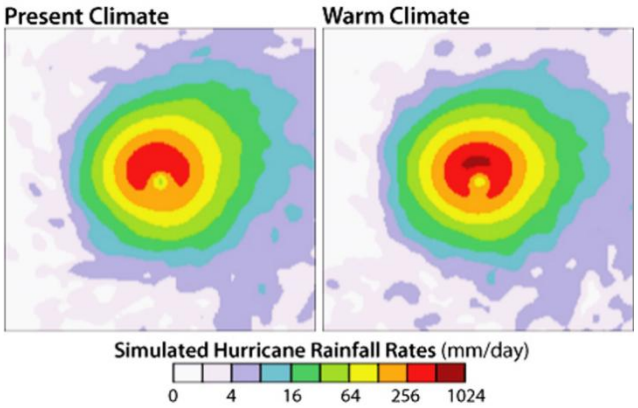

Figure 15-13: Hurricane rainfall rates with the present climate and a warmer climate.

Lastly, there is evidence that the locations where tropical cyclones reach their peak intensity has migrated poleward over the past 30 years as shown in Figure 15-14. This poleward shift is associated with the observed expansion of the tropics. Shading in this figure shows the 95% confidence bounds for the trend; not a huge shift poleward but a measurable change.

In summary, projected changes (not observed) associated with tropical cyclones are an increase in the number of category 4 and 5 hurricanes in some regions, an increase in precipitation associated with a moister, warmer atmosphere, the average location of their peak wind-intensity will migrate poleward in the western North Pacific Ocean, and the total number of all tropical cyclones will decrease or remain unchanged.

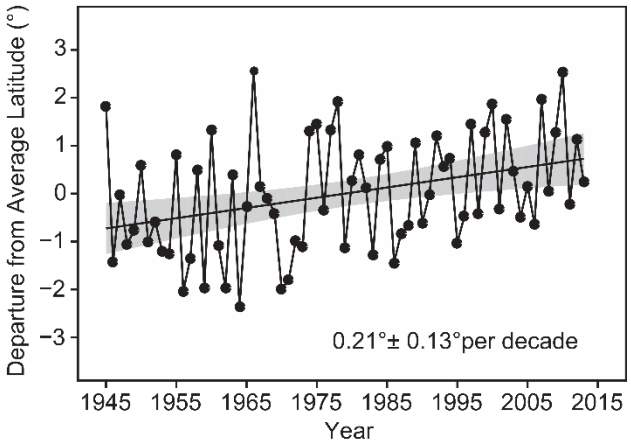

Figure 15-14: Migration of hurricanes poleward from 1945 to 2014.

15.2.7 – Extratropical (Midlatitude) Cyclones

Multiple studies have examined the frequency and intensity of midlatitude cyclones in both hemisphere with a wide range of results. Overall, any changes in the number of these cyclones over both hemispheres has a low confidence. The number and intensity of midlatitude cyclones is affected by large annual and decadal variations (natural climate variability), which makes finding a solid conclusion concerning frequency difficult. However, in recent decades the number of stronger extratropical cyclones has increased over the Southern Hemisphere, while the number of stronger cyclones has decreased in the Northern Hemisphere. Figure 15-15 contains graphs of these analyses for both the Southern and Northern Hemispheres. The top graphs are the total number of midlatitude cyclones for each hemisphere and the bottom graphs are the number of strong (<980 mb) systems.

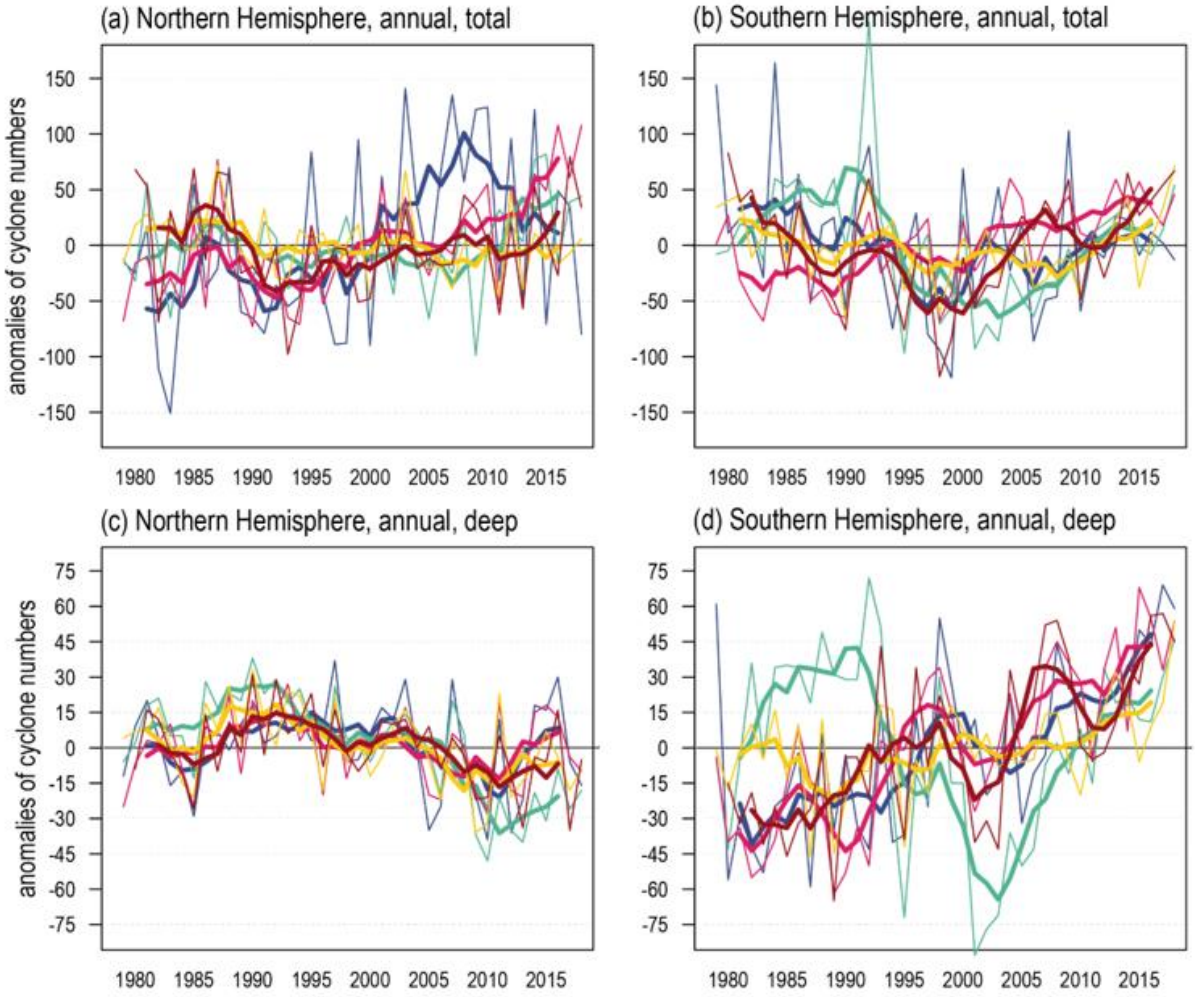

Figure 15-15: The total number of extratropical cyclones (a, b) and the number of strong cyclones (<980 mb) for both hemispheres. The thin lines are for each year. The thick lines are a five-year running average.

Several changes associated with midlatitudes cyclones that have higher confidence are a poleward shift of the storms. In other words, extratropical cyclones tracks are shifting to higher latitudes. As Earth warms, the greatest temperature gradient between the tropics and poles is

expected to shift northward as the warmer temperatures expand north. Thus, a slight shift poleward in the midlatitude cyclone storm track is to be expected.

Precipitation associated with midlatitude cyclones is projected to increase associated with the increases in atmospheric water vapor. This increase in precipitation is projected to be about 7% per degree of global warming. More details on projected precipitation were explored previously in section 14.3.2.

In summary, there is low confidence in any changes associated with the strength of extratropical cyclones, and medium confidence that changes in the future will continue to be small. Please note that the changes associated with the storm track location could cause some local strength variations. The increase in maximum precipitation rates has a high confidence that these rates will increase with warming.

15.2.8 – Wildfires

Wildfires are a global phenomenon caused by natural lightning and human ignition sources, and represent an important ecosystem process on our planet. Recent decades have seen a profound increase in forest fire activity over the western United States and Alaska. The frequency of large wildfires is influenced by a complex combination of natural and human factors. Temperature, soil moisture, relative humidity, wind speed, and vegetation (fuel density) are important aspects of the relationship between fire frequency and ecosystems. Forest management and fire suppression practices can also alter this relationship from what it was in the pre-industrial era. Changes in these control parameters can interact with each other in complex ways as the climate warms.

Figure 15-16 shows the total number of wildfires per year in the U.S. from 1983 to 2022. These totals include all reported wildfires, which can be as small as just a few acres. An average of approximately 70,000 wildfires occur per year. The two lines represent two different reporting systems. The National Interagency Fire Center consists of the land management agencies in the U.S. and is represented by the blue line. The Forest Service stopped collecting statistics (orange line) in 1997, and those statistics are shown here for comparison. The data do not show an obvious trend.

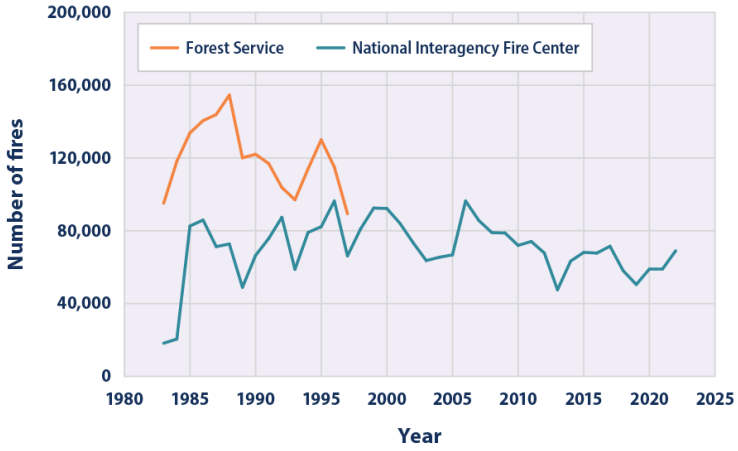

Figure 15-16: Wildfire frequency in the United States from 1983 to 2022. These graphs do not show an obvious trend.

However, the extent of areas burned by wildfires each year appears to have increased since the 1980s. According to National Interagency Fire Center data, of the 10 years with the largest acreage burned, all have occurred since 2004 including the peak years in 2015 and 2020. This period coincides with many of the warmest years on record nationwide. The largest increases have occurred during the spring and summer months. Figure 15-17 shows these changes in the annual wildfire-burned area (in millions of acres) from 1983 to 2022.

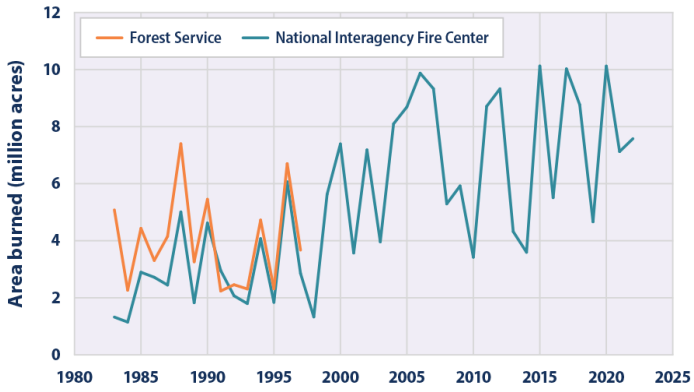

Figure 15-17: Areas burned by wildfires in the United States from 1983 to 2022. The area burned shows an increasing trend.

As stated previously, wildfires have many conditions associated with them. From a climate change standpoint, heatwaves, droughts, and less snow cover significantly affect fire conditions. However, humans greatly influence forest management and fire suppression practices, which significantly impacts wildfire conditions. This situation makes wildfire changes being fully attributed to climate change a difficult process.

In summary, the latest IPCC report states "There is medium confidence (50%) that weather conditions that promote wildfires (fire weather) have become more probable in southern Europe, northern Eurasia, the US, and Australia over the last century." However, favorable weather conditions for wildfires does not directly relate to more wildfires, since many other factors are involved.

15.2.9 – Severe Convective Storms (Thunderstorms and Tornadoes)

Detection of trends associated with severe convective storms is difficult due to changes in data quality and storm definitions. In the United States, observations of both tornadoes and hail show significant increases over the latter half of the 20th century, but these are widely understood to be artifacts of increased frequency of reporting rather than actual meteorological trends.

Environmental variables predictive of tornado formation, for example, do not coincide with the trends of tornadoes that occurred. Studies of trends in the United States find different results depending on the time period and spatial region chosen. Thus, there is no broad agreement on the detection of long-term trends in severe convective storm activity that might be related to anthropogenic climate change. In other words, an observed link between changes of severe thunderstorms and tornadoes and anthropogenic climate change has not been found.

Climate models have an equally difficult time projecting future convective storms. Thunderstorms have a short duration in time and cover a small area. The latest IPCC report summarizes this situation as "There is significant uncertainty about projected regional changes in tornadoes, hail, and lightning due to limited analysis of simulations". Currently, scientists' understanding of the effect of climate change on severe convective storms has the lowest confidence of any weather phenomena.

15.3 – Approaches for Dealing with Climate Change

Carbon dioxide concentrations in the atmosphere are directly affected by human activities. Atmospheric CO_2 concentrations adjust to human emissions of CO_2 over long time scales, spanning from decades to millennia. Estimates are that CO_2 resides in the atmosphere between 50 and 150 years before re-entering the carbon cycle elsewhere. The persistence of warming is longer than the atmospheric lifetime of CO_2 and other GHGs, owing in large part to the ocean. Climate change resulting from anthropogenic CO_2 emissions is unlikely to reverse in our

lifetimes. The world is committed to some degree of warming and associated climate change resulting from the emissions to date.

Climate change is a difficult problem to solve because our modern society was built with fossil fuel burning as an energy source. We still depend strongly on fossil fuel energy for everything from driving our cars and washing our laundry to charging our cell phones and heating our homes. Thus, the challenge is to decarbonize our economy. Because climate change is a global dilemma, most of the globe needs to agree on methods to deal with it. Hence, the reason for the Kyoto Protocol, the Paris Agreement, and other international efforts.

Three proactive approaches are discussed when trying to deal with climate change. These approaches are not mutually exclusive and can simultaneously be taken.

1. **Mitigation** is to reduce emissions.
2. **Adaptation** is to plan for the impacts and build for resiliency.
3. **Geoengineering** is to deliberately manipulate the climate system.

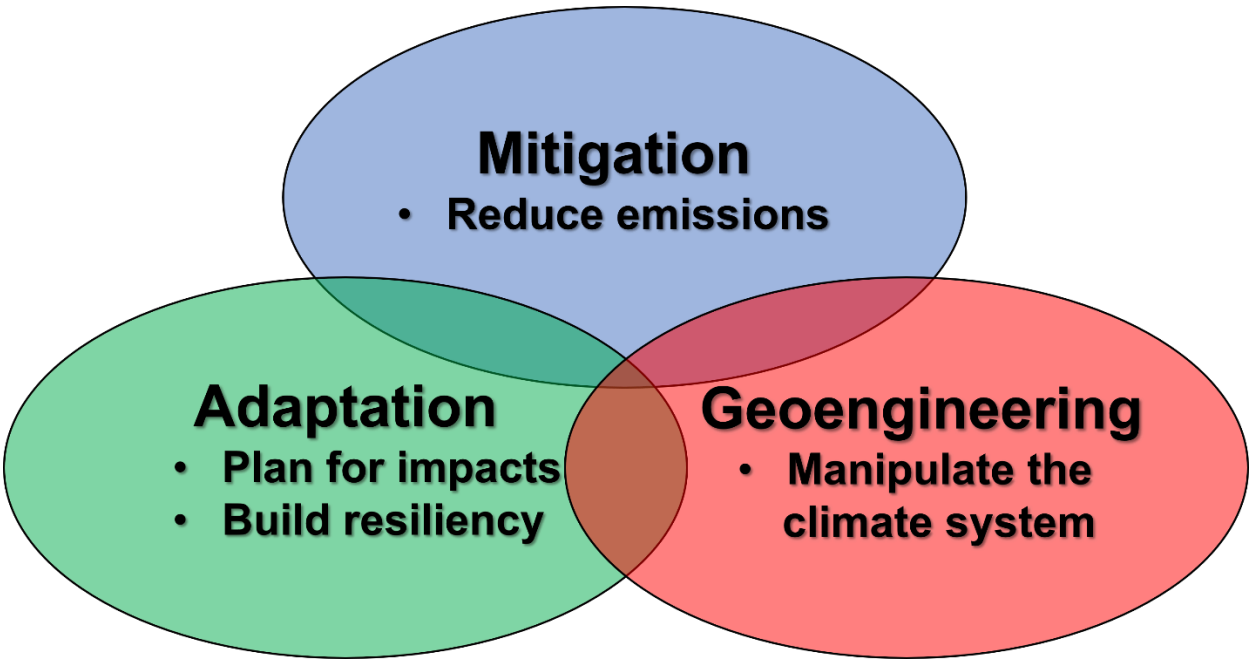

Reducing emissions is somewhat like preventing disease—exercise, eat well, and don't smoke. Adaptation is more like managing illness—take medicine to cope with symptoms and alleviate problems. Geoengineering is a little like organ transplantation—best avoided if at all possible but potentially better than nothing.

Each category consists of a broad family of options. In some cases, the boundaries between categories become a bit fuzzy. For example, efforts to reduce emissions might increase adaptive capacity and vice versa. Many experts characterize geoengineering approaches as mitigation or adaptation rather than as a separate category. However, the unique aspects of geoengineering merit a distinct category.

15.3.1 – Mitigation

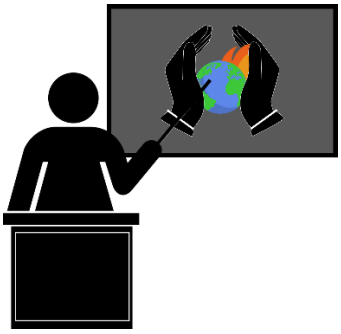

By reducing emissions, mitigation reduces society's future contributions to greenhouse gas concentrations in the atmosphere. Less emissions would reduce the changes to climate, and thereby increase the chances that any resulting societal impacts are manageable. Mitigation might also confer secondary benefits unrelated to climate change. For example, reducing emissions of greenhouse gases would likely reduce oil consumption and some traditional forms of air pollution. Using less oil would lessen a country's dependence on foreign oil and improve public health.

Unfortunately, mitigation has potential downsides. Mitigation actions could cause excessive energy prices or the premature retirement of capital equipment. Similarly, efforts to reduce emissions could lead to adverse secondary consequences. For example, policies to promote biofuel production could lead to inefficient uses of land, water, or agricultural crops. The use of biofuels can also exacerbate air pollution or degrade water quality.

Approaches to reducing emissions fall into several categories.

1. Pass regulations that set minimum energy-efficiency standards for cars or appliances or that prohibit the use of inefficient products.
2. Establish policies to encourage conservation of energy through public awareness campaigns, or subsidize climate-friendly choices.
3. Establish policies to fund the creation and deployment of low-emitting technologies like wind and solar energy or nuclear power.
4. Put a price on greenhouse gas emissions to encourage reductions.

All these approaches have much in common because emission prices and quantities are linked through market transactions. Common names given to these approaches are command and control regulations, carbon tax, and a cap-and-trade system. In each case, policymakers must determine the initial price or allowed quantity of emissions and how the price or quantity changes over time. Higher prices or lower quantities translate into larger, faster emission reductions, but may trigger larger price increases for energy and transportation.

Lastly, mitigation does not immediately reverse greenhouse gas concentrations. Carbon dioxide concentrations will take many decades to adjust to pre-industrial levels naturally even if emissions are curtailed immediately.

15.3.2 – Adaptation

Adaptation involves planning, building resilience, and improving society's capacity to recover from climate impacts. This approach helps reduce damages and disruptions from climate change. Additionally, adaptation may resolve threats already present from routine and severe weather events or from other natural hazards. A community will be able to handle threats regardless of what causes them, which is an important side benefit of efforts to build adaptive capacity.

Implementing adaptation policies successfully may require detailed consideration of location-specific factors, because climate change impacts will vary geographically. As a result, more centralized policy responses at the national or international level may be less effective for adaptation than for mitigation or geoengineering.

Nevertheless, centralized regulations have the potential to promote adaptive capacity by altering floodplain development, management of coastal zones, and insurance practices in ways that broadly account for climate change impacts. Similarly, more centralized approaches to disaster relief efforts, the establishment and design of wildlife reserves, and management of water and agricultural resources might be necessary for reducing some vulnerabilities to climate change.

Centralized adaptation policies can also support local and regional efforts. For example, a centralized repository could provide information and technical expertise about climate change vulnerabilities and response options. Alternatively, national and international policymakers could provide financial incentives for local adaptation planning and implementation. The goal of such efforts is to ensure that decision makers who best understand the local context also benefit from lessons learned in other areas.

15.3.3 – Geoengineering

Geoengineering refers to the deliberate, often global-scale manipulations of the climate system. Geoengineering might help lower greenhouse gas concentrations in the atmosphere, partially counteract the warming influence of increasing greenhouse gas concentrations, address specific climate change impacts, or offer desperation strategies in the event that abrupt, catastrophic, or otherwise unacceptable climate change impacts become evident.

However, the complexity of the climate system makes it challenging for scientists to fully identify and quantify the potential consequences associated with geoengineering. This approach could cause unintended and adverse consequences. Some of these consequences might even inadvertently compound rather than alleviate the dangers associated with climate change.

Even to the extent that the consequences of geoengineering could be well characterized, they would almost certainly differ between countries and individuals. This disparity raises complex legal, ethical, diplomatic, and national security. Furthermore, speculation on geoengineering's potential as a desperation strategy could distract from mitigation and adaptation efforts that may have a higher probability of contributing positively.

Nevertheless, two categories of geoengineering are most prevalent in scientific and policy discussions: solar radiation management and carbon removal and sequestration. Figure 15-18 illustrates the multitude of possible geoengineering methods.

The proposals for carbon dioxide removal and sequestration include:

a. fertilizing the ocean,
b. adding minerals to increase the ocean's alkalinity and enhance its ability to dissolve carbon dioxide,
c. accelerating the weathering of silicate rocks that can draw in atmospheric CO_2 when they dissolve in water,

d. directly capturing CO_2 from the air by chemical means,
e. building biomass-based power plants with carbon capture and storage capabilities, and
f. reforesting or planting new forests.

Solar radiation management aims to reflect more of the incoming sunlight back into space. These ideas include:

g. deploying space mirrors,
h. injecting aerosols into the stratosphere,
i. seeding marine clouds to make them more reflective,
j. brightening the ocean surface with microbubbles,
k. growing more reflective crops, and
l. whitening rooftops.

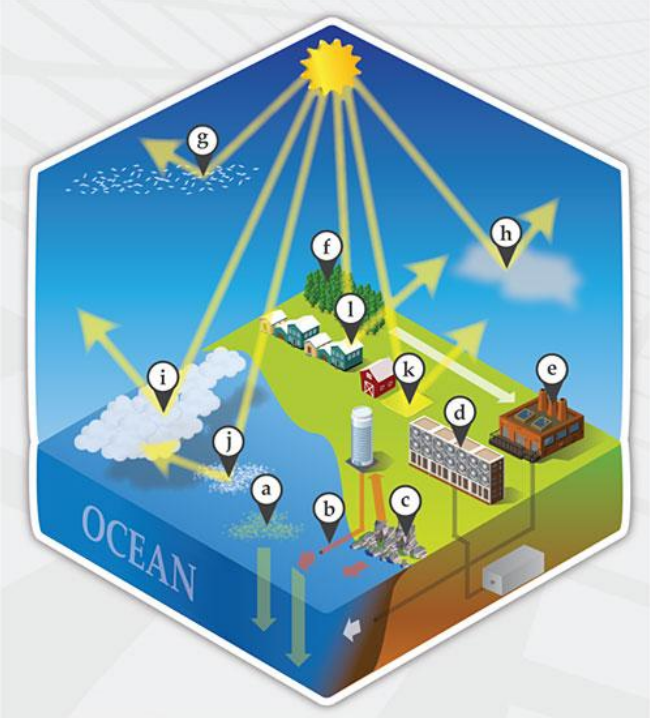

Figure 15-18: Illustration with the possible geoengineering methods. Proposals for carbon dioxide removal and sequestration are a-f. Incoming solar radiation management are g-l.

Chapter 15 Review Questions

1. What is necessary for reliably attributing an extreme weather event to anthropogenic climate change?
2. Rank weather events from highest to lowest in scientists' confidence that a specific weather event can be attributed to anthropogenic climate change.
3. What is the likelihood that human influence is the main contributor to the increase in heat waves and the decrease in cold waves?
4. What is the confidence level that humans have influenced changes in meteorological, hydrological, and agricultural droughts?
5. What is the projected increase in heavy precipitation per degree Celsius of global warming?
6. What is the confidence level that changes in the climate are influencing high river flows (floods) on the global scale?
7. Explaine the observed changes associated with hurricanes?
8. What are the climate model projections concerning hurricanes?
9. What are the climate model projections concerning extratropical (midlatitude) cyclones?
10. How have wildfire frequency and size changed since the 1980s?
11. What observed changes in severe convective storms can be attributed to anthropogenic climate change?
12. What are the three approaches for dealing with climate change, and briefly describe each.
13. What are four categories for reducing emissions.
14. List pros and cons associated with a mitigation approach to climate change.
15. Describe an adaptation approach to climate change.
16. Select two geoengineering approaches that may be reasonable to implement, and describe why these two approaches are feasible.

Chapter 16 – America's Climate Choices

Overview

This chapter is the shortest one in the book, and the topic covered is how do we deal with climate change? A topic in which a single solution or approach is not available to resolve it. Additionally, climate change is a political topic which leads to highly emotional responses from many people. Given this situation, this chapter explores the challenges associated with making decisions about climate change, discusses a possible framework for moving forward, and key elements in deciding what to do. The perspective used in this module is from a viewpoint of the United States as a whole, rather than what an individual person should do. However, many decisions the United States makes will affect individuals in this country and elsewhere.

Chapter objectives:

1. Understand that a single approach for resolving climate change is not possible.
2. Describe key elements needed for a country to make good climate choices.

16.1 – The Unique Challenges of Climate Change

The difficulty of developing sound strategies for responding to climate change, and of building public support for such strategies, stems in part from the inherent complexity of the issue. Some of this complexity relates to the physical science of climate change. However, understanding and responding to climate change also raises many social, economic, ethical, and political challenges.

There are complex linkages among emissions, concentrations, climate changes, and impacts. Projecting future climate change requires understanding numerous linkages among human activities, greenhouse gas (GHG) emissions, changes in atmospheric composition, the response of the climate system, and impacts on human and natural systems. The basic links in this chain are well understood, but some elements are much less so. As a result, the outcomes of actions to reduce emissions or to reduce the vulnerabilities of human and natural systems must often be presented in probabilistic or qualitative terms, rather than as certain predictions.

Lack of certainty about the details of future climate change is not a good justification for no action. People routinely take actions despite imperfect or incomplete knowledge about the future in situations, such as buying home insurance, saving for retirement, or planning business strategies. Likewise, people use probability data from weather forecasts to decide if they should take an umbrella to work, move a scheduled outdoor event indoors, or cancel a ball game.

There are significant time lags in the climate system. Climate change takes very long time periods (decades to millennia) for some aspects of the system to respond fully to changes in atmospheric GHG concentrations. This situation is because the world's oceans can store a large amount of heat, and because impacts such as sea level rise and the melting of ice sheets can take several centuries or even millennia to be fully expressed. Some GHGs (such as methane) are removed from the atmosphere within about a decade, but CO_2 persists much longer. Thus, a failure to reduce GHG emissions in the near-term will "lock in" a certain amount of future climate change for decades, if not centuries, to come.

There are also significant time lags in human response systems. GHG emissions are to a large extent built into societal infrastructure (e.g., buildings, power plants, settlement and transportation patterns) and into human habits and organizational routines, few of which change quickly. Market incentives affecting capital investments leave little room for considering consequences on century or longer time scale. Nevertheless, making major reductions in GHG emissions and preparing to adapt to the effects of climate change will require many changes. Mitigation efforts will likewise require significant changes in consumer choices, travel behavior, and other individual and household level decisions. Overcoming the inertia of the status quo in advancing these sorts of transformations will pose challenges for government, industry, agriculture, and individual citizens alike.

Many factors complicate and impede public understanding of climate change. Public understanding of climate change is important because public opinion underpins policy and because the public—as consumers, employers, and community members—can initiate, implement, and support actions to reduce GHG emissions and encourage adaptation. Fully understanding climate change is a difficult task even for scientific experts using voluminous data and complex mathematical models. People who have less experience with quantitative data and less time to develop such detailed understanding must rely on other sources that may or may not provide trustworthy information.

There will inevitably be additional risks and surprises. The climate system and human institutions that are affected by climate are exceedingly complex; consequently, anticipating all changes that may occur is impossible. Among the potential surprises are that climate change turns out to be more manageable than current projections suggest. Likewise, climate change could have more severe impacts than the values in the current projections.

16.2 – A Framework for Making Climate Choices

Risk management involves deciding what to do in light of this imperfect information. Of course, one option is always to do nothing. Most everyone ignores some risks in daily life, and the United States might choose to give little attention to the risks associated with climate change. Uncertainty is, after all, usually a two-edged sword. Future climate-related risks could be less serious than currently thought, but it is also possible that they will be even more serious. Even the most aggressive possible response could not remove all potential risks, since the world is already committed to some degree of climate change as a result of GHG emissions to date.

Making climate choices thus involves managing risks that may be quite substantial and that cannot be eliminated, yet are often difficult to assess precisely. Making choices under such conditions can seem very difficult in the abstract, yet most people make such decisions every day. For instance, people decide how fast to drive, knowing that driving faster saves time but

also uses more gas (or electricity), increases the chances of a speeding ticket, makes an accident more likely, and makes the consequences of an accident more severe.

In the case of climate change, appropriate strategies for reducing risks will change over time in light of new information, and so too will investments in different types of action. Historically, humans have responded to changing environments by a process of muddling through; that is, by taking an ad hoc approach to decision making as choices arise. In the modern era, techniques and approaches have been developed that allow decision makers to think through complex issues systematically. One prominent approach is the precautionary principle, which emphasizes avoidance of potentially serious or irreversible environmental harm, even when scientific uncertainties may be substantial. At the other extreme is what might be called "staying the course," or not taking any action until the need for action is fully established and the consequences of any action are fully understood. Another common approach is cost-benefit analysis and other related instruments that attempt to weigh the potential outcomes of taking (or not taking) action using a common metric, usually dollars discounted to present values.

All of these approaches present serious drawbacks in the context of climate change. In muddling through, for instance, decisions are generally driven by immediate events and the lessons learned from one's most recent experiences. Such an approach makes it difficult to thoughtfully consider long-term consequences of climate-related decisions.

Analyses based on the precautionary principle or "staying the course" both reflect a substantial aversion to risk. In the case of the precautionary principle, the goal is to minimize risks of future adverse consequences of climate change with little regard for present costs. In the case of "staying the course", the goal is to minimize the risks of incurring costs from responding to climate change with little regard for the risks of climate change. These approaches do not provide a way to decide among competing goals or to deal systematically with uncertainty.

Cost-benefit analysis has been applied in many evaluations of climate change policy and can provide some useful insights in some contexts. But using cost-benefit analyses as a primary basis for making climate choices is problematic for a number of reasons. The most prominent reason is that many of the costs of climate change impacts are difficult or impossible to quantify.

Any approach for dealing with climate change must reduce risk potential, be feasible, cost effective, equitable, fair, robust, and involve international considerations. Ultimately, any choice involves weighing multiple criteria. Decision makers will differ in their judgments about which criteria are most important and in their methods for dealing with uncertainties. Even when it is possible to characterize how different response actions rank under the different criteria, this information may not necessarily point to a preferred action or strategy. The successful application of this approach requires broad-based continuous learning by the scientific community together with decision makers in the government, the private sector, and the general public.

16.3 – Key Elements in Making Climate Choices

A comprehensive and effective response to climate change requires a diverse set of actions that evolve with new information and understanding. This set of actions involves:

- Limiting the magnitude of climate change (mitigation).

- Reducing the vulnerability to climate change impacts (adaptation).
- Investing to expand options and improve climate choices.
- Engaging with the international community.

Limiting the magnitude of climate change requires stabilizing atmospheric greenhouse gas (GHG) concentrations, which in turn requires reducing emissions of these gases so that their emissions are no greater than the rate at which they are naturally removed from the atmosphere. The basic opportunities available for reducing GHG emissions include restricting or modifying activities that release GHGs (e.g., burning of fossil fuels), removing CO_2 from the waste stream of large point sources of emissions and sequestering it underground (carbon capture and storage). For example, by managing agricultural soils or forests to increase the rate at which they sequester carbon. In addition, GHG emissions could potentially be offset by enhancing the reflection of solar radiation back to space (solar radiation management), which together with some post-emission GHG management strategies is referred to as geoengineering.

Solid, quantitative goals for limiting the magnitude of climate change offer the benefit of allowing all parties involved to have a common sense of purpose and a clear metric against which to measure progress. Finding agreement on quantitative targets is, however, an inevitably contentious process, and a failure to reach consensus on such targets can become a barrier to moving ahead with meaningful actions. Progress is of course possible to proceed with meaningful actions to limit GHG emissions in the absence of universally accepted quantitative goals. Nonetheless, it is important to understand the different types of goals that are being actively debated at national and international levels.

At the international level, a commonly discussed goal is the tolerable increase in global average surface temperature relative to pre-industrial times. For any given global temperature goal, corresponding goals can then be derived for:

1. Atmospheric GHG concentrations that would give a reasonable chance of meeting the temperature goal,
2. Global GHG emissions limits that would give a reasonable chance of meeting those GHG concentration goals,
3. National GHG emission limits that would collectively achieve the needed global emission reductions.

These relationships are complicated by a variety of scientific uncertainties and value judgments.

The nation's efforts to reduce GHG emissions depend to a large degree on private sector investments and on the behavioral and consumer choices of individual households. In general, there are four major tool chests from which to select policies for driving GHG emission reductions:

- pricing of emissions by means of a tax or cap-and-trade system;
- mandates or regulations, which includes full-scale programs of controls on emitters (for example through the Clean Air Act);
- public subsidies through the tax code, appropriations, or loan guarantees; and
- providing information and education and promoting voluntary measures.

As a matter of political reality, a comprehensive carbon-pricing strategy of the sort described above may not be feasible in the near term. A strategy relying solely on other types of policies would involve higher costs, but would still encourage near-term emission reductions and reduce the need to make costly reductions later.

Even if substantial global GHG emissions reductions are achieved, human societies will need to adapt to some degree to reduce vulnerability to climate change impacts. Choosing to do nothing now and simply adapt to climate change as it occurs, perhaps by accepting losses, would be an imprudent choice for a number of reasons. Even moderate climate change will be associated with a wide range of impacts on both human and natural systems, and the possibility of severe climate change with a host of adverse outcomes cannot be ruled out. Moreover, as climate change progresses, unforeseen events may pose serious adaptation challenges for regions, sectors, and groups that may not now seem particularly vulnerable. Thus, the United States should take proactive actions to mobilize the nation's capacity to adapt to future climate changes. This dual-path strategy will reduce the risks of future climate-related damages more than pursuing either path alone.

Like the challenge of reducing GHG emissions, the challenge of adaptation will be with America for decades. Accordingly, efforts need to include not just formulating an initial national adaptation strategy, but also creating durable institutions that can revise and improve that strategy over time.

A sound strategy for managing climate-related risks requires sustained investments in developing new knowledge and new technological capabilities. Investing to expand options and improve choices includes basic climate-related research and pre-commercial technology development. Because private firms and individuals typically do not stand to benefit commercially from such efforts, this action will need to be taken at the governmental level.

Important questions remain unanswered. Continuing research aimed at increasing our understanding of climate change processes, enhancing our ability to predict climate change, and increasing our understanding of how people affected are all areas where additional information is needed. Answering these questions provides better options and choices to move forward.

International agreements to limit GHG emissions requires rigorous methods to accurately estimate these emissions, monitor their changes over time, and verify them with independent data. To help assure that such efforts are carried out with transparency, consistency, and proper quality assurance in all countries, there is a need for active U.S. participation in international efforts.

The United States has a strong interest in ensuring an effective global response to climate change, because significant emission reductions are needed from all major emitting countries. Everyone can be affected by climate change impacts occurring elsewhere, since all nations are linked by shared natural resources and financial trade systems.

Responding to the risks of climate change is an important challenge facing the world today. Unfortunately, there is no "magic bullet" for dealing with this issue. No single solution or set of actions that can eliminate the risks we face. Climate choices will involve political and value judgments by decision makers and individuals everywhere. These choices, however, must be informed by sound scientific analyses, and combined with a concerted effort to learn from experience.

Chapter 16 Review Questions

1. What challenges make responding to climate change difficult?
2. Is anticipating all the changes that may occur in the Earth's climate system achievable? Why or why not?
3. Why is "staying the course" not the best choice for climate change?
4. What actions does a comprehensive and effective response to climate change require?

References, OER, and Public Domain Materials Used

Cover page images:
Cracked ground image is under Creative Commons Attribution 2.0 Generic and available at https://commons.wikimedia.org/wiki/File:Ladakh,_India_(14687115252).jpg. No modifications.

Lightning picture is under Creative Commons Attribution-Share Alike 3.0 and available at https://commons.wikimedia.org/wiki/File:Lightning_Pritzerbe_01_(MK).jpg. No modifications.

Tropical forest is under Creative Commons Attribution 4.0 and available at https://commons.wikimedia.org/wiki/File:Palawan,_Tropical_jungle_rainforest.jpg. No modifications.

Exploring Weather and Climate © 2025 by Glen Sampson is licensed under CC BY-NC 4.0. To view a copy of this license, visit https://creativecommons.org/licenses/by-nc/4.0/.

1.1
Some material originated from Khan Academy. All Khan Academy content is available for free at www.khanacademy.org.

1.3
Prime meridian map is public domain and is found at https://commons.wikimedia.org/wiki/File:Primemeridian.jpg

Other map projections: Strebe, CC BY-SA 3.0 <https://creativecommons.org/licenses/by-sa/3.0>, via Wikimedia Commons

1.3.1
METEO3 Course Author: Steven Seman (Assistant Teaching Professor, Department of Meteorology and Atmospheric Science, College of Earth and Mineral Sciences, The Pennsylvania State University). Some portions adapted from original course materials by David Babb and Lee M. Grenci. Creative Commons license (cc By-NC-SA 4.0), https://creativecommons.org/licenses/by-nc-sa/4.0/, accessed 3-21-2021 / Modifications were to clip segments and reduce text volume.

NASA MODIS hawaii.jpg – Public domain from NASA at https://eoimages.gsfc.nasa.gov/images/imagerecords/82000/82975/hawaii_tmo_2014026_lrg.jpg

1.4
Time zones: Goran tek-en, CC BY-SA 4.0 <https://creativecommons.org/licenses/by-sa/4.0>, via Wikimedia Commons

1.4.1
METEO3 Course Author: Steven Seman (Assistant Teaching Professor, Department of Meteorology and Atmospheric Science, College of Earth and Mineral Sciences, The Pennsylvania State University). Some portions adapted from original course materials by David Babb and Lee M. Grenci. Creative Commons license (cc By-NC-SA 4.0), https://creativecommons.org/licenses/by-nc-sa/4.0/, accessed 3-21-2021 / Modifications were to clip segments and reduce text volume.

Surface weather plot: Created with public money and in the public domain. Link to this chart is https://www.ametsoc.org/amsedu/dstreme/images/sfc-reg.html. This link is real-time data and chart is updated throughout a day.

Compass rose: I, Andrew pmk, CC BY-SA 3.0 <http://creativecommons.org/licenses/by-sa/3.0/>, via Wikimedia Commons

Station model key: Created with public money and in the public domain. Link to this chart is https://cimss.ssec.wisc.edu/sage/meteorology/lesson4/stationWx_plots.htm

1.4.2
METEO3 Course Author: Steven Seman (Assistant Teaching Professor, Department of Meteorology and Atmospheric Science, College of Earth and Mineral Sciences, The Pennsylvania State University). Some portions adapted from original course materials by David Babb and Lee M. Grenci. Creative Commons license (cc By-NC-SA 4.0), https://creativecommons.org/licenses/by-nc-sa/4.0/, accessed 3-21-2021 / Modifications were to clip segments and reduce text volume.

1.4.3
COMET resources are available for educational use at https://www.meted.ucar.edu/about.php
TMI polar-orbiting imagery is available from NASA at https://gpm.nasa.gov/data
Current GOES satellite images are available at https://www.star.nesdis.noaa.gov/goes/
The enhancement scale for Band 13 is described at https://www.star.nesdis.noaa.gov/goes/sector_band.php?sat=G16&sector=car&band=13&length=12

1.5
Some text and composition percentages used from the public domain NWS Jetstream at https://www.weather.gov/jetstream/atmos_intro

air glow.jpg – from NASA (public domain) at https://www.nasa.gov/sites/default/files/thumbnails/image/iss064e053173.jpg

co2_data_mlo.jpb – from NOAA (public domain) at https://www.noaa.gov/news/global-carbon-dioxide-growth-in-2018-reached-4th-highest-on-record

ch4_trend_all_gl.png – from NOAA (public domain) at https://www.esrl.noaa.gov/gmd/ccgg/trends_ch4/

1.6
Pressure versus altitude.jpg - Credit: Laura Guerin, Source: CK-12 Foundation, License: CC BY-NC 3.0. At https://flexbooks.ck12.org/cbook/ck-12-middle-school-physical-science-flexbook-2.0/section/12.3/primary/lesson/air-pressure-and-altitude-ms-ps

Mercury barometer.png - METEO3 Course Author: Steven Seman (Assistant Teaching Professor, Department of Meteorology and Atmospheric Science, College of Earth and Mineral Sciences, The Pennsylvania State University). Some portions adapted from original course materials by David Babb and Lee M. Grenci. Creative Commons license (cc By-NC-SA 4.0), https://creativecommons.org/licenses/by-nc-sa/4.0/, accessed 3-21-2021 / No modification to image.

1.7
Atmospheric layer diagrams are found at https://www.nesdis.noaa.gov/news/peeling-back-the-layers-of-the-atmosphere and https://www.noaa.gov/jetstream/atmosphere/layers-of-atmosphere

Text material support from https://climate.nasa.gov/news/2919/earths-atmosphere-a-multi-layered-cake/

2.1
METEO3 Course Author: Steven Seman (Assistant Teaching Professor, Department of Meteorology and Atmospheric Science, College of Earth and Mineral Sciences, The Pennsylvania State University). Some portions adapted from original course materials by David Babb and Lee M. Grenci. Creative Commons license (cc By-NC-SA 4.0), https://creativecommons.org/licenses/by-nc-sa/4.0/, accessed 3-21-2021 / Modifications were to clip segments and reduce text volume.

2.1.2
Water boiling. Photography. Britannica ImageQuest Encyclopædia with annotation added. Only available for non-commercial, educational purposes.

Heat transfer in the atmosphere diagram found at https://www.weather.gov/jetstream/heat

2.1.3
Figures and portions of the text modified from these web sites.
NASA public domain at https://science.nasa.gov/ems/02_anatomy and https://imagine.gsfc.nasa.gov/science/toolbox/emspectrum1.html.
NOAA, NWS public domain at https://www.noaa.gov/jetstream/satellites/electromagnetic-waves and https://www.noaa.gov/jetstream/satellites/absorb

2.1.4
NASA at https://solarsystem.nasa.gov/resources/681/solar-system-temperatures/ for Earth's temperature.

NASA at https://asd.gsfc.nasa.gov/archive/mwmw/mmw_bbody.html for some details on the radiation laws.

METEO3 Course Author: Steven Seman (Assistant Teaching Professor, Department of Meteorology and Atmospheric Science, College of Earth and Mineral Sciences, The Pennsylvania State University). Some portions adapted from original course materials by David Babb and Lee M. Grenci. Creative Commons license (cc By-NC-SA 4.0), https://creativecommons.org/licenses/by-nc-sa/4.0/, accessed 3-21-2021 / No modifications to Figure 2-7.

2.1.5
NOAA, NWS public domain at https://www.noaa.gov/jetstream/satellites/absorb

WikiCommons and is found at https://commons.wikimedia.org/wiki/ File:Atmospheric_Transmission.png. is associated with the GNU Free Documentation License.

NASA public domain at https://imagine.gsfc.nasa.gov/science/toolbox/emspectrum1.html

2.2.1 through 2.2.4
COMET program diagram available for educational use. See https://www.meted.ucar.edu/about_legal.php.

Figure 2-12 from WikiCommons https://commons.wikimedia.org/wiki/File:AxialTiltObliquity.png

NASA at https://earthobservatory.nasa.gov/features/EnergyBalance/page2.php. Figure 2-13 modified to show atmosphere.

Solstice and equinox illustrations from WikiCommons CC BY-SA 2.0

Figure 2-17 is public domain from NASA at https://earthobservatory.nasa.gov/features/EnergyBalance/page3.php

2.3.1
Figure 2-18 from WikiCommons at https://commons.wikimedia.org/wiki/File:Solar_Spectrum.png

Figure 2-19 from WikiCommons at https://upload.wikimedia.org/wikipedia/commons/9/91/Single_cloud_in_the_sky_over_Stora_H%C3%A4stn%C3%A4s%2C_Gotland_2.jpg Modified to add arrows for incoming and outgoing and cropped the picture.

2.3.2
Figure 2-20 from the University of Illinois WW2010 Project at http://ww2010.atmos.uiuc.edu/(Gh)/guides/mtr/opt/mch/sct.rxml

Visible spectrum and cumulus cloud photo from WikiCommons at https://commons.wikimedia.org/wiki/File:Linear_visible_spectrum.svg and https://commons.wikimedia.org/wiki/File:Cumulus-humilis.jpg

Atmospheric window and clouds capturing heat found at https://www.weather.gov/jetstream/.

2.4 sections
Incoming equals outgoing radiation from NASA at https://earthobservatory.nasa.gov/features/EnergyBalance/page1.php.

Earth's energy balance diagrams from https://www.weather.gov/jetstream/energy.

Figure 2-29: Ice cube and water glass photos from Image Quest.

Figure 2-30: *Public domain picture from WikiCommons at* https://commons.wikimedia.org/wiki/File:Small_greenhouse_with_grapevines_escaping_-_side_view.jpg Modified with longwave, shortwave and convection arrows and labels.

METEO3 Course Author: Steven Seman (Assistant Teaching Professor, Department of Meteorology and Atmospheric Science, College of Earth and Mineral Sciences, The Pennsylvania State University). Some portions adapted from original course materials by David Babb and Lee M. Grenci. Creative Commons license (cc By-NC-SA 4.0), https://creativecommons.org/licenses/by-nc-sa/4.0/, accessed 3-21-2021 / Modifications were to clip segments and reduce text volume.

3.1
Portions of the text originally from NOAA, NWS document Space Weather – Storms from the Sun.

Portions of the text originally from a NASA web page at https://solarsystem.nasa.gov/solar-system/sun/in-depth/#:~:text=The%20Sun%2C%20like%20others%20stars,%25%20hydrogen%20and%2027.4%25%20helium.

Sunspot cycle graph is *public domain from NOAA, NWS at https://www.swpc.noaa.gov/products/solar-cycle-progression*

Solar flare and CME images from NASA.

Aurora photo is public domain picture from WikiCommons, and can be found at https://commons.wikimedia.org/wiki/File:Polarlicht_2.jpg

Most text in 3.1.4 taken from NOAA, NWS document Space Weather – Storms from the Sun.

3.2
Mt. Hood photo is public domain from WikiCommons at https://commons.wikimedia.org/wiki/File:Mount_Hood_reflected_in_Mirror_Lake,_Oregon.jpg Annotated with the pressure symbols (P1 and P2).

Aneroid barometer diagram is public domain from WikiCommons at https://commons.wikimedia.org/wiki/File:Aneroid_Barometer_(PSF).png

Surface weather map from NOAA, National Weather Service at https://www.wpc.ncep.noaa.gov/archives/web_pages/sfc/sfc_archive_maps.php?arcdate=05/09/2021&selmap=2021050912&maptype=usfntsfc

Tire photos from public domain images on WikiCommons. Flat tire from https://commons.wikimedia.org/wiki/File:Flat_Tire.JPG Normal tire from https://commons.wikimedia.org/wiki/File:Jaguar_XJ_Roulette_(7x15%22)_alloy_wheel.jpg

500 mb weather map is a public domain image from NOAA, NWS and available at https://www.spc.noaa.gov/obswx/maps/

Figure 3-15 Mercator map is public domain from WikiCommons at https://commons.wikimedia.org/wiki/File:Mercator-projection.jpg Added 500mb heights annotation.

Figure 3-16 is public domain from NOAA and generated at https://psl.noaa.gov/cgi-bin/data/narr/plotday.pl

Section 3.2.7 – Portions of the text from NOAA at https://scijinks.gov/coriolis/

Earth image illustrating without and with rotation is public domain Earth globe from NASA at https://ti.arc.nasa.gov/tech/cas/advanced-exploration-knowledge-networks/world-wind/screenshots/globe/

3.3
Section 3.3.1 maps clipped from public domain Mercator map on WikiCommons at https://commons.wikimedia.org/wiki/File:Mercator-projection.jpg Modified by adding text, lines, arrows and labels. The 500 mb map from NOAA, NWS and available at https://www.spc.noaa.gov/obswx/maps/ Modified with annotation.

Vertical air motion diagram is public domain at NOAA, NWS https://www.noaa.gov/jetstream/synoptic/origin-of-wind

Trough illustrations are public domain at NOAA, NWS https://www.noaa.gov/jetstream/upper-air-charts/verses and https://www.noaa.gov/jetstream/upper-air-charts/basic-wave-patterns

4.1 and 4.2
Water molecules in various states from WikiCommons at https://commons.wikimedia.org/wiki/File:Water_molecule_3D.svg https://commons.wikimedia.org/wiki/File:Water_molecule_3D_with-signs.svg and https://commons.wikimedia.org/wiki/File:H-Br%C3%BCcken_f%C3%BChren_im_Eis_zu_regelm%C3%A4%C3%9Figen_Anordnung_im_Eis-Meolek%C3%BCl_(Kalottenmodell).png

American Meteorological Society (AMS) Glossary of Meteorology found at https://glossary.ametsoc.org/wiki/Welcome used in definitions throughout this section.

Vapor Pressure and temperature graph used in section 4.2.1 by Roland Stull, LibreTexts is licensed under CC BY-NC-SA . https://geo.libretexts.org/Bookshelves/Meteorology/Book%3A_Practical_Meteorology_(Stull)/04%3A_Water_Vapor/4.00%3A_Vapor_Pressure_at_Saturation

Data in saturated mixing ratio table from http://www.atmo.arizona.edu/students/courselinks/fall12/atmo336/lectures/sec1/Saturation_Mixing_Ratio_Tables.htm These tables are readily available or can be calculated from an equation.

The COMET copyright is only for use as educational materials. See https://www.meted.ucar.edu/index.php for details.

4.3
Contrail photo is public domain from Wikimedia Commons at https://commons.wikimedia.org/wiki/File:Contrail.fourengined.arp.jpg

Shower photo is public domain from Wikimedia Commons at https://commons.wikimedia.org/wiki/File:Il_dolce_corpo_di_Deborah_(1968)_-_Carroll_Baker_(1).jpg The original image was cropped.

RH and radius droplet size graph from "Nucleation of Liquid Droplets" by Roland Stull, LibreTexts is licensed under CC BY-NC-SA . Found at https://geo.libretexts.org/Bookshelves/Meteorology/Book%3A_Practical_Meteorology_(Stull)/07%3A_Precipitation_Processes/7.02%3A_Nucleation_of_Liquid_Droplets

Portions of the text in section 4.3 from “The COMET Program” and is found at https://www.meted.ucar.edu/norlat/snow/micro_ice/1.1.crystal_growth.htm. This material can only be accessed once logged into the COMET web site.

4.4
Map of sounding sites is public domain from NOAA, NWS at https://www.noaa.gov/jetstream/upperair/radiosondes.

Stuve example data is available from the University of Wyoming at http://weather.uwyo.edu/upperair/sounding.html. Annotated to identify the saturated layer.

Mount Rainier photo is public domain from Wikimedia Commons at https://commons.wikimedia.org/wiki/File:Mount_Rainier_panorama_3.jpg. Modified to illustrate orographic lift and subsidence warming /drying.

Terrain and vegetation image in public domain and from NASA MODIS at https://visibleearth.nasa.gov/images/62176/oregon-and-washington. Annotation was added to illustrate the rain shadow.

Convergence diagram in the public domain from NOAA, NWS at https://www.noaa.gov/jetstream/synoptic/origin-of-wind. Thermals diagram is at https://www.noaa.gov/jetstream/upperair/parcel-theory. Both modified to add a cloud over the rising air.

Fair weather cumulus cloud photo is in the public domain from NOAA. Obtained from COMET.

4.5
Most of the material from 4.5.1 can be found at https://www.noaa.gov/jetstream/upperair/bowls.

Thunderstorm photo from from Wikimedia Commons at https://commons.wikimedia.org/wiki/File:08-30-2020_Cumululonimbus_cloud.jpg. Modified to add annotations.

5.1
Portions of the text and artist renditions of clouds are from NOAA, NWS at https://www.noaa.gov/jetstream/clouds/four-core-types-of-clouds and https://www.noaa.gov/jetstream/clouds/ten-basic-clouds. Additionally, portions of this material can be found at COMET.

NOAA's cloud library is found at https://www.photolib.noaa.gov/Collections/National-Weather-Service/Weather-Wonders/Cloudy-Days/emodule/658/egallery/26/epage/3

The NOAA , NWS material references these two sources:

- Howard, L. 1803. On the Modifications of Clouds. J. Taylor, London.
- World Meteorological Organization 1956. International Cloud Atlas. Volumes I and II.

Definitions are found in the American Meteorological Society Glossary of Meteorology found at https://glossary.ametsoc.org/wiki/Welcome

Satellite image of cumulus clouds near a lake shore is found at https://visibleearth.nasa.gov/images/92313/massive-amounts-of-rain-in-michigan/92313f and cumulonimbus clouds at https://earthobservatory.nasa.gov/images/146761/cloud-building-over-hainan

Advection fog image is in the public domain from NASA and is found at https://earthobservatory.nasa.gov/images/79119/another-foggy-day-in-san-francisco.

Radiation fog image is in the public domain from NASA and is found at https://modis.gsfc.nasa.gov/gallery/individual.php?db_date=2020-12-22.

5.2
Some figures and text from PennState Meteo 300 Fundamentals of Atmospheric Science, Lesson 5 Cloud Physics by William H. Brune. Under a Creative Commons 4.0 license and is found at https://www.e-education.psu.edu/meteo300/

Virga photo is a public domain image from NOAA, NWS and is on Wikimedia Commons at https://commons.wikimedia.org/wiki/File:Virga.jpg

Droplet collision and thunderstorm water states figures from "Collision and Collection" by Roland Stull, LibreTexts is licensed under CC BY-NC-SA and can be found at https://geo.libretexts.org/Bookshelves/Meteorology/Book%3A_Practical_Meteorology_(Stull)/07%3A_Precipitation_Processes/7.06%3A_Collision_and_Collection Modified by clipping out the image title at the top.

Water droplet splitting figure is a public domain diagram from NASA and can be found at https://gpm.nasa.gov/education/articles/shape-of-a-raindrop

Ice and water vapor pressure graph from COMET. Modified to add the "H" and "L".

Definitions from the American Meteorological Society Glossary of Meteorology which can be found at https://glossary.ametsoc.org/wiki/Welcome

Rime ice on tree and snow flakes photos are in the public domain from Wikimedia Commons at https://commons.wikimedia.org/wiki/File:Rime_ice_on_Tree_Near_Beryl_Spring_(31681079222).jpg and https://upload.wikimedia.org/wikipedia/commons/d/d1/Snowflake_H%C3%B3pihe_%28100962989%29.jpeg.

5.3
Anatomy of a river graphic from American Rivers Organization and is found at https://www.americanrivers.org/rivers/discover-your-river/river-anatomy/.

Portions of text from the USGS at https://www.usgs.gov/special-topic/water-science-school/science/surface-runoff-and-water-cycle?qt-science_center_objects=0#qt-science_center_objects.

North America watershed map is in the public domain from the USGS at https://www.usgs.gov/special-topic/water-science-school/science/watersheds-and-drainage-basins?qt-science_center_objects=0#qt-science_center_objects.

5.4
Stream gage illustrations, photos and large portions of the text are from the USGS at https://www.usgs.gov/special-topic/water-science-school/science/how-streamflow-measured?qt-science_center_objects=0#qt-science_center_objects. The USGS frequently changes their web pages so their links are very perishable.

Peachtree Creek hydrograph in the public domain from the USGS and is found at https://www.usgs.gov/special-topic/water-science-school/science/how-much-water-flows-during-a-storm?qt-science_center_objects=0#qt-science_center_objects.

Santa Cruz hydrograph from the USGS at
https://nwis.waterdata.usgs.gov/az/nwis/uv/?cb_00060=on&cb_00065=on&format=gif_default&site_no=09486500&period=&begin_date=2014-10-03&end_date=2014-10-13
5.5
Illustrations, photo and portions of the text are from the USGS and are found at https://www.usgs.gov/special-topic/water-science-school/science/floods-and-recurrence-intervals?qt-science_center_objects=0#qt-science_center_objects and https://www.usgs.gov/special-topic/water-science-school/science/high-water-marks-and-flooding?qt-science_center_objects=0#qt-science_center_objects.

Inundation maps from NOAA.

Portions of the text are from the USGS and are found at https://www.usgs.gov/special-topic/water-science-school/science/floods-things-know?qt-science_center_objects=0#qt-science_center_objects.

6.1
The American Meteorological Society Glossary of Meteorology was referred to for definitions and is found at https://glossary.ametsoc.org/wiki/Welcome

Surface weather map from the United Kingdom Met Office in England. These charts can be found at https://www.metoffice.gov.uk/weather/maps-and-charts/surface-pressure.

Microburst damage photo in public domain image from Wikimedia Commons at https://commons.wikimedia.org/wiki/File:Milford,_CT_2009-07-31_wind_damage_4.jpg

6.2
The American Meteorological Society Glossary of Meteorology was referred to for definitions and is found at https://glossary.ametsoc.org/wiki/Welcome

Earth heating imbalance image from " General Circulation" by Roland Stull, LibreTexts is licensed under CC BY-NC-SA and is found at https://geo.libretexts.org/Bookshelves/Meteorology/Book%3A_Practical_Meteorology_(Stull)/11%3A_General_Circulation
Modified the image by clipping a portion out. Earth image used is from NASA.

Portions of the text on single-cell model information from Open Geography Education by R. Adam Dastrup is licensed under a Creative Commons Attribution 4.0 International License at https://www.opengeography.org/ch-10-climatic-disasters.html

Circulation diagrams from COMET and contain their copyright.

Zonal and meridional satellite image from CIRA at Colorado State University which is at https://rammb-slider.cira.colostate.edu/?sat=goes-16&sec=full_disk&x=5292&y=11528&z=0&angle=0&im=12&ts=1&st=0&et=0&speed=130&motion=loop&maps%5Bborders%5D=white&lat=1&p%5B0%5D=geocolor&opacity%5B0%5D=1&pause=0&slider=-1&hide_controls=0&mouse_draw=0&follow_feature=0&follow_hide=0&s=rammb-slider&draw_color=FFD700&draw_width=6
Modified with arrows indicating flow direction.

Three-cell model image and portions of the text in 6.2.2 from NOAA, NWS and can be found at https://www.noaa.gov/jetstream/global/global-atmospheric-circulations Image was modified to add labels.

ITCZ precipitation image and portions of the text from NASA at https://gpm.nasa.gov/science/observing-itcz-imerg Modified the image to increase the precipitation key size.

Visible full disk satellite image in the public domain from CIMMS at https://rammb-slider.cira.colostate.edu/?sat=goes-17&sec=full_disk&x=6848&y=11520&z=0&angle=0&im=12&ts=1&st=0&et=0&speed=130&motion=loop&maps%5Bborders%5D=white&lat=0&p%5B0%5D=geocolor&opacity%5B0%5D=1&pause=20210609224031&slider=-1&hide_controls=0&mouse_draw=0&follow_feature=0&follow_hide=0&s=rammb-slider&draw_color=FFD700&draw_width=6
Modified to add annotation and moved CIMMS mark.

ITCZ cross section image is associated with Creative Common 4.0 Meteo3 Course, Author: Steven Seman (Assistant Teaching Professor, Department of Meteorology and Atmospheric Science, College of Earth and Mineral Sciences, The Pennsylvania State

University). Some portions adapted from original course materials by David Babb and Lee M. Grenci.and is available at https://www.e-education.psu.edu/meteo3/sites/www.e-education.psu.edu.meteo3/files/images/lesson11/hadley_cross_section_lidar.png

Mercator map of Africa from Wikimedia Commons at https://commons.wikimedia.org/wiki/File:Mercator-projection.jpg

Horse latitude text in 6.2.2 from NOAA at https://oceanservice.noaa.gov/facts/horse-latitudes.html

July and January mean sea-level pressure map are public domain from NOAA, NWS and are available at https://www.cpc.ncep.noaa.gov/products/precip/CWlink/climatology/Sea-Lvl-Pressure.shtml

The ITCZ seasonal location map is domain map from Wikimedia Common at https://commons.wikimedia.org/wiki/File:ITCZ_january-july.png

Mean 500 mb maps for the Northern Hemisphere are public domain from NOAA, NWS at https://www.cpc.ncep.noaa.gov/products/precip/CWlink/climatology/Height-500-NH.shtml Modified to add latitude circles and arrows.

Many single day 500 mb charts are public domain from https://mag.ncep.noaa.gov/model-guidance-model-area.php# Modified to add latitude circles and arrows to indicate wind.

6.3
6-10-21 500mb map – Public domain from https://mag.ncep.noaa.gov/model-guidance-model-area.php# Modified to add latitude circles and arrows to indicate wind.

Jet stream illustrations and portions of the text are public domain, and can be found at https://www.noaa.gov/jetstream/global/jet-stream

Rossby waves, longwave, and shortwaves illustrations are in the public domain, and can be found at https://www.noaa.gov/jetstream/upper-air-charts/longwaves-and-shortwaves

Additional information on atmospheric rivers can be found at https://psl.noaa.gov/arportal/about/

6.4
Several illustrations have the COMET copyright.

6.5 and 6.5.1
mP precipitation diagram from "Airmasses" by Roland Stull, LibreTexts is licensed under CC BY-NC-SA and found at https://geo.libretexts.org/Bookshelves/Meteorology/Book%3A_Practical_Meteorology_(Stull)/12%3A_Fronts_and_Airmasses/12.01%3A_Section_2-. Modified by changing Olympic Mtns to coastal mtns, removed Puget Sound, added Sierra Nevada Mtns, and removed the numbers used in the sample application.

The American Meteorological Society Glossary of Meteorology was referred to for definitions and is found at https://glossary.ametsoc.org/wiki/Welcome.

Text about the history of the Norwegian cyclone model and mature-frontal-configuration.png are from " Airmasses" by Roland Stull, LibreTexts is licensed under CC BY-NC-SA and is found at https://geo.libretexts.org/Bookshelves/Meteorology/Book%3A_Practical_Meteorology_(Stull)/12%3A_Fronts_and_Airmasses/12.01%3A_Section_2-. Cross section diagram from " Geostrophic Adjustment - Part 3" by Roland Stull, LibreTexts is licensed under CC BY-NC-SA and is found at https://geo.libretexts.org/Bookshelves/Meteorology/Book%3A_Practical_Meteorology_(Stull)/12%3A_Fronts_and_Airmasses/12.03%3A_Section_4-. Modified to remove theta symbols.

6.5.2 and 6.5.3
Front diagrams from The COMET Program and has their copyright embedded.

Front characteristics diagram from " Surface Fronts" by Roland Stull, LibreTexts is licensed under CC BY-NC-SA and can be found at https://geo.libretexts.org/Bookshelves/Meteorology/Book%3A_Practical_Meteorology_(Stull)/12%3A_Fronts_and_Airmasses/12.02%3A_Section_3-. Modified wind image to add “frontal zone”. Modified cloud image to remove squall line.

Front slope diagram is under Creative Commons 4.0, Meteo3 Course Author: Steven Seman (Assistant Teaching Professor, Department of Meteorology and Atmospheric Science, College of Earth and Mineral Sciences, The Pennsylvania State University). Some portions adapted from original course materials by David Babb and Lee M. Grenci. Material can be found at https://www.e-education.psu.edu/meteo3/l7_p6.html. Modified image to add cold air and warm air labels.

6.5.4
Front diagram from The COMET Program and has their copyright embedded.

Stationary frontal zone is under Creative Commons 4.0, Meteo3 Course Author: Steven Seman (Assistant Teaching Professor, Department of Meteorology and Atmospheric Science, College of Earth and Mineral Sciences, The Pennsylvania State University).

Some portions adapted from original course materials by David Babb and Lee M. Grenci. Material can be found at https://www.e-education.psu.edu/meteo3/l7_p6.html.

6.5.5
Front diagram from The COMET Program and has their copyright embedded.

Cold and warm occlusions and portions of the text are in the public domain from NOAA, NWS and can be found at https://www.noaa.gov/jetstream/wxmaps.

Occlusion clouds and precipitation diagram from "Occluded Fronts and Midtropospheric Fronts" by Roland Stull, LibreTexts is licensed under CC BY-NC-SA and is found at https://geo.libretexts.org/Bookshelves/Meteorology/Book%3A_Practical_Meteorology_(Stull)/12%3A_Fronts_and_Airmasses/12.05%3A_Section_6-. Clipped image to only use the cloud and precipitation portion.

6.5.6
Figures and portions of the text are in the public domain from NOAA, NWS and can be found at https://www.noaa.gov/jetstream/wxmaps.

7.1
Portions of the text are from " Cyclone Characteristics" by Roland Stull, LibreTexts is licensed under CC BY-NC-SA and is found at https://geo.libretexts.org/Bookshelves/Meteorology/Book%3A_Practical_Meteorology_(Stull)/13%3A_Extratropical_Cyclones/13.00%3A_Section_1-.

Bombogenesis terminology in the public domain from NOAA, NOS and is found at https://oceanservice.noaa.gov/facts/bombogenesis.html.

Images from The COMET Program have their copyright embedded.

Some images in section 7.1.5 are under Creative Commons 4.0, Meteo3 Course Author: Steven Seman (Assistant Teaching Professor, Department of Meteorology and Atmospheric Science, College of Earth and Mineral Sciences, The Pennsylvania State University). Some portions adapted from original course materials by David Babb and Lee M. Grenci and can be found at https://www.e-education.psu.edu/meteo3/l7_p7.html.

Figure 7-15 is public domain from NOAA and also available on the COMET website.

COMET storm track map modified by adding information for Hatteras Low and Nor'easter.

Lake effect diagram is from NOAA, NESDIS at https://www.nesdis.noaa.gov/about/k-12-education/ice-snow/what-lake-effect-snow, and satellite image from Colorado State University at https://www.cira.colostate.edu/, and the snow depth analysis from NOAA, NWS at https://www.nohrsc.noaa.gov/snowfall_v2/.

7.2
Image of Earth is public domain from NASA and Wikimedia Commons at https://commons.wikimedia.org/wiki/File:Earth_Eastern_Hemisphere.jpg.

7.3
Image are from the COMET program and have their copyright embedded.

All other images are in the public domain from federal government agencies: NWCG and NGDC within NOAA.

7.4
The American Meteorological Society Glossary of Meteorology was used as a reference for definitions and can be found at https://glossary.ametsoc.org/wiki/Welcome.

Monsoon location map – Reference is embedded in the image and is given here with more details.
Li, J. P., and Q. C. Zeng, 2005: A new monsoon index, its interannual variability and relation with monsoon precipitation. Climatic and Environmental Research, 10(3): 351-365.

Low-level NAM moisture is public domain from NOAA, NWS at https://www.weather.gov/twc/Monsoon.

NOAA publication was used for monsoon precipitation dates – The North American Monsoon. Reports to the Nation on our Changing Planet. NOAA/National Weather Service, August 2004.

Monthly 500 mb map are public domain from NOAA, NWS at https://www.weather.gov/twc/Monsoon.

Tucson-monthly-precip.png – Data from the NWS and can be found at https://www.weather.gov/twc/TucsonMonthlyNormalExtremes.

8.1
Portions of the text are in the public domain from NOAA, NWS and is found at https://www.noaa.gov/jetstream/lightning.

Lightning map is in public domain from NASA and can be found at https://earthobservatory.nasa.gov/images/2002/where-lightning-strikes

Lightning photo is in the public domain from NOAA and can be found on Wikimedia Commons at https://commons.wikimedia.org/wiki/File:Lightning_in_Dallas_2015.jpg.

NLDN sensor photo is in the public domain from NASA and can be found at https://ghrc.nsstc.nasa.gov/lightning/lightning_primer.html#.

GLM data examples are in the public domain from NOAA and CIRA, and have their logos embedded.

Charge distribution in a CB from Creative Commons: METEO3, Course Author: Steven Seman (Assistant Teaching Professor, Department of Meteorology and Atmospheric Science, College of Earth and Mineral Sciences, The Pennsylvania State University). Some portions adapted from original course materials by David Babb and Lee M. Grenci. Found at https://www.e-education.psu.edu/meteo3/l8_p4.html

Lightning formation steps and portions of the text are public domain and can be found at https://www.noaa.gov/jetstream/lightning/how-lightning-is-created/jetstream-max-lightning-process-keeping-in-step. Modified the images by adding labels.

Lightning striking a tree is in the public domain from NOAA, NWS and has their name embedded. This image is available from The COMET Program and was used on a lightning safety poster for years. Modified by adding labels.

Illustration of TLEs and red sprite photo are public domain from https://www.nssl.noaa.gov/education/svrwx101/lightning/types/.

Blue jet photo from Creative Commons 4.0, created by National Optical-Infrared Astronomy Research Laboratory on Mauna Kea, Hawaii. Can be found on Wikimedia Commons at https://commons.wikimedia.org/wiki/File:Red_sprite_blue_jet_NOIRLab.jpg.

Lightning safety graphs and pie charts in public domain from NOAA, NWS and can be found at https://www.weather.gov/media/safety/Analysis06-19.pdf.

8.2 to 8.2.2
Annual thunderstorm climatology map copyrighted and used with permission. Koehler, Thomas L. “Cloud-to-Ground Lightning Flash Density and Thunderstorm Day Distributions over the Contiguous United States Derived from NLDN Measurements: 1993–2018.” Monthly Weather Review, vol. 148, no. 1, 2019, pp. 313–332., https://doi.org/10.1175/MWR-D-19-0211.1.

A few portions of the text and illustrations are in the public domain from NOAA, NWS and can be found at https://www.noaa.gov/jetstream/thunderstorms/ingredients-for-thunderstorm and https://www.noaa.gov/jetstream/thunderstorms/life-cycle-of-thunderstorm and https://www.noaa.gov/jetstream/tstrmtypes.

TCU photo is a public domain image from NOAA and can be found at https://photolib.noaa.gov/Collections/National-Weather-Service/Weather-Wonders/Cloudy-Days/emodule/658/eitem/2554.

CB photo is a public domain image from NOAA and can be found at https://photolib.noaa.gov/Collections/National-Weather-Service/Weather-Wonders/Cloudy-Days/emodule/658/eitem/2553.

Anvil remnants photo is a public domain image from NOAA and can be found at https://photolib.noaa.gov/Collections/National-Weather-Service/Weather-Wonders/Cloudy-Days/emodule/658/eitem/2531.

The COMET Program images have their copyright embedded.

Mature basic thunderstorm illustrations are from Creative Commons " Thunderstorm Characteristics" by Roland Stull, LibreTexts is licensed under CC BY-NC-SA. Can be found at https://geo.libretexts.org/Bookshelves/Meteorology/Book%3A_Practical_Meteorology_(Stull)/14%3A_Thunderstorm_Fundamentals/14.00%3A_Section_1-. Modified to remove some labels.

Squall line radar image and portions of the text are public domain from NOAA, NSSL and can be found at https://www.nssl.noaa.gov/education/svrwx101/thunderstorms/types/.

MCC radar image is public domain from CIMMS, University of Wisconsin and can be found at https://cimss.ssec.wisc.edu/satellite-blog/archives/24506.

8.2.3
Artist rendition of a supercell is public domain from NOAA, NWS and can be found at https://www.noaa.gov/jetstream/tstrmtypes.

Supercell cross section is from Creative Commons " Thunderstorm Characteristics" by Roland Stull, LibreTexts is licensed under CC BY-NC-SA. Can be found at

https://geo.libretexts.org/Bookshelves/Meteorology/Book%3A_Practical_Meteorology_(Stull)/14%3A_Thunderstorm_Fundamentals/14.00%3A_Section_1-. Modified to remove Cu labels from flanking line, enhanced V-notch, added a V-notch label and removed beaver tail notation.

WER radar image is public domain from NOAA, NWS and can be found at https://www.spc.noaa.gov/faq/tornado/radscel.htm.

Hail formation diagram, size table and portions of the text on hail are public domain from NOAA, NWS and can be found at https://www.noaa.gov/jetstream/hail.

8.2.4
Outflow boundary image is in the public domain from NOAA, NWS and can be found at https://www.weather.gov/gid/29139.

Portions of derecho text and image are in public domain from NOAA, NWS and can be found at https://www.nssl.noaa.gov/education/svrwx101/thunderstorms/types/.

Microburst illustration is from The COMET Program and has their logo embedded.

Microburst hazard to aircraft diagram and the associated text are in the public domain from NOAA, NWS and can be found at https://www.noaa.gov/jetstream/wind_damage.

8.3
Portions of the text and images are public domain from NOAA, NWS and can be found at https://www.noaa.gov/jetstream/doppler/how-radar-works.

WSR-88D photos are in the public domain and originally from the NOAA photo library at https://photolib.noaa.gov/Collections.

Additional dual polarization information and animations in the public domain from NOAA, NWS at https://www.weather.gov/bmx/radar_dualpol.

8.4
Much of the information is in the public domain from NOAA, NWS and can be found at https://www.noaa.gov/jetstream/doppler. This link is to top level material with additional material available from this webpage.

Radar beam information is in the public domain from NOAA, NWS and can be found at https://www.noaa.gov/jetstream/radar-beams.

Images from The COMET Program have their logo embedded.

Beam blockage image is public domain originally from NOAA, NWS and was found at https://meted.ucar.edu (The COMET Program)

8.4.5
All images originated from The COMET Program. Bright band diagram was annotated with approximate dBZ changes.

9.1
Tornado picture in public domain from NOAA, NWS and can be found at https://www.nssl.noaa.gov/education/svrwx101/tornadoes/types/

Tornado probability maps in domain from NOAA, NWS and can be found at https://www.spc.noaa.gov/new/SVRclimo/climo.php?parm=allTorn

Annual tornadoes in each state, wind shear diagrams, mesocyclone top view and some portions of the text in the public domain from NOAA, NWS and can be found at https://www.noaa.gov/jetstream/thunderstorms/thunderstorm-hazards-tornadoes

Tornado shape diagram from Creative commons, " Tornadoes" by Roland Stull, LibreTexts is licensed under CC BY-NC-SA . Found at https://geo.libretexts.org/Bookshelves/Meteorology/Book%3A_Practical_Meteorology_(Stull)/15%3A_Thunderstorm_Hazards/15.03%3A_Section_4-

Rotation entrainment diagrams from Creative Commons, Steven Seman (Assistant Teaching Professor, Department of Meteorology and Atmospheric Science, College of Earth and Mineral Sciences, The Pennsylvania State University). Some portions adapted from original course materials by David Babb and Lee M. Grenci. Images can be found at https://www.e-education.psu.edu/meteo3/l9_p5.html and https://www.e-education.psu.edu/meteo3/l9_p9.html

QLCS image and animation is in the public domain from NOAA, NWS and can be found at https://www.nssl.noaa.gov/education/svrwx101/tornadoes/types/

The COMET Program illustrations have their copyright embedded.

Definition of dust devils is from the American Meteorological Society, Glossary of Meteorology which can be found at https://glossary.ametsoc.org/wiki/Dust_devil

Portions of the text on dust devils from The COMET Program and can be found at https://www.meted.ucar.edu/mesoprim/dust/print.php#page_5-5-0

Dust devil photo is in the public domain from NASA and is available on Wikimedia Commons at https://commons.wikimedia.org/wiki/File:Dust_devil.jpg

TVS radar products are in the public domain from NOAA, NWS and can be found at https://www.weather.gov/bmx/event_04272011ohatchee. Circles and arrows were added for easier analysis.

Tornado graphs and portions of the text are in the public domain from NOAA, NCDC, and NSSL. These graphs were originally on their web pages, but are now available in online databases.

9.2
Tropical storm basins from Creative Commons, " Intensity and Geographic Distribution" by Roland Stull, LibreTexts is licensed under CC BY-NC-SA . Can be found at https://geo.libretexts.org/Bookshelves/Meteorology/Book%3A_Practical_Meteorology_(Stull)/16%3A_Tropical_Cyclones/16.01%3A_Section_2-. Modified by adding numbers to the basins.

Tropical storm statistics originally from https://www.aoml.noaa.gov/physical-oceanography-division/.

Tropical storm fuel and size figures, hurricane diagram, Wilma eye replacement, and portions of the text are in the public domain from NOAA, NWS at https://www.noaa.gov/jetstream/tropical/tropical-cyclone-introduction and https://www.noaa.gov/jetstream/tropical/tropical-cyclone-introduction/tropical-cyclone-structure.

Average sea surface temperature maps are in the public domain from NOAA, NESDIS and can be found at https://www.ospo.noaa.gov/Products/ocean/sst/monthly_mean.html.
The COMET Program materials and have their copyright embedded.

Hot tower reproduction is in the public domain from NASA and can be found at https://svs.gsfc.nasa.gov/cgi-bin/details.cgi?aid=3413. Added “Hot Tower” annotation.

Storm designations and category definitions are from NOAA, NHC and can be found at https://www.nhc.noaa.gov/aboutgloss.shtml#t and https://www.nhc.noaa.gov/aboutsshws.php.

Hurricane track and monthly area maps are in the public domain from NOAA, NWS and can be found at https://www.nhc.noaa.gov/climo/.

Hurricane landfall wind graph and Gulf Stream image are in the public domain from NOAA, NWS/NHC and NOS. Gulf Stream image can be found at https://oceanservice.noaa.gov/education/tutorial_currents/media/supp_cur04d.html.

Hurricane wind shear image is in the public domain and is originally from NASA MODIS.

Portions of the hurricane name text are from the WMO website.

9.3
Portions of the text are in the public domain from NOAA, NWS and can be found at https://www.noaa.gov/jetstream/tc-hazards.

Hurricane Andrew damage photos are in the public domain from NOAA, NWS/NHC and can be found at https://www.nhc.noaa.gov/1992andrew.html.

Right-front quadrant illustration is in the domain from NOAA, AOML and can be found at https://www.aoml.noaa.gov/hrd-faq/#tc-rightside-winds. Annotation added.

Hurricane Katrina tornado map is in the public domain from NOAA, NWS and can be found at https://www.weather.gov/media/publications/assessments/Katrina.pdf.

Atlantic hurricane deaths chart is in the public domain from NOAA, NWS and can be found at https://www.noaa.gov/education/resource-collections/weather-atmosphere/hurricanes.

Photo of house that survived Hurricane Ike is in the public domain from NOAA, NWS and can be found at https://www.noaa.gov/jetstream/tc-potential.

Precipitation associated with Hurricane Katrina is in the public domain from NOAA, NWS and can be found at https://www.wpc.ncep.noaa.gov/tropical/rain/katrina2005.html.

Tropical storms images associated with Arizona are in the public domain from NOAA, NWS and can be found at https://www.weather.gov/twc/tropical.

Photo of NHC building is in the public domain from NOAA, NWS and can be found at https://www.nhc.noaa.gov/aboutintro.shtml.

Hurricane Earl forecast is in the public domain from NOAA, NWS and can be found at https://www.nhc.noaa.gov/archive/2010/EARL_graphics.shtml.

Atlantic and Pacific Ocean tropical storm counts are in the public domain from NOAA, NWS and can be found at https://www.nhc.noaa.gov/climo/.

10.1
Refraction and reflection diagram is from Creative Commons, " Ray Geometry" by LibreTexts and is licensed under CC BY-NC-SA. The diagram can be found at https://geo.libretexts.org/Bookshelves/Meteorology/Book%3A_Practical_Meteorology_(Stull)/22%3A_Atmospheric_Optics/22.00%3A_New_Page.

Diffraction diagram and portions of the text from WW2010, Department of Atmospheric Sciences at the University of Illinois at Urbana-Champaign, and can be found at http://ww2010.atmos.uiuc.edu/(Gh)/guides/mtr/opt/mch/diff.rxml.

Definitions from the American Meteorological Society Glossary of Meteorology, which can be found at https://glossary.ametsoc.org/wiki/Welcome.

Corona around the Moon photo from Creative Commons 2.0 generic license; photo is by BLM Nevada and can be found on Wikimedia Commons at https://commons.wikimedia.org/wiki/File:Moon_corona_Over_Black_Rock_City_(21031738371).jpg.

Glory photo is Creative Commons 3.0; photo is by Reeftraveler and can be found on Wikimedia Commons at https://commons.wikimedia.org/wiki/File:Glory_of_the_Pilot.jpg.

Light spectrum diagram is in the public domain and can be found on Wikimedia Commons at https://commons.wikimedia.org/wiki/File:Linear_visible_spectrum.svg.

Definitions from the American Meteorological Society Glossary of Meteorology which can be found at https://glossary.ametsoc.org/wiki/Welcome.

Highway inferior mirage photo from Britannica ImageQuest, Encyclopædia Britannica, 25 May 2016. https://quest.eb.com/search/107_293899/1/107_293899/cite.

Green flash and superior mirage diagrams from Creative Commons, "Mirages" by LibreTexts is licensed under CC BY-NC-SA and can be found at https://geo.libretexts.org/Bookshelves/Meteorology/Book%3A_Practical_Meteorology_(Stull)/22%3A_Atmospheric_Optics/22.6%3A_Mirages. Modified to adjust the labeling.

Green flash photo is from Creative Commons 3.0; photo by Brocken Inaglory and can be found on Wikimedia Commons at https://commons.wikimedia.org/wiki/File:GreenFlash.jpg.

Superior mirage photo is from Creative Commons by Juris Sennikovs and is on Wikimedia Commons at https://commons.wikimedia.org/wiki/File:Superior_mirage_of_ships_in_the_Gulf_of_Riga.jpg.

Rainbow illustrations and portions of the text – Creative Commons, “Liquid-Drop Optics” by LibreTexts is licensed under CC BY-NC-SA and can be found at https://geo.libretexts.org/Bookshelves/Meteorology/Book%3A_Practical_Meteorology_(Stull)/22%3A_Atmospheric_Optics/22.01%3A_New_Page. The cloud was rainbow observers diagram was modified.

Secondary rainbow photo by Alexis Dworsky from Creative Commons photograph, and can be found on Wikimedia Commons at https://commons.wikimedia.org/wiki/File:Regenbogen_%C3%BCber_dem_Lipno-Stausee.JPG.

Halo photo is in the public domain and can be found on Wikimedia Commons at https://commons.wikimedia.org/wiki/File:Halo_L%C3%A4ngental.jpg.

Sun pillar diagram and small portions of the text - Creative Commons, “Ice Crystal Optics” by LibreTexts is licensed under CC BY-NC-SA and can be found at https://geo.libretexts.org/Bookshelves/Meteorology/Book%3A_Practical_Meteorology_(Stull)/22%3A_Atmospheric_Optics/22.02%3A_New_Page.

Sun dogs photo is in the public domain from the U.S. Fish and Wildlife Service and can be found at https://commons.wikimedia.org/wiki/File:Sundog_at_Minnesota_Valley_National_Wildlife_Refuge_(11225736674).jpg.

Sun pillar photo is in the public domain from NOAA and can be found on Wikimedia Commons at https://commons.wikimedia.org/wiki/File:Sun_pillar5_-_NOAA.jpg.

South Pole photograph is in the public domain from NOAA and can be found on Wikimedia Commons at https://commons.wikimedia.org/wiki/File:Sun_halo_optical_phenomenon_edit.jpg.

10.2
Agency logos are from the agency's websites.

NOAA supercomputer photo is public domain from https://www.nco.ncep.noaa.gov/.

Target with arrows figures and portions of the text – Creative Commons; Steven Seman (Assistant Teaching Professor, Department of Meteorology and Atmospheric Science, College of Earth and Mineral Sciences, The Pennsylvania State University). Some portions adapted from original course materials by David Babb and Lee M. Grenci. This information is found at https://www.e-education.psu.edu/meteo3/node/2284.

Spaghetti diagrams are in the public domain from NCEP, NOAA and the current charts can be found at https://psl.noaa.gov/map/images/ens/ens.html.

Many definitions originated from the American Meteorological Society Glossary of Meteorology which can be found at https://glossary.ametsoc.org/wiki/Welcome.

Forecast types figure is in the public domain from the NWS, NOAA and can be found for any city at https://www.weather.gov/.

Seasonal outlook classes of probabilities reference – Public domain from NWS, NOAA and can be found at https://www.cpc.ncep.noaa.gov/products/predictions/long_range/tools.html.

Seasonal outlook maps – Public domain from NWS, NOAA and the current versions can be found at https://www.cpc.ncep.noaa.gov/products/predictions/long_range/seasonal.php?lead=1.

11.1
Definitions reference is the American Meteorological Society Glossary of Meteorology which can be found at https://glossary.ametsoc.org/wiki/Climate.

Map of Koppen-Geiger classification over North America - Creative Commons; Beck, H.E., Zimmermann, N. E., McVicar, T. R., Vergopolan, N., Berg, A., & Wood, E. F. - "Present and future Köppen-Geiger climate classification maps at 1-km resolution". Nature Scientific Data. DOI:10.1038/sdata.2018.214. Map modified to fit on a page better.

Portions of the text are in the public domain from NOAA and can be found at https://www.climate.gov/maps-data/primer/how-do-scientists-classify-different-types-climate.

Global maps of average temperature and seasonal temperature range are Creative Commons; Image created by Robert A. Rohde for Berkeley Earth and can be found on Wikimedia Commons at https://commons.wikimedia.org/wiki/File:Annual_Average_Temperature_Map.png and https://commons.wikimedia.org/wiki/File:Average_Seasonal_Temperature_Range.png.

Three-cell illustration is in the public domain from NOAA, NWS and can be found at https://www.noaa.gov/jetstream/global/jet-stream.

All climographs are from Climograph images - Laura Zepner, Pierre Karrasch, Felix Wiemann & Lars Bernard (2020) ClimateCharts.net – an interactive climate analysis web platform, International Journal of Digital Earth, DOI: 10.1080/17538947.2020.1829112. Images can be obtained at https://climatecharts.net/.

Data source used for the climograph images is public domain from NWS, NOAA at https://www.ncdc.noaa.gov/ghcnm.

Ocean currents image is in the public domain from NOAA, NWS and can be found at https://www.noaa.gov/jetstream/ocean/circulations/jetstream-max-major-ocean-currents.

Tucson, Arizona temperature data maintained by the University of Utah, Department of Atmospheric Sciences and can be found at https://mesowest.utah.edu/.

Death Valley photo is available from Arizona State University and can be found at https://wmo.asu.edu/content/northern-hemisphere-highest-temperature. See https://wmo.asu.edu/content/world-lowest-temperature for information on the world's coldest temperature.

11.2
Clouds and temperature illustration is in the public domain from NOAA, NWS and can be found at https://www.noaa.gov/jetstream/atmosphere/energy,

Seattle, WA temperature data maintained by the University of Utah, Department of Atmospheric Sciences and can be found at https://mesowest.utah.edu/.

Heat Index chart and portions of the text are in the public domain from NOAA, NWS and can be found at https://www.weather.gov/safety/heat-index.

Wind Chill chart and portions of the text are in the public domain from NOAA, NWS and can be found at https://www.weather.gov/safety/cold-wind-chill-chart.

11.3
U.S. Koppen-Geiger climate groups and portions of the text are in the public domain from NOAA, NWS and can be found at https://www.noaa.gov/jetstream/global/climate-zones. Changed map annotation for consistency.

Portions of the text – Creative Commons, Physical Geography and Natural Disasters by R. Adam Dastrup, MA, GISP is licensed under a Creative Commons Attribution-NonCommercial-ShareAlike 4.0 International License. Can be found at https://slcc.pressbooks.pub/physicalgeography/chapter/10-3/.

World Koppen Classification map – Creative Commons, by Peel, M. C., Finlayson, B. L., and McMahon, T. A. (University of Melbourne). Can be found on Wikimedia Commons at https://commons.wikimedia.org/wiki/File:World_K%C3%B6ppen_Classification.svg.

11.3.1
Koppen_World_Map_A – Creative Commons, by Peel, M. C., Finlayson, B. L., and McMahon, T. A. (University of Melbourne). Can be found on Wikimedia Commons at https://commons.wikimedia.org/wiki/File:Koppen_World_Map_A.png.

Portions of the text – Creative Commons, Physical Geography and Natural Disasters by R. Adam Dastrup, MA, GISP is licensed under a Creative Commons Attribution-NonCommercial-ShareAlike 4.0 International License. Can be found at https://slcc.pressbooks.pub/physicalgeography/chapter/10-3/.

World map for locations – Public domain by Styx and can be found on Wikimedia Commons at https://commons.wikimedia.org/wiki/File:World_location_map.svg. Annotated with city location.

Climograph images - Laura Zepner, Pierre Karrasch, Felix Wiemann & Lars Bernard (2020) ClimateCharts.net – an interactive climate analysis web platform, International Journal of Digital Earth, DOI: 10.1080/17538947.2020.1829112. Images can be obtained at https://climatecharts.net/

Gabon photo – Creative Commons by Wikifrédéric and can be found on Wikimedia Commons at https://commons.wikimedia.org/wiki/File:V%C3%A9g%C3%A9tationLibreville.jpg.

Mumbai photo – Public domain photo by Rudolphfurtado and can be found on Wikimedia Commons at https://commons.wikimedia.org/wiki/File:Skyscrapers_of_Mumbai_viewed_from_%27National_Park,_Borivili.jpg.

11.3.2
Koppen_World_Map_B – Creative Commons, by Peel, M. C., Finlayson, B. L., and McMahon, T. A. (University of Melbourne). Can be found on Wikimedia Commons at https://commons.wikimedia.org/wiki/File:Koppen_World_Map_B_new2.png

Portions of the text – Creative Commons, Physical Geography and Natural Disasters by R. Adam Dastrup, MA, GISP is licensed under a Creative Commons Attribution-NonCommercial-ShareAlike 4.0 International License. Can be found at https://slcc.pressbooks.pub/physicalgeography/chapter/10-3/.

World-map for locations – Public domain by Styx and can be found on Wikimedia Commons at https://commons.wikimedia.org/wiki/File:World_location_map.svg Annotated with city location.

Climograph images - Laura Zepner, Pierre Karrasch, Felix Wiemann & Lars Bernard (2020) ClimateCharts.net – an interactive climate analysis web platform, International Journal of Digital Earth, DOI: 10.1080/17538947.2020.1829112. Images can be obtained at https://climatecharts.net/.

Yuma photo – Public domain from the U.S. Customs and Border Protection and can be found on Wikimedia Commons at https://commons.wikimedia.org/wiki/File:Border_wall_in_the_Imperial_Sand_Dunes,_20_miles_west_of_Yuma,_AZ_-_48537286061.jpg.

Prescott photo – Creative Commons by Mike Peel (www.mikepeel.net) and can be found on Wikimedia Commons at https://commons.wikimedia.org/wiki/File:Prescott_National_Forest_region_2015_017.jpg.

11.3.3
Koppen-Geiger_Map_C.png – Creative Commons by Beck, Hylke E.; E. Zimmermann, Niklaus; McVicar, Tim R.; Vergopolan, Noemi; Berg, Alexis; Wood, Eric F. (2018): "Present and future Köppen-Geiger climate classification maps at 1-km resolution". Nature Scientific Data. DOI:10.1038/sdata.2018.214. Can be found on Wikimedia Commons at https://commons.wikimedia.org/wiki/File:Koppen-Geiger_Map_C_present.svg.

World locations map – Public domain by Styx and can be found on Wikimedia Commons at https://commons.wikimedia.org/wiki/File:World_location_map.svg Annotated with city location.

Climograph images - Laura Zepner, Pierre Karrasch, Felix Wiemann & Lars Bernard (2020) ClimateCharts.net – an interactive climate analysis web platform, International Journal of Digital Earth, DOI: 10.1080/17538947.2020.1829112. Images can be obtained at https://climatecharts.net/ Modified Jerusalem (Csa) climograph because it was labeled incorrectly as Cfa.

Jerusalem photo – Public domain and can be found on Wikimedia Commons at https://commons.wikimedia.org/wiki/File:Jerusalem-1712855.jpg .

New Orleans photo – Public domain by Carol M. Highsmith and can be found on Wikimedia Commons at https://commons.wikimedia.org/wiki/File:City_Park,_New_Orleans,_Louisiana_LCCN2011630537.tif.

Dublin photo – Public domain and can be found on Wikimedia Commons at https://commons.wikimedia.org/wiki/File:Fairview_015.JPG.

11.3.4
Portions of the text – Creative Commons, Physical Geography and Natural Disasters by R. Adam Dastrup, MA, GISP is licensed under a Creative Commons Attribution-NonCommercial-ShareAlike 4.0 International License. Can be found at https://slcc.pressbooks.pub/physicalgeography/chapter/10-3/.

Koppen World Map D group – Creative Commons, by Peel, M. C., Finlayson, B. L., and McMahon, T. A. (University of Melbourne). Can be found on Wikimedia Commons at https://commons.wikimedia.org/wiki/File:Koppen_World_Map_D.png.

World map for locations – Public domain by Styx and can be found on Wikimedia Commons at https://commons.wikimedia.org/wiki/File:World_location_map.svg. Annotated with city location.

Climograph images - Laura Zepner, Pierre Karrasch, Felix Wiemann & Lars Bernard (2020) ClimateCharts.net – an interactive climate analysis web platform, International Journal of Digital Earth, DOI: 10.1080/17538947.2020.1829112. Images can be obtained at https://climatecharts.net/.

New York City photo – Public domain and can be found on Wikimedia Commons at https://commons.wikimedia.org/wiki/File:Central_Park,_New_York_City,_2006_006.jpg. Cropped the date/time off the bottom of the photo.

11.3.5 and 11.3.6
Portions of the text – Creative Commons, Physical Geography and Natural Disasters by R. Adam Dastrup, MA, GISP is licensed under a Creative Commons Attribution-NonCommercial-ShareAlike 4.0 International License. Can be found at https://slcc.pressbooks.pub/physicalgeography/chapter/10-3/.

Koppen classificaton world map E group – Public domain by みれでぃー and can be found on Wikimedia at https://commons.wikimedia.org/wiki/File:Koppen_classification_worldmap_E.png

World map locations – Public domain by Styx and can be found on Wikimedia Commons at https://commons.wikimedia.org/wiki/File:World_location_map.svg. Annotated with city location.

Climograph images - Laura Zepner, Pierre Karrasch, Felix Wiemann & Lars Bernard (2020) ClimateCharts.net – an interactive climate analysis web platform, International Journal of Digital Earth, DOI: 10.1080/17538947.2020.1829112. Images can be obtained at https://climatecharts.net/. Corrected the “EF” label on the climograph.

Barrow photo – Creative Commons with no author. Image can be found on Wikimedia Commons at https://commons.wikimedia.org/wiki/File:Barrow_AK.jpg. Note this Wikimedia entry has malicious links on its page so tread with care.

Vostok photo – Public domain from NASA and can be found at https://visibleearth.nasa.gov/images/82672/flying-over-vostok-station/82675l.

Map and climate division references are in the public domain from NCDC, NOAA and can be found at https://www.ncdc.noaa.gov/monitoring-references/maps/us-climate-divisions.php.

12.1
General pollution definitions from the American Meteorological Society, Glossary of Meteorology which can be found at https://glossary.ametsoc.org/wiki/Welcome.

EPA definitions and descriptions of the agency roles are in public domain from the EPA and can be found at https://www.epa.gov/indoor-air-quality-iaq/technical-overview-volatile-organic-compounds and https://www.epa.gov/regulatory-information-topic/regulatory-and-guidance-information-topic-air.

2022 pollution the growth graphs are in the public domain from the EPA and can be found at https://www.epa.gov/air-trends/air-quality-national-summary.

12.1.1
Most of the text is public domain from the EPA and can be found at https://www.epa.gov/co-pollution.

Data for CO Air Quality graph – Public domain from the EPA and can be found at https://www.epa.gov/air-trends/carbon-monoxide-trends.

Global CO maps are public domain from NASA and can be found at https://earthobservatory.nasa.gov/global-maps/MOP_CO_M.

12.1.2
Most of the text is in the public domain from the EPA and can be found at https://www.epa.gov/lead-air-pollution/basic-information-about-lead-air-pollution#how and https://www.epa.gov/lead/learn-about-lead#effects.

Data for Lead Air Quality graph is inn the public domain from the EPA and can be found at https://www.epa.gov/air-trends/lead-trends.

12.1.3
Portions of the text are in the public domain from the EPA and can be found at https://www.epa.gov/no2-pollution.

Portions of the text are available for educational use from UCAR and can be found at https://scied.ucar.edu/learning-zone/air-quality/nitrogen-oxides.

Aerial View of Photochemical Smog over Mexico City is from Creative Commons by Fidel Gonzalez and can be found on Wikimedia Commons at https://commons.wikimedia.org/wiki/File:AerialViewPhotochemicalSmogMexicoCity_2.jpg.

Data for NO2 Air Quality graph is in the public domain from the EPA and can be found at https://www.epa.gov/air-trends/nitrogen-dioxide-trends.

12.1.4
Portions of the text are available for educational use from UCAR and can be found at https://scied.ucar.edu/learning-zone/air-quality/sulfur-oxides.

Portions of the text are in the public domain from the EPA and can be found at https://www.epa.gov/so2-pollution.

Data for SO_2 Air Quality graph is in the public domain from the EPA and can be found at https://www.epa.gov/air-trends/sulfur-dioxide-trends.

12.1.5
Portions of the text and the ozone illustration are in the public domain from the EPA, and can be found at https://www.epa.gov/ground-level-ozone-pollution/ground-level-ozone-basics#wwh.

Portions of the text are available for educational use from UCAR and can be found at https://scied.ucar.edu/learning-zone/air-quality/ozone.

Data for Ozone Air Quality graph is in the public domain from the EPA, and can be found at https://www.epa.gov/air-trends/ozone-trends.

12.1.6 and 12.1.7
Portions of the 12.1.6 text and PM scale illustration are in the public domain from the EPA and can be found at https://www.epa.gov/pm-pollution/particulate-matter-pm-basics and https://www.epa.gov/pm-pollution/health-and-environmental-effects-particulate-matter-pm.

Data for PM air quality graphs are in the public domain from the EPA and can be found at https://www.epa.gov/air-trends/particulate-matter-pm25-trends and https://www.epa.gov/air-trends/particulate-matter-pm10-trends.

NASA aerosol optical depth image and a portion of the description text are in the public domain at https://earthobservatory.nasa.gov/global-maps/MODAL2_M_AER_OD.

Portions of the 12.1.7 text and AQI table in the public domain from the EPA, and can be found at https://www.airnow.gov/aqi/aqi-basics/.

12.2
Portions of the text are in the public domain from NWS, NOAA and can be found at https://www.weather.gov/wrn/summer-article-clearing-the-air.

Portions of the text are available for educational use from UCAR and can be found at https://scied.ucar.edu/learning-zone/air-quality/how-weather-affects-air-quality.

Normal and inversion pollution graphics are available from the Canadian Government for non-commercial use and can be found at https://www.canada.ca/en/environment-climate-change/services/air-pollution/issues/smog-causes-effects/winter.html.

Acid rain pathway diagram, pH scale, and portions of the text are in the public domain from the EPA and can be found at https://www.epa.gov/acidrain/what-acid-rain and https://www.epa.gov/acidrain/effects-acid-rain.

Acidity precipitation maps are in the public domain from the EPA and can be found at https://www3.epa.gov/castnet/precipchem.html.

12.3
Definition reference – American Meteorological Society, Glossary of Meteorology which can be found at https://glossary.ametsoc.org/wiki/Welcome.

Heat island diagrams and portions of the text are in the public domain from the EPA, and can be found at https://www.epa.gov/heatislands/learn-about-heat-islands and https://www.epa.gov/heatislands/measuring-heat-islands and https://www.epa.gov/heatislands/heat-island-cooling-strategies.

Providence heat island imagery is in the public domain from NASA and can be found at https://earthobservatory.nasa.gov/images/47704/urban-heat-islands.

Phoenix heat island information reference - "Urban Heat Island Research in Phoenix, Arizona: Theoretical Contributions and Policy Applications." Bulletin of the American Meteorological Society, vol. 93, no. 4, 2012, https://doi:10.1175/BAMS-D-11-00011.1.

NYC satellite images are in the public domain from NASA and can be found at https://landsat.visibleearth.nasa.gov/view.php?id=6800.

Impervious surface area study is in the public domain from NASA and can be found at https://www.earthobservatory.nasa.gov/images/86440/vegetation-limits-city-warming-effects.

12.4
Portions of the text are from "Introduction to Climate Science" by Andreas Schmittner is licensed under a Creative Commons Attribution-NonCommercial 4.0 International License.

Portions of the text and the carbon cycle diagram are in the public domain from NASA and DOE, and can be found at https://earthobservatory.nasa.gov/features/CarbonCycle.

Portions of the text, photosynthesis/respiration, and air-sea CO2 exchange diagrams are from Creative Commons by Drs. Timothy Bralower and David Bice, Pennsylvania State University and can be found at https://www.e-education.psu.edu/earth103/.

Tree carbon diagram from Creative Commons by Valerie Martin, TERC and can be found at https://serc.carleton.edu/eslabs/carbon/1a.html.

Phytoplankton references are in the public domain from NOS, NOAA and can be found at https://oceanservice.noaa.gov/facts/phyto.html.

White Cliffs of Dover photo is from Creative Commons by Immanuel Giel and can be found on Wikimedia Commons at https://commons.wikimedia.org/wiki/File:White_Cliffs_of_Dover_02.JPG.

Forest changes map is from M. C. Hansen, et al. "High-Resolution Global Maps of 21st-Century Forest Cover Change." Science, vol. 342, no. 6160, Nov. 2013, pp. 850–853.

12.5
All the images and portions of the text are in the public domain from the EIA (Energy Information Administration) and can be found at:
https://www.eia.gov/energyexplained/us-energy-facts/
https://www.eia.gov/energyexplained/renewable-sources/
https://www.eia.gov/energyexplained/what-is-energy/sources-of-energy.php
https://www.eia.gov/energyexplained/units-and-calculators/british-thermal-units.php
https://www.eia.gov/energyexplained/us-energy-facts/images/consumption-by-source-and-sector.pdf
https://www.eia.gov/energyexplained/energy-and-the-environment/where-greenhouse-gases-come-from.php
https://www.eia.gov/tools/faqs/faq.php?id=82&t=11

GHG infographic is in the public domain from the EPA and can be found at https://cfpub.epa.gov/ghgdata/inventoryexplorer/.

13.1
Portions of the text and several images are from "Introduction to Climate Science" by Andreas Schmittner, and is licensed under a Creative Commons Attribution-NonCommercial 4.0 International License.

Portions of the text are in the public domain from NCDC, NOAA and can be found at https://www.ncei.noaa.gov/news/what-is-paleoclimatology.

Colorized pollen image is in the public domain from Dartmouth Electron Microscope Facility and can be found on Wikimedia Commons at https://commons.wikimedia.org/wiki/File:Misc_pollen_colorized.jpg.

Tree ring photo is in the public domain from Wikimedia Commons and can be found at https://commons.wikimedia.org/wiki/File:Tree_rings_pattern_(Unsplash).jpg. Cropped the original to display the tree rings better.

Portions of the text are in the public domain from NCDC, NOAA and can be found at https://www.ncei.noaa.gov/news/how-can-tree-rings-teach-us-about-climate, and https://www.ncei.noaa.gov/news/how-can-corals-teach-us-about-climate, and https://www.ncei.noaa.gov/news/how-can-pollen-teach-us-about-climate.

Coral pictures are in the public domain from NOAA and can be found at https://coralreef.noaa.gov/gallery/welcome.html.

Carbon-14 decay graph is from the USGS and can be found at https://va.water.usgs.gov/va123/3age-D.html.

Bee photograph is from Creative Commons by Forest Wander and can be found on Wikimedia Commons at https://commons.wikimedia.org/wiki/File:Macro_Bee_Pollen.jpg.

13.2 and 13.2.1
Images and portions of the text are in the public domain from NASA and can be found at https://earthobservatory.nasa.gov/features/Paleoclimatology_OxygenBalance.

“Introduction to Climate Science” by Andreas Schmittner is licensed under a Creative Commons Attribution-NonCommercial 4.0 International License, and is used as a reference.

Portions of the text are in the public domain from NCDC, NOAA and can be found at https://www.ncei.noaa.gov/news/how-can-ice-teach-us-about-climate.

Reference used here and is available for educational use from UCAR at https://scied.ucar.edu/learning-zone/how-climate-works/investigating-past-climates.

Antarctic ice core site map are in the public domain and originated from DOE. These maps were originally from https://cdiac.ess-dive.lbl.gov/trends/co2/ice_core_co2.html but are no longer present.

Ice core with bubble photo is public domain from NASA and can be found at https://climate.nasa.gov/news/2616/core-questions-an-introduction-to-ice-cores/.

Ice layers photo credit: Kendrick Taylor, Chief Scientist, WAIS Divide Ice Core Project Research Professor, Desert Research Institute, Nevada System of Higher Education and can be found at https://www.nsf.gov/news/news_images.jsp?cntn_id=118546&org=NSF.

Volcanic layer photo credit: Heidi Roop, NSF and can be found at https://icecores.org/about-ice-cores.

13.2.2
Images and portions of the text are available for educational use from UCAR and can be found at https://scied.ucar.edu/learning-zone/how-climate-works/investigating-past-climates.

Text on sedimentary rocks and evaporites is from Creative Commons by Drs. Timothy Bralower and David Brice at Penn State University, course Earth 103, and can be found at https://www.e-education.psu.edu/earth103/node/991.

13.2.3
Geologic column table is in the public domain from the NPS and can be found at https://www.nps.gov/subjects/geology/time-scale.htm. Modified by clipping North American Events column.

Graphs and most of the text – Public domain from NOAA and can be found at https://www.climate.gov/news-features/climate-qa/whats-hottest-earths-ever-been.

paleo-CO2 graphs - IPCC AR6 WG1 Physical Science Basis, Figure 2.3 page 183 which can be found at https://www.ipcc.ch/report/ar6/wg1/. Formal citation is: Gulev, S. K., P. W. Thorne, J. Ahn, F. J. Dentener, C. M. Domingues, S. Gerland, D. Gong, D. S. Kaufman, 26 H. C. Nnamchi, J. Quaas, J. A. Rivera, S. Sathyendranath, S. L. Smith, B. Trewin, K. von Shuckmann, R. S. 27 Vose, 2021, Changing State of the Climate System. In: Climate Change 2021: The Physical Science Basis. 28 Contribution of Working Group I to the Sixth Assessment Report of the Intergovernmental Panel on Climate 29 Change [Masson-Delmotte, V., P. Zhai, A. Pirani, S. L. Connors, C. Péan, S. Berger, N. Caud, Y. Chen, L. 30 Goldfarb, M. I. Gomis, M. Huang, K. Leitzell, E. Lonnoy, J. B. R. Matthews, T. K. Maycock, T. Waterfield, 31 O. Yelekçi, R. Yu and B. Zhou (eds.)].

13.2.4
LGM illustration is public domain from NOAA and can be found at https://www.climate.gov/news-features/climate-qa/whats-coldest-earths-ever-been.

Ice age graph over billions of years is from the Utah Geological Survey which is part of the State of Utah government. Graphs and can be found at https://geology.utah.gov/map-pub/survey-notes/glad-you-asked/ice-ages-what-are-they-and-what-causes-them/. This graph was modified from several sources including Dynamical Paleoclimatology: Generalized Theory of Global Climate Change, 2002, by Barry Saltzman.

Antarctic ice core graphs from Introduction to Climate Science by Andreas Schmittner is licensed under a Creative Commons Attribution-NonCommercial 4.0 International License. Modified the graphs by highlighting the interglacial periods. These graphs used the following references:

- Jouzel, J., et al. (2007) Orbital and millennial Antarctic climate variability over the past 800,000 years, Science, 317 (5839), 793-796, doi:10.1126/science.1141038.
- Lüthi, D., et al. (2008), High-resolution carbon dioxide concentration record 650,000-800,000 years before present, Nature, 453(7193), 379-382, doi:10.1038/nature06949.
- Lisiecki, L. E., and M. E. Raymo (2005), A Pliocene-Pleistocene stack of 57 globally distributed benthic δ18O records, Paleoceanography, 20(1), PA1003, doi:10.1029/2004pa001071.

13.3.1
Portions of the text from UCAR and can be found at https://scied.ucar.edu/learning-zone/how-climate-works/how-volcanoes-influence-climate.

Aerosol satellite images and stratosphere photos are public domain from NASA and are available at https://earthobservatory.nasa.gov/images/1510/global-effects-of-mount-pinatubo, and https://earthobservatory.nasa.gov/features/AstronautPinatubo/astronaut_pinatubo2.php.

13.3.2
Portions of the text is in the public domain from NASA and can be found at https://earthobservatory.nasa.gov/images/7122/chilly-temperatures-during-the-maunder-minimum.

Maunder Minimum graph is in the public domain from NASA and can be found at https://solarscience.msfc.nasa.gov/images/ssn_yearly.jpg.

Proxy-based temperature graph is in the public domain from NASA and can be found at https://earthobservatory.nasa.gov/features/GlobalWarming/page3.php.

Portions of the text and temperature/solar activity graph is in the public domain from NASA and can be found at https://science.nasa.gov/earth/climate-change/there-is-no-impending-mini-ice-age/.

13.3.3 through 13.3.5
Large portions of the text and all the images - Introduction to Climate Science by Andreas Schmittner is licensed under a Creative Commons Attribution-NonCommercial 4.0 International License. Modified the ETP-cycles image to highlight the interglacial periods.

Image and portions of the text – Public domain form the USGS and can be found at https://pubs.usgs.gov/gip/dynamic/historical.html.

Portions of the text – Available for educational use from UCAR and can be found at https://scied.ucar.edu/learning-zone/how-climate-works/how-geosphere-rocks-climate.
Polar vortex images and portions of the text are in the public domain from NOAA and can be found at https://www.climate.gov/news-features/understanding-climate/understanding-arctic-polar-vortex, and https://www.climate.gov/news-features/event-tracker/how-polar-vortex-related-arctic-oscillation.

13.4
Ocean currents image is public domain from NOAA and can be found at https://oceanexplorer.noaa.gov/facts/currents.html.

Thermocline image and portions of the text are public domain from NOS, NOAA and can be found at https://oceanservice.noaa.gov/facts/thermocline.html.

Ocean gyres map is available for educational use from the NGA and COMET program and has their copyright embedded.

Thermohaline Circulation map is public domain from NASA and can be found on Wikimedia Commons at https://commons.wikimedia.org/wiki/File:Thermohaline_Circulation_2.png.

Portions of the text are available for educational use from UCAR and can be found at https://scied.ucar.edu/video/ocean-move-thermohaline-circulation.

Upwelling illustration and portions of the text are in the public domain from NOS, NOAA and can be found at https://oceanservice.noaa.gov/education/tutorial_currents/03coastal4.html.

Equatorial Pacific Ocean data is in the public domain from PMEL, NOAA and can be found at https://www.pmel.noaa.gov/tao/drupal/disdel/,

Walker circulation images and portions of the ENSO text are public domain from NOAA, NWS and can be found at https://www.noaa.gov/jetstream/tropical/enso, https://www.noaa.gov/jetstream/tropical/enso/enso-patterns, https://www.noaa.gov/jetstream/enso_impacts.

SST anomaly maps (Figure 13-42) are public domain from ESRL, NOAA but are no longer on the web.

Portions of the PDO text and pdo_warm_cold.png are in the public domain from PSL, NOAA and can be found at https://psl.noaa.gov/pdo/. Labeled negative and positive phases on the image.

Portions of the PDO text are from COMET and can be found in Introduction to Tropical Meteorology, Chapter 4. When logged into METED the link is https://www.meted.ucar.edu/tropical/textbook_2nd_edition/navmenu.php?tab=5&page=3.1.0.

Portions of the PDO text and PDO graph are in the public domain from NCDC, NOAA and can be found at https://www.ncdc.noaa.gov/teleconnections/pdo/.

Reference used for AMO text can be found on the UK Met Office Climate Dashboard website at https://www.metoffice.gov.uk/hadobs/monitoring/climate_modes.html#:~:text=AMO%20%2D%20Atlantic%20Multidecadal%20Oscillation,they%20are%20colder%20than%20average.

Historical AMO animation with AMO Index (Figures 13-47 and 13-48) are in the public domain from NASA and can be found at https://svs.gsfc.nasa.gov/4895.

14.1 – 14.1.2
Land use change simulation and maps along with their descriptions - Pielke, Roger A., et al. “Land’s Complex Role in Climate Change.” Physics Today, vol. 69, no. 11, 1 Nov. 2016, pp. 40–46., https://doi:10.1063/pt.3.3364.

IPCC AR6 WG1 Summary for Policy Makers, Figure SPM.2 on page 8 which can be found at https://www.ipcc.ch/report/ar6/wg1/. The formal citation is: IPCC, 2021: Summary for Policymakers. In: Climate Change 2021: The Physical Science Basis. Contribution of Working Group I to the Sixth Assessment Report of the Intergovernmental Panel on Climate Change [Masson-Delmotte, V., P. Zhai, A. Pirani, S.L. Connors, C. Péan, S. Berger, N. Caud, Y. Chen, L. Goldfarb, M.I. Gomis, M. Huang, K. Leitzell, E. Lonnoy, J.B.R. Matthews, T.K. Maycock, T. Waterfield, O. Yelekçi, R. Yu, and B. Zhou (eds.)]. In Press.

GHG-concentrations graphs are in the public domain from the U.S. Global Change Research Program (multiple government agencies) and can be found at https://nca2009.globalchange.gov/2000-years-greenhouse-gas-concentrations/index.html.

Portions of the cloud feedback text are from: Introduction to Climate Science by Andreas Schmittner is licensed under a Creative Commons Attribution-NonCommercial 4.0 International License.

Global temperature anomalies graph is in the public domain from NCDC, NOAA and can be found at https://www.ncdc.noaa.gov/sotc/global/202306.

Some portions of the 14.1.2 text is in the public domain from NOAA and can be found at https://www.climate.gov/news-features/understanding-climate/climate-change-global-temperature. The content of this web page does change consistently.

14.1.3
Ocean heat images and portions of the text are in the public domain from NOAA and can be found at https://www.climate.gov/news-features/understanding-climate/climate-change-ocean-heat-content.

Changes in Earth’s heat content – From the IPCC AR6 WG1, Chapter 9 – page 244. The formal citation is: Fox-Kemper, B., H. T. Hewitt, C. Xiao, G. Aðalgeirsdóttir, S. S. Drijfhout, T. L. Edwards, N. R. Golledge, M. Hemer, R. E. Kopp, G. Krinner, A. Mix, D. Notz, S. Nowicki, I. S. Nurhati, L. Ruiz, J-B. Sallée, A. B. A. Slangen, Y. Yu, 2021, Ocean, Cryosphere and Sea Level Change. In: Climate Change 2021: The Physical Science Basis. Contribution of Working Group I to the Sixth Assessment Report of the Intergovernmental Panel on Climate Change [Masson-Delmotte, V., P. Zhai, A. Pirani, S. L. Connors, C. Péan, S. Berger, N. Caud, Y. Chen, L. Goldfarb, M. I. Gomis, M. Huang, K. Leitzell, E. Lonnoy, J. B. R. Matthews, T. K. Maycock, T. Waterfield, O. Yelekçi, R. Yu and B. Zhou (eds.)]. Cambridge University Press. In Press.

Ocean acidification and portions of the text are in the public domain from NOAA and can be found at https://www.noaa.gov/education/resource-collections/ocean-coasts/ocean-acidification and https://www.pmel.noaa.gov/co2/file/Hawaii%20Carbon%20Dioxide%20Time-Series.

Oscillation paragraph reference - IPCC AR6 WG1 Summary for Policy Makers, Human Influence on Modes of Climate Variability, Chapter 3, section 3.7 which can be found at https://www.ipcc.ch/report/ar6/wg1/. The formal citation is: Eyring, V., N.P. Gillett, K.M. Achuta Rao, R. Barimalala, M. Barreiro Parrillo, N. Bellouin, C. Cassou, P.J. Durack, Y. Kosaka, S. McGregor, S. Min, O. Morgenstern, and Y. Sun, 2021: Human Influence on the Climate System. In Climate Change 2021: The Physical Science Basis. Contribution of Working Group I to the Sixth Assessment Report of the Intergovernmental Panel on Climate Change [Masson-Delmotte, V., P. Zhai, A. Pirani, S.L. Connors, C. Péan, S. Berger, N. Caud, Y. Chen, L. Goldfarb, M.I. Gomis, M. Huang, K. Leitzell, E. Lonnoy, J.B.R. Matthews, T.K. Maycock, T. Waterfield, O. Yelekçi, R. Yu, and B. Zhou (eds.)]. Cambridge University Press, Cambridge, United Kingdom and New York, NY, USA, pp. 423–552, doi: 10.1017/9781009157896.005.

14.1.4

Portions of the text and images are in the public domain from NOAA and can be found at https://www.climate.gov/news-features/understanding-climate/climate-change-minimum-arctic-sea-ice-extent, and https://arctic.noaa.gov/Report-Card/Report-Card-2020/ArtMID/7975/ArticleID/891/Sea-Ice.

14.1.5
Portions of the text and images are in the public domain from NOAA and can be found at https://www.climate.gov/news-features/understanding-climate/climate-change-glacier-mass-balance, and https://arctic.noaa.gov/Report-Card/Report-Card-2020/ArtMID/7975/ArticleID/906/Glaciers-and-Ice-Caps-Outside-Greenland.

Anthropogenic attribution of glacial melt reference- Marzeion, B., et al. “Attribution of Global Glacier Mass Loss to Anthropogenic and Natural Causes.” Science, vol. 345, no. 6199, 2014, pp. 919–921., https://www.science.org/doi/10.1126/science.1254702.

14.1.6
Portions of the text are from National Snow and Ice Data Center (NSIDC) which is sponsored by NASA, NSF, and NOAA. These references are found at https://nsidc.org/learn/what-cryosphere#anchor-ice-sheets.

Antarctic map from NASA and produced by the British Antarctic Survey and can be found at https://blogs.nasa.gov/icebridge/2014/11/19/east-and-west-the-geography-of-antarctica/ and is also available from the USGS at https://lima.usgs.gov/download.php.

14.1.7
Portions of the text and all the images are in the public domain from the EPA and can be found at https://www.epa.gov/climate-incoverdicators/climate-change-indicators-snow-cover.

Portions of the text are in the public domain from NOAA and can be found at https://www.climate.gov/news-features/understanding-climate/climate-change-spring-snow-cover.

14.1.8
Portions of the text and figures are in the public domain from the EPA and NOAA at https://www.epa.gov/climate-indicators/climate-change-indicators-sea-level, and https://www.climate.gov/news-features/understanding-climate/climate-change-global-sea-level.

14.2
GCM image and portions of the text are in the public domain from NOAA and can be found at https://www.climate.gov/maps-data/primer/climate-models.

Portions of the text - Introduction to Climate Science by Andreas Schmittner, which is licensed under a Creative Commons Attribution-NonCommercial 4.0 International License.

SRES-RCP scenario graphs are from the IPCC AR5 WG1 Box1.1-Figure3 which can be found at https://www.ipcc.ch/report/ar5/wg1/introduction/figbox1-1-3/.

SSP scenario text and associated graph - Chen, D., M. Rojas, B. H. Samset, K. Cobb, A. Diongue Niang, P. Edwards, S. Emori, S. H. Faria, E. Hawkins, P. Hope, P. Huybrechts, M. Meinshausen, S. K. Mustafa, G. K. Plattner, A. M. Tréguier, 2021, Framing, Context, and Methods Supplementary Material. In: Climate Change 2021: The Physical Science Basis. Contribution of Working Group I to the Sixth Assessment Report of the Intergovernmental Panel on Climate Change [Masson-Delmotte, V., P. Zhai, A. Pirani, S. L. Connors, C. Péan, S. Berger, N. Caud, Y. Chen, L. Goldfarb, M. I. Gomis, M. Huang, K. Leitzell, E. Lonnoy, J. B. R. Matthews, T. K. Maycock, T. Waterfield, O. Yelekçi, R. Yu and B. Zhou (eds.)]. Found in Chapter 1 at https://www.ipcc.ch/report/ar6/wg1/#FullReport.

14.2.1
Large portions of the CMIP text and video can be found at the World Climate Research Programme at https://www.wcrp-climate.org/wgcm-cmip.

14.2.2
Most of the text is from Introduction to Climate Science by Andreas Schmittner, and is licensed under a Creative Commons Attribution-NonCommercial 4.0 International License.

Some portions of the text and Figure 14-26 are from IPCC AR5 WG1 FAQ 10.1, and can be found at: https://www.ipcc.ch/report/ar5/wg1/detection-and-attribution-of-climate-change-from-global-to-regional/, and Chapter 10 at https://www.ipcc.ch/site/assets/uploads/2018/02/WG1AR5_Chapter10_FINAL.pdf, pages 894-895.

14.3 – 14.3.3
All historical information on the IPCC and their work can be found at https://www.ipcc.ch/.

Images are from IPCC AR6 WG1, Summary for Policy Makers and Chapter 4 at https://www.ipcc.ch/report/ar6/wg1/. The downloads for the Physical Basis Reports are found at https://www.ipcc.ch/report/ar6/wg1/downloads/, and separate zip files are available with the figures.

14.3.4 and 14.3.5

All figures are from IPCC AR6 WG1, Chapter 9 which can be found at https://www.ipcc.ch/report/ar6/wg1/#FullReport, and can be downloaded at https://www.ipcc.ch/report/ar6/wg1/downloads/. The formal citation is: Fox-Kemper, B., H.T. Hewitt, C. Xiao, G. Aðalgeirsdóttir, S.S. Drijfhout, T.L. Edwards, N.R. Golledge, M. Hemer, R.E. Kopp, G. Krinner, A. Mix, D. Notz, S. Nowicki, I.S. Nurhati, L. Ruiz, J.-B. Sallée, A.B.A. Slangen, and Y. Yu, 2021: Ocean, Cryosphere and Sea Level Change. In Climate Change 2021: The Physical Science Basis. Contribution of Working Group I to the Sixth Assessment Report of the Intergovernmental Panel on Climate Change [Masson-Delmotte, V., P. Zhai, A. Pirani, S.L. Connors, C. Péan, S. Berger, N. Caud, Y. Chen, L. Goldfarb, M.I. Gomis, M. Huang, K. Leitzell, E. Lonnoy, J.B.R. Matthews, T.K. Maycock, T. Waterfield, O. Yelekçi, R. Yu, and B. Zhou (eds.)]. Cambridge University Press, Cambridge, United Kingdom and New York, NY, USA, pp. 1211–1362, doi:10.1017/9781009157896.011.

15.1 and 15.2
Portions of the text and figures are in the public domain from the EPA and can be found at https://www.epa.gov/climate-indicators/weather-climate, and from the National Academy of Sciences, "Attribution of Extreme Weather Events in the Context of Climate Change", 2016; can be found at https://www.nap.edu/catalog/21852/attribution-of-extreme-weather-events-in-the-context-of-climate-change. An update of this NAS publication was started in 2025.

15.2.1
Portions of the text and all figures are in the public domain from the EPA and can be found at https://www.epa.gov/climate-indicators/climate-change-indicators-heat-waves and https://www.epa.gov/climate-indicators/climate-change-indicators-high-and-low-temperatures.

Observed increases of hot extremes are from the IPCC, AR6, Physical Science Basis, Chapter 11 which is available at https://www.ipcc.ch/report/ar6/wg1/#FullReport. The formal citation is: Seneviratne, S.I., X. Zhang, M. Adnan, W. Badi, C. Dereczynski, A. Di Luca, S. Ghosh, I. Iskandar, J. Kossin, S. Lewis, F. Otto, I. Pinto, M. Satoh, S.M. Vicente-Serrano, M. Wehner, and B. Zhou, 2021: Weather and Climate Extreme Events in a Changing Climate. In Climate Change 2021: The Physical Science Basis. Contribution of Working Group I to the Sixth Assessment Report of the Intergovernmental Panel on Climate Change [Masson-Delmotte, V., P. Zhai, A. Pirani, S.L. Connors, C. Péan, S. Berger, N. Caud, Y. Chen, L. Goldfarb, M.I. Gomis, M. Huang, K. Leitzell, E. Lonnoy, J.B.R. Matthews, T.K. Maycock, T. Waterfield, O. Yelekçi, R. Yu, and B. Zhou (eds.)]. Cambridge University Press, Cambridge, United Kingdom and New York, NY, USA, pp. 1513–1766, doi:10.1017/9781009157896.013.

15.2.2
Number of days below freezing is from the Fifth National Climate Assessment and can be found at https://nca2023.globalchange.gov/chapter/2/#fig-2-7.

Portion of the text and the cold days graph is in the public domain from the EPA and can be found at https://www.epa.gov/climate-indicators/climate-change-indicators-high-and-low-temperatures.

Observed decreases of cold extremes – IPCC, AR6, Physical Science Basis, Chapter 11 which is available at https://www.ipcc.ch/report/ar6/wg1/#FullReport. The formal citation is: Seneviratne, S.I., X. Zhang, M. Adnan, W. Badi, C. Dereczynski, A. Di Luca, S. Ghosh, I. Iskandar, J. Kossin, S. Lewis, F. Otto, I. Pinto, M. Satoh, S.M. Vicente-Serrano, M. Wehner, and B. Zhou, 2021: Weather and Climate Extreme Events in a Changing Climate. In Climate Change 2021: The Physical Science Basis. Contribution of Working Group I to the Sixth Assessment Report of the Intergovernmental Panel on Climate Change [Masson-Delmotte, V., P. Zhai, A. Pirani, S.L. Connors, C. Péan, S. Berger, N. Caud, Y. Chen, L. Goldfarb, M.I. Gomis, M. Huang, K. Leitzell, E. Lonnoy, J.B.R. Matthews, T.K. Maycock, T. Waterfield, O. Yelekçi, R. Yu, and B. Zhou (eds.)]. Cambridge University Press, Cambridge, United Kingdom and New York, NY, USA, pp. 1513–1766, doi:10.1017/9781009157896.013.

15.2.3
Portions of the text are from the older Fourth National Climate Assessment which can be found at https://science2017.globalchange.gov/chapter/8/.

Portions of the text on PDSI are available for educational use from UCAR and can be found at https://climatedataguide.ucar.edu/climate-data/palmer-drought-severity-index-pdsi.

Portions of the text and PDSI-chart.png are in the public domain from the EPA and can be found at https://www.epa.gov/climate-indicators/climate-change-indicators-drought.

General reference material used – IPCC, AR6, Physical Science Basis, Chapter 11 which is available at https://www.ipcc.ch/report/ar6/wg1/#FullReport. The formal citation is: Seneviratne, S.I., X. Zhang, M. Adnan, W. Badi, C. Dereczynski, A. Di Luca, S. Ghosh, I. Iskandar, J. Kossin, S. Lewis, F. Otto, I. Pinto, M. Satoh, S.M. Vicente-Serrano, M. Wehner, and B. Zhou, 2021: Weather and Climate Extreme Events in a Changing Climate. In Climate Change 2021: The Physical Science Basis. Contribution of Working Group I to the Sixth Assessment Report of the Intergovernmental Panel on Climate Change [Masson-Delmotte, V., P. Zhai, A. Pirani, S.L. Connors, C. Péan, S. Berger, N. Caud, Y. Chen, L. Goldfarb, M.I. Gomis, M. Huang, K. Leitzell, E. Lonnoy, J.B.R. Matthews, T.K. Maycock, T. Waterfield, O. Yelekçi, R. Yu, and B. Zhou (eds.)]. Cambridge University Press, Cambridge, United Kingdom and New York, NY, USA, pp. 1513–1766, doi:10.1017/9781009157896.013.

15.2.4
Portions of the text and heavy-precip bar graph are from the EPA and can be found at https://www.epa.gov/climate-indicators/climate-change-indicators-heavy-precipitation.

Annual heaviest daily precipitation amount map is from the Fifth National Climate Assessment and can be found at https://nca2023.globalchange.gov/chapter/2/#fig-2-8.

Confidence level on global heavy precipitation is from the IPCC, AR6, Chapter 11 which is available at https://www.ipcc.ch/report/ar6/wg1/#FullReport. The formal citation is: Seneviratne, S.I., X. Zhang, M. Adnan, W. Badi, C. Dereczynski, A. Di Luca, S. Ghosh, I. Iskandar, J. Kossin, S. Lewis, F. Otto, I. Pinto, M. Satoh, S.M. Vicente-Serrano, M. Wehner, and B. Zhou, 2021: Weather and Climate Extreme Events in a Changing Climate. In Climate Change 2021: The Physical Science Basis. Contribution of Working Group I to the Sixth Assessment Report of the Intergovernmental Panel on Climate Change [Masson-Delmotte, V., P. Zhai, A. Pirani, S.L. Connors, C. Péan, S. Berger, N. Caud, Y. Chen, L. Goldfarb, M.I. Gomis, M. Huang, K. Leitzell, E. Lonnoy, J.B.R. Matthews, T.K. Maycock, T. Waterfield, O. Yelekçi, R. Yu, and B. Zhou (eds.)]. Cambridge University Press, Cambridge, United Kingdom and New York, NY, USA, pp. 1513–1766, doi:10.1017/9781009157896.013.

15.2.5
Portions of the text and river flooding map are from the EPA and can be found at https://www.epa.gov/climate-indicators/climate-change-indicators-river-flooding.

Portions of the text are from the Fourth National Climate Assessment which can be found at https://science2017.globalchange.gov/chapter/8/. The Fourth National Climate Assessment seemed to have more relevant information on flooding than the latest one.

Quote from the IPCC, AR6, Physical Science Basis, chapter 11, page 11-64 and can be found at https://www.ipcc.ch/report/ar6/wg1/#FullReport.

15.2.6
Portions of the text are from the National Academy of Sciences, “Attribution of Extreme Weather Events in the Context of Climate Change”, pages 109-110, 2016; and can be found at https://www.nap.edu/catalog/21852/attribution-of-extreme-weather-events-in-the-context-of-climate-change. An update of this NAS publication was started in 2025.

Portions of the text and HurricaneRainfall graphic are from NOAA and can be found at https://www.climate.gov/news-features/features/will-hurricanes-change-world-warms.

General reference and for projected changes – IPCC, AR6, Physical Science Basis, Chapter 11 which can be found at https://www.ipcc.ch/report/ar6/wg1/#FullReport (page 88). The formal citation is: Seneviratne, S.I., X. Zhang, M. Adnan, W. Badi, C. Dereczynski, A. Di Luca, S. Ghosh, I. Iskandar, J. Kossin, S. Lewis, F. Otto, I. Pinto, M. Satoh, S.M. Vicente-Serrano, M. Wehner, and B. Zhou, 2021: Weather and Climate Extreme Events in a Changing Climate. In Climate Change 2021: The Physical Science Basis. Contribution of Working Group I to the Sixth Assessment Report of the Intergovernmental Panel on Climate Change [Masson-Delmotte, V., P. Zhai, A. Pirani, S.L. Connors, C. Péan, S. Berger, N. Caud, Y. Chen, L. Goldfarb, M.I. Gomis, M. Huang, K. Leitzell, E. Lonnoy, J.B.R. Matthews, T.K. Maycock, T. Waterfield, O. Yelekçi, R. Yu, and B. Zhou (eds.)]. Cambridge University Press, Cambridge, United Kingdom and New York, NY, USA, pp. 1513–1766, doi:10.1017/9781009157896.013.

Poleward change graphic is from the Fourth National Climate Assessment at https://science2017.globalchange.gov/chapter/9/.

15.2.7
Portion of the text are from the IPCC, AR6, WG1, Physical Science Basis, Chapters 2, 8 and 11 which can be found at https://www.ipcc.ch/report/ar6/wg1/#FullReport. The graph is a modified Figure 8.12 in Chapter 8. The formal citations are:
(Chapter 2) Gulev, S.K., P.W. Thorne, J. Ahn, F.J. Dentener, C.M. Domingues, S. Gerland, D. Gong, D.S. Kaufman, H.C. Nnamchi, J. Quaas, J.A. Rivera, S. Sathyendranath, S.L. Smith, B. Trewin, K. von Schuckmann, and R.S. Vose, 2021: Changing State of the Climate System. In Climate Change 2021: The Physical Science Basis. Contribution of Working Group I to the Sixth Assessment Report of the Intergovernmental Panel on Climate Change [Masson-Delmotte, V., P. Zhai, A. Pirani, S.L. Connors, C. Péan, S. Berger, N. Caud, Y. Chen, L. Goldfarb, M.I. Gomis, M. Huang, K. Leitzell, E. Lonnoy, J.B.R. Matthews, T.K. Maycock, T. Waterfield, O. Yelekçi, R. Yu, and B. Zhou (eds.)]. Cambridge University Press, Cambridge, United Kingdom and New York, NY, USA, pp. 287–422, doi:10.1017/9781009157896.004.

(Chapter 8) Douville, H., K. Raghavan, J. Renwick, R.P. Allan, P.A. Arias, M. Barlow, R. Cerezo-Mota, A. Cherchi, T.Y. Gan, J. Gergis, D. Jiang, A. Khan, W. Pokam Mba, D. Rosenfeld, J. Tierney, and O. Zolina, 2021: Water Cycle Changes. In Climate Change 2021: The Physical Science Basis. Contribution of Working Group I to the Sixth Assessment Report of the Intergovernmental Panel on Climate Change [Masson-Delmotte, V., P. Zhai, A. Pirani, S.L. Connors, C. Péan, S. Berger, N. Caud, Y. Chen, L. Goldfarb, M.I. Gomis, M. Huang, K. Leitzell, E. Lonnoy, J.B.R. Matthews, T.K. Maycock, T. Waterfield, O. Yelekçi, R. Yu, and B. Zhou (eds.)]. Cambridge University Press, Cambridge, United Kingdom and New York, NY, USA, pp. 1055–1210, doi:10.1017/9781009157896.010.

(Chapter 11) Seneviratne, S.I., X. Zhang, M. Adnan, W. Badi, C. Dereczynski, A. Di Luca, S. Ghosh, I. Iskandar, J. Kossin, S. Lewis, F. Otto, I. Pinto, M. Satoh, S.M. Vicente-Serrano, M. Wehner, and B. Zhou, 2021: Weather and Climate Extreme Events in a Changing Climate. In Climate Change 2021: The Physical Science Basis. Contribution of Working Group I to the Sixth Assessment Report of the Intergovernmental Panel on Climate Change [Masson-Delmotte, V., P. Zhai, A. Pirani, S.L. Connors, C. Péan, S. Berger, N. Caud, Y. Chen, L. Goldfarb, M.I. Gomis, M. Huang, K. Leitzell, E. Lonnoy, J.B.R. Matthews, T.K. Maycock, T. Waterfield, O. Yelekçi, R. Yu, and B. Zhou (eds.)]. Cambridge University Press, Cambridge, United Kingdom and New York, NY, USA, pp. 1513–1766, doi:10.1017/9781009157896.013.

15.2.8
Portions of the text are from the Fourth National Climate Assessment, Chapter 8, which can be found at https://science2017.globalchange.gov/chapter/8/. The formal citation for this chapter is Wehner, M.F., J.R. Arnold, T. Knutson, K.E. Kunkel, and A.N. LeGrande, 2017: Droughts, floods, and wildfires. In: Climate Science Special Report: Fourth National Climate Assessment, Volume I [Wuebbles, D.J., D.W. Fahey, K.A. Hibbard, D.J. Dokken, B.C. Stewart, and T.K. Maycock (eds.)]. U.S. Global Change Research Program, Washington, DC, USA, pp. 231-256, https://doi:10.7930/J0CJ8BNN. The Fifth National Climate Assessment, Chapter 7, contains more detailed information on wildfires at https://nca2023.globalchange.gov/chapter/7/, but was not used as a formal reference.

Portions of the text and wildfire graphs are from the EPA and can be found at https://www.epa.gov/climate-indicators/climate-change-indicators-wildfires.

Changes in fire weather conditions is from the IPCC, AR6, Physical Science Basis, Chapter 12 which is available at https://www.ipcc.ch/report/ar6/wg1/#FullReport. The formal citation is: Ranasinghe, R., A.C. Ruane, R. Vautard, N. Arnell, E. Coppola, F.A. Cruz, S. Dessai, A.S. Islam, M. Rahimi, D. Ruiz Carrascal, J. Sillmann, M.B. Sylla, C. Tebaldi, W. Wang, and R. Zaaboul, 2021: Climate Change Information for Regional Impact and for Risk Assessment. In Climate Change 2021: The Physical Science Basis. Contribution of Working Group I to the Sixth Assessment Report of the Intergovernmental Panel on Climate Change [Masson-Delmotte, V., P. Zhai, A. Pirani, S.L. Connors, C. Péan, S. Berger, N. Caud, Y. Chen, L. Goldfarb, M.I. Gomis, M. Huang, K. Leitzell, E. Lonnoy, J.B.R. Matthews, T.K. Maycock, T. Waterfield, O. Yelekçi, R. Yu, and B. Zhou (eds.)]. Cambridge University Press, Cambridge, United Kingdom and New York, NY, USA, pp. 1767–1926, doi:10.1017/9781009157896.014.

15.2.9
Portions of the text are from the National Academy of Sciences, “Attribution of Extreme Weather Events in the Context of Climate Change”, 2016; can be found at https://www.nap.edu/catalog/21852/attribution-of-extreme-weather-events-in-the-context-of-climate-change.

Quote from the IPCC, AR6, Physical Science Basis, Chapter 11, page 11-104 and can be found at https://www.ipcc.ch/report/ar6/wg1/#FullReport. The formal citation is: Seneviratne, S.I., X. Zhang, M. Adnan, W. Badi, C. Dereczynski, A. Di Luca, S. Ghosh, I. Iskandar, J. Kossin, S. Lewis, F. Otto, I. Pinto, M. Satoh, S.M. Vicente-Serrano, M. Wehner, and B. Zhou, 2021: Weather and Climate Extreme Events in a Changing Climate. In Climate Change 2021: The Physical Science Basis. Contribution of Working Group I to the Sixth Assessment Report of the Intergovernmental Panel on Climate Change [Masson-Delmotte, V., P. Zhai, A. Pirani, S.L. Connors, C. Péan, S. Berger, N. Caud, Y. Chen, L. Goldfarb, M.I. Gomis, M. Huang, K. Leitzell, E. Lonnoy, J.B.R. Matthews, T.K. Maycock, T. Waterfield, O. Yelekçi, R. Yu, and B. Zhou (eds.)]. Cambridge University Press, Cambridge, United Kingdom and New York, NY, USA, pp. 1513–1766, doi:10.1017/9781009157896.013.

15.3
Portions of the text are from the Fourth National Climate Assessment, Chapter 14, which can be found at https://science2017.globalchange.gov/chapter/14/. The formal citation for this chapter is DeAngelo, B., J. Edmonds, D.W. Fahey, and B.M. Sanderson, 2017: Perspectives on climate change mitigation. In: Climate Science Special Report: Fourth National Climate Assessment, Volume I [Wuebbles, D.J., D.W. Fahey, K.A. Hibbard, D.J. Dokken, B.C. Stewart, and T.K. Maycock (eds.)]. U.S. Global Change Research Program, Washington, DC, USA, pp. 393-410, https://doi10.7930/J0M32SZG.

Portions of the text are from “Introduction to Climate Science” by Andreas Schmittner and is licensed under a Creative Commons Attribution-NonCommercial 4.0 International License.

Another text reference – Higgins, Paul A. “How to Deal with Climate Change.” Physics Today, vol. 67, no. 10, 2014, pp. 32–37., https://doi.org/10.1063/pt.3.2548.

Climate change mitigation and adaptation illustrations are in the public domain from Wikimedia Commons at https://commons.wikimedia.org/wiki/File:Teaching_climate_change_mitigation_(blackboard)_icon.png, and https://commons.wikimedia.org/wiki/File:Teaching_climate_change_mitigation_(blackboard)_icon.png

16
National Research Council 2011. America's Climate Choices. Washington, DC: The National Academies Press. https://doi.org/10.17226/12781. Section 16.1 - text is composed from excerpts of Chapter 3, pages 29-37; Section 16.2 - text is composed from excerpts of Chapter 4, pages 39-50; and Section 16.3 - text is composed from excerpts of Chapter 5, pages 51-79.

Exploring Weather and Climate © 2025 by Glen Sampson is licensed under CC BY-NC-SA 4.0. To view a copy of this license, visit https://creativecommons.org/licenses/by-nc-sa/4.0/.